Seismic Performance of Chevron Concentrically Braced Frames with Weak Beams

Andrew D. Sen

A thesis
submitted in partial fulfillment of the
requirements for the degree of

Master of Science in Civil Engineering

University of Washington

2014

Committee:

Charles W. Roeder

Dawn E. Lehman

Jeffrey W. Berman

Program Authorized to Offer Degree:
Department of Civil and Environmental Engineering

©Copyright 2014
Andrew D. Sen

University of Washington

Abstract

Seismic Performance of Chevron Concentrically Braced Frames with Weak Beams

Andrew D. Sen

Chair of the Supervisory Committee:
Professor Charles W. Roeder
Civil and Environmental Engineering

Steel concentrically braced frames are lateral seismic force resisting systems that have been historically popular. Despite extensive deployment and continued service of these systems, little research has focused on the seismic performance and rehabilitation of older braced frames, termed non-seismic concentrically braced frames (NCBFs). Such frames were designed prior to the advent of capacity design standards and lack details and brace section geometry that promote ductility and sustain resistance, such as adequate gusset plate rotational clearance, minimum weld toughness, and brace compactness limits. Beams in NCBFs with braces in chevron configurations (V and inverted V) are commonly unable to develop the design brace unbalanced load specified in the 2010 AISC Seismic Provisions that arises after brace buckling. NCBFs with these weak beams are the primary subject of this research program. Two-story experimental specimens with braces in the inverted V configuration were tested at the National Center for Research on Earthquake Engineering in Taiwan to examine the seismic response of a prototypical existing NCBF and three rehabilitation schemes. The results show that poor brace compactness and connection details can be highly detrimental to system performance, but weak beam braced frames with ductile details can achieve good ductility while maintaining strength. Numerical models of the specimens, developed in Abaqus, simulate the observed response well and provide a validated basis for future analyses.

TABLE OF CONTENTS

Page

List of Figures vi

List of Tables xiii

Chapter 1: Introduction 1
1.1 Background 1
1.2 Evolution of CBF Design 2
1.3 NEES Project Overview 4
1.4 Research Objectives 5
1.5 Document Overview 5

Chapter 2: Infrastructure and Literature Review 7
2.1 Introduction 7
2.2 Infrastructure Review 7
2.3 Experimental Research 11
2.3.1 United States/Japan: Full-Scale Six-Story Building (Foutch et al. 1987; Roeder 1989) 11
Findings 11
Commentary 13
2.3.2 United States/Japan: Half-Scale Three-Story Building (Fukuta et al. 1989) . 13
Findings 14
Commentary 16
2.4 Computational Research 16
2.4.1 HP Building: 1994 Northridge Case Study (Rai and Goel 2003) 16
Findings 17
Commentary 18
2.4.2 Numerical Analysis of Chevron Braced Frames (Khatib et al. 1988) 19
Findings 19
Commentary 20

2.4.3 Effect of Beam Strength on Chevron Braced Frame Performance (Tremblay and Robert 2000, 2001) . . . 20
Findings . . . 21
Commentary . . . 22

Chapter 3: Experimental Specimen Design . . . 23
3.1 Introduction . . . 23
3.2 Overview of Limit States . . . 24
3.2.1 Uniform Force Method . . . 25
Corner gusset plates not welded to shear tabs . . . 27
Corner gusset plates welded to shear tabs . . . 28
Mid-span gusset plates . . . 29
3.2.2 Beam Axial-Flexural Interaction . . . 29
3.3 Component Material Properties . . . 31
3.4 Specimen Demand-to-Capacity Ratios . . . 32
3.5 TNCBF1-N-HSS Design . . . 35
3.5.1 General Constraints . . . 36
3.5.2 Connections . . . 38
3.5.3 Beam Details . . . 40
3.5.4 OpenSEES Analyses . . . 42
3.5.5 Abaqus Analyses . . . 44
3.5.6 Final Details . . . 48
3.6 TNCBF1-R-HSS Design . . . 49
3.7 TNCBF1-R-WF Design . . . 52
3.8 TNCBF2-D-HSS Design . . . 55
3.9 Experimental Setup . . . 58
3.9.1 Out-of-Plane Reaction Frame . . . 58
3.9.2 Actuator Load Path and Edge Beams . . . 59
3.9.3 Loading Protocol . . . 60
3.9.4 Base and Anchor Plates . . . 62
3.10 Instrumentation . . . 64
3.10.1 Frame . . . 66
3.10.2 Braces . . . 67
3.10.3 Beams . . . 67
3.10.4 Columns . . . 69

3.10.5 Whitewash 69

Chapter 4: Experimental Observations 71
4.1 Introduction 71
4.2 Performance State Overview 72
4.2.1 Yielding 75
4.2.2 Brace Buckling and Fracture 76
4.2.3 Brace Splice Connection Damage and Failure 77
4.2.4 Gusset Plate Cracking 78
4.2.5 Beam and Column Interface Weld and Base Metal Damage 79
4.3 TNCBF1-N-HSS Observations 80
4.3.1 Overview of Cyclic Response 80
4.3.2 Detailed Cyclic Response 87
Initial State (Roof Drift $\leq 0.35\%$) 87
Severe Damage State (Roof Drift $> 0.35\%$) 87
4.4 TNCBF1-R-HSS Observations 91
4.4.1 Overview of Cyclic Response 91
4.4.2 Detailed Cyclic Response 99
Initial State (Roof Drift $\leq 0.26\%$) 99
Moderate Damage State ($0.26\% <$ Roof Drift $\leq 0.89\%$) 99
Severe Damage State (Roof Drift $> 0.89\%$) 102
4.5 TNCBF1-R-WF Observations 107
4.5.1 Overview of Cyclic Response 107
4.5.2 Detailed Cyclic Response 115
Initial State (Roof Drift $\leq 0.26\%$) 115
Moderate Damage State ($0.26 <$ Roof Drift $\leq 0.62\%$) 115
Severe Damage State (Roof Drift $> 0.62\%$) 116
4.6 TNCBF2-D-HSS Observations 120
4.6.1 Overview of Cyclic Performance 120
4.6.2 Detailed Cyclic Performance 128
Initial State (Roof Drift $\leq 0.26\%$) 128
Moderate Damage State ($0.26\% <$ Roof Drift $\leq 1.07\%$) 128
Severe Damage State (Roof Drift $> 1.07\%$) 130

Chapter 5: Experimental Analysis . . . 135
5.1 Introduction . . . 135
5.1.1 Backbone Curve Description . . . 136
5.2 System Response . . . 136
5.2.1 Damage Progression . . . 136
5.2.2 Force-Drift Response . . . 137
Comparison to TCBF2 . . . 140
5.2.3 Energy Dissipation . . . 141
Comparison to TCBF2 . . . 143
5.3 Brace Response . . . 146
5.3.1 Brace Axial Force . . . 146
Predicting Maximum Axial Force in Tension . . . 146
5.3.2 Brace Vertical Unbalanced Force . . . 154
5.3.3 Brace Elongation . . . 157
5.3.4 Brace Out-of-Plane Mid-Span Deflection . . . 159
5.3.5 Brace Effective Length Factors . . . 164
5.4 Beam Response . . . 166
5.4.1 Beam Mid-Span Deflection . . . 166
5.4.2 Beam Torsion . . . 169
5.5 Frame Response . . . 173
5.5.1 Story Shear Contribution . . . 173
Predicting Maximum Lateral Resistance of Braces . . . 173
5.5.2 Brace Unbalance-Beam Deflection Response . . . 177
5.6 Connection Response . . . 180
5.6.1 Gusset Plate Rotation . . . 180
5.6.2 Beam-to-Column Connection Rotation . . . 184

Chapter 6: Numerical and Experimental Response Comparison . . . 187
6.1 Introduction . . . 187
6.2 Model Details . . . 187
6.2.1 Overview . . . 187
6.2.2 Elements and Meshing . . . 187
6.2.3 Material Models . . . 188
6.2.4 Boundary Conditions . . . 189
6.2.5 Brace Imperfection . . . 189

6.2.6 Composite Action . . . 191
6.3 TNCBF1-N-HSS Response Comparisons . . . 192
6.3.1 Observed Yielding . . . 194
6.4 TNCBF1-R-HSS Response Comparisons . . . 196
6.5 TNCBF1-R-WF Response Comparisons . . . 201
6.6 TNCBF2-D-HSS Response Comparisons . . . 206

Chapter 7: Summary and Conclusions . . . 212
7.1 Introduction . . . 212
7.2 Summary . . . 212
7.3 Conclusions . . . 214
7.3.1 Response of Existing NCBFs and Rehabilitation Priority . . . 214
7.3.2 Rehabilitation Scheme Evaluation . . . 217
7.3.3 Evaluation Recommendations . . . 217
7.4 Future Work . . . 218

Appendix A: Specimen Drawings . . . 221
A.1 TNCBF1-N-HSS . . . 221
A.2 TNCBF1-R-HSS . . . 246
A.3 TNCBF1-R-WF . . . 259
A.4 TNCBF2-D-HSS . . . 273
A.5 General Test Setup . . . 295

Appendix B: Sample Calculations . . . 311
B.1 Sample Design Calculations . . . 311
B.1.1 Brace Demands . . . 311
B.1.2 Connection Demand-to-Capacity Ratios . . . 312
Brace Limit States . . . 312
Connection Limit States . . . 315
B.1.3 Beams . . . 324
Axial-Flexural Interaction . . . 324

LIST OF FIGURES

Figure Number Page

1.1 Common CBF configurations . . . 2
1.2 Experimental setup at various NCBF testing locations . . . 4

2.1 Example NCBF elevations in building inventory . . . 9
2.2 Connection limit states by DCR (Sloat 2014) . . . 10
2.3 Elevation and brace connection details in six-story US/Japan specimen (Foutch et al. 1987) . . . 12
2.4 Elevation and slab and loading details in three-story US/Japan specimen (Fukuta et al. 1989) . . . 15
2.5 Idealized elevation and reported damage of North Hollywood HP building (Rai and Goel 2003) . . . 17
2.6 Pushover curves for simulated original and rehabilitated structures (Rai and Goel 2003) . . . 18
2.7 Typical analytical model used in Tremblay and Robert (2000, 2001) . . . 21

3.1 Test frame overview . . . 23
3.2 Assumed gusset plate load distribution for corner connections . . . 27
3.3 Assumed gusset plate load distribution for mid-span connections . . . 30
3.4 86WA3A corner gusset plate connection . . . 39
3.5 92WA2A corner gusset plate connection . . . 39
3.6 92WA2A mid-span gusset plate connection . . . 40
3.7 TNCBF1 second story corner connections at first story beam . . . 42
3.8 OpenSEES model of initial design . . . 43
3.9 OpenSEES first story drift hystereses . . . 45
3.10 Typical Abaqus model of initial design . . . 46
3.11 von Mises stress fields of models listed in Table 3.10 . . . 47
3.12 TNCBF1-N-HSS first story corner gusset plate details . . . 48
3.13 TNCBF1-N-HSS second story corner gusset plate details . . . 48
3.14 TNCBF1-N-HSS first story mid-span gusset plate details . . . 49
3.15 TNCBF1-N-HSS second story mid-span gusset plate details . . . 49

3.16 TNCBF1-R-HSS first story corner gusset plate details 50
3.17 TNCBF1-R-HSS first story mid-span gusset plate details 50
3.18 TNCBF1-R-HSS connection repair measures 52
3.19 TNCBF1-R-WF first story corner gusset plate details 53
3.20 TNCBF1-R-WF first story mid-span gusset plate details 53
3.21 TNCBF1-R-WF first story beam-to-column connection repairs 54
3.22 TNCBF2-D-HSS first story corner gusset plate details 56
3.23 TNCBF2-D-HSS second story corner gusset plate details 56
3.24 TNCBF2-D-HSS first story mid-span gusset plate details 57
3.25 TNCBF2-D-HSS second story mid-span gusset plate details 57
3.26 Typical slab blockout around corner gusset plates 58
3.27 Experimental setup 59
3.28 Out-of-plane frame interfaces 60
3.29 Actuator-to-specimen load path at second story 61
3.30 Frame edge beams 61
3.31 Loading protocol with test ends labeled 62
3.32 Base setup 63
3.33 Methods of determining brace out-of-plane displacement using string potentiometers 68
3.34 Column strain gauge schematic and derived shear and moment fields 70

4.1 Roof and story heights and displacements 71
4.2 Frame location notation 75
4.3 Examples of yielding 76
4.4 Examples of local buckling (BC) 77
4.5 Examples of brace fracture (BF) 77
4.6 Examples of brace splice connection damage 78
4.7 Example of plate cracking 79
4.8 Example of gusset plate interface weld and base metal damage 79
4.9 Example of beam interface weld and base metal damage 80
4.10 TNCBF1-N-HSS overview 81
4.11 TNCBF1-N-HSS roof drift history 81
4.12 TNCBF1-N-HSS load history 82
4.13 TNCBF1-N-HSS base shear-roof drift hysteresis 83
4.14 TNCBF1-N-HSS base shear-story drift hystereses 83
4.15 TNCBF1-N-HSS initial yielding at column base, Y1 (0.27% story drift) 87
4.16 TNCBF1-N-HSS buckling and tearing of 1F south brace 88

4.17 TNCBF1-N-HSS fracture of 1F south brace, BF (0.46% first story drift at fracture) 89
4.18 TNCBF1-N-HSS transverse first story slab crack due to upward beam deflection (0.99% first story drift) . . . 89
4.19 TNCBF1-N-HSS yielding from beam (link) rotation, Y2 (1.15% first story drift) . . 90
4.20 TNCBF1-N-HSS first story north brace beam mid-span connection fracture, BFs (-1.24% story drift) . . . 91
4.21 TNCBF1-N-HSS miscellaneous observations . . . 91
4.22 TNCBF1-R-HSS overview . . . 92
4.23 TNCBF1-R-HSS roof drift history . . . 93
4.24 TNCBF1-R-HSS load history . . . 93
4.25 TNCBF1-R-HSS base shear-roof drift hysteresis . . . 94
4.26 TNCBF1-R-HSS base shear-story drift hystereses . . . 94
4.27 TNCBF1-R-HSS first story yielding, Y1 (0.29% first story drift) . . . 99
4.28 TNCBF1-R-HSS south first story out-of-plane brace buckling . . . 100
4.29 TNCBF1-R-HSS north first story gusset plate elliptical yielding (1.10% first story drift) . . . 100
4.30 TNCBF1-R-HSS first story corner gusset plate weld (W) and base metal (WB) damage . . . 101
4.31 TNCBF1-R-HSS first story beam yielding, Y2 (-0.94% story drift) . . . 102
4.32 TNCBF1-R-HSS first story column yielding . . . 102
4.33 TNCBF1-R-HSS first story brace damage progression . . . 103
4.34 TNCBF1-R-HSS south first story corner gusset plate weld crack (post-test) . . . 104
4.35 TNCBF1-R-HSS first story beam yielding, Y3 (post-test) . . . 105
4.36 TNCBF1-R-HSS first story beam-to-column connection damage . . . 105
4.37 TNCBF1-R-HSS column and gusset plate yielding at bases, Y3 (post-test) . . . 106
4.38 TNCBF1-R-HSS concrete spalling around north second story brace corner connection (−0.46% second story drift) . . . 106
4.39 TNCBF1-R-HSS north second story brace splice connection damage, Bs2 (−0.46% second story drift) . . . 107
4.40 TNCBF1-R-WF overview . . . 108
4.41 TNCBF1-R-WF roof drift history . . . 108
4.42 TNCBF1-R-WF load history . . . 109
4.43 TNCBF1-R-WF base shear-roof drift hysteresis . . . 110
4.44 TNCBF1-R-WF base shear-story drift hystereses . . . 110
4.45 TNCBF1-R-WF first story yielding accelerated by thermal stresses, Y1 (0.17 story drift level) . . . 116

4.46 TNCBF1-R-WF first story brace buckling, B1 . . . 117
4.47 TNCBF1-R-WF north second story brace splice connection damage . . . 118
4.48 TNCBF1-R-WF second story brace splice connection fracture . . . 119
4.49 Beam base metal tear at bottom of shear tab (−1.22% story drift) . . . 120
4.50 TNCBF1-R-WF first story beam-to-column connection fracture . . . 120
4.51 TNCBF2-D-HSS overview . . . 121
4.52 TNCBF2-D-HSS roof drift history . . . 121
4.53 TNCBF2-D-HSS load history . . . 122
4.54 TNCBF2-D-HSS base shear-roof drift hysteresis . . . 123
4.55 TNCBF2-D-HSS base shear-story drift hystereses . . . 123
4.56 TNCBF2-D-HSS typical initial gusset plate yielding, Y1 (0.26% first story drift) . . . 128
4.57 TNCBF2-D-HSS south first story brace buckling progression . . . 129
4.58 TNCBF2-D-HSS south first story beam mid-span, Y2 (−1.72% first story drift) . . . 130
4.59 TNCBF2-D-HSS first story corner gusset plate column interface weld cracks, Wc . . . 131
4.60 TNCBF2-D-HSS typical first story slab crack around block-out (2.57% first story drift) . . . 131
4.61 TNCBF2-D-HSS first story beam-to-column connection regions, Y2 (post-test) . . . 132
4.62 TNCBF2-D-HSS column yielding and local buckling at bases, Y3 (2.57% first story drift) . . . 132
4.63 TNCBF2-D-HSS first story gusset plates, Y3 (post-test) . . . 133
4.64 TNCBF2-D-HSS second story gusset plates, Y3 (post-test) . . . 134

5.1 Backbone curve (hysteretic envelope) example . . . 135
5.2 Damage state progression of TNCBF frames . . . 137
5.3 Base shear-roof drift backbone curve . . . 138
5.4 Base shear-first story drift backbone curve . . . 139
5.5 Base shear-second story drift backbone curve . . . 139
5.6 Base shear-story drift backbones from TNCBF and TCBF2 tests . . . 140
5.7 Cumulative frame energy dissipated . . . 141
5.8 Cumulative first story energy dissipated . . . 142
5.9 Cumulative second story energy dissipated . . . 142
5.10 TNCBF2-D-HSS cumulative energy dissipated decomposed by component type . . . 143
5.11 Cumulative energy dissipated in TNCBF and TCBF2 tests . . . 145
5.12 Cyclic energy dissipated in TNCBF and TCBF2 tests . . . 145
5.13 TNCBF1-N-HSS brace elongation hystereses . . . 147
5.14 TNCBF1-R-HSS brace elongation hystereses . . . 148

5.15 TNCBF1-R-WF brace elongation hystereses . . . 149
5.16 TNCBF2-D-HSS brace elongation hystereses . . . 150
5.17 Plastic mechanism for braced frame beam . . . 151
5.18 TNCBF2-D-HSS first story brace axial force hystereses with effective brace yield force in tension . . . 153
5.19 TNCBF1-N-HSS brace unbalanced force hystereses . . . 155
5.20 TNCBF1-R-HSS brace unbalanced force hystereses . . . 155
5.21 TNCBF1-R-WF brace unbalanced force hystereses . . . 156
5.22 TNCBF2-D-HSS brace unbalanced force hystereses . . . 156
5.23 TNCBF1-R-WF first story brace elongation curves . . . 157
5.24 TNCBF2-D-HSS brace elongation curves . . . 158
5.25 TNCBF1-N-HSS brace out-of-plane mid-span hystereses . . . 160
5.26 TNCBF1-R-HSS brace out-of-plane mid-span hystereses . . . 161
5.27 TNCBF1-R-WF brace out-of-plane mid-span hystereses . . . 162
5.28 TNCBF2-D-HSS brace out-of-plane mid-span hystereses . . . 163
5.29 TNCBF1-N-HSS beam vertical deflection hystereses . . . 167
5.30 TNCBF1-R-HSS beam vertical deflection hystereses . . . 167
5.31 TNCBF1-R-WF beam vertical deflection hystereses . . . 168
5.32 TNCBF2-D-HSS beam vertical deflection hystereses . . . 168
5.33 Beam torsional rotation geometry . . . 169
5.34 TNCBF1-N-HSS beam mid-span torsional rotation . . . 171
5.35 TNCBF1-R-HSS beam mid-span torsional rotation . . . 171
5.36 TNCBF1-R-WFS beam mid-span torsional rotation . . . 172
5.37 TNCBF2-D-HSS beam mid-span torsional rotation . . . 172
5.38 Column shear contribution to story shear backbone curves . . . 174
5.39 Brace lateral resistance backbones normalized by plastic load case . . . 175
5.40 Brace lateral resistance backbones normalized by plastic load case . . . 176
5.41 TNCBF1-N-HSS brace unbalanced force-beam vertical deflection hystereses . . . 178
5.42 TNCBF1-R-HSS brace unbalanced force-beam vertical deflection hystereses . . . 178
5.43 TNCBF1-R-WF brace unbalanced force-beam vertical deflection hystereses . . . 179
5.44 TNCBF2-D-HSS brace unbalanced force-beam vertical deflection hystereses . . . 179
5.45 Gusset plate rotation geometry . . . 181
5.46 TNCBF1-N-HSS gusset plate out-of-plane rotation hystereses . . . 181
5.47 TNCBF1-R-HSS gusset plate out-of-plane rotation hystereses . . . 182
5.48 TNCBF1-R-WF gusset plate out-of-plane rotation hystereses . . . 182

5.49 TNCBF2-D-WF gusset plate out-of-plane rotation hystereses 183
5.50 Joint rotation mechanisms 184
5.51 TNCBF1-N-HSS first story beam-to-column connection rotation 185
5.52 TNCBF1-R-HSS first story beam-to-column connection rotation 185
5.53 TNCBF1-R-WFS first story beam-to-column connection rotation 186
5.54 TNCBF2-D-HSS first story beam-to-column connection rotation 186

6.1 Abaqus model boundary conditions 190
6.2 TNCBF1-N-HSS Abaqus model 192
6.3 TNCBF1-N-HSS experimental and simulated roof drift hystereses 193
6.4 TNCBF1-N-HSS experimental and simulated story drift hystereses 193
6.5 TNCBF1-N-HSS experimental and simulated beam mid-span deflection hystereses . 194
6.6 TNCBF1-N-HSS experimental and simulated first story brace mid-span deflection hystereses 194
6.7 TNCBF1-N-HSS south first story corner gusset plate at 0.44% roof drift 195
6.8 TNCBF1-N-HSS south first story beam end at 0.71% roof drift 195
6.9 TNCBF1-R-HSS Abaqus model 196
6.10 TNCBF1-R-HSS experimental and simulated roof drift hystereses 197
6.11 TNCBF1-R-HSS experimental and simulated story drift hystereses 197
6.12 TNCBF1-R-HSS experimental and simulated beam mid-span deflection hystereses . 198
6.13 TNCBF1-R-HSS experimental and simulated first story brace mid-span deflection hystereses 198
6.14 TNCBF1-R-HSS north first story corner gusset plate at test end 199
6.15 TNCBF1-R-HSS north first story mid-span gusset plate at test end 199
6.16 TNCBF1-R-HSS first story beam at test end 200
6.17 TNCBF1-R-HSS south first story beam-to-column connection region at test end . . 200
6.18 TNCBF1-R-WF Abaqus model 201
6.19 TNCBF1-R-WF experimental and simulated roof drift hystereses 202
6.20 TNCBF1-R-WF experimental and simulated story drift hystereses 202
6.21 TNCBF1-R-WF experimental and simulated beam mid-span deflection hystereses . 203
6.22 TNCBF1-R-WF experimental and simulated first story brace mid-span deflection hystereses 203
6.23 TNCBF1-R-WF south first story brace at base region at 0.17% roof drift 204
6.24 TNCBF1-R-WF south first story corner gusset plate at 0.35% roof drift 204
6.25 TNCBF1-R-WF south first story beam-to-column connection region at test end . . 205

6.26 TNCBF1-R-WF south second story column near beam-to-column connection at test end . . . 205
6.27 TNCBF2-D-HSS Abaqus model . . . 206
6.28 TNCBF2-D-HSS experimental and simulated roof drift hystereses . . . 207
6.29 TNCBF2-D-HSS experimental and simulated story drift hystereses . . . 207
6.30 TNCBF2-D-HSS experimental and simulated beam mid-span deflection hystereses . 208
6.31 TNCBF2-D-HSS experimental and simulated first story brace mid-span deflection hystereses . . . 208
6.32 TNCBF2-D-HSS experimental and simulated second story brace mid-span deflection hystereses . . . 209
6.33 TNCBF2-D-HSS south base plate region at test end . . . 210
6.34 TNCBF2-D-HSS north base plate region at test end . . . 210
6.35 TNCBF2-D-HSS south first story beam-to-column region at test end . . . 211

B.1 Whitmore section diagram . . . 316
B.2 Flexural buckling diagram based on Whitmore width . . . 318

LIST OF TABLES

Table Number Page

1.1 Pre-1988 (NCBF) and present (SCBF) design criteria . . . 3

2.1 Chevron NCBF building inventory details compiled by Sloat (2014) . . . 8
2.2 Members, geometry, and beam interaction values in six-story US/Japan specimen . 13
2.3 Members, geometry, and beam interaction values in three-story US/Japan specimens 15

3.1 Limit states and corresponding resistance expressions for AISC and balanced design approaches (Roeder et al. 2011b) . . . 25
3.2 Notation for symbols in Table 3.1 . . . 26
3.3 Steel material properties . . . 32
3.4 Concrete material properties . . . 32
3.5 Component demand-to-capacity ratios[a] in TNCBF test series . . . 34
3.6 TNCBF1-R-HSS knife plate demand-to-capacity ratios[a] . . . 35
3.7 Brace compactness ratios (λ/λ_{hd}) . . . 35
3.8 Unfactored DCRs for shared shear tab reference connections (Sloat 2014) . . . 41
3.9 List of OpenSEES analyses . . . 43
3.10 List of Abaqus analyses . . . 46
3.11 Loading protocol . . . 62
3.12 Overview of sensor descriptions and uses . . . 65

4.1 Performance state notation modified from Lumpkin (2009) . . . 73
4.2 Frame location notation . . . 74
4.3 Description of labels in Figs. 4.13 and 4.14 . . . 83
4.4 TNCBF1-N-HSS peak lateral resistances and drifts . . . 84
4.5 TNCBF1-N-HSS performance state progression . . . 85
4.6 Description of labels in Figs. 4.25 and 4.26 . . . 94
4.7 TNCBF1-R-HSS peak lateral resistances and drifts . . . 95
4.8 TNCBF1-R-HSS performance state progression . . . 96
4.9 Description of labels in Figs. 4.43 and 4.44 . . . 110
4.10 TNCBF1-R-WF peak lateral resistances and drifts . . . 111
4.11 TNCBF1-R-WF performance state progression . . . 112

4.12 Description of labels in Figs. 4.54 and 4.55 123
4.13 TNCBF2-D-HSS peak lateral resistances and drifts 124
4.14 TNCBF2-D-HSS performance state progression 125

5.1 Variables in plastic mechanism to predict brace force 152
5.2 TNCBF2-D-HSS variables for beam plastic analysis 153
5.3 Brace effective length factors 164
5.4 Beam mid-span deflection maxima and residuals 166

6.1 Abaqus model steel material properties 188
6.2 Abaqus model concrete material properties 189
6.3 Brace imperfection amplitudes and directions 190

7.1 Rehabilitation priority of tested NCBF deficiencies 215

ACKNOWLEDGMENTS

I would like to acknowledge my advisors and supervisory committee, Professors Charles Roeder, Jeffrey Berman, and Dawn Lehman, who have provided considerable support and guidance during the course of my master's degree and offered invaluable feedback on the content of this thesis. Further, they provided initial funding for my degree and steered me toward securing an external fellowship. I am truly grateful for their continued interest in my success as an academic and as an individual.

I would also like to extend my sincere gratitude to Professor Keh-Chyuan Tsai of National Taiwan University (NTU) and the National Center for Research on Earthquake Engineering (NCREE), who facilitated experimental testing and extended generous hospitality during my two visits to Taiwan. These trips were made especially productive thanks to the laboratory staff at NCREE, including Chao-Hsien Li and An-Chien Wu, who managed specimen construction and instrumentation on a day-to-day basis. In addition, Professor Tsai's graduate students at NTU ("KC 512") were extremely helpful in installing instrumentation, collecting observations, and generally ensuring that I had a great experience.

Many students at the University of Washington (UW) also provided significant help as friends and colleagues. In particular, Dan Sloat, Molly Johnson, and Ryan Ballard, my fellow graduate students on this research project, were and continue to be valuable assets. I would also like thank Kelli Slaven and Meredith Clarke, who ventured abroad with me to help instrument specimens and collect data. There are countless other former and current UW graduate students who have made a positive impact during my first few years in Seattle–it is probably true that if they are reading these acknowledgments, then they know who they are.

Monetary support from the National Science Foundation through the George E. Brown, Jr. Network for Earthquake Engineering Simulation (CMMI #1208002) and my Gradaute Research Fellowship (DGE #1256082) is also much appreciated. The experimental testing presented in this

thesis would also not have been possible without steel donations made by the American Institute of Steel Construction.

Finally, and perhaps most importantly, I would like to thank my family–my parents, David and Pamela Sen and my brother, Jeremy Sen–for their unwavering love and support from across the country.

Chapter 1
INTRODUCTION

1.1 Background

The concentrically braced frame (CBF) lateral force resisting system is a mainstay in steel construction. CBFs have long been used to resist wind, seismic, and other lateral forces; they are attractive because they exhibit considerable strength and stiffness, have traditionally been economical, and are familiar to engineers, architects, and fabricators. The majority of the lateral resistance provided by CBFs is provided by the braces, which are oriented diagonally like a truss. However, braced frames should not be thought of as trusses, as in seismic events, the braces are intended to yield in tension and buckle in compression, acting as ductile fuses to dissipate energy. Since the tensile and compressive responses of the braces differ, they are typically used in pairs, as in Fig. 1.1, to achieve a symmetric response. In the design of special concentrically braced frames (SCBFs), the standard in CBF design in regions of high seismicity, restrictions are placed on connection details, brace configuration, and the geometry of the structural shapes that comprise the frame to ensure a ductile response.

In recent years, a wealth of SCBF-focused research has sought to maximize the seismic performance of braced frames and advance the state of the practice. This has led to the development of improved gusset plate rotational clearance models (Lehman et al. 2008) and a balanced design procedure (BDP) that promotes ductility (Roeder et al. 2011b). Yet, significantly less research has examined the performance of older braced frames designed prior to the adoption of the 1988 Uniform Building Code (ICBO 1988), which introduced capacity design principles into code for the first time–principles that laid the foundation for current seismic design. Lacking a capacity design philosophy, these older, "non-seismic" concentrically braced frames (NCBFs) have been recognized by the engineering community as vulnerable to earthquake loading. Due to the historical prevalence of braced frame construction, many NCBFs are still in service today in areas of high seismic risk, while some have been retrofitted or repaired to upgrade performance.

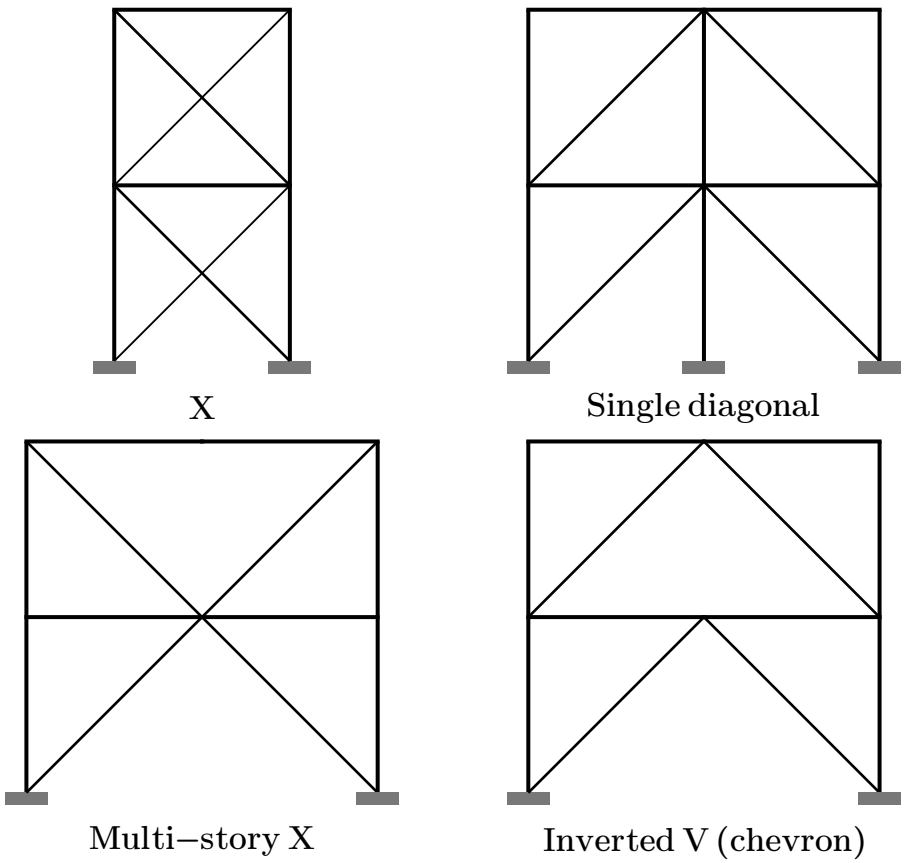

Figure 1.1: Common CBF configurations

1.2 Evolution of CBF Design

Unrehabilitated NCBFs have obviously not benefited from the numerous design advances in the past several decades. NCBF braces were selected as today based on reduced seismic forces, but the connections, beams, and columns were sized for the design seismic load as well. In modern design, these components are designed such that their capacities exceed the expected brace demands (i.e., the tensile and compressive capacities of the braces). Braces are sized based on their compressive capacities, typically governed by buckling. As a result, the tensile yield strength of the brace is almost certainly greater than the force associated with the seismic loads. Significant changes have also been made to brace section and connection detailing limits, including more stringent brace slenderness and compactness criteria as well as the addition of provisions for gusset plate rotational

clearance. Further, in many cases, design spectral accelerations have increased in magnitude since 1988, and the existing braces may not provide suitable lateral resistance.

Code evolution was not limited to braces and connections. The 1997 Seismic Provisions (AISC 1997) introduced consideration for the brace unbalanced force in chevron (V and inverted V) configuration braced frames. Prior to brace buckling, opposing braces remain elastic and develop axial forces equal in magnitude. However, when braces buckle, strength in compression degrades while the force developed in tension remains stable (and may in fact increase).The brace forces were balanced in the elastic case, but the post-buckling response produces an unbalanced load condition and a resultant downward (vertical) force arises at the beam mid-span. This brace unbalanced force can generate substantial bending moment in the beam and lead to an undesirable collapse mechanism if plastic hinges form in the beam. AISC 341-10 (AISC 2010a) mandates that the braced frame beam be able to develop a design unbalanced load where one brace yields in tension and the other is at 30% of its critical buckling load in compression. This provision often results in the use of large and expensive beam sections.

Major design changes since 1988 are summarized in Table 1.1.

Table 1.1: Pre-1988 (NCBF) and present (SCBF) design criteria

Citerion	Pre-1988 (NCBF)	Present (SCBF)
Brace slenderness	–	$KL/r \lesssim 100$
Brace compactness	–	Compactness ratio $\leq \lambda_{\text{hd}}$
Gusset plate	Design for brace force from seismic load	Design for expected brace capacity
Gusset plate rotational clearance	–	$2t_{\text{p}}$ linear (AISC) or $8t_{\text{p}}$ elliptical at corner gusset plates and $6t_{\text{p}}$ vertical at mid-span gusset plates (BDP)
Columns	Design for brace force from seismic load	Design for expected brace capacity
Beams	Design for brace force from seismic load	Design for expected brace capacity (unbalanced load)

1.3 NEES Project Overview

The research presented in this document belongs to a larger collaborative effort involving the University of Washington (UW); the University of California, Berkeley; and the National Center for Research on Earthquake Engineering (NCREE) in Taipei, Taiwan. Funding is provided by the National Science Foundation (NSF) through the George E. Brown, Jr. Network for Earthquake Engineering Simulation (NEES). Large-scale experimental testing is performed at each of the aforementioned sites to evaluate the performance of existing braced frames and potential rehabilitation methods. Pictures of each of the test setups are shown in Fig. 1.2. Testing at the University of Washington of one-story single-diagonal specimens is primarily intended to examine brace and connection performance. Two-story testing at nees@berkeley investigates system performance of exsisting and rehabilitated NCBFs with weak beams, one weak axis column, and loading at both stories. Finally, experiments conducted at NCREE–the focus of this report–explore the performance of two-story inverted V-braced existing and repaired weak beam NCBFs designed with various degrees of composite action, brace types, and connection details.

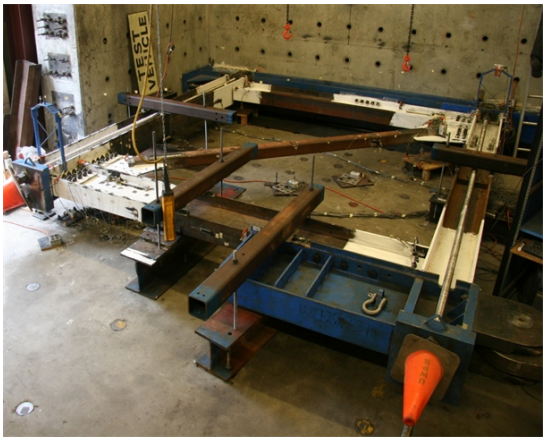

(a) UW, courtesy of Molly Johnson



(b) Berkeley, courtesy of Jiun-Wei Lai



(c) NCREE

Figure 1.2: Experimental setup at various NCBF testing locations

1.4 Research Objectives

In line with the overarching goal of the international research collaboration, the objectives specific to the work presented herein include:

- Experimentally evaluate the performance of existing NCBFs with weak beams.
- Experimentally evaluate the performance of several rehabilitation measures for NCBFs with weak beams. Repair or retrofit that does not require invasive action (e.g., beam reinforcement, slab removal, etc.) is preferred.
- Quantify composite action developed in the absence of shear connectors.
- Determine the effects of weak beams on system and component response.
- Determine critical limit states or details highly detrimental to frame performance.
- Compare the performance of existing and rehabilitated NCBFs to SCBFs.
- Validate the response of finite element models simulating the experimental specimens.
- Propose design and analysis recommendations for practicing engineers based on experimental observations and analyses.

1.5 Document Overview

To address the stated research objectives, this report is divided into six additional chapters. Chapter 2 provides a review of existing weak beam NCBF infrastructure and pertinent experimental and computational previous research efforts. Descriptions of experimental specimen design, including preliminary numerical analyses, as well as the test setup at NCREE are included in Chapter 3. Observations from each of the four tests are documented in Chapter 4. Chapter 5 builds upon the observations through comprehensive analyses of experimental data collected by instrumentation. Chapter 6 compares the response of finite element models of each specimen developed by Lingli Pan in Abaqus (Dassault Systèmes 2013) to the test results. Finally, Chapter 7 contains a summary

of the research conducted as well as conclusions drawn from this work. Appdendix A includes the specimen construction and instrumentation drawings and Appendix B provides sample calculations used to evaluate component limit states.

Chapter 2

INFRASTRUCTURE AND LITERATURE REVIEW

2.1 Introduction

This chapter introduces weak beam NCBF infrastructure and weak beam-related previous research. A relatively limited amount of research has attempted to quantify weak beam effects on braced frame performance; experimental research on this subject was largely conducted as part of an international collaboration between the United States and Japan.

2.2 Infrastructure Review

Sloat (2014) conducted an extensive review of NCBF infrastructure. In all, the limit states and member attributes of 12 low- to mid-rise buildings were analyzed. Of these buildings, 8 contain chevron bracing, all of which have weak beams relative the brace unbalance load. Beam strength was evaluated on the basis of axial-flexural interaction (Eq. 2.1), unfactored ($\phi = 1.0$) beam capacities, and the axial forces and moments associated with the AISC (2010a) design horizontal and vertical brace unbalanced load components (Eqs. 2.2 and 2.3). An interaction value greater than one indicates that the beam is weak with respect to the unbalanced load. Details of the frames, including their unfactored brace axial-flexural interaction values, are listed in Table 2.1 and Fig. 2.1 depicts four examples of NCBF elevations. The expected yield strengths (i.e., $R_{\mathrm{y}}F_{\mathrm{y}}$) of the steel were used in the interaction calculations and composite action was neglected. Only interaction values calculated for stories with chevron braces are shown.

$$\frac{P_{\mathrm{r}}}{P_{\mathrm{c}}} + \frac{8}{9}\frac{M_{\mathrm{r}}}{M_{\mathrm{c}}} \leq 1.0 \tag{2.1}$$

$$H_{\mathrm{unbal}} = (R_{\mathrm{y}}F_{\mathrm{y}}A_{\mathrm{g}} + 0.3F_{\mathrm{cre}}A_{\mathrm{g}})\cos\gamma \tag{2.2}$$

$$V_{\mathrm{unbal}} = (R_{\mathrm{y}}F_{\mathrm{y}}A_{\mathrm{g}} - 0.3F_{\mathrm{cre}}A_{\mathrm{g}})\sin\gamma \tag{2.3}$$

Table 2.1: Chevron NCBF building inventory details compiled by Sloat (2014)

Building	Date	State	Occupant	Stories	Brace type(s)	Connection type(s)	Beam interaction (DCR)
83CA3A	10/1983	CA	Corporate HQ	3	HSS, WF	Bolted "mega" gusset	6.32, 4.52
82TN4A	11/1982	TN	Corporate HQ	3, 5	HSS, pipe	Bolted shared shear tab	1.55, 1.06, 0.94
88CA3A	1/1988	CA	Research	2, 3	HSS, pipe	Bolted "mega" gusset	8.84, 6.66
80CA4A	9/1980	CA	Office	4	HSS, WF	Beam only	1.73, 1.53, 1.14
86WA3A	6/1986	WA	Hospital	3	HSS	Welded shared shear tab	3.76, 1.61
83CA2A	5/1983	CA	Office	2	HSS	Fully welded	4.35, 3.32
86CA4A	8/1986	CA	Office	4	HSS	Bolted double angle	5.91, 3.30, 3.52, 3.25
92WA2A	2/1992	WA	School	2, 3	HSS	Welded shared shear tab	3.84, 5.09

NCBF deficiencies are of course not limited to beams. Widespread connection limit states failing to develop brace capacities are reported by Sloat (2014), shown graphically in Fig. 2.2. In addition, 7 of the 12 buildings analyzed had non-seismically compact braces.

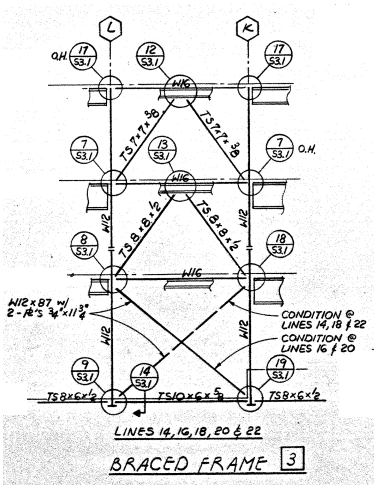

(a) 83CA3A

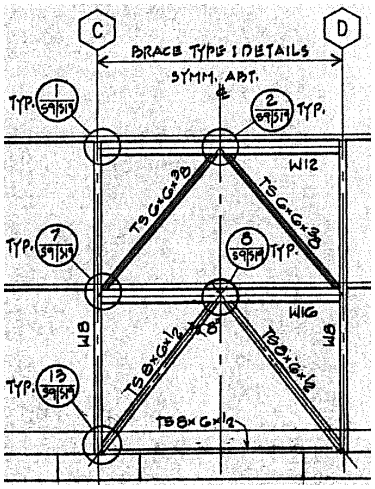

(b) 88CA3A

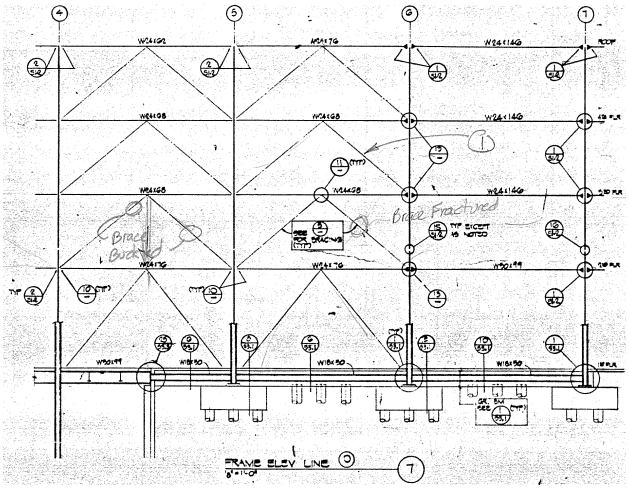

(c) 86CA4A

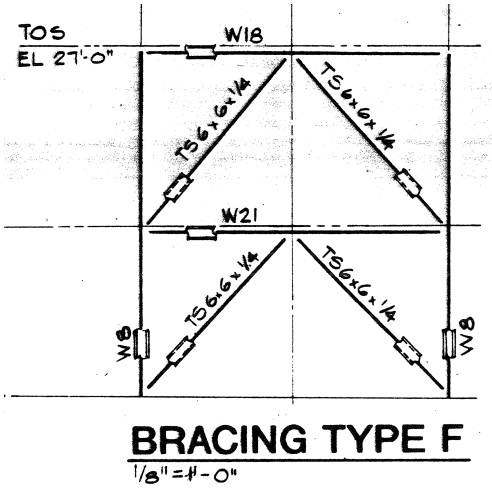

(d) 92WA2A

Figure 2.1: Example NCBF elevations in building inventory

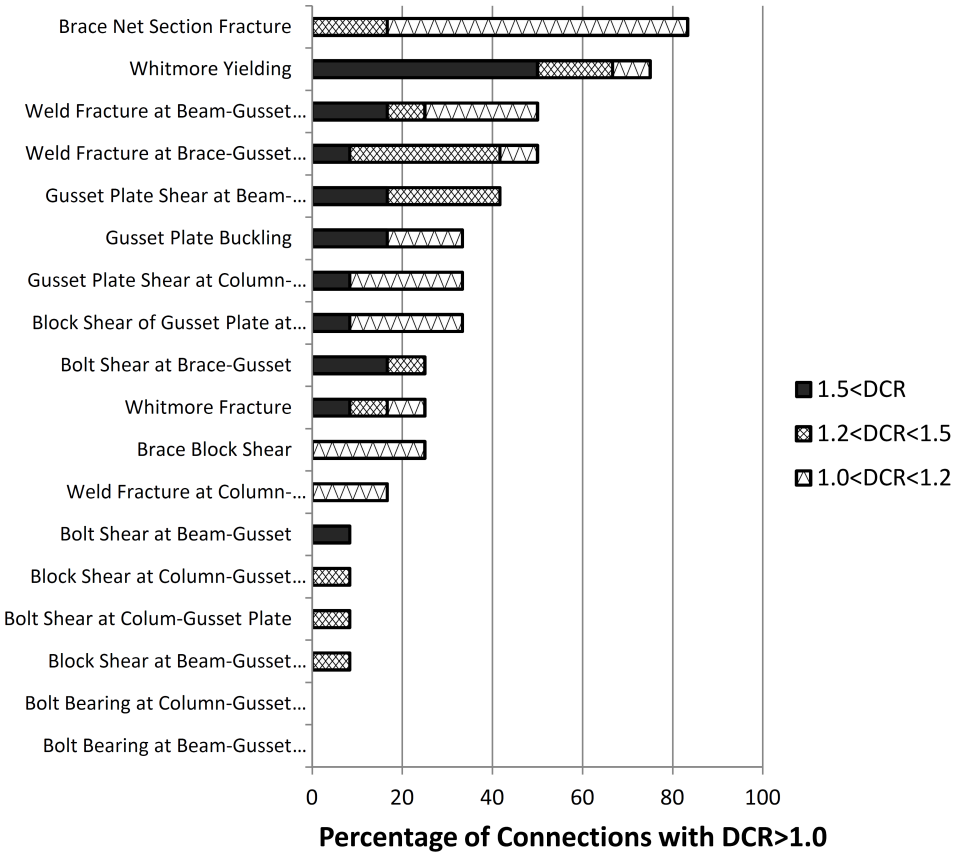

Figure 2.2: Connection limit states by DCR (Sloat 2014)

2.3 Experimental Research

2.3.1 United States/Japan: Full-Scale Six-Story Building (Foutch et al. 1987; Roeder 1989)

As part of the United States/Japan Cooperative Earthquake Research Program Utilizing Large-Size Testing Facilities, a six-story chevron configuration NCBF was tested on May 18, 1981 at the Large Size Structures Laboratory in Tsukuba, Japan. The setup and results of the research program are described by Foutch et al. (1987) and Roeder (1989). The frame represented a blend of current practice in the United States and Japan at the time of testing. The structure consisted of two-by-two bays with the CBF located in one bay. The frame elevation and brace connection details are reproduced in Fig. 2.3. The beams were designed for composite action with moment resisting beam-to-column connections. The beam splice detail in the braced frame is unusual, but it has been used in NCBF construction in the United States. As is seen in the elevation in Fig. 2.3, the bay width measured from the column centerlines of the braced bays is 7500 mm; story heights and frame member dimensions are listed in Table 2.2 along with unfactored demand-to-capacity ratios (DCRs) for beam axial-flexural interaction due to the brace load combination defined in the Seismic Provisions (AISC 2010a). Brace yield and critical buckling loads are calculated based on documented yield strengths from coupon tests and compression force at buckling in the experiment. Every beam in the braced frame of the specimen has a beam axial-flexural interaction value greater than one, meaning it is unable to develop this load and fails to meet SCBF requirements. The frame was pseudodynamically loaded with actuators at each floor using the Miyagi-ken-Oki acceleration record scaled to simulate a small, moderate, and severe earthquake.

Findings

- In the moderate test, where a peak acceleration of approximately 0.25 g was reached, both second story braces buckled and one brace buckled on the third and fifth floors. However, the first story beam web tore at the beam splice. At other floors, the beam splice did not fail, but less severe damage in the form of prying and panel distortion was noted. The adverse response of the beam splice was judged to be caused by the development of high shear force and bending moment at the splice location as well as brace end rotation after buckling, though it should be noted that the latter did not occur on the first story.

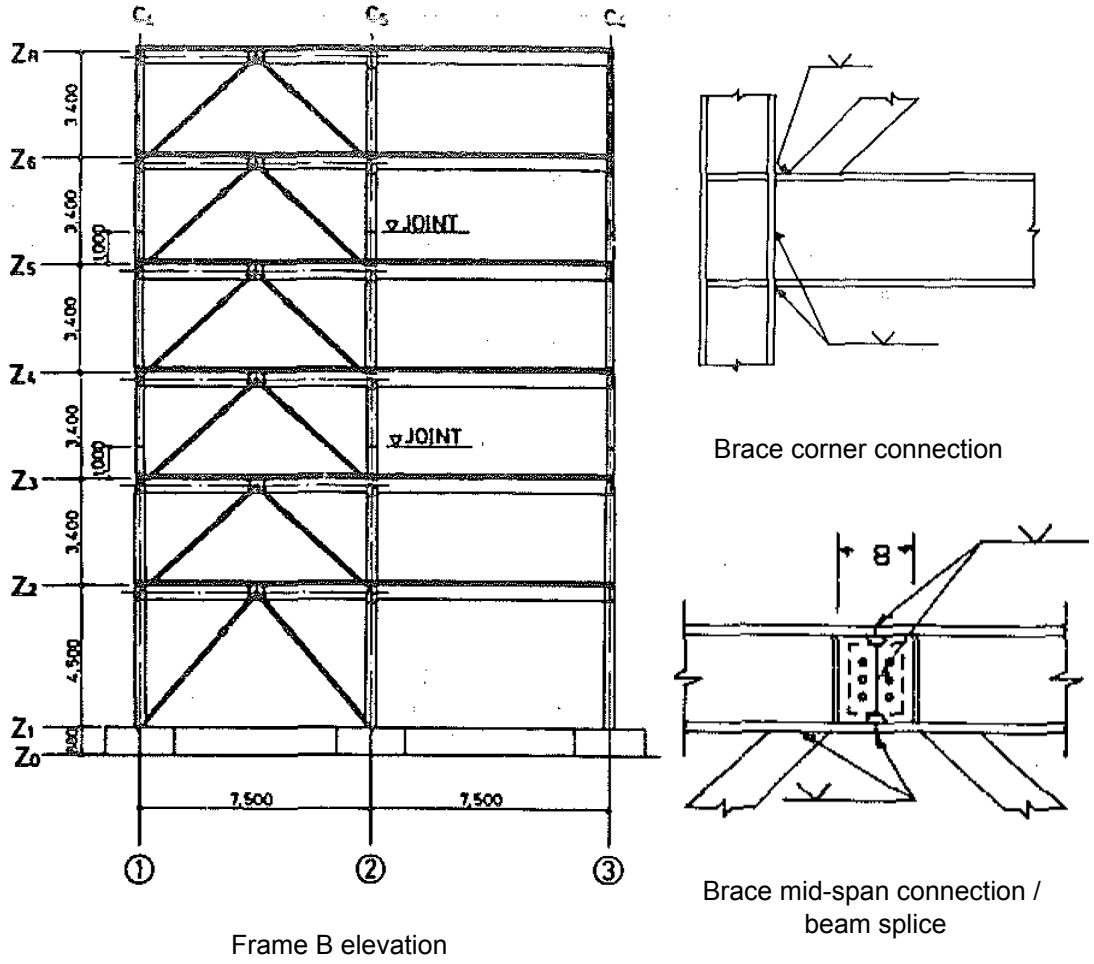

Figure 2.3: Elevation and brace connection details in six-story US/Japan specimen (Foutch et al. 1987)

- Brace buckling and yielding are major sources of energy dissipation, but as they tear and fracture, beams and columns can become important secondary energy dissipaters in dual lateral force resisting systems. This was illustrated in the final test, where the braces dissipated approximately 80% of the frame's energy initially but only about 60% by the end of the test.

- Composite action increases initial strength and stiffness, but it is less effective under cyclic loading. The development of slab cracks was matched with the reduction of the slab effective width derived from strain gauge data.

Table 2.2: Members, geometry, and beam interaction values in six-story US/Japan specimen

Story	Story height (mm)	Beam	Brace	Interaction (DCR)
6F	3400	W16×31	ST4×4×3/16	1.43[a]
5F	3400	W18×35	ST4×4×3/16	1.11
4F	3400	W18×35	ST5×5×1/4	1.81
3F	3400	W18×40	ST6×6×1/4	1.83
2F	3400	W18×40	ST6×6×1/4	1.83
1F	4500	W18×40	ST6×6×1/2	3.77

[a] P_{cr} estimated using $K = 0.82$, $L =$ centerline length

Commentary

The beam splice was clearly identified as a weakness in the system; in fact, the current provisions (AISC 2010a) require continuous beams in chevron configuration SCBFs and OCBFs. However, this research did not evaluate the performance of more commonly used continuous beams that may not be able to develop the AISC-specified brace unbalanced load. Significant beam mid-span force and deformation demands were observed and possible sources were identified, providing some insight into the response of continuous beams in CBFs.

2.3.2 United States/Japan: Half-Scale Three-Story Building (Fukuta et al. 1989)

In another effort in the United States/Japan Cooperative Earthquake Research Program Utilizing Large-Scale Testing Facilities, a series of half-scale three-story inverted V-braced frame specimens were tested at Japan's Building Research Institute. The tests and results are described by Fukuta et al. (1989). Six frames were tested under quasistatic loading–five with inverted V configuration braces and one without braces. All beam-to-column connections were designed to resist bending moment and various beam sizes, brace sizes, and levels of composite action were studied. The first two frames tested had beams designed for composite action and were intended to represent the first three stories of the six-story United States/Japan inverted V-braced frame described by Foutch et al. (1987) and Roeder (1989). The frames had bay widths of 3750 mm and Table 2.3 presents story heights, beam and brace sections, and axial-flexural interaction values for the five braced

frames tested. Axial-flexural interaction is calculated using the brace yield strengths determined from coupon tests and assuming the brace effective length factor, K, to be 0.82 where brace length is taken from centerline-to-centerline. This K value is the average effective length factor observed in the related full-scale six-story tests (Roeder 1989). As can be seen, all first and second story beams had interaction values greater than one, indicating that these beams would be unable to develop the design brace unbalanced load.

Based on the results of the tests, a hysteresis model was developed that accounts for brace-beam interaction using plastic analysis. The dual lateral force resisting system is decomposed into its moment and braced frame components. Story shear contribution from the brace in tension, Q_{bt} in Eq. 2.4, is governed by the strength of the beam, Q_{g} in Eq. 2.5, and the shear contribution from the brace in compression, Q_{bc}. It can be seen that the effect of the beam strength is at most ($Q_{\mathrm{g,max}}$) the lateral resistance of the moment frame in a sway mechanism where plastic hinges form in the beam.

$$Q_{\mathrm{bt}}(X) = -Q_{\mathrm{bc}}(X) - Q_{\mathrm{g}}(X) \leq P_{\mathrm{y}} \cos\theta \tag{2.4}$$

$$Q_{\mathrm{g}}(X) \leq Q_{\mathrm{g,max}} = \frac{2M_{\mathrm{gp}}}{h} \tag{2.5}$$

Findings

- Composite action (i.e., beam strength) does not affect the lateral load at which braces buckle.
- Stronger beams allow greater brace force and elongation to develop in tension, leading to greater lateral resistance of the story at post-buckled drifts.
- Braces in weak beam frames do not achieve gross area yielding in tension, meaning brace damage is mostly accrued in compression.
- The proposed braced frame hysteresis model predicts the lateral force-drift response of the test frames reasonably well.

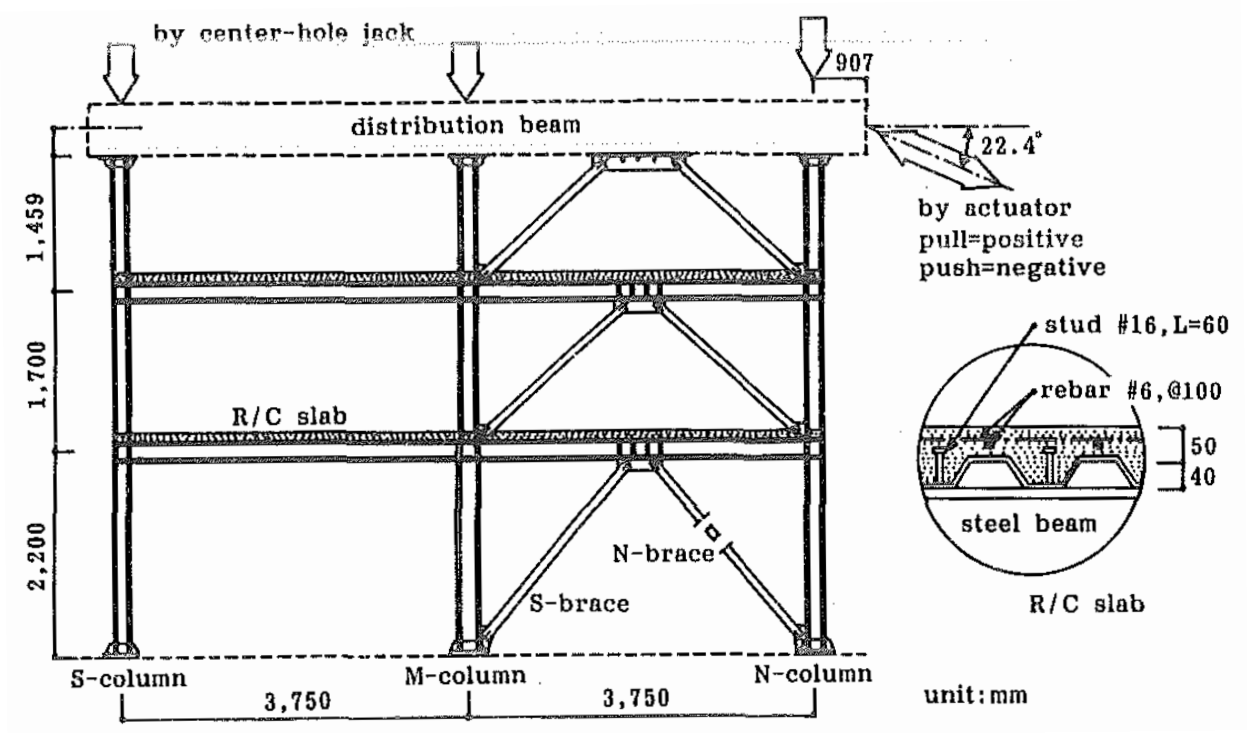

Figure 2.4: Elevation and slab and loading details in three-story US/Japan specimen (Fukuta et al. 1989)

Table 2.3: Members, geometry, and beam interaction values in three-story US/Japan specimens

Story	Frame No.	Story height (mm)	Beam	Brace (d×b×t)	Interaction (DCR)[a]
3F		1459	Rigid	□−105×45×4.5	$\ll 1$
2F	1,2,3	1700	W8×10	□−105×45×4.5	1.82
1F		2200	W8×13	□−110×55×4.5	1.92
3F		1459	Rigid	□−70×35×6.0	$\ll 1$
2F	4	1700	W8×10	□−70×35×6.0	2.31
1F		2200	W8×13	□−70×40×9.0	2.80
3F		1459	Rigid	□−105×45×4.5	$\ll 1$
2F	5	1700	W8×13	□−105×45×4.5	1.60
1F		2200	W10×17	□−110×55×4.5	1.17

[a] P_{cr} estimated using $K = 0.58$, L = centerline length

Commentary

This set of half-scale experiments provides the most comprehensive data on weak beam braced frames available. Although the first and second story beams were weak with respect to the unbalanced load, the frames showed good ductility and energy dissipation. Important conclusions were drawn that focused on the effect of the weak beam on the response of the braces and the entire frame. However, dual lateral force resisting systems are less common in the United States than in Japan; most NCBFs reviewed in the infrastructure survey do not appear to have moment resisting beam-to-column connections. In addition, the proposed hysteresis model appears to under-predict story shear at post-buckled drifts and therefore may not provide appropriate demand estimates for capacity design. While the advent of faster and accessible computing resources has lessened the necessity for such models, accurate demand estimates that do not require finite element analysis may be attractive to practicing engineers.

2.4 Computational Research

2.4.1 HP Building: 1994 Northridge Case Study (Rai and Goel 2003)

In the 1994 Northridge earthquake, a four-story building with concentrically braced frame lateral systems was moderately damaged, as noted by Fig. 2.5. The building was located in North Hollywood and owned by Hewlett-Packard; a detailed description of the actual recorded damage and rehabilitation efforts is provided by Kelly et al. (2000). Rai and Goel (2003) conducted analyses of the original north-south frame as well as rehabilitated frames using SNAP-2DX. The rehabilitated frames, in order of economic cost, included (i) concrete fill in braces, (ii) reconfiguration to two-story X-bracing, and (iii) beam strength upgrade to SCBF requirements. Beams, columns, and braces were modeled one-to-one (i.e., one beam in the actual frame was represented by one line element in the model) using beam-column and brace hysteresis models. A fracture life model was also implemented for braces. Linear modal analyses and nonlinear pushover and time history analyses were performed as part of the research program. Three ground motions from the Northridge earthquake were studied–the North Hollywood, Newhall, and Sylmar ground motions. These unscaled motions had peak ground accelerations of 0.31g, 0.59g, and 0.84g, respectively.

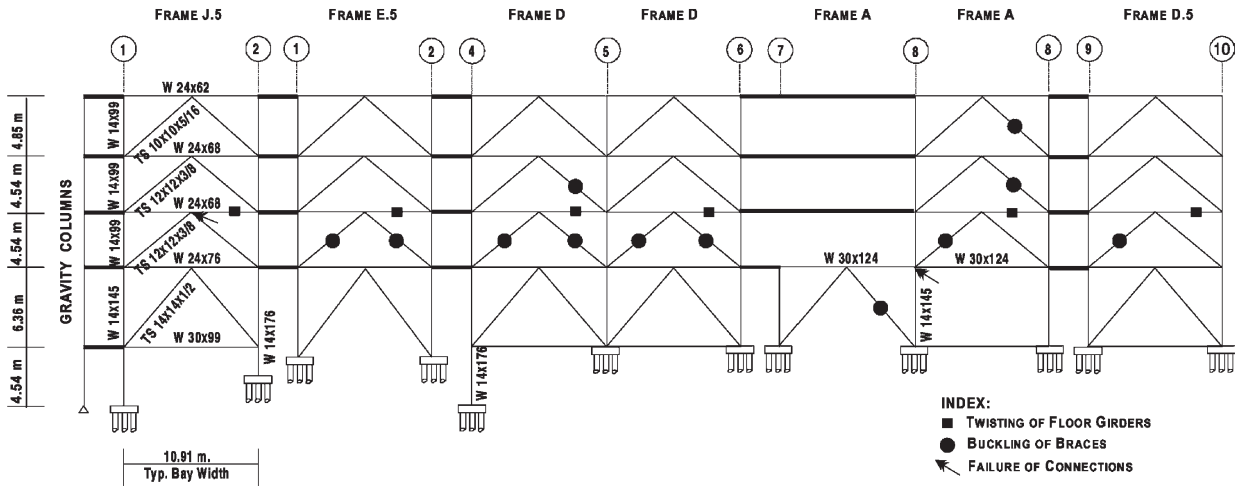

Figure 2.5: Idealized elevation and reported damage of North Hollywood HP building (Rai and Goel 2003)

Findings

- The simulation using the nearby North Hollywood ground motion predicted plastic hinging in five of the six second story beams and widespread brace buckling–far more damage than was observed in the actual event, where no beam hinging occurred and brace buckling was most prevalent on the second story. Nonetheless, the vulnerability of the second story to soft story behavior was clearly identified by the model.

- According to the simulation, a repeat of the North Hollywood event with the unrepaired frame would have caused significant damage but not collapse.

- The model of the existing structure developed complete collapse mechanisms when subjected to the severe Newhall and Sylmar ground motions.

- Filling the braces with concrete can lead to significant performance gains with relatively little expense. Brace fracture life improvements should be addressed in any level of retrofit.

- Both two-story X reconfiguration and beam upgrading led to more stable frame lateral resistance after brace buckling, as seen in Fig. 2.6. The former retrofit achieved greater base

shear due to better load redistribution among the stories after brace buckling, but all second story beams formed plastic hinges due to the brace unbalanced loads.

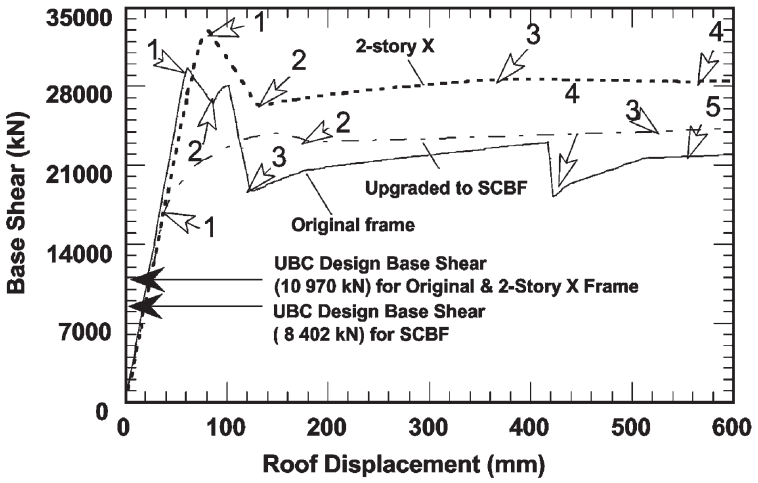

Figure 2.6: Pushover curves for simulated original and rehabilitated structures (Rai and Goel 2003)

Commentary

This numerical study addresses the performance and rehabilitation of an NCBF in a comprehensive manner. However, the scope of the research was rather limited: only one brace line of one building was studied and the acceleration records used in the analyses were taken from one event. NCBF design varies considerably, so analyses including more building archetypes, design details, and ground motions could provide more precise conclusions. In addition, the models developed in SNAP-2DX were coarse in resolution and seemed to overestimate damage to the structure. The results of the analysis using the North Hollywood ground motion did not match the level of damage observed in the actual event. The validity of the analyses could also be strengthened through experimental research.

2.4.2 Numerical Analysis of Chevron Braced Frames (Khatib et al. 1988)

A numerical study by Khatib et al. (1988) was conducted to examine the inelastic behavior of concentrically braced frames with braces in the chevron configuration. The study consisted of a review of existing brace models (particularly the post-buckling response), quasistatic simulation using a stiffness-driven system model, dynamic simulation, and parametric studies. Design methods of optimizing chevron braced frame performance and the performance of different bracing configurations were also studied using numerical simulation. Most pertinent to the research presented in this document is the stiffness-driven system model, which introduced an approach for classifying beams as stiff or flexible relative to the braces using chevron braced frame kinematics. With this model, the effect of beam stiffness on frame resistance and stiffness could be theoretically quantified. A stiff beam leads to a positive post-buckling frame stiffness and satisfies Eq. 2.6, where K_{bm} is the beam stiffness with respect to its vertical degree of freedom at its mid-span, K_{br} is the brace axial stiffness in tension, K_{bb} is the brace axial post-buckled stiffness in compression (generally negative), and θ is the brace-to-beam angle. Eq. 2.7 gives the relationship between the change in lateral frame displacement and vertical beam deflection as a function of the beam and brace stiffnesses. This allowed for the development of pushover curves from which the effects of beam stiffness and brace slenderness on frame response can be studied.

$$K_{\mathrm{bm}} \geq \frac{-4K_{\mathrm{br}}K_{\mathrm{bb}}\sin^2\theta}{K_{\mathrm{br}}+K_{\mathrm{bb}}} \tag{2.6}$$

$$\Delta_{\mathrm{bm}} = \frac{\Delta_{\mathrm{t}}\sin\theta\cos\theta(K_{\mathrm{br}}+K_{\mathrm{bb}})}{K_{\mathrm{bm}}+(K_{\mathrm{br}}-K_{\mathrm{bb}})\sin^2\theta} \tag{2.7}$$

Findings

Based on the quasistatic stiffness-driven analysis of chevron braced frames, the following findings were made:

- Frame response after brace buckling is highly dependent on beam stiffness and brace slenderness. A hardening frame force-deformation response after brace buckling, which was considered to be most desirable, can be achieved with a stiff beam and slender braces (approximately

$KL/r \geq 130$ for A36 steel).

- Implementation of stiff beam systems may be limited by the catalog of structural shapes available and the large compression forces that could develop in columns.

- Intermediate slenderness braces (approximately $60 \leq KL/r \leq 130$ for A36 steel) result in substantial force redistributions after buckling and should be avoided in design. Stocky compact braces (approximately $KL/r \leq 60$) are preferred.

However, the other analyses described in the report produced conflicting results. For instance, the performance optimization procedure for chevron braced frames produced a design with intermediate slenderness braces and flexible beams in one case. Yet, intermediate slenderness braces were not recommended previously due to force redistribution issues. The dynamic analyses suggested that stiff beams with slender braces performed poorly, but this combination was recommended in the quasistatic analyses, though it was recognized as potentially impractical.

Commentary

The numerous discrepancies on the inelastic response of chevron braced frames between the different analysis techniques does not provide much clarity on the subject. This is recognized by the authors. In addition, the issue of beam strength is not directly studied, though its effects are postulated. All beams in the study were assumed to be stiff or flexible with respect to brace stiffness *and* strong with respect to the brace unbalanced load. The effect of composite action was also not studied. However, sound relationships between brace, beam, and lateral stiffness were developed, which may serve as a basis for future work.

2.4.3 Effect of Beam Strength on Chevron Braced Frame Performance (Tremblay and Robert 2000, 2001)

Tremblay and Robert (2000, 2001) studied the effect of beam strength on the performance of chevron configuration CBFs using nonlinear time history analyses conducted in Drain-2D. The analyses were designed with a view towards generating code recommendations specific to chevron braced frames. Four different design scenarios were examined for 2-, 4-, 8-, and 12-story buildings: nominal

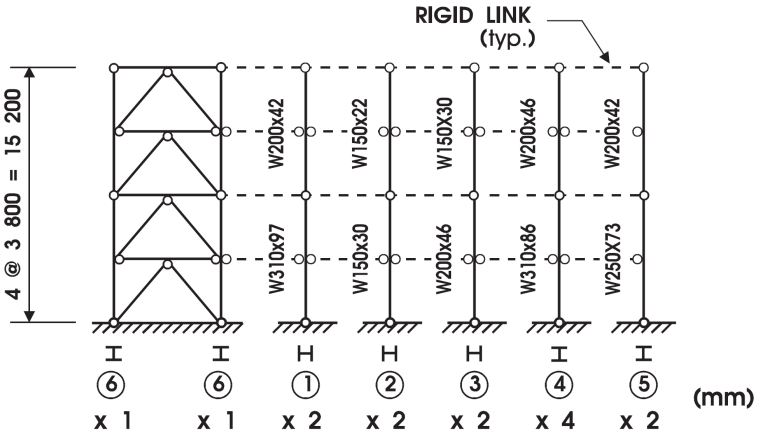

Figure 2.7: Typical analytical model used in Tremblay and Robert (2000, 2001)

ductility braced frames (NDBFs) where the beams are not designed for the brace unbalanced loads and ductile braced frames with beams designed for the brace unbalanced loads considering 100%, 80%, and 60% of the brace yield load ($A_g F_y$) in the tension brace (DBF-100, DBF-80, and DBF-60). The NDBF buildings designed complied with CSA-S16.1-94 (CSA 1994). P-Δ effects were included in the models. The input ground motions consisted of 5 west coast motions and 1 simulated motion. Two scale factors were used to create two ensembles of the six motions, one scaled to represent design demands and the other scaled to represent stronger motions.

Findings

- Soft story collapse, defined in this study when story drift exceeds 10%, spurred instability in several of the analyses. The first and second stories were most vulnerable because the ground motion affects these stories first, leading to drift concentration, and the P-Δ effects are greatest.

- Dynamic instability occurred most often in taller buildings with weaker beams. NDBF frames, particularly the 8- and 12-story varieties, had the most instances of dynamic instability. The DBF frames were more stable in general, but instability still occurred in all of the 12-story models in both ground motion ensembles.

- Based on the prevalence of dynamic instability, it was recommended that NDBF systems be limited to 2 stories in height. DBF-60 systems were recommended to be limited to 4 stories in height. DBF-100 systems were recommended to be limited to 8 stories in height.

Commentary

The analyses presented by Tremblay and Robert indicate that chevron braced frames, particularly those with weak beams, are prone to dynamic instability. This is a serious concern, but these results have not been experimentally validated. This research is also focused on new design and not the performance of older systems (i.e., NCBFs), which could face other vulnerabilities.

Chapter 3

EXPERIMENTAL SPECIMEN DESIGN

3.1 Introduction

In this chapter, the design rationale for the experimental specimens is discussed. The limit states that govern CBF design are introduced along with the material properties and demand-to-capacity ratios of each specimen. The design of each specimen is detailed with an emphasis on the first specimen, since it was the subject of numerous computational analyses performed to validate the design. Finally, the test setup and instrumentation are discussed.

The experimental research program was composed of four tests of specimens with the general form seen in Fig. 3.1. The test series was designed to examine the system response of chevron braced

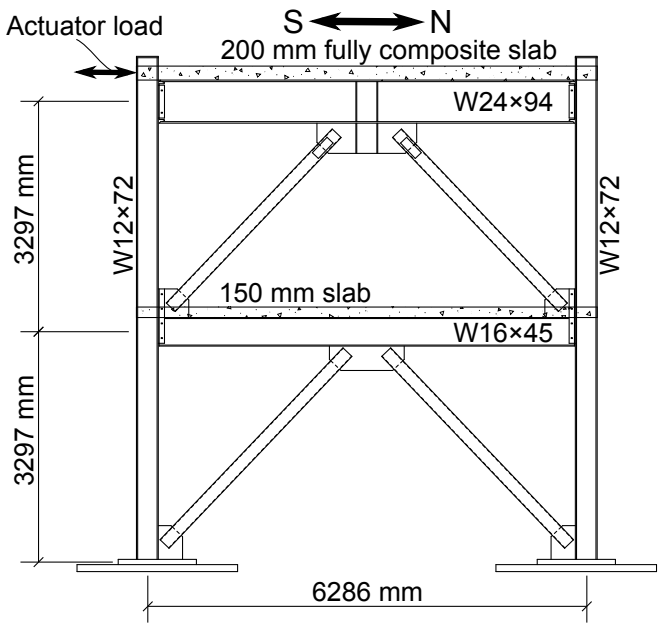

(a) Typical frame dimensions and members



(b) Frame picture

Figure 3.1: Test frame overview

fraems with beams that are too weak to resist the unbalanced loads that develop after brace buckling in chevron braced frames; that is, they are weak beam-strong brace systems. This deficiency is common in NCBFs, as consideration of the unbalanced load did not enter code until the 1992 AISC Seismic Provisions. Testing this system level issue demands a specimen complete enough to reasonably capture the response interactions between the system's individual components; this was accomplished with two-story single-bay braced frame with braces in the inverted V configuration. Brace type, connection details, and slab details varied according to the specific objectives of each test. All tests were conducted at the National Center for Research Engineering (NCREE) in Taiwan between July 2013 and January 2014.

The test series is given the base name "TNCBF," where "T" is prepended to "NCBF" to indicate two-story testing in Taiwan and to differentiate the series from concurrent single-bay single-diagonal NCBF testing at the University of Washington. Modifiers are appended to designate frame classes (Ductile, Non-ductile, or Repair) and brace type (HSS or WF). The specimens are also numerically identified as "1" or "2"; specimens with the same number contained the same first story beam. The specimen names TNCBF1-N-HSS, TNCBF1-R-HSS, TNCBF1-R-WF, and TNCBF2-D-HSS therefore broadly describe the features of the tests; more detailed explanations are provided later in this chapter.

3.2 Overview of Limit States

Limit states were evaluated on the basis of demand-to-capacity ratios (DCRs) using capacity design principles, as would be common for SCBFs, to guide specimen design and compare predicted and observed response. In some cases, the design demand-to-capacity ratios exceeded one in order to simulate NCBF deficiencies. Demands are calculated based on brace capacities (yielding in tension or buckling in compression). The capacity of the component with respect to each limit state is calculated using design expressions.

Two design approaches are used to evaluate connections–AISC and balanced design, which are presented in Table 3.1 with notation provided in Table 3.2. The AISC approach is based on the Specifications for Structural Steel Buildings (AISC 2010b) and resistance (ϕ) factors are applied to the appropriate expressions. Interface welds are evaluated using the uniform force method (UFM) to distribute brace forces. The second approach uses the balanced design procedure (BDP) proposed

by Roeder et al. (2011b), which seeks to establish a clear yielding hierarchy while suppressing brittle failure modes using balance (β) factors applied to resistance expressions that are largely similar to those of AISC. Critically, however, interface welds are evaluated based on the capacity of the gusset plate and not the brace forces, recognizing that the gusset plate demands are deformation-based and not force-based when brace buckling occurs.

Table 3.1: Limit states and corresponding resistance expressions for AISC and balanced design approaches (Roeder et al. 2011b)

	AISC design		Balanced design	
Limit state	Resistance (ϕR_n)	ϕ	Resistance (βR_n)	β
Whitmore yielding	$\phi F_y B_w t_p$	0.90	$\beta R_y F_y B_w t_p$	1.0
Brace net section fracture	$\phi U(R_{tb} F_{ub} A_{nb} + F_{up} A_{gp})$	0.75	$\beta U(R_{tb} F_{ub} A_{nb} + F_{up} A_{gp})$	0.95
Brace-to-gusset weld	$\phi(0.6) F_{EXX} N_w L_c (0.707) w_2$	0.75	Same as AISC	0.75
Brace-to-gusset base metal	$\phi(0.6) F_u N_s L_c t_f$	0.75	Same as AISC	0.75
Plate block shear	$\phi\{(0.6 F_u A_{nv} + U_{bs} F_u A_{nt}) \leq (0.6 F_y A_{gv} + U_{bs} F_u A_{nt})\}$	0.75	$\beta\{(0.6 F_u A_{nv} + U_{bs} F_u A_{nt})\}$	0.85
Whitmore fracture	$\phi F_u B_w t_p$	0.75	$\beta F_u B_w t_p$	0.85
Gusset plate buckling	$\phi B_w t_p F_{cr}$	0.90	$\beta B_w t_p F_{cr}$	0.90
Interface welds	$\phi(0.6) F_{EXX}[1 + 0.5(\sin\gamma)^{1.5}] 2 L_w (0.707) w_1 \geq$ UFM	0.75	$2(1.5)\beta(0.6) F_{EXX}(0.707) w_1 \geq R_y F_y t_p$	0.75

3.2.1 Uniform Force Method

The development and application of the limit state expressions for braced frame connections has been discussed extensively in the literature (Roeder et al. 2011b; Lumpkin 2009; Sloat 2014) and will not be reviewed here. However, the application of the UFM to distribute brace forces to the gusset plates and their welds requires some explanation, since this distribution is not necessarily obvious in connections not designed using the method. The process for analyzing existing connections is outlined in the Steel Construction Manual (2010c). In design, the UFM seeks gusset plate geometry that eliminates moments at the interfaces. A connection designed with an alternate procedure does not satisfy this in general, as the centroids of the gusset-to-beam and -column connections, α and β, may violate Eq. 3.1, where e_b and e_c are the half-depths of the beam and column and θ is the brace-to-column angle. Consequently, in the UFM, moments must exist on either or both connections to

Table 3.2: Notation for symbols in Table 3.1

ϕ	Resistance factor for AISC approach
β	Balance factor for BDP approach
F_{y}	Yield strength of component
F_{u}	Ultimate strength of component
F_{ub}	Ultimate strength of brace
F_{up}	Ultimate strength of plate
F_{cr}	Flexural buckling stress
F_{EXX}	Electrode classification number
R_y	Ratio of expected to nominal yield strength
R_{tb}	Ratio of expected to nominal ultimate strength of brace
A_{nb}	Net area of brace
A_{gp}	Gross area of plate(s)
A_{nv}	Net area in shear
A_{nt}	Net area in tension
B_{w}	Width of Whitmore section
t_{p}	Thickness of plate
t_{f}	Thickness of flange
N_{w}	Number of weld lines
N_{s}	Number of shear surfaces
L_{c}	Length of splice
L_{w}	Length of weld line
w_1	Weld leg size at gusset plate interface
w_2	Weld leg size at brace splice
γ	Loading angle

ensure equilibrium.

$$\alpha - \beta = e_{\mathrm{b}} \tan\theta - e_{\mathrm{c}} \tag{3.1}$$

The vertical and horizontal (variables V and H) beam and column (subscripts b and c) forces from the UFM for a brace load P are given in Eqs. 3.2 through 3.5 where r is the norm of the vector sum of the centroid-to-work point distances.

$$V_{\mathrm{c}} = \frac{\beta}{r} P \tag{3.2}$$

$$H_{\mathrm{c}} = \frac{e_{\mathrm{c}}}{r} P \tag{3.3}$$

$$V_{\mathrm{b}} = \frac{e_{\mathrm{b}}}{r} P \tag{3.4}$$

$$H_{\mathrm{b}} = \frac{\alpha}{r} P \tag{3.5}$$

$$r = \sqrt{(\alpha + e_{\mathrm{c}})^2 + (\beta + e_{\mathrm{b}})^2} \tag{3.6}$$

Corner gusset plates not welded to shear tabs

Some corner gusset plates in the tests interface with a column and base plate or beam directly. It is assumed that moment exists in both vertical and horizontal connections, as in Fig. 3.2, because they are welded with the same size fillet weld and probably share similar flexural rigidity. The dimensions $\bar{\alpha}$ and $\bar{\beta}$ represent the actual connection centroids and α and β represent the ideal centroids of the connections given by Eqs. 3.7 through 3.11.

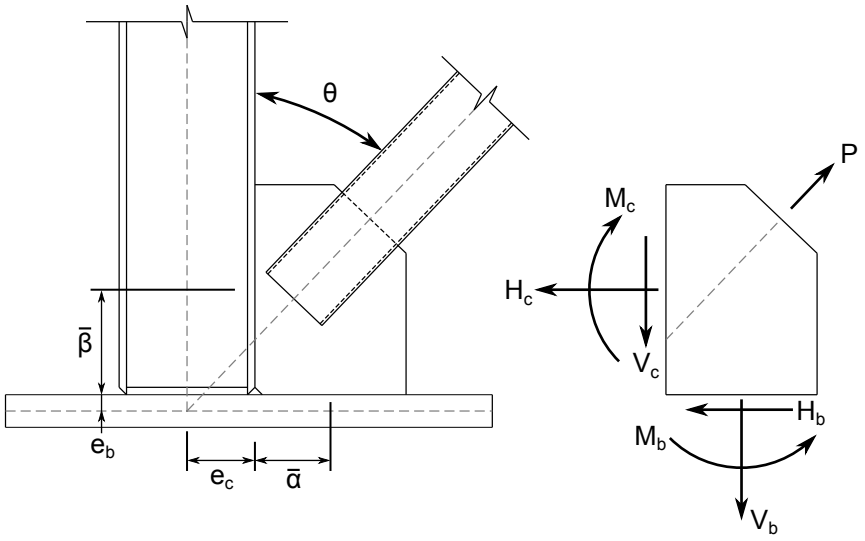

Figure 3.2: Assumed gusset plate load distribution for corner connections

$$\alpha = \frac{K' \tan\theta + K\left(\frac{\bar{\alpha}}{\bar{\beta}}\right)^2}{D} \tag{3.7}$$

$$\beta = \frac{K' - K\tan\theta}{D} \tag{3.8}$$

$$K = e_{\mathrm{b}} \tan\theta - e_{\mathrm{c}} \tag{3.9}$$

$$K' = \alpha\left(\tan\theta + \frac{\bar{\alpha}}{\bar{\beta}}\right) \tag{3.10}$$

$$D = \tan^2\theta + \left(\frac{\bar{\alpha}}{\bar{\beta}}\right)^2 \tag{3.11}$$

The locations of the ideal centroids can then be used in the standard UFM equations to find the vertical and horizontal forces at each connection. The moments result from the eccentricities of the actual and ideal centroids (Eqs. 3.12 and 3.13).

$$M_{\mathrm{b}} = V_{\mathrm{b}}\left(\alpha - \bar{\alpha}\right) \tag{3.12}$$

$$M_{\mathrm{c}} = H_{\mathrm{c}}\left(\beta - \bar{\beta}\right) \tag{3.13}$$

The weld demands are then computed using the maximum traction vector composed of the longitudinal and transverse stresses.

Corner gusset plates welded to shear tabs

The UFM is largely the same for corner gusset plates with shear tabs as for those without, except that no moment is assumed to transfer through the shear tab-to-column connection (i.e., $\beta = \bar{\beta}$). A moment at the beam-to-shear tab connection is still generally required to satisfy equilibrium of the system. As in the above case, the ideal centroid of the beam connection must be found to

compute the moment. This relation is given in Eq. 3.14 and the remaining loads are calculated as previously.

$$\alpha = K + \bar{\beta} \tan\theta \tag{3.14}$$

Mid-span gusset plates

The force distribution through mid-span gusset plates is considerably different since the plates connect only to a beam. Mid-span gusset plates, and therefore their weld lines, are centered with the work point in the beam. However, the lines of action of the braces are eccentric with respect to the connection centroid. This eccentricity is computed by Eq. 3.15. Additionally, it should be noted that the forces from two braces, one in tension (P_t) and one in compression (P_c), must be distributed. These forces are typically not equal for braced frames. AISC 341-10 (2010a) requires that the brace in tension reach its expected yield strength, $R_\mathrm{y} F_\mathrm{y} A_\mathrm{g}$, and the brace in compression reach 1.1 times its expected brace strength in compression, typically $1.1(1.14) F_\mathrm{cre} A_\mathrm{g}$. Note that F_cre is the flexural buckling stress of the brace according to Chapter E of AISC 360-10 (2010b) where F_y is replaced with $R_\mathrm{y} F_\mathrm{y}$. This system is depicted in Fig. 3.3.

$$\alpha = e_\mathrm{b} \tan\theta \tag{3.15}$$

The moment produced by the two braces is given by either equality in Eq. 3.16 and the remaining loads are calculated as previously.

$$M_\mathrm{b} = (P_\mathrm{t} + P_\mathrm{c})\, \alpha \cos\theta = (P_\mathrm{t} + P_\mathrm{c})\, e_\mathrm{b} \sin\theta \tag{3.16}$$

3.2.2 Beam Axial-Flexural Interaction

In chevron configuration SCBFs, the beam limit state of axial-flexural interaction must be checked against the brace unbalanced load. AISC 360-10 (2010b) provides the inequality to evaluate axial-flexural interaction in Section H1, given in Eq. 3.17, where P_r and P_c represent the required and available axial strengths and M_r and M_c represent the required and available flexural strengths. The available strengths include resistance factors, often 0.9 in both axial and flexural modes, in

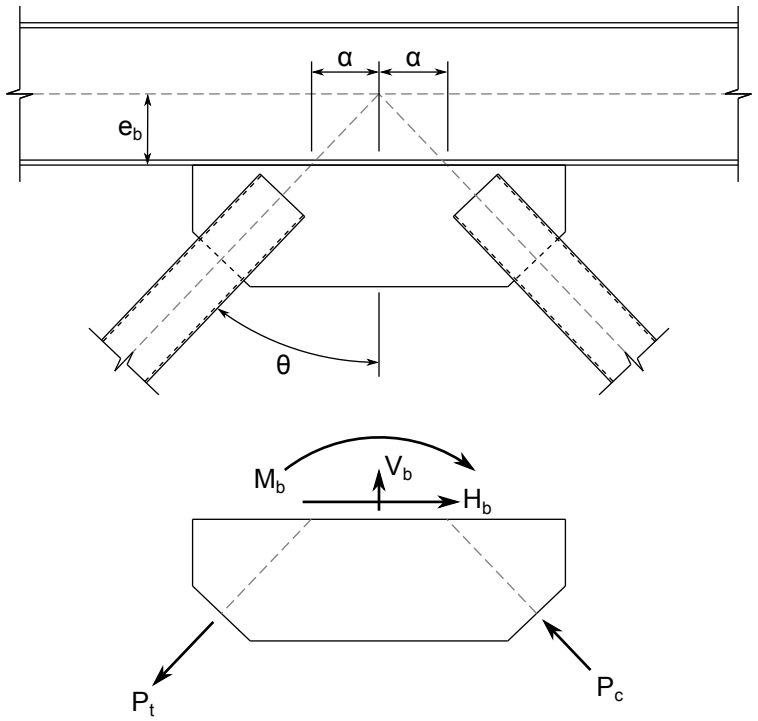

Figure 3.3: Assumed gusset plate load distribution for mid-span connections

design situations.

$$\frac{P_{\mathrm{r}}}{P_{\mathrm{c}}} + \frac{8}{9}\frac{M_{\mathrm{r}}}{M_{\mathrm{c}}} \leq 1.0 \tag{3.17}$$

Beam flexural demands are greatest after brace buckling due to strength degradation in compression paired with strength stability, or even growth, in tension. The AISC Seismic Provisions (2010a) stipulate that the unbalanced load be calculated using 30 percent of the expected critical buckling load in compression and the expected yield force in tension. Thus, the horizontal resultant is given by Eq. 3.18 and the vertical resultant is given by Eq. 3.19, where γ is the brace-to-beam angle. In the unbuckled load case, the demand equations are similar in form, but the maximum compressive force is the lesser of $1.14F_{\mathrm{cre}}A_{\mathrm{g}}$ and $R_{\mathrm{y}}F_{\mathrm{y}}A_{\mathrm{g}}$.

$$H_{\mathrm{unbal}} = (R_{\mathrm{y}}F_{\mathrm{y}}A_{\mathrm{g}} + 0.3F_{\mathrm{cre}}A_{\mathrm{g}})\cos\gamma \tag{3.18}$$

$$V_{\text{unbal}} = (R_{\text{y}} F_{\text{y}} A_{\text{g}} - 0.3 F_{\text{cre}} A_{\text{g}}) \sin \gamma \tag{3.19}$$

Beam capacities depend on composite action with the slab. In compression, out-of-plane beam buckling is unlikely to control capacity due to restraint provided by the slab (if shear connectors are present) and lateral bracing; that is, the buckling load may exceed yielding of the full section in compression. However, in the load cases presented above, the beam is in compression and tension on either side of its mid-span, where the horizontal force acts. Thus, the beam strength in tension, $R_{\text{y}} F_{\text{y}} A_{\text{g}}$, typically controls axial strength for beams with composite slabs. Non-composite slabs are assumed in this study to provide no lateral restraint, so the axial strength of non-composite beams may be governed by weak axis buckling instead. Flexural capacity depends on composite action as well as end fixity. It is also assumed in the proceeding calculations that if the beam has moment connections at its ends, the brace unbalanced load induces negative moments at these ends and slab contribution is negligible since the top of the composite section (i.e., the slab) is in tension. If the beam has simple connections, composite action is considered since the beam undergoes positive bending and the compressive strength of the concrete is activated.

3.3 Component Material Properties

Structural steel shapes and plates used in the TNCBF test series are listed in Table 3.3 and is assumed to have an elastic modulus of 200 GPa (29000 ksi). Their yield and ultimate tensile strengths, F_{y} and F_{u}, are listed along with the material overstrength (ratio of actual to nominal strengths). Concrete compressive strengths, f_{c}, were found from cylinder tests performed off-site and are listed in Table 3.4. The time elapsed between pouring and the compression tests and specimen tests is given, recognizing that the concrete gains strength over time; thus, the given strengths are less than or equal to those when the frames were tested.

Table 3.3: Steel material properties

TNCBF**X**	Section	Material	F_y (MPa)	F_u (MPa)	$F_y/F_{y,nom}$	$F_u/F_{u,nom}$
1,2	W12×72	A992	395	506	1.14	1.13
1,2	W24×94	A992	460	535	1.33	1.19
2	W16×45	A992	411	521	1.19	1.16
1	W16×45	A992	414	519	1.20	1.16
1	HSS7×7×1/4	A500 Gr B	443	508	1.39	1.27
1,2	HSS5×5×3/8	A500 Gr C	438	504	1.27	1.18
1	H175×175×7.5×11	SN400B	333	459	1.42	1.15
1	10 mm plate	A572 Gr 50[a]	395	513	1.14	1.15
2	12 mm plate	A572 Gr 50[a]	445	548	1.29	1.22
1	12 mm plate	A572 Gr 50[a]	337	504	0.98	1.13
1	15 mm plate	A572 Gr 50[a]	424	541	1.23	1.21
1	20 mm plate	A572 Gr 50[a]	416	536	1.21	1.20

[a] Taiwanese equivalent

Table 3.4: Concrete material properties

		Elapsed time since pour (days)		
Specimen	Story	Cylinder	Frame	Min. f_c (MPa)
TNCBF1-N-HSS	1	10	11	33.1
	2	10	11	35.1
TNCBF1-R-HSS	1	13	32	36.4
	2	13	32	37.3
TNCBF1-R-WF	1	13	53	36.4
	2	13	53	37.3
TNCBF2-D-HSS	1	25	25	39.2
	2	13	200	37.3

3.4 Specimen Demand-to-Capacity Ratios

The braced frame limit states described above were used to develop the demand-to-capacity ratios (DCRs) in Tables 3.5 and 3.6 for each component of each specimen, as detailed in Sections 3.5 through 3.8. Each limit state is approached from three points of view at most: (i)

unfactored (or $\phi = 1.0$) DCRs computed using the AISC expressions and the uniform force method (UFM), (ii) factored DCRs computed using the AISC expressions and resistance factors and the UFM, and (iii) factored DCRs computed using the BDP expressions and balance factors. The unfactored DCRs are presented to help identify yielding and failure hierarchies without the conservatism usually introduced by resistance factors. The factored DCRs are presented to facilitate direct comparisons to the respective design approaches.

The demands are calculated using measured material properties and buckling loads of the braces. Brace demands are not increased beyond their strengths calculated from measured yield stresses, contrary to AISC 341-10 (2010a) where connections subjected to compression brace loading must be analyzed for 1.1×1.14 the critical buckling load.

Comparing brace compactness, λ, to the limit for highly ductile members in AISC 341 (2010a), λ_{hd}, can be accomplished with a ratio serving much the same purpose as demand-to-capacity ratios. These values are presented in Table 3.7. Ratios exceeding one, like DCRs, could lead to potentially poor performance due to severe strain accumulation in non-compact sections after buckling.

Table 3.5: Component demand-to-capacity ratios[a] in TNCBF test series

		TNCBF1-N-HSS				TNCBF1-R-HSS				TNCBF1-R-WF				TNCBF2-D-HSS			
		First story		Second story		First story		Second story		First story		Second story		First story		Second story	
Component	Limit state	Corner	Mid-span	Corner	Mid-span	Corner	Mid-span	Corner	Mid-span	Corner	Mid-span	Corner	Mid-span	Corner	Mid-span	Corner	Mid-span
Brace	Block shear rupture	0.96 (1.28) [1.28]	0.96 (1.28) [1.28]	0.96 (1.28) [1.28]	0.84 (1.12) [1.12]	0.59 (0.79) [0.79]	0.59 (0.79) [0.79]	0.96 (1.28) [1.28]	0.84 (1.12) [1.12]	0.50 (0.67) [0.67]	0.50 (0.67) [0.67]	0.96 (1.28) [1.28]	0.84 (1.12) [1.12]	0.58 (0.77) [0.77]	0.58 (0.77) [0.77]	0.58 (0.77) [0.77]	0.58 (0.77) [0.77]
	Net section rupture	1.25 (1.67) [1.32]	1.25 (1.67) [1.32]	1.25 (1.67) [1.32]	0.88 (1.17) [0.93]	0.92 (1.23) [0.97]	0.92 (1.23) [0.97]	0.92[b] (1.23[b]) [0.97[b]]	0.88 (1.17) [0.93]	0.74 (0.99) [0.78]	0.74 (0.99) [0.78]	0.92[b] (1.23[b]) [0.97[b]]	0.88 (1.17) [0.93]	0.87 (1.16) [0.92]	0.87 (1.16) [0.92]	0.87 (1.16) [0.92]	0.87 (1.16) [0.92]
	Splice weld rupture	0.77 (1.03) [1.03]	0.77 (1.03) [1.03]	0.77 (1.03) [1.03]	0.68 (0.91) [0.91]	0.71 (0.95) [0.95]	0.71 (0.95) [0.95]	0.77 (1.03) [1.03]	0.68 (0.91) [0.91]	0.62 (0.83) [0.83]	0.62 (0.83) [0.83]	0.77 (1.03) [1.03]	0.68 (0.91) [0.91]	1.26[c] (1.68[c]) [1.68[c]]	1.26[c] (1.68[c]) [1.68[c]]	1.26[c] (1.68[c]) [1.68[c]]	1.26[c] (1.68[c]) [1.68[c]]
Gusset plate	Whitmore yielding	0.91 (1.01) [0.91]	0.95 (1.06) [0.95]	0.94 (1.04) [0.94]	0.82 (0.91) [0.82]	0.85 (0.94) [0.85]	0.88 (0.98) [0.88]	0.94 (1.04) [0.94]	0.82 (0.91) [0.82]	0.87 (0.97) [0.87]	0.88 (0.98) [0.88]	0.94 (1.04) [0.94]	0.82 (0.91) [0.82]	0.72 (0.80) [0.72]	0.75 (0.83) [0.75]	0.72 (0.80) [0.72]	0.72 (0.80) [0.72]
	Whitmore fracture	0.63 (0.84) [0.74]	0.66 (0.88) [0.78]	0.63 (0.84) [0.74]	0.56 (0.75) [0.66]	0.67 (0.89) [0.79]	0.69 (0.92) [0.81]	0.63 (0.84) [0.74]	0.56 (0.75) [0.66]	0.67 (0.89) [0.79]	0.68 (0.91) [0.80]	0.63 (0.84) [0.74]	0.56 (0.75) [0.66]	0.59 (0.79) [0.69]	0.60 (0.80) [0.71]	0.59 (0.79) [0.69]	0.59 (0.79) [0.69]
	Flexural buckling	0.78 (0.87) [0.87]	1.01 (1.12) [1.12]	$\ll 1$	0.80 (0.89) [0.89]	0.57 (0.63) [0.63]	$\ll 1$	$\ll 1$	0.80 (0.89) [0.89]	0.68 (0.76) [0.76]	0.63 (0.70) [0.70]	$\ll 1$	0.80 (0.89) [0.89]	0.49 (0.54) [0.54]	0.46 (0.51) [0.51]	0.49 (0.54) [0.54]	0.48 (0.53) [0.53]
	Block shear rupture	0.76 (1.01) [0.71]	0.76 (1.01) [0.71]	0.76 (1.01) [0.71]	0.71 (0.95) [0.65]	0.76 (1.01) [0.76]	0.76 (1.01) [0.76]	0.76 (1.01) [0.71]	0.71 (0.95) [0.65]	0.77 (1.03) [0.71]	0.77 (1.03) [0.71]	0.76 (1.01) [0.71]	0.71 (0.95) [0.65]	0.66 (0.88) [0.67]	0.66 (0.88) [0.67]	0.66 (0.88) [0.67]	0.66 (0.88) [0.67]
	Beam interface weld	0.51 (0.68) [1.09]	0.76 (1.01) [1.09]	0.66 (0.88) [1.09]	0.37 (0.49) [0.68]	0.32 (0.43) [0.99]	0.50 (0.67) [0.99]	0.66 (0.88) [1.09]	0.37 (0.49) [0.68]	0.32 (0.43) [0.77]	0.45 (0.60) [0.77]	0.66 (0.88) [1.09]	0.37 (0.49) [0.68]	0.28 (0.37) [0.89]	0.40 (0.53) [0.89]	0.31 (0.41) [0.89]	0.32 (0.43) [0.89]
	Column or shear tab interface weld	0.74 (0.99) [1.09]		0.80 (1.07) [2.19]		0.51 (0.68) [0.99]		0.80 (1.07) [2.19]		0.41 (0.55) [0.77]		0.80 (1.07) [2.19]		0.36 (0.48) [0.89]		0.27 (0.36) [0.89]	
Shear tab	Beam or gusset plate interface weld			1.78 (2.38)				1.78 (2.38)				1.78 (2.38)					
	Column interface weld			0.54 (0.71) [1.09]				0.54 (0.71) [1.09]				0.54 (0.71) [1.09]					
Beam	Axial-flexural interaction	2.52 (2.80)		0.42 (0.47)		2.66 (2.96)		0.42 (0.47)		2.55 (2.83)		0.42 (0.47)		1.43 (1.59)		0.44 (0.49)	

[a] AISC DCR (AISC DCR/ϕ) [BDP DCR/β] – All demands based on measured properties if available; AISC capacities based on resistance expressions in AISC specifications and UFM; BDP capacities based on resistance expressions proposed by Roeder et al. (2011b).

[b] Net section reinforcement plates added, but cracks initiated in previous test(s).

[c] Inadvertently low capacity in drawings due to weld size specification error, but as-built capacity likely adequate.

Inadequate DCR by at least one evaluation method.

Table 3.6: TNCBF1-R-HSS knife plate demand-to-capacity ratios[a]

Limit State	Corner and mid-span
Gross section yielding	0.88 (0.98) [0.88]
Gross section fracture	0.68 (0.91) [0.80]
Flexural buckling	0.59 (0.66) [0.66]
Block shear rupture at brace	0.36 (0.48) [0.42]
Block shear rupture at gusset plate	0.46 (0.61) [0.54]
Splice weld rupture at brace	0.69 (0.92) [0.92]
Splice weld rupture at gusset plate	0.69 (0.92) [0.92]

[a] AISC DCR (AISC DCR/ϕ) [BDP DCR/β] – All demands based on measured properties if available; AISC capacities based on resistance expressions in AISC specifications and UFM; BDP capacities based on resistance expressions proposed by Roeder et al. (2011b).

Table 3.7: Brace compactness ratios ($\lambda/\lambda_{\text{hd}}$)

Specimen	1F	2F
TNCBF1-N-HSS	2.27	2.27
TNCBF1-R-HSS	0.94	2.27
TNCBF1-R-WF	1.08	2.27
TNCBF2-D-HSS	0.94	0.94

3.5 TNCBF1-N-HSS Design

TNCBF1-N-HSS was developed to simulate an existing chevron configuration NCBF with a weak first story beam. Since this was the first specimen to be tested at NCREE, its general design also served as the basis for the rest of the frames in the test series. Numerical studies were performed in OpenSEES and Abaqus to determine the adequacy of the design in meeting the test objectives and to provide more refined predictions for lateral force and deformation capacity of the system to inform the experimental setup. The objectives of TNCBF1-N-HSS are listed below:

- Capture...

  - Seismic response of a typical inverted V-NCBF system.
  - Weak beam-strong brace behavior.
  - Behavior of gusset plates and braces partially embedded in slabs.

- Evaluate...
  - Performance of non-seismically compact braces and any interaction with weak beam-strong brace condition.
  - Effect of low ductility braces on system response.
  - Relative importance of braced frame limit states.
  - Impact of connection deficiencies on braced frame behavior.
  - Impact of connection welds lacking minimum toughness requirements.
  - Effect of low rotational clearance on braces, connections, and adjacent framing members.
  - Performance of nominally non-composite slab under cyclic loading.

3.5.1 General Constraints

The design of the frame was intended to satisfy basic test objectives within the limitations of the laboratory environment. The general form of the specimen is therefore a result of accommodating the following factors:

- Frame Geometry
  - Consistency with previous multi-story SCBFs tested at NCREE (Roeder et al. 2011a; Lumpkin et al. 2012) to aid performance comparisons.
  - Strong wall and strong floor tie-down spacing of one meter on center.
  - Available laboratory equipment (e.g., anchor plates).
  - Realistic aspect ratios (bay width-to-story height).

- Braces

  - Axial force limited by actuator strength.

- Beams

  - Weak first story beam with unfactored demand-to-capacity ratio greater than one and consistent with many actual NCBFs.
  - Strong second story beam with demand-to-capacity ratio less than one and consistent with SCBF requirements to deliver actuator load, limit damage, and permit reuse.

- Columns

  - Sufficient axial and flexural strength to permit reuse.

Based on the above, a preliminary design with 6756 mm bay widths and 3454 mm story heights was developed with W12×72 columns. To design the beams, HSS7×7×1/4 braces were used to compute the unbalanced load at the beam mid-span. This brace section is a non-seismically compact hollow structural section (HSS), with a width-to-thickness ratio of 27.0 that exceeds AISC 341-10's criterion for highly ductile members of 13.8, considering nominal yield strength. Nonetheless, its gross area (and thereby yield strength) is nearly equal to that of braces used in the TCBF tests (Roeder et al. 2011a; Lumpkin et al. 2012); with similar brace angles, the lateral resistances achieved in the test series are more directly comparable.

Two first story beam sections were considered, W16×45 and W14×26, with approximate axial-flexural interaction unfactored demand-to-capacity ratios (DCRs) of 3 and 6 considering pinned ends, respectively. Sloat (2014) reports that the majority of the NCBF systems in the building surveyed have DCRs greater than one, of which most have interaction DCRs between two and four. A W24×94 second story beam was selected with a non-composite axial-flexural interaction DCR less than 0.5, providing a strong beam-weak brace condition at the second story. While this is not representative of many NCBFs, nor is a stronger roof beam common in practice, the load distribution through the second story columns and braces was intended to provide reasonable boundary conditions at the first story, where the braces could buckle and place large demands on the weak beam. A fully composite slab was provided at the second story due to its critical role in delivering the actuator load to the frame.

3.5.2 Connections

The specimen was designed with a mix of existing (older) and current connections to meet the different test objectives. Current connections were used at the second story beam to reduce potential demands on the beam, which was expected to be used in multiple tests. This consisted of welded unreinforced flange moment connections at the beam ends, where the beam flanges were connected to the column flanges and web with complete joint penetration (CJP) welds, and balanced design gusset plate connections at the beam mid-span. In addition, the columns were CJP welded to the base plates, since this is a critical force transfer mechanism. Welds for these connections were performed with AWS E71T-1 wire, which meets minimum toughness requirements for demand-critical welds in the Seismic Provisions (AISC 2010a).

Connections from two buildings, built in 1986 and 1992, served as the basis for the remaining existing connections: first and second story corner gusset plates, first story mid-span gusset plates, and first story beam-to-column connections. These buildings, identified as 86WA3A and 92WA2A in Sloat (2014), utilize the welded continuous shear tab connections shown in Figs. 3.4 and 3.5 at corner gusset plates where braces, beams, and columns intersect. The shear tab is continuous along the beam and gusset plates, which is accommodated by coping half of one beam flange. Sloat documents that 86WA3A suffers from limit state deficiencies in brace net section and splice weld rupture and gusset plate Whitmore yielding and beam interface weld rupture. Unfactored DCRs for 92WA2A exceeded one in these limit states as well as brace block shear rupture and shear tab-to-gusset and -beam weld rupture. It can also be seen in the drawings that brace end clearance was minimal with respect to the shear tab edge.

The 86WA3A and 92WA2A connections are the references for the first and second story corner gusset plates of TNCBF1-N-HSS. This type of connection was also the subject of thorough evaluation and retrofit testing by Sloat (2014) at the University of Washington. These tests are designated NCBF1 and NCBF1-R1 through -R5. Unique to the TNCBF1 tests, the second story corner gusset plates and adjacent braces are partially embedded in the slab as in Fig. 3.7b. Slabs in modern braced frames are blocked out at the gusset plate to allow for out-of-plane rotation, but this was not a concern in older designs. The impact of the restraint provided by the slab is unclear for gusset plate connections, but Roeder (1989) reports effective length factors between 0.73 and

0.93 for both in- and out-of-plane buckling braces welded directly to beams and fully embedded in slabs (taking length as the brace centerline length).

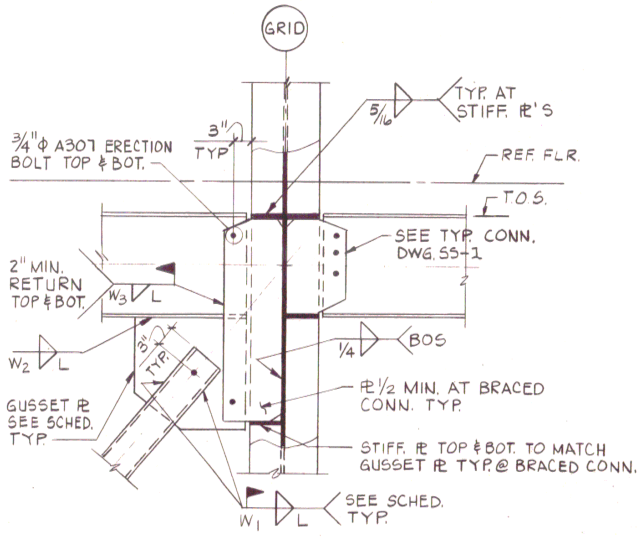

Figure 3.4: 86WA3A corner gusset plate connection

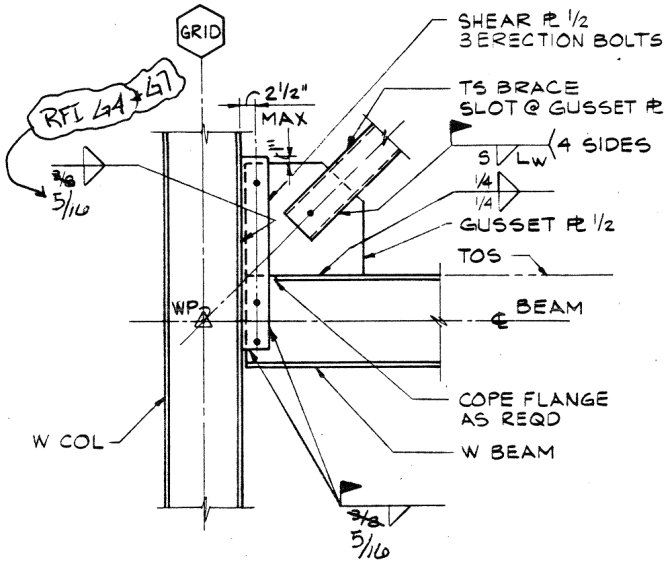

Figure 3.5: 92WA2A corner gusset plate connection

Mid-span gusset plate connections in NCBFs generally vary less in style than corner gusset plate connections. Braces typically meet at the beam mid-span at a continuous rectangular gusset plate without stiffeners. As with the corner gusset plates, adequate rotational clearance is not provided and the braces terminate very close to the beam flange as in Fig. 3.6. The typical mid-span gusset plate connection in 92WA2A serves as the reference connection for the mid-span gusset plate for the first story of TNCBF1-N-HSS.

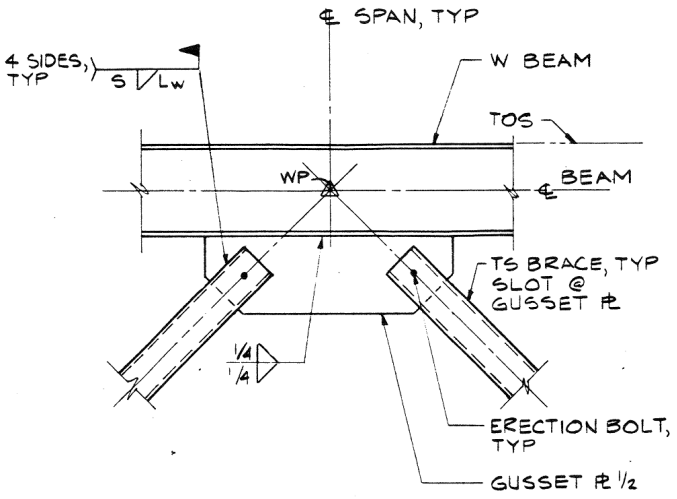

Figure 3.6: 92WA2A mid-span gusset plate connection

While the aforementioned connections were the basis of the TNCBF1-N-HSS existing connections, some practical exceptions were made to their design to prevent predictable brittle failure modes such as splice and interface weld rupture because these limit states have been well-documented.

3.5.3 Beam Details

Since the intent of the TNCBF test series is to simulate system level behavior, TNCBF1-N-HSS contained beam details commonly found in the NCBF infrastructure review (Sloat 2014). Some NCBFs do not utilize shear connectors and in other cases, the quantity of shear connectors used is unclear in available drawings. In beams without shear connectors, the only source of shear transfer between metal deck and slab systems and beams may be puddle welds between the deck

Table 3.8: Unfactored DCRs for shared shear tab reference connections (Sloat 2014)

Component	Limit state	86WA3A	92WA2A
Brace	Block shear rupture	0.64	1.09
	Net section rupture	1.07	1.25
	Splice weld rupture	1.25	1.42
Gusset plate	Whitmore yielding	1.14	1.62
	Flexural buckling	0.45	0.64
	Block shear rupture	0.86	0.97
	Shear yielding at beam interface	0.54	0.57
	Beam interface weld	1.65	2.03
Shear tab	Gusset and beam interface weld	0.64	1.42
	Column interface weld rupture	0.83	0.90

and beam flange. The shear capacity of these puddle welds is not easily quantified and perhaps unreliable under cyclic loading. To test this detail, no shear connectors were included on the first story beam and the deck was tack welded along its length at approximately 150 mm intervals, as shown in Fig. 3.7a. Fig. 3.7b shows the same connection partially covered by the concrete slab; as was previously discussed, the slabs were not blocked out around gusset plates to permit out-of-plane rotation. Shear studs were welded to the floor beams to facilitate load transfer and enable composite support of gravity loads. Their contribution to composite behavior of the braced frame beam is not considered.

Many TNCBFs with braces in chevron configurations also lack lateral bracing at the brace-to-beam intersection. This violates a requirement in the AISC Seismic Provisions (2010a) that aims to prevent lateral-torsional buckling of the beam. This location is especially vulnerable due to torsion that may be introduced by brace buckling and out-of-plane brace deflection, and significant damage has been reported at this location in at least one seismic event (Kelly et al. 2000). The first story beam of TNCBF1-N-HSS was braced at its third-points but not at its midpoint to mimic the deficient lateral bracing of NCBFs.

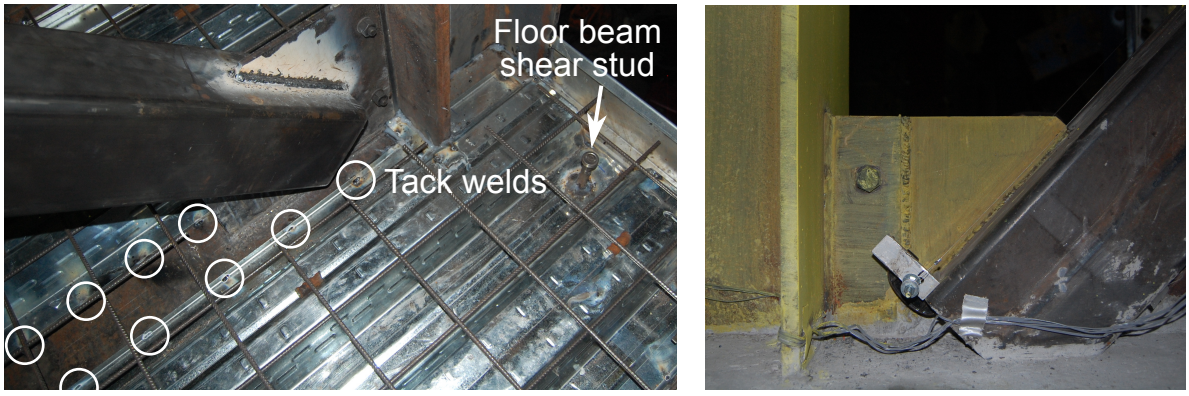

(a) Tack welds between deck and first story beam

(b) Brace and connection partially embedded in slab

Figure 3.7: TNCBF1 second story corner connections at first story beam

3.5.4 OpenSEES Analyses

OpenSEES models were developed by Keith Palmer to verify the feasibility of the proposed design alternatives. Line element models were created, so most connection and test setup details were naturally omitted. However, the models utilized techniques proposed by Hsiao (2012):

- Braces, beams, and columns were modeled using nonlinear fiber based beam-column elements.
- Gusset plate connections were modeled with nonlinear rotational springs whose strength and stiffness properties were defined by gusset plate geometry and yield strength.
- Rigid end zones were introduced in the beams and columns along the lengths of the gusset plates.
- Braces were given initial sinusoidal deflections of amplitude $L/500$ where L is the brace length using the BraceMake Tool command language (Tcl) procedure.

In addition, the work points and beam mid-spans were restrained against out-of-plane translation. The beam mid-spans were also restrained against torsional rotation. The prototype model is depicted in Fig. 3.8. The models developed are summarized in Table 3.9. The main parameters studied were first story beam strength, composite action, beam-to-column connection details, and

base fixity. Since the test frame was intended to have a W24×94 beam at the second floor, which would not be representative of weak beam NCBFs, an analysis with a W14×26 second floor beam was also performed (model O-W14-RF).

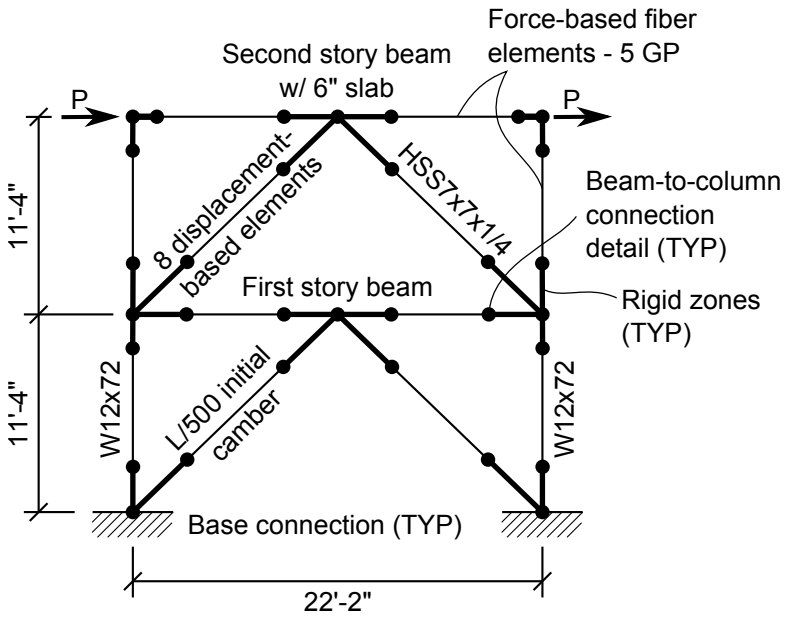

Figure 3.8: OpenSEES model of initial design

Table 3.9: List of OpenSEES analyses

Model	First story beam	Second story beam	First story composite slab thickness (in)	Beam-to-column connection	Base connection
O-W14-1	W14×26	W24×94	6	Fixed	Fixed
O-W14-2	W14×26	W24×94	6	Pinned	Fixed
O-W14-3	W14×26	W24×94	0	Fixed	Fixed
O-W16-1	W16×45	W24×94	6	Fixed	Fixed
O-W16-2	W16×45	W24×94	6	Pinned	Fixed
O-W16-3	W16×45	W24×94	0	Fixed	Fixed
O-W16-4	W16×45	W24×94	0	Pinned	Fixed
O-W16-5	W16×45	W24×94	6	Fixed	Pinned
O-W14-RF	W14×26	W14×26	6	Fixed	Fixed

The analyses suggested that braces on both stories would buckle in all cases. Varying beam strength, composite action, and beam-to-column connection fixity had predictable effects:

- The weaker W14x26 beam resulted in greater mid-span deflections and demand-to-capacity ratios than the W16x45 beam. For the case of pinned beam-to-column connections, the maximum mid-span deflection of the W14x26 beam was approximately 1.5 in greater, reaching a peak vertical displacement of about 2.25 in.

- The absence of the composite slab increased mid-span deflections in the beams.

- Pinned beam-to-column connections resulted in greater mid-span deflections and lower lateral resistance and stiffness.

All models generally show good ductility and energy dissipation, but it is worth noting that a brace fracture model was not implemented. Since the brace is non-seismically compact, its fracture life is hindered by severe strain concentrations where local buckling occurs (Goel 1992), so resistance is overestimated at larger drifts. Results between the realistic frame, O-W14-RF, and the comparable test frame, O-W14-1, show that the strong second story beam did not significantly alter the first story behavior, validating the proposed test configuration. The lateral force-drift response of the first story is plotted in Fig. 3.9.

3.5.5 Abaqus Analyses

The Abaqus models, listed in Table 3.10, were developed by Lingli Pan to study the effects of first story beam strength and more specific connection details–specifically the gusset plate thickness and geometry. Gusset plate geometry is related to splice length, so longer splice lengths correspond to larger gusset plates and larger Whitmore sections. Since the primary test objectives involve the behavior of the weak beam and not necessarily the brace-to-gusset connections, this analytical study was intended to eliminate details that lead to obvious connection failure modes. In these continuum models, the gusset plates and shear tabs were modeled as drawn with fixed constraints along welds. Additionally, the models included edge beams on either side of the slabs and the

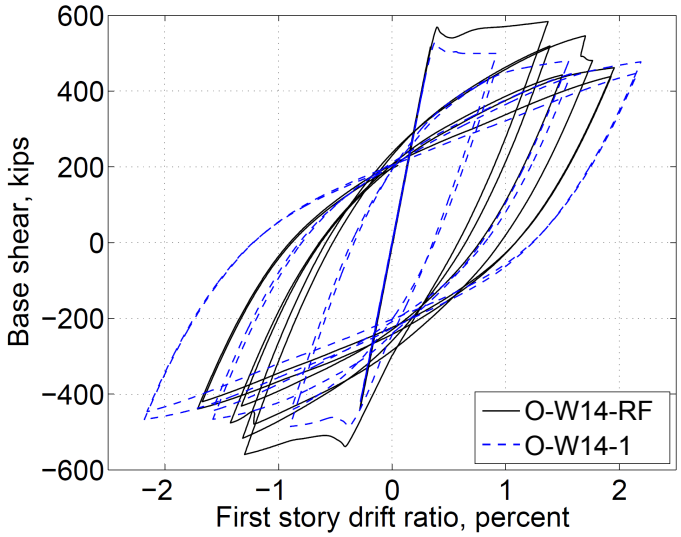

Figure 3.9: OpenSEES first story drift hystereses

load was applied at the south end of the second story edge beams. A typical model is depicted in Fig. 3.10. Each model contained these general characteristics:

- Steel members were modeled as shell elements (S4R) with trilinear constitutive relationships with kinematic hardening. The points of the material models were defined by expected yield and tensile strengths of the steel, $R_y F_y$ and $R_t F_u$, and elastic and strain hardening moduli of 200 and 0.2 GPa.

- Concrete slabs were modeled as solid elements (C3D8R) using the concrete damaged plasticity material model in Abaqus. A compressive strength of 34.5 MPa and a tensile strength of 3.45 MPa were specified. The elastic modulus followed the ACI recommended relation for normal-weight concrete ($E_c = 4700\sqrt{f_c}$). Default properties were used to characterize concrete damage in the absence of experimental data that could be used to calibrate these values.

- The concrete slabs were continuously tied to the beams to provide full composite action.

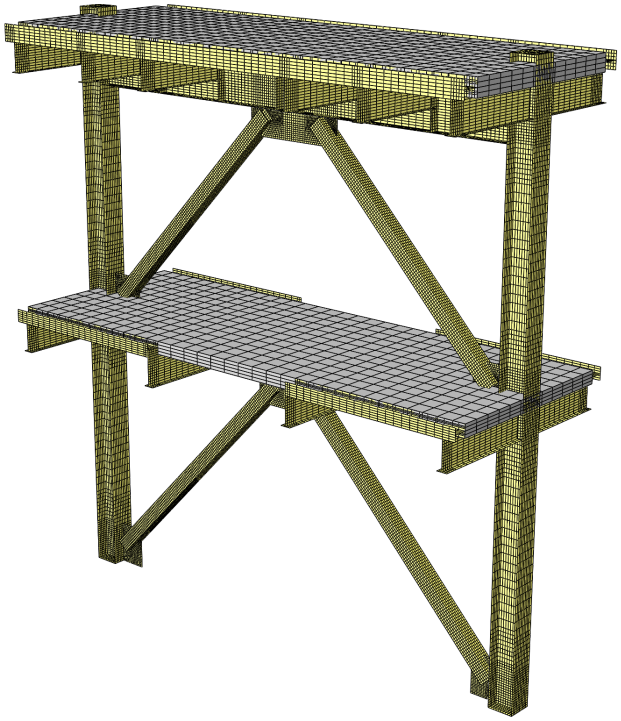

Figure 3.10: Typical Abaqus model of initial design

Table 3.10: List of Abaqus analyses

Model	First story beam	Gusset plate thickness (mm)	Brace-to-gusset plate splice length (mm)
A-W14-1	W14×26	9.5	229
A-W14-2	W14×26	12.7	229
A-W14-3	W14×26	12.7	254
A-W16-1	W16×45	9.5	229
A-W16-2	W16×45	12.7	229
A-W16-3	W16×45	12.7	254

From the stress fields in Fig. 3.11, it is clear that yielding in the first story beam is extensive when either the W14×26 or W16×45 beam is used. Maximum mid-span deflection of the first story beam was approximately 79 to 83 mm in the W14×26 models and 58 to 60 mm in the W16×45 models. The analyses suggested significant beam damage would occur with either beam, but the less deficient W16×45 was chosen for further study. The potential deformation of the W14×26

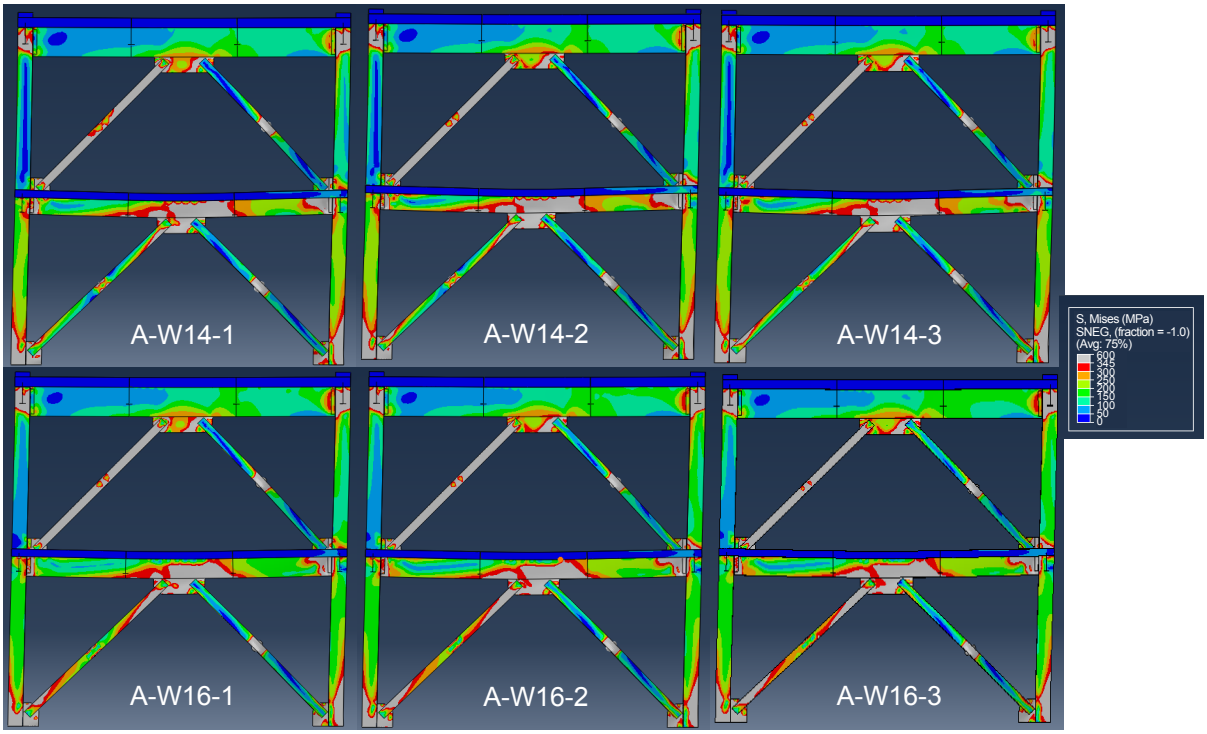

Figure 3.11: von Mises stress fields of models listed in Table 3.10

would be excessive, limiting reuse of the beam for multiple tests. The designs with the W16×45 first story beam were fine-tuned to satisfy dimensional constraints in the laboratory, which led to 6286 mm bay widths and 3297 story heights and slightly different connection geometry.

Two additional analyses were performed based on the updated designs with connection details matching A-W16-1 and A-W16-3 in Table 3.10. These changes represented two levels of connection deficiency. The analyses showed that with a gusset plate thickness of 9.5 mm and splice length of 229 mm, gusset plate buckling occurred at the first story mid-span prior to brace buckling. However, with a gusset plate thickness of 12.7 mm and a splice length of 254 mm, brace buckling occurred. In both cases, the second story braces did not buckle. Nonetheless, this was acceptable because the first story behavior was of greater interest in the test.

3.5.6 Final Details

Aided by the series of OpenSEES and Abaqus analyses, the details of TNCBF1-N-HSS were finalized; they can be found in Figs. 3.12 through 3.15. A W16×45 first story beam was selected with a 150 mm non-composite slab. Gusset plates were sized to 12 mm to alleviate flexural buckling concerns and splice lengths were set at 254 mm. The splice length is short with respect to the brace block shear and splice weld rupture limit states by AISC and BDP standards, though the unfactored DCRs for both are below 1.0.

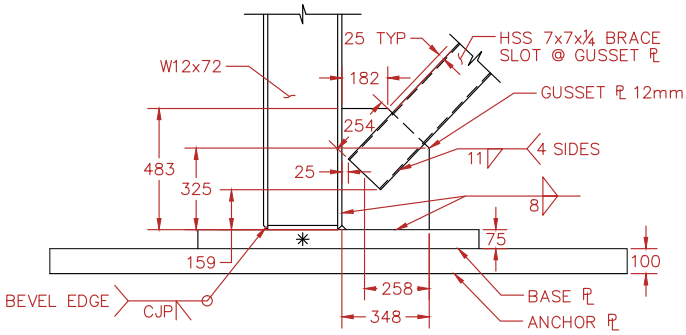

Figure 3.12: TNCBF1-N-HSS first story corner gusset plate details

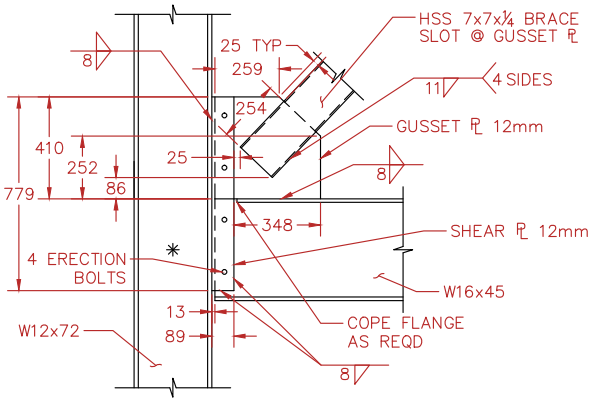

Figure 3.13: TNCBF1-N-HSS second story corner gusset plate details

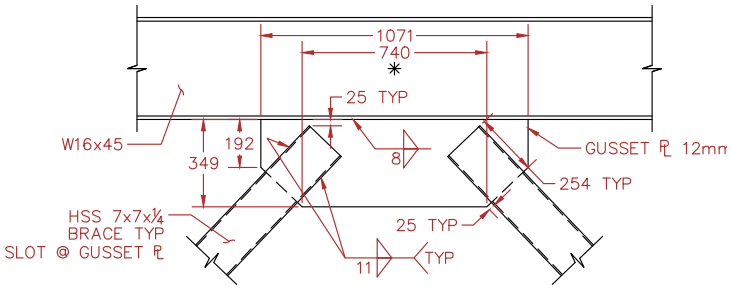

Figure 3.14: TNCBF1-N-HSS first story mid-span gusset plate details

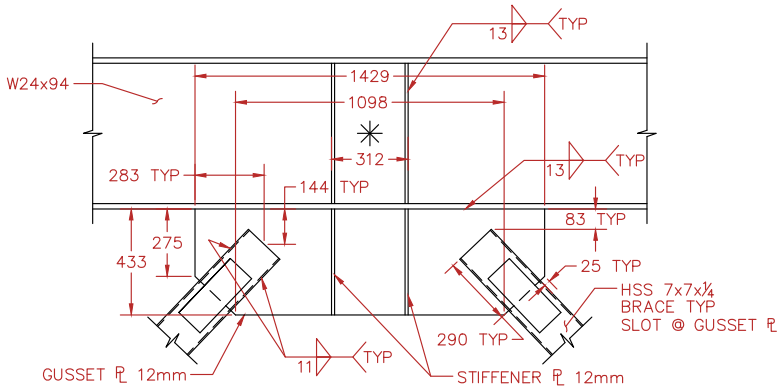

Figure 3.15: TNCBF1-N-HSS second story mid-span gusset plate details

3.6 TNCBF1-R-HSS Design

TNCBF1-R-HSS was designed as a repair of the first story of TNCBF1-N-HSS with in-plane buckling braces. The first story braces of TNCBF1-N-HSS were damaged, so these members and their connections were removed and replaced with seismically compact HSS5×5×3/8 braces with connections details shown in Figs. 3.16 and 3.17. Unlike conventional out-of-plane buckling brace connections, plastic hinges were not designed to develop in the gusset plates; instead, hinges were intended to form in the knife plates with rotation in the plane of the frame. A square HSS brace (equal radii of gyration in the section's local axes) was used in this design, so the knife plate connections must induce the desired buckling mode. Frames with in-plane buckling braces have been shown to perform similarly to those with out-of-plane buckling braces Lumpkin (2009). In-plane buckling retrofits may prove beneficial in NCBFs with thin gusset plates and deficient interface

welds, since the knife plates would protect the existing welds by eliminating out-of-plane gusset plate deformation and reducing associated stresses on the welds. Such a retrofit may be economical since only the braces would need to be removed. The in-plane buckling action of the braces would have the added benefit of preventing damage to adjacent wall systems, which would occur with out-of-plane buckling braces.

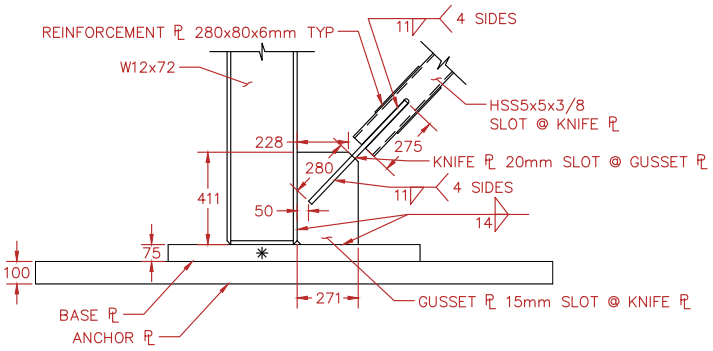

Figure 3.16: TNCBF1-R-HSS first story corner gusset plate details

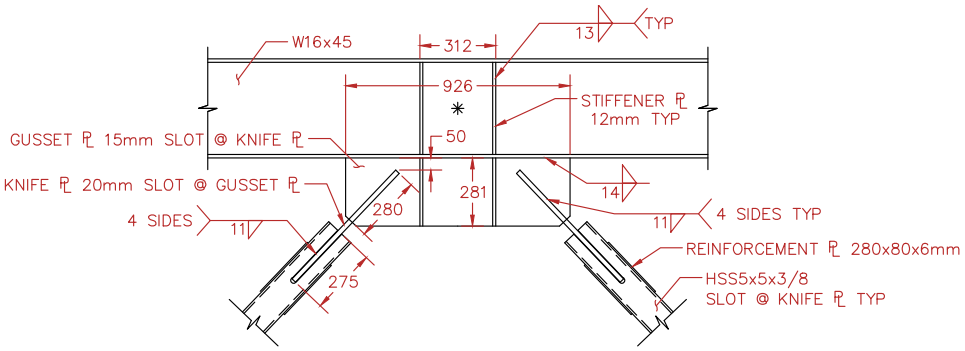

Figure 3.17: TNCBF1-R-HSS first story mid-span gusset plate details

The design followed recommendations by Roeder et al. (2013) and Tsai et al. (2013), utilizing a $3t_{kp}$ knife plate clearance ($3.25t_{kp}$ as-built). As-built DCRs for the gusset plates, braces, and beams are found in Table 3.5, and knife plate DCRs are documented in Table 3.6. Using the BDP, the gusset plates were sized to 15 mm and the knife plates to 20 mm. The knife plate thickness was controlled by the limited width of the plate; the plate width was not to exceed the flange

width of either the beam or column to fit within a theoretical existing wall system. Due to the knife plate geometry, its Whitmore section reduces to its gross section, which was used to check yielding, fracture, and buckling. The usual limit states of plate block shear and splice weld rupture were also checked at the gusset and brace interfaces. Additionally, the knife and gusset plates were slotted and inset to prevent the need for net section reinforcement. The gusset plates were given 50 mm horizontal and vertical clearances at corner and mid-span connections, respectively. This clearance was thought to be sufficiently small to discourage out-of-plane brace buckling while providing reasonable clearance for welding. Care was taken in welding the knife plates so that splice welds were not returned into the intended plastic hinge zone. Previous experiments with in-plane buckling knife plates demonstrated significant damage at the toes of the return welds due to stress concentrations in the region (Roeder et al. 2013).

While the existing columns, first story beam, second story braces, and second story beam remained, some repairs were required. The first story beam-to-column connections were slightly damaged in the previous test, specifically the beam-to-shear tab welds. Areas where these welds cracked were backgouged and replaced with notch-tough AWS E71T-1 weld metal, seen in Fig. 3.18a. Cracks at the net section of the second story braces had initiated at the corner connections in TNCBF1-N-HSS, so net section reinforcement plates were added to attempt to prevent further damage. This measure, pictured in Fig. 3.18b, was aimed at eliminating the potential for net section rupture and the development of new net section cracks. However, it is important to note that no repair was made to address the existing weld or base metal cracks, which could still grow under cyclic loading. Splice weld and block shear rupture deficiencies at the second story corner connections were not affected.

Considering the repair efforts outlined above, the objectives of TNCBF1-R-HSS are to:

- Capture...
  - Seismic response of a rehabilitated inverted V-NCBF system.
  - Weak beam-strong brace behavior.
  - Behavior of gusset plates and braces partially embedded in slabs.
- Evaluate...



(a) Beam-to-shear tab weld repair (b) New net section reinforcement plates

Figure 3.18: TNCBF1-R-HSS connection repair measures

- Performance of in-plane buckling repair and any interaction with weak beam-strong brace condition.
- Relative importance of braced frame limit states.
- Impact of addition of net section reinforcement plates after some net section damage has occurred.
- Performance of repaired beam-to-column connection welds.
- Performance of nominally non-composite and previously cracked slab under repeated cyclic loading.

3.7 TNCBF1-R-WF Design

The third specimen, TNCBF1-R-WF, was designed immediately following the testing of TNCBF1-R-HSS, where the first story braces were damaged. These braces and their connections were removed and replaced with Taiwanese H175×175×7.5×11 wide flange braces (similar in geometry to W6×25) with 10 mm gusset plates designed for out-of-plane buckling. Typical connection details are shown in Figs. 3.19 and 3.20. Wide flange braces have been shown to have greater deformation capacity than HSS braces since the deformations due to local buckling are better distributed, resulting in less severe strain concentrations (Lumpkin 2009). The gusset plates were designed using the BDP (Roeder et al. 2011b) with $8t_p$ elliptical and $6t_p$ vertical clearances at the corner and mid-span

connections, as recommended by Lehman et al. (2008) and Lumpkin et al. (2012). DCRs for these new members and an updated DCR for the first story beam are provided in Table 3.5.

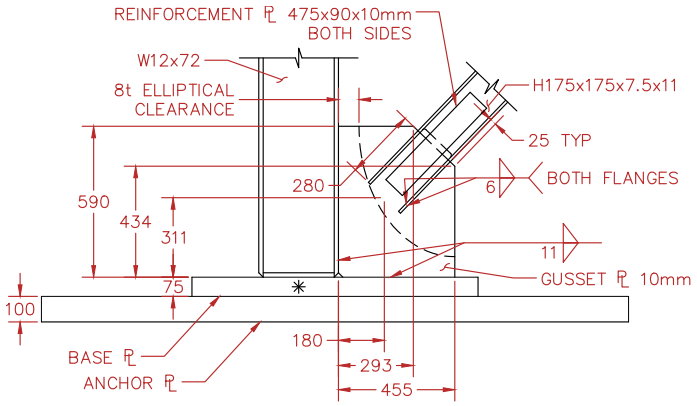

Figure 3.19: TNCBF1-R-WF first story corner gusset plate details

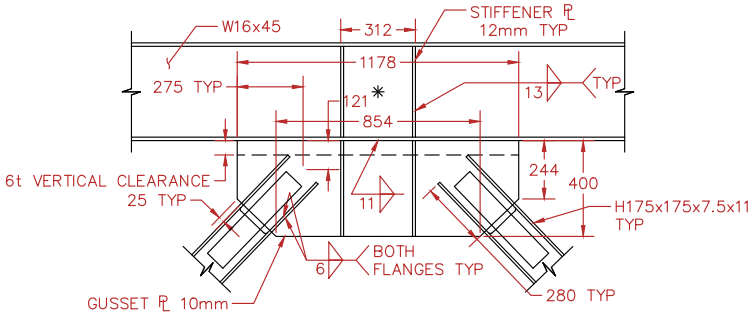

Figure 3.20: TNCBF1-R-WF first story mid-span gusset plate details

The existing beams and columns were retained, though the first story beam retained about 38 mm of residual downward displacement. This residual displacement was considered in the design of the new braces and gusset plates. The first story beam-to-column connections damaged in TNCBF1-N-HSS were also damaged in TNCBF1-R-HSS, despite the use of tougher weld metal; this was a result of significant rotation at the beam-to-column connection. However, in addition to the beam-to-shear tab welds, the column-to-shear tab welds were damaged. The repair procedure for these welds was the same as for TNCBF1-R-HSS: the damaged welds were backgouged and replaced with AWS E71T-1 metal. In order to prevent the bottom flange of the first story beam

from contacting the adjacent column flange, 30 mm by 30 mm sections were cutout from the lower ends of the beam. Both of these repair measures are depicted in Fig. 3.21.

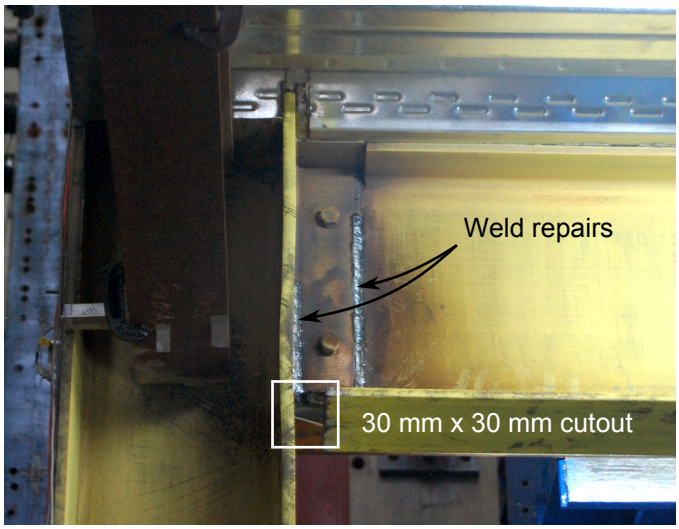

Figure 3.21: TNCBF1-R-WF first story beam-to-column connection repairs

The objectives of TNCBF1-R-WF, which are much the same as TNCBF1-R-HSS, are listed below:

- Capture...
  - Seismic response of a rehabilitated inverted V-NCBF system.
  - Weak beam-strong brace behavior.
  - Behavior of gusset plates and braces partially embedded in slabs.
- Evaluate...
  - Performance of wide flange braces with weak beam-strong brace condition.
  - Relative importance of braced frame limit states.
  - Impact of addition of net section reinforcement plates after some net section damage has occurred.

  - Performance of repaired beam-to-column connection welds.
  - Performance of nominally non-composite and previously cracked slab under repeated cyclic loading.

3.8 TNCBF2-D-HSS Design

TNCBF2-D-HSS was designed several months after the completion of testing TNCBF1-R-WF, where all four braces and the first story beam were damaged beyond repair, necessitating the removal of these components and their connections. Thus, this specimen utilized new braces and gusset plates at both stories and a new first story beam, while the existing columns and second story beam were reused. The main goal of the test was to evaluate the performance of an inverted V-braced frame with a weak beam and ductile details in order to provide a ductile (best case scenario) baseline for weak beam CBF performance. The objectives of TNCBF2-D-HSS are listed below:

- Capture...
  - Seismic response of a heavily rehabilitated inverted V-NCBF or a new inverted V-CBF with SCBF details and a weak beam.
  - Weak beam-strong brace behavior.
- Evaluate...
  - Performance of weak beam versus strong beam with moment connections.
  - Relative importance of braced frame limit states.
  - Performance of partially composite slab under cyclic loading.

Essentially, the frame was designed as an SCBF, but the first story beam was weak with respect to the brace unbalanced load. All braces were HSS5×5×3/8 sections whose connections, found in Figs. 3.22 through 3.25 were designed according to the BDP (Roeder et al. 2011b) using 12 mm gusset plates. Unlike the previous specimens, the second story corner gusset plates in Fig. 3.23 were designed to be welded only to the adjacent beam and columns and not to a shear tab. Welded

flange welded web (WFWW) moment resisting connections were used for the first story beam-to-column connections, just as the existing second story beam-to-column connections. The corner gusset plates were designed with $8t_p$ elliptical clearances and the mid-span gusset plates with $6t_p$ vertical clearances. At the second story corner connections, the slab was blocked out around the gusset plates as in Fig. 3.26 to permit rotation.

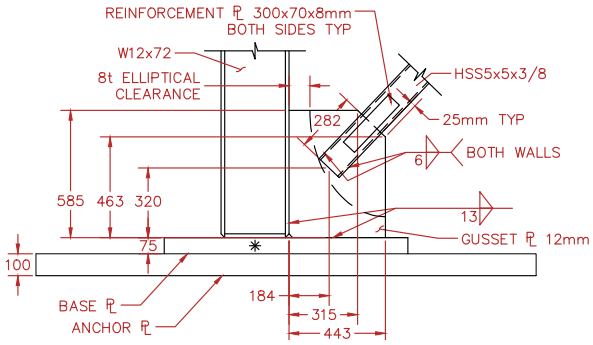

Figure 3.22: TNCBF2-D-HSS first story corner gusset plate details

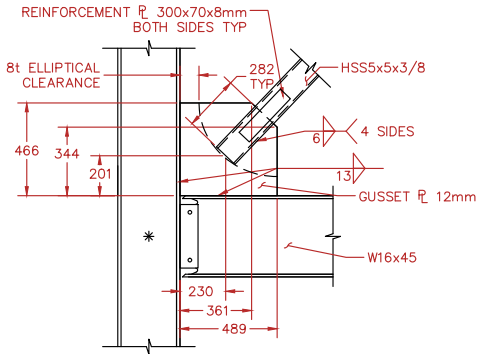

Figure 3.23: TNCBF2-D-HSS second story corner gusset plate details

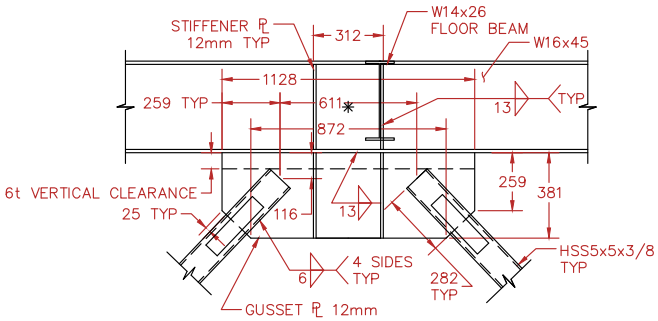

Figure 3.24: TNCBF2-D-HSS first story mid-span gusset plate details

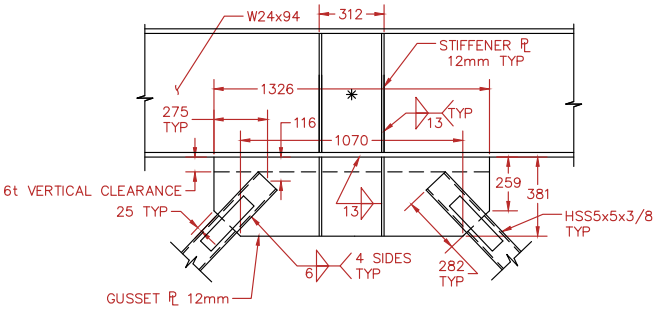

Figure 3.25: TNCBF2-D-HSS second story mid-span gusset plate details



Figure 3.26: Typical slab blockout around corner gusset plates

3.9 Experimental Setup

The experimental setup, designed by NCREE researchers Chao-Hsien Li and An-Chien Wu, was largely the same as that used for the TCBF2 test series, which is explained in Lumpkin (2009). The test setup was generally intended to provide realistic loading and boundary conditions.

3.9.1 Out-of-Plane Reaction Frame

The out-of-plane reaction frame is depicted in Fig. 3.27 (blue/dark shading) and can be seen surrounding the specimen in Fig. 3.1b. The frame's primary purpose was to prevent significant out-of-plane beam movement brought about by geometric and loading eccentricities and brace buckling. It consisted of four wide flange columns east and west of the frame. Beams and braces were bolted to the columns to provide additional contact surfaces and stiffness. This frame was not attached to the specimen but points of contact were provided at specific locations to provide lateral support. Grease was applied at these support points to reduce frictional forces.

On the first story, and unique from the TCBF2 test series, two wide flange beams east and west of the specimen serve as reaction surfaces for large edge plates bolted to the ends of the inner floor beams. These edge plates, shown in Fig. 3.28a, were provided to limit torsional rotation of the first story beam, as an actual floor diaphragm might, during significant vertical excursions. Out-of-plane lacing on the first story was used in TNCBF1-N-HSS only; it was removed from later tests to provide adequate clearance for brace buckling.

At the second story, the beam was restrained at the locations of the out-of-plane columns only as in Fig. 3.28b. Since significant beam deformation was not expected at the second story, with its strong beam, the slab edge beams interfaced with plates attached to the columns with threaded rods. Additionally, rollers were attached to transverse beams to resist twisting action of the beam. Prior to testing, the contact surfaces on the out-of-plane frame were adjusted so that they nearly touched the adjacent surfaces on the specimen by repositioning the anchor rods.

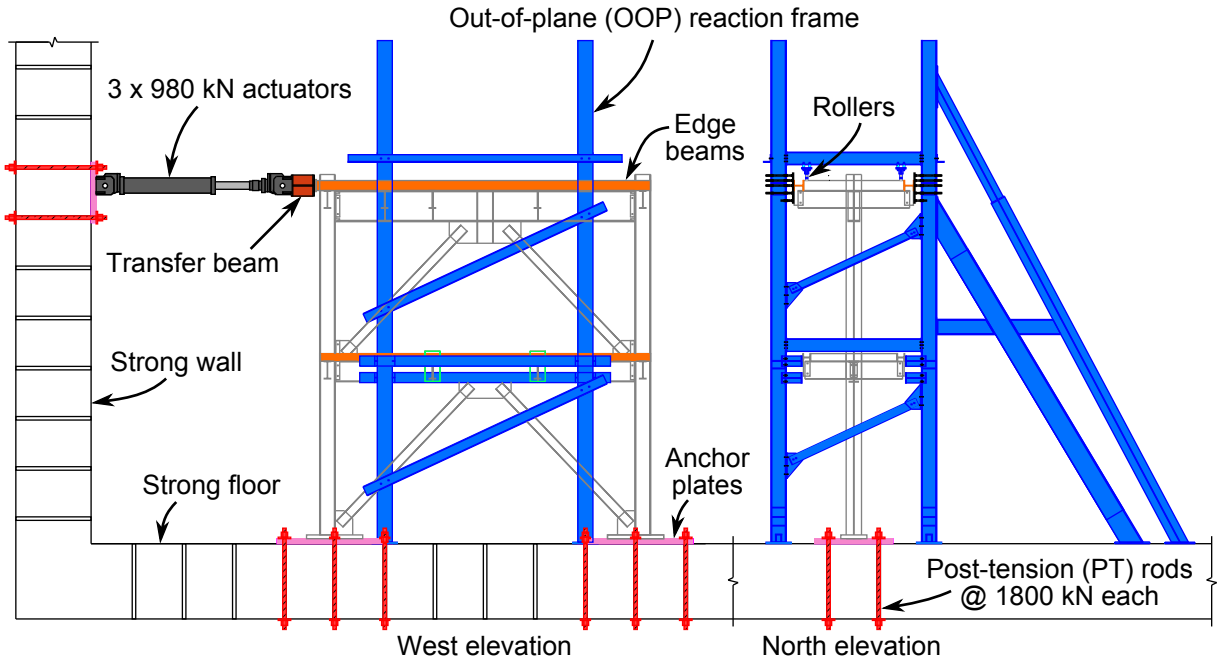

Figure 3.27: Experimental setup

3.9.2 Actuator Load Path and Edge Beams

The specimens' lateral load followed the path diagrammed in Fig. 3.29. Three 980 kN actuators located at the south end of the second story loaded the specimens. The actuators were directed north such that north displacement corresponded to a pushing action (actuators in compression) and south displacement corresponded to a pulling action (actuators in tension). The east and west actuators followed the displacement of the central actuator. Forces induced by the actuators were transferred through a load beam and then through two edge beams bounding the concrete

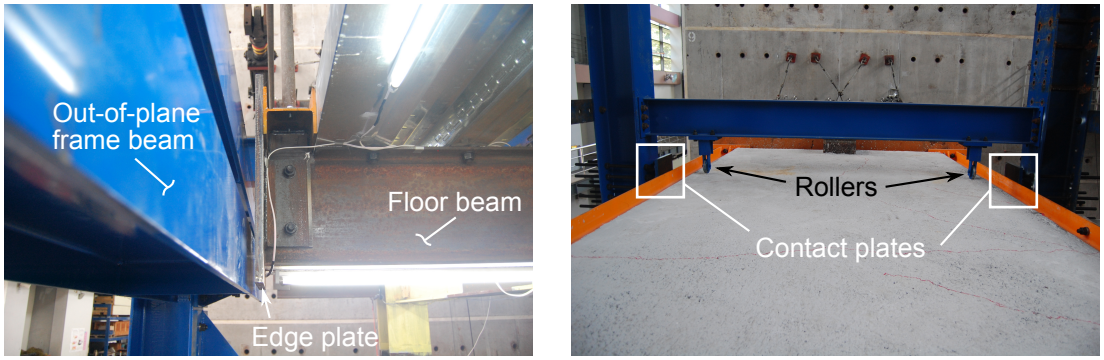

(a) First story edge plate interface (b) Second story edge beam interface

Figure 3.28: Out-of-plane frame interfaces

slab continuous along the length of the bay. The edge beams delivered shear to the slab through densely spaced (150 mm on center) 19 mm-diameter shear studs. The resulting diaphragm load was transferred to the braced frame through a double row of shear studs on the second story beam with the same spacing. Through this system, the force is more uniformly distributed to the beam and compatibility between the edge beams and the rest of the second story system effectively stiffens the braced frame beam. The first story was not loaded by actuators and therefore did not require a robust force distribution system through the slab edges. To avoid stiffening the intentionally weak first story beam, which was expected to undergo significant vertical excursions, the edge beams were not extended into the middle third of the bay. The different edge beam systems can be seen prior to erection of the out-of-plane frame in Fig. 3.30.

3.9.3 Loading Protocol

The actuators were programmed to follow the displacement-controlled reversed cyclic loading protocol in Fig. 3.31 and Table 3.11 using LVDTs attached at the opposite end of the slab as references. The loading protocol was based on a yield roof drift, Δ_y, of 25 mm, determined from preliminary Abaqus analyses. Up to ductility 2.5, the increase in amplitude was limited to $0.25\Delta_y$ to ensure that enough data would be collected in the event of significant at a low drift level, as might be the case for TNCBF1-N-HSS, a frame with non-ductile details.

This loading configuration was not representative of an actual structure under seismic excitation.

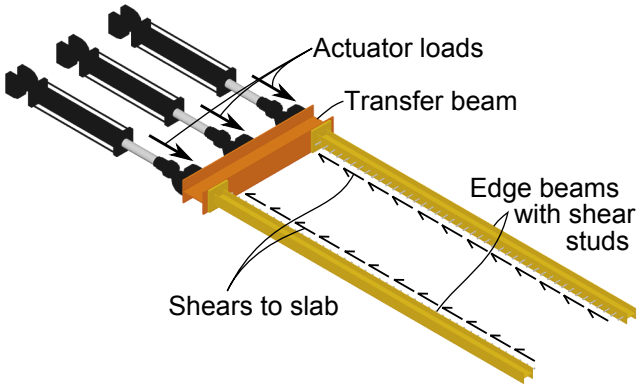

Figure 3.29: Actuator-to-specimen load path at second story

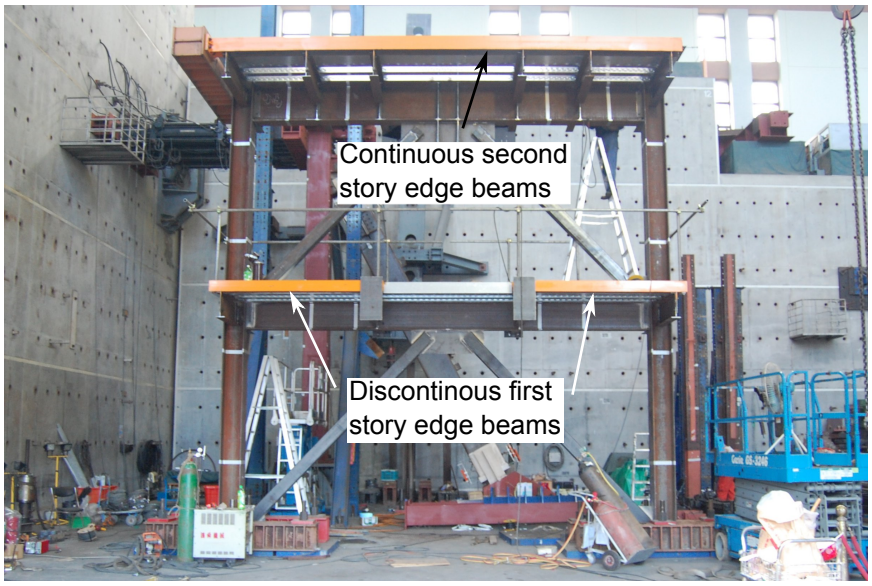

Figure 3.30: Frame edge beams

In a more realistic first mode load distribution, inertial forces would develop at the first story such that the first story shear would exceed the second story shear, which may necessitate larger braces to provide adequate lateral resistance. The specimens' braces, however, were selected to have similar yield strengths since the story shears were equivalent.

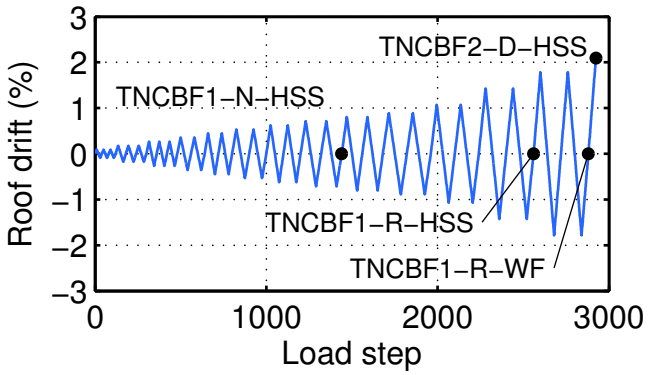

Figure 3.31: Loading protocol with test ends labeled

Table 3.11: Loading protocol

Ductility, Δ/Δ_y	Cycles	Roof drift (%)	Roof disp. (mm)	Test end
0.25	3	0.09	6.25	
0.5	3	0.18	12.50	
0.75	3	0.27	18.75	
1	2	0.36	25.00	
1.25	2	0.45	31.25	
1.5	2	0.54	37.50	
1.75	2	0.62	43.75	
2	2	0.71	50.00	TNCBF1-N-HSS
2.25	2	0.80	56.25	
2.5	2	0.89	62.50	
3	2	1.07	75.00	
4	2	1.43	100.00	TNCBF1-R-HSS
5	2	1.79	125.00	TNCBF1-R-WF
6	1/2	2.14	150.00	TNCBF2-D-HSS

3.9.4 Base and Anchor Plates

The axial forces, shear forces, and moments that developed in the specimens were reacted through 75 mm base plates connected to 100 mm anchor plates through a grid of 30 mm-diameter anchor rods. This connection was capacity designed for the maximum column and first story brace demands.

The originally-designed base plates were extended with 40 mm plates due to uplift concern. The extensions were welded to the base plates with complete joint penetration (CJP) welds and are shown in Fig. 3.32b.

Three anchor plates were used at each column. The base plate rods threaded into wider central anchor plates and the base plate extension rods threaded into narrower outer anchor plates. The sets of anchor plates were bridged with two transfer beams east and west of the columns and anchored to the strong floor with 6-1800 kN post-tension rods per column as is seen in Fig. 3.32c.

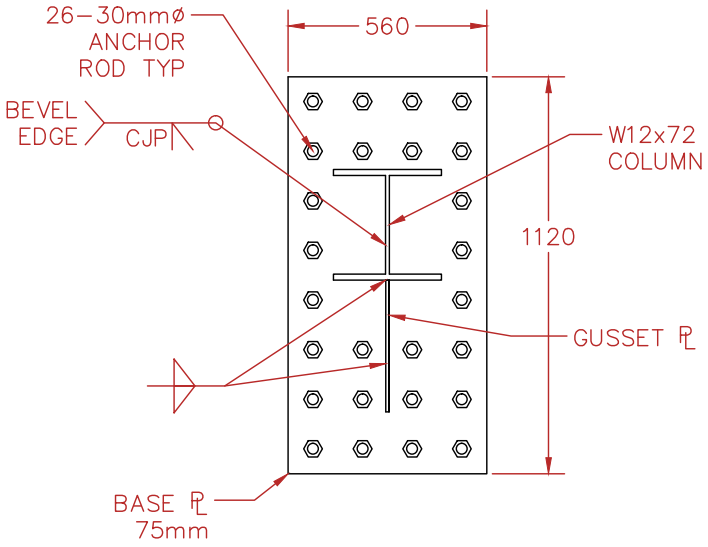

(a) Base plate sketch

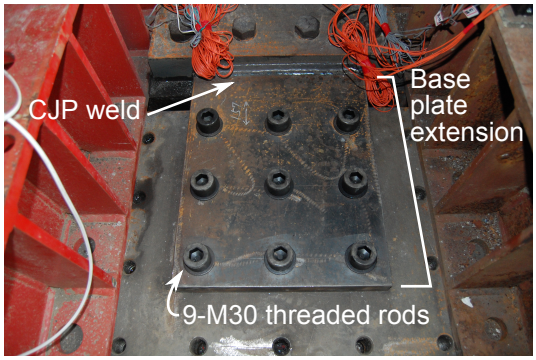

(b) Base plate extension

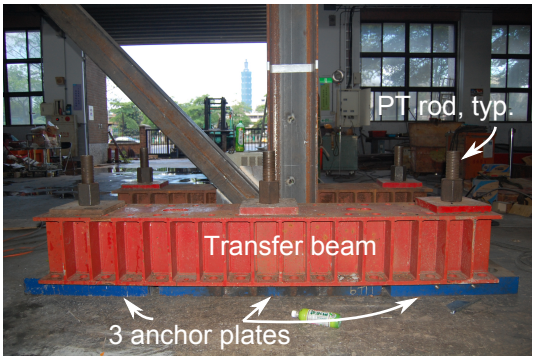

(c) Anchorage system

Figure 3.32: Base setup

3.10 Instrumentation

Physical and optical sensors, listed fully in Table 3.12, were applied to each specimen with little variation between tests. Data from these two sets of sensors was collected with two separate data acquisition units. In general, physical sensors measure voltage differentials caused by geometric changes in the instrument. Each physical sensor is calibrated prior to testing so that the voltage output by the instrument has physical meaning, such as strain or displacement. The types of physical sensors used in the tests include strain gauges, linear variable displacement transducers (LVDTs), string potentiometers, inclinometers, dial gauges, and load cells.

Optical sensors were also employed using the NDI Optotrak system, which uses a camera to record the spatial position of light emitting diode (LED) markers attached to various components of the specimen. This form of data collection is advantageous in that the measurement device–the camera–does not require direct contact with the specimen, only the LED markers. This attribute is particularly useful when space is limited and traditional physical sensors would be unwieldy. Results derived from each of these two instrumentation types are generally consistent, which in part validates the accuracy of both systems. The instrumentation specifically applied to certain components of each specimen will be described in detail below.

Table 3.12: Overview of sensor descriptions and uses

Sensor	Photo	Locations	Derived quantity
Uniaxial strain gauge (TML)	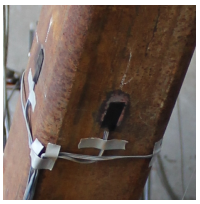	Braces Beams Columns	Axial force Axial and shear force, moment Axial and shear force, moment
Triaxial strain gauge rosette (TML)	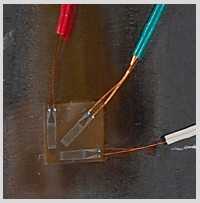	Columns	Shear force
Linear variable displacement transducer (TML)		Beams Gusset plates	Mid-span vertical displacement Out-of-plane rotation
Linear variable displacement transducer (Temposonic)		2F slab end	2F lateral displacement
String potentiometer (Celesco)	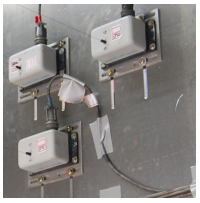	1F slab ends Braces Gusset plates	1F lateral displacement Out-of-plane displacement, elongation and shortening Out-of-plane rotation
Inclinometer (Jewell)		Beams Columns Knife plates	In-plane rotation In-plane rotation In-plane rotation

Continued on next page

Table 3.12 – continued from previous page

Sensor	Photo	Locations	Derived quantity
Dial gauge (Peacock)		Base plates	Slip, uplift
		Anchor plates....	Slip, uplift
Internal load cell (MTS)	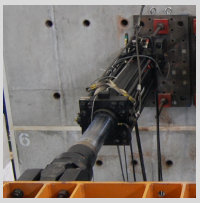	Actuators.....	Applied lateral force
Optotrak LED marker (NDI)		1F braces.....	Out-of-plane displacement, rotation
		1F beams.....	3D displacement and rotation
		Gusset plates	Out-of-plane rotation
		Knife plates	In-plane rotation

3.10.1 Frame

Internal load cells in the actuators at the roof were used to determine base and story shears. The base and story shears are equivalent under this loading protocol because the load is applied at the top of the frame only. Such a load distribution is atypical in frames subjected to seismic excitation, but it is economical and efficient for the purposes of experimental testing. Temposonic linear variable displacement transducers (LVDTs) were mounted to a reference column two meters from the frame and opposite of the actuators to measure roof displacement. These LVDTs were also used to control the actuator displacement, since the internal displacement transducers in the actuators may capture displacements that are not associated with the frame (e.g. slip or uplift of actuator anchor plates, load beam deformation, etc.). String potentiometers were attached to reference columns to measure displacement at the first story. At both stories, the sensors were mounted at the mid-depth of the slabs.

3.10.2 Braces

For each brace, there are three important quantities of interest: axial force, elongation and shortening, and out-of-plane displacement. Axial force was measured indirectly using uniaxial strain gauges located on the brace walls at the lower quarter-point of each brace. Force was calculated by assuming that the stress-strain relationship in the steel was bilinear and fitted to stress-strain curves from coupon tension tests. Brace elongation and shortening was measured using string potentiometers mounted at one end of each brace. The string was extended along the length of the brace and attached to the opposite end. It should be noted that brace elongation and shortening is not the axial deformation of the brace (i.e., along its deformed longitudinal axis), but rather the change in length from brace end-to-brace end.

Out-of-plane displacement of the brace was measured via two methods shown in Fig. 3.33. D_i, C_i, d_i, and s_i are determined from the initial geometry (measured by hand; e.g., d_o) and string potentiometer data collected at each time step, i. The first method is indirect and based on trigonometry and uses the brace elongation and shortening string potentiometer and a second similarly arranged potentiometer that contacts a pin at the brace mid-span, where out-of-plane movement is expected to be largest. The pin catches the second string when the brace buckles out-of-plane and a triangle can be constructed using the string potentiometer set. From the triangle, out-of-plane displacement ($\delta_{\mathrm{oop},1}$) can be derived. However, this method is prone to error magnification due to the trigonometric relations involved. A more direct measure of out-of-plane displacement was used in all tests but TNCBF1-N-HSS. It involves mounting a string potentiometer to a reference column (in this case, a column of the frame resisting out-of-plane movement) that extends to the mid-span of the brace. The results from this measure ($\delta_{\mathrm{oop},2}$) were found to be more accurate than those from the former method when compared to hand measurements at different stages of the test.

3.10.3 Beams

The behavior of the bottom beam subjected to the brace unbalanced load at its mid-span is of particular interest, so this location was heavily instrumented with LED markers and redundant physical instruments. The LEDs captured vertical displacements as well as in-plane and torsional rotation of the beam. Vertical displacements at the mid-spans of both beams were also captured

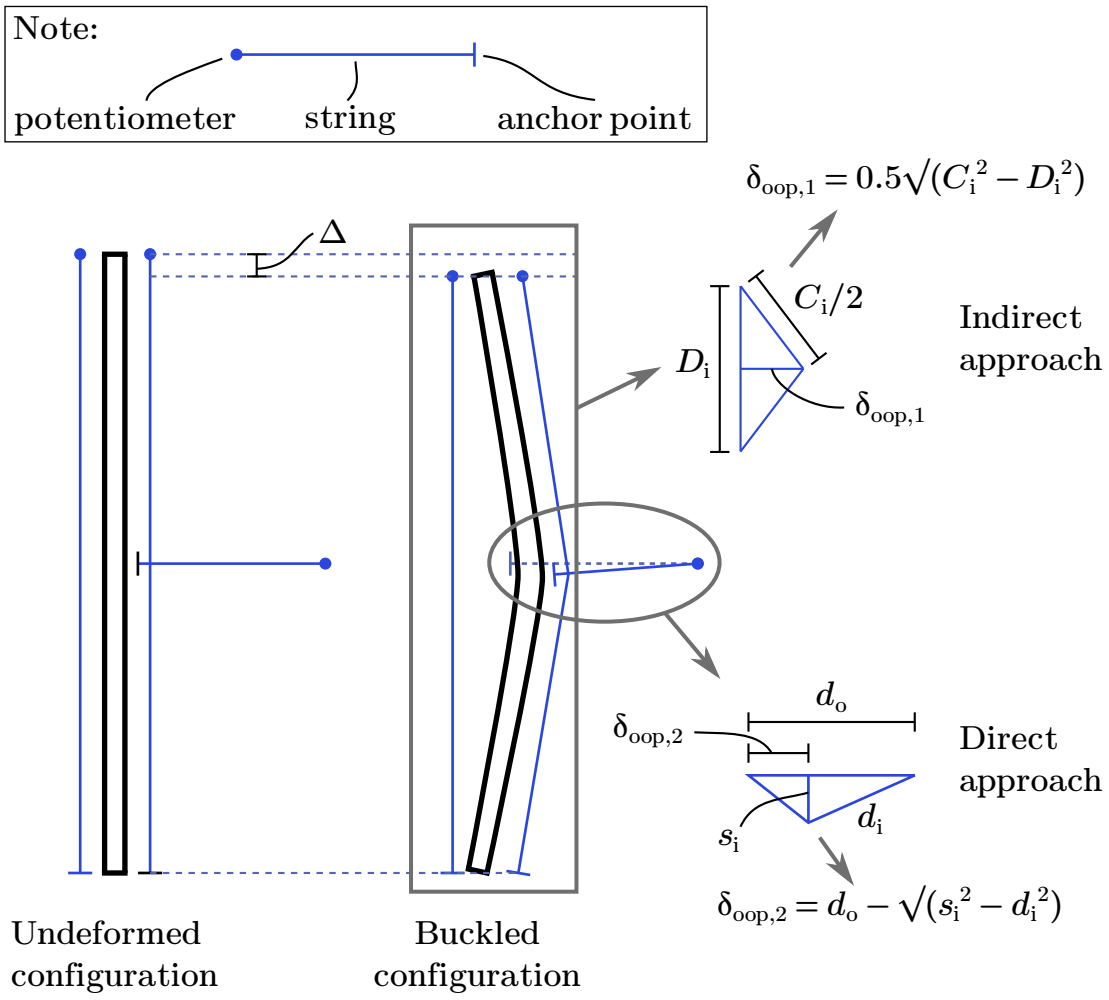

Figure 3.33: Methods of determining brace out-of-plane displacement using string potentiometers

with LVDTs located at the bottom flanges. On the bottom beam, inclinometers were mounted to the beam webs in the connection regions, including the mid-span gusset plates.

The beams were also instrumented with uniaxial strain gauages to attempt to capture their axial force, shear, and moment distributions. However, deriving these quantities from strain gauge data is complicated in the presence of a partially composite slab. Stain gauges were placed inside the slab and on the bottom of the deck to attempt to quantify behavior across the composite cross section, but the data from these instruments was ultimately not useful. Since the data from the

strain gauges on the steel alone does not provide a complete response, the desired quantities could not be computed.

3.10.4 Columns

The most critical instrumentation on the columns was the uniaxial and triaxial strain gauges. These were applied to attempt to capture the same internal forces and moments as in the beams. Since the columns are bare steel, their section behavior is much simpler and these quantities are extracted relatively easily. Moments were calculated using uniaxial strain gauge pairs on the extreme fibers at different locations along the columns, typically 336 to 400 mm from adjacent gusset plates or beams. The moment distribution along the length of the column is linear, so column shear is constant and may also be computed; this concept is represented in Fig. 3.34. The triaxial strain gauge rosettes provided an alternative method for calculating shear, and in general, these two methods produced consistent results. The triaxial strain gauge data is most often presented henceforth because they were located at the mid-height of each story where no yielding occurred. The uniaxial strain gauge pairs were located closer to the ends of the columns where the steel yielded in some cases.

3.10.5 Whitewash

Selected areas of the frame were whitewashed to detect yielding. When hot rolled steel yields, mill scale (an artifact of hot rolling) located on the surface of the steel debonds (flakes). Whitewash that is applied to the surface provides contrast to bare steel exposed by mill scale flaking. The whitewash used in these tests was dyed yellow to improve picture quality.

The whitewash plans for each specimen are found in Appendix A. Whitewash was applied in areas where yielding was anticipated; in general, this includes beam and column connections and surrounding vicinities, gusset plates, and braces. HSS braces are cold formed and do not have mill scale, so these components were not whitewashed.

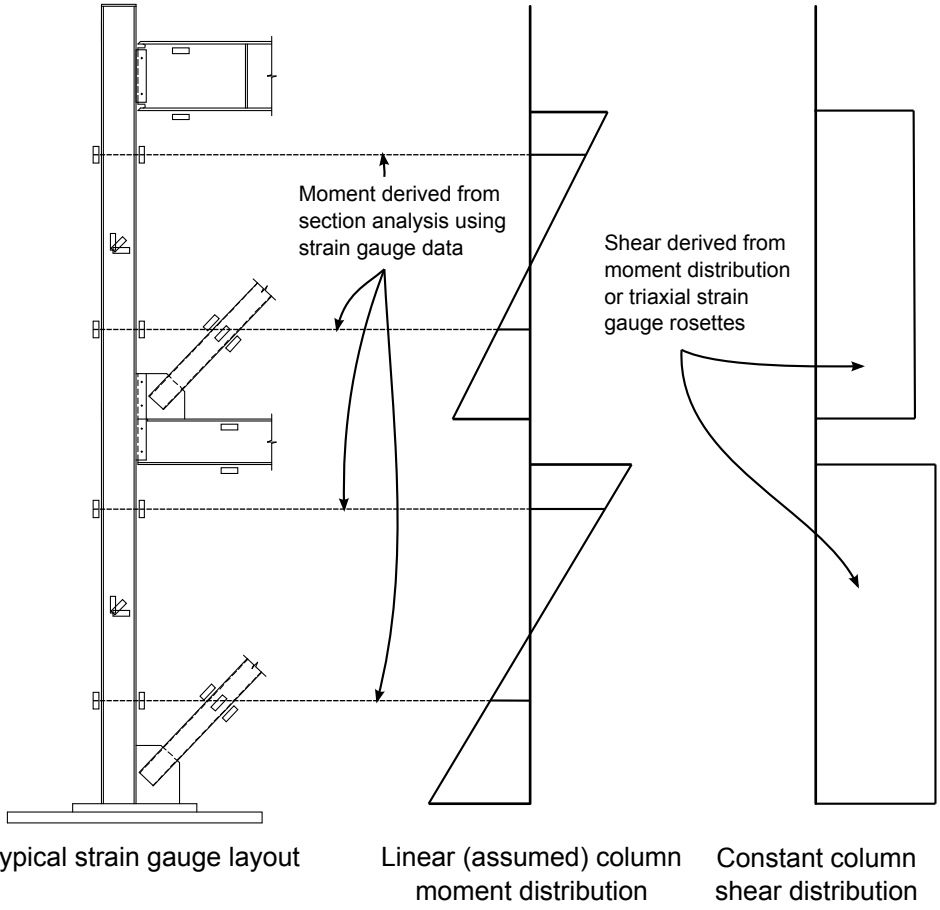

Figure 3.34: Column strain gauge schematic and derived shear and moment fields

Chapter 4

EXPERIMENTAL OBSERVATIONS

4.1 Introduction

In this chapter, the performance states used to identify the observations are defined first. For each test, an overview of the test is provided along with load and drift time histories and hystereses. Since the frame is only loaded at the second story, actuator load, first story shear, second story shear, and base shear are all equivalent. Drift is the ratio of the lateral displacement of the roof (Δ_r) or story (Δ_1 or Δ_2) to the roof or story height; it is presented throughout this document as a percentage. Fig. 4.1 illustrates the story and roof heights for the TNCBF specimens and provides a lateral displacement schematic. From the figure, percent drift can be calculated using lateral displacement measurements in millimeters at any time step by Eqs. 4.1 through 4.3. Note that Δ_2 is the difference between the roof displacement and first story displacement.

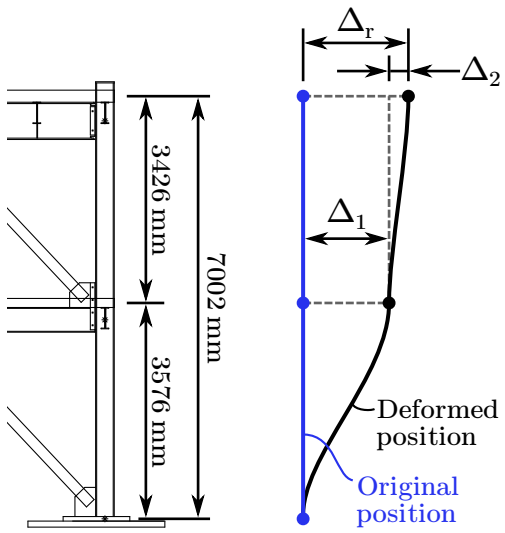

Figure 4.1: Roof and story heights and displacements

$$\delta_{\mathrm{r}} = \frac{\Delta_{\mathrm{r}}}{7002} \times 100\% \tag{4.1}$$

$$\delta_1 = \frac{\Delta_1}{3576} \times 100\% \tag{4.2}$$

$$\delta_2 = \frac{\Delta_2}{3426} \times 100\% \tag{4.3}$$

A detailed review of the cyclic response is then divided into at most three frame state categories: initial, moderate damage, and severe damage. The drifts associated with each of these categories are dependent on the observed damage, so damage state drift intervals do not necessarily match from test-to-test. In the initial state, the frame is primarily elastic. The frame enters the moderate damage state when it sustains damage that does not compromise the integrity of the frame, maintaining strength and stiffness (e.g. brace buckling). The severe damage state is defined by fracture or other damage that leads to a rapid reduction in frame performance (e.g. brace local buckling or significant weld cracking).

4.2 Performance State Overview

Various performance states that pertain to yielding, buckling, and connection damage are used to support the test observations. The performance states used in this chapter are listed in Table 4.1 and are based on those developed by Lumpkin (2009). The most significant modification is the inclusion of brace splice connection performance states, since NCBFs have much higher potential for connection damage than SCBFs. Each performance state is described in greater detail below.

Table 4.1: Performance state notation modified from Lumpkin (2009)

Label	Description	Detailed description
Y1	Initial yielding	Yield lines first visible and/or cover no more than half the component width; may be highly localized
Y2	Moderate yielding	Yield lines cover more than half the component width but not the entire width
Y3	Severe yielding	Yield lines cover the entire width of the member or large, concentrated areas of yielding are visible
B1	Initial buckling	Brace buckling does not exceed the member depth
B2	Moderate buckling	Brace buckling greater than the member depth
B3	Severe buckling	Brace buckling greater than twice the member depth
BC	Local buckling	Brace local buckling occurred at the plastic hinge location
BF	Brace fracture	Brace fracture in tension at the plastic hinge location
Bs1	Initial brace splice crack	Initial damage to the brace slotted splice weld connection, usually minor transverse cracking at the net section
Bs2	Moderate brace splice crack	Propagation of crack along length of brace (parallel to splice)
BFs	Splice connection fracture	Loss of tensile resistance due to damage to the splice connection, usually a combination of weld and base metal crack propagation
PC	Plate cracking	Cracks visible on gusset plate at brace end
Wc	Weld crack at column	Gusset plate or shear tab weld to column is cracked; crack length is appended to the label
Wb	Weld crack at beam	Gusset plate or shear tab weld to beam is cracked; crack length is appended to the label
Ws	Weld crack at shear tab	Gusset plate or beam weld to shear tab is cracked; crack length is appended to the label
WBc	Base metal crack at column	Base metal at column interface is cracked; crack length is appended to the label
WBb	Base metal crack at beam	Base metal at beam interface is cracked; crack length is appended to the label
Wbs	Base metal crack at shear tab	Base metal at shear tab interface is cracked; crack length is appended to the label

The frame location notation used in the performance state tables in this chapter is described by Table 4.2. The shaded locations in Fig. 4.2 show the different areas of interest in the performance state tables. For instance, the shaded lower left-hand corner box corresponds to the region abbreviated as "1S-L."

Table 4.2: Frame location notation

Label	Meaning
1	First story
2	Second story
S	South
N	North
L	Lower
U	Upper
E	End
M	Mid-span

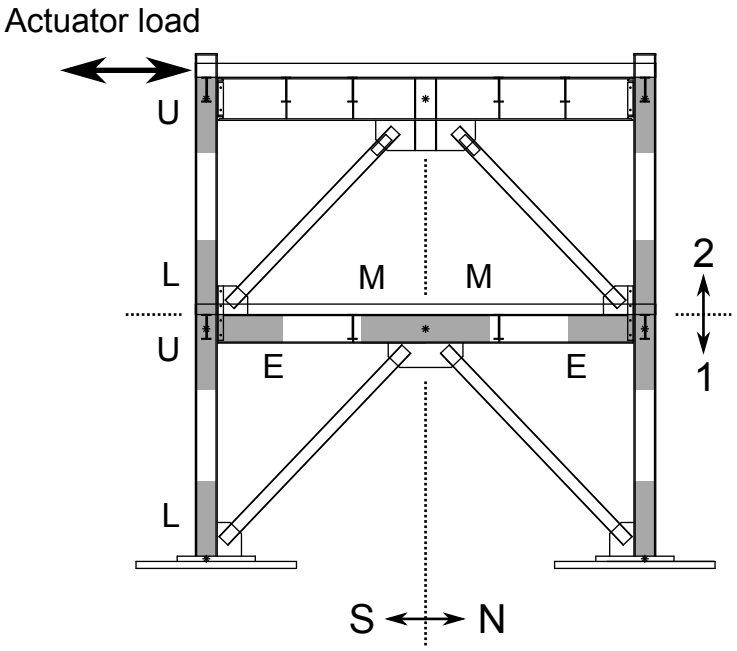

Figure 4.2: Frame location notation

4.2.1 Yielding

Yielding is generally detected by the flaking of whitewash on gusset plates, beams, and columns. Examples of yielding are depicted in Fig. 4.3. Gusset plate yielding is induced by tension and/or flexural action in compression due to brace end rotation. Beam and column yielding usually results from web and flange local buckling due to combined axial and flexural demand. Column yielding may occur in panel zones due to shear. Brace yielding is not included in this classification. Yielding of HSS braces can be detected through strain gauge readings, though it should be noted that post-yield measurements have been found to be less reliable, as the strain gauge glue is likely to debond from the surface of the brace at post-yield strains and confound the results. Wide flange braces suffer from the same strain gauge issues, but they can be whitewashed to detect yielding. However, in reverse cyclic loading of the braces, buckling is likely to occur prior to gross section yielding, and the deformation from buckling inevitably produces local yielding, particularly at the brace mid-span. Thus, yielding of the gross section in tension is difficult to detect by whitewash alone.

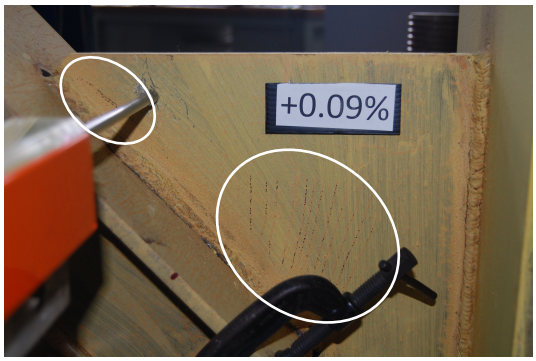

(a) Initial yielding (Y1)



(b) Moderate yielding (Y2)



(c) Severe yielding (Y3)

Figure 4.3: Examples of yielding

4.2.2 Brace Buckling and Fracture

The initiation of brace buckling is not always visually distinguishable from elastic deformations, but it can be easily identified in the data by axial strength loss of the brace in compression. Later stages of buckling are defined by the out-of-plane displacement of the brace at its mid-span, where the maximum displacement occurs, relative to its depth. This displacement is measured using string potentiometers. Local buckling (BC) is identified by cupping at the brace mid-span in HSS braces. A plastic hinge develops as one brace wall deforms inward and the adjacent walls protrude out, causing severe strain accumulation at these locations. In wide flange braces, the flanges deform on the compressive side of the resulting plastic hinge. The local buckling modes of HSS and wide flange braces are pictured in Fig. 4.4.

Brace fracture, seen in Fig. 4.5, occurs in tension due to severe strain accumulation due to local



(a) HSS brace

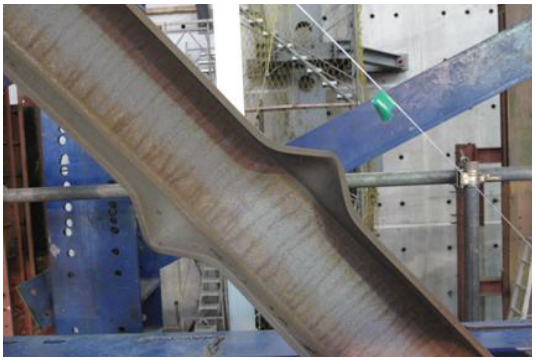

(b) WF brace (Lumpkin 2009)

Figure 4.4: Examples of local buckling (BC)

buckling. Preceding rupture, tearing typically initiates on the compressive face of the plastic hinge, where deformation is most severe.

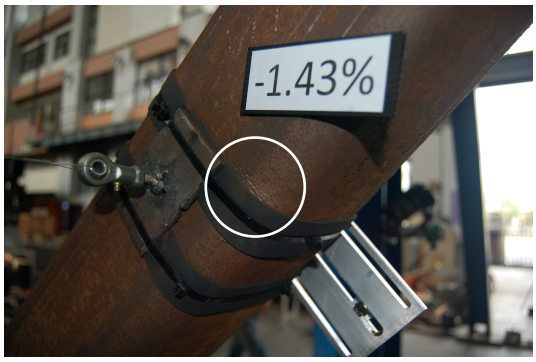

(a) Teraing prior to fracture

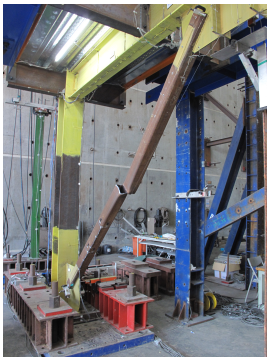

(b) Complete brace fracture

Figure 4.5: Examples of brace fracture (BF)

4.2.3 Brace Splice Connection Damage and Failure

Damage to the brace splice connection arises due to weld and brace base metal cracking. The various levels of damage are depicted in Fig. 4.6. The initial crack (Bs1) is transverse and forms at the net section, specifically at the toe of the weld at the end of the brace slot. In Bs2, the crack turns and propagates along the brace length in the weld, base metal, or both. Additionally,

cracks may form at the opposite end of the splice due to the eccentricity introduced by the initial crack. When the connection is damaged such that it loses load carrying capacity, BFs is reached. Failure may be progressive (i.e., load drops incrementally with each cycle until complete fracture) or sudden.



(a) Crack initiation (Bs1)

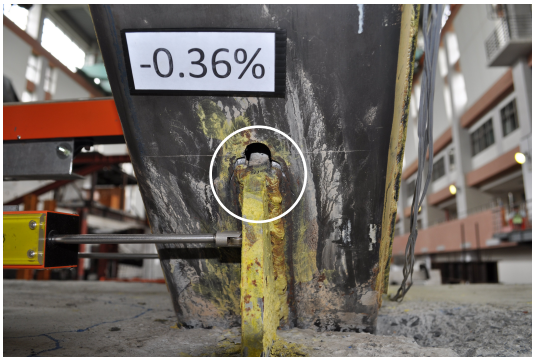

(b) Crack propagation (Bs2)



(c) Connection fracture (BFs)

Figure 4.6: Examples of brace splice connection damage

4.2.4 Gusset Plate Cracking

Gusset plate cracking refers to the initiation of transverse cracks in the plate at the toe of the splice weld at the brace end, as in Fig. 4.7. When braces buckle, these cracks initiate due to stress concentrations and significant inelastic deformation at the plastic hinge in the plate. This is not considered a severe performance state and is typically observed just prior to brace fracture.

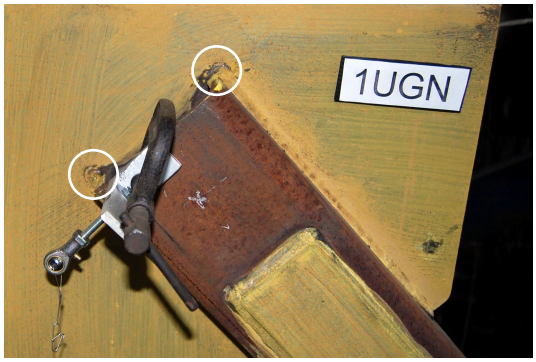

(a) Plate crack locations



(b) Plate crack magnified

Figure 4.7: Example of plate cracking

4.2.5 Beam and Column Interface Weld and Base Metal Damage

Gusset-to-beam and -column interface welds are subjected to significant demands primarily due to rotation. When highly ductile braces are employed, tearing of gusset plate interface welds is not uncommon due to significant deformation demands from brace buckling. Note that for this reason, balance-designed welds are sized for the capacity of the gusset plate and not the brace axial force. In the performance state tables presented in this section, interface weld and base metal damage is documented with the crack length. For example, "Wb-4cm" indicates a 4 cm beam interface weld crack. Two examples of damage at the gusset interface are shown in Fig. 4.8.



(a) Beam interface weld damage (Wb)



(b) Column interface base metal damage (WBc)

Figure 4.8: Example of gusset plate interface weld and base metal damage

Weld and base metal damage also occurs in beams and shear tabs due to large in-plane rotations resulting from beam deformation induced by brace unbalanced loads and frame story drift (joint opening and closing). This damage may be viewed as more severe due to the critical nature of beam-to-column connections in preserving structural integrity. Two examples of damage at the beam interface are shown in Fig. 4.9.

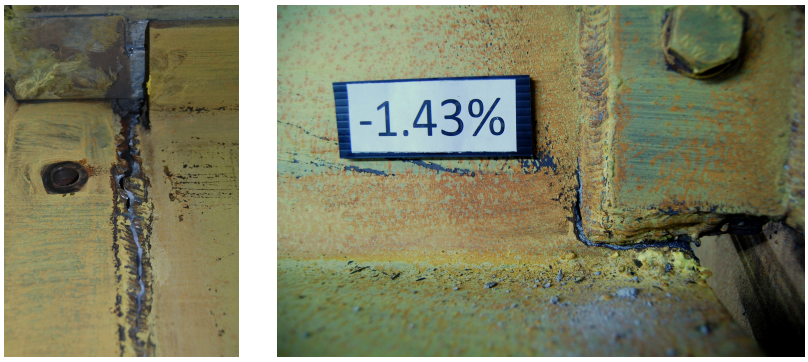

(a) Shear tab interface weld damage (Ws)

(b) Shear tab interface base metal damage (WBs)

Figure 4.9: Example of beam interface weld and base metal damage

4.3 TNCBF1-N-HSS Observations

4.3.1 Overview of Cyclic Response

The specimen TNCBF1-N-HSS, shown in Fig. 4.10, was tested on July 20, 2013 and was designed as a prototypical NCBF with a weak beam and braces in the inverted V configuration. This frame was intended to serve as a non-ductile baseline to examine how an existing NCBF might perform if it is not rehabilitated. Critical deficiencies in this specimen included non-seismically compact HSS7×7×1/4 braces and non-seismic (and presumably non-ductile) connections. The load and roof drift histories can be found in Figs. 4.12 and 4.11. Roof and story drift hystereses are presented in Figs. 4.13 and 4.14. Key events are labeled on the hystereses and described in Table 4.3.

As can be seen by the hystereses, inelastic deformation was concentrated in the first story while the second story remained essentially elastic. On the first story, one brace buckled and fractured at nearly 0.5% story drift. The remaining first story brace did not buckle, resulting in eccentrically



Figure 4.10: TNCBF1-N-HSS overview

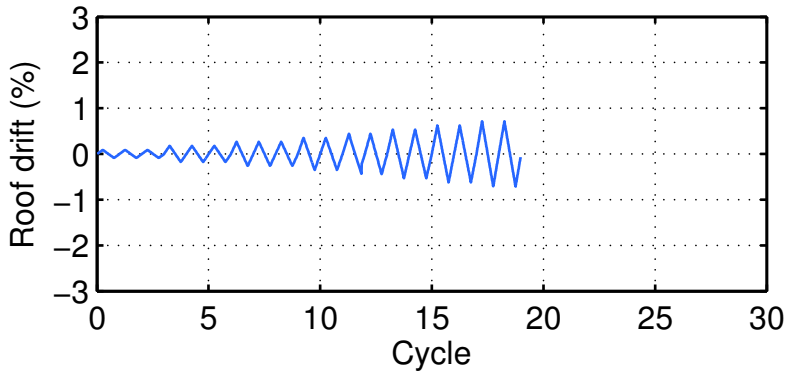

Figure 4.11: TNCBF1-N-HSS roof drift history

braced frame (EBF) behavior for several cycles, but its mid-span connection failed at just over 1% story drift. The test was ended at the corresponding roof drift level of 0.71% to prevent further damage, as the frame had lost significant lateral resistance.

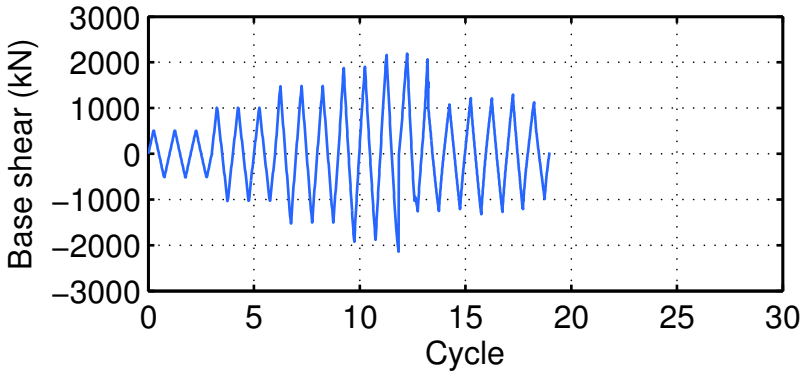

Figure 4.12: TNCBF1-N-HSS load history

Peak resistances (actuator force, story shear, and base shear are equivalent) and drifts within each cycle are shown in Table 4.4. After brace fracture, the frame lost almost half its lateral resistance, though a marginal amount was regained due to the EBF mechanism. The performance states reached in each cycle are tabulated in detail in Table 4.5.

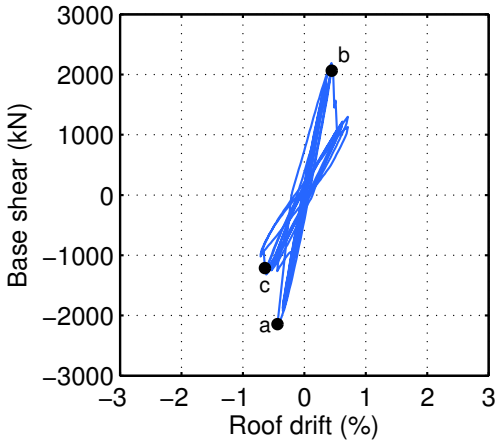

Figure 4.13: TNCBF1-N-HSS base shear-roof drift hysteresis

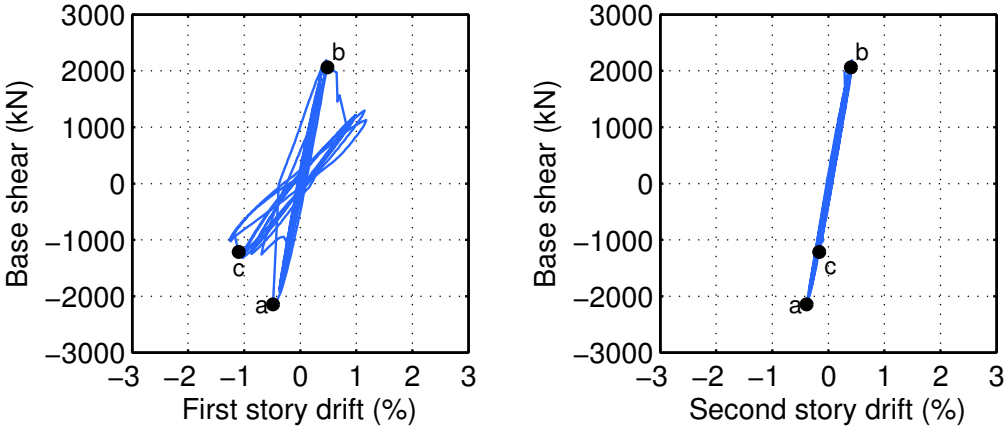

(a) First story

(b) Second story

Figure 4.14: TNCBF1-N-HSS base shear-story drift hystereses

Table 4.3: Description of labels in Figs. 4.13 and 4.14

Label	Location	Event	Roof drift (%)	Story drift (%)
a	1F south brace	Buckling Local buckling	−0.44	−0.48
b	1F south brace	Complete fracture	+0.42	+0.46
c	1F north brace	Connection fracture	−0.61	−1.04

Table 4.4: TNCBF1-N-HSS peak lateral resistances and drifts

	Resistance (kN)		Roof drift (%)		1F drift (%)		2F drift (%)	
Cycle	Max.	Min.	Max.	Min.	Max.	Min.	Max.	Min.
1	502	−508	0.08	−0.08	0.08	−0.09	0.09	−0.08
2	501	−508	0.08	−0.08	0.08	−0.09	0.09	−0.08
3	500	−505	0.08	−0.08	0.08	−0.09	0.08	−0.08
4	1008	−1035	0.17	−0.17	0.18	−0.18	0.17	−0.16
5	1008	−1031	0.17	−0.17	0.18	−0.18	0.17	−0.16
6	1006	−1030	0.17	−0.17	0.18	−0.18	0.17	−0.16
7	1477	−1530	0.26	−0.26	0.27	−0.27	0.25	−0.25
8	1484	−1508	0.26	−0.26	0.27	−0.27	0.26	−0.25
9	1485	−1505	0.26	−0.26	0.27	−0.27	0.25	−0.25
10	1873	−1925	0.35	−0.35	0.37	−0.37	0.34	−0.33
11	1903	−1880	0.35	−0.35	0.36	−0.37	0.34	−0.32
12	2164	−2144	0.44	−0.44	0.48	−0.48	0.41	−0.39
13	2192	−1262	0.44	−0.44	0.46	−0.69	0.42	−0.18
14	2063	−1250	0.53	−0.53	0.83	−0.87	0.41	−0.17
15	1081	−1213	0.53	−0.53	0.84	−0.88	0.21	−0.17
16	1217	−1321	0.62	−0.62	0.99	−1.03	0.24	−0.19
17	1212	−1275	0.62	−0.62	0.99	−1.03	0.24	−0.19
18	1297	−1211	0.71	−0.71	1.15	−1.24	0.26	−0.17
19	1129	−990	0.71	−0.71	1.18	−1.25	0.23	−0.14

Table 4.5: TNCBF1-N-HSS performance state progression

Drift (%)		Braces				Corner gusset plates				Mid-span gusset plates				Beams				Columns								Drift range (%)	
Roof	1F 2F	1S	1N	2S	2N	1S	1N	2S	2N	1S	1N	2S	2N	1S-E	1S-M	1N-M	1N-E	1S-L	1S-U	2S-L	2S-U	1N-L	1N-U	2N-L	2N-U	Roof	1F 2F
0.08	0.08 0.09																									0.17	0.17
−0.08	−0.09 −0.08																										0.16
0.08	0.08 0.09																									0.17	0.17
−0.08	−0.09 −0.08																										0.16
0.08	0.08 0.08																									0.17	0.17
−0.08	−0.09 −0.08																										0.16
0.17	0.18 0.17																									0.35	0.36
−0.17	−0.18 −0.16																										0.33
0.17	0.18 0.17																									0.35	0.36
−0.17	−0.18 −0.16																										0.33
0.17	0.18 0.17																									0.35	0.36
−0.17	−0.18 −0.16																										0.33
0.26	0.27 0.25					Y1						Y1						Y1				Y1				0.52	0.54
−0.26	−0.27 −0.25						Y1						Y1														0.50
0.26	0.27 0.26																									0.52	0.54
−0.26	−0.27 −0.25																										0.50
0.26	0.27 0.25																									0.52	0.54
−0.26	−0.27 −0.25																										0.50
0.35	0.37 0.34																									0.70	0.74
−0.35	−0.37 −0.33																										0.66
0.35	0.36 0.34										Y1															0.70	0.74
−0.35	−0.37 −0.32																										0.66
0.44	0.48 0.41	Bs1								Y1																0.88	0.96
−0.44	−0.48 −0.39	BC	Bs1			Y2															Y1				Y1		0.79

Continued on next page

Table 4.5 – continued from previous page

Drift (%)		Braces				Corner gusset plates				Mid-span gusset plates				Beams				Columns								Drift range (%)	
Roof	1F 2F	1S	1N	2S	2N	1S	1N	2S	2N	1S	1N	2S	2N	1S-E	1S-M	1N-M	1N-E	1S-L	1S-U	2S-L	2S-U	1N-L	1N-U	2N-L	2N-U	Roof	1F 2F
0.44	0.46 0.42						Y2																			0.88	1.16
−0.44	−0.69 −0.18																										0.60
0.53	0.83 0.41	BF		Bs1																						1.06	1.70
−0.53	−0.87 −0.17				Bs1									Y1					Y1								0.58
0.53	0.84 0.21																									1.06	1.72
−0.53	−0.88 −0.17																										0.39
0.62	0.99 0.24														Y1	Y1										1.24	2.02
−0.62	−1.03 −0.19		Bs2																								0.44
0.62	0.99 0.24																									1.24	2.03
−0.62	−1.03 −0.19																										0.43
0.71	1.15 0.26													Y2				Y2								1.42	2.39
−0.71	−1.24 −0.17		BFs																								0.43
0.71	1.18 0.23																									1.42	2.43
−0.71	−1.25 −0.14																										0.37

4.3.2 Detailed Cyclic Response

Initial State (Roof Drift $\leq 0.35\%$)

In the initial state, all components remained primarily elastic except for highly localized instances of yielding. The first detected yielding occurred at the 0.26% roof drift level in the first story corner and second story mid-span gusset plates, as well as the column bases (Fig. 4.15).

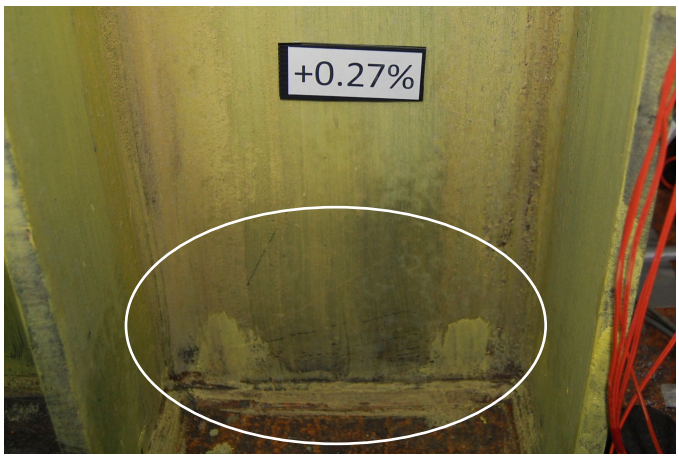

Figure 4.15: TNCBF1-N-HSS initial yielding at column base, Y1 (0.27% story drift)

Severe Damage State (Roof Drift $> 0.35\%$)

The severe damage state of TNCBF1-N-HSS corresponds to roof drift levels greater than 0.44%. For TNCBF1-N-HSS, there is no moderate damage state. At the first positive excursion to 0.44% roof drift, 0.48% first story drift was achieved and small net section cracks developed in the south first story brace (Bs1). While driving the frame to -0.44% roof drift, the first story south brace buckled violently out-of-plane and local buckling was immediately observed (BC). In addition, net section cracks developed in the north first story brace, just as the south brace. Large vibrations induced by buckling activated a hydraulic interlock in the actuator controller and the frame was automatically unloaded to zero force. No data was collected during this unexpected event. The command displacement tolerance was increased to a larger but safe value to prevent similar problems in the future. Fig. 4.16a shows the brace after unloading with obvious local buckling of the brace

walls. The south first story brace, though heavily damaged, survived the remaining cycle at the same roof drift level without fracturing, though tearing at the location of local buckling occurred (Fig. 4.16b).

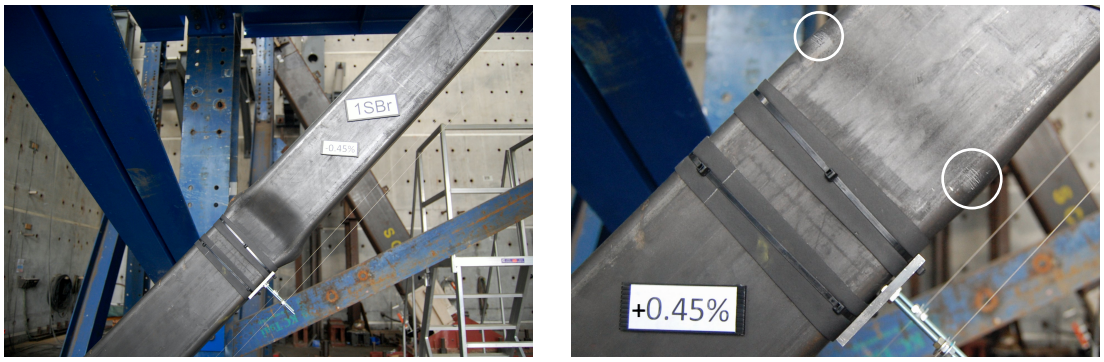

(a) Global and local buckling of 1F south brace, BC (-0.48% first story drift)

(b) Brace tearing at corners (0.46% first story drift)

Figure 4.16: TNCBF1-N-HSS buckling and tearing of 1F south brace

While loading the frame to the next roof drift level, 0.53%, the first story south brace fractured. The brace fractured at 0.42% roof drift, shown in Fig. 4.17, which was less than the previous roof drift level. This suggests that strain accumulation due to local buckling was extremely severe, which matches the observed state. The observed rapid tensile fracture after buckling is not surprising, as it is characteristic of non-compact braces Goel (1992) and is a critical contributor to the reduced ductility of the frame. This event resulted in a drop in lateral resistance of 982 kN and a considerable decline in story stiffness.

In the subsequent cycles, the north first story brace did not buckle in compression or yield in tension. The weak beam was unable to develop either of these loads; thus, the brace force was limited by the strength of the beam. Since the remaining first story brace did not buckle, the first story behaved as an EBF with the south half of the first story beam acting as a long, flexible link. As a result, the bottom beam underwent significant vertical excursions in this mode–up to about 30 mm upward and 17 mm downward. This caused the first story slab to crack along its width just north of the mid-span, shown opened approximately 4 mm in Fig. 4.18.

A marginal amount of force was developed in the south brace in compression as the fractured brace ends impacted during negative drifts. In addition, Y2 yielding occurred at 0.71% roof drift

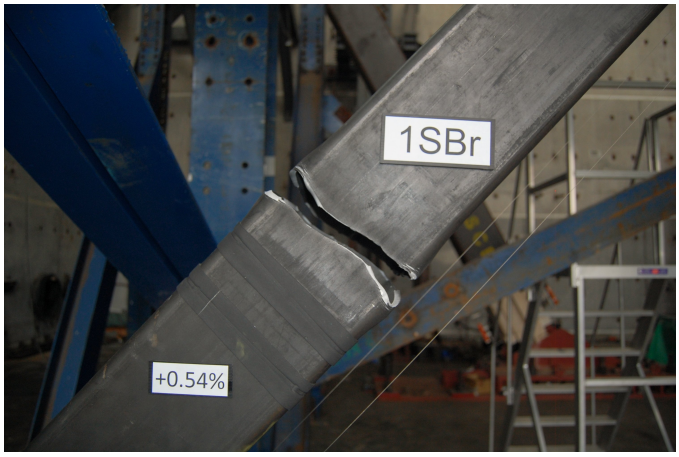

Figure 4.17: TNCBF1-N-HSS fracture of 1F south brace, BF (0.46% first story drift at fracture)



Figure 4.18: TNCBF1-N-HSS transverse first story slab crack due to upward beam deflection (0.99% first story drift)

at the south beam-to-column connection of the first story beam due to link rotation (Fig. 4.19). A crack in the shear tab-to-beam weld also developed at the lower end as a result of the high rotational demands.

At ±0.53% roof drift, net section cracks also developed in the second story braces at the corner connections. No cracks initiated at the mid-span connections where adequate net section reinforcement was provided. These cracks did not grow throughout the remainder of the test, however, the net section cracks at the north first story brace propagated in tension (Bs2) at −0.62% roof drift



Figure 4.19: TNCBF1-N-HSS yielding from beam (link) rotation, Y2 (1.15% first story drift)

or −1.03% first story drift. This led rapidly to fracture of the connection at the next drift level at −0.71% roof drift. The eventual fracture mechanism was a combination of weld and base metal crack growth as shown in Fig. 4.20. With the east weld lines were still intact, the crack propagated transversely and not along the length of the brace. This created an eccentric load path through the brace, causing the brace end at the beam mid-span to rotate out-of-plane. Even so, the connection was considered to fail as the residual brace force was marginal.

The test was ended at the conclusion of the second cycle at 0.71% roof drift. A few other observations are worth noting. The south column reached Y2 yielding at its base during the final two cycles, but this was not severe damage and it was not expected to impact the performance of future tests. In addition, the south first story corner gusset plate yielded significantly in an elliptical pattern due to self-impact of the fractured brace. No interface weld or base metal damage was discovered at this location, but drawing conclusions from this response is not appropriate since the brace delivered essentially no force through the connection; the observed gusset plate deformation occurred due to brace end rotation alone as the fractured brace ends contacted in negative drift excursions.



(a) Top view



(b) Bottom view

Figure 4.20: TNCBF1-N-HSS first story north brace beam mid-span connection fracture, BFs (-1.24% story drift)



(a) South column at base (1.15% first story drift)



(b) 1F south corner gusset plate (post-test)

Figure 4.21: TNCBF1-N-HSS miscellaneous observations

4.4 TNCBF1-R-HSS Observations

4.4.1 Overview of Cyclic Response

TNCBF1-R-HSS, shown in Fig. 4.22, was tested on August 10, 2013 and was intended to evaluate the performance of an in-plane buckling HSS brace repair designed with the BDP. The beams,

columns, and second story braces and connections from TNCBF1-N-HSS were reused in this test but the first story was rehabilitated with in-plane buckling braces. Previous weld damage was also repaired. The load and roof drift histories can be found in Figs. 4.24 and 4.23. Roof and story drift hystereses are presented in Figs. 4.25 and 4.26. Key events are annotated on the hystereses and described in Table 4.6.



Figure 4.22: TNCBF1-R-HSS overview

Like in the test of TNCBF1-N-HSS, inelastic deformation was concentrated in the first story and the second story remained essentially elastic. Both first story braces buckled and fractured, but they buckled out-of-plane and not in-plane, contrary to the design intent. Despite the unanticipated buckling mode and weak beam, a first story drift range of 4.70% was achieved prior to partial brace fracture, which is comparable to SCBFs (Roeder et al. 2011a; Lumpkin et al. 2012). Both first story braces partially fractured in tension due to strain accumulation at the locations of local buckling. The test was ended after two cycles at the 1.43% roof drift level.

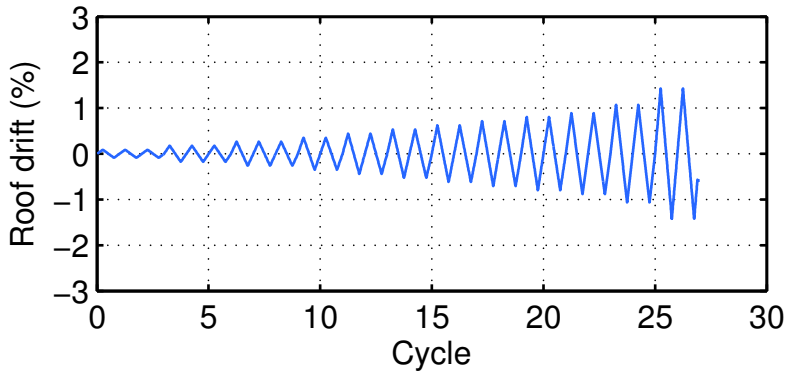

Figure 4.23: TNCBF1-R-HSS roof drift history

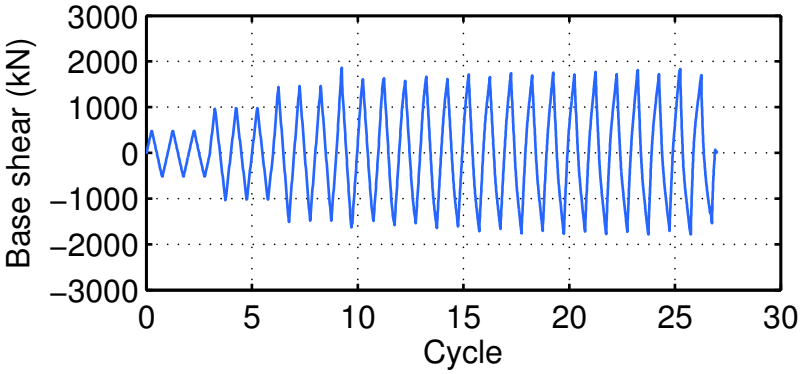

Figure 4.24: TNCBF1-R-HSS load history

Peak resistances and drifts within each cycle are shown in Table 4.7. The lateral resistance of the frame was stable through the loading protocol. The performance states reached in each cycle are tabulated in detail in Table 4.8. Pre-existing damage incurred in TNCBF1-N-HSS is noted in the tables since all components except for the first story braces and gusset plates were reused, though this damage did not have a noticeable impact on performance.

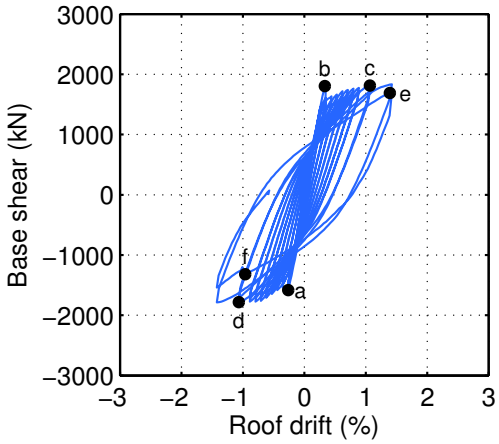

Figure 4.25: TNCBF1-R-HSS base shear-roof drift hysteresis

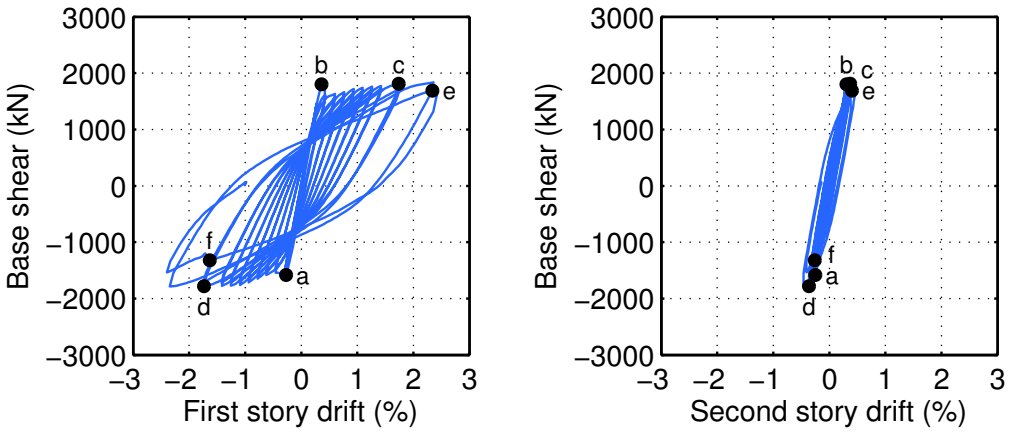

(a) First story

(b) Second story

Figure 4.26: TNCBF1-R-HSS base shear-story drift hystereses

Table 4.6: Description of labels in Figs. 4.25 and 4.26

Label	Location	Event	Roof drift (%)	Story drift (%)
a	1F south brace	Buckling	−0.26	−0.25
b	1F north brace	Buckling	+0.33	+0.31
c	1F north brace	Local buckling	+1.07	+1.74
d	1F south brace	Local buckling	−1.06	−1.73
e	1F south brace	Partial fracture	+1.39	+2.34
f	1F north brace	Partial fracture	−0.96	−1.63

Table 4.7: TNCBF1-R-HSS peak lateral resistances and drifts

	Resistance (kN)		Roof drift (%)		1F drift (%)		2F drift (%)	
Cycle	Max.	Min.	Max.	Min.	Max.	Min.	Max.	Min.
1	477	−512	0.08	−0.08	0.09	−0.09	0.08	−0.07
2	478	−513	0.08	−0.08	0.09	−0.09	0.08	−0.08
3	478	−510	0.08	−0.08	0.09	−0.09	0.08	−0.08
4	964	−1036	0.17	−0.17	0.19	−0.19	0.16	−0.16
5	977	−1019	0.17	−0.17	0.18	−0.19	0.16	−0.16
6	977	−1021	0.17	−0.17	0.18	−0.19	0.16	−0.16
7	1444	−1515	0.26	−0.26	0.29	−0.28	0.24	−0.24
8	1465	−1483	0.26	−0.26	0.28	−0.29	0.25	−0.23
9	1462	−1484	0.26	−0.26	0.28	−0.28	0.25	−0.24
10	1859	−1631	0.35	−0.35	0.43	−0.45	0.31	−0.25
11	1609	−1490	0.35	−0.35	0.43	−0.46	0.27	−0.23
12	1633	−1582	0.44	−0.44	0.60	−0.62	0.28	−0.25
13	1575	−1544	0.44	−0.44	0.61	−0.62	0.26	−0.25
14	1663	−1646	0.53	−0.53	0.77	−0.78	0.29	−0.27
15	1618	−1608	0.53	−0.53	0.78	−0.78	0.28	−0.26
16	1718	−1712	0.62	−0.62	0.94	−0.94	0.30	−0.28
17	1661	−1667	0.62	−0.62	0.94	−0.94	0.29	−0.27
18	1742	−1761	0.71	−0.71	1.10	−1.09	0.31	−0.30
19	1694	−1708	0.71	−0.71	1.11	−1.10	0.30	−0.29
20	1760	−1772	0.80	−0.80	1.26	−1.26	0.32	−0.31
21	1715	−1724	0.80	−0.80	1.27	−1.26	0.31	−0.31
22	1772	−1775	0.89	−0.88	1.42	−1.42	0.33	−0.33
23	1721	−1726	0.89	−0.88	1.43	−1.42	0.32	−0.32
24	1811	−1784	1.07	−1.06	1.74	−1.73	0.37	−0.36
25	1721	−1708	1.07	−1.06	1.76	−1.75	0.35	−0.35
26	1835	−1786	1.43	−1.42	2.36	−2.34	0.46	−0.46
27	1701	−1538	1.43	−1.42	2.44	−2.40	0.41	−0.41

Table 4.8: TNCBF1-R-HSS performance state progression

Drift (%)	Braces				Corner gusset plates				Mid-span gusset plates				Beams				Columns								Drift range (%)
Roof 1F / 2F	1S	1N	2S	2N	1S	1N	2S	2N	1S	1N	2S	2N	1S-E	1S-M	1N-M	1N-E	1S-L	1S-U	2S-L	2S-U	1N-L	1N-U	2N-L	2N-U	Roof 1F / 2F
Pre-existing damage			Bs1	Bs1							Y1	Y1	Y2	Y1	Y1		Y2	Y1		Y1	Y1		Y1		N/A
0.08 0.09 / 0.08																									0.17 0.18 / 0.15
−0.08 −0.09 / −0.07																									
0.08 0.09 / 0.08																									0.17 0.18 / 0.15
−0.08 −0.09 / −0.08																									
0.08 0.09 / 0.08																									0.17 0.18 / 0.15
−0.08 −0.09 / −0.08																									
0.17 0.19 / 0.16																									0.35 0.37 / 0.31
−0.17 −0.19 / −0.16						Y1											Y1				Y1	Y1			
0.17 0.18 / 0.16																									0.35 0.37 / 0.32
−0.17 −0.19 / −0.16																									
0.17 0.18 / 0.16																									0.35 0.37 / 0.32
−0.17 −0.19 / −0.16																									
0.26 0.29 / 0.24					Y1				Y1	Y1				Y1	Y1										0.52 0.57 / 0.48
−0.26 −0.28 / −0.24																									
0.26 0.28 / 0.25																									0.52 0.56 / 0.48
−0.26 −0.29 / −0.23																									
0.26 0.28 / 0.25																									0.52 0.56 / 0.48
−0.26 −0.28 / −0.24																									
0.35 0.43 / 0.31		B1				Y2																			0.70 0.88 / 0.56
−0.35 −0.45 / −0.25	B1								Y2	Y2															
0.35 0.43 / 0.27																									0.70 0.89 / 0.50
−0.35 −0.46 / −0.23																									
0.44 0.60 / 0.28		B2											Y1					Y1							0.88 1.23 / 0.52
−0.44 −0.62 / −0.25	B2				Y2																				

Continued on next page

Table 4.8 – continued from previous page

Drift (%)		Braces				Corner gusset plates				Mid-span gusset plates				Beams				Columns								Drift range (%)	
Roof	1F 2F	1S	1N	2S	2N	1S	1N	2S	2N	1S	1N	2S	2N	1S-E	1S-M	1N-M	1N-E	1S-L	1S-U	2S-L	2S-U	1N-L	1N-U	2N-L	2N-U	Roof	1F 2F
0.44 −0.44	0.61 0.26 −0.62 −0.25																									0.88	1.24 0.51
0.53 −0.53	0.77 0.29 −0.78 −0.27																									1.06	1.55 0.55
0.53 −0.53	0.78 0.28 −0.78 −0.26																									1.06	1.56 0.54
0.62 −0.62	0.94 0.30 −0.94 −0.28					Wb-1cm									Y2				Y2				Y2			1.24	1.88 0.58
0.62 −0.62	0.94 0.29 −0.94 −0.27					Wb-5cm																				1.24	1.89 0.56
0.71 −0.71	1.10 0.31 −1.09 −0.30					Wb-6cm					Y3							Y2		Y1		Y2				1.42	2.19 0.61
0.71 −0.71	1.11 0.30 −1.10 −0.29																									1.42	2.21 0.59
0.80 −0.80	1.26 0.32 −1.26 −0.31	B3	B3			Wb-8.5cm	Y3															Y3				1.60	2.52 0.63
0.80 −0.80	1.27 0.31 −1.26 −0.31																									1.60	2.53 0.62
0.89 −0.88	1.42 0.33 −1.42 −0.33					Wb-9.5cm																				1.77	2.84 0.66
0.89 −0.88	1.43 0.32 −1.42 −0.32					Wb-10cm																				1.78	2.86 0.65
1.07 −1.06	1.74 0.37 −1.73 −0.36	BC	BC			Y3 Wb-12cm										Y2		Y3								2.13	3.47 0.74

Continued on next page

Table 4.8 – continued from previous page

Drift (%)		Braces				Corner gusset plates				Mid-span gusset plates				Beams				Columns								Drift range (%)	
Roof	1F 2F	1S	1N	2S	2N	1S	1N	2S	2N	1S	1N	2S	2N	1S-E	1S-M	1N-M	1N-E	1S-L	1S-U	2S-L	2S-U	1N-L	1N-U	2N-L	2N-U	Roof	1F 2F
1.07	1.76 0.35						WBc- 3cm																			2.13	3.50 0.70
−1.06	−1.75 −0.35																										
1.43	2.36 0.46						PC									Y3	Y2									2.85	4.70 0.91
−1.42	−2.34 −0.46				Bs2		PC, Wb- 15cm																				
1.43	2.44 0.41	BF					WBc- 3.5cm												Y3				Y3			2.85	4.83 0.82
−1.42	−2.40 −0.41		BF			Wc- 4cm								Wb- 7cm			Wb- 11cm						Ws- 9cm				

4.4.2 Detailed Cyclic Response

Initial State (Roof Drift $\leq 0.26\%$*)*

Up to the 0.35% roof drift level, the frame remained primarily elastic. Very minor yielding was observed at the first story gusset and knife plates (Fig. 4.27a). The column flanges and webs yielded at their bases, as expected due to the pre-existing damage. Yielding also initiated in the beam's web near its mid-span, as in Fig. 4.27b, likely influenced by heat effects from torch cutting the previous gusset plates and welding new gusset plates and stiffeners at the same location. Small brace deformations were recorded in compression, but these were elastic and not associated with strength loss due to buckling. Such deformation may be attributed to initial out-of-straightness of the members.



(a) South first story corner knife plate (b) Beam web

Figure 4.27: TNCBF1-R-HSS first story yielding, Y1 (0.29% first story drift)

Moderate Damage State ($0.26\% <$ *Roof Drift* $\leq 0.89\%$*)*

The moderate damage state spans from initial brace buckling to the precipice of brace local buckling on the first story. The first story's north brace buckled out-of-plane at 0.43% story drift and its south brace, shown in Fig. 4.28a, buckled out-of-plane at -0.45% first story drift. These events coincided with increased yielding of the gusset plates largely due to brace end rotation. Gusset plate yielding was most extensive in elliptically-shaped regions between the braces and gusset plate edges as seen in Fig. 4.29. At the corner gusset plates of the first story, this elliptical clearance

was $0.55t_p$ in width, much less than the recommended $8t_p$ width recommended by Lehman et al. (2008). The mid-span gusset plates had no measurable elliptical clearance, though yielding still took an elliptical form. In the photos, yield lines outside the elliptical region indicate yielding due to the brace tensile force.

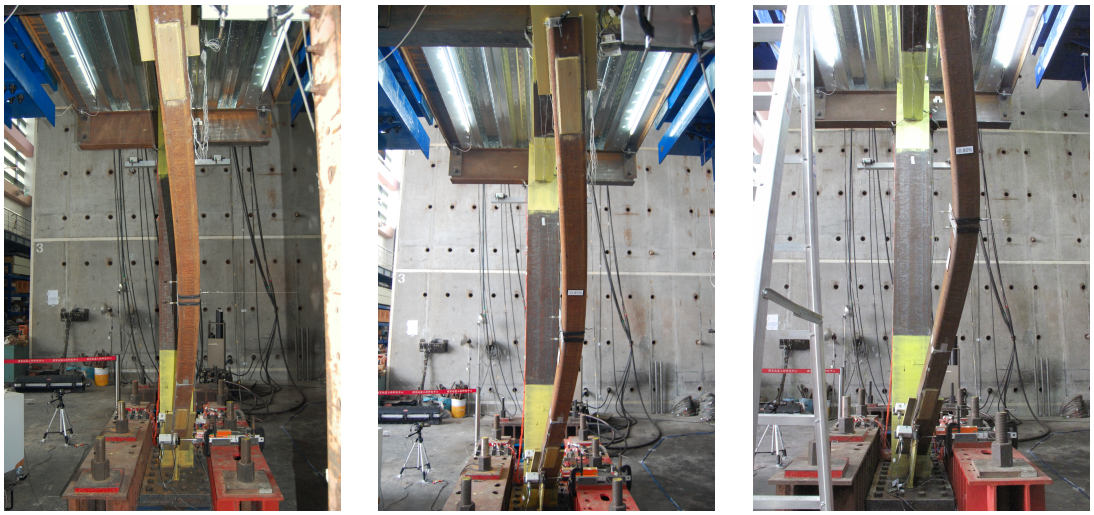

(a) B1 (−0.45% first story drift) (b) B2 (−0.62% first story drift) (c) B3 (−1.26% first story drift)

Figure 4.28: TNCBF1-R-HSS south first story out-of-plane brace buckling

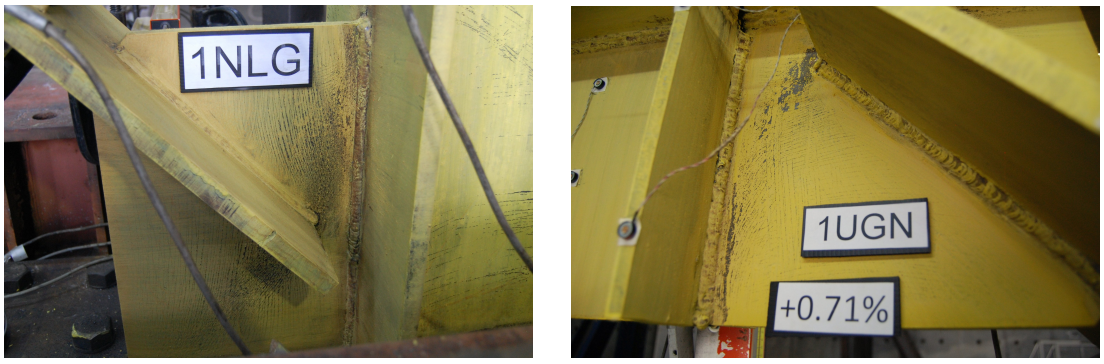

(a) Mid-span (b) Corner

Figure 4.29: TNCBF1-R-HSS north first story gusset plate elliptical yielding (1.10% first story drift)

With the exception of the light initial yielding previously mentioned, the knife plates remained

elastic and acted like rigid brace ends. Thus, brace end rotation on the first story was actually knife plate end rotation. The buckling regime of the south first story brace prior to local buckling is depicted in Fig. 4.28.

At −0.94% first story drift, a weld crack in the south corner gusset plate formed due to gusset plate rotation. The initial crack length was 1 cm, which grew to 5 cm in the second cycle at the same drift level. In subsequent cycles, crack growth was relatively stable, as shown in Fig. 4.30, extending only in compression half-cycles. Weld cracks in other components did not form until the severe damage state described below.

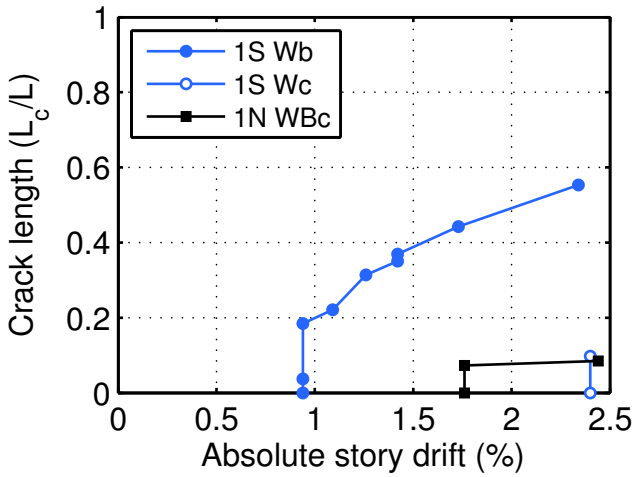

Figure 4.30: TNCBF1-R-HSS first story corner gusset plate weld (W) and base metal (WB) damage

A moderate amount of beam yielding was observed at the first story due to downward vertical deflection induced by the brace unbalanced load. New beam yielding locations in this damage state were limited to the flanges of the first story beam, as can be seen in Fig. 4.31. Column yielding at the bases and first story beam-to-column connections, shown in Fig. 4.32, was significantly greater than beam yielding. The columns were stronger than the first story beam, but the slab and gusset plates adjacent to the connection may have helped limit damage to the beam.

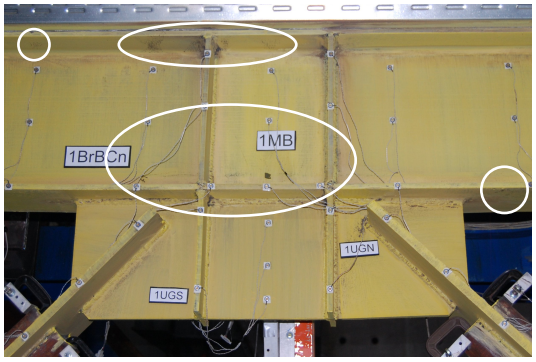

Figure 4.31: TNCBF1-R-HSS first story beam yielding, Y2 (-0.94% story drift)

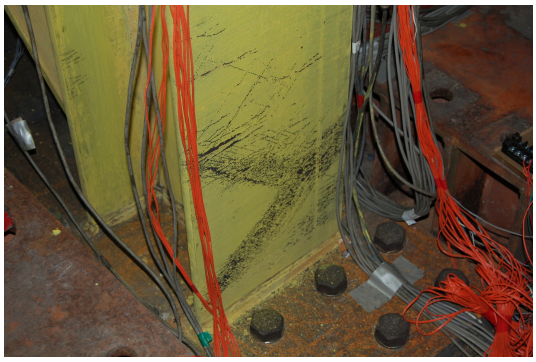

(a) North base, Y3 (1.27% story drift)



(b) South beam-to-column connection, Y2 (1.10% story drift)

Figure 4.32: TNCBF1-R-HSS first story column yielding

Severe Damage State (Roof Drift $> 0.89\%$*)*

The severe damage state began with local buckling of the first story braces at approximately $\pm 1.75\%$ first story drift. This is considered severe because local buckling accumulates high strains in the affected regions, leading to fracture in tension. Even after the first story braces developed local buckling, the lateral resistance of the frame remained stable. The typical damage progression of these braces is shown in Fig. 4.33. Unlike the braces of TNCBF1-N-HSS, however, the braces in TNCBF1-R-HSS met the highly ductile compactness limit for HSS braces (AISC 2010a). With greater compactness, strain accumulation is less severe and fracture life is significantly improved. Comparing the event tables for the two tests, Tables 4.3 and 4.6, it can be seen that the braces in

this test sustained much greater lateral drifts prior to fracture. It should be noted that the braces in TNCBF1-R-HSS did not fracture completely; only the cupped region of each brace fractured as in Fig. 4.33c. After both first story braces partially fractured, resistance dropped by about 250 kN at the peak displacement and the brace in tension clearly developed substantial load through the reduced cross section.

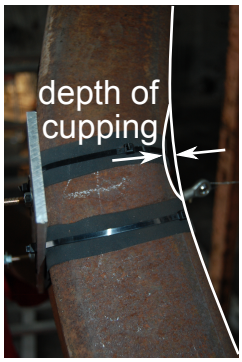

(a) North brace cupping, BC (1.76% first story drift)



(b) North brace tearing (−2.34% first story drift)



(c) South brace partial fracture, BF (2.44% first story drift)

Figure 4.33: TNCBF1-R-HSS first story brace damage progression

As shown previously in Fig. 4.30, damage to the south first story corner gusset plate welds increased substantially but in a stable manner in the severe damage state. Over half the gusset plate-to-base plate weld tore due to large rotational demands (Fig. 4.34), yet the weld never ruptured, showing the effectiveness of tough welds sized for the capacity of the gusset plate even when gusset plate clearance is marginal. Minor weld and base metal cracks developed at the corner gusset

plate-to-column interfaces near the end of the test, but these did not grow to more than 4 cm in length.

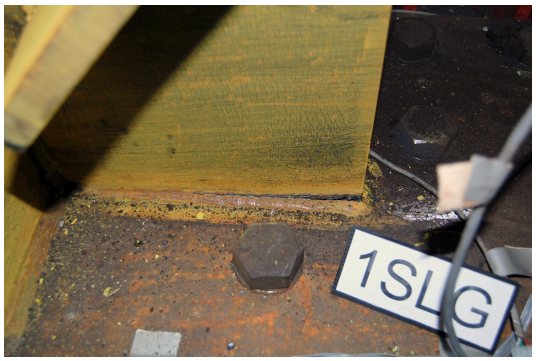

Figure 4.34: TNCBF1-R-HSS south first story corner gusset plate weld crack (post-test)

Further beam yielding occurred at the first story due to pull-down as well as torsional rotation of the beam brought about by brace end rotation. A post-test photograph of the beam mid-span is shown in Fig. 4.35. Torsional beam deformation was not anticipated since the braces were intended to buckle in the plane of the frame. The deformation, however, helps identify the cause of out-of-plane brace buckling. In-plane buckling with square HSS braces is dependent upon the relative flexibility of the gusset and knife plate connections (i.e., the knife plate connection should be less stiff than the gusset plate connection). This was intended to be ensured geometrically by limiting gusset plate clearance and requiring adequate ($3t_{\mathrm{kp}}$) knife plate clearance. For this specimen, the mid-span gusset plate connection flexibility was underestimated, largely due to the low torsional stiffness of the beam, a function of the cross section geometry and limited lateral bracing. The torsional deformation of the beam likely protected the gusset plate-to-beam welds of the mid-span connections, where no weld or base metal damage was observed.

First story beam deflection imposed in-plane rotational demands on the beam-to-column connections, causing significant weld damage, shown in Fig. 4.36. In the final cycle a maximum of 2.44% first story drift was reached and cracks developed in the beam-to-shear tab welds that were 7 cm and 11 cm in length on the south and north ends of the beam, respectively. In addition, the first story column-to-shear tab weld at the north end of frame developed a 9 cm-long weld crack.

Fig. 4.36 also shows significant beam and column yielding at the first story beam-to-column

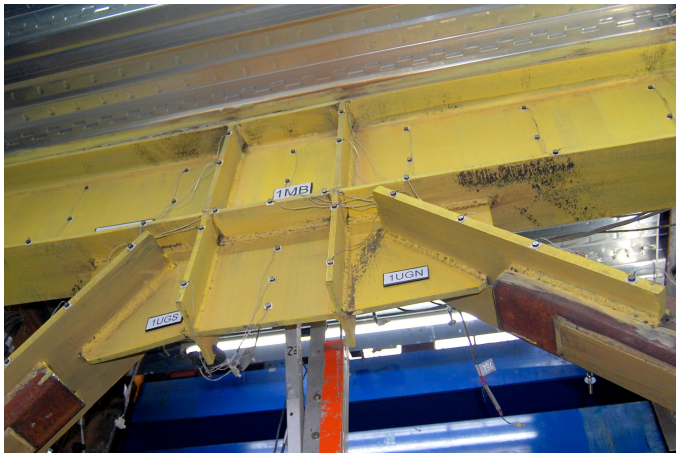

Figure 4.35: TNCBF1-R-HSS first story beam yielding, Y3 (post-test)

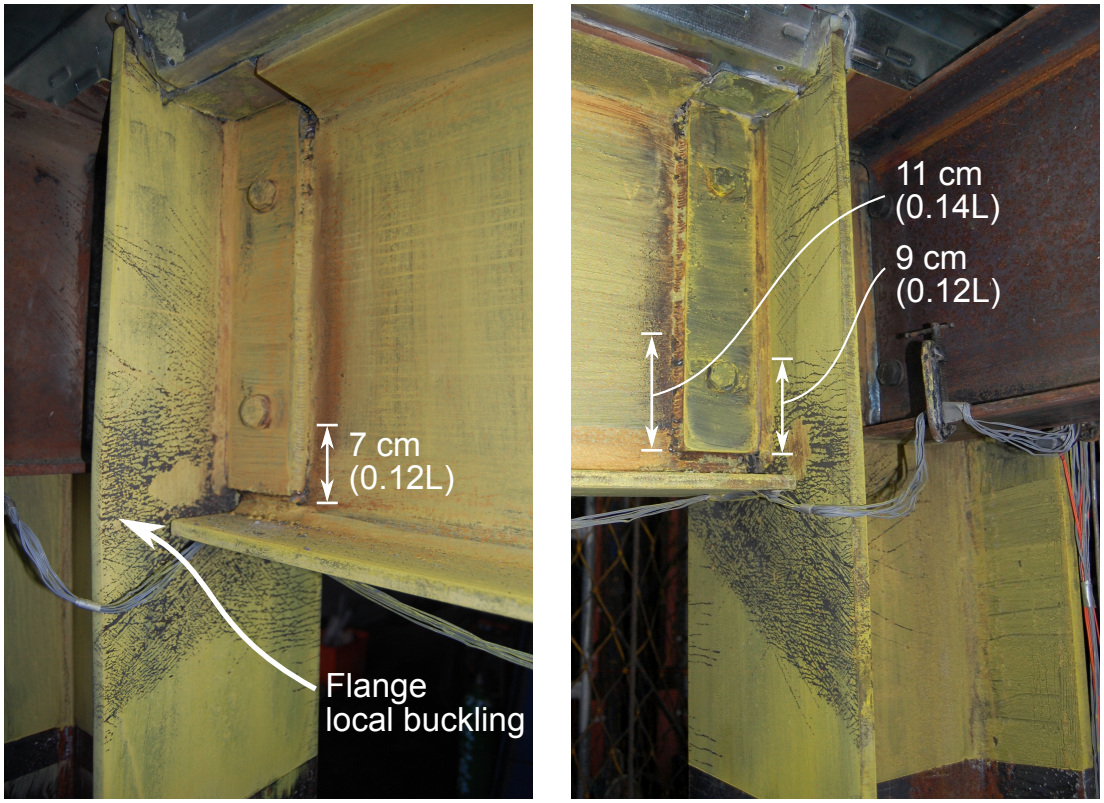

(a) South end (post-test)

(b) North end (post-test)

Figure 4.36: TNCBF1-R-HSS first story beam-to-column connection damage

connection. Yielding was most severe in the columns within the first story and local buckling occurred in the south column's inner flange at its base and near the beam-to-column connection. Beam web yielding also occurred in the regions adjacent to the shear tabs. This damage was expected, as the beam flange was coped on one side to accommodate the shear tab, lowering its flexural capacity.

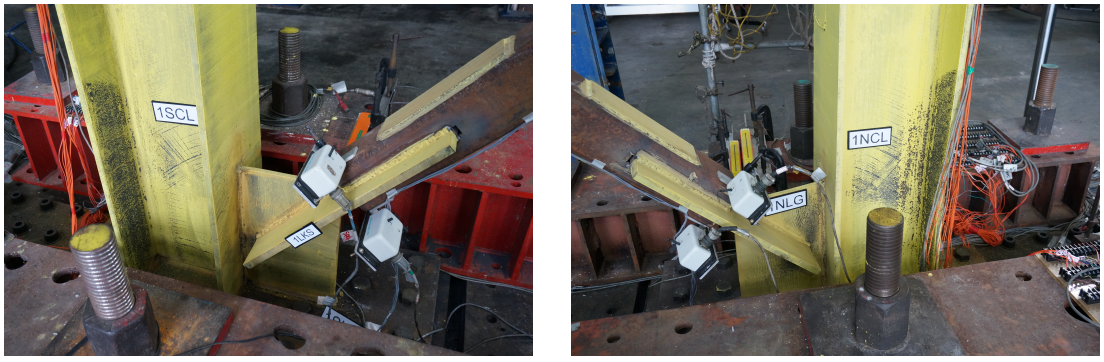

(a) South base (b) North base

Figure 4.37: TNCBF1-R-HSS column and gusset plate yielding at bases, Y3 (post-test)

Inelastic behavior on the second story was marginal, but non-negligible. The most significant event occurred at −1.42% roof drift (−0.46% second story drift), when a portion of the slab around the north second story brace spalled (Fig. 4.38) and a net section crack initiated in TNCBF1-N-HSS at that location propagated slightly down the length of the brace as shown in Fig. 4.39.

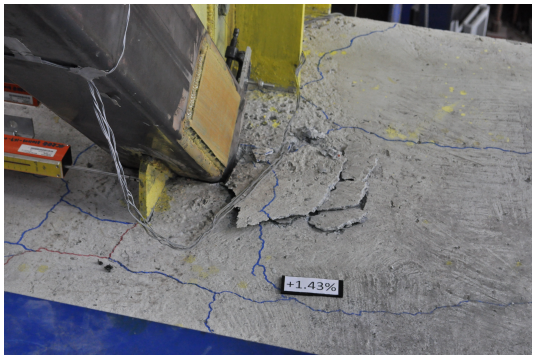

Figure 4.38: TNCBF1-R-HSS concrete spalling around north second story brace corner connection (−0.46% second story drift)

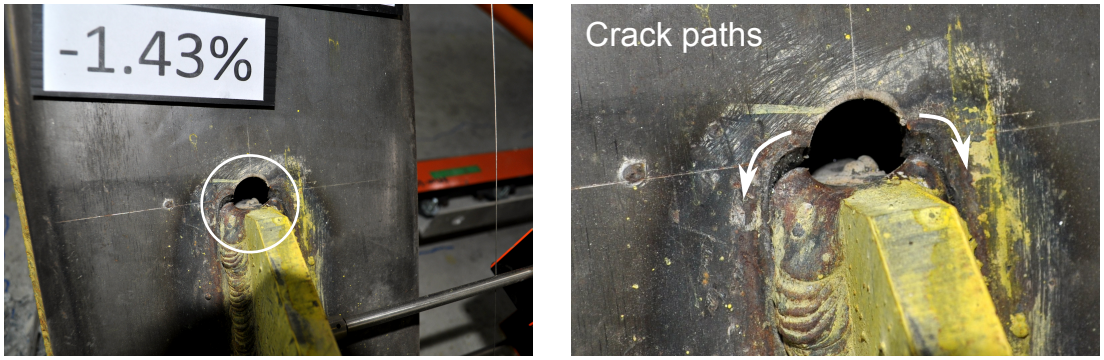

(a) Net section crack propagation (b) Magnified view

Figure 4.39: TNCBF1-R-HSS north second story brace splice connection damage, Bs2 (−0.46% second story drift)

4.5 TNCBF1-R-WF Observations

4.5.1 Overview of Cyclic Response

TNCBF1-R-WF, depicted in Fig. 4.40, was tested at NCREE on August 31, 2013. The experiment was conducted to evaluate the performance of a wide flange brace repair on the first story with conventional out-of-plane buckling connections designed using the BDP. The beams, columns, and second story braces and connections from TNCBF1-N-HSS and TNCBF1-R-HSS were reused in this test and repairs were only made to the first story. The load and roof drift histories can be found in Figs. 4.42 and 4.41, while the roof and story drift hystereses are presented in Figs. 4.43 and 4.44. Key events are annotated on the hystereses and described in Table 4.9.

In contrast to previous tests, lateral drift was not concentrated in the first story, yet the overall response was poor. The first story wide flange braces buckled as desired; the second story braces did not buckle, but their corner brace splice connections failed in tension. Following this fracture, the second story behaved as a weak column-strong beam moment frame. The second story maintained enough strength and stiffness to permit further inelastic deformation of the first story braces. However, substantial weld cracking at the first story beam-to-column connections precluded brace fracture and the test was ended prior to the inevitable complete fracture of the connections.

Peak lateral resistances and drifts are documented in Table 4.10 and detailed accounts of performance state progressions are given in Table 4.11. Pre-existing damage incurred in TNCBF1-N-HSS



Figure 4.40: TNCBF1-R-WF overview

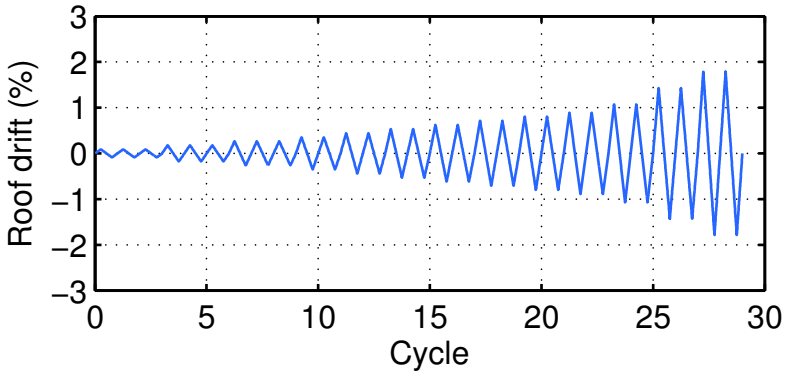

Figure 4.41: TNCBF1-R-WF roof drift history

and TNCBF1-R-HSS is noted in the tables since all components except the first story braces and gusset plates were reused. In general, frame member yielding in previous tests did not have a noticeable impact on performance, but second story brace splice connection damage and beam-to-column

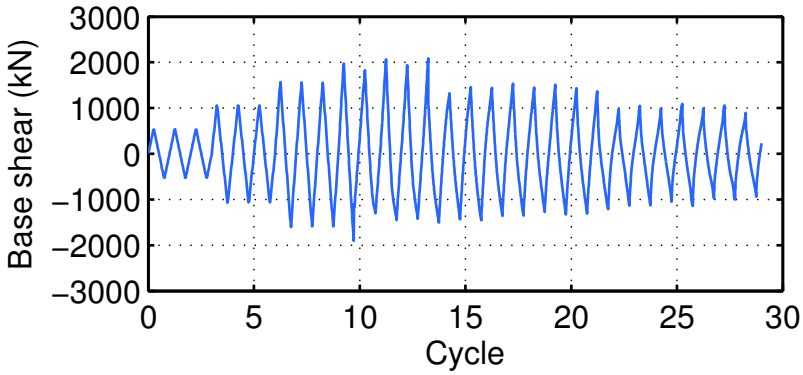

Figure 4.42: TNCBF1-R-WF load history

connection damage (yielding in previous tests and heat effects from welding and backgouging) clearly limited strength and ductility of the frame.

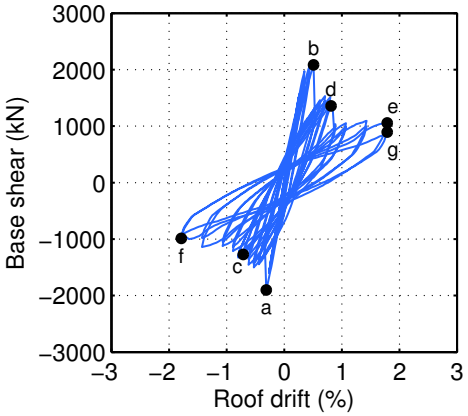

Figure 4.43: TNCBF1-R-WF base shear-roof drift hysteresis

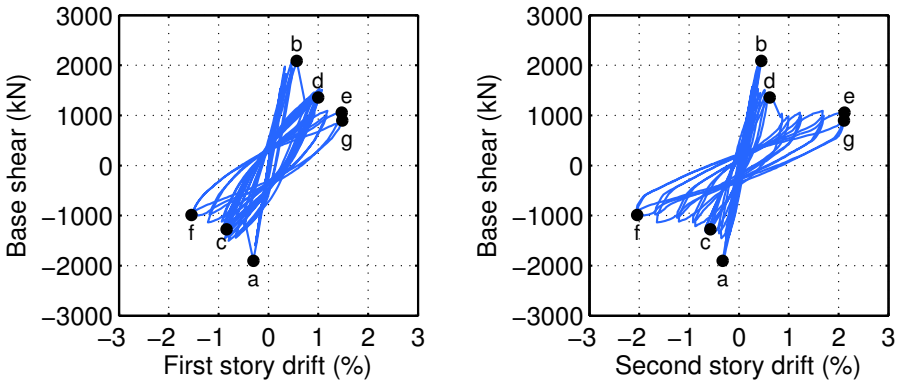

(a) First story

(b) Second story

Figure 4.44: TNCBF1-R-WF base shear-story drift hystereses

Table 4.9: Description of labels in Figs. 4.43 and 4.44

Label	Location	Event	Roof drift (%)	Story drift (%)
a	1F south brace	Buckling	−0.31	−0.30
b	1F north brace	Buckling	+0.51	+0.57
c	2F north brace	Connection fracture	−0.71	−0.57
d	2F south brace	Connection fracture	+0.81	+0.62
e	1F north brace	Local buckling	+1.79	+1.47
f	1F south brace 1F beam south	Local buckling Connection partial fracture	−1.79	−1.54
g	1F beam north	Connection partial fracture	+1.79	+1.48

Table 4.10: TNCBF1-R-WF peak lateral resistances and drifts

	Resistance (kN)		Roof drift (%)		1F drift (%)		2F drift (%)	
Cycle	Max.	Min.	Max.	Min.	Max.	Min.	Max.	Min.
1	528	−520	0.08	−0.08	0.08	−0.09	0.09	−0.08
2	527	−523	0.08	−0.08	0.08	−0.09	0.09	−0.08
3	526	−520	0.08	−0.08	0.08	−0.09	0.09	−0.08
4	1055	−1074	0.17	−0.17	0.17	−0.17	0.18	−0.17
5	1058	−1067	0.17	−0.17	0.17	−0.17	0.18	−0.17
6	1057	−1063	0.17	−0.17	0.17	−0.18	0.18	−0.17
7	1570	−1603	0.26	−0.26	0.26	−0.26	0.27	−0.26
8	1564	−1588	0.26	−0.26	0.26	−0.26	0.27	−0.26
9	1555	−1590	0.26	−0.26	0.25	−0.26	0.27	−0.26
10	1974	−1903	0.35	−0.35	0.33	−0.49	0.38	−0.33
11	1829	−1305	0.35	−0.35	0.35	−0.51	0.35	−0.19
12	2068	−1446	0.44	−0.44	0.47	−0.66	0.42	−0.22
13	1937	−1420	0.44	−0.44	0.48	−0.66	0.40	−0.21
14	2086	−1503	0.53	−0.53	0.77	−0.80	0.45	−0.25
15	1323	−1437	0.53	−0.53	0.77	−0.79	0.28	−0.25
16	1458	−1454	0.62	−0.62	0.92	−0.87	0.32	−0.35
17	1441	−1357	0.62	−0.62	0.92	−0.83	0.31	−0.40
18	1530	−1353	0.71	−0.71	1.03	−0.88	0.38	−0.53
19	1447	−1273	0.71	−0.71	0.99	−0.84	0.43	−0.57
20	1509	−1330	0.80	−0.80	1.07	−0.93	0.52	−0.67
21	1435	−1308	0.80	−0.80	1.03	−0.92	0.56	−0.67
22	1366	−1212	0.89	−0.89	1.01	−0.90	0.86	−0.88
23	983	−1135	0.89	−0.89	0.79	−0.86	0.99	−0.92
24	1053	−1124	1.07	−1.07	0.92	−0.94	1.22	−1.20
25	993	−1047	1.07	−1.07	0.90	−0.90	1.25	−1.24
26	1093	−1139	1.43	−1.43	1.18	−1.22	1.68	−1.65
27	996	−981	1.43	−1.43	1.17	−1.18	1.70	−1.68
28	1056	−1001	1.79	−1.79	1.47	−1.54	2.12	−2.04
29	895	−936	1.79	−1.79	1.48	−1.52	2.11	−2.06

Table 4.11: TNCBF1-R-WF performance state progression

Drift (%)	Braces				Corner gusset plates				Mid-span gusset plates				Beams				Columns								Drift range (%)
Roof 1F / 2F	1S	1N	2S	2N	1S	1N	2S	2N	1S	1N	2S	2N	1S-E	1S-M	1N-M	1N-E	1S-L	1S-U	2S-L	2S-U	1N-L	1N-U	2N-L	2N-U	Roof 1F / 2F
Pre-existing damage			Bs1	Bs2							Y1	Y1	Y2	Y2	Y3	Y2	Y3	Y3	Y1	Y1	Y3	Y3			N/A
0.08 0.08 / 0.09 −0.08 −0.09 / −0.08					Y1				Y1																0.17 0.17 / 0.17
0.08 0.08 / 0.09 −0.08 −0.09 / −0.08						Y1				Y1															0.17 0.17 / 0.17
0.08 0.08 / 0.09 −0.08 −0.09 / −0.08																									0.17 0.17 / 0.17
0.17 0.17 / 0.18 −0.17 −0.17 / −0.17															Y1		Y1				Y1				0.34 0.34 / 0.35
0.17 0.17 / 0.18 −0.17 −0.17 / −0.17																									0.35 0.34 / 0.35
0.17 0.17 / 0.18 −0.17 −0.18 / −0.17																									0.34 0.34 / 0.35
0.26 0.26 / 0.27 −0.26 −0.26 / −0.26																			Y1				Y1		0.52 0.52 / 0.53
0.26 0.26 / 0.27 −0.26 −0.26 / −0.26																									0.52 0.52 / 0.53
0.26 0.25 / 0.27 −0.26 −0.26 / −0.26																									0.52 0.52 / 0.53
0.35 0.33 / 0.38 −0.35 −0.49 / −0.33	B1			Bs2	Y3				Y3																0.70 0.82 / 0.70
0.35 0.35 / 0.35 −0.35 −0.51 / −0.19																									0.70 0.86 / 0.54
0.44 0.47 / 0.42 −0.44 −0.66 / −0.22	B2					Y2				Y2				Y1											0.88 1.12 / 0.63

Continued on next page

Table 4.11 – continued from previous page

Drift (%)		Braces				Corner gusset plates				Mid-span gusset plates				Beams				Columns								Drift range (%)	
Roof	1F 2F	1S	1N	2S	2N	1S	1N	2S	2N	1S	1N	2S	2N	1S-E	1S-M	1N-M	1N-E	1S-L	1S-U	2S-L	2S-U	1N-L	1N-U	2N-L	2N-U	Roof	1F 2F
0.44	0.48 0.40																									0.88	1.14 0.61
−0.44	−0.66 −0.21																										
0.53	0.77 0.45		B1	Bs2			Y3				Y3															1.06	1.57 0.70
−0.53	−0.80 −0.25		B2																								
0.53	0.77 0.28																									1.06	1.57 0.54
−0.53	−0.79 −0.25																										
0.62	0.92 0.32																									1.24	1.79 0.67
−0.62	−0.87 −0.35																										
0.62	0.92 0.31																									1.24	1.75 0.71
−0.62	−0.83 −0.40																										
0.71	1.03 0.38																		Ws- 1cm							1.42	1.91 0.91
−0.71	−0.88 −0.53				BFs																						
0.71	0.99 0.43																									1.42	1.83 1.00
−0.71	−0.84 −0.57																										
0.80	1.07 0.52																									1.60	2.00 1.18
−0.80	−0.93 −0.67																										
0.80	1.03 0.56																									1.60	1.96 1.23
−0.80	−0.92 −0.67																										
0.89	1.01 0.86			BFs																						1.78	1.91 1.74
−0.89	−0.90 −0.88																				Y1				Y1		
0.89	0.79 0.99																									1.78	1.65 1.91
−0.89	−0.86 −0.92																										
1.07	0.92 1.22																									2.14	1.86 2.43
−1.07	−0.94 −1.20													Y1, Ws- 6cm													

Continued on next page

Table 4.11 – continued from previous page

Drift (%)		Braces				Corner gusset plates				Mid-span gusset plates				Beams				Columns								Drift range (%)	
Roof	1F 2F	1S	1N	2S	2N	1S	1N	2S	2N	1S	1N	2S	2N	1S-E	1S-M	1N-M	1N-E	1S-L	1S-U	2S-L	2S-U	1N-L	1N-U	2N-L	2N-U	Roof	1F 2F
1.07	0.90 1.25																									2.14	1.80 2.49
−1.07	−0.90 −1.24																										
1.43	1.18 1.68																				Y2				Y2	2.86	2.40
−1.43	−1.22 −1.65													Ws-7cm			Y1, Ws-2cm, WBs-15cm										3.33
1.43	1.17 1.70																									2.86	2.35
−1.43	−1.18 −1.68													Y2, Ws-8cm													3.38
1.79	1.47 2.12		BC											WBs-15cm			Ws-8cm									3.58	3.02
−1.79	−1.54 −2.04	BC												Y3, Ws-22cm				Y2			Y3				Y3		4.16
1.79	1.48 2.11																Y2, Ws-19cm									3.58	3.01
−1.79	−1.52 −2.06																										4.17

4.5.2 Detailed Cyclic Response

Initial State (Roof Drift $\leq 0.26\%$*)*

The global response of TNCBF1-R-WF remained primarily elastic up to the 0.26% roof drift level. In the elastic cycles conducted to test the instrumentation ($\pm 0.08\%$ roof drift), light yielding was observed in some heat affected zones of the first story gusset plates, braces, and beam, particularly those with geometric discontinuities. Typical examples are shown in Fig. 4.45. Yielding around the brace splice under such low loading is explained by the close spacing of the welds. This led to repeated thermal stresses on the adjacent components, which were relatively thin (10 mm gusset plates, 11 mm brace flanges, and 7.5 mm brace webs). Yielding was also observed in the 9 mm-thick first story beam web at its mid-span, another location of significant thermal stress due to fabrication, as was seen in TNCBF1-R-HSS.

Moderate Damage State ($0.26 <$ *Roof Drift* $\leq 0.62\%$*)*

The frame transitioned to the moderate damage when the south first story brace buckled suddenly at -0.30% first story drift. When this occurred, its gusset plates immediately developed heavy elliptical yielding (Y3). The north first story brace buckled later at 0.57% first story drift, and its gusset plates yielded similarly to those of the south brace. These buckling events, shown in Fig. 4.46, resulted in rapid decreases in the frame's lateral strength.

Brace splice damage on the second story increased at both the north and south corner connections. The damage progression in the north connection is shown in Fig. 4.47. In the north brace, cracks emanating from the net section propagated on both the top and bottom faces of the brace at -0.33% second story drift. After this event, the frame resistance at positive peaks (i.e., north displacement) exceeded that of negative peaks. Crack propagation in the south brace began at 0.42% second story drift on its top face only. Then, at 0.45% second story drift, cracks were discovered in the brace base metal originating from the brace end embedded in the slab. During this cycle, the difference in resistance between positive and negative excursions reached a maximum at 622 kN. At -0.25% second story drift (second story drift decreased when the first story braces buckled), another crack originating from the brace end formed in one of the top splice welds. With numerous cracks in the connection weld and base metal, some crack growth occurred when the brace was

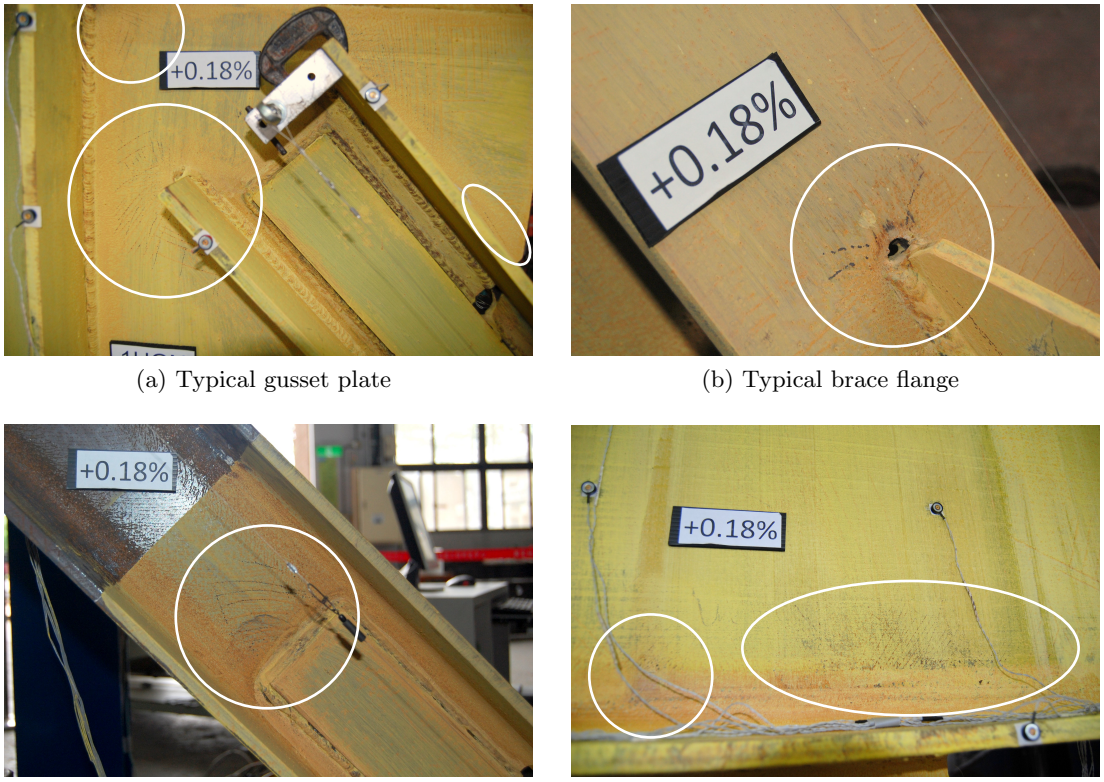

(a) Typical gusset plate

(b) Typical brace flange

(c) Typical brace web

(d) Typical beam web

Figure 4.45: TNCBF1-R-WF first story yielding accelerated by thermal stresses, Y1 (0.17 story drift level)

in compression as a result of the eccentricity of the damaged connection. These aforementioned cracks extended significantly at −0.40% second story drift when displacement in the north brace also caused slab spalling in the surrounding area.

Severe Damage State (Roof Drift $> 0.62\%$*)*

Essentially all tensile capacity of the north second story corner brace splice connection was lost at −0.57% second story drift in the second cycle at the 0.71% roof drift level. The connection fracture, shown in Fig. 4.48a, was very similar to that of the north first story mid-span brace splice connection in TNCBF1-N-HSS with cracks propagating through both weld and base metal. The south second story corner brace splice connection cracks propagated minimally until the frame was displaced to 0.89% roof drift. During this loading, the connection ruptured at 0.62% second story

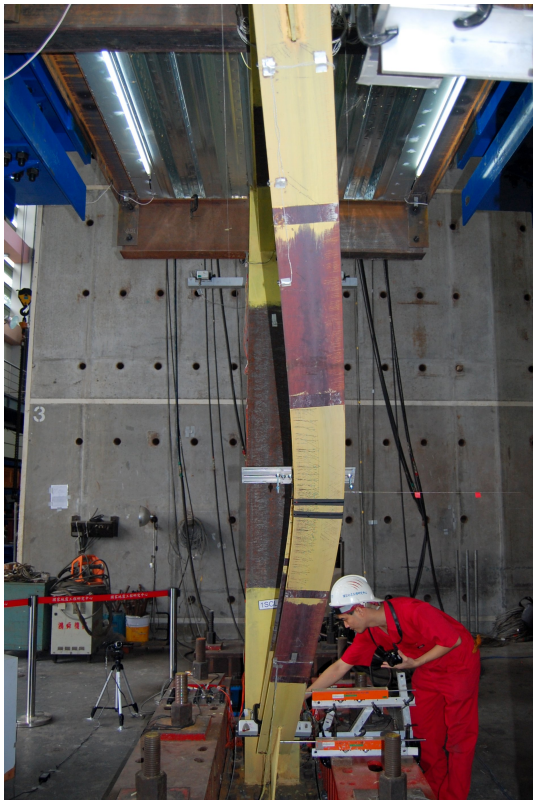

(a) South brace (-0.49% story drift)



(b) North brace (0.77% story drift)

Figure 4.46: TNCBF1-R-WF first story brace buckling, B1

drift, losing all tensile capacity. The failed south connection is shown in Fig. 4.48b. This rapid fracture was in contrast with that of the south connection, which failed in a much more progressive manner as story drift increased. These differences illustrate the inherent unpredictability of crack propagation through the brace and especially the weld metal lacking minimum Charpy V-notch toughness for demand critical welds. Following connection fracture, the frame was able to resist about 1000 kN of force.

With the second story corner splice connections failed, the braces could not develop tensile force. A small amount of compressive force was delivered through the braces as they impacted the first story slab. However, the second story behavior in the severe damage state was generally that of a moment frame with plastic hinges beginning to develop in the columns just below the second story beam.

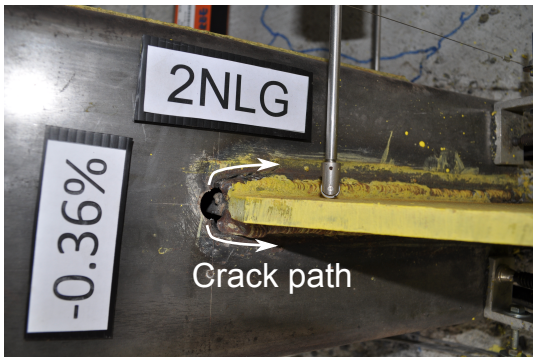

(a) Top of brace (−0.33% second story drift)

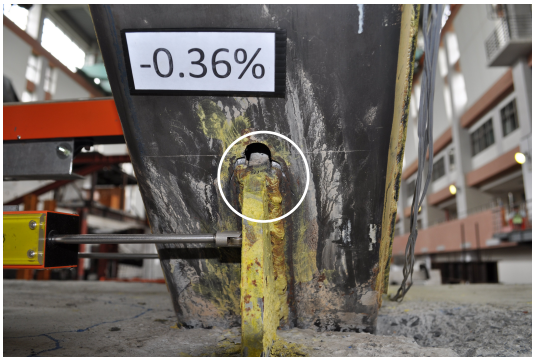

(b) Bottom of brace (−0.33% second story drift)



(c) Bottom of brace (−0.49% second story drift)



(d) Bottom of brace magnified (−0.49% second story drift)



(e) Top of brace (−0.40% second story drift)



(f) Bottom of brace (−0.40% second story drift)

Figure 4.47: TNCBF1-R-WF north second story brace splice connection damage

Although the first story was clearly stiffer than the second, first story drift continued to increase, along with brace and beam deflection. Rotational demands at the ends of the first story beam also increased, resulting in crack initiation in the south beam-to-shear tab weld at −0.94% first story

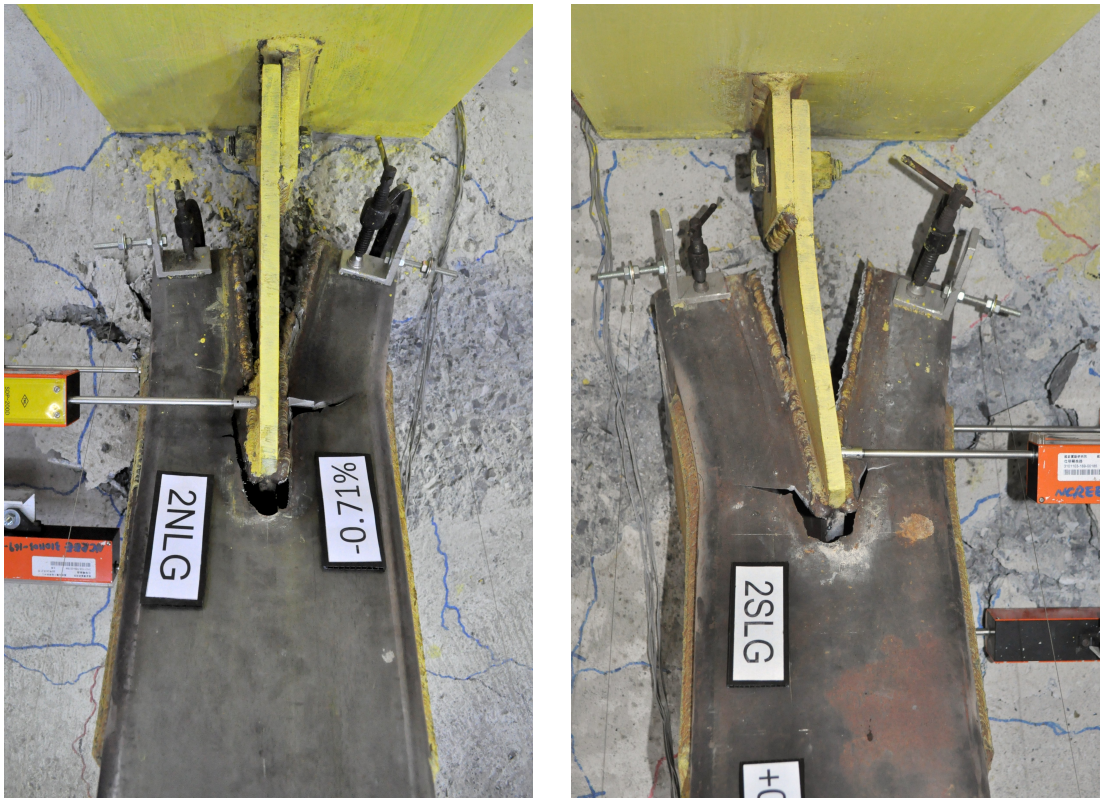

(a) North brace (−0.53% second story drift) (b) South brace (0.86% second story drift)

Figure 4.48: TNCBF1-R-WF second story brace splice connection fracture

drift. At −1.22% first story drift, weld and beam base metal damage was observed at the north beam-to-column connection. The beam base metal damage, shown in Fig. 4.49, was in an L-shape along the bottom edge of the shear tab. This base metal damage may have been expedited by the repeated backgouging and welding of the shear tab to repair weld damage in TNCBF1-N-HSS and TNCBF1-R-HSS. Similar damage occurred at 1.47% story drift at the south connection. At −1.54% and 1.48% first story drift, the south and north first story beam-to-column connections failed, as the rotational demands due to beam vertical deflection fractured the shear tab erection bolts, resulting in significant crack propagation. This damage is displayed in Fig. 4.50. The second cycle at 1.79% roof drift was completed and the test was ended due to the severe damage to the frame.

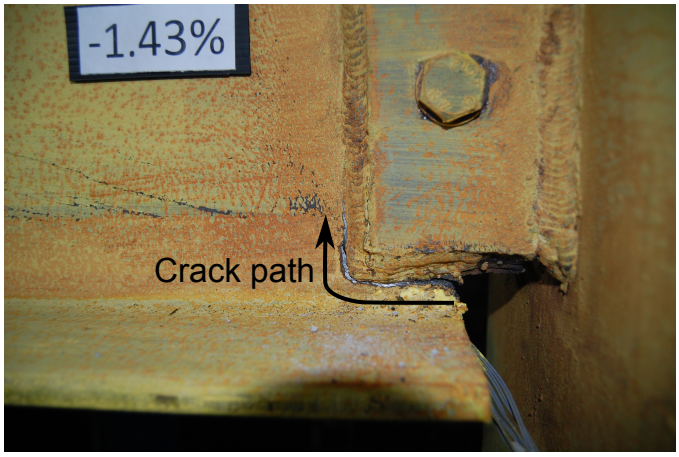

Figure 4.49: Beam base metal tear at bottom of shear tab (−1.22% story drift)

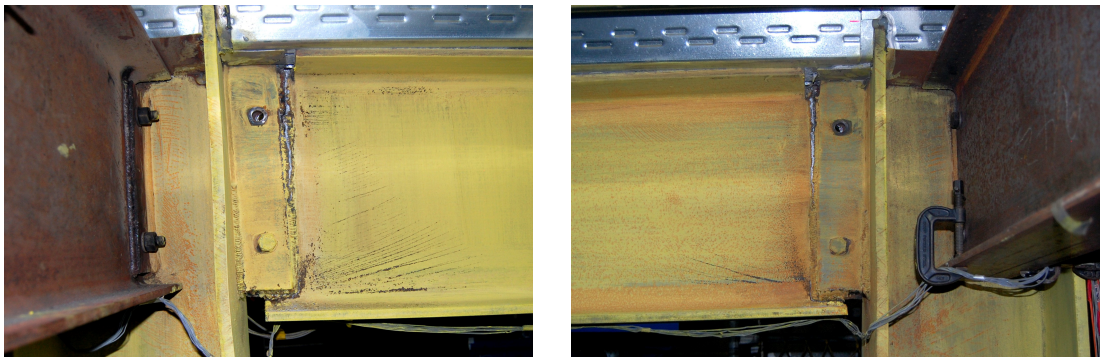

(a) South connection (−1.54% first story drift) (b) North connection (1.48% first story drift)

Figure 4.50: TNCBF1-R-WF first story beam-to-column connection fracture

4.6 TNCBF2-D-HSS Observations

4.6.1 Overview of Cyclic Performance

TNCBF2-D-HSS, shown in Fig. 4.51, was tested on January 25, 2014. The experiment was intended to capture the performance of a weak beam braced frame with details consistent with well-performing SCBFs. Only the columns and second story beam and slab were reused from the TNCBF1 tests, while the first story beam and slab, all braces, and all gusset plates were new. The load and roof drift time histories can be found in Figs. 4.53 and 4.52. Base shear-roof and -story drift hystereses are presented in Figs. 4.54 and 4.55 with annotated key events described in

Table 4.12.



Figure 4.51: TNCBF2-D-HSS overview

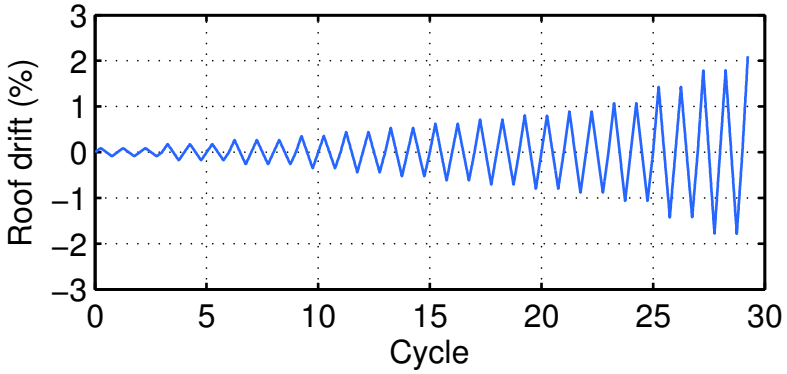

Figure 4.52: TNCBF2-D-HSS roof drift history

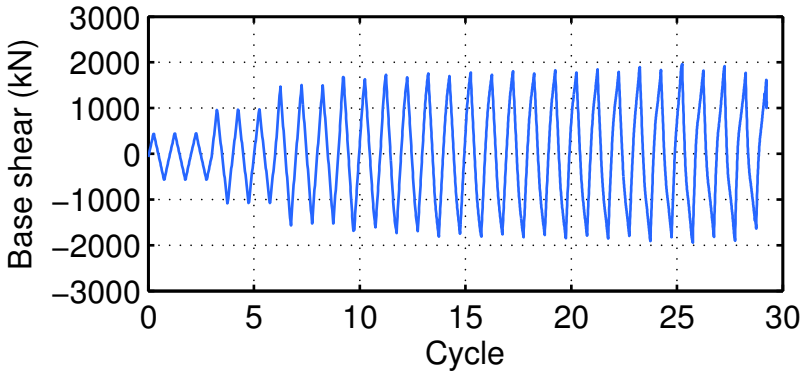

Figure 4.53: TNCBF2-D-HSS load history

Both braces on each story buckled in compression, but lateral drift was greatest in the first story. Since the first story underwent the greatest deformation, it follows that its braces were more heavily damaged than their counterparts on the second story, and they eventually fractured in tension at the locations of local buckling, where the test was ended. Even so, the north second story brace did develop local buckling at its mid-span in the final peak loading. Lateral resistance steadily increased even after the braces buckled, plateauing as local buckling in the first story braces intensified.

Peak lateral resistances and drifts are found in Table 4.13, while cyclic performance state progressions are provided in Table 4.14. Damage to the columns sustained in the TNCBF1 tests is noted in the tables.

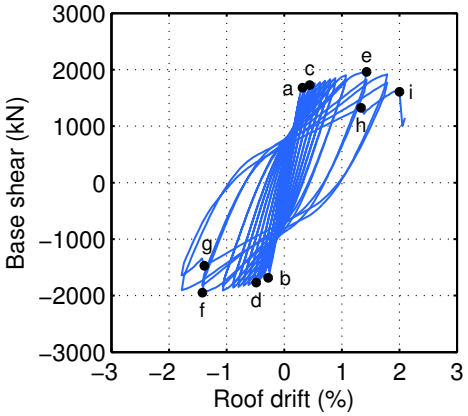

Figure 4.54: TNCBF2-D-HSS base shear-roof drift hysteresis

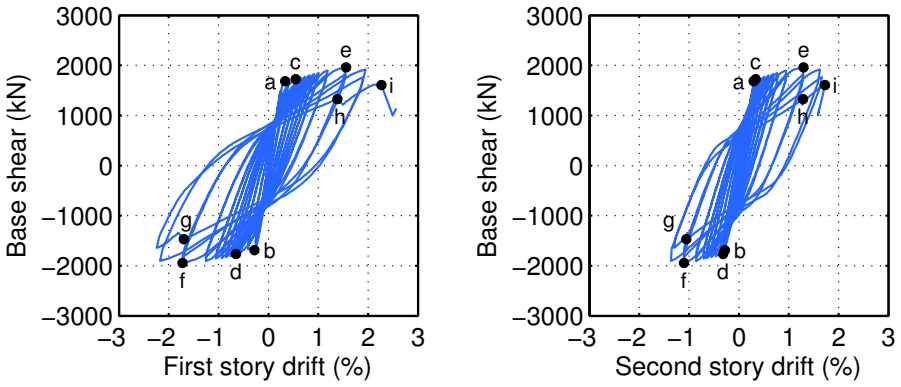

(a) First story

(b) Second story

Figure 4.55: TNCBF2-D-HSS base shear-story drift hystereses

Table 4.12: Description of labels in Figs. 4.54 and 4.55

Label	Location	Event	Roof drift (%)	Story drift (%)
a	1F north brace	Buckling	+0.32	+0.34
b	1F south brace	Buckling	−0.28	−0.28
c	2F north brace	Buckling	+0.44	+0.34
d	2F south brace	Buckling	−0.49	−0.32
e	1F north brace	Local buckling	+1.43	+1.56
f	1F south brace	Local buckling	−1.42	−1.72
g	1F north brace	Partial fracture	−1.38	−1.70
h	1F south brace	Partial fracture	+1.34	+1.39
i	1F south brace 2F north brace	Complete fracture Local buckling	+2.00	+2.27

Table 4.13: TNCBF2-D-HSS peak lateral resistances and drifts

	Resistance (kN)		Roof drift (%)		1F drift (%)		2F drift (%)	
Cycle	Max.	Min.	Max.	Min.	Max.	Min.	Max.	Min.
1	434	−567	0.08	−0.08	0.08	−0.08	0.09	−0.09
2	442	−564	0.09	−0.08	0.08	−0.08	0.09	−0.09
3	442	−567	0.08	−0.08	0.08	−0.08	0.09	−0.09
4	961	−1084	0.17	−0.17	0.17	−0.17	0.18	−0.18
5	966	−1078	0.17	−0.17	0.17	−0.17	0.18	−0.17
6	970	−1080	0.17	−0.17	0.17	−0.17	0.18	−0.18
7	1472	−1566	0.26	−0.26	0.26	−0.25	0.27	−0.27
8	1502	−1525	0.26	−0.26	0.25	−0.25	0.27	−0.27
9	1497	−1526	0.26	−0.26	0.25	−0.26	0.28	−0.26
10	1682	−1687	0.35	−0.35	0.40	−0.41	0.30	−0.29
11	1632	−1611	0.35	−0.35	0.40	−0.41	0.30	−0.28
12	1727	−1738	0.44	−0.44	0.55	−0.56	0.33	−0.31
13	1673	−1691	0.44	−0.44	0.55	−0.58	0.33	−0.29
14	1755	−1810	0.53	−0.53	0.65	−0.69	0.41	−0.36
15	1698	−1749	0.53	−0.53	0.64	−0.69	0.42	−0.36
16	1778	−1811	0.62	−0.62	0.73	−0.76	0.51	−0.47
17	1731	−1765	0.62	−0.62	0.74	−0.75	0.50	−0.48
18	1804	−1827	0.71	−0.71	0.82	−0.85	0.59	−0.55
19	1757	−1778	0.71	−0.71	0.83	−0.85	0.59	−0.56
20	1829	−1848	0.80	−0.79	0.91	−0.94	0.69	−0.64
21	1782	−1792	0.80	−0.80	0.92	−0.94	0.68	−0.64
22	1848	−1858	0.89	−0.88	1.01	−1.06	0.77	−0.70
23	1794	−1803	0.89	−0.88	1.01	−1.05	0.77	−0.71
24	1901	−1910	1.07	−1.06	1.19	−1.26	0.95	−0.86
25	1831	−1830	1.07	−1.06	1.18	−1.26	0.96	−0.86
26	1961	−1947	1.43	−1.42	1.56	−1.72	1.30	−1.10
27	1820	−1820	1.43	−1.42	1.56	−1.72	1.30	−1.10
28	1917	−1906	1.79	−1.78	1.95	−2.18	1.62	−1.36
29	1768	−1642	1.79	−1.78	1.90	−2.24	1.67	−1.30
30	1619		2.10		2.57		1.73	

Table 4.14: TNCBF2-D-HSS performance state progression

Drift (%)	Braces				Corner gusset plates				Mid-span gusset plates				Beams				Columns								Drift range (%)
Roof 1F / 2F	1S	1N	2S	2N	1S	1N	2S	2N	1S	1N	2S	2N	1S-E	1S-M	1N-M	1N-E	1S-L	1S-U	2S-L	2S-U	1N-L	1N-U	2N-L	2N-U	Roof 1F / 2F
Pre-existing damage																	Y3	Y3	Y1	Y1	Y3	Y3			N/A
0.08 0.08 / 0.09 −0.08 −0.08 / −0.09																									0.17 0.17 / 0.17
0.09 0.08 / 0.09 −0.08 −0.08 / −0.09																									0.17 0.17 / 0.17
0.08 0.08 / 0.09 −0.08 −0.08 / −0.09																									0.17 0.17 / 0.17
0.17 0.17 / 0.18 −0.17 −0.17 / −0.18					Y1	Y1	Y1	Y1			Y1	Y1													0.35 0.34 / 0.35
0.17 0.17 / 0.18 −0.17 −0.17 / −0.17																									0.35 0.34 / 0.35
0.17 0.17 / 0.18 −0.17 −0.17 / −0.18																									0.35 0.33 / 0.36
0.26 0.26 / 0.27 −0.26 −0.25 / −0.27																	Y1								0.52 0.51 / 0.54
0.26 0.25 / 0.27 −0.26 −0.25 / −0.27																									0.52 0.50 / 0.55
0.26 0.25 / 0.28 −0.26 −0.26 / −0.26																									0.52 0.51 / 0.54
0.35 0.40 / 0.30 −0.35 −0.41 / −0.29		B1							Y1	Y2				Y1	Y1						Y1	Y1			0.70 0.81 / 0.59
0.35 0.40 / 0.30 −0.35 −0.41 / −0.28																									0.70 0.82 / 0.58
0.44 0.55 / 0.33 −0.44 −0.56 / −0.31		B2				Y2													Y1				Y1		0.88 1.11 / 0.64

Continued on next page

Table 4.14 – continued from previous page

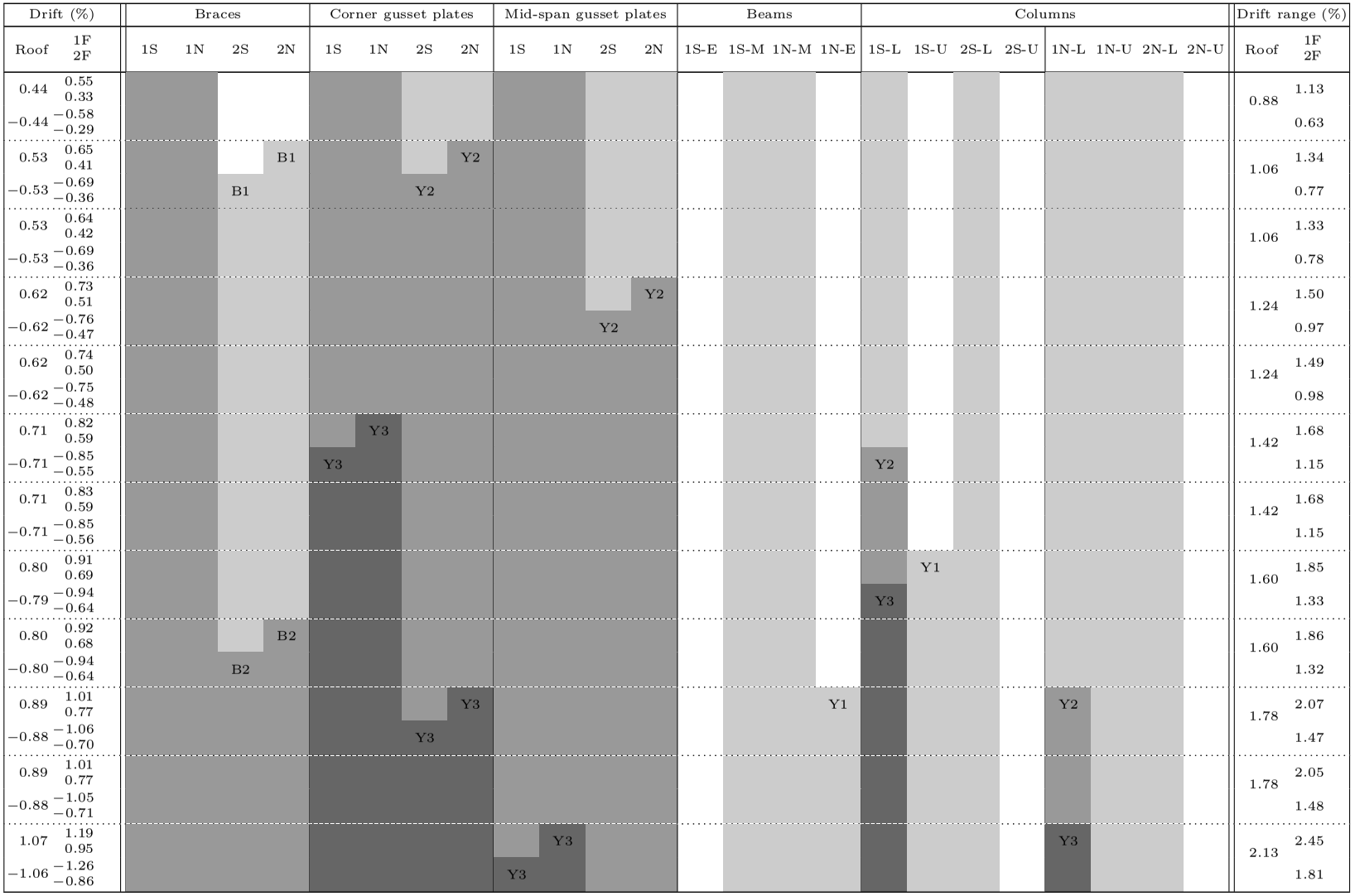

Continued on next page

Table 4.14 – continued from previous page

Drift (%)		Braces				Corner gusset plates				Mid-span gusset plates				Beams				Columns								Drift range (%)	
Roof	1F 2F	1S	1N	2S	2N	1S	1N	2S	2N	1S	1N	2S	2N	1S-E	1S-M	1N-M	1N-E	1S-L	1S-U	2S-L	2S-U	1N-L	1N-U	2N-L	2N-U	Roof	1F 2F
1.07	1.18 0.96																									2.14	2.44
−1.06	−1.26 −0.86	B3																									1.81
1.43	1.56 1.30	Bs1	B3, BC				Wc- 2cm									Y2									Y1	2.85	3.28
−1.42	−1.72 −1.10	BC													Y2						Y1						2.40
1.43	1.56 1.30						Wc- 4cm																			2.85	3.28
−1.42	−1.72 −1.10					Wc- 1cm								Y2													2.40
1.79	1.95 1.62				B3												Y2						Y2		Y2	3.57	4.12
−1.78	−2.18 −1.36			B3															Y2		Y2						2.98
1.79	1.90 1.67																									3.57	4.15
−1.78	−2.24 −1.30		BF																								2.97
2.10	2.57 1.73	BF			BC					PC	PC															N/A	

4.6.2 Detailed Cyclic Performance

Initial State (Roof Drift $\leq 0.26\%$*)*

In the initial state, the frame remained essentially elastic on both stories. Yielding initiated in the first and second story corner gusset plates as well as the second story mid-span gusset plates, but it was mostly confined to the heat affected zones around the ends of the splice welds as in Fig. 4.56. Minor web yielding also occurred at the base of the south column. The extent of this initial yielding was small such that it is indistinguishable in the hysteretic response of the frame.



(a) Yielding locations (b) Magnified brace end

Figure 4.56: TNCBF2-D-HSS typical initial gusset plate yielding, Y1 (0.26% first story drift)

Moderate Damage State ($0.26\% <$ *Roof Drift* $\leq 1.07\%$*)*

Brace buckling marks the beginning of the moderate damage state, which extends up to the drift level just prior to local buckling. Both first story braces buckled in the first cycle at 0.35% roof drift, which corresponds to about 0.40% first story drift. The buckling progression of the south first story brace is shown in Fig. 4.57. Yielding along elliptical fold lines in the gusset plates connecting these braces to the frame increased (Y2) due to gusset plate rotation, and yielding in the first story beam initiated at its mid-span due to the brace unbalanced load.

The second story braces buckled at the first cycle at 0.53% roof drift at nearly the same story drift as the first story braces. Following the same performance state progression, gusset plate yielding increased in the second story gusset plates shortly thereafter.



(a) B1 (−0.41% first story drift)



(b) B2 (−0.56% first story drift)

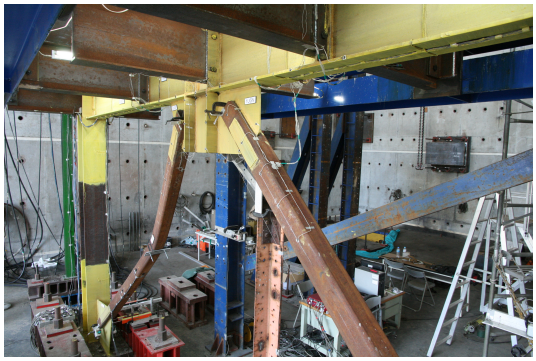

(c) B3 (−1.26% first story drift)



(d) BC (−1.72% first story drift)

Figure 4.57: TNCBF2-D-HSS south first story brace buckling progression

Gusset plate yielding at the corners of the first story became severe (Y3) beyond 0.82% first story drift. However, the second story gusset plates reached severe yielding earlier at 0.77% and −0.70% second story drift. This makes sense, as the second story braces should deliver greater tensile forces to the gusset plates since the second story beam is strong enough to resist the brace unbalanced load. The first story brace force was limited by the beam strength, so most first story gusset plate yielding developed due to plastic hinging in compression. Mid-span gusset plate severe yielding did not occur until just under 1.00% first story drift, which may indicate that the mid-span connections were more flexible than the corner connections on the first story. The corner gusset plates were welded to the column bases and base plates, where fixity should be considerable compared to the beam mid-span. Consequently, deformation may concentrate in the first story corner gusset plates but may be distributed among the gusset plates and beam at the first story

mid-span.

At the base of the south column, yielding became moderate (Y2) at −0.85% first story drift and severe (Y3) at −0.94% first story drift. This yielding progression occurred at lower drifts than in previous tests, but their true performance is muddled by previous severe damage, including flange local buckling. By the end of the moderate damage state, yielding in the columns near the first story beam-to-column connections had initiated, but it did not grow significantly.

Severe Damage State (Roof Drift > 1.07%*)*

In the severe damage state, the first story braces developed local buckling at their mid-spans at 1.56% and −1.72% story drift in the north and south braces, respectively. These events coincided with moderate yielding at the mid-span of the first story beam (Fig. 4.58) and slight weld damage along the corner gusset plate column interfaces (Fig. 4.59). No such damage occurred at the mid-span gusset plates, but as mentioned above, the increased fixity at the bases may be responsible for greater damage.



Figure 4.58: TNCBF2-D-HSS south first story beam mid-span, Y2 (−1.72% first story drift)

At −1.72% and 1.95% first story drift, the first story beam ends developed moderate (Y2) yielding. This damage is consistent with the regions of maximum moment for a beam with fixed ends. It should also be noted that the first story slab at the beam ends developed large cracks emanating from the gusset plate block-out to the slab edge as shown in Fig. 4.60. Similar damage has been observed in previous SCBF tests with slab block-outs (Lumpkin 2009). The columns near both the first and second story beam ends also developed moderate yielding in the first cycle at



(a) Wc-4cm (1.56% first story drift)



(b) Wc-1cm (−1.72% first story drift)

Figure 4.59: TNCBF2-D-HSS first story corner gusset plate column interface weld cracks, Wc

1.79% roof drift. Column yielding was expected at the second story beam-to-column connections since the flexural capacity of the beam exceeded that of the columns. This was nominally not the case on the first story, though the damage seen in Fig. 4.61 suggests that their actual flexural capacities were closer.



Figure 4.60: TNCBF2-D-HSS typical first story slab crack around block-out (2.57% first story drift)

The north and south first story braces fractured at their mid-spans at −2.24% and 2.57% first story drift, respectively, where the test was ended to prevent further damage to the frame. At the final drift peak, column damage was significant at the bases and local buckling in the flanges was observed (Fig. 4.62). Photographs depicting the extent of yielding in the gusset plates are found in Fig. 4.63 for the first story and Fig. 4.64 for the second story.

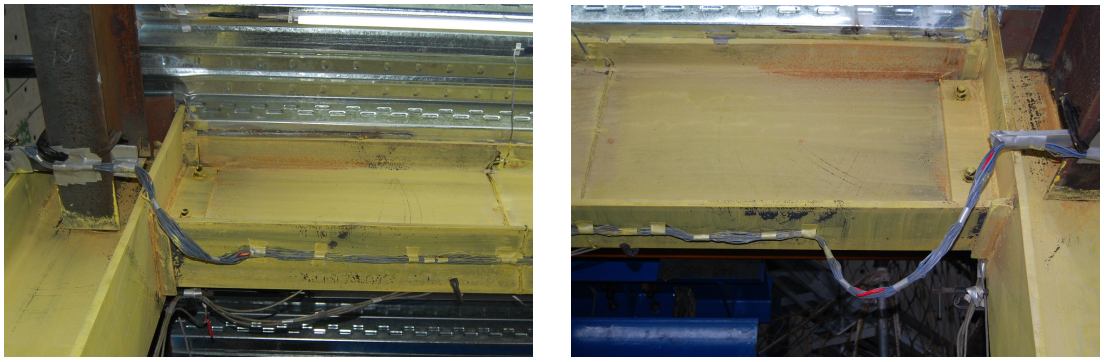

(a) South end (b) North end

Figure 4.61: TNCBF2-D-HSS first story beam-to-column connection regions, Y2 (post-test)

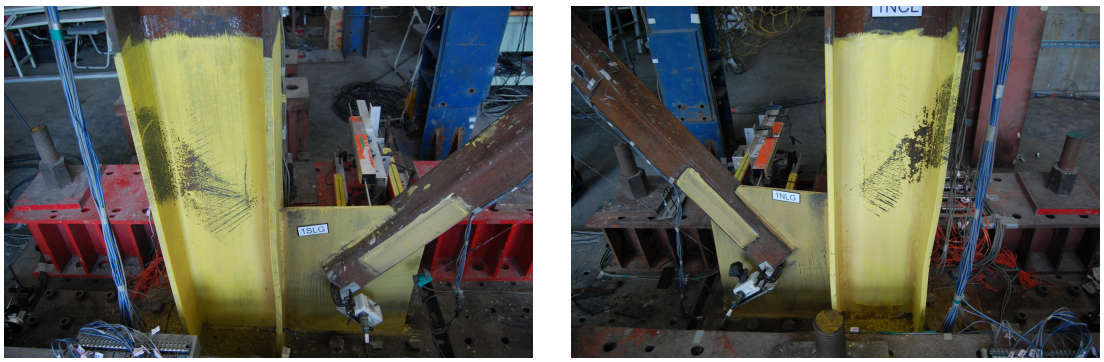

(a) South base (b) North base

Figure 4.62: TNCBF2-D-HSS column yielding and local buckling at bases, Y3 (2.57% first story drift)



(a) South corner



(b) North corner



(c) South mid-span



(d) North mid-span

Figure 4.63: TNCBF2-D-HSS first story gusset plates, Y3 (post-test)



(a) South corner



(b) North corner



(c) South mid-span



(d) North mid-span

Figure 4.64: TNCBF2-D-HSS second story gusset plates, Y3 (post-test)

Chapter 5

EXPERIMENTAL ANALYSIS

5.1 Introduction

The results of analyses performed using data collected from testing at NCREE are presented in this chapter. Data collected from both instrumentation and written observations (e.g., weld crack length) is used to support the interpretation of both system and local responses. Local response analyses focus on the cyclic behavior of braces, beams, columns, and connections. Comparisons between TNCBF specimens are made to demonstrate the effectiveness of the various rehabilitation schemes. Further, the results are compared to those from the TCBF2 series, a set of three-story multi-story X configuration SCBFS (Lumpkin 2009).

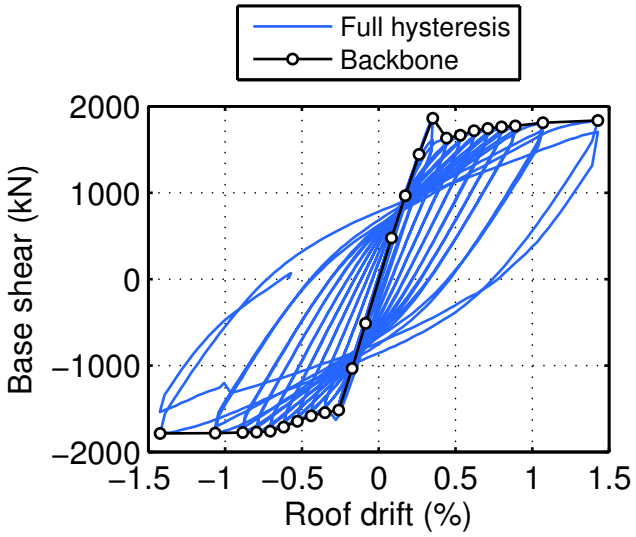

Figure 5.1: Backbone curve (hysteretic envelope) example

5.1.1 Backbone Curve Description

Some results in this chapter are presented in the form of backbone curves (hysteretic envelopes), where only data collected at the peaks of the first cycle of each displacement amplitude level is plotted. Only completed cycles were used to develop the backbones. These succinct representations of response reduce clutter in the plots, facilitating comparisons between tests. Nonetheless, it should be recognized that important information is lost in the backbone curves–in particular, the shape and size of the hysteretic loops is ignored, which is associated with energy dissipation. An example of how the backbone compares to the full response is shown in Fig. 5.1. Data from both the TNCBF and TCBF2 specimens used to develop these plots is available on NEEShub (NEES 2014).

5.2 System Response

5.2.1 Damage Progression

The damage state progression of each story of each frame is represented graphically in Fig. 5.2 to provide a relative sense of the performance of each specimen. The story damage states are defined just as the frame damage states in Chapter 4. Typically, this means the moderate damage state begins at brace buckling (B1) and the severe damage state begins at brace local buckling (BC). The progression is plotted with respect to story drift range and each story is represented with a bar (each specimen's stories read from the bottom up). The drift range shown is the one achieved prior to the cycle when the next damage state occurred. Fracture is also indicated at the end of the bars to note that it occurred in the next cycle (not the drift range where the marker is located). Drift ranges achieved in post-fracture cycles on each story are not included.

Fig. 5.2 highlights the poor performance of TNCBF1-N-HSS and TNCBF1-R-WF, which were only able to sustain drift ranges less than 2% prior to fracture. However, the first story of TNCBF1-R-HSS and both stories of TNCBF2-D-HSS perform similarly to the TCBF2 tests in terms of damage and ductility. The presence of the weak beam does not appear to lead to brace local buckling at lower drifts or hinder brace fracture life. The most direct comparisons can be made between TNCBF1-R-HSS (first story only), TNCBF2-D-HSS, and TCBF2-HSS. TNCBF1-R-HSS contained the weakest beam, as it lacked shear connectors and moment connections. Yet, its first story achieved the greatest story drift range prior to brace fracture among similar specimens.

On the other hand, Fig. 5.2 suggests greater damage concentration in a given story. The results from TNCBF1-R-HSS should be interpreted cautiously because the second story braces were much stockier than the first story braces, but soft story behavior is still apparent in TNCBF2-D-HSS, which had the same braces on both stories.

5.2.2 Force-Drift Response

The base shear-roof drift and -story drift backbone curves for the TNCBF tests are plotted in Figs. 5.3 through 5.5. The base shear-roof drift backbones highlight the low ductility of TNCBF1-N-HSS and significant lateral strength degradation in TNCBF1-N-HSS and TNCBF1-R-WF. TNCBF1-RHSS and TNCBF2-D-HSS both show reasonably good performance, as strength was maintained up to the end of the tests. However, roof drift is not necessarily an appropriate metric since soft story behavior in the first story was intentional. For instance, TNCBF2-D-HSS reaches greater roof

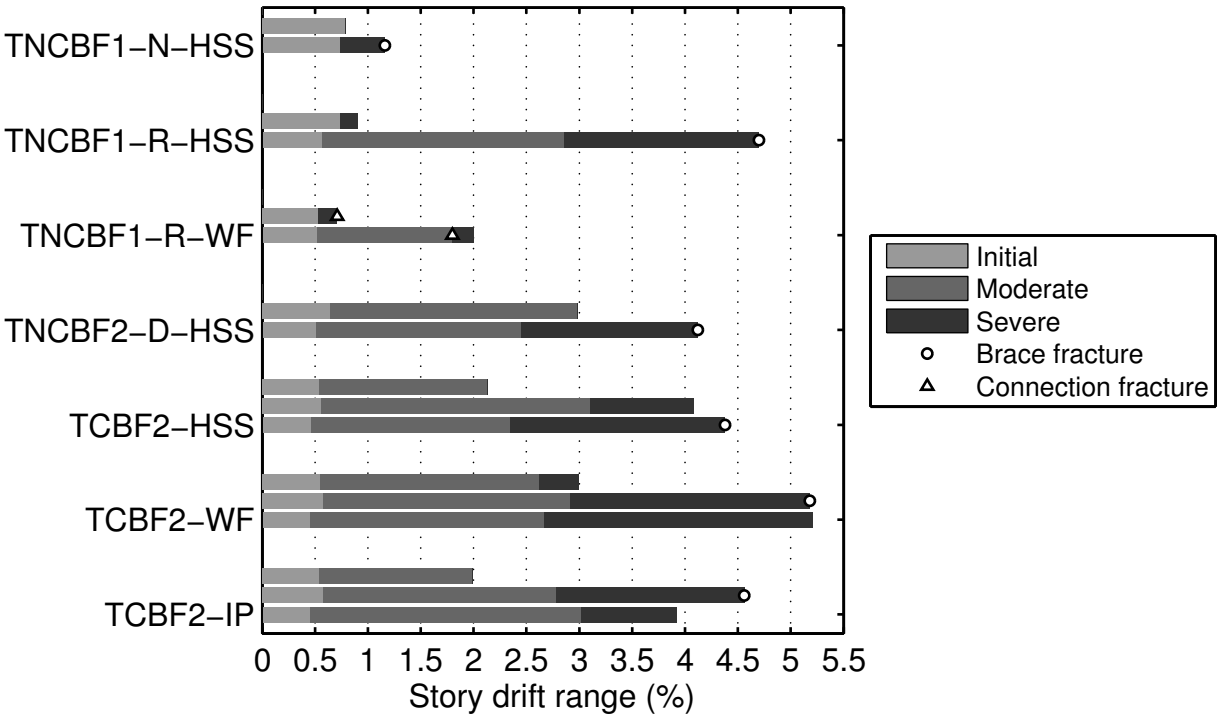

Figure 5.2: Damage state progression of TNCBF frames

drifts than TNCBF1-R-HSS, but the latter specimen remained nearly elastic on its second story while its first story drift exceeded that of all specimens.

The first story backbones shows similar responses between TNCBF1-N-HSS and TNCBF1-R-WF as well as TNCBF1-R-HSS and TNCBF2-D-HSS. Both TNCBF1-N-HSS and TNCBF1-R-WF experienced large strength drops due to brace buckling. TNCBF1-N-HSS regained some strength in its EBF mode and TNCBF1-R-WF recovered as brace deformation grew larger. However, it is clear that in TNCBF1-R-WF, strength was lost on the first story as its beam-to-column connections suffered greater damage. TNCBF2-D-HSS was slightly stronger than TNCBF1-R-HSS, which may be attributable to composite action between the beam and slab. This strengthens the beam and in turn the braces can develop greater tensile forces.

The second story backbones vary significantly. TNCBF1-N-HSS and TNCBF1-R-HSS both remained mostly elastic, with the latter developing a small amount of inelastic behavior at later drifts. TNCBF1-R-WF lost a considerable amount of strength through brace splice connection

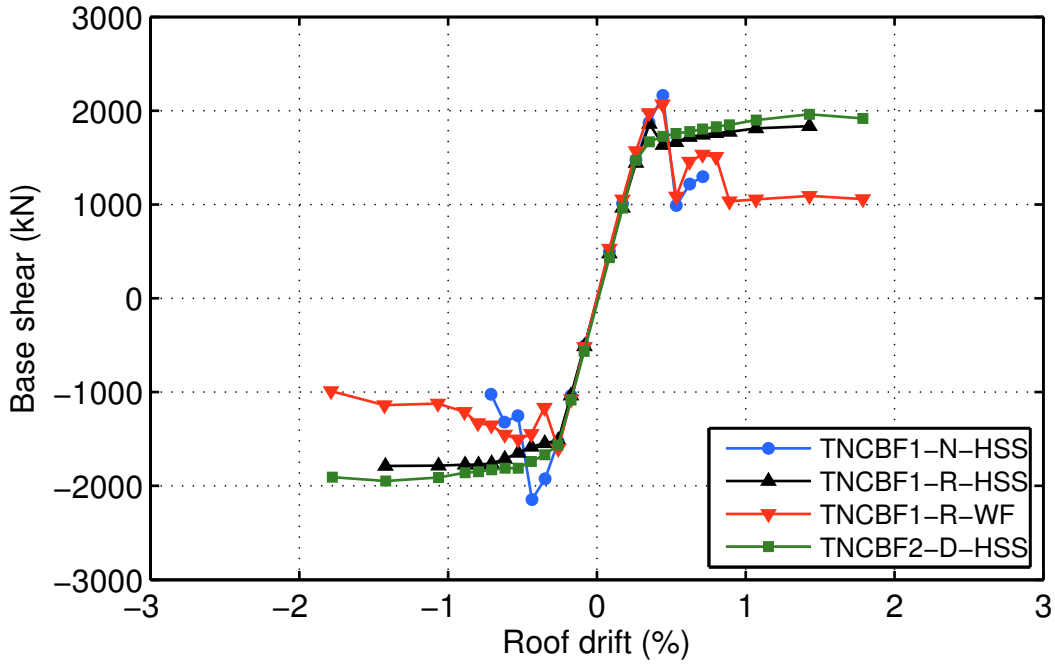

Figure 5.3: Base shear-roof drift backbone curve

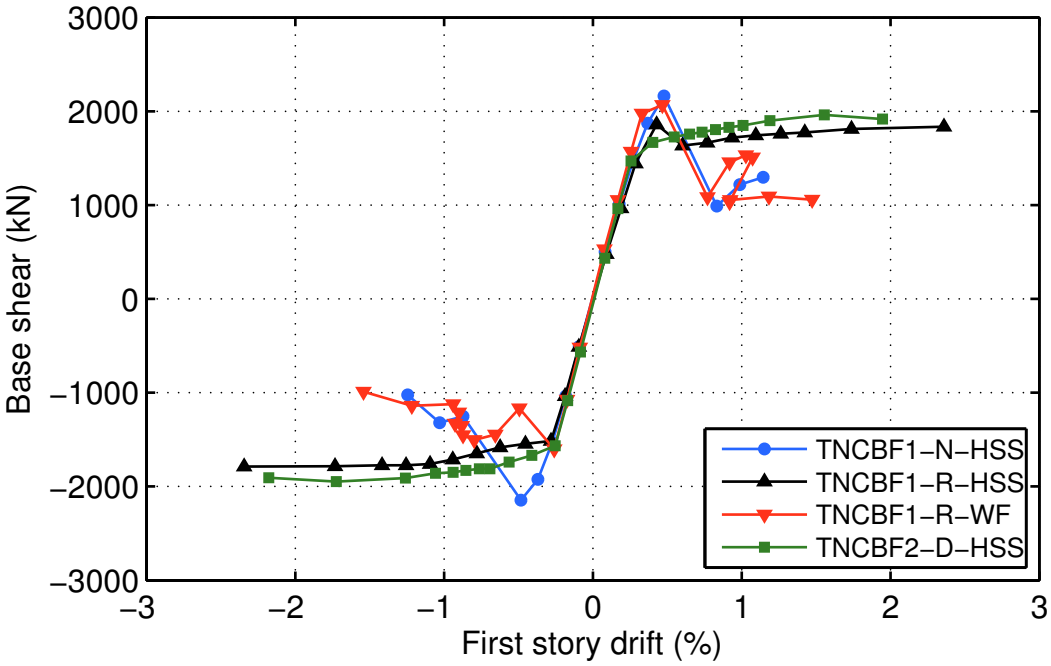

Figure 5.4: Base shear-first story drift backbone curve

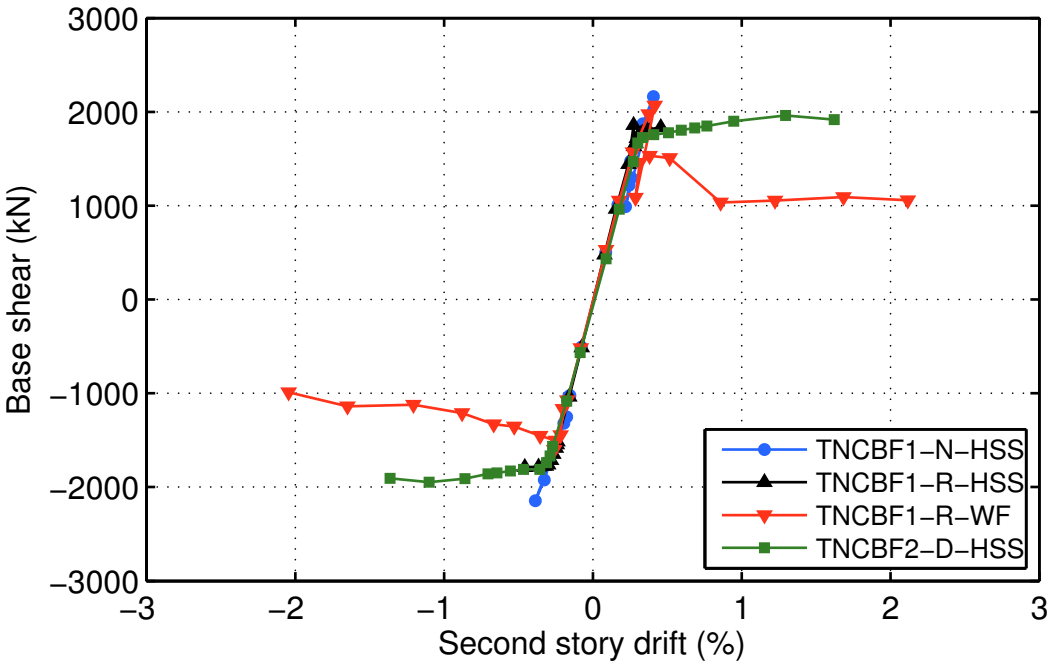

Figure 5.5: Base shear-second story drift backbone curve

fracture. Its behavior past about 1% drift was that of a moment frame, which was considerably weaker and less stiff than its initial braced configuration. TNCBF2-D-HSS shows typical braced frame behavior where braces buckle but story shear (the same as base shear in this loading) remains stable as long as the brace does not fracture.

Comparison to TCBF2

The best performing TNCBF stories are plotted with all TCBF2 stories in gray in Fig. 5.6. The weak beam stories (1F) of the TNCBF tests developed slightly weaker lateral resistance than all stories of the TCBF2 tests, with TCBF2-HSS having the greatest difference. However, TCBF2-HSS was also stronger than any of the other TCBF2 tests, which generally still developed strong and ductile responses. Some of the strength discrepancy between the TNCBF and TCBF2 series can be attributed to the column sections used. The TCBF2 series used W12×106 columns while the TNCBF series used weaker W12×72 columns. The contribution of the columns to story shear increases after brace buckling; this is discussed in more detail later in the chapter.

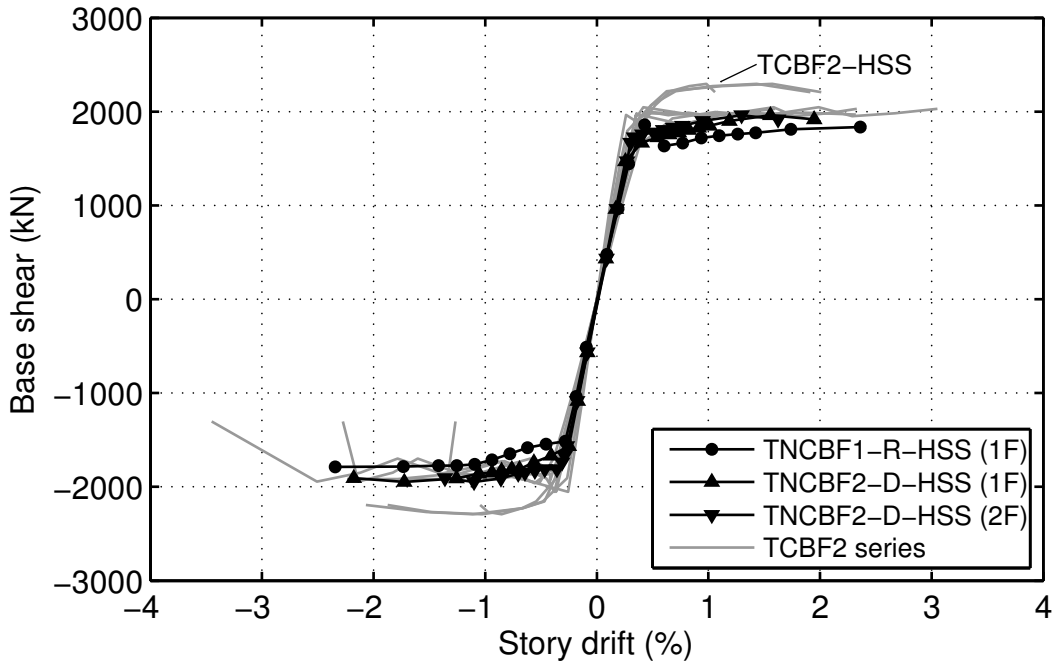

Figure 5.6: Base shear-story drift backbones from TNCBF and TCBF2 tests

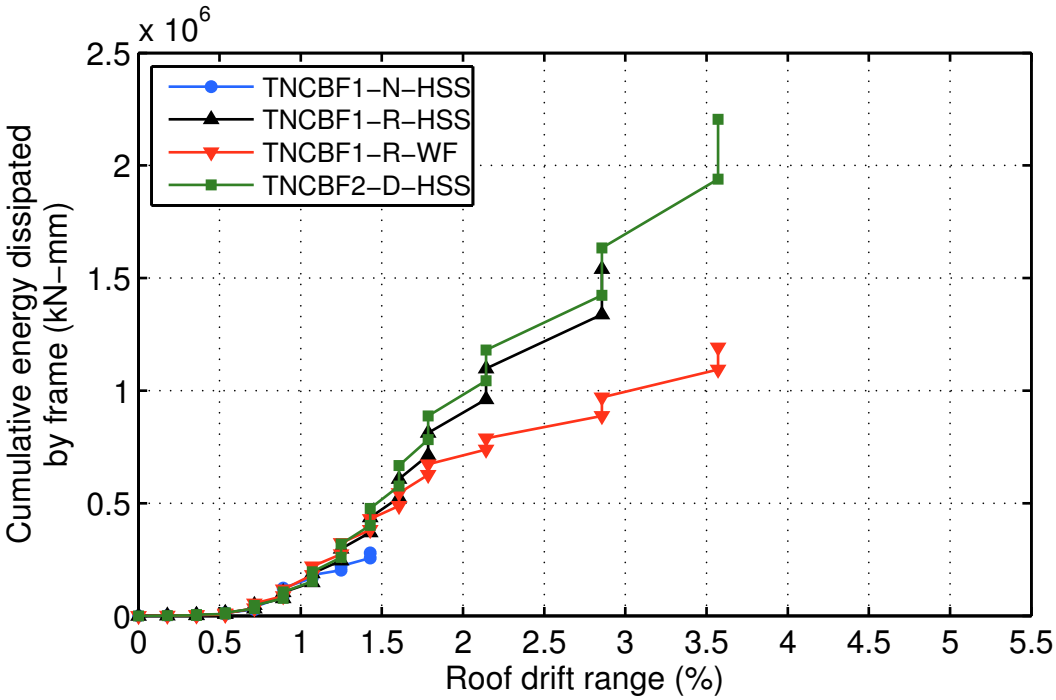

Figure 5.7: Cumulative frame energy dissipated

5.2.3 Energy Dissipation

The extent of energy dissipated is generally a good indication of performance. In quasistatic loading, as in the tests presented in this thesis, energy dissipated is associated with rate-independent damping. This damping reduces the response of the structure to dynamic loading. Energy dissipated per cycle is calculated as the area enclosed by the force-displacement hysteresis produced in that cycle (zero drift to zero drift). Cumulative energy dissipated by the frames as well as individual stories in TNCBF tests are plotted in Figs. 5.7 through 5.9, where it can be seen that TNCBF1-R-HSS and TNCBF2-D-HSS dissipated the most energy by far. The story energy dissipated by post-fracture EBF (TNCBF1-N-HSS first story) and moment frame (TNCBF1-R-WF second story) action was markedly less than that of the braced frame action in the first story of TNCBF1-R-HSS and both stories of TNCBF2-D-HSS.

In SCBFs, experimental research has shown that braces are responsible for approximately 80% of the total energy dissipated, while yielding of the gusset plates and framing members constitutes

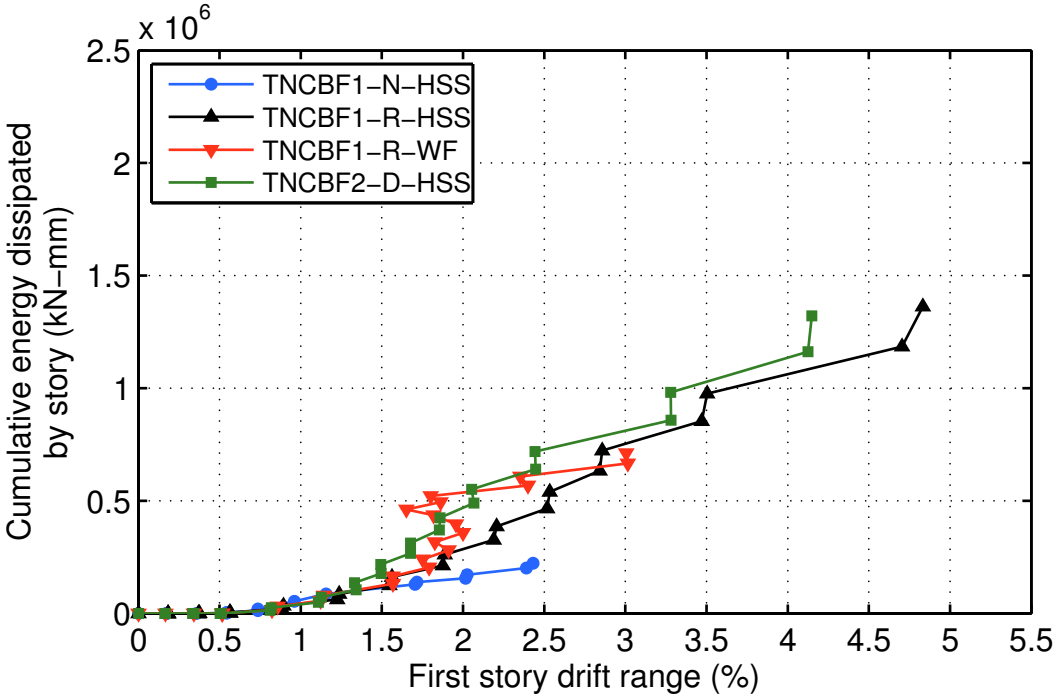

Figure 5.8: Cumulative first story energy dissipated

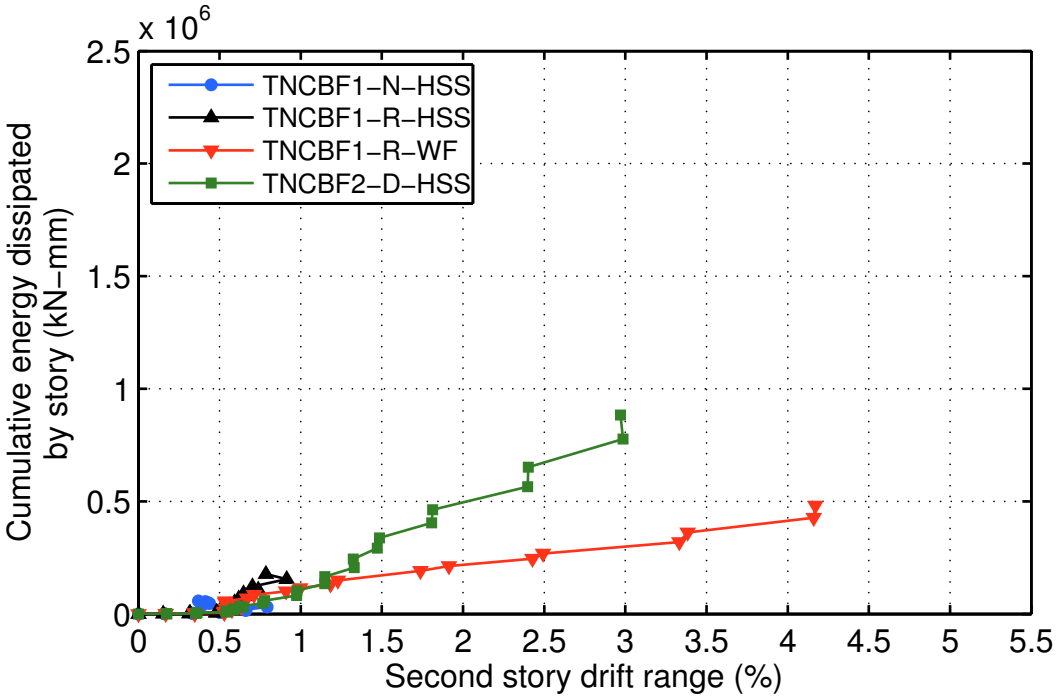

Figure 5.9: Cumulative second story energy dissipated

the remainder (Kotulka 2007; Powell 2010). However, the proportion of energy dissipated by braces may be less in weak beam NCBFs, as inelastic deformation from braces in tension is expected to concentrate in the beams and not the braces. To investigate this behavior, the energy dissipated by each story of TNCBF2-D-HSS was decomposed into columns (from column shear and story displacement), beams (from brace unbalanced force and beam mid-span deflection), and braces and connections (from subtraction of column and beam energy dissipated from story energy dissipated). The decomposed story energy dissipation plots presented in Fig. 5.10 show that in this test, the energy dissipated by the beam was relatively small, even on the first story where the beam was weak. On the other hand, the contribution of the columns in energy dissipation was much greater on the first story. This data is consistent with the observed greater yielding in the first story columns than the beam.

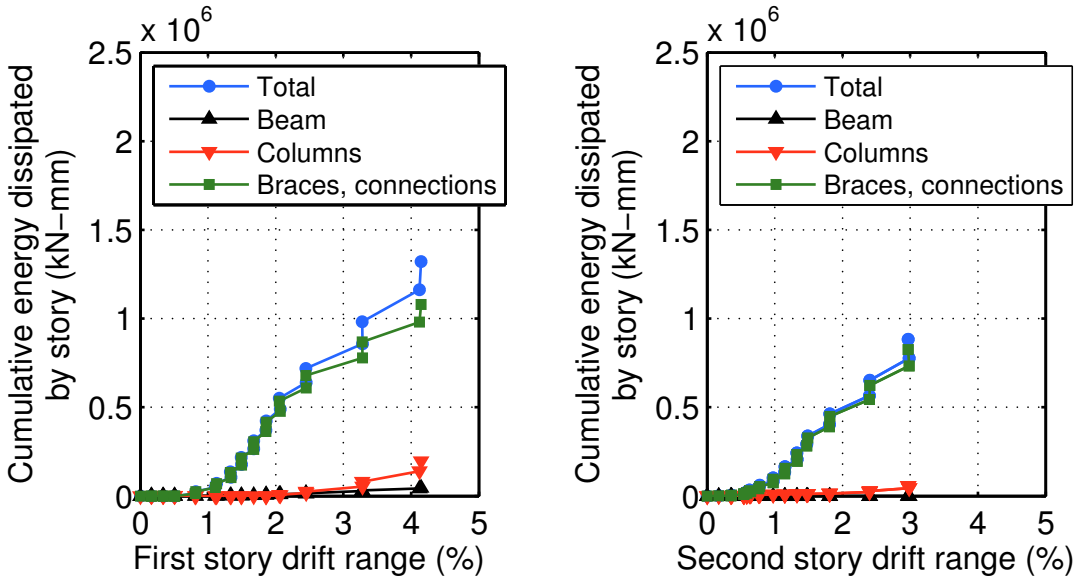

(a) First story (weak beam) (b) Second story (strong beam)

Figure 5.10: TNCBF2-D-HSS cumulative energy dissipated decomposed by component type

Comparison to TCBF2

The cumulative energy dissipated by the selected TNCBF stories in Fig. 5.11 was typically greater than the TCBF2 tests at the same drift ranges; however, direct comparisons cannot be made

because the loading protocols in the two test series are different. Since the TNCBF protocol features more cycles at lower drifts, it makes sense that more energy was dissipated. Comparing energy dissipated by individual cycles and not cumulative energy dissipated (Fig. 5.12) reveals that the best performing TNCBF stories dissipated similar amounts of energy in each cycle at the same drift levels as the TCBF2 stories.

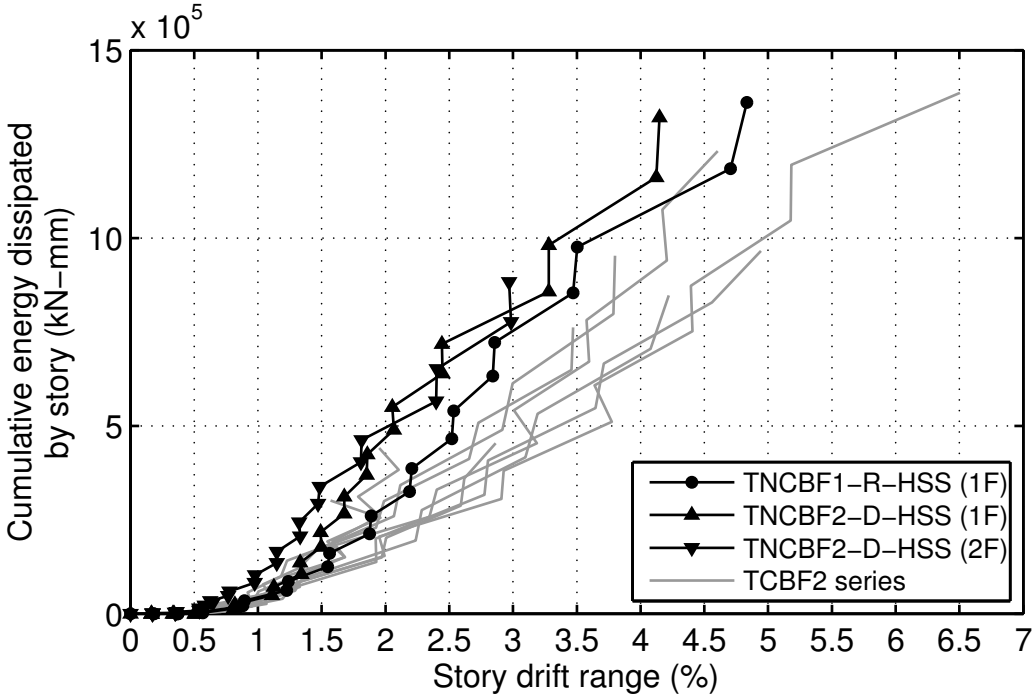

Figure 5.11: Cumulative energy dissipated in TNCBF and TCBF2 tests

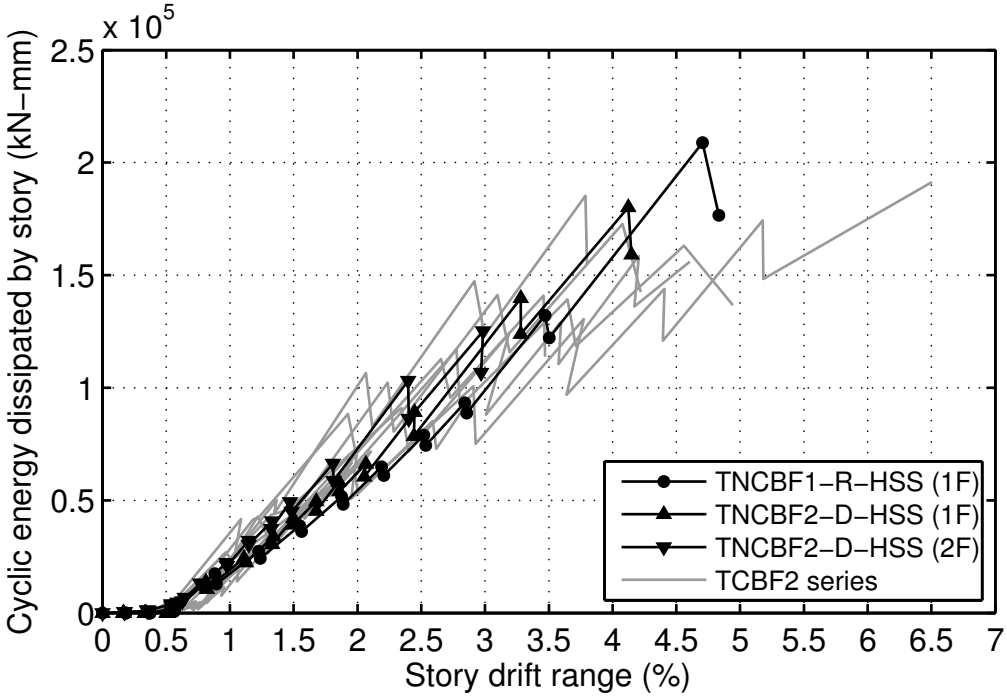

Figure 5.12: Cyclic energy dissipated in TNCBF and TCBF2 tests

5.3 Brace Response

5.3.1 Brace Axial Force

Story drift-brace axial force hystereses are plotted in Figs. 5.13 through 5.16. Brace axial forces were derived from sets of strain gauges attached to each brace wall for HSS braces and each flange and side of web for wide flange braces. These strain gauges were located at the lower quarter-point of each brace. From the recorded strain histories, stress histories were produced assuming an elastic perfectly plastic constitutive relationship with material yield stresses found from coupon tests. The yield and critical buckling (assuming pinned-pinned ends, $K = 1$) forces of each brace are marked on the plots as references.

By examining the plots, one can immediately see that in stories with weak beams, the braces do not yield in tension over their entire areas. This is an expected outcome in a weak beam chevron braced frame, as the beam is deemed weak by virtue of its inability to develop the design brace unbalanced load. In direct contrast, tensile yielding can be seen in the north second story brace of TNCBF2-D-HSS, shown in Fig. 5.16b. The corresponding south brace clearly yielded, but most of its post-yield behavior could not be extracted from its own strain gauges, likely due to debonding. In place of the south brace strain gauge-derived force, this brace's axial force was back-calculated from the actuator force, column shears, and north brace axial force. As can be seen in Fig. 5.16b, this quantity does not reach P_y, likely as a result of error in the measurements used to derive it. Still, the shape of the south brace hysteresis using back-calculated brace axial force rather than the brace strain gauge-derived quantity appears to more accurately represent response. The line style of the south brace axial force and quantities derived using it presented later (e.g. brace unbalanced load), is dashed to indicate lower confidence in the measured response.

Predicting Maximum Axial Force in Tension

The ability to predict the maximum achievable brace force in tension for weak beam NCBFs may be useful in determining the actual demands on the brace connections and framing members. In the case of retrofit, evaluating existing components with a demand based on an "effective" yield force in tension may indicate that some components are not deficient and do not require rehabilitation, though they may not be able to develop the full tensile capacity of the brace. This effective yield

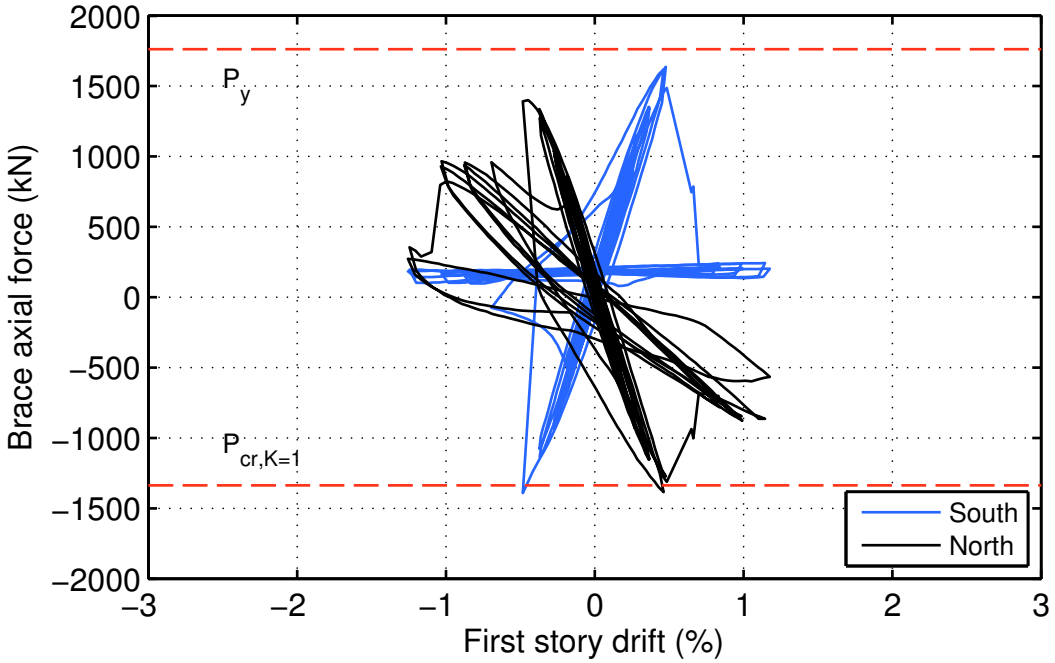

(a) First story (north brace did not buckle)

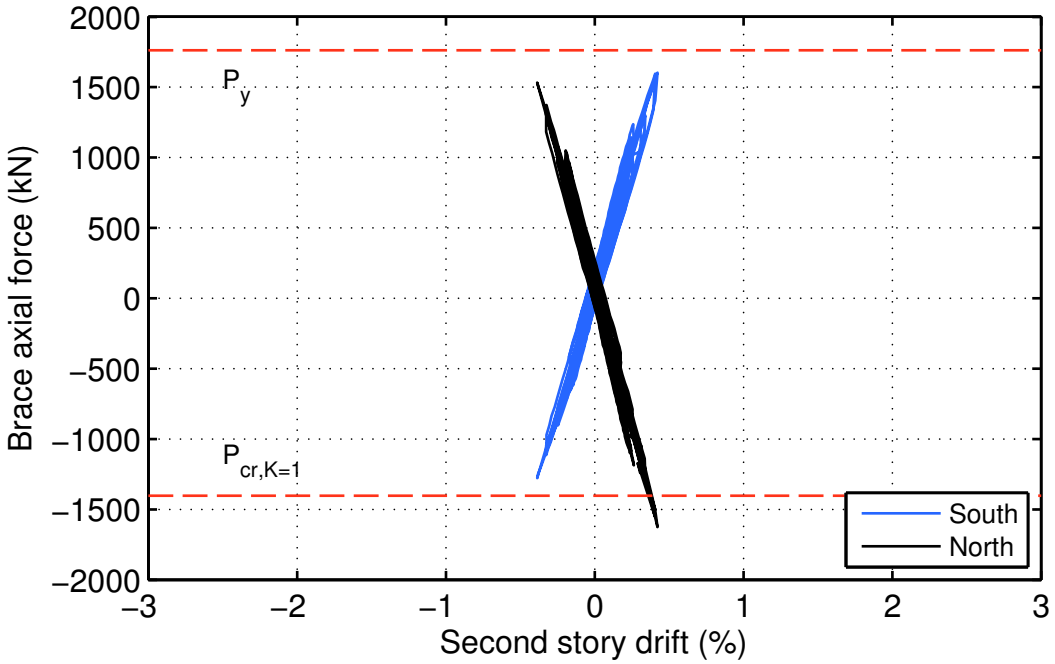

(b) Second story

Figure 5.13: TNCBF1-N-HSS brace elongation hystereses

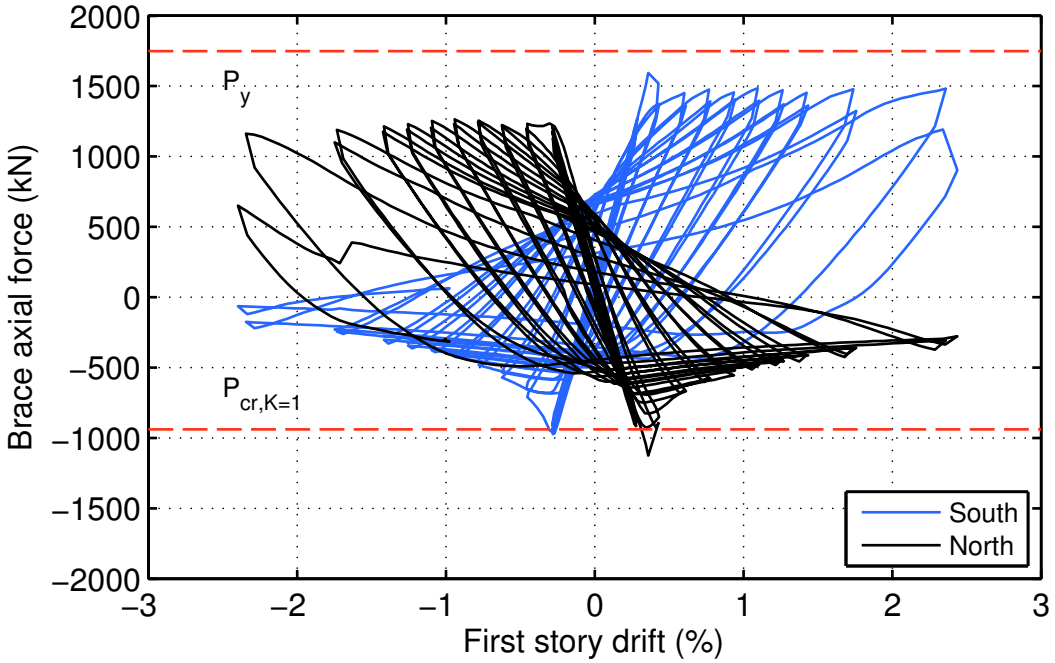

(a) First story (south brace instrumentation error)

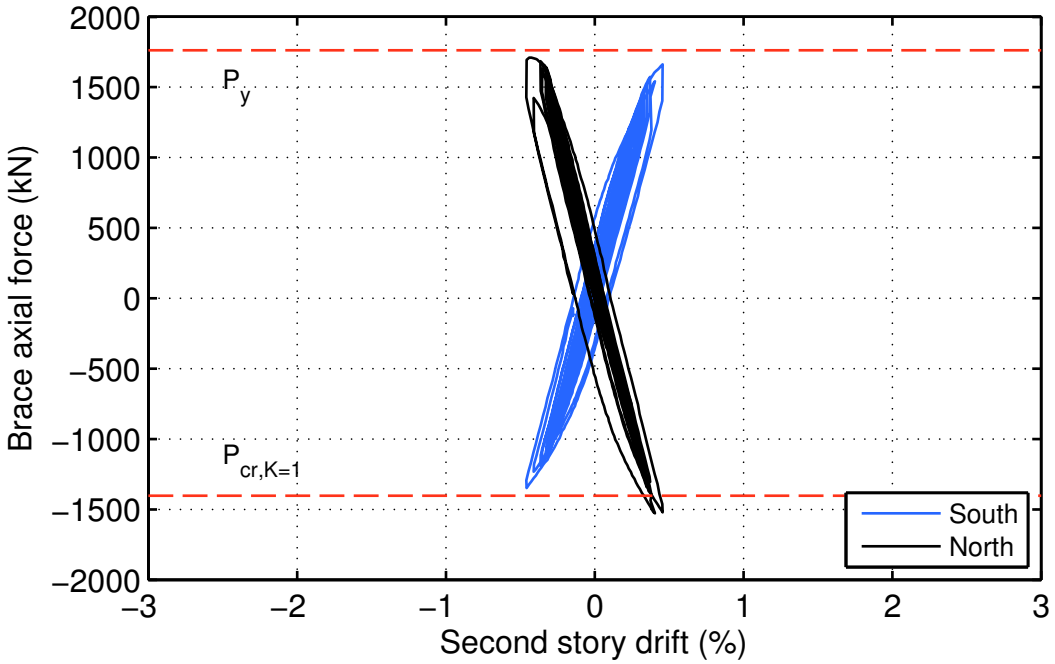

(b) Second story

Figure 5.14: TNCBF1-R-HSS brace elongation hystereses

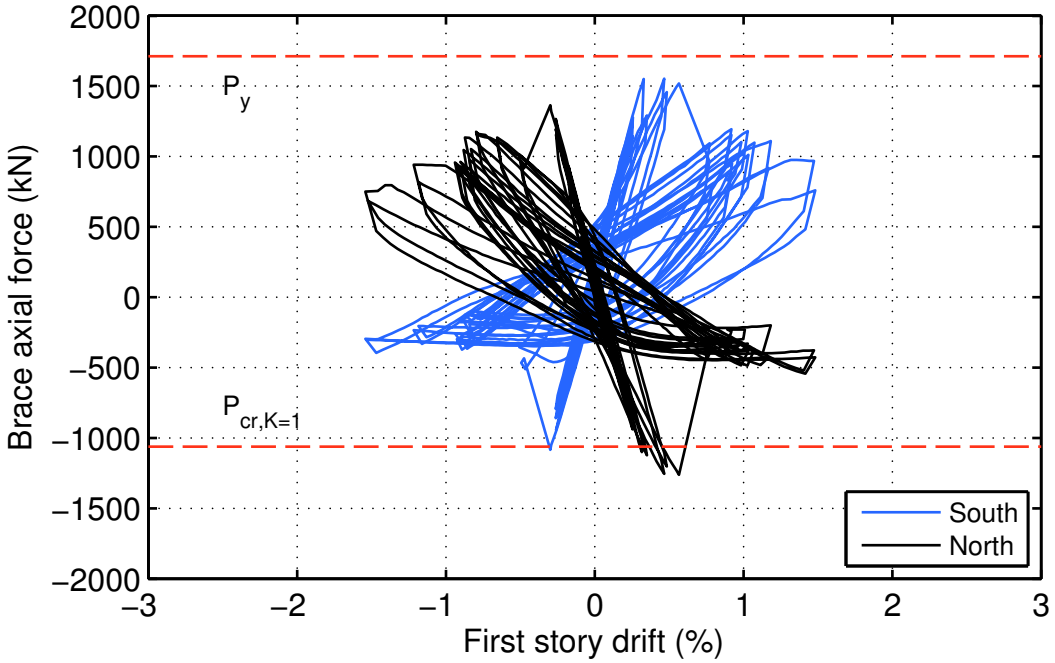

(a) First story

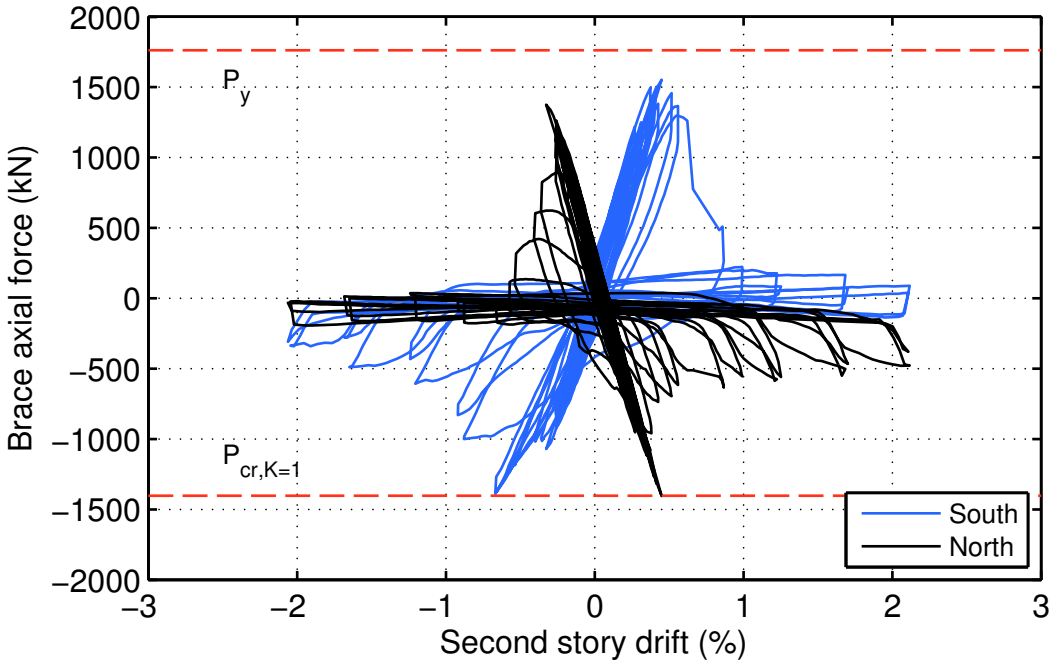

(b) Second story

Figure 5.15: TNCBF1-R-WF brace elongation hystereses

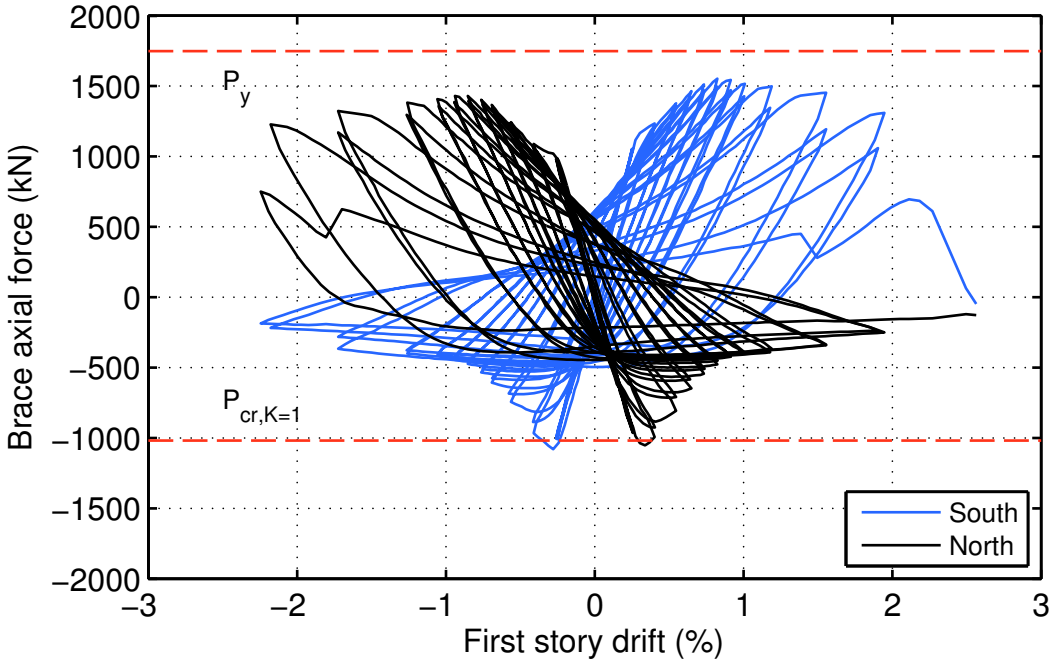

(a) First story

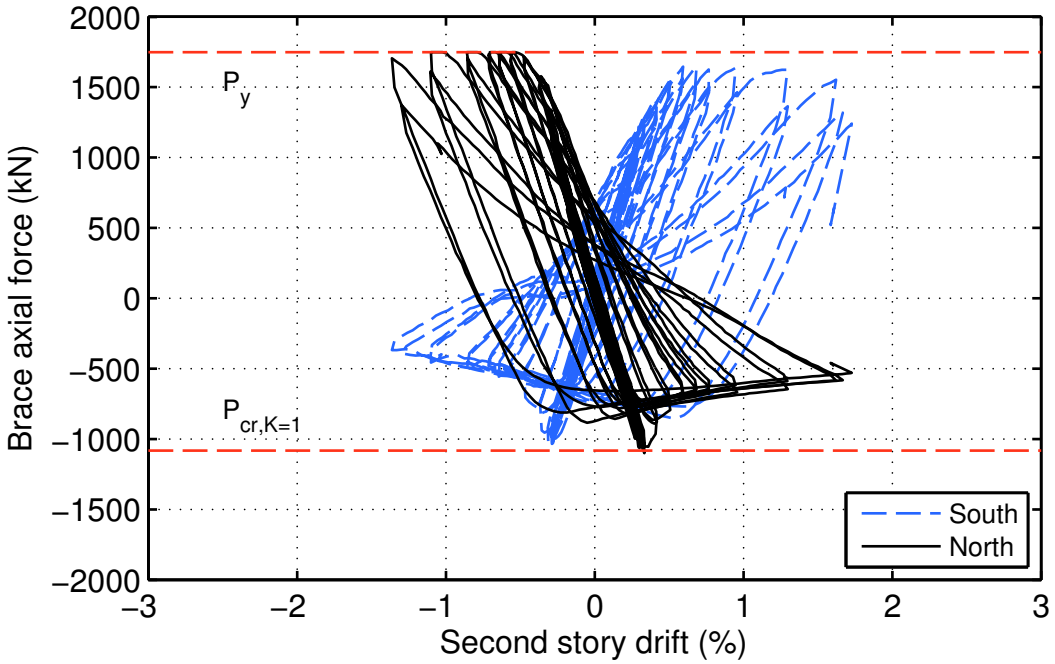

(b) Second story

Figure 5.16: TNCBF2-D-HSS brace elongation hystereses

force in tension corresponds to beam yielding instead of brace yielding, recognizing that beam strength may control demand.

The effective yield force, $P_{y,eff}$, can be determined from plastic analysis of the general beam mechanism shown in Fig. 5.17. The variables required to analyze the mechanism are listed in Table 5.1. The plastic moment capacity of the beam at its ends and mid-span may differ due to the degree of composite action of the slab under positive bending.

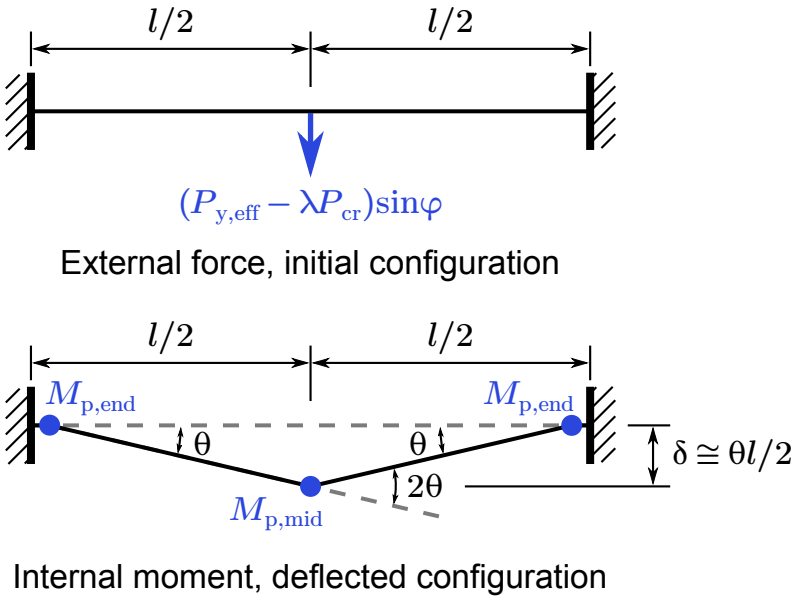

Figure 5.17: Plastic mechanism for braced frame beam

Given the model presented in Fig. 5.17, an expression for $P_{y,eff}$ can be determined by equating external and internal virtual work.

$$\sum W_{EXT} = \sum W_{INT} \tag{5.1}$$

$$(P_{y,eff} - \lambda P_{cr})\,\delta \sin\phi = M_{p,mid}(2\theta) + 2M_{p,end}\theta \tag{5.2}$$

$$(P_{y,eff} - \lambda P_{cr})\,\frac{\theta l}{2} \sin\phi = 2\theta\,(M_{p,mid} + M_{p,end}) \tag{5.3}$$

Isolating $P_{y,eff}$ in Eq. 5.3 and enforcing that the effective yield force of the brace due to the weak

Table 5.1: Variables in plastic mechanism to predict brace force

Variable	Description	Comments
$P_{\text{y,eff}}$	Brace effective yield force in tension	Unknown prior to analysis
P_{cr}	Brace critical buckling load	
$M_{\text{p,end}}$	Beam plastic moment capacity at ends	0 for pinned ends
$M_{\text{p,mid}}$	Beam plastic moment capacity at mid-span	May include composite action
l	Beam clear span	
λ	Proportion of P_{cr} at $P_{\text{y,eff}}$	< 1
ϕ	Brace-to-beam angle	

beam cannot exceed the yield force of the brace leads to the desired expression in Eq. 5.4.

$$P_{\text{y,eff}} = \lambda P_{\text{cr}} + \frac{4\left(M_{\text{p,mid}} + M_{\text{p,end}}\right)}{l \sin\phi} \leq P_{\text{y}} \tag{5.4}$$

To validate this model for determining the maximum brace force in tension, the first story of TNCBF2-D-HSS is examined. This particular frame was selected because unlike the TNCBF1 tests, its beam end connections and composite action are well defined. The plastic moment capacity of the beam at its ends is taken to be the plastic moment capacity of the steel alone, since negative bending is expected to occur at the ends. The plastic moment capacity of the beam at its mid-span is taken to be the plastic moment capacity of the partially composite section. A compressive strength degradation of 30% ($\lambda = 0.3$) was assumed, since this matches the expected post-buckling brace strength in the Seismic Provisions (AISC 2010a). These values, along with the frame geometry, are defined in Table 5.2.

Substituting the values in Table 5.2 in Eq. 5.4 results in an effective brace yield force in tension of 1663 kN. Note that the yield strength of the brace is 1748 kN. The effective yield force is marked as a dashed line on the plot of the measured brace axial force versus story drift for the first story of TNCBF2-D-HSS in Fig. 5.18. This plot suggests that $P_{\text{y,eff}}$ is a better prediction of the maximum brace force in tension than the yield strength of the brace. The difference in force is small in this instance, but it could be significant for weaker beams. Further analyses are required to validate this method for use in practice.

Table 5.2: TNCBF2-D-HSS variables for beam plastic analysis

Variable	Value	
P_{cr}	1069	kN
$M_{\text{p,end}}$	558750	kN-mm
$M_{\text{p,mid}}$	886908	kN-mm
l	5948	mm
λ	0.3	
ϕ	46.4	degrees

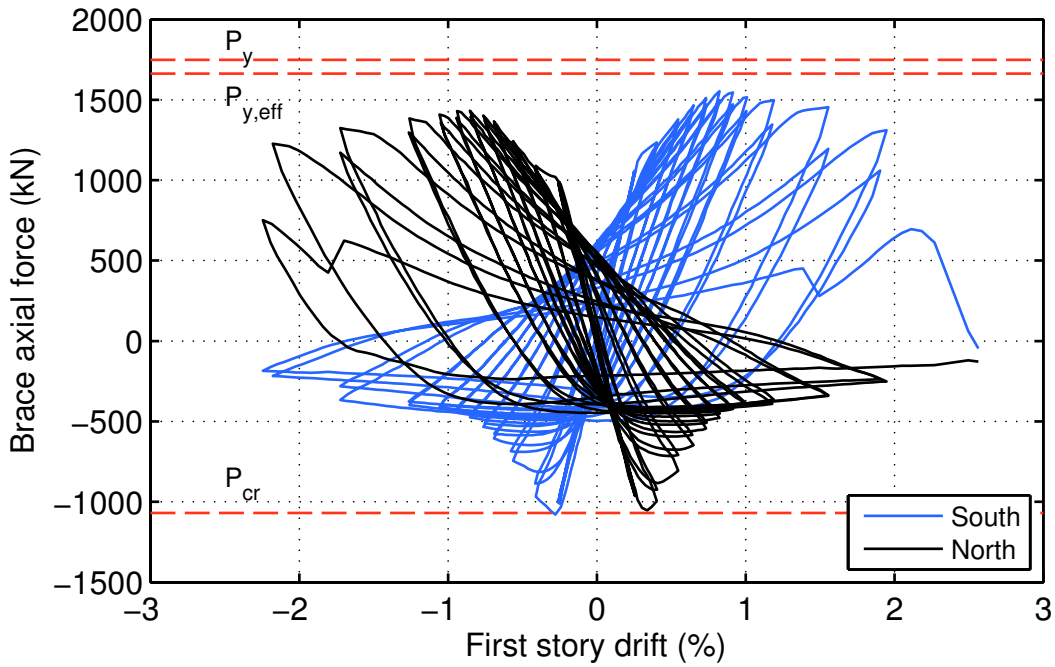

Figure 5.18: TNCBF2-D-HSS first story brace axial force hystereses with effective brace yield force in tension

5.3.2 Brace Vertical Unbalanced Force

Brace vertical unbalanced force hystereses are plotted in Figs. 5.19 through 5.22. The unbalanced forces are calculated using the vertical in-plane components of the brace axial forces. Positive and negative force indicate the force was directed upward and downward, respectively.

In TNCBF1-N-HSS, the first story unbalanced force was directed upward in positive drifts and downward in negative drifts after the south brace fractured. This makes sense considering the post-fracture EBF behavior. Interestingly, the magnitude of the maximum negative unbalanced force was greater than that of the positive unbalanced force, which indicates some composite activation of the slab in positive bending, even though the first story contained no shear connectors.

The first story response of TNCBF1-R-HSS may be considered typical for CBFs, where the unbalanced force at both positive and negative drift peaks is negative, tending to pull the beam down. The magnitude of the force continued to increase until brace fracture (the final cycle), indicating that the beam did not reach its plastic capacity. Throughout load reversal, positive unbalanced loads occur since the braces reload in compression faster than in tension.

TNCBF1-R-WF shows the expected CBF brace unbalanced force response initially on the first story, but the force decreases at later drifts (approximately greater than 1% in magnitude). However, considering the observed damage in the first story beam, this was due to beam-to-column connection damage and not plastic hinging. As weld and base metal cracks developed in the beam-to-column connections, they could no longer resist moment, altering the plastic capacity of the beam. The second story response is highly atypical, but can be explained by fracture of the corner brace splice connections. After the connections fractured, the braces could not develop tensile force but could develop compressive force via bearing on the first story slab.

Both stories of TNCBF2-D-HSS behaved largely as described for the first story of TNCBF1-R-HSS. It appears that the second story developed high positive unbalance forces, but this may result from inaccurate readings in the south brace strain gauges.

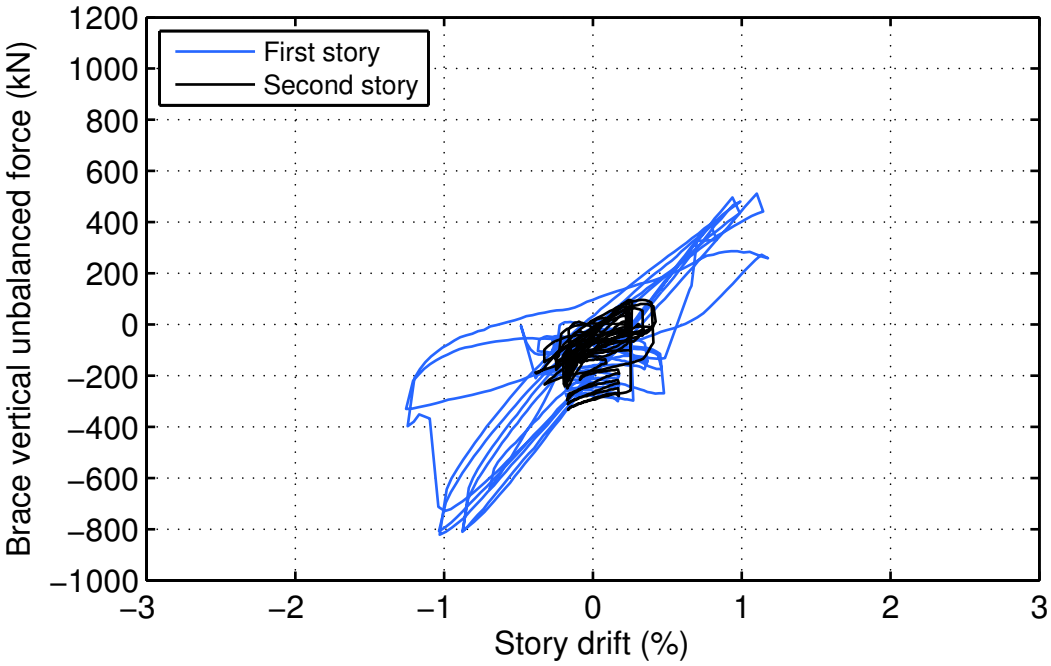

Figure 5.19: TNCBF1-N-HSS brace unbalanced force hystereses

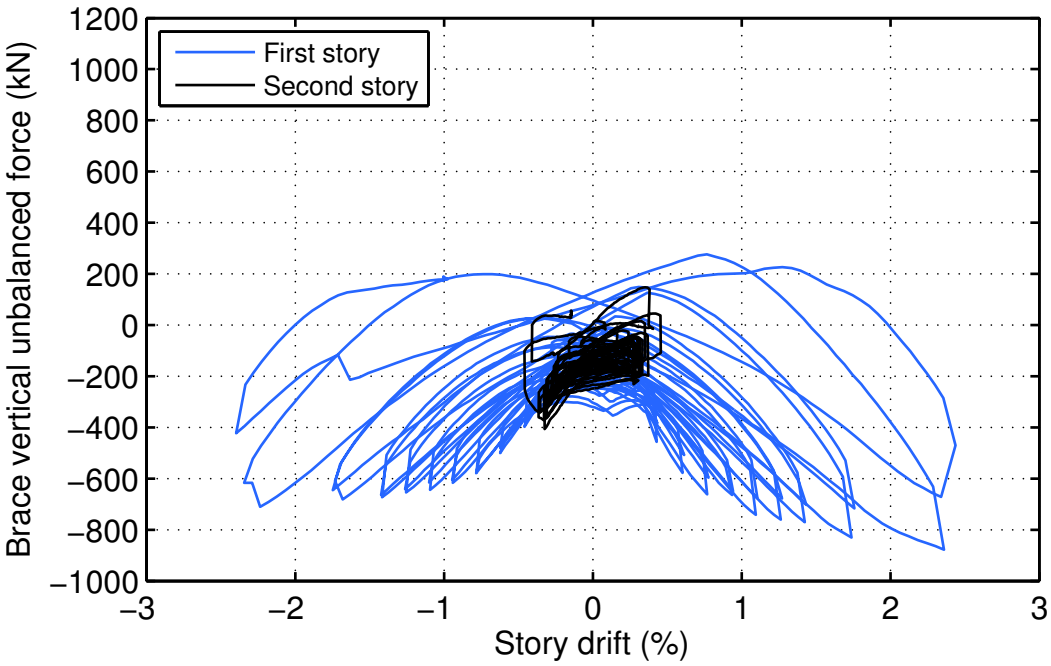

Figure 5.20: TNCBF1-R-HSS brace unbalanced force hystereses

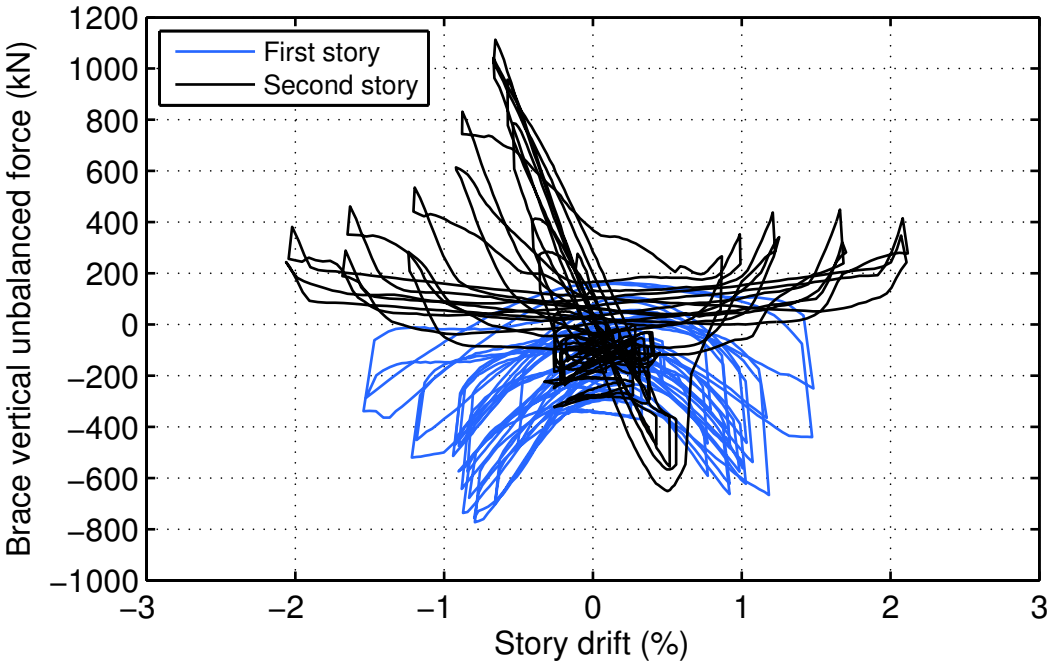

Figure 5.21: TNCBF1-R-WF brace unbalanced force hystereses

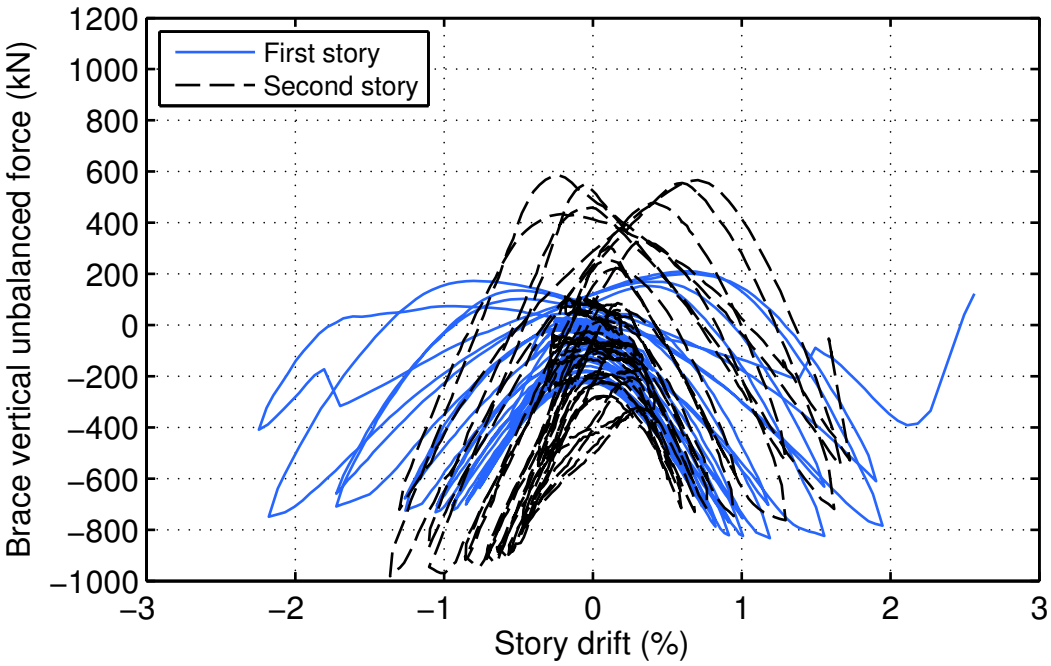

Figure 5.22: TNCBF2-D-HSS brace unbalanced force hystereses

5.3.3 Brace Elongation

Brace elongation curves are plotted in Figs. 5.23 and 5.24. Elongation was measured directly using string potentiometers along each brace's longitudinal axis. Data from TNCBF1-N-HSS is not shown due to the very brief nature of inelastic brace response prior to fracture. Data from TNCBF1-R-HSS is not available because the string potentiometers along the first story brace lengths were arranged to measure in-plane buckling; out-of-plane buckling of the braces interfered with the ability to measure elongation. The second stories from TNCBF1 specimens are not shown because the braces did not buckle.

The plots show, as expected, that braces connected to weak beams (Figs. 5.23 and 5.24a) do not elongate in tension as much as braces connected to strong beams (Fig. 5.24b). Conversely, weak beams deflect downward after brace buckling, resulting in greater shortening in compression.

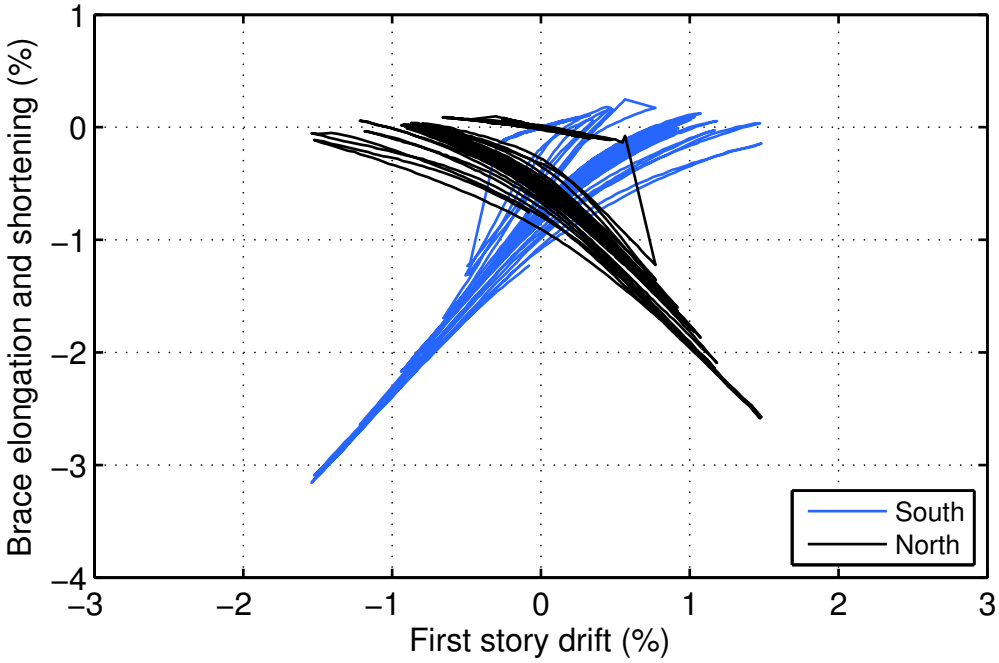

Figure 5.23: TNCBF1-R-WF first story brace elongation curves

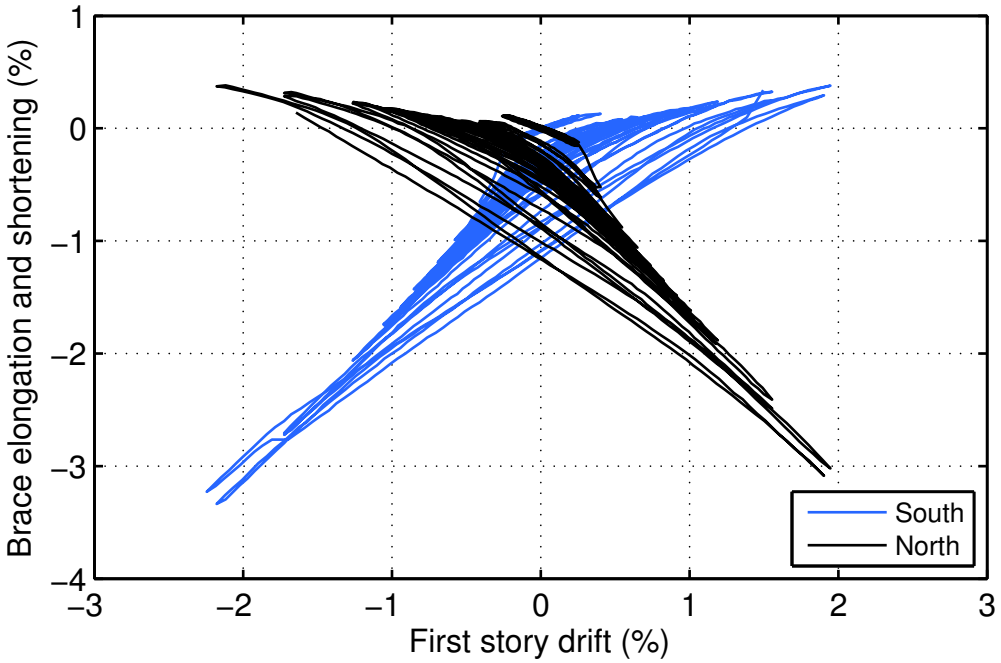

(a) First story

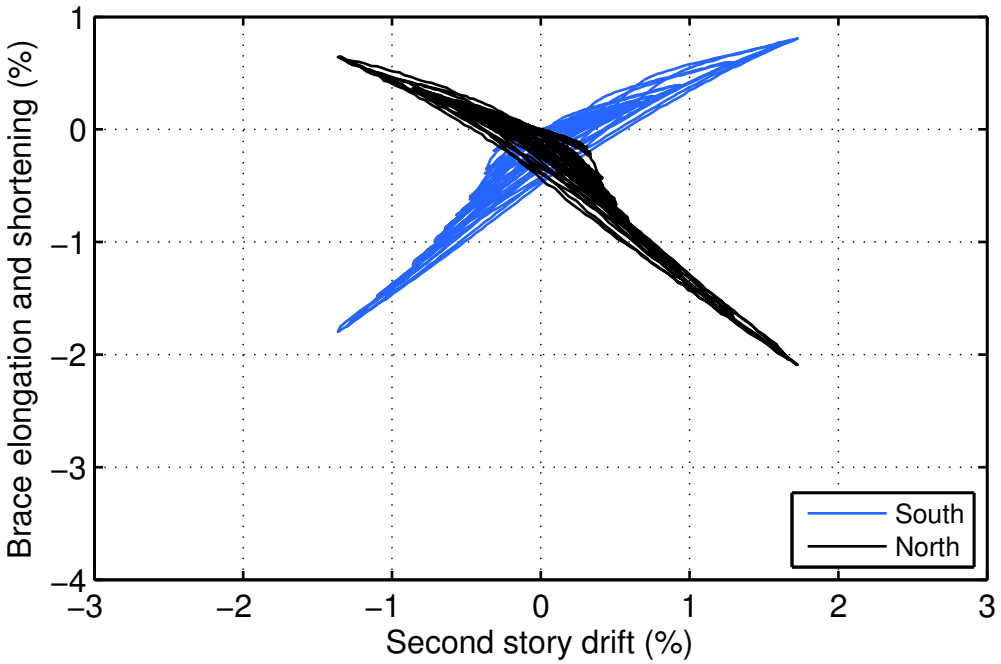

(b) Second story

Figure 5.24: TNCBF2-D-HSS brace elongation curves

5.3.4 Brace Out-of-Plane Mid-Span Deflection

The brace out-of-plane mid-span deflection hystereses for all braces that buckled are plotted in Figs. 5.25 through 5.28. In TNCBF1-N-HSS, this was measured using two string potentiometers oriented along the length of the brace, with one displacing out-of-plane with the brace and the other remaining in-plane measuring elongation. This method is suitable in theory, but less effective in practice due to error magnification when deriving deflection from the data (hence the considerable noise at small deformations in Fig. 5.25). In all other tests, out-of-plane deflection was measured directly with a string potentiometer oriented out-of-plane on a reference column. This method is less prone to error and hand measurements of brace deflection from the tests confirm the accuracy of the results.

The plots show that initial deflection due to brace buckling of HSS braces was less than that of wide flange braces. In addition, residual deflection when the braces were in tension was greater for wide flange braces. Braces connected to strong beams show a propensity to return to zero deflection in tension, as such braces yield and elongate in tension.

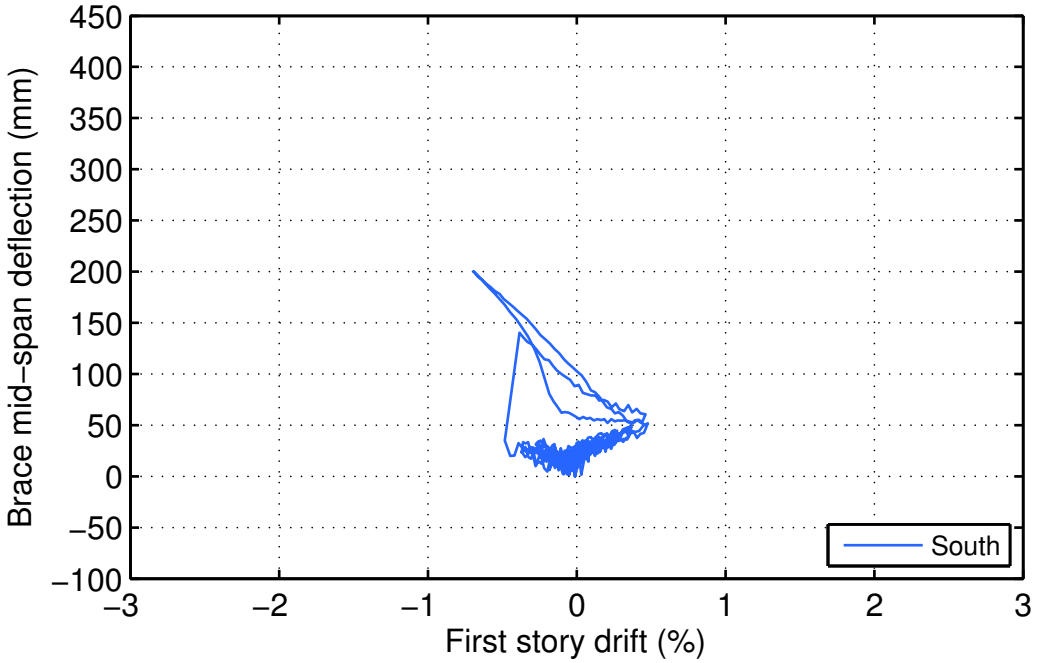

(a) First story

Braces did not buckle

(b) Second story

Figure 5.25: TNCBF1-N-HSS brace out-of-plane mid-span hystereses

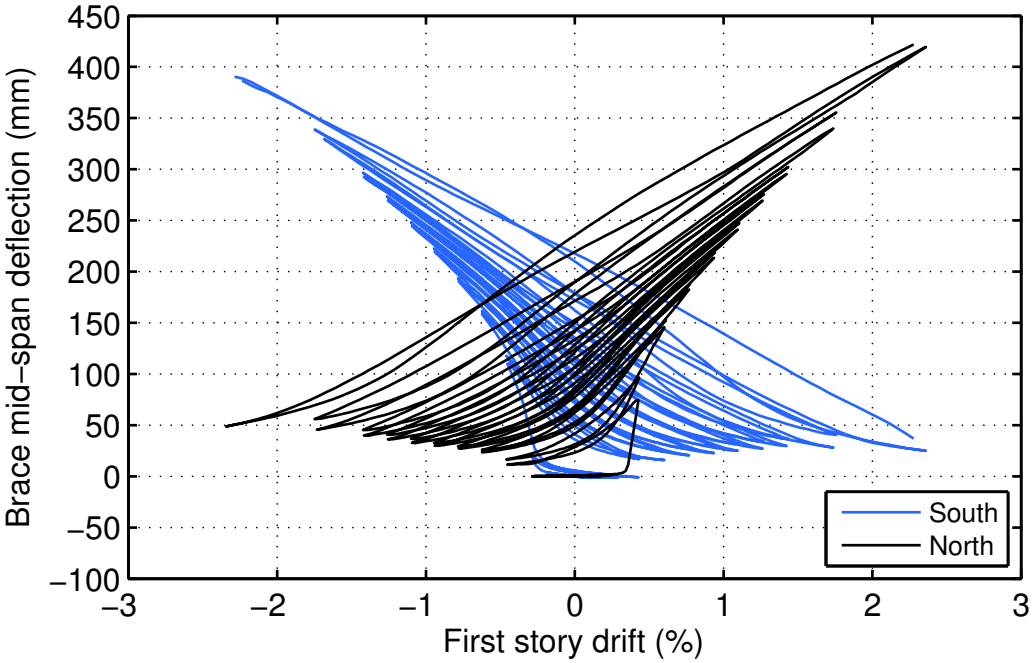

(a) First story

Braces did not buckle

(b) Second story

Figure 5.26: TNCBF1-R-HSS brace out-of-plane mid-span hystereses

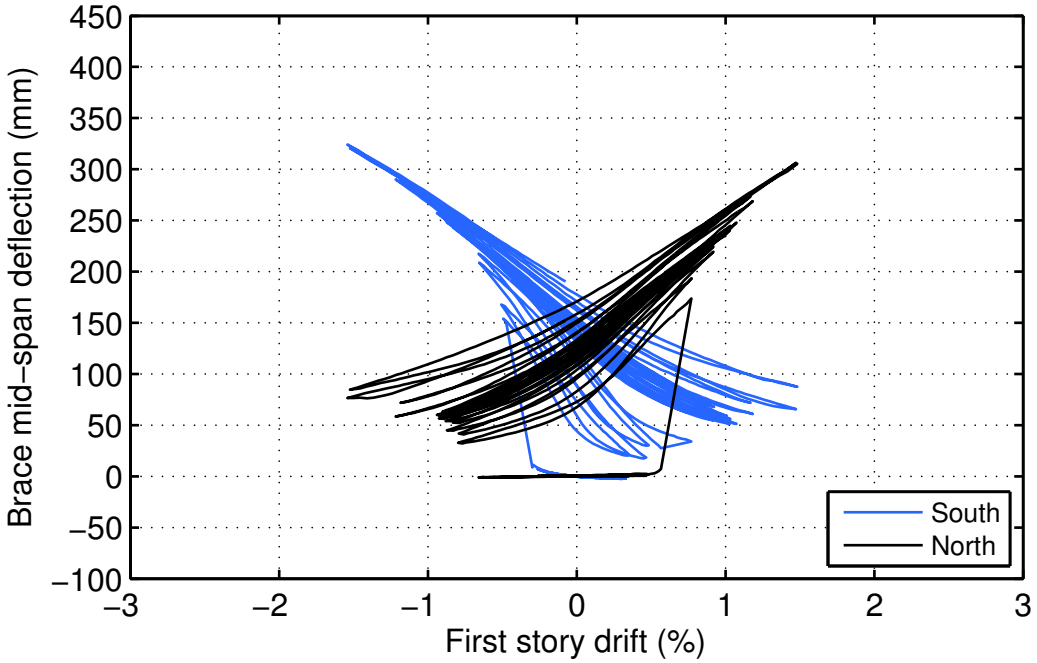

(a) First story

Braces did not buckle

(b) Second story

Figure 5.27: TNCBF1-R-WF brace out-of-plane mid-span hystereses

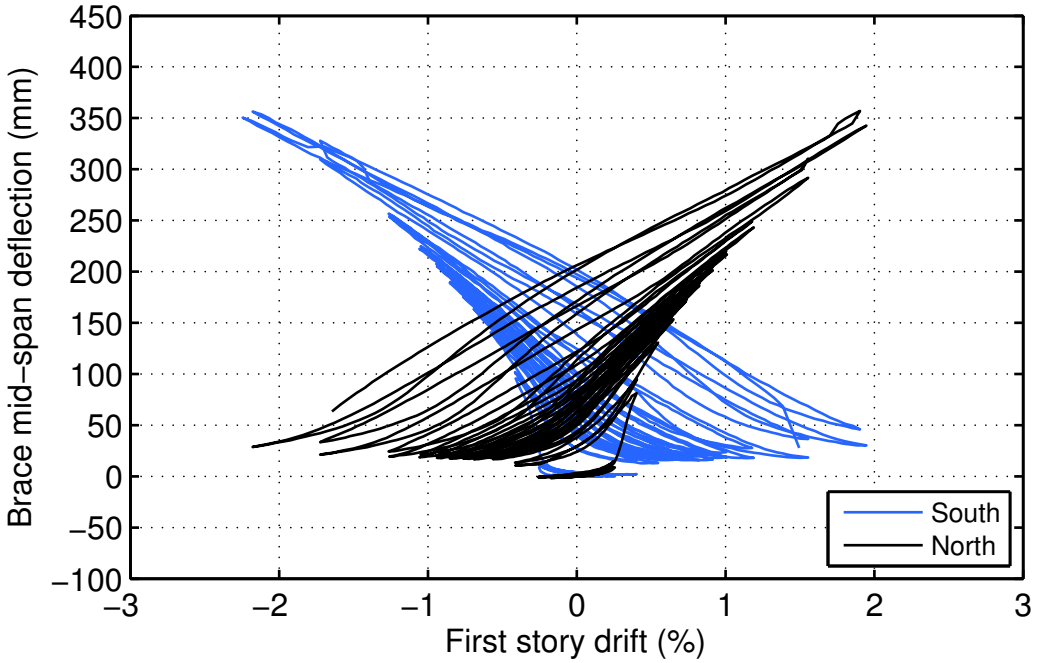

(a) First story

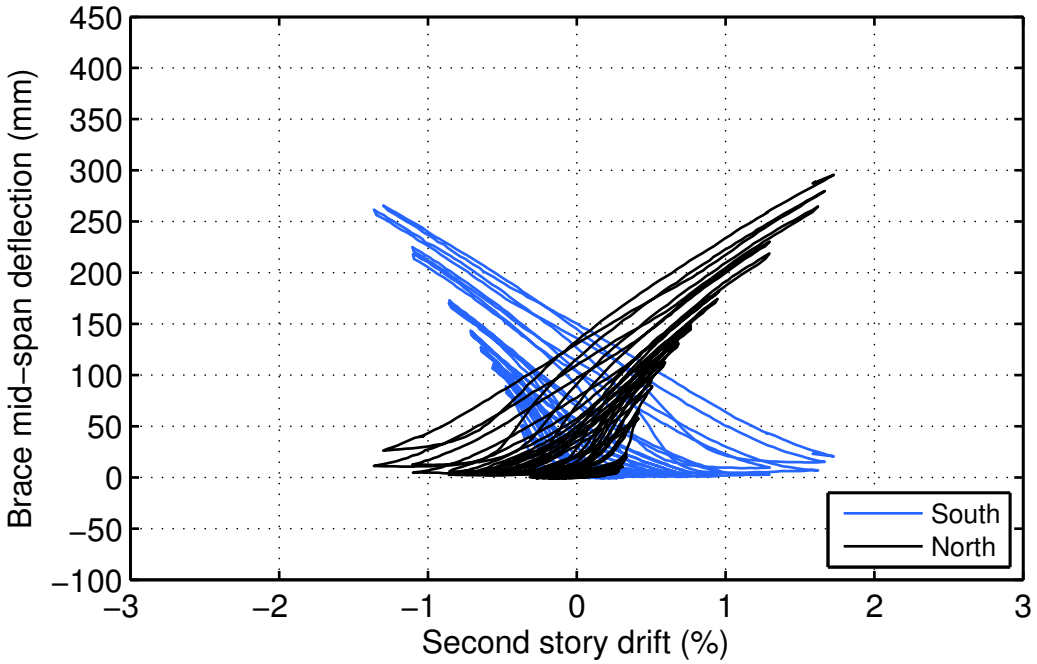

(b) Second story

Figure 5.28: TNCBF2-D-HSS brace out-of-plane mid-span hystereses

5.3.5 Brace Effective Length Factors

The brace effective length factors shown in Table 5.3 are back-calculated from the experimental critical buckling load of each brace. In all cases except the first story of TNCBF1-R-HSS, the brace end-to-end distance was used as the brace length. For the first story of TNCBF1-R-HSS, the knife plates acted as rigid brace ends when the braces buckled out-of-plane, so the knife plate end-to-end distance was used as the brace length. The yield stresses of the members are derived from coupon tests.

Table 5.3: Brace effective length factors

Specimen	Location	$P_{c,max}$ (kN)	Length, L (mm)	Effective length factor, K	Story buckling sequence
TNCBF1-N-HSS	1S	1392	3796	0.92	1
TNCBF1-R-HSS	1S	973.9	3885	0.97	1
	1N	1127	3885	0.84	2
TNCBF1-R-WF	1S	1085	3592	1.08	1
	1N	1261	3592	0.80	2
TNCBF2-D-HSS	1S	1079	3619	0.94	2
	1N	1054	3619	0.97	1
	2S	1061	3409	1.02	2
	2N	1100	3409	0.98	1

The calculated brace effective lengths help elucidate the fixity of the gusset plate connections. The first story gusset plates of TNCBF1-N-HSS had very little rotational clearance, the effective length factor of the south brace was still close to the theoretical pinned-pinned case ($K = 1$) at 0.92. The weak beam may have affected this response by increasing the flexibility of the mid-span connection. This same reasoning is thought to be the reason why the first story braces buckled out-of-plane in TNCBF1-R-HSS, yet the effective length factors of the braces were less than 1 and do not seem to confirm that the effective length of the brace extended into the beam. On the other hand, the rotational clearance of the gusset plates were low to attempt to induce in-plane buckling, which would tend to shift the effective length factor less than 1. The bottom end of the brace

The results from TNCBF1-R-WF are not intuitive. The gusset plates were designed using the

BDP (Roeder et al. 2011b) and Lehman et al. (2008) recommend a K value of 1 for determining the critical buckling load of braces with adequate clearance. An effective length factor greater than 1, as seen in the south brace, is not surprising given the flexibility of weak beam on the first story; however, the north brace had an effective length factor of 0.80. Possible reasons for such a low effective length factor include strain gauge inaccuracy (from which the brace forces are derived), minimal brace out-of-straightness prior to buckling, and buckling sequence. The latter The calculated effective length factors for TNCBF2-D-HSS are near 1 for braces on both stories, which confirms the findings by Lehman et al. (2008).

5.4 Beam Response

5.4.1 Beam Mid-Span Deflection

Beam deformation is expected to be severe in weak beam NCBFs with predominantly downward deflection due to the brace unbalanced load after buckling. Excessive deflections may be detrimental to non-structural systems and significant residual deformation may necessitate repair. The deflection at the beam mid-span was measured on both stories for each test using LVDTs, and their hysteretic responses are plotted in Figs. 5.29 through 5.32. Peak downward and upward deflections as well as residual deflections are documented in Table 5.4.

Table 5.4: Beam mid-span deflection maxima and residuals

Specimen	Story	Max. downward (mm)	Max. upward (mm)	Residual[a] (mm)
TNCBF1-N-HSS	1F	16.7	30.3	−3.1
	2F	0.8	6.4	0.5
TNCBF1-R-HSS	1F	62.4	0.6	−34.7
	2F	3.2	3.1	−0.8
TNCBF1-R-WF	1F	31.9	5.0	−11.9
	2F	3.5	7.3	0.1
TNCBF2-D-HSS	1F	49.4	0.2	−23.3
	2F	9.5	1.4	−1.3

[a] Residual deflection relative to beginning of test

Most first story deflection in TNCBF1-N-HSS (Fig. 5.29) is associated with the EBF mechanism that developed after fracture of the south first story brace. Its greatest deflection was upward and due to the activation of composite action under positive bending. Downward deflection of the first story was greatest in TNCBF1-R-HSS, since nearly all inelastic deformation was concentrated in the first story. Even so, the total maximum deflection of TNCBF1-R-WF (i.e. including residual from TNCBF1-R-HSS) was slightly higher than TNCBF1-R-HSS. As expected, the magnitude of deflection of the strong second story beam was consistently less than that of the weak first story beam. In TNCBF2-D-HSS, when both sets of braces buckled, the first story beam deflection was often over twice as large as the second story beam deflection at comparable story drifts.

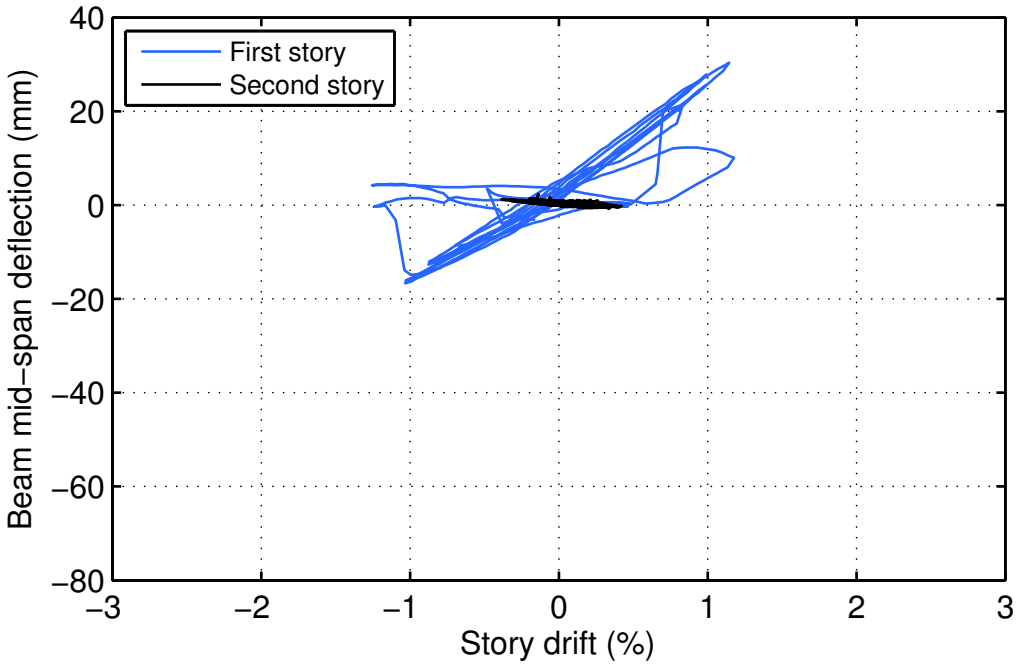

Figure 5.29: TNCBF1-N-HSS beam vertical deflection hystereses

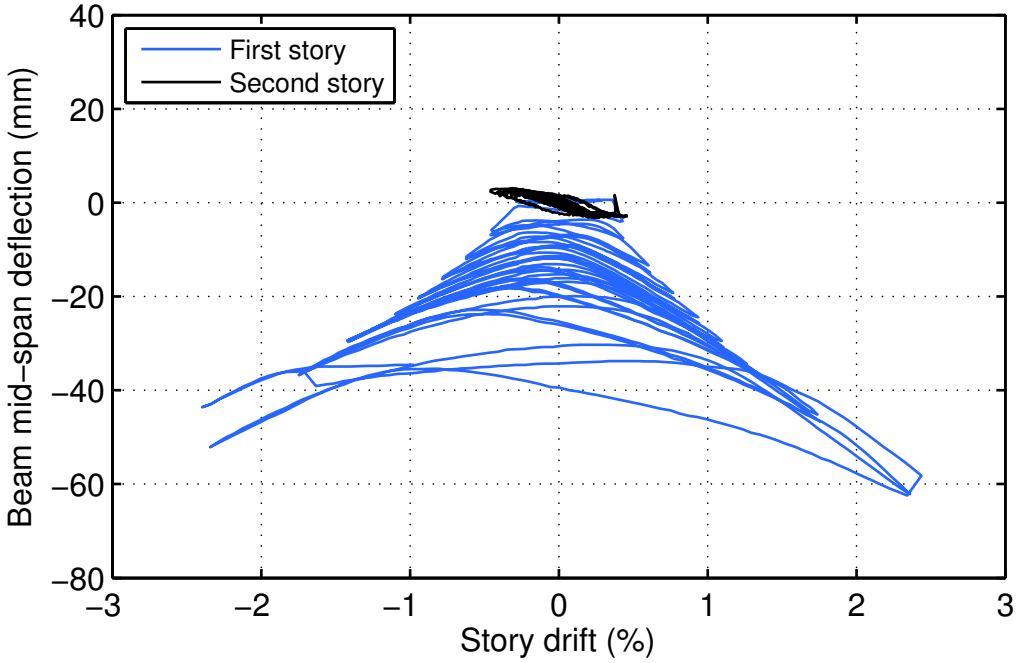

Figure 5.30: TNCBF1-R-HSS beam vertical deflection hystereses

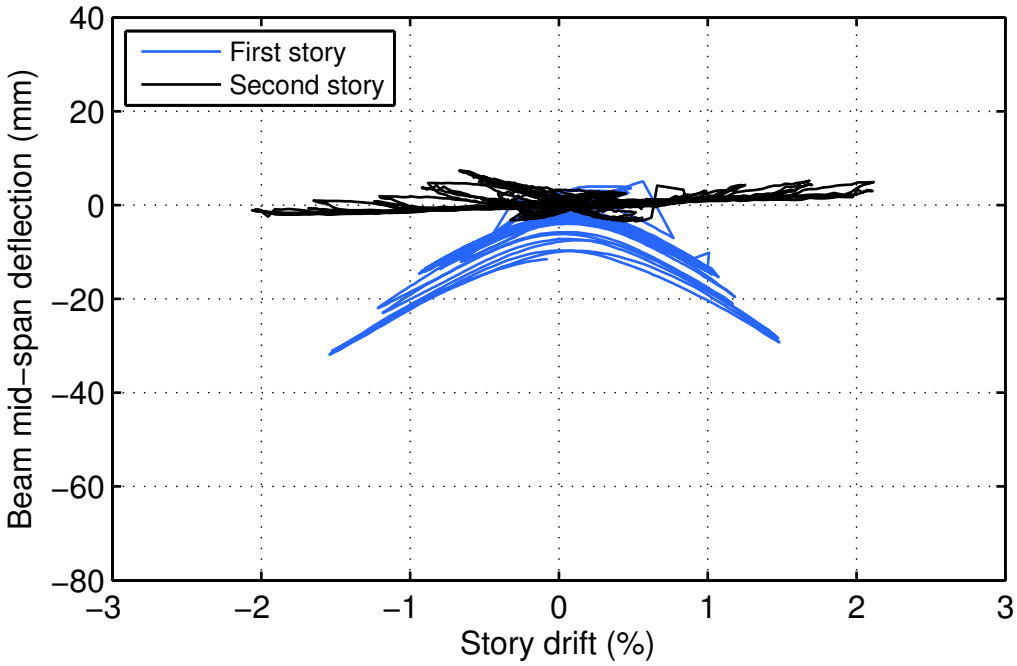

Figure 5.31: TNCBF1-R-WF beam vertical deflection hystereses

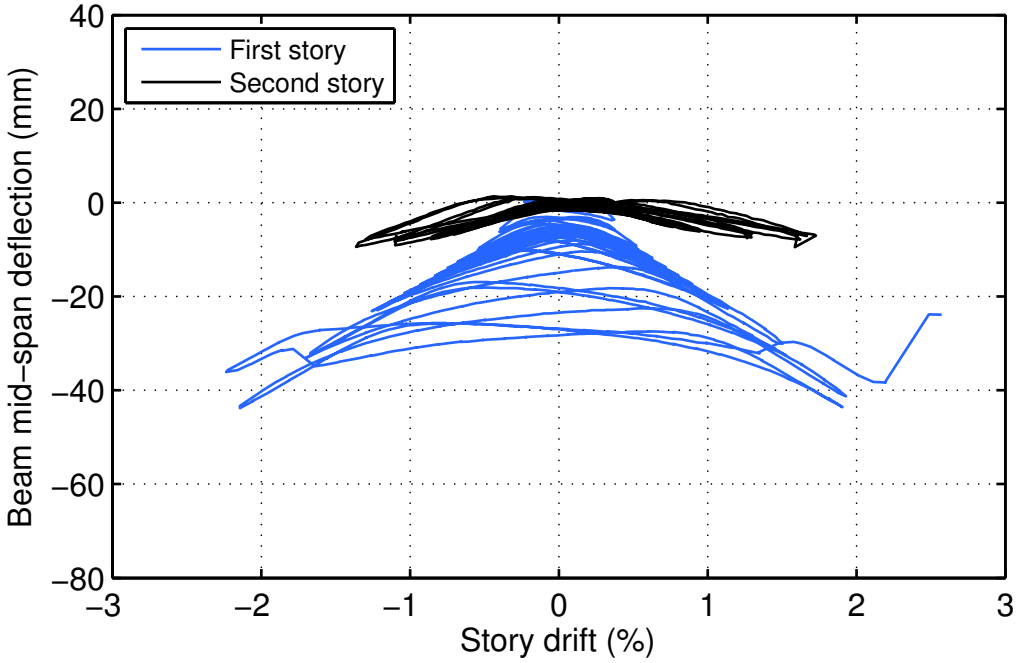

Figure 5.32: TNCBF2-D-HSS beam vertical deflection hystereses

5.4.2 Beam Torsion

The AISC Seismic Provisions 2010a recognizes that beams in chevron braced frames are particularly susceptible to lateral-torsional buckling since buckled braces direct a portion of their axial load out-of-plane. Hence, beam lateral bracing must be provided at the brace intersection in SCBFs. Many NCBFs fail to meet this requirement and may incur inelastic torsional deformation and/or lateral-torsional buckling in the event of brace buckling. Note that when both braces buckle in the same direction, their out-of-plane force components tend to negate one another; when the braces buckle in opposing directions, their out-of-plane force components coalesce. However, in general, buckling direction is not controlled in braced frames.

Beam mid-span torsional rotation was measured using Optotrak LEDs. Rotation was derived considering the geometry in Fig. 5.33. The locations x and y are can be derived directly from the Optotrak output, which gives the coordinates of each LED at each time step. The angle between any two LEDs is then given by Eq. 5.5 and the angle of rotation at step i is given by Eq. 5.6. Note that the locations of the LEDs on the section are arbitrary, but accidentally capturing web deformation was avoided by using LEDs located on web stiffeners when possible.

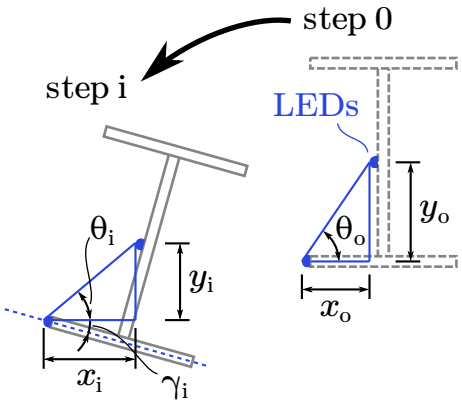

Figure 5.33: Beam torsional rotation geometry

$$\theta = \text{atan}(y/x) \tag{5.5}$$

$$\gamma_{\mathrm{i}} = \theta_{\mathrm{o}} - \theta_{\mathrm{i}} \tag{5.6}$$

The TNCBF1 first story beams were not braced at their mid-spans but the TNCBF2-D-HSS first story beam was. Plots of the torsional rotation hystereses of these beams are shown in Figs. 5.34 through 5.37. In TNCBF1-N-HSS, torsional rotation was small but limited by the ductility of the frame. The most torsional deformation occurred in TNCBF1-R-HSS, which makes sense because its gusset plates had low rotational clearances and the braces buckled in opposing directions. The first story braces of TNCBF1-R-WF also buckled in opposing directions, but torsional rotation was much smaller, as might be expected due to greater gusset plate rotational clearance. Torsional rotation of the first story beam of TNCBF2-D-HSS was the smallest among the tests due to adequate gusset plate rotational clearnace, braces buckling in the same direction, and lateral bracing at the beam mid-span.

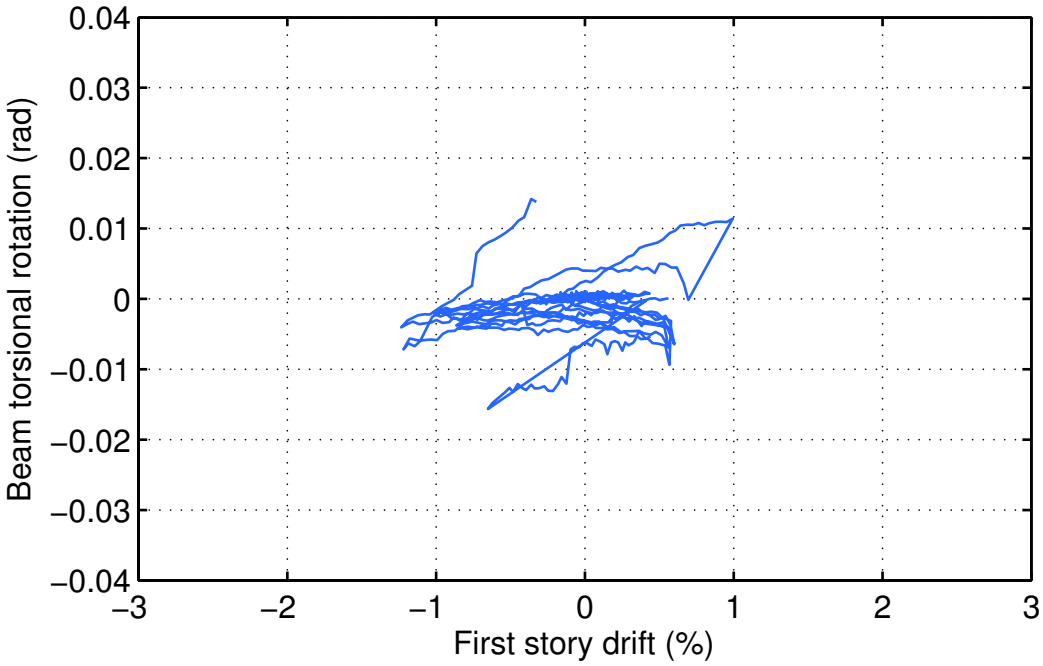

Figure 5.34: TNCBF1-N-HSS beam mid-span torsional rotation

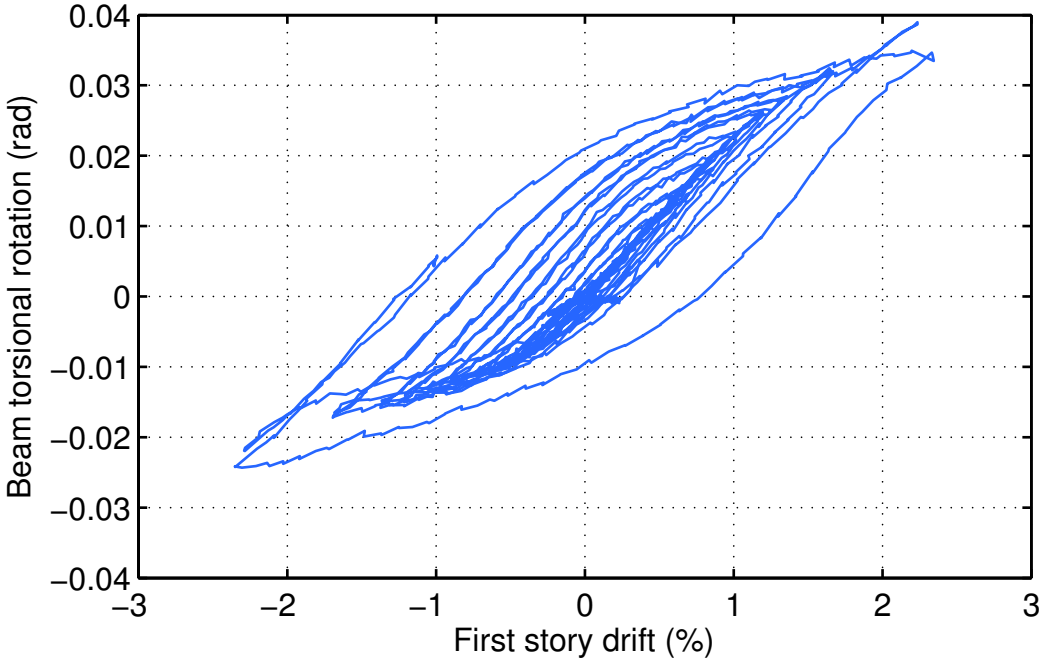

Figure 5.35: TNCBF1-R-HSS beam mid-span torsional rotation

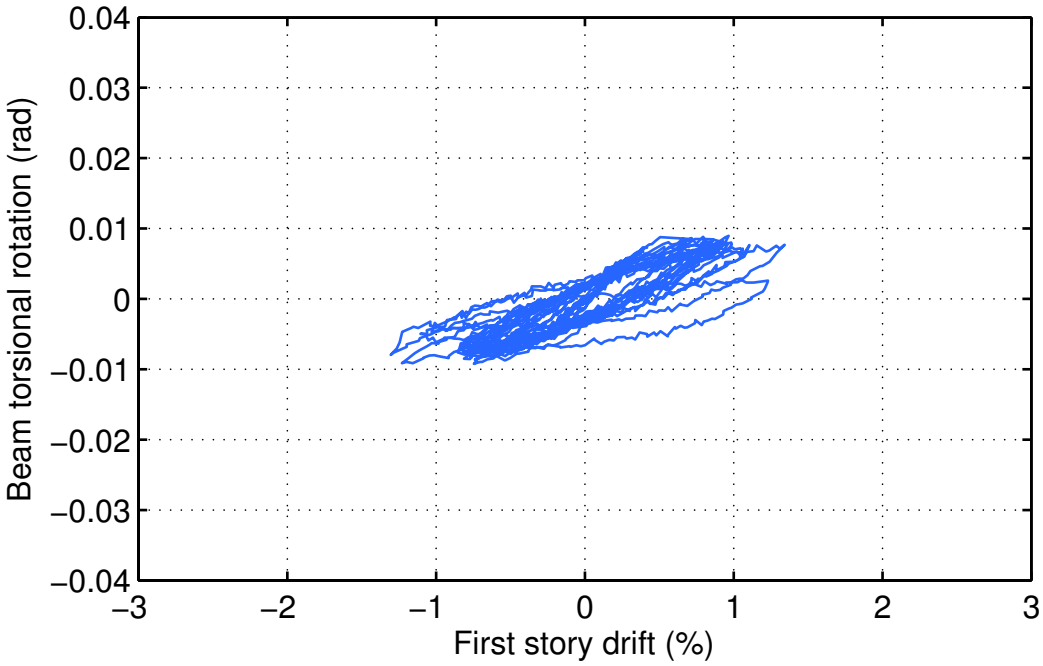

Figure 5.36: TNCBF1-R-WFS beam mid-span torsional rotation

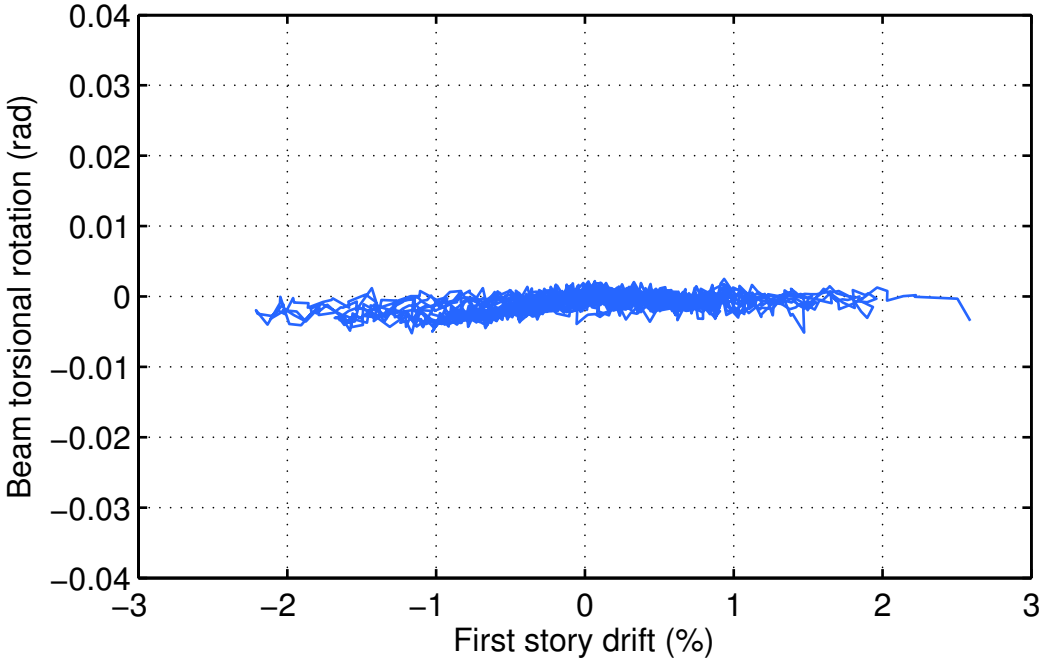

Figure 5.37: TNCBF2-D-HSS beam mid-span torsional rotation

5.5 Frame Response

5.5.1 Story Shear Contribution

In CBFs, the braces are designed as the primary lateral force resisting members, but the frame invariably contributes to story shear as well, particularly after the braces buckle. When a brace buckles, the force it is able to resist in compression degrades beyond the critical buckling load in further cycles. This is recognized in the Seismic Provisions (AISC 2010a), where the beam in chevron configuration CBFs must be analyzed for the unbalanced load, assuming the compression brace has degraded to 30% of its critical buckling load. It is clear that the lateral resistance of the braces must lessen after buckling, yet before brace fracture, the lateral resistance of the entire story remains stable, as Fig. 5.6 demonstrates. The additional resistance must come from the frame, and often the columns become secondary lateral force resisting members. This is especially the case in weak column-strong beam frames, which may be particularly common in SCBFs due to design for the unbalanced load.

Fig. 5.38 shows the column shear contribution to story shear for the ductile stories in the TNCBF series–the first story of TNCBF1-R-HSS and both stories of TNCBF2-D-HSS. Prior to brace buckling, the columns constitute around 5 to 10% of the total story shear. After brace buckling, the contribution of column shear steadily increases. The first stories of TNCBF1-R-HSS and TNCBF2-D-HSS, each with weak beams, responded similarly and approached 50% story shear carried by the columns. The second story columns of TNCBF2-D-HSS resisted a significantly lower proportion of story shear than its first story counterparts. This effect is attributed to greater strength degradation of the first story (weak beam) braces. In either case, however, the columns clearly participate in lateral force resistance after brace buckling and their strength may have a considerable effect on CBF performance.

Predicting Maximum Lateral Resistance of Braces

It is clear from the above discussion that braces in braced frames are not the sole contributors to lateral resistance of the frame. However, for design purposes, the braces are intended to resist the entire lateral load. Plastic analysis suggests that the maximum lateral resistance provided by the braces occurs when opposing braces yield in tension and buckle in compression simultaneously. To

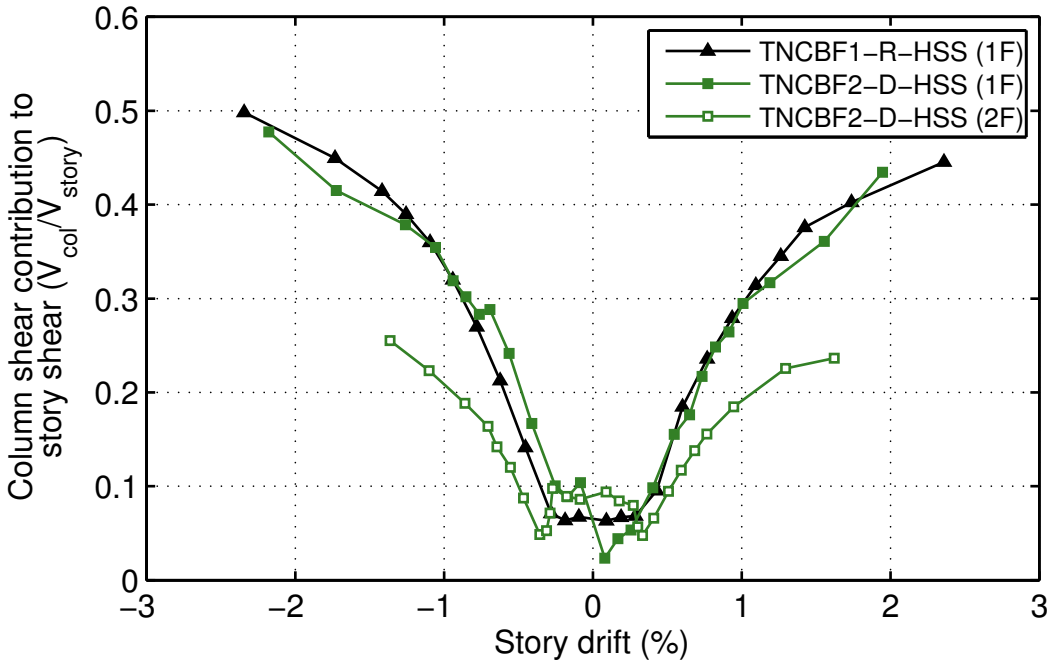

Figure 5.38: Column shear contribution to story shear backbone curves

evaluate the adequacy of this assumption, the lateral resistance of the braces was calculated as the difference of the base shear and column shears. Resistance was then normalized by the plastic load case given by Eq. 5.7. Fig. 5.39 shows backbones of brace lateral resistance normalized by Eq. 5.7 for the best performing TNCBF tests and the TCBF2 tests. None of the frames reached the plastic load case. TCBF2-WF reached 92% of the plastic lateral resistance, the most of all the analyzed specimens. On the other end of the spectrum, the maximum lateral resistance of the first story of TNCBF2-D-HSS was just 74% of the load–a very large difference.

$$V_{\mathrm{br,p}} = (P_{\mathrm{y}} + P_{\mathrm{cr}}) \cos \phi \tag{5.7}$$

Since none of the TNCBF or TCBF2 specimens were achieved the plastic limit, it is logical to conclude that the weak beams tested did not limit combined brace strength. Examining the brace force hystereses in Figs. 5.13 through 5.16 reveals that brace buckling and yielding do not coincide. Just prior to buckling, braces are typically elastic and consequently carry the same magnitude of

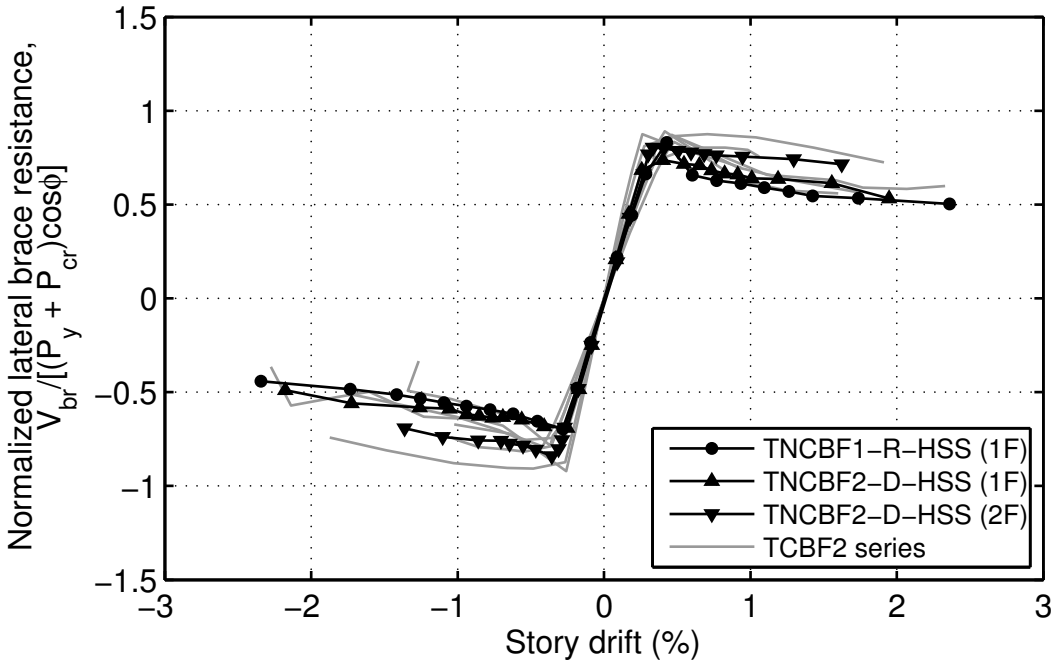

Figure 5.39: Brace lateral resistance backbones normalized by plastic load case

force. However, after buckling, the force in the compression brace drops immediately and degrades in future cycles. Thus, even if a brace does yield in tension, as in the second story of TNCBF2-D-HSS, the compression brace is no longer at its critical buckling load. With this in mind, the maximum lateral brace resistance a frame may achieve may occur at the moment just before brace buckling, when the braces are still elastic. In this case, the lateral resistance of the braces are given by Eq. 5.8. Brace lateral resistance backbones normalized by Eq. 5.8 are shown in Fig. 5.40. On average, the maximum resistance tends to be closer to this elastic capacity. Data analysis of more experimental and computational data is required to validate this idea and more research should be conducted to determine why some frames exceed the proposed limit.

$$V_{\mathrm{br,e}} = 2P_{\mathrm{cr}} \cos\phi \tag{5.8}$$

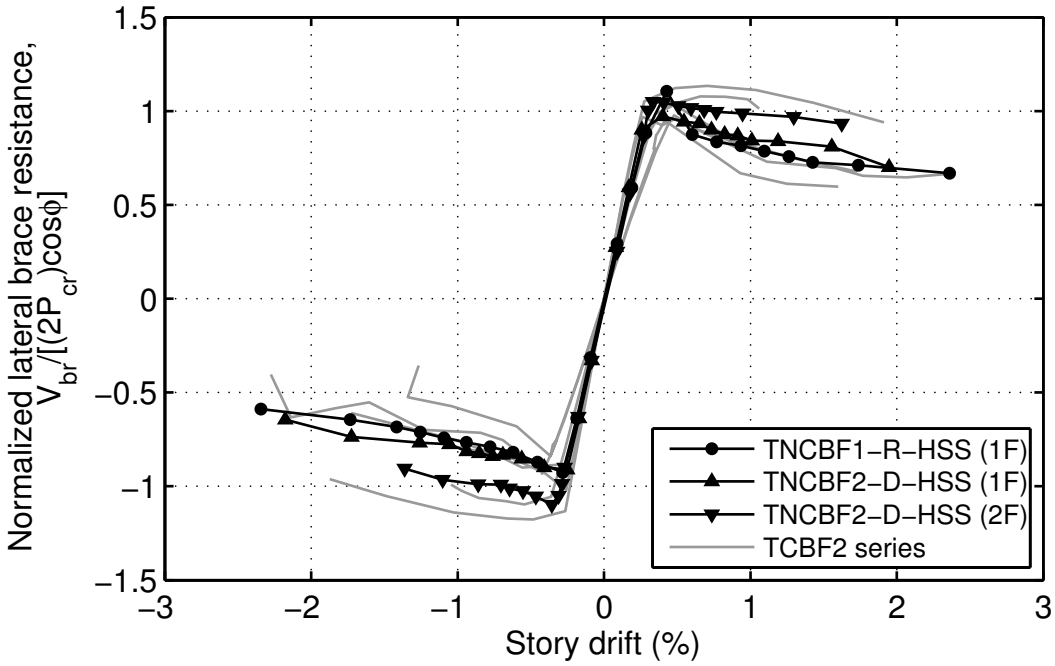

Figure 5.40: Brace lateral resistance backbones normalized by plastic load case

5.5.2 Brace Unbalance-Beam Deflection Response

To better understand the influence of the brace vertical unbalanced force on beam mid-span deflection, these two quantities are plotted as hystereses in Figs. 5.41 through 5.44. The second story beams for all specimens remained primarily elastic with only slight hysteretic responses. The first story hysteresis for TNCBF1-N-HSS shows that the beam was both stronger and stiffer in downward excursions (positive bending) due to composite action achieved with tack welds only. The response of the first story beam in TNCBF1-R-HSS was inelastic, but the amount of energy dissipated per cycle was not large (evaluated by the size and fullness of the hysteretic loops) since the unbalanced load does not fully reverse in each cycle, keeping the loading range much lower than a brace or column. Much different behavior can be seen on the first story of TNCBF1-R-WF, where the beam mid-span deflection continued to increase throughout the test despite decreasing unbalanced force. This is likely a consequence of beam-to-column connection damage, which impaired the ability of the connections to resist moment. A stiffer first story beam response is apparent for TNCBF2-D-HSS, which had well-defined moment connections unlike the other first story beams.

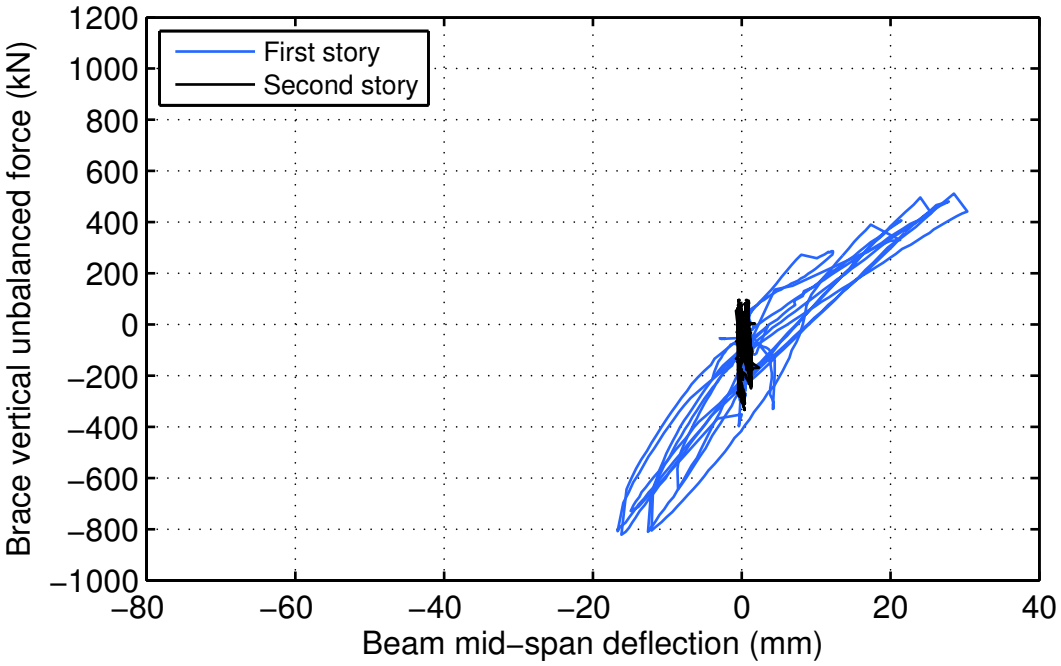

Figure 5.41: TNCBF1-N-HSS brace unbalanced force-beam vertical deflection hystereses

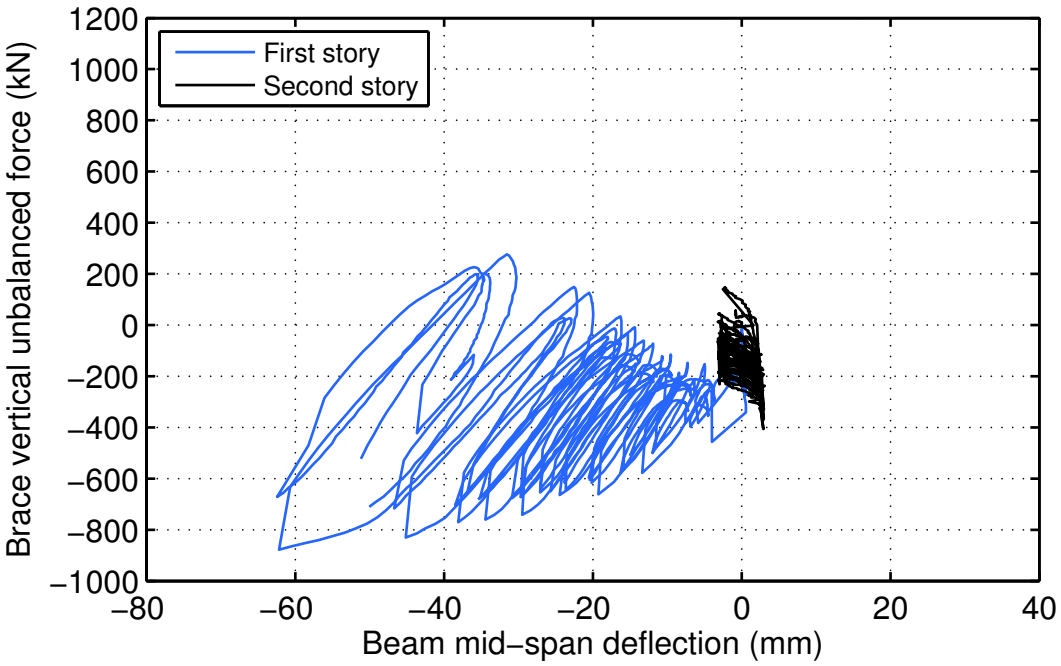

Figure 5.42: TNCBF1-R-HSS brace unbalanced force-beam vertical deflection hystereses

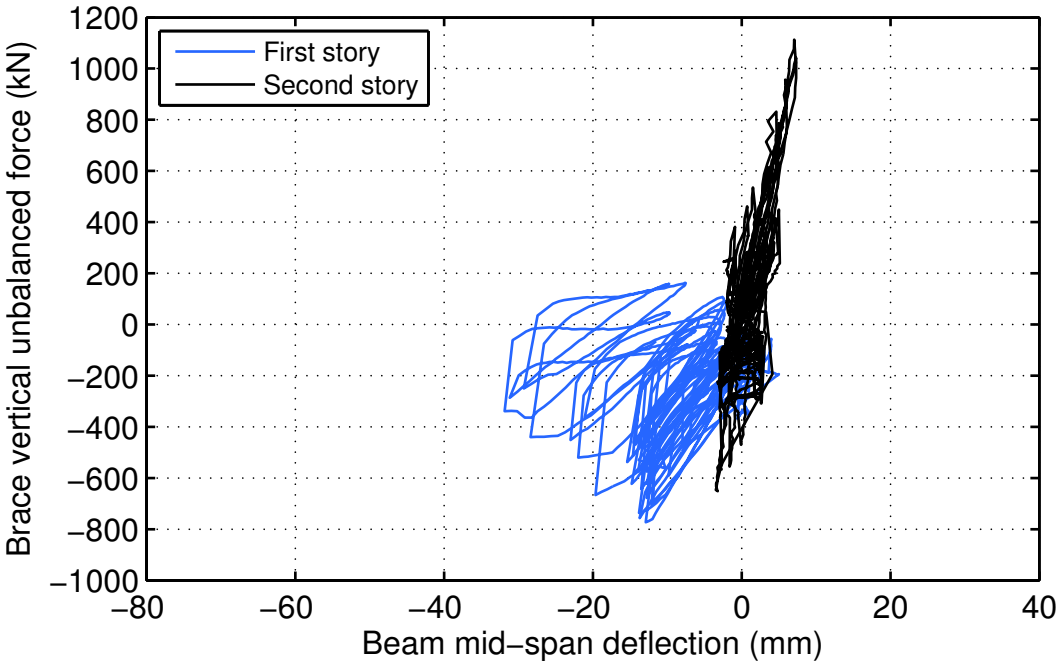

Figure 5.43: TNCBF1-R-WF brace unbalanced force-beam vertical deflection hystereses

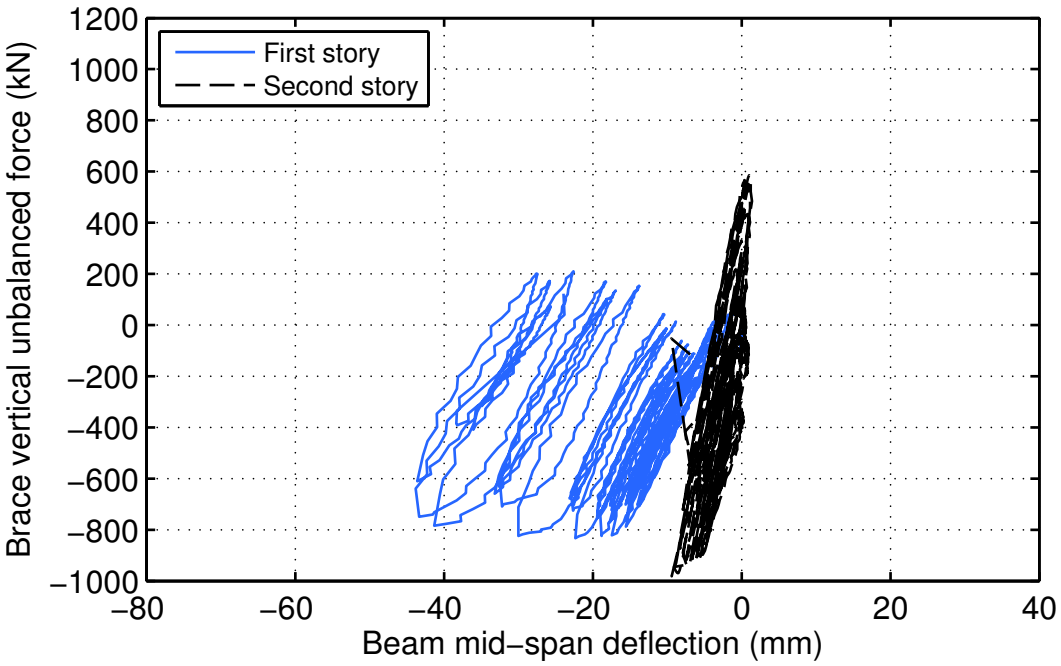

Figure 5.44: TNCBF2-D-HSS brace unbalanced force-beam vertical deflection hystereses

5.6 Connection Response

5.6.1 Gusset Plate Rotation

When braces buckle out-of-plane, their adjacent gusset plates deform to accommodate brace end rotation. This rotation was measured in the tests using sensors located on the gusset plates and braces as in Fig. 5.45. If two sensors were used as shown on the left-hand side of the figure, the corresponding gusset plate rotation, θ_{gp}, is approximated by Eq. 5.9. If three sensors were used, the gusset plate rotation can be more accurately calculated as Eq. 5.10. If two optical sensors are used, the rotation is calculated similarly to Eqs. 5.5 and 5.6, except y is replaced by d_3.

$$\theta_{\text{gp}} = \text{atan}\left(\frac{(s_{\text{i}} + s_{\text{j}})/2}{d_1}\right) \tag{5.9}$$

$$\theta_{\text{gp}} = \text{atan}\left(\frac{(s_{\text{i}} + s_{\text{j}})/2 - s_{\text{k}}}{d_2}\right) \tag{5.10}$$

Plots of gusset plate rotation hystereses are provided in Figs. 5.46 through 5.49. The first story corner gusset plate rotation could not be obtained due to instrumentation error and gusset plates connecting to braces that did not buckle are omitted. Gusset plate rotations appear to be about the same at the corner and mid-span brace ends, suggesting that the deflected shape of the brace was essentially symmetric about its midpoint. In addition, the shapes of the hystereses appear to be about the same as those of the corresponding brace out-of-plane deflection hystereses, as expected from kinematics.

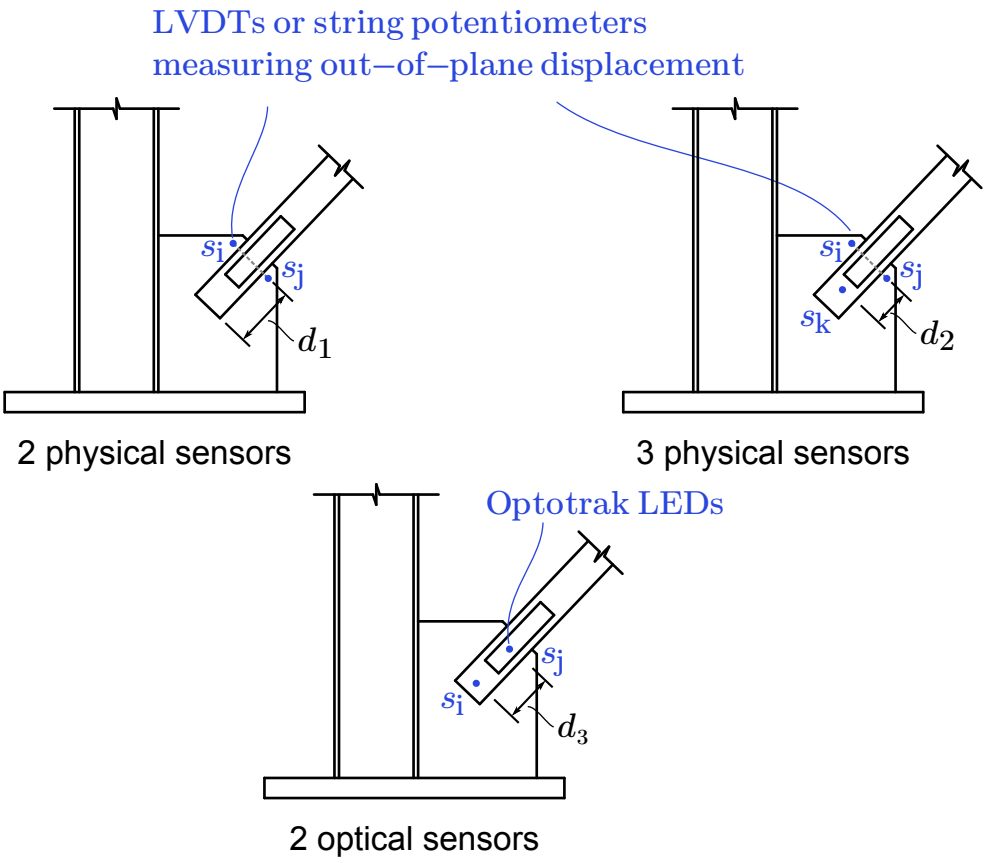

Figure 5.45: Gusset plate rotation geometry

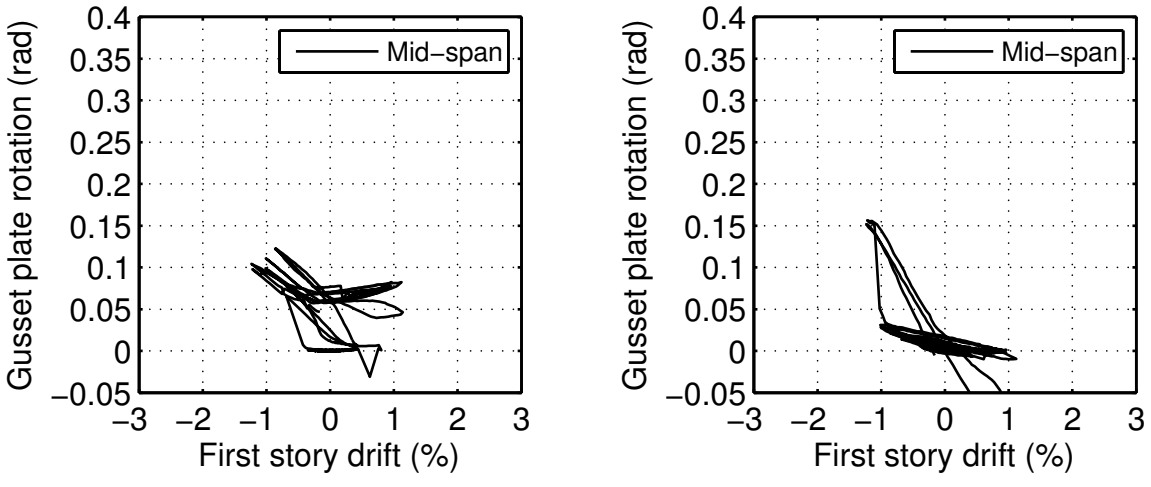

(a) First story south

(b) First story north

Figure 5.46: TNCBF1-N-HSS gusset plate out-of-plane rotation hystereses

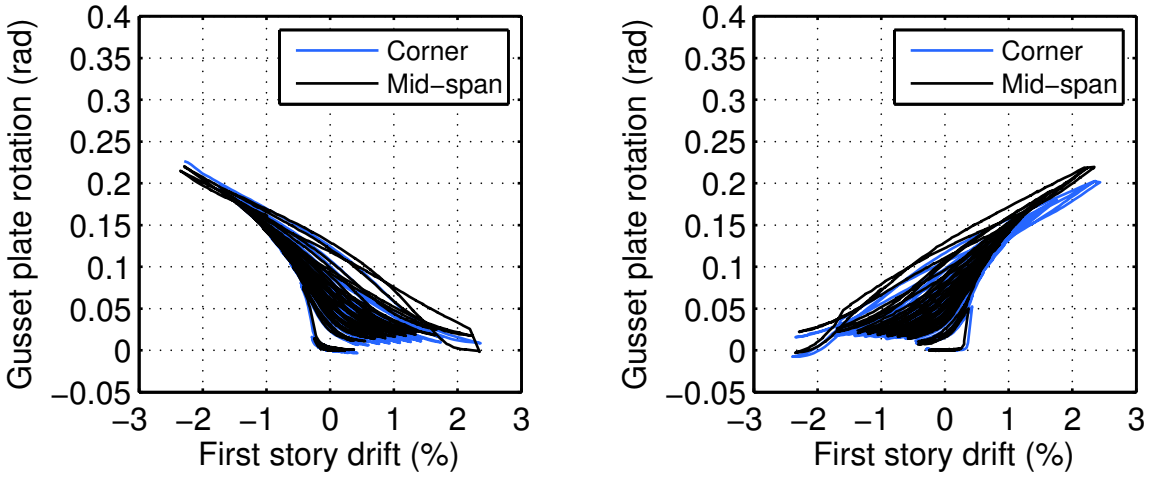

(a) First story south

(b) First story north

Figure 5.47: TNCBF1-R-HSS gusset plate out-of-plane rotation hystereses

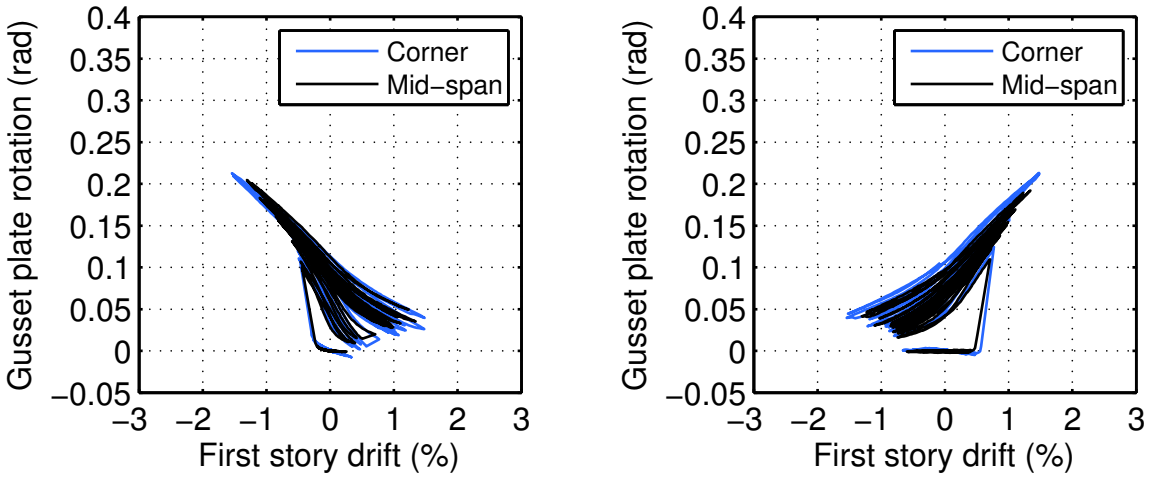

(a) First story south

(b) First story north

Figure 5.48: TNCBF1-R-WF gusset plate out-of-plane rotation hystereses

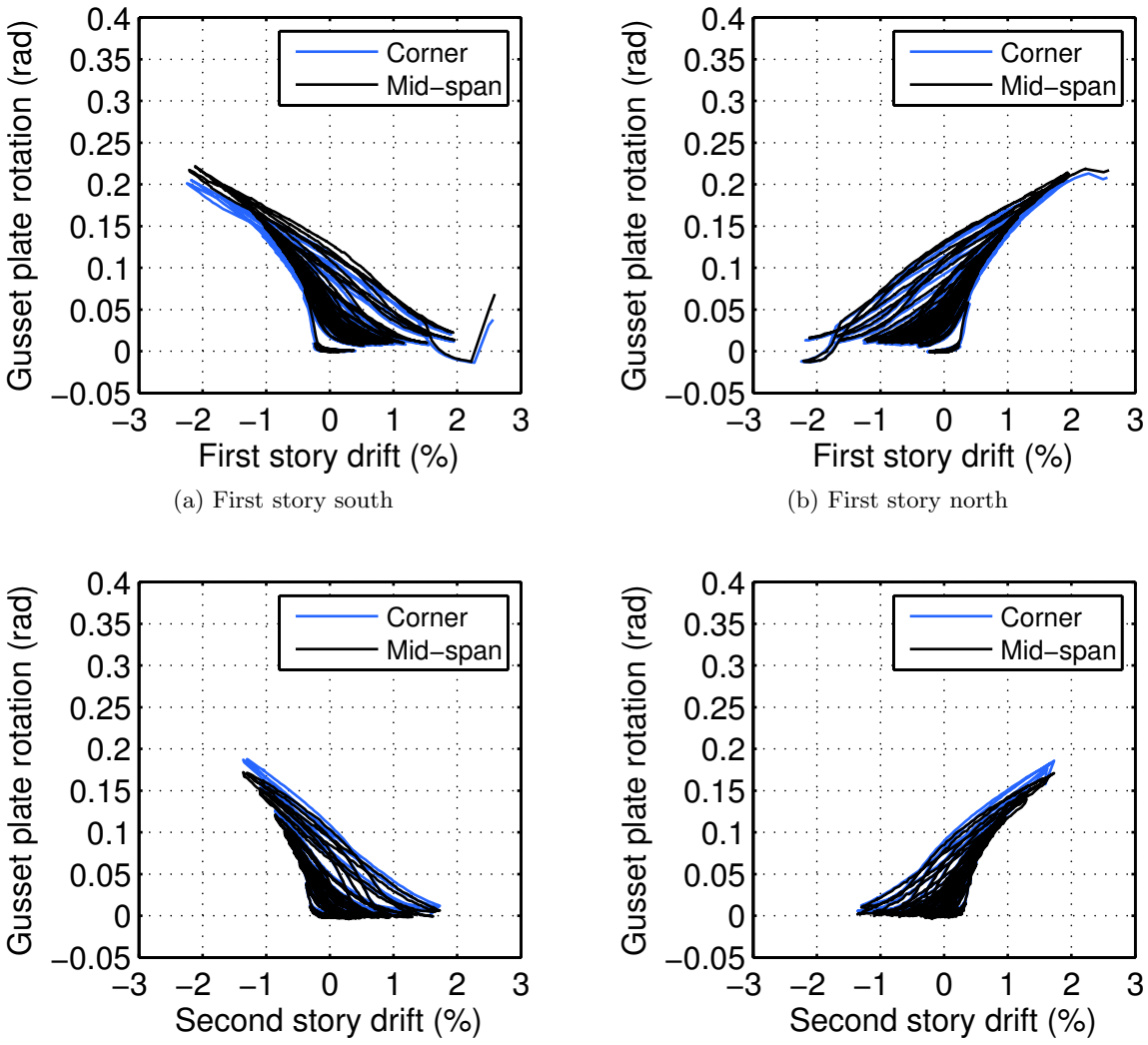

(a) First story south

(b) First story north

(c) Second story south

(d) Second story north

Figure 5.49: TNCBF2-D-WF gusset plate out-of-plane rotation hystereses

5.6.2 Beam-to-Column Connection Rotation

Beam-to-column connections rotations in chevron braced frames are dominated by two mechanisms: frame action and beam pull-down. The combination of frame action and beam pull-down can lead to one joint closing significantly. Consider the frame drifting to the right, as in Fig. 5.50. The right joint undergoes closing from both frame action and beam deflection, but these two mechanisms counteract each other on the left-hand side. The first story beam-to-column connection rotations are plotted in Figs. 5.51 through 5.54. These rotations are derived from inclinometers located on the columns and on the beam outside the connection region. The difference between these two inclinometer measurements provides the rotation of the beam-to-column connection alone. Both south and north end rotations are plotted except for the north end of TNCBF1-R-WF, which could not be obtained due to malfunctioning instrumentation. As expected, when beam pull-down is significant as in TNCBF1-R-HSS and TNCBF1-R-WF, beam-to-column connection rotation at a given drift concentrates on one side of the frame. The first story beam-to-column connections of TNCBF2-D-HSS were moment connections and underwent almost no rotation.

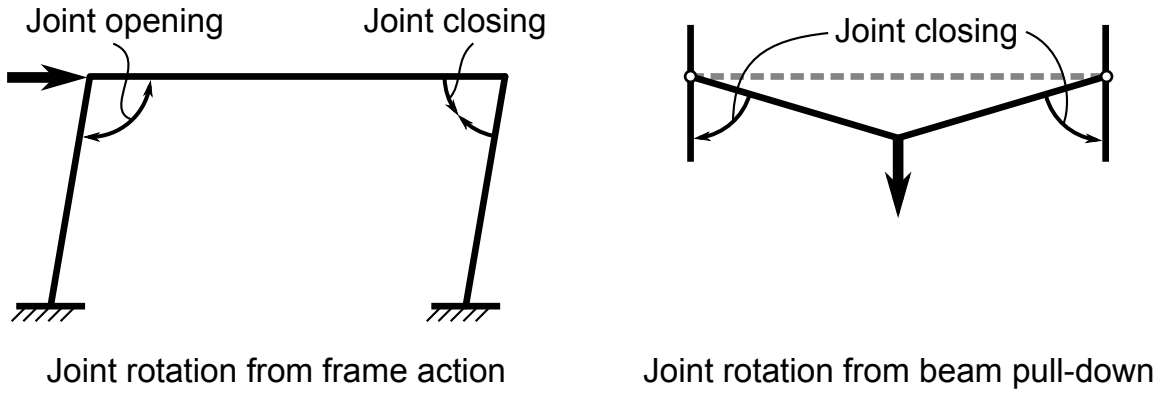

Figure 5.50: Joint rotation mechanisms

Beam-to-column connections can clearly be subjected to large rotational demands in weak beam CBFs. Thus, to ensure ductile performance, connections should be able to sustain large rotations or resist bending moments such that plastic hinges form in the beam. However, the rotational capacities of many NCBF connections are not well quantified, as a variety of connection types exist with relatively little experimental evaluation.

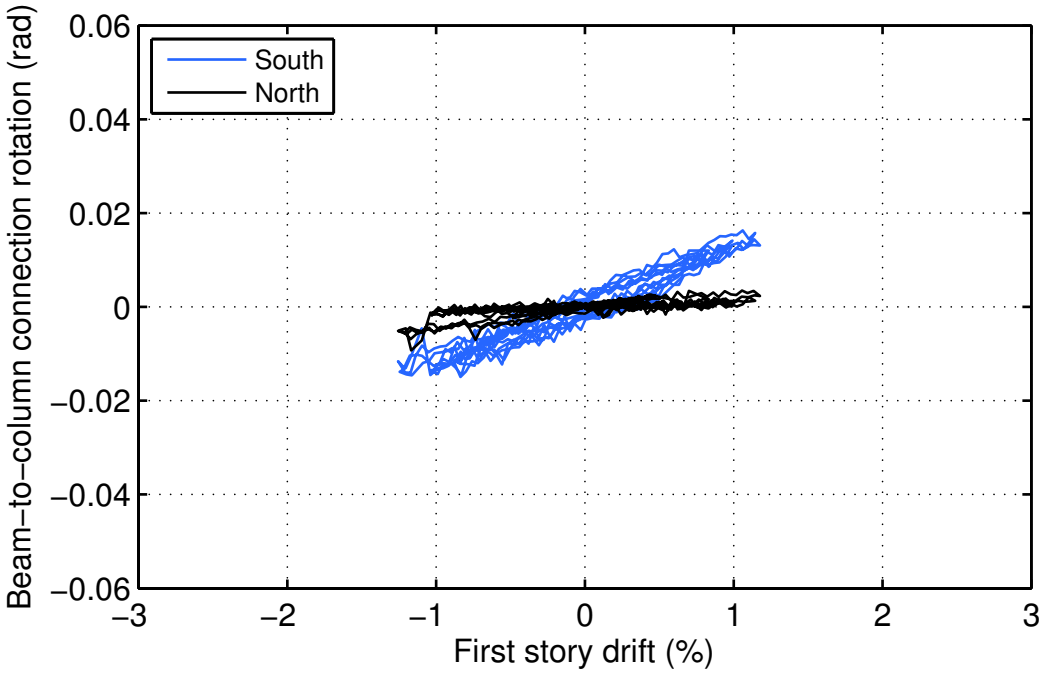

Figure 5.51: TNCBF1-N-HSS first story beam-to-column connection rotation

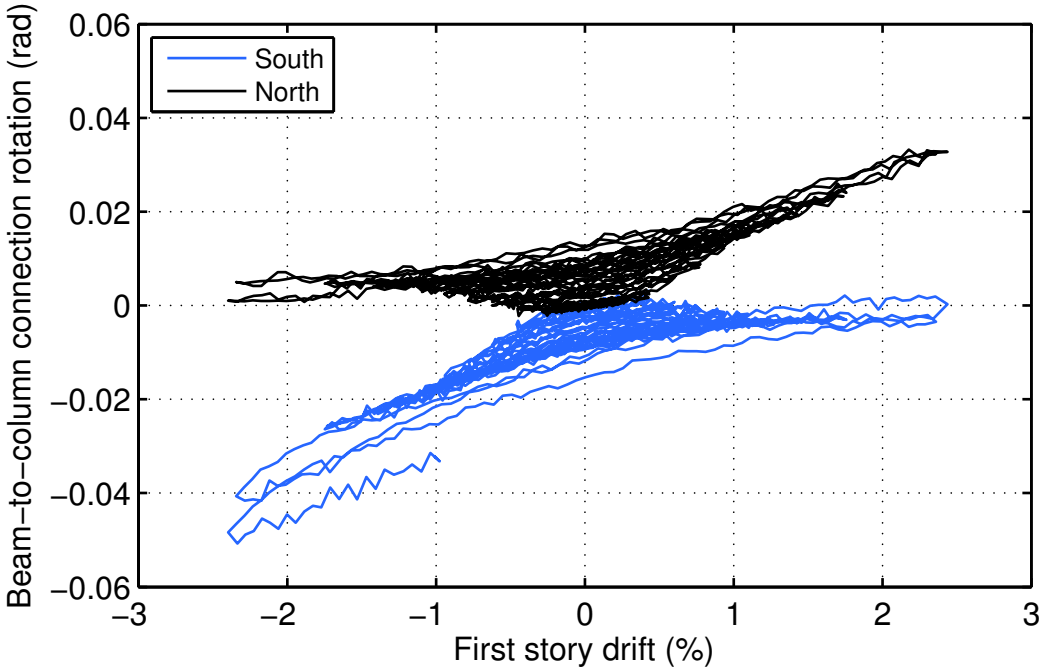

Figure 5.52: TNCBF1-R-HSS first story beam-to-column connection rotation

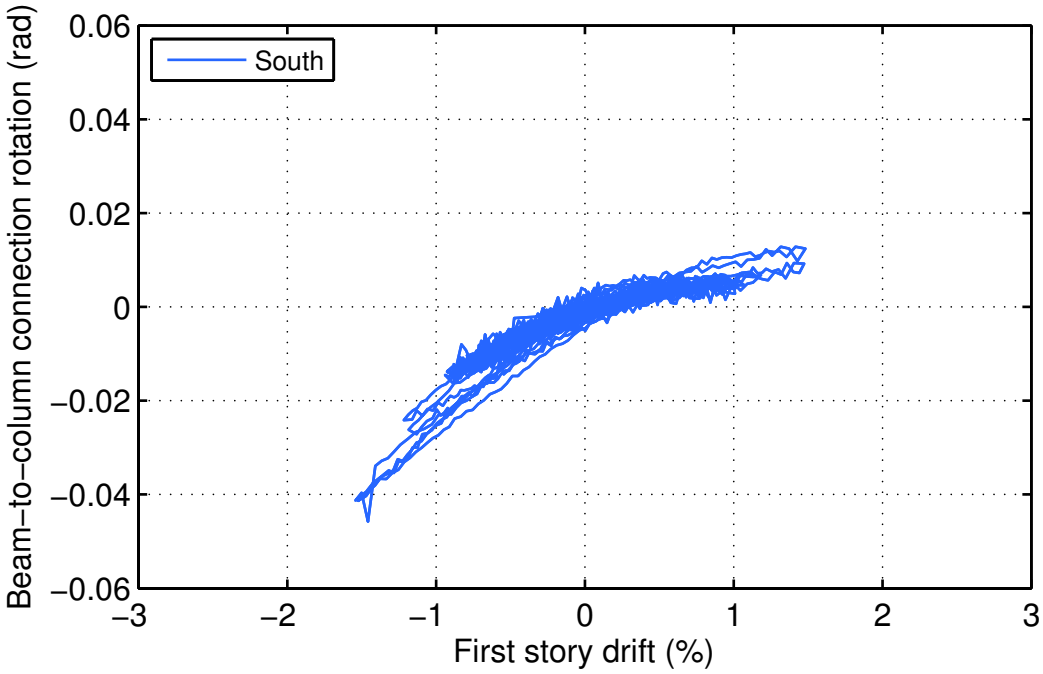

Figure 5.53: TNCBF1-R-WFS first story beam-to-column connection rotation

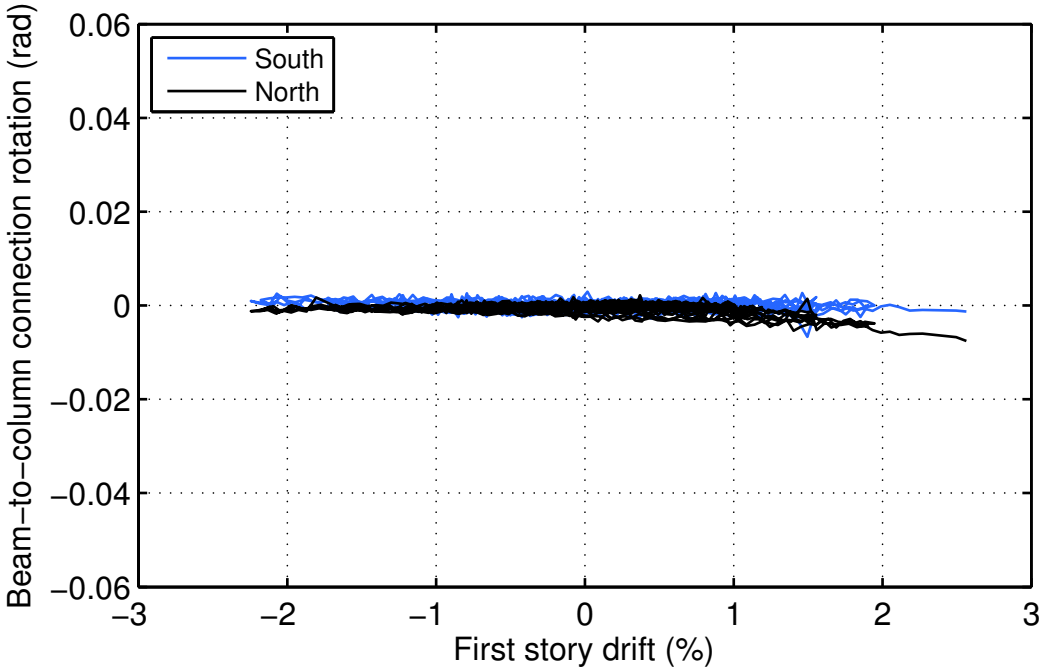

Figure 5.54: TNCBF2-D-HSS first story beam-to-column connection rotation

Chapter 6

NUMERICAL AND EXPERIMENTAL RESPONSE COMPARISON

6.1 Introduction

In support of the experimental specimens tested at NCREE, high resolution finite element models were developed in Abaqus (Dassault Systèmes 2013) by Ph.D candidate Lingli Pan from Tongji University. For each test, comparisons are made between the recorded experimental data and observations and the corresponding simulated results in Abaqus. The hysteretic responses analyzed include base shear, roof drift, story drift, beam deflection, and brace deflection. In addition, banded contour plots of the von Mises stress fields in Abaqus are presented in conjunction with photographs of whitewash flaking in order to match locations of yielding.

6.2 Model Details

6.2.1 Overview

As mentioned in Chapter 3, Abaqus models were developed throughout the design process to verify the expected response of each specimen prior to testing. The models presented here bear many of the same attributes as the initial models, however, they have been refined to (i) include material properties derived from steel coupon and concrete cylinder tests, (ii) simulate fracture via element deactivation at corresponding drifts, and (iii) simulate the observed buckling directions. The loading protocol (Fig. 3.31), location of applied force (north end of second story slab), and location of displacement control (south end of second story slab) were the same as in the tests.

6.2.2 Elements and Meshing

All steel is modeled with S4R shell elements and the concrete slabs are modeled with C3D8R solid elements. Element meshes are refined in areas expected to encounter steep stress gradients. Specifically, meshes sizes are approximately 30 mm by 40 mm for braces, finer than 25 mm by 25 mm for plates, and about 150 mm by 150 mm for slabs.

6.2.3 Material Models

A bilinear kinematic hardening material model is used for steel elements with yield stress, ultimate stress, and ultimate strain values determined from analyses of coupon tension tests. For all steel materials, Young's modulus, E_s, is 200 GPa and Poisson's ratio, ν_s, is 0.3. The remaining material properties for steel are listed in Table 6.1.

Table 6.1: Abaqus model steel material properties

Member	TNCBF series	Yield stress, F_y (MPa)	Ultimate stress, F_u (MPa)	Ultimate strain, ϵ_u (mm/mm)
W12×72 flange	1,2	381	499	0.1605
W12×72 web	1,2	445	530	0.1009
W16×45 flange	1	408	523	0.1486
W16×45 web	1	423	515	0.1569
W24×94 flange	1,2	452	526	0.1364
W24×94 web	1,2	472	547	0.1335
HSS7×7×1/4	1	443	508	0.1053
HSS5×5×3/8	1,2	438	504	0.0652
H175×175×7.5×11 flange	1	325	454	0.1847
H175×175×7.5×11 web	1	363	477	0.1530
10 mm plate	1	395	513	0.1587
12 mm plate	1	337	504	0.1615
12 mm plate	2	445	548	0.1609
15 mm plate	1	424	541	0.1513
20 mm plate	1	416	536	0.1517

The concrete slabs are modeled with the concrete damaged plasticity model in Abaqus. Compressive strengths are the same as those found in Table 3.4, but no data is available to calibrate the remaining model parameters. Since the response of the frame is dominated by steel, the default parameters found in Table 6.2, are used in the models. In addition, the tensile strength of the concrete, f_t, is set to 10% of the compressive strength, Young's modulus, E_c, is $57000\sqrt{f_c}$, and Poisson's ratio, ν_c, is 0.2.

Table 6.2: Abaqus model concrete material properties

Parameter	Value	
Dilation angle	31	deg
Eccentricity	0.1	
f_{b0}/f_{c0}	1.16	
K	2/3	
Viscosity parameter	0.001	

6.2.4 Boundary Conditions

The boundary conditions and restraints imposed on the model mimic the experimental setup. The bottom face of the base plates are fixed in all degrees of freedom. The edge beams are fixed against out-of-plane translation and rotation where the actual frame would contact the out-of-plane reaction frame. In the TNCBF1 series specimens, the second story corner gusset plates and adjacent brace ends were partially embedded in the first story slab. This is simulated by tieing the gusset plate and slab translational degrees of freedom in the region of the embedded region.

6.2.5 Brace Imperfection

Brace imperfection is introduced to simulate initial out-of-straightness and seed the buckling directions observed in the tests. Elastic buckling analyses are conducted prior to the cyclic loading protocol to determine the buckled shapes of the braces with the specified amplitude of deflection as a proportion of the brace length, L. Buckling is not seeded in braces that did not buckle in the tests. Only out-of-plane buckling is seeded in the model of TNCBF1-R-HSS, which was designed for in-plane buckling, since in-plane buckling did not occur in the test. The amplitudes and directions of the imperfections are found in Table 6.3. In most cases, the amplitude of the deflected shape is $L/500$. For TNCBF1-R-WF, the amplitude is decreased to $L/5000$ in the south first story brace to simulate buckling at the same story drift as in the test. For the same purpose, imperfection is not introduced in the north first story brace. The imperfection of the second story braces of TNCBF2-D-HSS is increased to $L/400$ to achieve brace buckling.

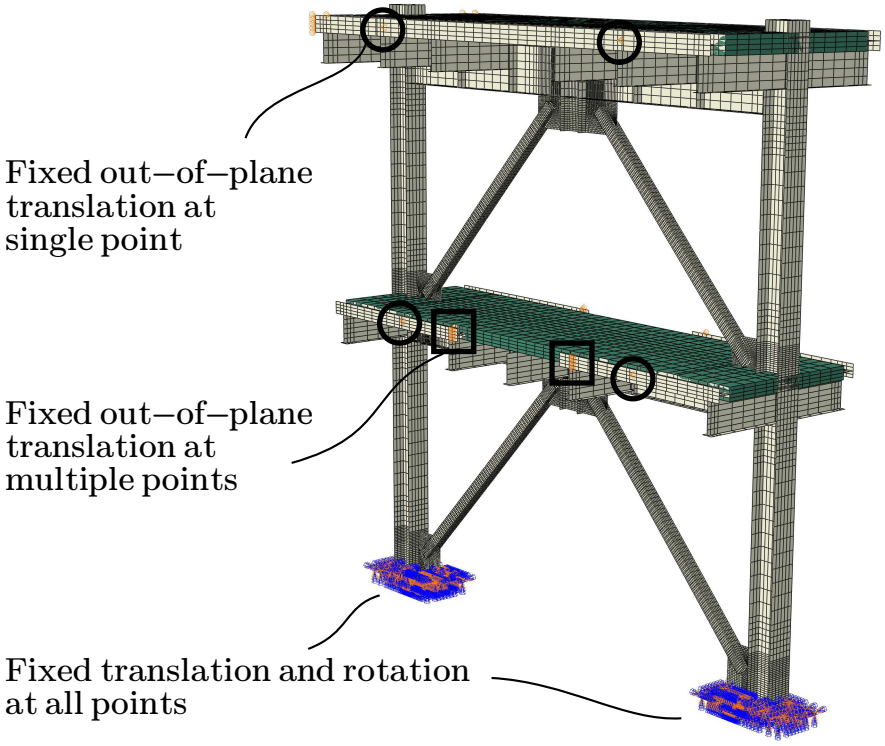

Figure 6.1: Abaqus model boundary conditions

Table 6.3: Brace imperfection amplitudes and directions

Specimen	Story	Brace	Amplitude	Direction
TNCBF1-N-HSS	1F	S	$L/500$	West
TNCBF1-R-HSS	1F	S	$L/500$	West
	1F	N	$L/500$	East
TNCBF1-R-WF	1F	S	$L/5000$	West
TNCBF2-D-HSS	1F	S	$L/500$	West
	1F	N	$L/500$	West
	2F	S	$L/400$	East
	2F	N	$L/400$	East

6.2.6 Composite Action

The first stories of the TNCBF1 specimens are not modeled with composite action, since no shear studs were used in the tests and the shear resistance afforded by the puddle welds is unknown but likely minimal. However, the first story of TNCBF2-D-HSS and the second stories of all specimens do have shear studs and modeling composite action is appropriate. This is accomplished by tieing the beam and slab translational degrees of freedom at shear stud locations throughout the specimen.

6.3 TNCBF1-N-HSS Response Comparisons

Fig. 6.2 shows the model produced to simulate TNCBF1-N-HSS. The lateral force-displacement response of the simulation matches the experimental response well, as shown by Figs. 6.3 and 6.4. Elements at the mid-span of the south first story brace are deactivated to simulate fracture after the 0.45% roof drift level cycles, however connection fracture in the north first story brace is not modeled. This is apparent as the test results and simulated results diverge at larger drifts, where the actual frame response was dominated by weaker and less stiff moment frame behavior on the first story after connection fracture. The simulated first story beam response in Fig. 6.5 does not match the experimental behavior well in negative (downward) excursions due to the fact that composite action is not modeled. This is further validation that the nominally non-composite slab on the first story of TNCBF1-N-HSS did provide some composite action in the test. The south first story brace deflections are slightly different in magnitude, but such little data is available for the brace due to its rapid progression to fracture.

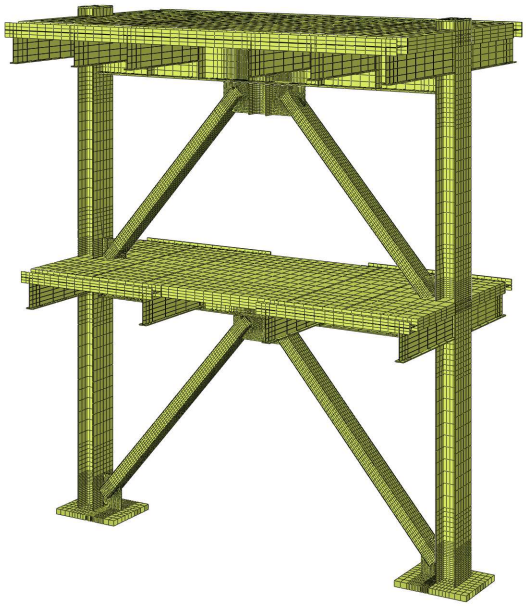

Figure 6.2: TNCBF1-N-HSS Abaqus model

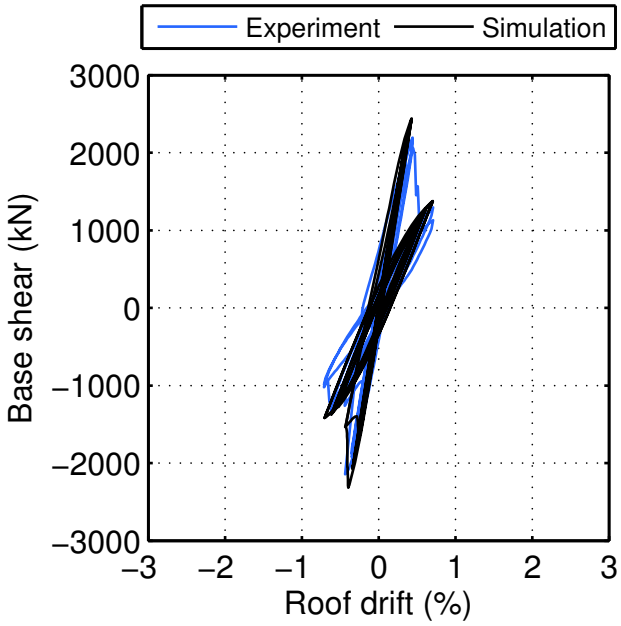

Figure 6.3: TNCBF1-N-HSS experimental and simulated roof drift hystereses

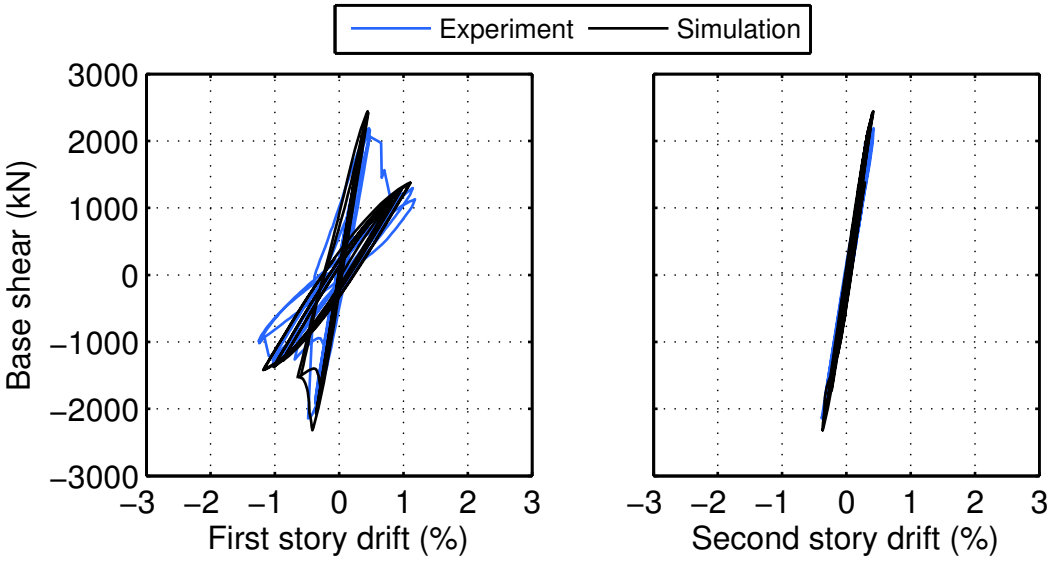

Figure 6.4: TNCBF1-N-HSS experimental and simulated story drift hystereses

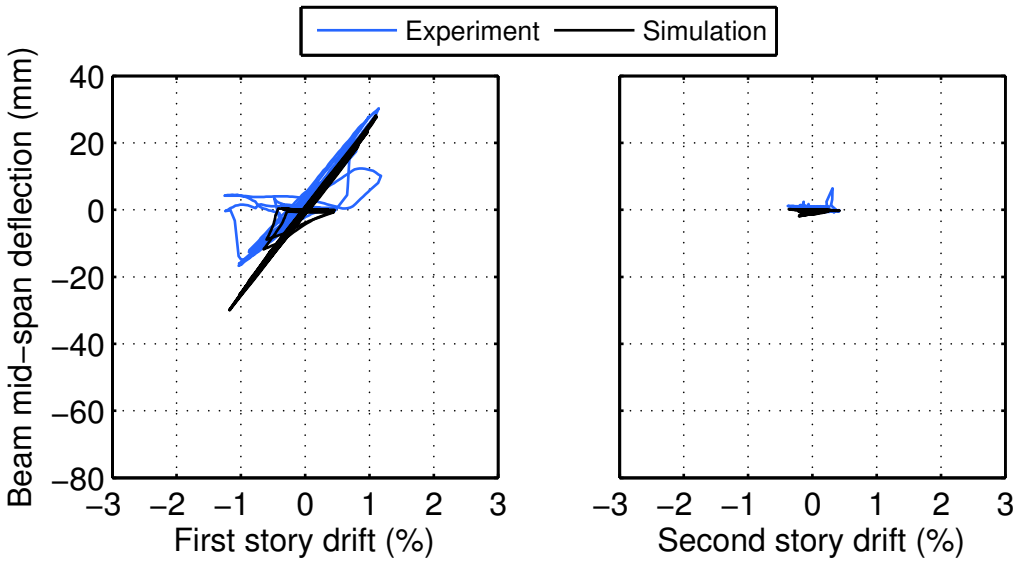

Figure 6.5: TNCBF1-N-HSS experimental and simulated beam mid-span deflection hystereses

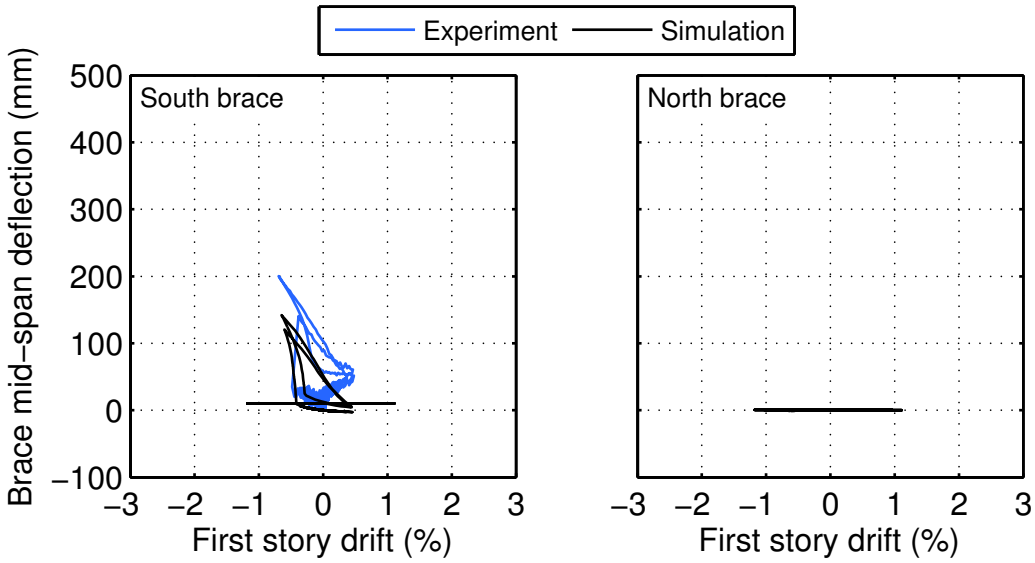

Figure 6.6: TNCBF1-N-HSS experimental and simulated first story brace mid-span deflection hystereses

6.3.1 Observed Yielding

Contour plots of the stress fields reveal similar yielding locations in the Abaqus analysis and test. Beam web yielding appears to be slightly less prominent in Fig. 6.8b than in the actual test, but

heat effects from welding may have introduces initial stresses not present in the model.

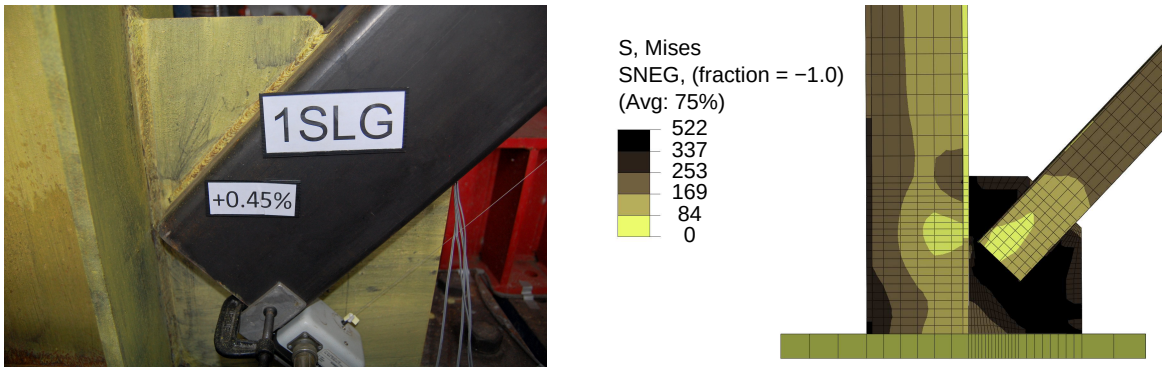

(a) Experiment photograph

(b) Simulated von Mises stress field (MPa); gusset plate $F_y = 337$ MPa

Figure 6.7: TNCBF1-N-HSS south first story corner gusset plate at 0.44% roof drift

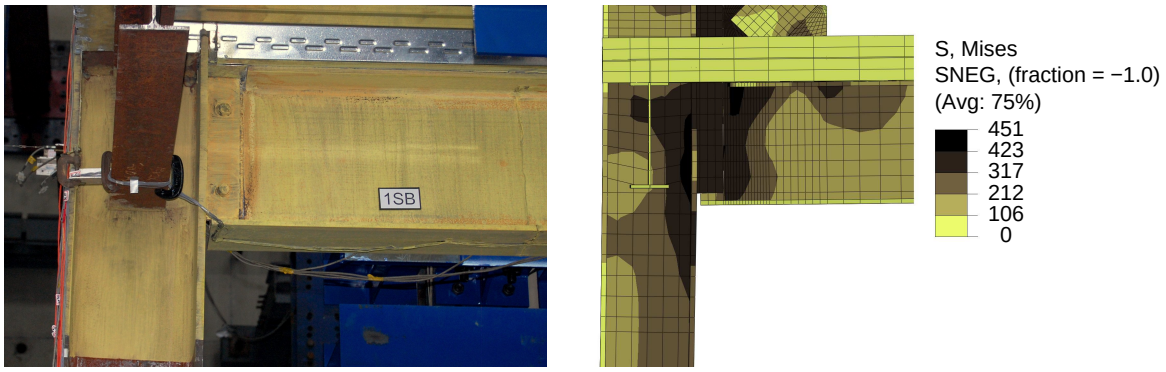

(a) Experiment photograph

(b) Simulated von Mises stress field (MPa); beam web $F_y = 423$ MPa

Figure 6.8: TNCBF1-N-HSS south first story beam end at 0.71% roof drift

6.4 TNCBF1-R-HSS Response Comparisons

Fig. 6.9 shows the Abaqus model produced to simulate TNCBF1-R-HSS. Since fracture in the test did not occur until the final drift level, no elements were deactivated in the model. The experimental and simulated responses in Figs. 6.10 through 6.13 generally match well. The simulated response was slightly stiffer through reloading, though the base shear values at drift peaks remain almost indistinguishable. The first story beam (Fig. 6.12) reached greater deflections in the test, which could be influenced by loss of composite action and beam-to-column connection damage that reduced its fixity. The first story brace mid-span deflection hystereses show similar behavior, though in the experiment, the braces appear to straighten further in tension.

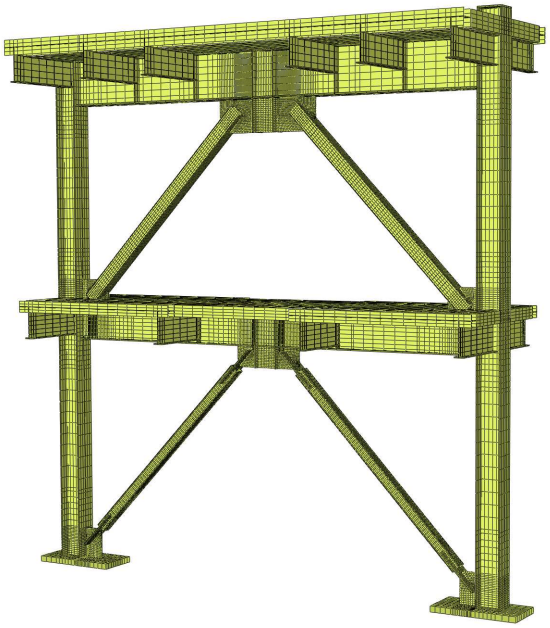

Figure 6.9: TNCBF1-R-HSS Abaqus model

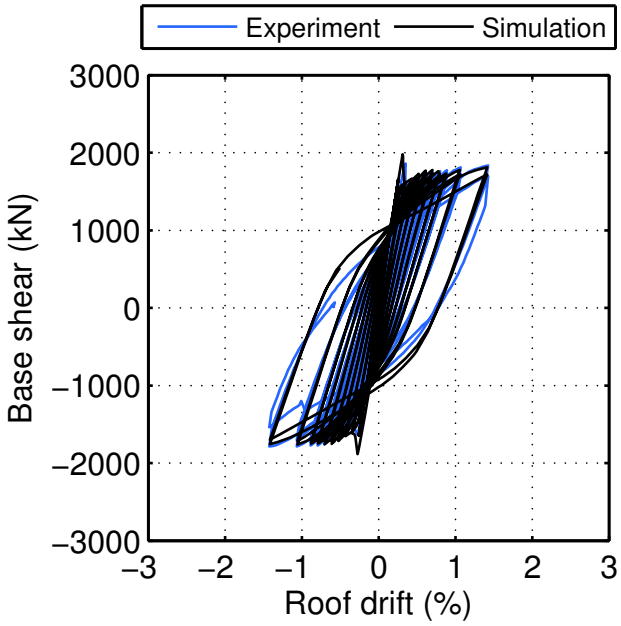

Figure 6.10: TNCBF1-R-HSS experimental and simulated roof drift hystereses

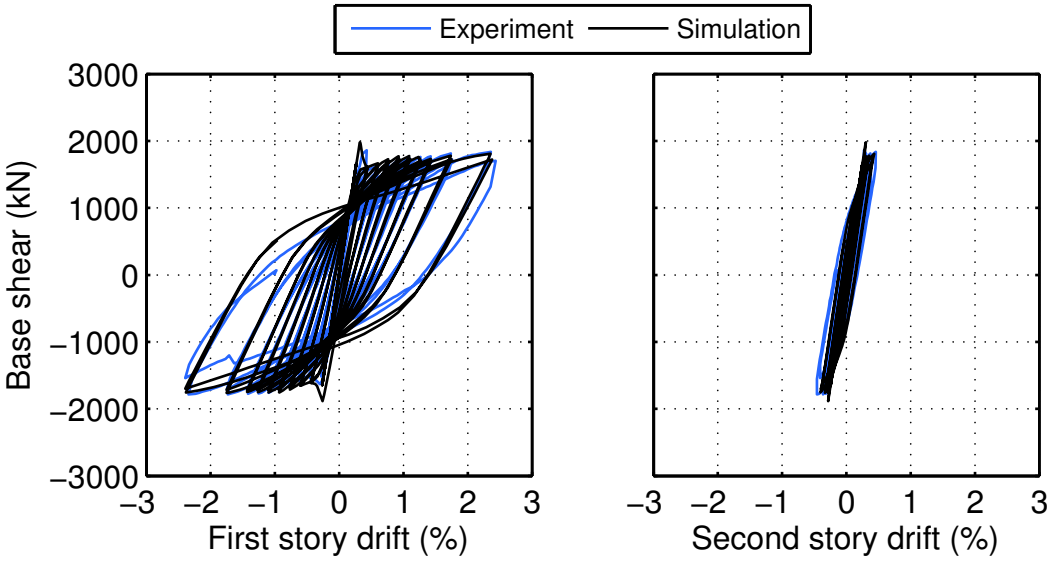

Figure 6.11: TNCBF1-R-HSS experimental and simulated story drift hystereses

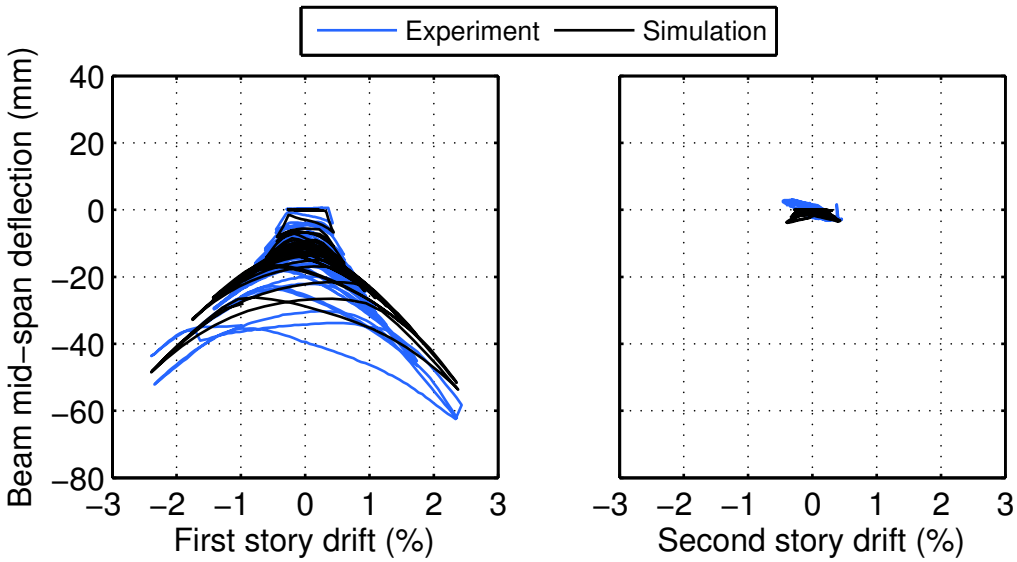

Figure 6.12: TNCBF1-R-HSS experimental and simulated beam mid-span deflection hystereses

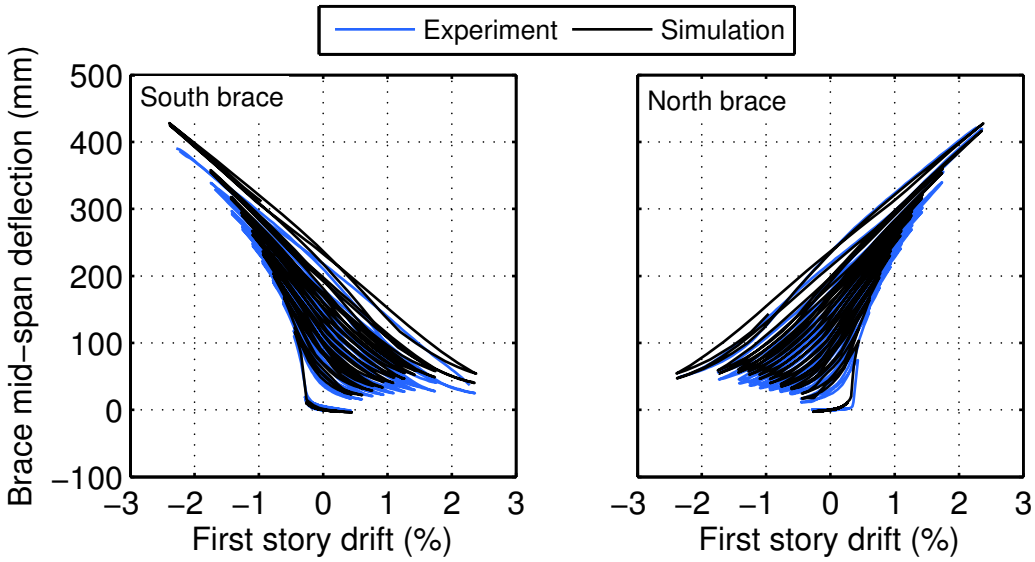

Figure 6.13: TNCBF1-R-HSS experimental and simulated first story brace mid-span deflection hystereses

The contour plots in Figs. 6.14 through 6.17 also match the whitewash flaking from the tests with reasonable accuracy, but local deformation of the column flange in Figs. 6.14 and 6.17 is

highly exaggerated (deformation is unscaled in the figures). At the column bases, this may be partly explained by higher fixity in the model, where the base plates are fully fixed at all nodes. In the test, the base plates were bolted to anchor plates that were post-tensioned to the strong floor, an overall more flexible system that is also prone to slip. At the first story beam-to-column connection, the welds are modeled as translational ties between the elements, but some weld cracking occurred in the test, reducing the fixity of the connection. Yielding at the first story beam mid-span (Fig. 6.16) is captured at the same locations as in the test.

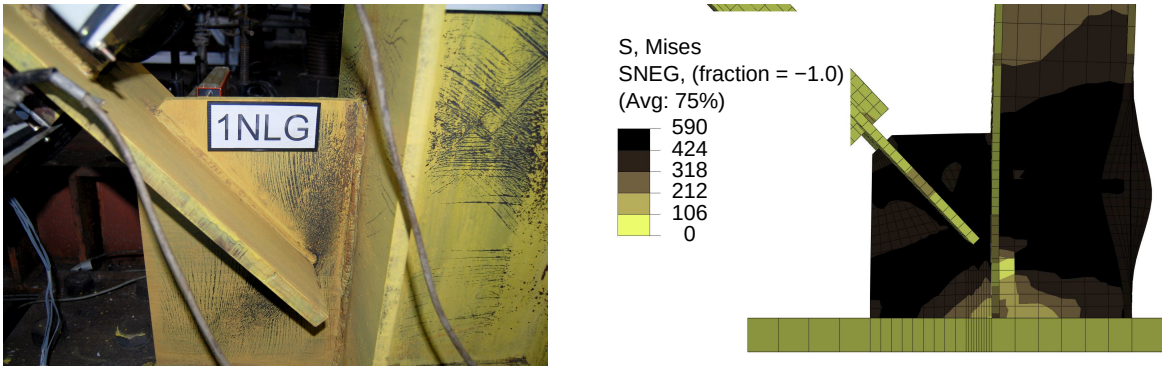

(a) Experiment photograph

(b) Simulated von Mises stress field (MPa); gusset plate $F_y = 424$ MPa

Figure 6.14: TNCBF1-R-HSS north first story corner gusset plate at test end

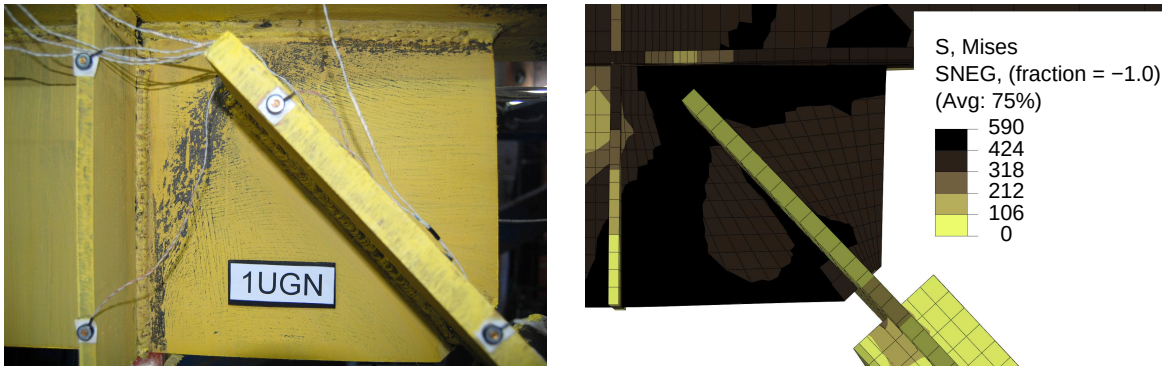

(a) Experiment photograph

(b) Simulated von Mises stress field (MPa); gusset plate $F_y = 424$ MPa

Figure 6.15: TNCBF1-R-HSS north first story mid-span gusset plate at test end

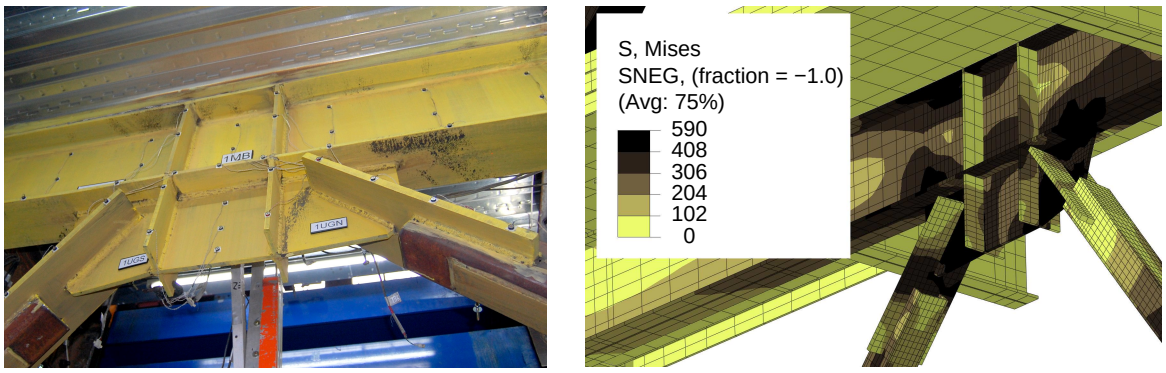

(a) Experiment photograph

(b) Simulated von Mises stress field (MPa); beam flange $F_y = 408$ MPa

Figure 6.16: TNCBF1-R-HSS first story beam at test end

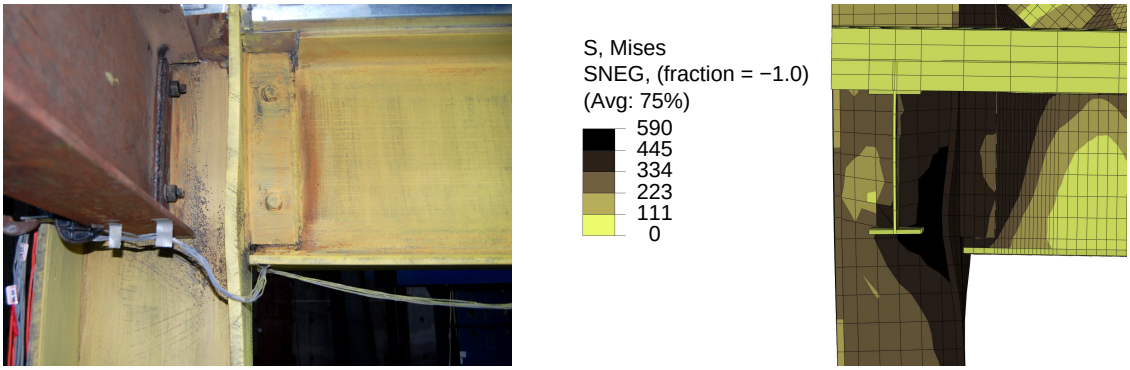

(a) Experiment photograph

(b) Simulated von Mises stress field (MPa); column web $F_y = 445$ MPa

Figure 6.17: TNCBF1-R-HSS south first story beam-to-column connection region at test end

6.5 TNCBF1-R-WF Response Comparisons

Fig. 6.18 depicts the model used to simulate TNCBF1-R-WF. The residual beam deflection from TNCBF1-R-HSS, approximately 35 mm, was simulated in the model geometry and the north and south second story brace ends were deactivated after 0.71% and 0.80% roof drift cycles, respectively, in accordance with the connection fracture events of the test. The lateral force-displacement responses in Figs. 6.19 and 6.20 match well up to the point of brace connection fracture on the second story, but the simulated response is weaker and less stiff afterward. In the test, the second story braces continued to develop compressive forces as they contacted the slab following connection fracture, but this behavior is not modeled in Abaqus. Consequently, the second story reached higher drifts than in the test and the first story reached lower drifts. Beam mid-span deflection, seen in Fig. 6.21, is also underestimated in the analysis. On the first story, the demand from the brace unbalanced force is lower, resulting in less beam deflection. On the second story, small upward vertical excursions resulting from brace compression due to contact with the slab is not captured.

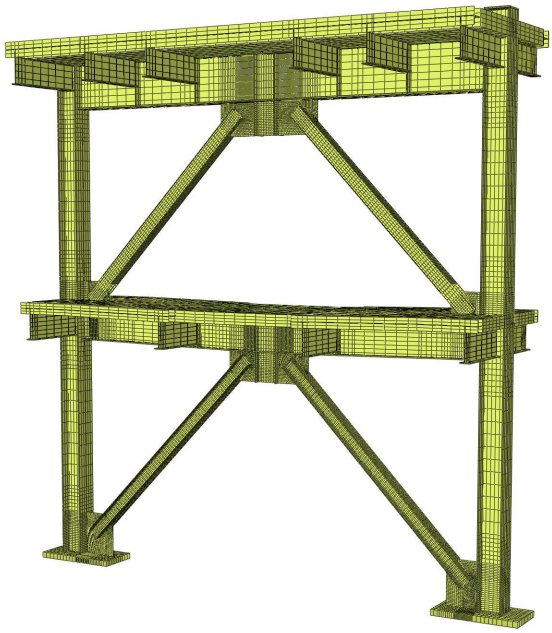

Figure 6.18: TNCBF1-R-WF Abaqus model

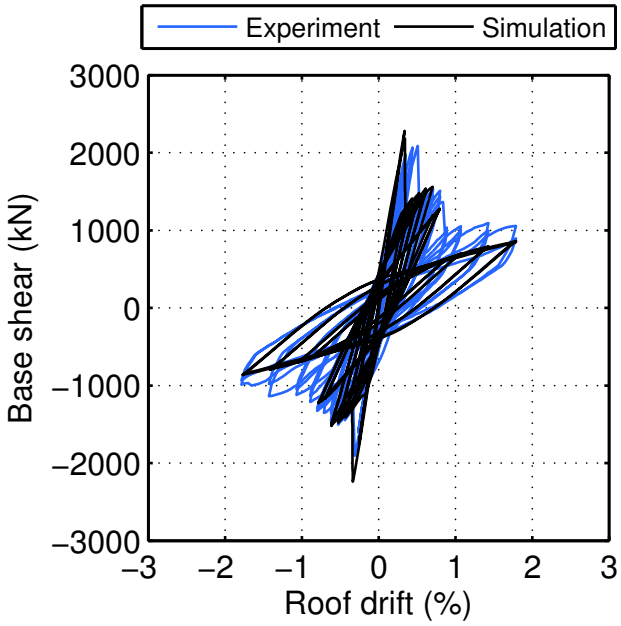

Figure 6.19: TNCBF1-R-WF experimental and simulated roof drift hystereses

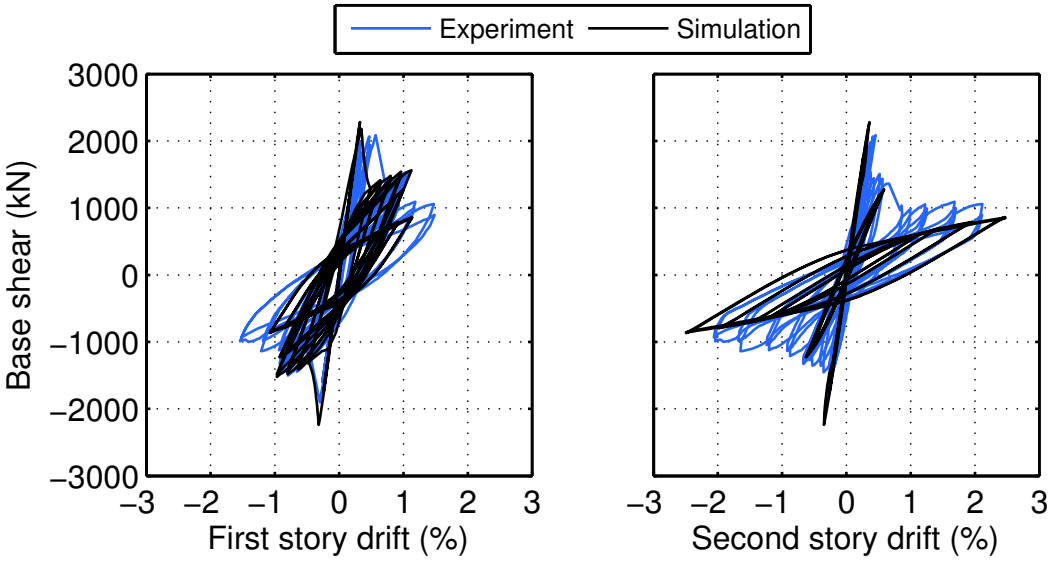

Figure 6.20: TNCBF1-R-WF experimental and simulated story drift hystereses

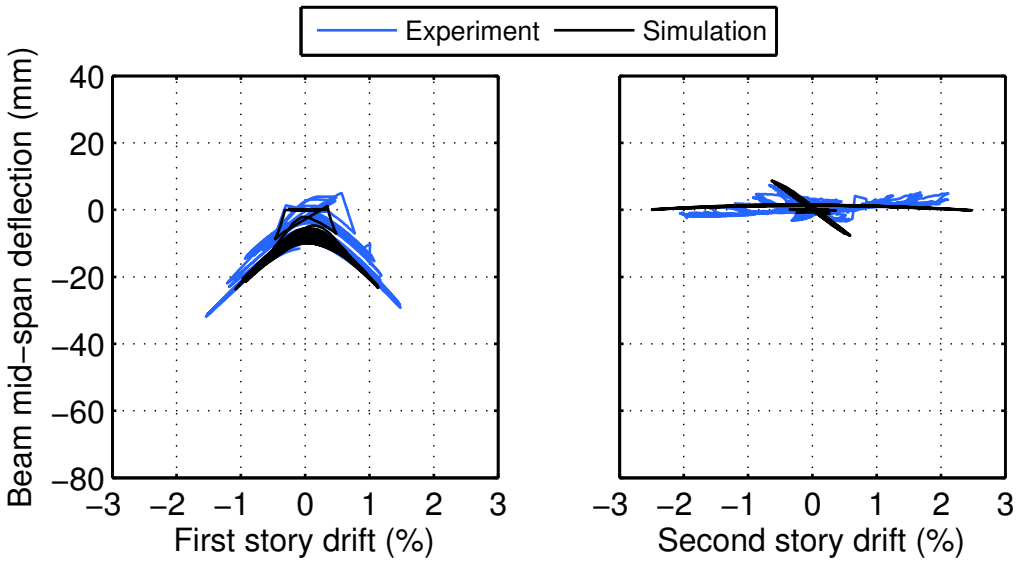

Figure 6.21: TNCBF1-R-WF experimental and simulated beam mid-span deflection hystereses

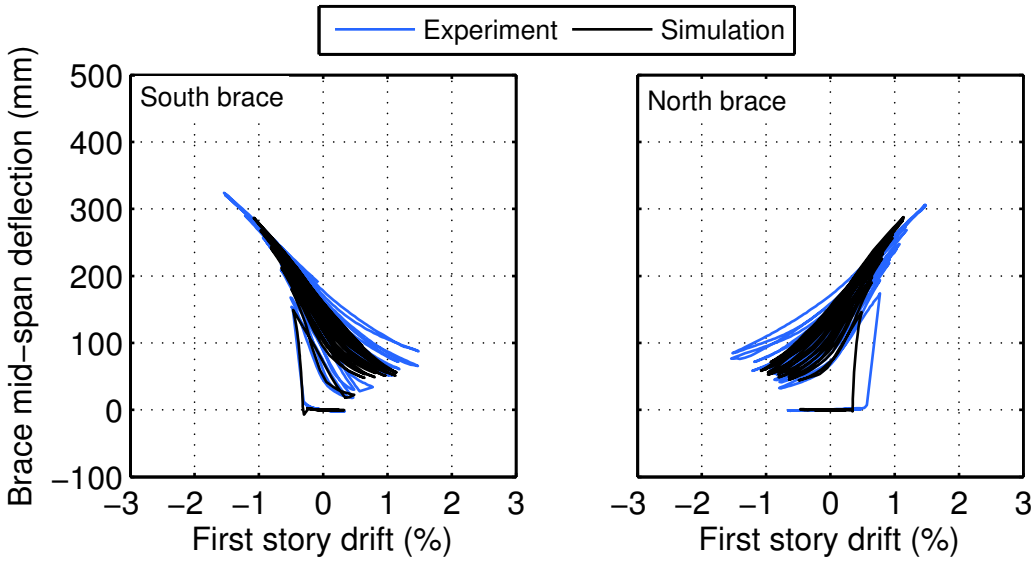

Figure 6.22: TNCBF1-R-WF experimental and simulated first story brace mid-span deflection hystereses

Despite clear difficulties in capturing the frame response after brace connection fracture, the von Mises stress field plots in Figs. 6.23 through 6.26 are informative. Fig. 6.23 shows yielding in

the brace web just outside the net section reinforcement plate in the test and a stress concentration at the same location in the simulation. Yielding likely occurred in the test due to heat effects from welding. Fig. 6.24 shows experimental and simulated elliptical yielding of the south first story corner gusset plate when the adjacent brace buckled. Beam yielding is not as extensive in the analysis as in the test, but locations of stress concentrations in the beam web are still identified in the model in Fig. 6.25. Column panel zone yielding due to moment frame action on the second story is also captured by the model, as shown in Fig. 6.26.

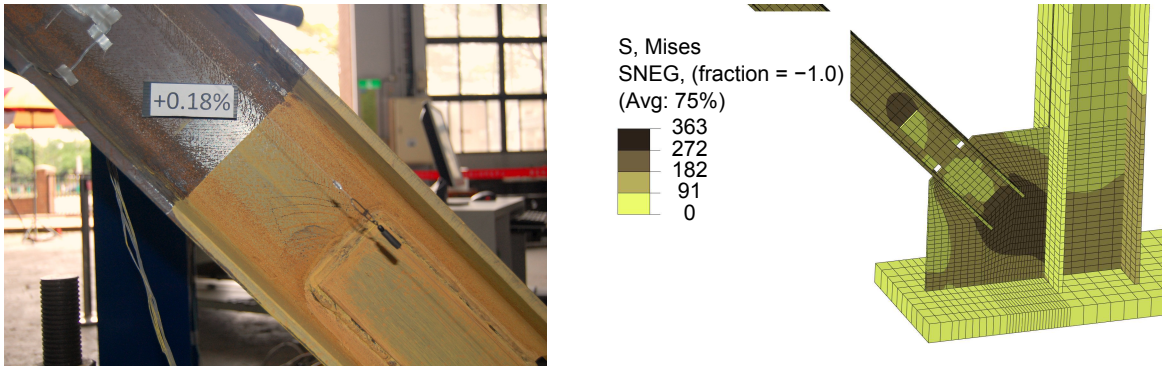

(a) Experiment photograph

(b) Simulated von Mises stress field (MPa); brace web $F_y = 363$ MPa

Figure 6.23: TNCBF1-R-WF south first story brace at base region at 0.17% roof drift

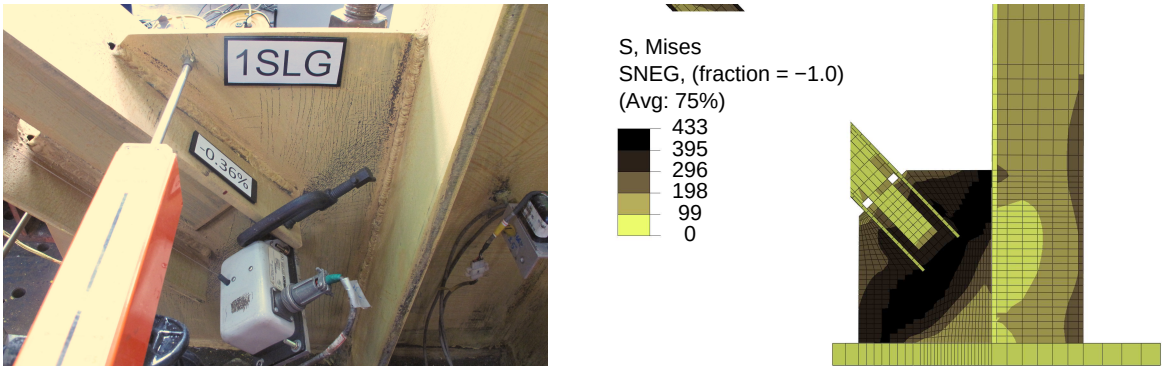

(a) Experiment photograph

(b) Simulated von Mises stress field (MPa); gusset plate $F_y = 395$ MPa

Figure 6.24: TNCBF1-R-WF south first story corner gusset plate at 0.35% roof drift

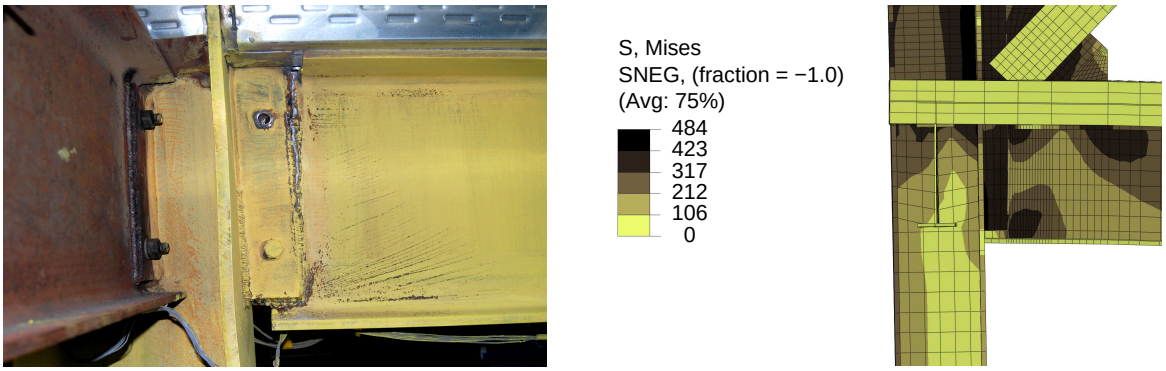

(a) Experiment photograph

(b) Simulated von Mises stress field (MPa); beam web $F_y = 423$ MPa

Figure 6.25: TNCBF1-R-WF south first story beam-to-column connection region at test end

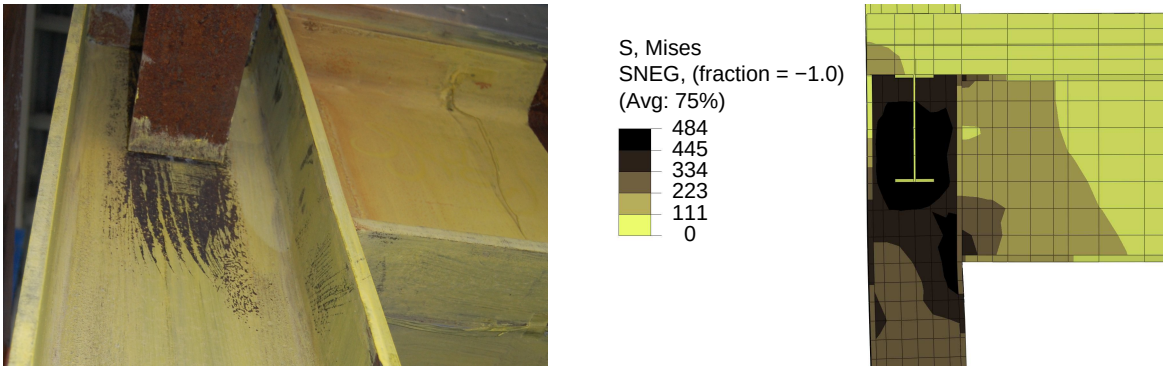

(a) Experiment photograph

(b) Simulated von Mises stress field (MPa); column web $F_y = 445$ MPa

Figure 6.26: TNCBF1-R-WF south second story column near beam-to-column connection at test end

6.6 TNCBF2-D-HSS Response Comparisons

Fig. 6.27 shows the Abaqus model produced to simulate TNCBF2-D-HSS. Like in TNCBF1-R-HSS, fracture did not occur in the test until the final drift level, so no elements were deactivated in the model. The simulated response is stronger and stiffer than that of the experiment, as can be seen in Figs. 6.28 and 6.29. A soft story develops at the first story, but the second story still undergoes significant inelastic deformation, just as in the test. However, the first story beam deflection hystereses in Fig. 6.30 underestimates response even though the extent of composite action on the first story is quantified better for TNCBF2-D-HSS than any other test. Brace deflection on both stories, plotted in Figs. 6.31 and 6.32, matched the experimental results closely.

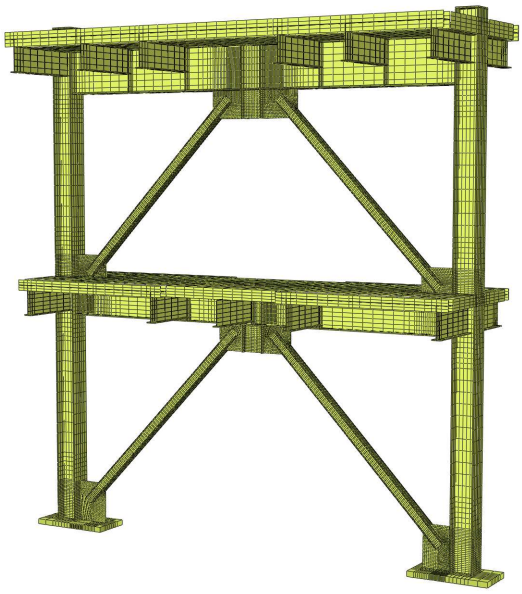

Figure 6.27: TNCBF2-D-HSS Abaqus model

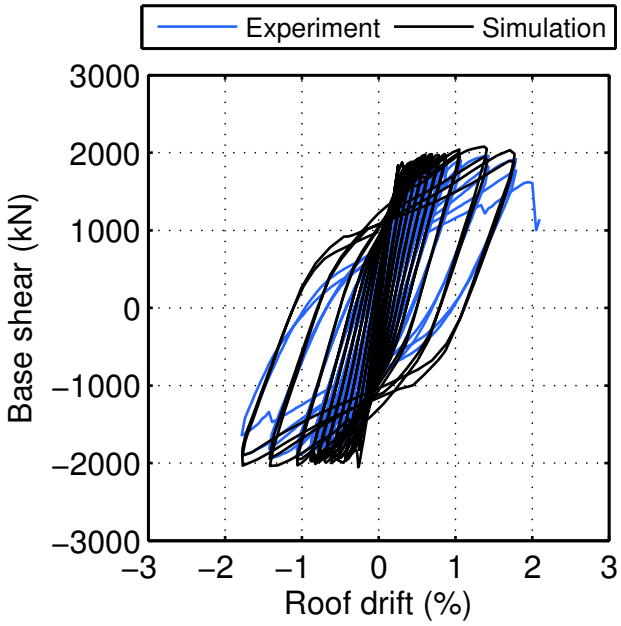

Figure 6.28: TNCBF2-D-HSS experimental and simulated roof drift hystereses

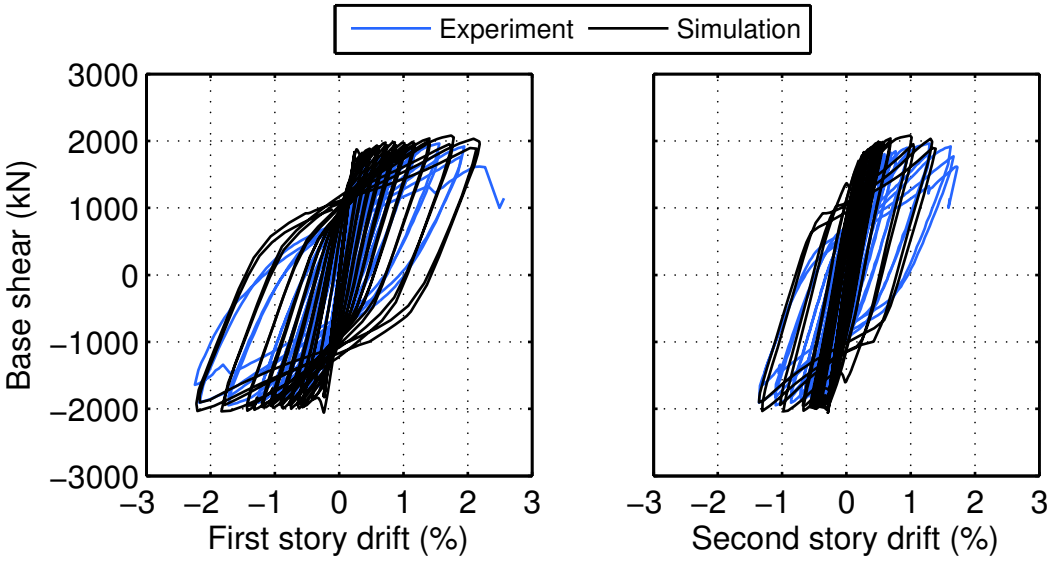

Figure 6.29: TNCBF2-D-HSS experimental and simulated story drift hystereses

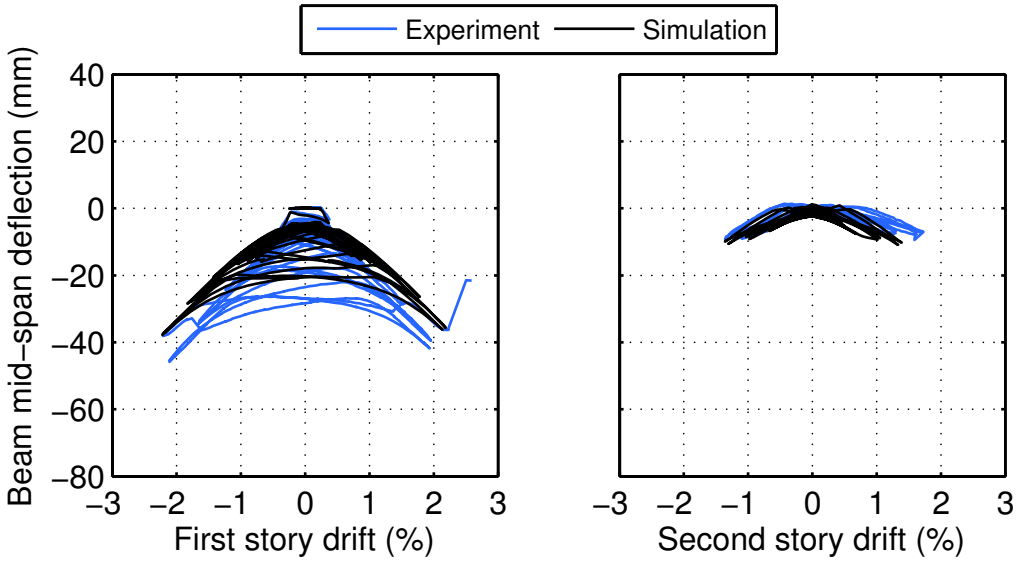

Figure 6.30: TNCBF2-D-HSS experimental and simulated beam mid-span deflection hystereses

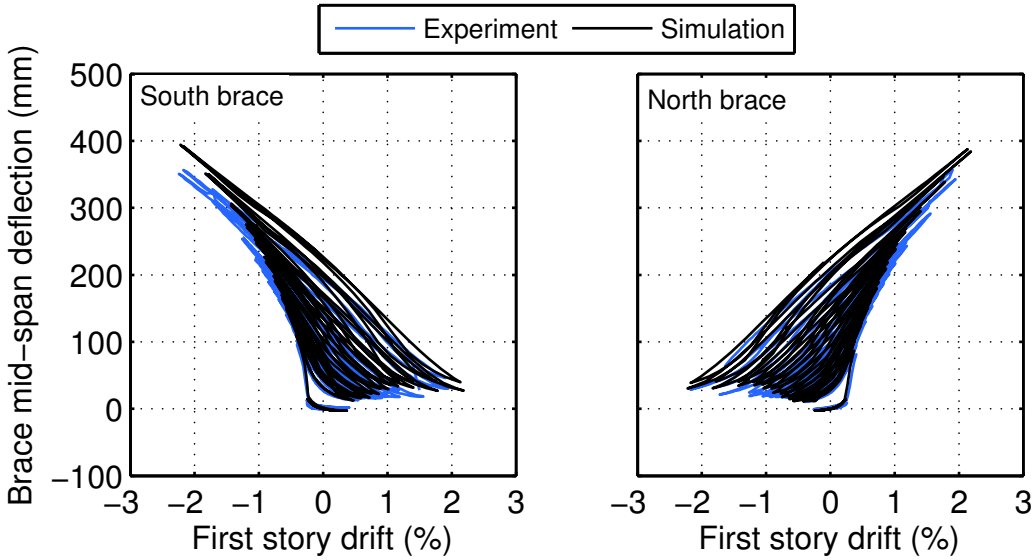

Figure 6.31: TNCBF2-D-HSS experimental and simulated first story brace mid-span deflection hystereses

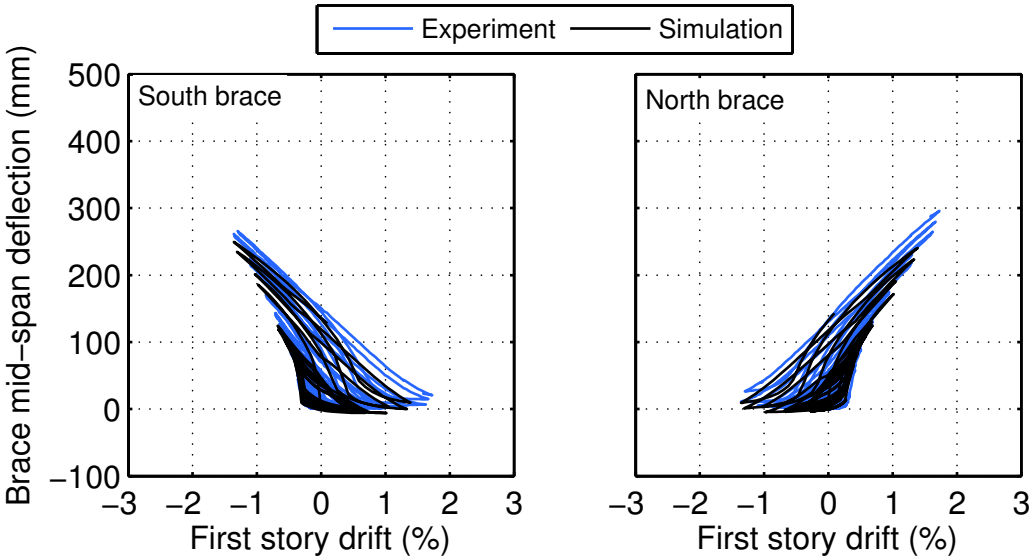

Figure 6.32: TNCBF2-D-HSS experimental and simulated second story brace mid-span deflection hystereses

The column web von Mises stress fields in Figs. 6.33 and 6.34 show yielding patterns similar to those observed in the test. Yet, as was noted for the TNCBF1-R-HSS models, the local deformation of the column flange is highly exaggerated in the simulation. Fig. 6.35 does not show significant yielding in the beam web, but the contours shows high stress in regions where yielding was observed in the test–the column panel zone, the column web at the bottom flange of the beam, and the adjacent gusset plate.



(a) Experiment photograph

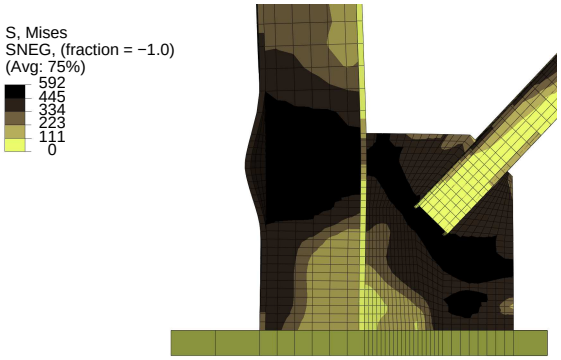

(b) Simulated von Mises stress field (MPa); column web $F_y = 445$ MPa

Figure 6.33: TNCBF2-D-HSS south base plate region at test end



(a) Experiment photograph

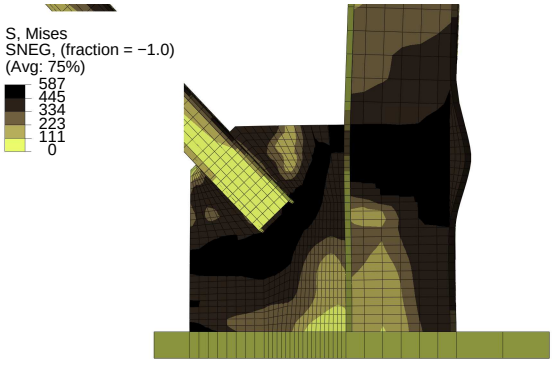

(b) Simulated von Mises stress field (MPa); column web $F_y = 445$ MPa

Figure 6.34: TNCBF2-D-HSS north base plate region at test end

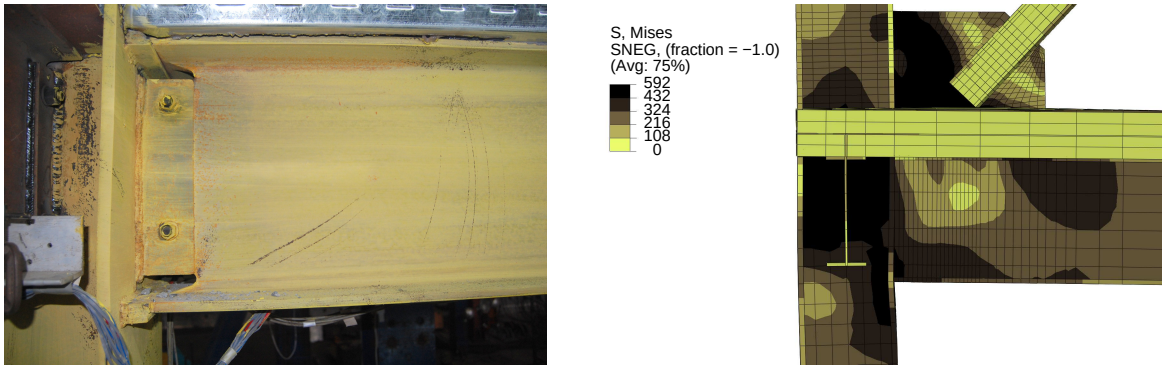

(a) Experiment photograph

(b) Simulated von Mises stress field (MPa); beam web $F_y = 432$ MPa

Figure 6.35: TNCBF2-D-HSS south first story beam-to-column region at test end

Chapter 7
SUMMARY AND CONCLUSIONS

7.1 Introduction

This chapter contains a brief summary of the work completed as part of this research as well as conclusions drawn from the observations and analyses. Specifically, the effect of the weak beam on the response of the test specimens is discussed along with recommendations for frame rehabilitation, analysis, and future work.

7.2 Summary

The research presented in this thesis is part of an international research collaboration between the University of Washington; University of California, Berkeley; and National Center for Research on Earthquake Engineering (NCREE) in Taiwan to further the understanding of the behavior of non-seismic concentrically braced frames (NCBFs). The ultimate goal of the collaboration is to deliver evaluation and rehabilitation recommendations to practicing engineers and researchers. To examine the performance of chevron configuration NCBFs with weak beams, data from four full-scale tests performed at NCREE were collected and analyzed. The test specimens consisted of two-story frames with inverted V-bracing and weak first-story beams. The second story beams were fully-composite and strong with respect to the design brace unbalanced force in all specimens. The first specimen was intended to represent an existing NCBF with non-ductile details, typical of braced frames designed prior to about 1988. The final three specimens examined rehabilitation scenarios for NCBFs using a variety of brace, connection, and composite slab details. Results from these tests were compared with those of three-story multi-story X-configuration SCBFs (Lumpkin et al. 2012) with similar test setups using data available on NEEShub (NEES 2014). Data from continuum models produced by Lingli Pan that represented the experimental specimens was also analyzed and compared to the experimental data.

Under the imposed quasistatic reversed cyclic loading protocol, the responses of the experimental

specimens were highly varied. The weak first story beam did not severely impair the performance of any specimens directly, but it was nonetheless influential in each test, as described below.

- **TNCBF1-N-HSS:** The ductility of the frame was limited by the rapid degradation of the non-compact brace ($b/t = 2.27\lambda_{\text{hd}}$) that buckled. Local buckling of the brace cross section coincided with global buckling along its length, accumulating large strains at the brace mid-span immediately and leading to brace fracture at a relative low deformation, less than 0.5% story drift. After fracture, the weak beam, with an axial-flexural interaction demand-to-capacity ratio (DCR) of 2.52, prevented buckling of the remaining brace, as the beam was not strong enough to develop the critical buckling load of the brace. This initiated an eccentrically braced frame (EBF) mechanism on the first story that was weaker and less stiff than the initial CBF response. The EBF mechanism persisted until connection fracture in the remaining brace at 1.04% story drift. The ensuing moment frame response was weaker and less stiff than the EBF response, showing that the weak beam marginally improved the post-fracture performance of the frame.

- **TNCBF1-R-HSS:** The first story of the specimen represented a repair with in-plane buckling braces. However, the braces buckled out-of-plane in the test. The torsional stiffness of the first story beam was relatively low as a consequence of the low torsional constant of the cross section and lack of lateral support at its mid-span, where the braces intersect. The beam's flexibility in this vicinity may have led to the unintended buckling mode. The beam was also deficient compared to the design brace unbalanced load, with an axial-flexural interaction DCR of 2.66. Despite these two factors, the first story response was ductile and lateral resistance was maintained up to brace at a story drift range comparable to SCBFs, 4.70%. Though the beam may have been partially responsible for the initiation of out-of-plane buckling, its participation in the mid-span connection through beam twist appeared to limit weld damage to the adjacent gusset plates, which had low rotational clearance. The weak beam underwent significant downward vertical deflection due to the brace unbalanced load, up to 63 mm, leading to large rotational demands at its ends and weld cracking in its beam-to-column connections.

- **TNCBF1-R-WF:** The first story of the specimen represented a repair with out-of-plane buckling wide flange braces. The desired buckling response was achieved on the first story, but the second story corner brace connections fractured prior to brace buckling. These connections had been retrofitted with brace net section reinforcement plates, but not before the development of net section cracking in previous tests. Repeated cycling in TNCBF1-N-HSS, TNCBF1-R-HSS, and TNCBF1-R-WF led to crack growth and eventually complete fracture of the brace splice connections at -0.57% and 0.62% story drift. Like TNCBF1-R-HSS, large rotational demands at the ends of the weak beam developed due to pull-down from the brace unbalanced load, but beam-to-column connection damage was further exacerbated by the unbraced nature of the second story and heat effects from multiple weld repairs. The first story beam-to-shear tab connections fractured around 1.5% story drift, though the beam was still connected to the columns through the beam-to-gusset plate welds. Gravity loads, which were not simulated in the test, could further threaten the integrity of the connection.

- **TNCBF2-D-HSS:** Both stories of the specimen represented a repair with details known to provide highly ductile performance. The first story beam was partially composite, though evaluating axial-flexural interaction considering its non-composite capacity and the design brace unbalanced load results in a DCR of 1.43. Brace buckling occurred on both stories, though the story drift distribution was weighted towards the first story. A first story drift range of 4.12% was achieved prior to brace fracture, which is only slightly less than that of SCBFs. The weak beam limited the tensile force developed by the first story braces and deflected up to 50 mm prior to brace fracture. In contrast, the strong beam on the second story was able to develop the yield strength of the braces. In concordance with these observations, the first story braces underwent less elongation and more shortening than the second story braces.

7.3 Conclusions

7.3.1 Response of Existing NCBFs and Rehabilitation Priority

The cyclic responses of the test specimens, particularly TNCBF1-N-HSS and TNCBF1-R-WF, suggest that the seismic performance of existing NCBFs may be poor due to strength and stiffness

Table 7.1: Rehabilitation priority of tested NCBF deficiencies

Priority	Deficiency	Geometric Limit or Limit State	Normalized Value or Unfactored DCR Tested
1	Brace compactness	Compactness ratio, $(b/t)/\lambda_{hd}$	2.27
2	Beam-to-column connections	Rotational capacity, θ/θ_c	> 1
		Shear tab-to-beam weld (UFM)	1.78
		Shear tab-to-column weld (UFM)	0.54
3	Brace splice connections	Brace net section rupture	1.25
		Brace block shear rupture	0.96
		Splice weld rupture	0.77
4	Beam strength	Axial-flexural interaction	2.66

degradation at modest story drift ranges (less than 1.2%). The ductility of NCBFs is substantially lower than that of SCBFs, where over 4% story drift range can be achieved if yielding mechanisms and failure modes are well-controlled (Lumpkin 2009). Several common NCBF deficiencies were simulated in the experiments and their contributions to the behavior of the frame are described below. The relative impacts of these component deficiencies also provides a basis for a rehabilitation priority, with "1" being the most important deficiency to address. An overview of the rehabilitation priority and associated deficiencies tested is provided in Table. 7.1.

1. **Brace compactness:** HSS braces with non-seismically compact cross sections ($b/t > \lambda_{hd}$) are highly detrimental to frame performance. Such braces have limited fracture life after buckling, which could lead to brace fracture at low story drifts and, consequently, dramatic reductions in lateral strength and stiffness. Consequently, brace compactness should be addressed in a minimum retrofit. The impact of braces with poor fracture life is so severe that issues due to other deficiencies would likely not manifest themselves. This retrofit could include brace replacement or concrete in-fill of HSS braces; the latter has been studied by Liu and Goel (1988) and Sloat (2014). These findings experimentally validate those of Rai and Goel (2003) for braced frame retrofit.

2. **Beam-to-column connections:** Beam-to-column connections in chevron configuration frames are subjected to large rotations due to frame action and beam deflection. Connections lacking adequate rotational capacity or moment resistance can develop damage (weld cracking, base metal tearing, bolt fracture, etc.) that reduces beam stiffness and may compromise structural integrity. Gravity loads were not simulated but would increase rotational demand. While beam-to-column connection retrofit appears less important, it could provide more stable lateral strength and stiffness when large beam deflections are expected and could help mitigate damage and post-earthquake repair costs.

3. **Brace splice connections:** Deficiencies in brace-to-gusset plate connections, specifically the limit states of brace net section, brace block shear, and weld rupture, can result in connection fracture when the brace is in tension. In instances where this occurred in testing, cracks initiated at the brace net section and propagated towards the brace end until complete fracture. Although this is a brittle failure mechanism that results in the loss of a brace in the system, it should be noted that this only occurred in cases where the braces did not buckle in the tests. Brace buckling may concentrate inelastic deformation elsewhere in the brace or connection and reduce the potential for fracture at the brace splice connection. Thus, the importance of brace splice connection retrofit is unclear but likely less critical than brace compactness and beam-to-column connection rehabilitation.

4. **Beam strength:** Beams in chevron configuration frames that do not satisfy the strength requirements of the Seismic Provisions (AISC 2010a) can undergo significant deflections after brace buckling due to the unbalanced load. Deflections as large as $L/100$ were recorded at the beam mid-span. Greater beam flexibility decreases the ultimate lateral resistance of the braces in a story but ductility is not necessarily reduced and the beam can serve as an additional energy dissipating element. While beams may be deficient with respect to design demands, beam strengthening, stiffening, or replacement does not appear to be necessary within the limits of the tested DCRs.

7.3.2 Rehabilitation Scheme Evaluation

The performance of TNCBF1-R-HSS, in which an in-plane buckling retrofit was installed on the first story, and TNCBF2-D-HSS, in which an out-of-plane (conventional) buckling retrofit was installed on both stories provides some insight into the impact of the respective rehabilitation schemes relative to the performance of TNCBF1-N-HSS, the specimen representing an existing NCBF.

- **In-plane buckling:** Retrofitting NCBFs with in-plane buckling may be desirable where gusset plate interface welds are undersized and/or existing gusset plate geometry does not permit adequate out-of-plane rotational clearance, as plastic hinging would be restricted to the knife plates and not the gusset plates. This was not achieved in the specimen TNCBF1-R-HSS, which implemented a knife plate repair with square HSS braces, where the braces buckled out-of-plane. The use of square HSS braces can be problematic in the context of in-plane buckling because the cross section radii of gyration are equal for both in- and out-of-plane actions. As a result, the initiation of in-plane buckling relies upon connection stiffness, which can be difficult to quantify. NCBFs may have additional connection flexibility that promotes out-of-plane buckling due to low torsional constants in weak beams and limited lateral bracing of beams at brace intersections.

- **Brace and connection replacement:** Retrofitting NCBFs with SCBF-standard braces and connections while preserving existing beams, including those that are weak, can improve the performance of an individual braced frame story. Although the beams may not be able to develop the design brace unbalanced load, which may result in large deflections, they can still achieve story ductility comparable to chevron configuration SCBFs with strong beams and multi-story X configuration SCBFs as long as the braces and connections have ductile characteristics.

7.3.3 Evaluation Recommendations

- When performing limit state analyses of NCBF components, it should be recognized that weak beams may limit the maximum tensile force achieved by the brace. The proposed beam plastic analysis model in Chapter 5 appears to provide an accurate method of predicting this

force through the expression given in Eq. 5.4. This approach requires further validation, but in general, using an effective brace yield force controlled by beam strength and the post-buckled strength of the brace in compression rather than the yield force of the brace section could provide a basis for accepting limit state capacities that would otherwise be deficient.

- The maximum lateral resistance provided by the braces in chevron and multi-story X configuration systems is overestimated by the plastic analysis load case where one brace yields in tension and the other reaches its critical buckling load in compression. These two events may occur in a braced frame bay, but they are not coincident. The brace in tension typically does not achieve its maximum force (P_{y} or $P_{\mathrm{y,eff}}$) until later drifts, when the force in the opposing compression brace has likely degraded. An alternative approach is to consider the lateral resistance provided by the braces just prior to brace buckling, where the brace forces reach P_{cr} in tension and compression. This approach underestimates lateral resistance in some cases, but the error is generally less than the overestimation from the plastic analysis case (i.e., it is generally a better estimate). These two approaches provide upper and lower bounds on brace lateral resistance. Thus, for capacity design, the plastic analysis case provides a conservative estimation of *demand*. However, when evaluating the ultimate lateral *capacity* of the frame, the pre-buckling case is conservative.

7.4 Future Work

The following recommendations are made for future work based upon limitations of the research presented in this thesis and new concerns that have been identified related to the system performance of existing and rehabilitated NCBFs.

- Experimental and analytical investigation of the performance of chevron braced frames with weaker and more flexible beams. The specimens presented in this thesis used the same beam section, though composite action varied. The experimental results suggest that beams with interaction values less than or equal to 2.66 (TNCBF1-R-HSS) can still allow good ductility and maintenance of strength of stiffness, which is contrary to some of the reasoning behind code requirements. Still, there may be a quantifiable limit at which low beam strength negatively impacts system performance to an unacceptable degree.

- Experimental investigation of the performance of existing and rehabilitated NCBF brace-to-beam/column connections subjected to demands from weak beam deformation as well as post-buckled brace deformation. In the testing regime presented in this thesis, a soft story was intended to form on the first story; when the welded shear tab connection was tested, the second story braces did not buckle and place additional demands on the corner gusset plate and shear tab connections. For the same reason, the effect of the partial slab embedment of the corner connections and brace ends was not studied, which may be of interest.

- Experimental investigation of the effect of load history on system performance. Reversed cyclic increasing amplitude load histories, which were used in the experiments, are often used in structural engineering to gauge seismic performance. However, this load history does not simulate an actual ground motion and may mask some failure mechanisms and diminish the importance of certain deficiencies.

- Experimental and analytical investigation of the effect of column strength on NCBF performance. Axially weak columns relative to brace capacities have been reported in the infrastructure review by Sloat (2014); this deficiency may present more serious performance drawbacks than weak beams. In post-buckled states, the braces contribute less to the lateral resistance of the frame due to degradation of compressive strength and eventually fracture in tension, requiring an increasing amount of shear to be carried through the columns to maintain a stable response.

- Continued experimental investigation of the performance of existing and rehabilitated NCBF brace connection classes. Thus far, welded shared shear tabs (Sloat 2014) and bolted shear tabs (Johnson 2014) have been evaluated, but several other connection classes remain untested, included bolted gusset plates that also serve as beam-to-column connections.

- Refinement of the finite element models developed by Lingli Pan in Abaqus (Dassault Systèmes 2013). In particular, a brace fracture criterion should be implemented in order to provide accurate response predictions.

- Analytical parametric studies on the impact of frame member strength, brace slenderness, beam lateral bracing, and other details on the seismic performance of NCBFs using high fidelity models (e.g., continuum models developed in Abaqus).

- Nonlinear time history analyses of existing and rehabilitated NCBFs to evaluate performance under dynamic loading and develop collapse fragility curves to quantify the effectiveness of various rehabilitation schemes. These analyses would also investigate the prevalence of soft story collapse in chevron braced frames with weak beams, an issue identified in previous research (Tremblay and Robert 2001).

Appendix A

SPECIMEN DRAWINGS

This appendix includes specimen construction and instrumentation drawings for the specimens described in this report, TNCBF1-N-HSS, TNCBF1-R-HSS, TNCBF1-R-WF, and TNCBF2-D-HSS. The construction drawings, designated "SK," were used by professional fabricators to build each specimen at the National Center for Research on Earthquake Engineering in Taiwan. The instrumentation drawings, designated "IN," were used to apply physical and optical sensors and whitewash the specimens. The test setup drawings produced by Chao-Hsien Li are also included in this appendix.

A.1 TNCBF1-N-HSS

The specimen drawings for TNCBF1-N-HSS are found below. This was the first specimen tested at NCREE in this test series, so this drawing set includes the complete frame.

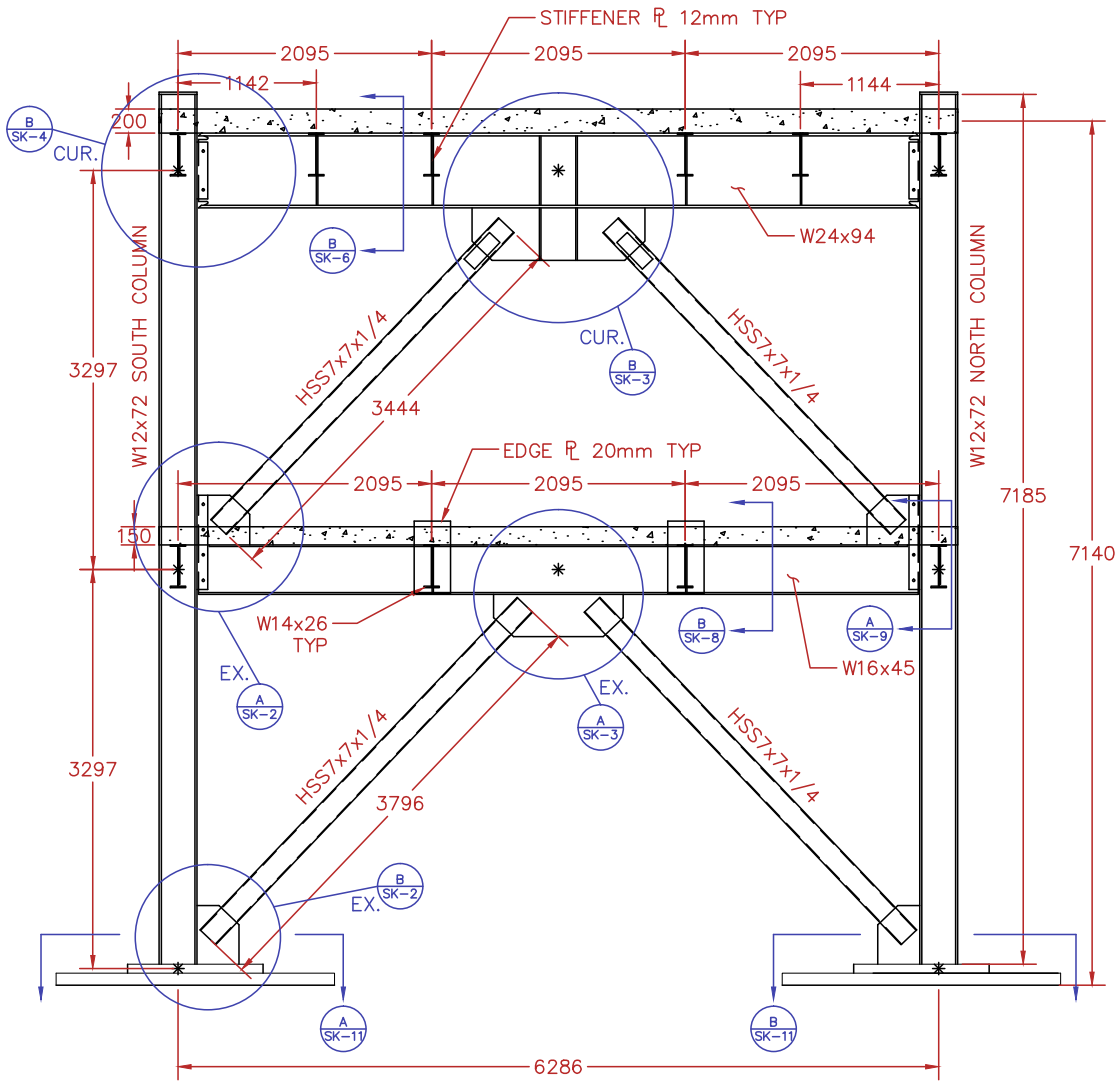

NOTES:
- CALLOUTS DESIGNATED "EX." USE AWS E71T-7 OR EQUIVALENT (NO CVN IMPACT REQUIREMENT) FOR FILLET WELDS ONLY
- CALLOUTS DESIGNATED "CUR." TO SATISFY AISC DEMAND CRITICAL AWS E71T-8 OR EQUIVALENT FOR FILLET WELDS ONLY
- ALL OTHER WELDS (STIFFENER PLATE FILLET WELDS, CJP WELDS, ETC.) TO SATISFY AISC DEMAND CRITICAL AWS E71T-8 OR EQUIVALENT
- CONCRETE SLABS TO HAVE SPECIFIED COMPRESSIVE STRENGTH OF 6.0 KSI

SCALE: 1mm = 50mm

TNCBF1-N-HSS: NON-DUCTILE DETAILS/HSS BRACES

NEESR: SEISMIC REHAB. OF VULNERABLE BRACED FRAMES

DWG: SK-1

DRAWN BY: ADS
DESIGNED BY: ADS
DATE: 6/27/2013
REVISED: 9/8/2014
CONTACT: ADSEN@UW.EDU

A
SK–2

2F CORNER GUSSET PLATE DETAIL
SCALE: 1mm = 20mm

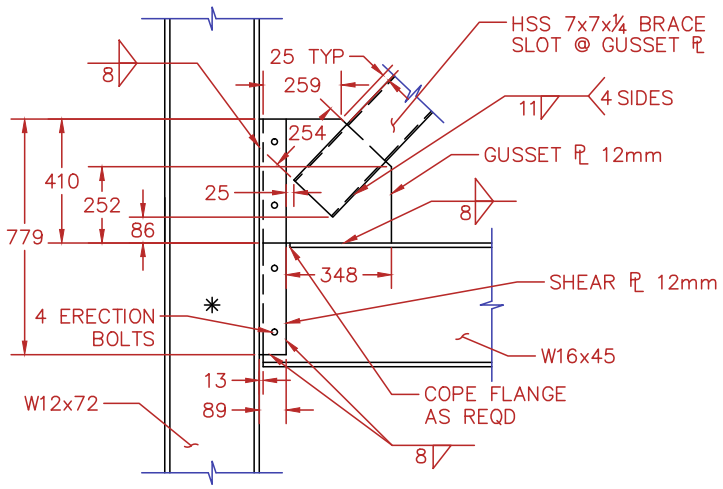

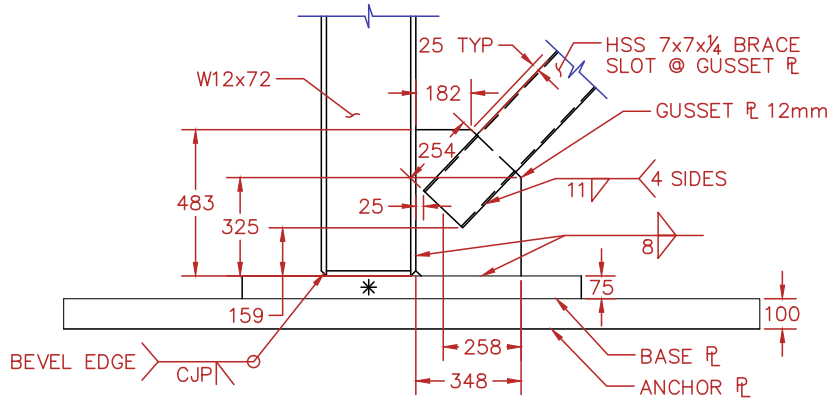

B
SK–2

1F CORNER GUSSET PLATE DETAIL
SCALE: 1mm = 20mm

NOTES:
–ALL PLATE STEEL A572 GR 50 OR EQUIVALENT
–ALL ROLLED SHAPES TO BE A992 OR EQUIVALENT
–ALL BRACES TO BE A500 GR B/C OR EQUIVALENT
–ALL WELDS AS DESIGNATED IN SK–1
–ALL STRUCTURAL BOLTS TO BE F10T

TNCBF1-N-HSS: NON-DUCTILE DETAILS/HSS BRACES

NEESR: SEISMIC REHAB. OF VULNERABLE BRACED FRAMES

DRAWN BY: ADS
DESIGNED BY: ADS
DATE: 6/27/2013
REVISED: 9/8/2014
CONTACT: ADSEN@UW.EDU

DWG: SK-2

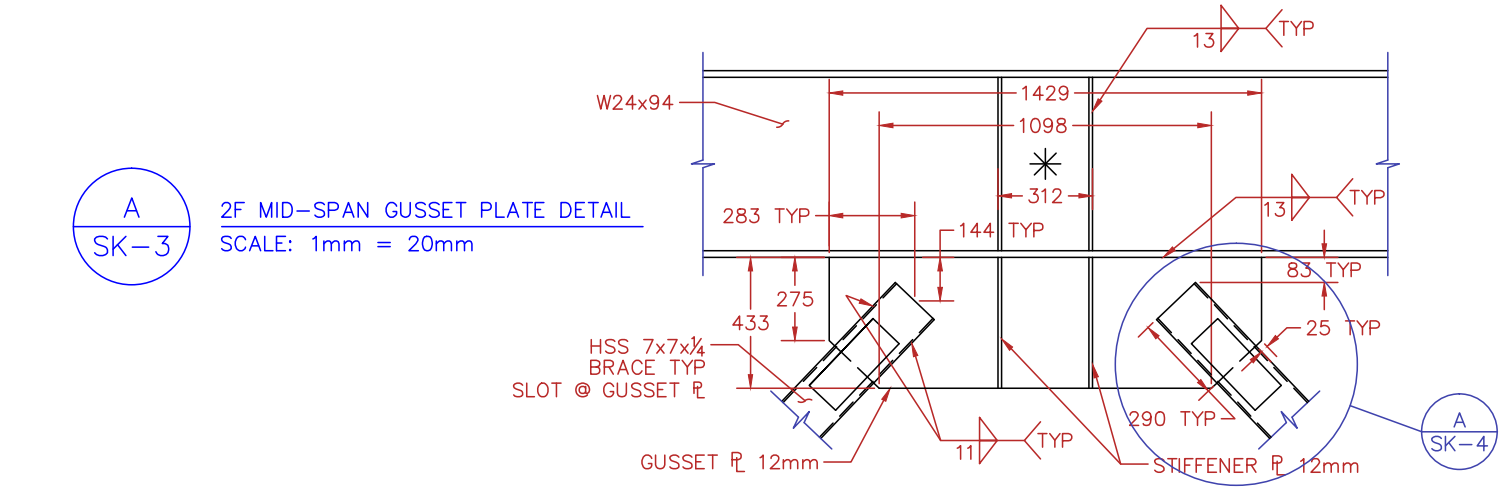

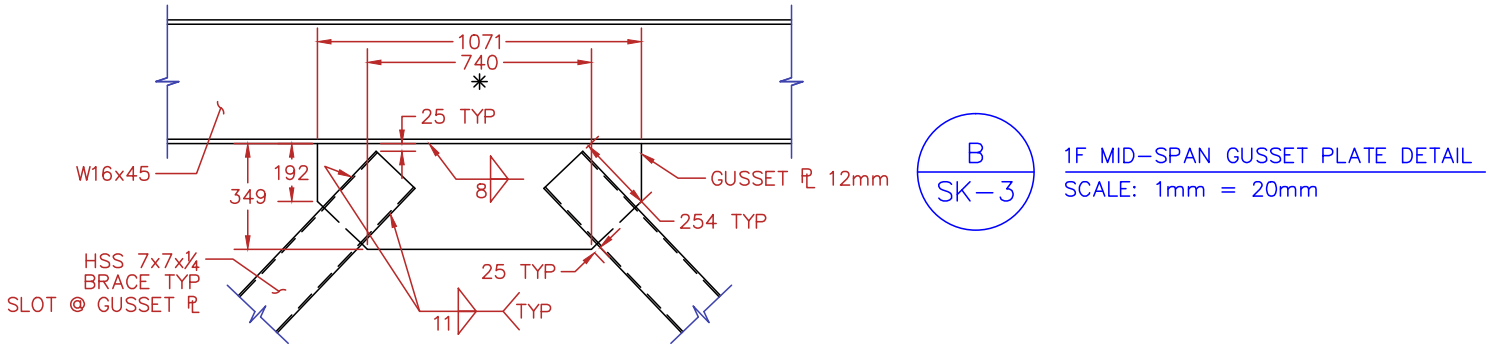

NOTES:
- ALL PLATE STEEL A572 GR 50 OR EQUIVALENT
- ALL ROLLED SHAPES TO BE A992 OR EQUIVALENT
- ALL BRACES TO BE A500 GR B/C OR EQUIVALENT
- ALL WELDS AS DESIGNATED IN SK–1
- ALL STRUCTURAL BOLTS TO BE F10T

TNCBF1-N-HSS: NON-DUCTILE DETAILS/HSS BRACES

NEESR: SEISMIC REHAB. OF VULNERABLE BRACED FRAMES

DRAWN BY: ADS
DESIGNED BY: ADS
DATE: 6/27/2013
REVISED: 9/8/2014
CONTACT: ADSEN@UW.EDU

DWG: SK-3

A
SK–4

NET SECTION REINFORCEMENT DETAIL
SCALE: 1mm = 20mm

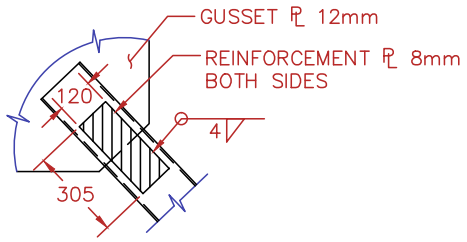

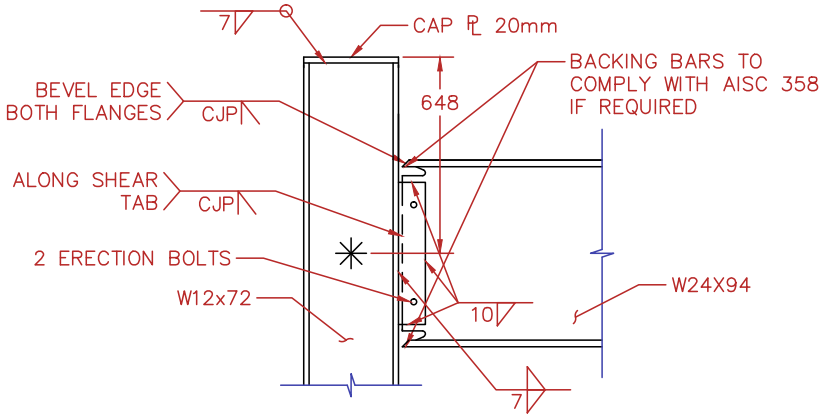

B
SK–4

2F BEAM–TO–COLUMN CONN. DETAIL
SCALE: 1mm = 20mm

C
SK–4

BRACE SLOT DETAIL
SCALE: 1mm = 20mm

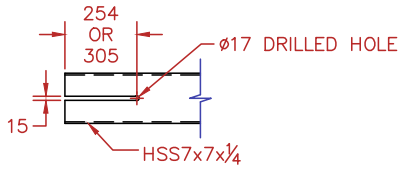

NOTES:
–ALL PLATE STEEL A572 GR 50 OR EQUIVALENT
–ALL ROLLED SHAPES TO BE A992 OR EQUIVALENT
–ALL BRACES TO BE A500 GR B/C OR EQUIVALENT
–ALL WELDS AS DESIGNATED IN SK–1
–ALL STRUCTURAL BOLTS TO BE F10T

TNCBF1-N-HSS: NON-DUCTILE DETAILS/HSS BRACES

NEESR: SEISMIC REHAB. OF VULNERABLE BRACED FRAMES

DRAWN BY: ADS
DESIGNED BY: ADS
DATE: 6/27/2013
REVISED: 9/8/2014
CONTACT: ADSEN@UW.EDU

DWG: SK-4

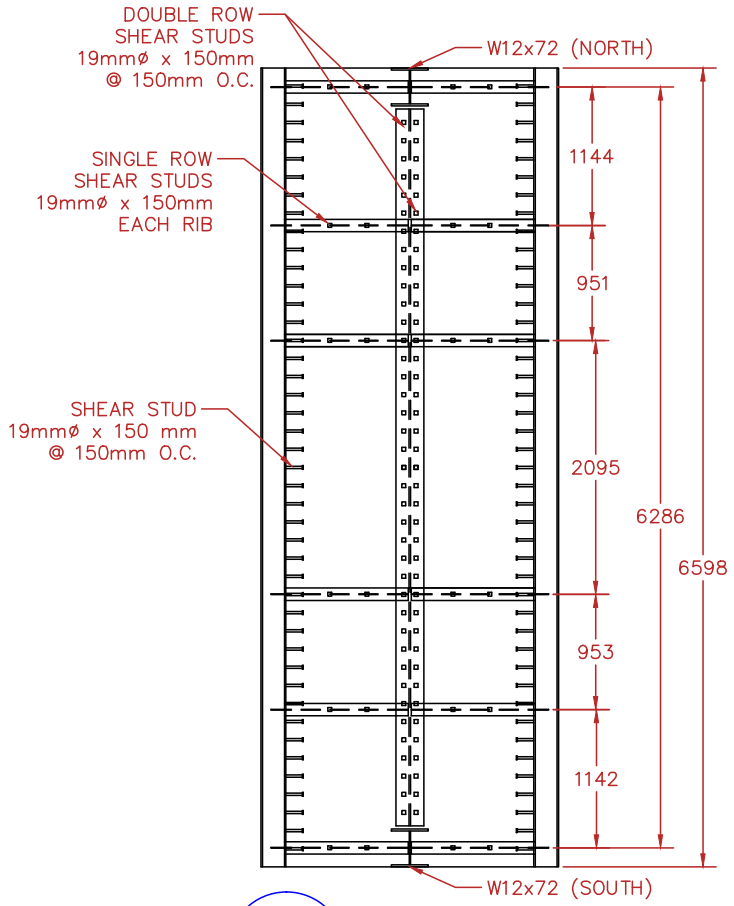

A
SK–5

2F SLAB PLAN
SCALE: 1mm = 50mm

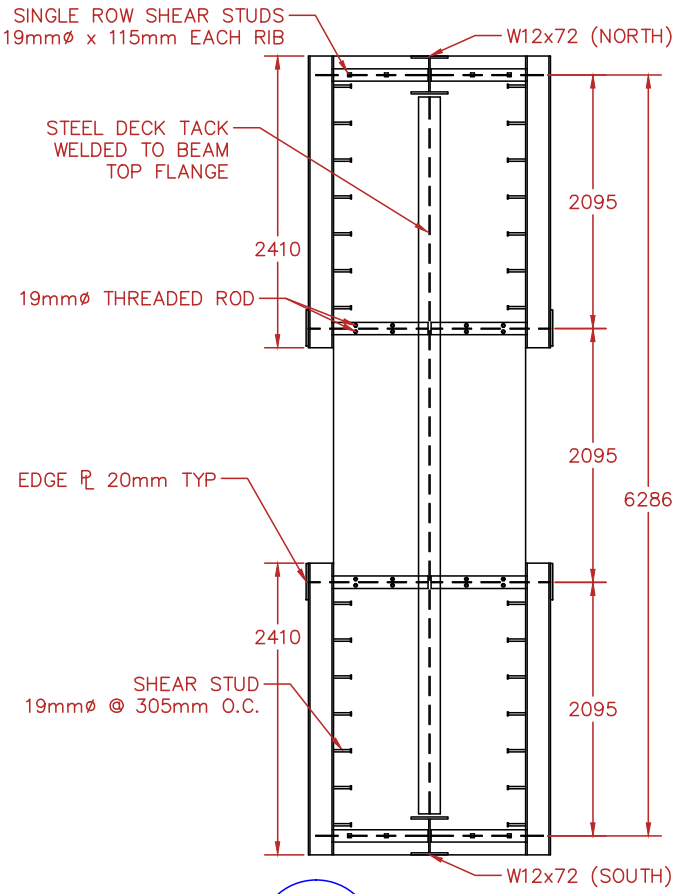

B
SK–5

1F SLAB PLAN
SCALE: 1mm = 50mm

NOTES:
–ALL PLATE STEEL A572 GR 50 OR EQUIVALENT
–ALL ROLLED SHAPES TO BE A992 OR EQUIVALENT
–ALL BRACES TO BE A500 GR B/C OR EQUIVALENT
–ALL WELDS AS DESIGNATED IN SK–1
–ALL STRUCTURAL BOLTS TO BE F10T

TNCBF1-N-HSS: NON-DUCTILE DETAILS/HSS BRACES

NEESR: SEISMIC REHAB. OF VULNERABLE BRACED FRAMES

DRAWN BY: ADS
DESIGNED BY: ADS
DATE: 6/27/2013
REVISED: 9/8/2014
CONTACT: ADSEN@UW.EDU

DWG: SK-5

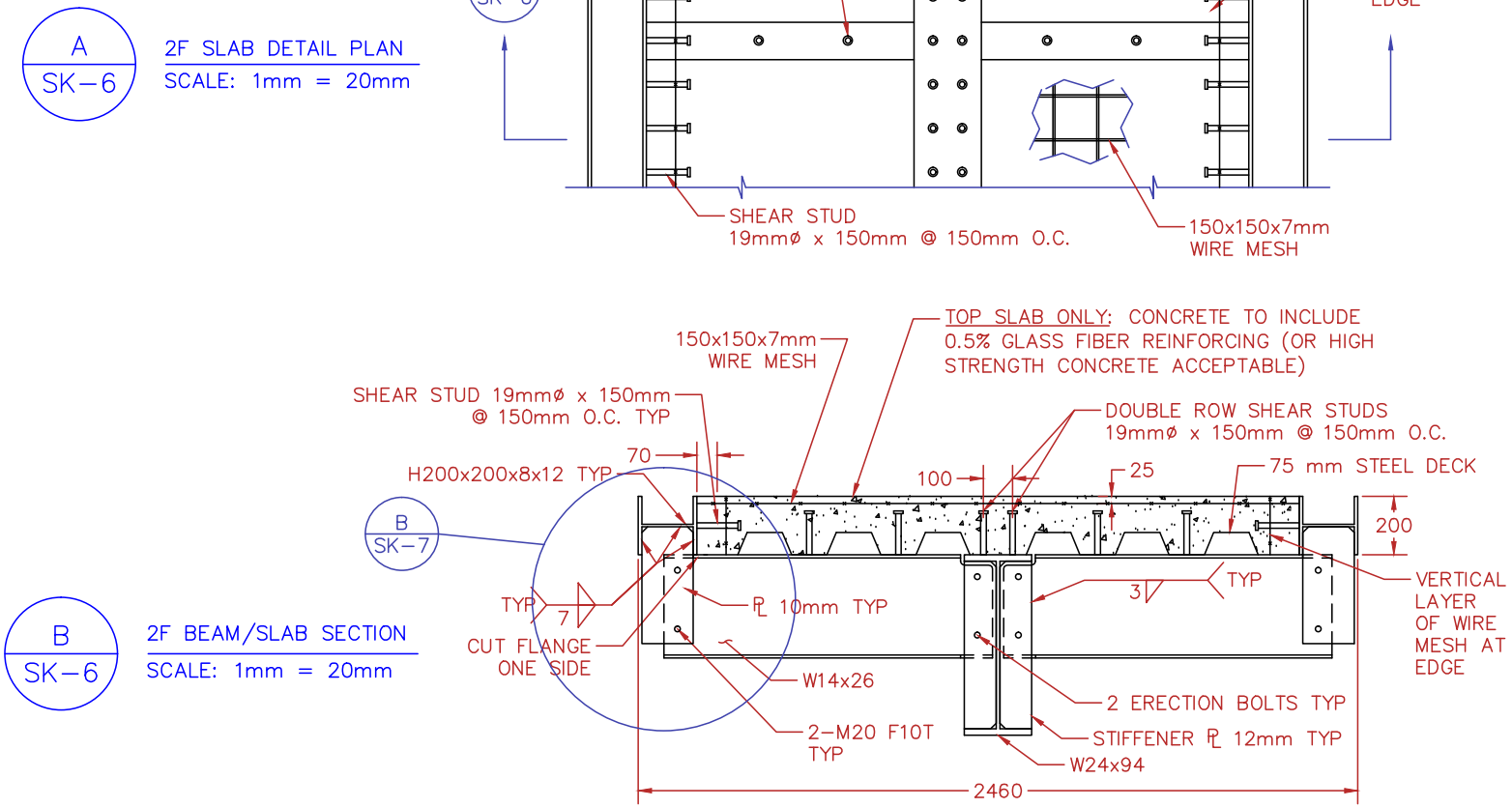

NOTES:
- ALL PLATE STEEL A572 GR 50 OR EQUIVALENT
- ALL ROLLED SHAPES TO BE A992 OR EQUIVALENT
- ALL BRACES TO BE A500 GR B/C OR EQUIVALENT
- ALL WELDS AS DESIGNATED IN SK–1
- ALL STRUCTURAL BOLTS TO BE F10T

TNCBF1-N-HSS: NON-DUCTILE DETAILS/HSS BRACES

NEESR: SEISMIC REHAB. OF VULNERABLE BRACED FRAMES

DRAWN BY: ADS
DESIGNED BY: ADS
DATE: 6/27/2013
REVISED: 9/8/2014
CONTACT: ADSEN@UW.EDU

DWG: SK-6

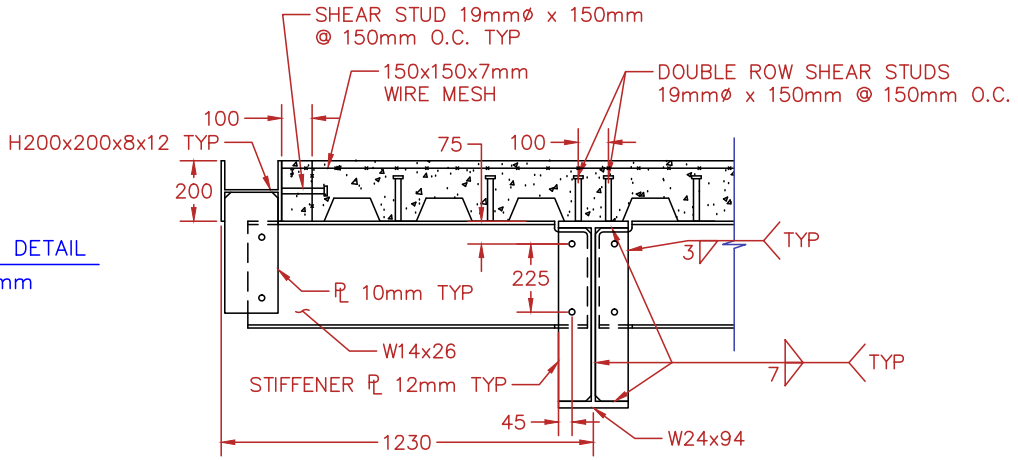

A / SK–7

2F BEAM STIFFENER DETAIL

SCALE: 1mm = 20mm

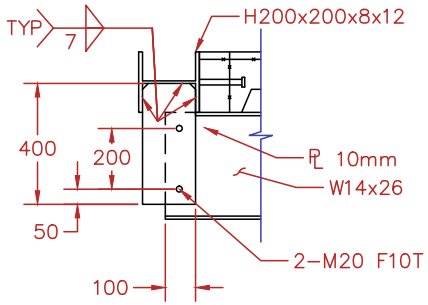

B / SK–7

2F BEAM/SLAB EDGE DETAIL

SCALE: 1mm = 20mm

NOTES:
- ALL PLATE STEEL A572 GR 50 OR EQUIVALENT
- ALL ROLLED SHAPES TO BE A992 OR EQUIVALENT
- ALL BRACES TO BE A500 GR B/C OR EQUIVALENT
- ALL WELDS AS DESIGNATED IN SK–1
- ALL STRUCTURAL BOLTS TO BE F10T

TNCBF1-N-HSS: NON-DUCTILE DETAILS/HSS BRACES

NEESR: SEISMIC REHAB. OF VULNERABLE BRACED FRAMES

DRAWN BY: ADS
DESIGNED BY: ADS
DATE: 6/27/2013
REVISED: 9/8/2014
CONTACT: ADSEN@UW.EDU

DWG: SK-7

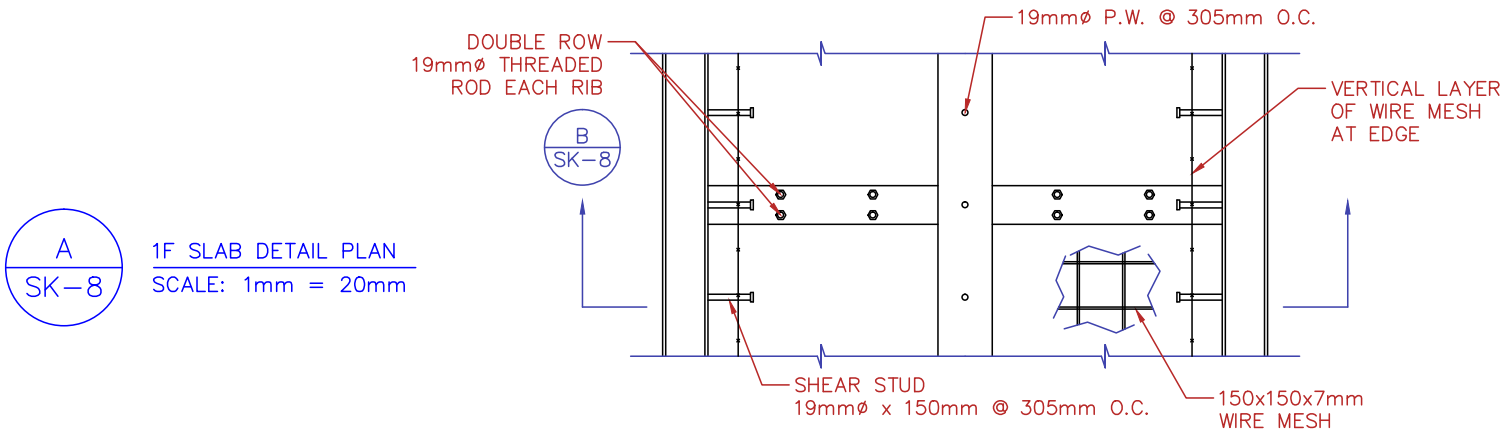

A
SK–8

1F SLAB DETAIL PLAN
SCALE: 1mm = 20mm

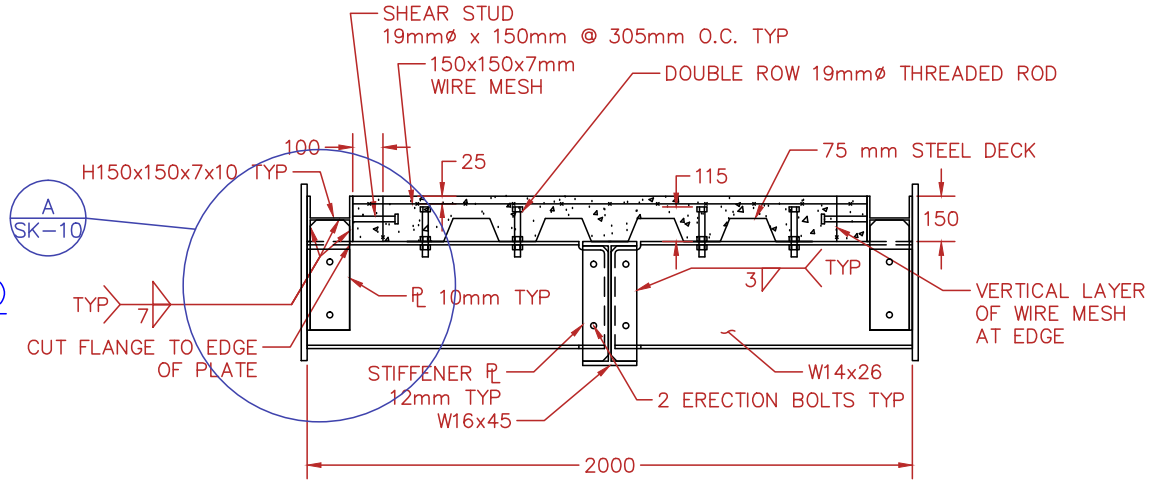

B
SK–8

1F BEAM/SLAB SECTION
(INTERIOR FLOOR BEAMS)
SCALE: 1mm = 20mm

NOTES:
–ALL PLATE STEEL A572 GR 50 OR EQUIVALENT
–ALL ROLLED SHAPES TO BE A992 OR EQUIVALENT
–ALL BRACES TO BE A500 GR B/C OR EQUIVALENT
–ALL WELDS AS DESIGNATED IN SK–1
–ALL STRUCTURAL BOLTS TO BE F10T

TNCBF1-N-HSS: NON-DUCTILE DETAILS/HSS BRACES

NEESR: SEISMIC REHAB. OF VULNERABLE BRACED FRAMES

DRAWN BY: ADS
DESIGNED BY: ADS
DATE: 6/27/2013
REVISED: 9/8/2014
CONTACT: ADSEN@UW.EDU

DWG: SK-8

A
SK–9

1F BEAM/SLAB SECTION
(EXTERIOR FLOOR BEAMS)

SCALE: 1mm = 20mm

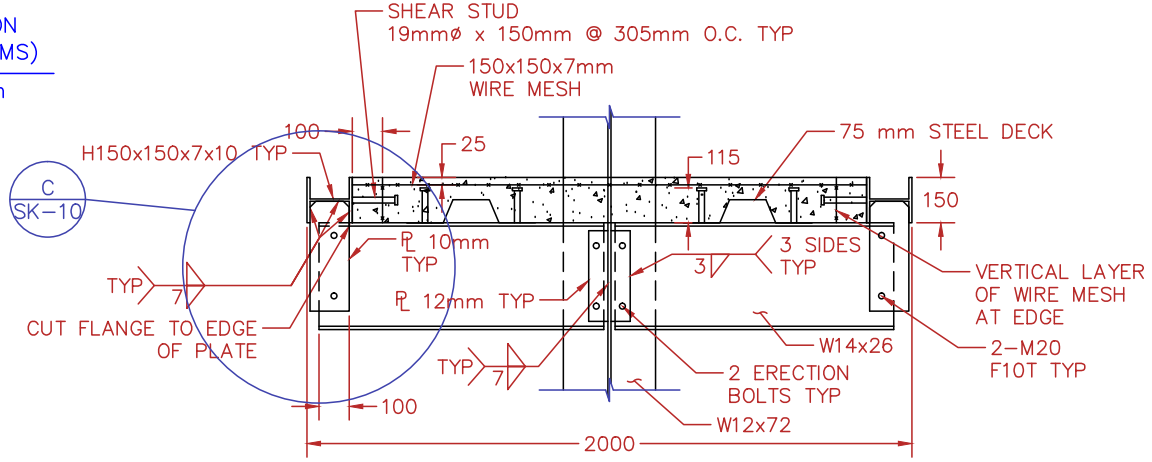

B
SK–9

TYPICAL FLOOR BEAM–TO–COLUMN CONNECTION

SCALE: 1mm = 20mm

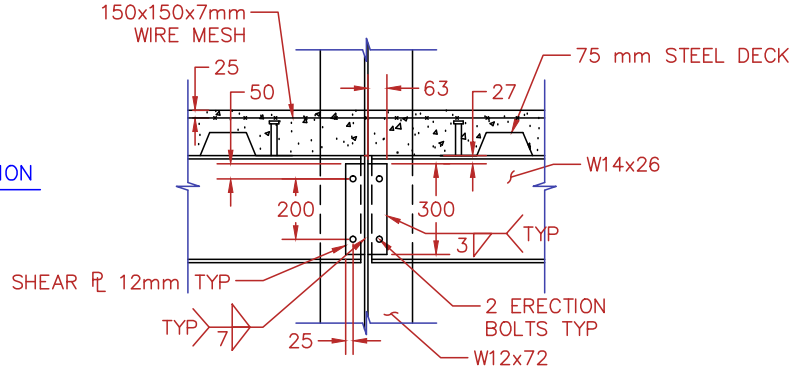

NOTES:
–ALL PLATE STEEL A572 GR 50 OR EQUIVALENT
–ALL ROLLED SHAPES TO BE A992 OR EQUIVALENT
–ALL BRACES TO BE A500 GR B/C OR EQUIVALENT
–ALL WELDS AS DESIGNATED IN SK–1
–ALL STRUCTURAL BOLTS TO BE F10T

TNCBF1-N-HSS: NON-DUCTILE DETAILS/HSS BRACES

NEESR: SEISMIC REHAB. OF VULNERABLE BRACED FRAMES

DRAWN BY: ADS
DESIGNED BY: ADS
DATE: 6/27/2013
REVISED: 9/8/2014
CONTACT: ADSEN@UW.EDU

DWG: SK-9

A
SK–10

1F EDGE PLATE DETAIL
SCALE: 1mm = 20mm

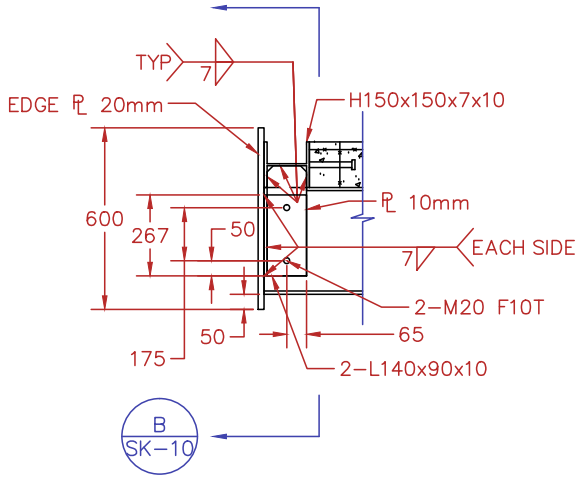

B
SK–10

1F INTERIOR FLOOR BEAM SECTION
SCALE: 1mm = 20mm

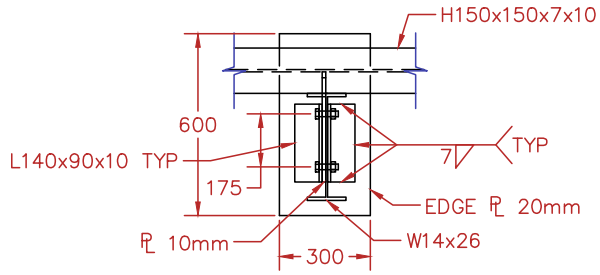

C
SK–9

1F BEAM EDGE BEAM DETAIL
(EXTERIOR FLOOR BEAMS)
SCALE: 1mm = 20mm

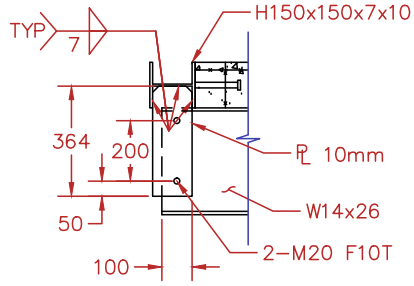

NOTES:
–ALL PLATE STEEL A572 GR 50 OR EQUIVALENT
–ALL ROLLED SHAPES TO BE A992 OR EQUIVALENT
–ALL BRACES TO BE A500 GR B/C OR EQUIVALENT
–ALL WELDS AS DESIGNATED IN SK–1
–ALL STRUCTURAL BOLTS TO BE F10T

TNCBF1-N-HSS: NON-DUCTILE DETAILS/HSS BRACES

NEESR: SEISMIC REHAB. OF VULNERABLE BRACED FRAMES

DRAWN BY: ADS
DESIGNED BY: ADS
DATE: 6/27/2013
REVISED: 9/8/2014
CONTACT: ADSEN@UW.EDU

DWG: SK-10

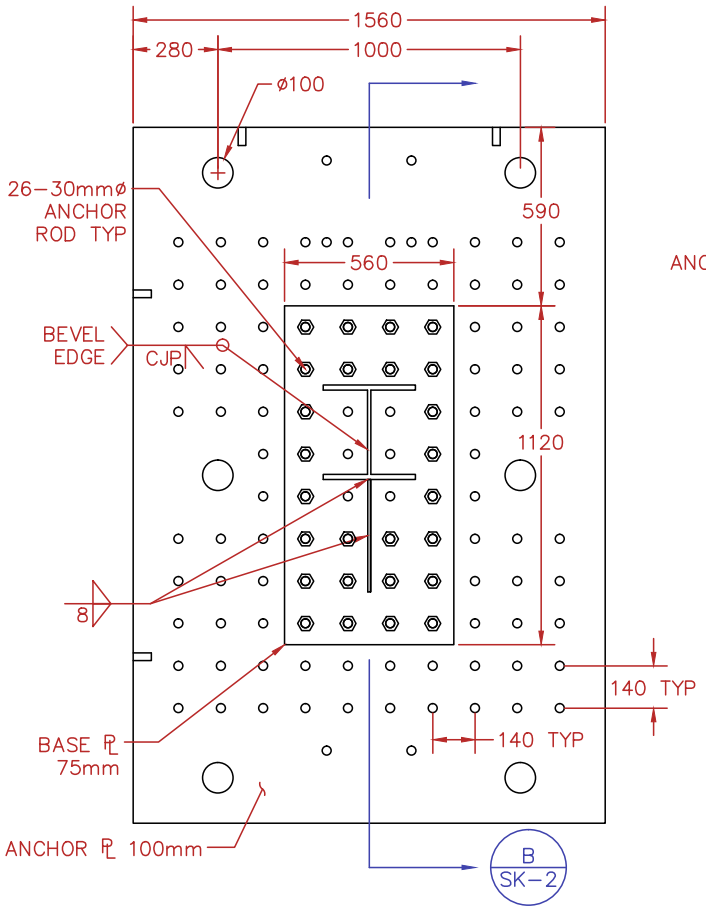

A
SK–11

SOUTH BASE PLATE DETAIL
SCALE: 1mm = 20mm

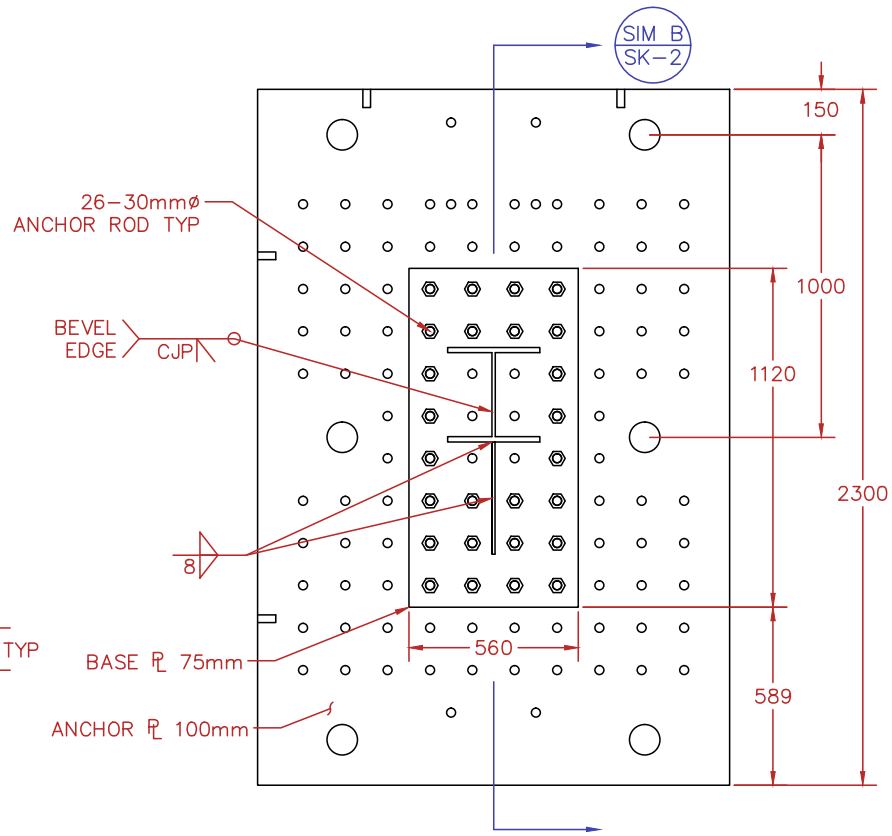

B
SK–11

NORTH BASE PLATE DETAIL
SCALE: 1mm = 20mm

NOTES:
–ALL PLATE STEEL A572 GR 50 OR EQUIVALENT
–ALL ROLLED SHAPES TO BE A992 OR EQUIVALENT
–ALL BRACES TO BE A500 GR B/C OR EQUIVALENT
–ALL WELDS AS DESIGNATED IN SK–1
–ALL STRUCTURAL BOLTS TO BE F10T

TNCBF1-N-HSS: NON-DUCTILE DETAILS/HSS BRACES

NEESR: SEISMIC REHAB. OF VULNERABLE BRACED FRAMES

DRAWN BY: ADS
DESIGNED BY: ADS
DATE: 6/27/2013
REVISED: 9/8/2014
CONTACT: ADSEN@UW.EDU

DWG: SK-11

A
SK–12

2F BEAM FABRICATION DETAIL
SCALE: 1mm = 50mm

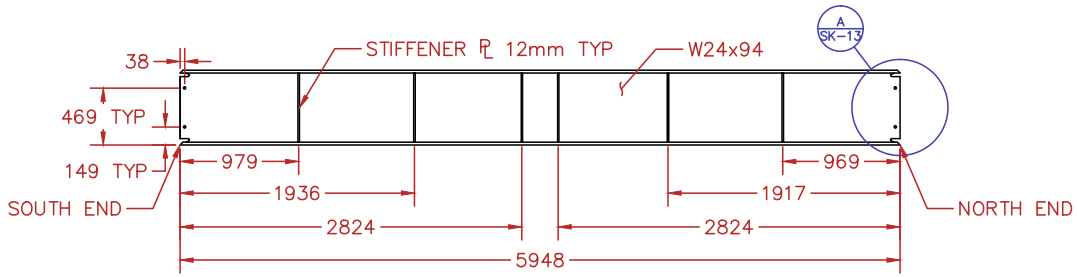

B
SK–12

1F BEAM FABRICATION DETAIL
SCALE: 1mm = 50mm

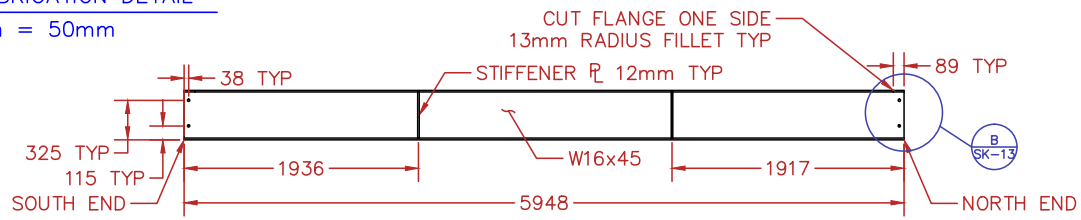

NOTES:
–ALL PLATE STEEL A572 GR 50 OR EQUIVALENT
–ALL ROLLED SHAPES TO BE A992 OR EQUIVALENT
–ALL BRACES TO BE A500 GR B/C OR EQUIVALENT
–ALL WELDS AS DESIGNATED IN SK–1
–ALL STRUCTURAL BOLTS TO BE F10T

TNCBF1-N-HSS: NON-DUCTILE DETAILS/HSS BRACES

NEESR: SEISMIC REHAB. OF VULNERABLE BRACED FRAMES

DRAWN BY: ADS
DESIGNED BY: ADS
DATE: 6/27/2013
REVISED: 9/8/2014
CONTACT: ADSEN@UW.EDU

DWG: SK-12

A
SK–13

2F BEAM END DETAIL
SCALE: 1mm = 20mm

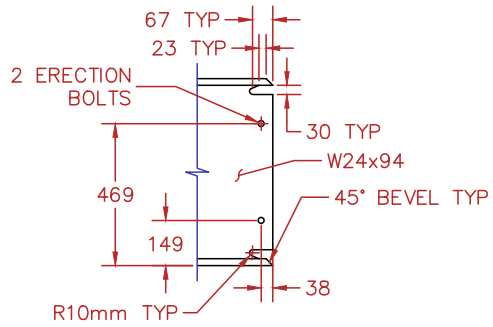

B
SK–13

1F BEAM END DETAIL
SCALE: 1mm = 20mm

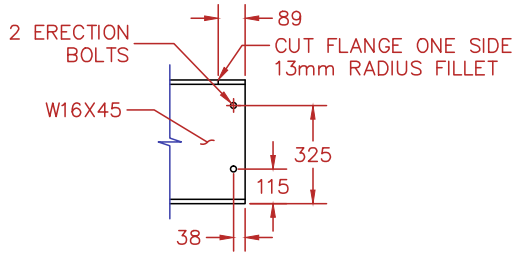

NOTES:
–ALL PLATE STEEL A572 GR 50 OR EQUIVALENT
–ALL ROLLED SHAPES TO BE A992 OR EQUIVALENT
–ALL BRACES TO BE A500 GR B/C OR EQUIVALENT
–ALL WELDS AS DESIGNATED IN SK–1
–ALL STRUCTURAL BOLTS TO BE F10T

TNCBF1-N-HSS: NON-DUCTILE DETAILS/HSS BRACES

NEESR: SEISMIC REHAB. OF VULNERABLE BRACED FRAMES

DRAWN BY: ADS
DESIGNED BY: ADS
DATE: 6/27/2013
REVISED: 9/8/2014
CONTACT: ADSEN@UW.EDU

DWG: SK-13

A
SK–14

2F INTERIOR FLOOR BEAM
FABRICATION DETAIL

SCALE: 1mm = 20mm

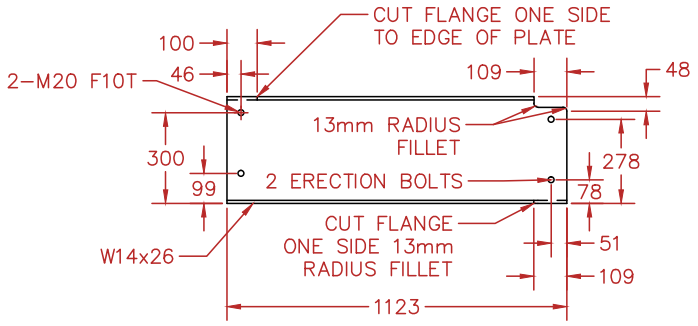

B
SK–14

2F EXTERIOR FLOOR BEAM
FABRICATION DETAIL

SCALE: 1mm = 20mm

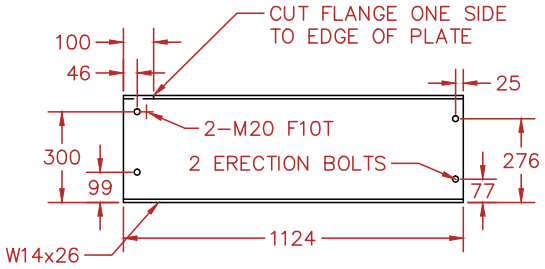

NOTES:
–ALL PLATE STEEL A572 GR 50 OR EQUIVALENT
–ALL ROLLED SHAPES TO BE A992 OR EQUIVALENT
–ALL BRACES TO BE A500 GR B/C OR EQUIVALENT
–ALL WELDS AS DESIGNATED IN SK–1
–ALL STRUCTURAL BOLTS TO BE F10T

TNCBF1-N-HSS: NON-DUCTILE DETAILS/HSS BRACES

NEESR: SEISMIC REHAB. OF VULNERABLE BRACED FRAMES

DRAWN BY: ADS
DESIGNED BY: ADS
DATE: 6/27/2013
REVISED: 9/8/2014
CONTACT: ADSEN@UW.EDU

DWG: SK-14

A
SK–15

1F INTERIOR FLOOR BEAM
FABRICATION DETAIL

SCALE: 1mm = 20mm

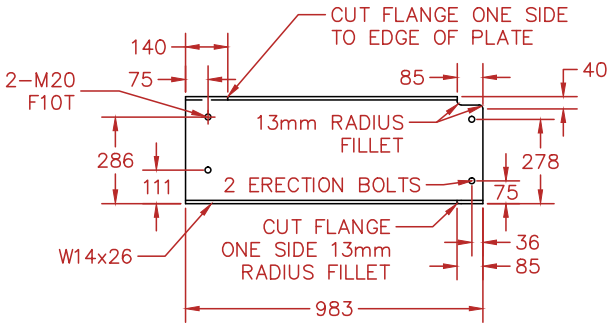

B
SK–15

1F EXTERIOR FLOOR BEAM
FABRICATION DETAIL

SCALE: 1mm = 20mm

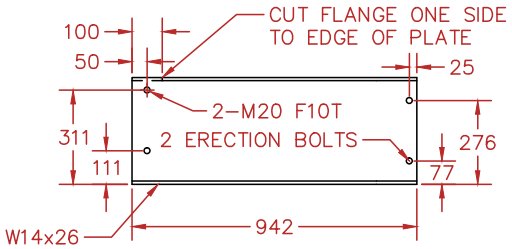

NOTES:
–ALL PLATE STEEL A572 GR 50 OR EQUIVALENT
–ALL ROLLED SHAPES TO BE A992 OR EQUIVALENT
–ALL BRACES TO BE A500 GR B/C OR EQUIVALENT
–ALL WELDS AS DESIGNATED IN SK–1
–ALL STRUCTURAL BOLTS TO BE F10T

TNCBF1-N-HSS: NON-DUCTILE DETAILS/HSS BRACES

NEESR: SEISMIC REHAB. OF VULNERABLE BRACED FRAMES

DRAWN BY: ADS
DESIGNED BY: ADS
DATE: 6/27/2013
REVISED: 9/8/2014
CONTACT: ADSEN@UW.EDU

DWG: SK-15

A
SK–16

2F CORNER GUSSET PLATE CONNECTION
FABRICATION DETAIL

SCALE: 1mm = 20mm

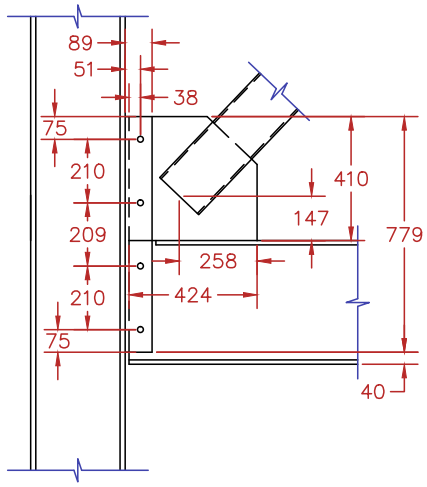

NOTES:
–ALL PLATE STEEL A572 GR 50 OR EQUIVALENT
–ALL ROLLED SHAPES TO BE A992 OR EQUIVALENT
–ALL BRACES TO BE A500 GR B/C OR EQUIVALENT
–ALL WELDS AS DESIGNATED IN SK–1
–ALL STRUCTURAL BOLTS TO BE F10T

TNCBF1-N-HSS: NON-DUCTILE DETAILS/HSS BRACES

NEESR: SEISMIC REHAB. OF VULNERABLE BRACED FRAMES

DRAWN BY: ADS
DESIGNED BY: ADS
DATE: 6/27/2013
REVISED: 9/8/2014
CONTACT: ADSEN@UW.EDU

DWG: SK-16

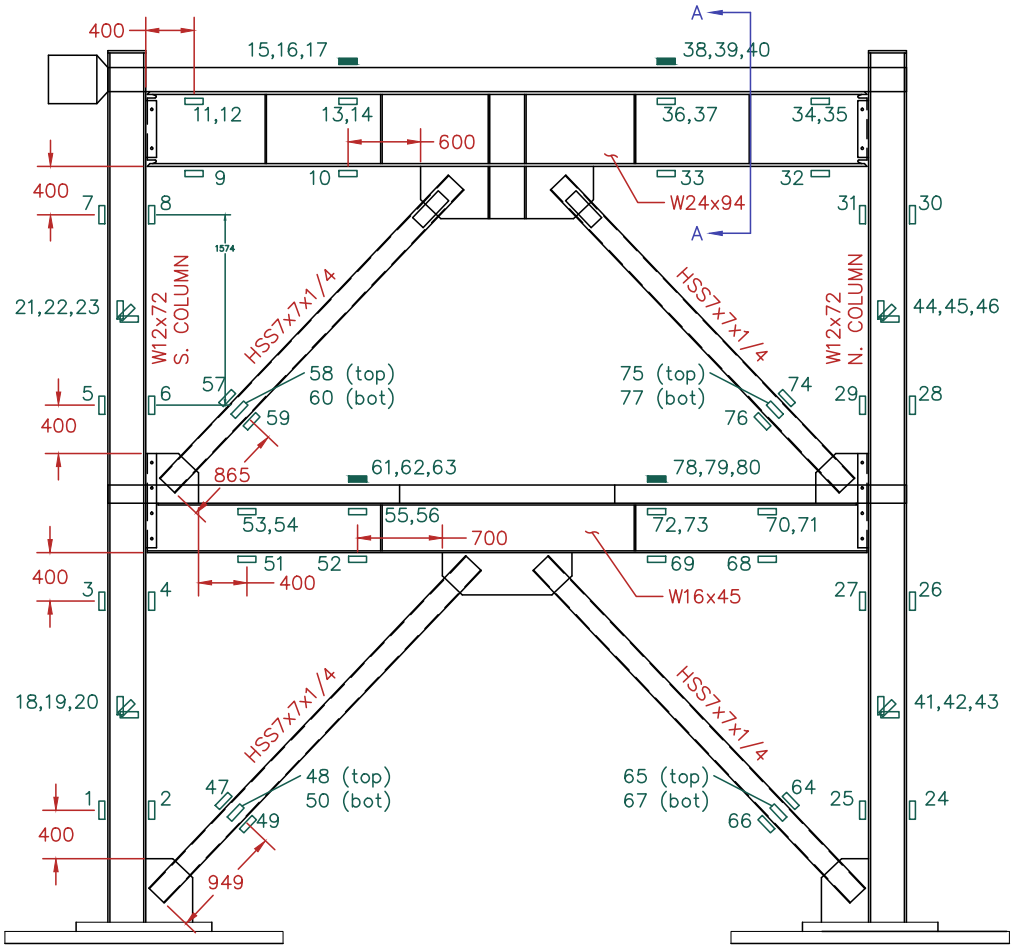

STRAIN GAUGE LAYOUT
SCALE: 1mm = 50mm

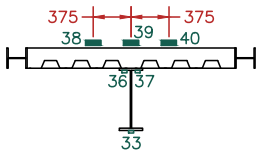

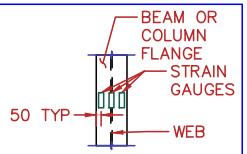

NOTE: LOCATE SG ON CENTER OF FLANGE OR UNDERSIDE OF FLANGE 50mm FROM EDGE AS NECESSARY.

KEY
- STEEL UNIAXIAL STRAIN GAUGE
- CONCRETE UNIAXIAL STRAIN GAUGE
- TRIAXIAL STRAIN GAUGE

	LABEL	LOCATION		LABEL	LOCATION
1	SG 1	S COLUMN	24	SG 24	N COLUMN
2	SG 2	S COLUMN	25	SG 25	N COLUMN
3	SG 3	S COLUMN	26	SG 26	N COLUMN
4	SG 4	S COLUMN	27	SG 27	N COLUMN
5	SG 5	S COLUMN	28	SG 28	N COLUMN
6	SG 6	S COLUMN	29	SG 29	N COLUMN
7	SG 7	S COLUMN	30	SG 30	N COLUMN
8	SG 8	S COLUMN	31	SG 31	N COLUMN
9	SG 9	S TOP BEAM	32	SG 32	N TOP BEAM
10	SG 10	S TOP BEAM	33	SG 33	N TOP BEAM
11	SG 11	S TOP BEAM*	34	SG 34	N TOP BEAM*
12	SG 12	S TOP BEAM*	35	SG 35	N TOP BEAM*
13	SG 13	S TOP BEAM*	36	SG 36	N TOP BEAM*
14	SG 14	S TOP BEAM*	37	SG 37	N TOP BEAM*
15	SG 15	S TOP SLAB	38	SG 38	N TOP SLAB
16	SG 16	S TOP SLAB	39	SG 39	N TOP SLAB
17	SG 17	S TOP SLAB	40	SG 40	N TOP SLAB
18	SG 18	S COL BOT 0°	41	SG 41	N COL BOT 0°
19	SG 19	S COL BOT 45°	42	SG 42	N COL BOT 45°
20	SG 20	S COL BOT 90°	43	SG 43	N COL BOT 90°
21	SG 21	S COL TOP 0°	44	SG 44	N COL TOP 0°
22	SG 22	S COL TOP 45°	45	SG 45	N COL TOP 45°
23	SG 23	S COL TOP 90°	46	SG 46	N COL TOP 90°

	LABEL	LOCATION		LABEL	LOCATION
47	SG 47	S BOT BRACE	64	SG 64	N BOT BRACE
48	SG 48	S BOT BRACE	65	SG 65	N BOT BRACE
49	SG 49	S BOT BRACE	66	SG 66	N BOT BRACE
50	SG 50	S BOT BRACE	67	SG 67	N BOT BRACE
51	SG 51	S BOT BEAM	68	SG 68	N BOT BEAM
52	SG 52	S BOT BEAM	69	SG 69	N BOT BEAM
53	SG 53	S BOT BEAM*	70	SG 70	N BOT BEAM*
54	SG 54	S BOT BEAM*	71	SG 71	N BOT BEAM*
55	SG 55	S BOT BEAM*	72	SG 72	N BOT BEAM*
56	SG 56	S BOT BEAM*	73	SG 73	N BOT BEAM*
57	SG 57	S TOP BRACE	74	SG 74	N TOP BRACE
58	SG 58	S TOP BRACE	75	SG 75	N TOP BRACE
59	SG 59	S TOP BRACE	76	SG 76	N TOP BRACE
60	SG 60	S TOP BRACE	77	SG 77	N TOP BRACE
61	SG 61	S BOT SLAB	78	SG 78	N BOT SLAB
62	SG 62	S BOT SLAB	79	SG 79	N BOT SLAB
63	SG 63	S BOT SLAB	80	SG 80	N BOT SLAB

* LOCATE STRAIN GAUGE AT UNDERSIDE OF BEAM FLANGE

TNCBF1-N-HSS: NON-DUCTILE DETAILS/HSS BRACES

NEESR: SEISMIC REHAB. OF VULNERABLE BRACED FRAMES

DWG: IN-1

DRAWN BY: ADS
DESIGNED BY: ADS
DATE: 6/27/2013
REVISED: 9/10/2014
CONTACT: ADSEN@UW.EDU

KEY

- POTENTIOMETER PERPENDICULAR TO PLANE
- POTENTIOMETER IN DIRECTION OF ARROW
- TILTMETER (T)
- NDI OPTOTRAK LED TARGET (N)

ABBREVIATIONS

N	NORTH
S	SOUTH
E	EAST
W	WEST
BOT	BOTTOM
MID	MIDDLE
COL	COLUMN
BR	BRACE
PL	PLATE
OOP	OUT OF PLANE
IP	IN PLANE
DIAG	DIAGONAL
DISP	DISPLACEMENT
ROT	ROTATION
PT	POINT
WP	WORK POINT
L	LOWER
U	UPPER

TILTMETER DESIGNATIONS

○	DESCRIPTION	RANGE +/−
T1	1F S COL ROT L	5°
T2	1F S COL ROT L	10°
T3	1F S COL FLANGE AT BEAM	10°
T4	1F S COL ROT U	10°
T5	1F S COL ROT U	10°
T6	2F BEAM ROT MID S SIDE	10°
T7	2F BEAM ROT MID S SIDE	5°
T8	1F BEAM ROT S SIDE	5°
T9	1F BEAM ROT S SIDE	10°
T10	1F BEAM ROT MID S SIDE	5°
T11	1F BEAM ROT MID S SIDE	10°
T12	1F SLAB ROT S SIDE E	5°
T13	1F SLAB ROT S SIDE W	5°
T14	1F N COL ROT L	5°
T15	1F N COL ROT L	5°
T16	1F N COL FLANGE AT BEAM	10°
T17	1F N COL ROT U	10°
T18	1F N COL ROT U	10°
T19	2F BEAM ROT MID N SIDE	10°
T20	2F BEAM ROT MID N SIDE	5°
T21	1F BEAM ROT N SIDE	5°
T22	1F BEAM ROT N SIDE	10°
T23	1F BEAM ROT MID N SIDE	5°
T24	1F BEAM ROT MID N SIDE	10°
T25	1F SLAB ROT N SIDE E	5°
T26	1F SLAB ROT N SIDE W	5°
T27	1F SLAB ROT MID E	10°
T28	1F SLAB ROT MID W	10°
T29	2F SLAB ROT N SIDE E	5°
T30	2F SLAB ROT N SIDE W	5°

NDI OPTOTRAK LED DESIGNATIONS

●	DESCRIPTION	●	DESCRIPTION
N1	1F S BR OOP 1/4 PT	N25	1F BEAM MID GRID
N2	1F S BR OOP	N26	1F BEAM MID GRID
N3	1F S BR OOP	N27	1F MID GP GRID
N4	1F S BR OOP	N28	1F BEAM MID GRID
N5	1F S BR OOP	N29	1F BEAM MID GRID
N6	1F MID GP GRID	N30	1F BEAM MID GRID
N7	1F MID GP GRID	N31	1F BEAM MID GRID
N8	1F MID GP GRID	N32	1F BEAM MID GRID
N9	1F MID GP GRID	N33	1F BEAM MID GRID
N10	1F MID GP GRID	N34	1F BEAM MID GRID
N11	1F MID GP GRID	N35	1F BEAM MID GRID
N12	1F MID GP GRID	N36	1F BEAM MID GRID
N13	1F MID GP GRID	N37	1F MID GP GRID
N14	1F MID GP GRID	N38	1F MID GP GRID
N15	1F BEAM MID GRID	N39	1F MID GP GRID
N16	1F BEAM MID GRID	N40	1F MID GP GRID
N17	1F BEAM MID GRID	N41	1F MID GP GRID
N18	1F BEAM MID GRID	N42	1F MID GP GRID
N19	1F BEAM MID GRID	N43	1F MID GP GRID
N20	1F BEAM MID GRID	N44	1F N BR OOP
N21	1F BEAM MID GRID	N45	1F N BR OOP
N22	1F BEAM MID GRID	N46	1F N BR OOP
N23	1F BEAM MID GRID	N47	1F N BR OOP
N24	1F BEAM MID GRID	N48	1F N BR OOP 1/4 PT

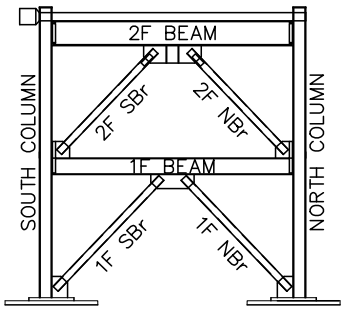

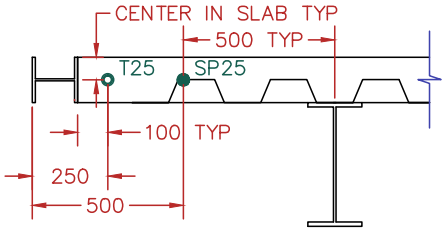

TYPICAL SLAB END INSTRUMENTATION DETAIL

NOTE: LOCATE INCLINOMETERS ON OUTSIDE EDGE OF EACH SLAB

TNCBF1-N-HSS: NON-DUCTILE DETAILS/HSS BRACES

NEESR: SEISMIC REHAB. OF VULNERABLE BRACED FRAMES

DRAWN BY: ADS
DESIGNED BY: ADS
DATE: 6/27/2013
REVISED: 9/10/2014
CONTACT: ADSEN@UW.EDU

DWG: IN-2

POTENTIOMETER DESIGNATIONS

●	DESCRIPTION	TYPE	RANGE +/−	FREEDOM
L1	1F S COR BR OOP CENTER	TML	50mm	
L2	1F S COR GP OOP EDGE	TML	100mm	
L3	1F S COR GP OOP EDGE	TML	100mm	
L4	2F S COR BR BR CENTER	TML	100mm	HORIZ
L5	2F S COR GP OOP EDGE	TML	100mm	HORIZ
L6	2F S COR GP OOP EDGE	TML	100mm	HORIZ
L7	ALUMINUM PL OOP S	TML	25mm	
L9	ALUMINUM PL OOP N	TML	25mm	
L10	1F N COR BR CENTER	TML	100mm	
L11	1F N COR GP OOP EDGE	TML	100mm	
L12	1F N COR GP OOP EDGE	TML	100mm	
L13	2F N COR BR OOP CENTER	TML	100mm	HORIZ
L14	2F N COR GP OOP EDGE	TML	100mm	HORIZ
L15	2F N COR GP OOP EDGE	TML	100mm	HORIZ
L16	2F BEAM DRIFT E SIDE	TEMPO	250mm	
L17	2F BEAM DRIFT W SIDE	TEMPO	250mm	
L18	2F BEAM VERT DISP	TML	150mm	HORIZ
L19	1F BEAM VERT DISP	TML	150mm	HORIZ

●	DESCRIPTION	TYPE	RANGE +/−	FREEDOM
SP1	2F BEAM S OOP ROT	STRING	125mm	HORIZ
SP2	2F BEAM MID OOP	STRING	125mm	HORIZ
SP3	2F BEAM N OOP ROT	STRING	250mm	HORIZ
SP4	1F S BRACE DIAG/OOP	STRING	250mm	HORIZ
SP5	1F S BRACE DIAG/OOP	STRING	250mm	HORIZ
SP6	2F S BRACE DIAG/OOP	STRING	250mm	HORIZ
SP7	2F S BRACE DIAG/OOP	STRING	250mm	HORIZ
SP8	2F S BRACE QUARTER PT	STRING	250mm	HORIZ
SP9	2F S GP OOP BOT EDGE	STRING	125mm	HORIZ
SP10	2F S GP OOP S EDGE	STRING	125mm	HORIZ
SP11	2F S GP OOP CENTER	STRING	125mm	HORIZ
SP12	2F MID TOP GP OOP	STRING	125mm	HORIZ
SP13	1F S BEAM DRIFT E SIDE	STRING	250mm	
SP14	1F S BEAM DRIFT W SIDE	STRING	250mm	
SP15	1F N BRACE DIAG/OOP	STRING	250mm	HORIZ
SP16	1F N BRACE DIAG/OOP	STRING	250mm	HORIZ
SP18	2F N BRACE DIAG/OOP	STRING	250mm	HORIZ
SP19	2F N BRACE DIAG/OOP	STRING	250mm	HORIZ
SP20	2F N BRACE QUARTER PT	STRING	250mm	HORIZ
SP21	2F N GP OOP BOT EDGE	STRING	125mm	HORIZ
SP22	2F N GP OOP N EDGE	STRING	125mm	HORIZ
SP23	2F N GP OOP CENTER	STRING	125mm	HORIZ
SP24	1F N BEAM DRIFT WP	STRING	250mm	
SP25	1F N BEAM DRIFT E SIDE	STRING	250mm	
SP26	1F N BEAM DRIFT W SIDE	STRING	250mm	

●	DESCRIPTION	TYPE	RANGE +/−	FREEDOM
D1	S ANCHOR PL SLIP	DIAL	25mm	
D2	S ANCHOR PL UPLIFT	DIAL	25mm	
D3	S BASE PL SLIP	DIAL	25mm	
D4	S BASE PL UPLIFT	DIAL	25mm	
D5	N ANCHOR PL SLIP	DIAL	25mm	
D6	N ANCHOR PL UPLIFT	DIAL	25mm	
D7	N BASE PL SLIP	DIAL	25mm	
D8	N BASE PL UPLIFT	DIAL	25mm	
D9	ACTUATOR BASE PL UPLIFT	DIAL	25mm	
D10	ACTUATOR BASE PL SLIP	DIAL	25mm	

ABBREVIATIONS

N	NORTH
S	SOUTH
E	EAST
W	WEST
BOT	BOTTOM
MID	MIDDLE
COL	COLUMN
BR	BRACE
PL	PLATE
OOP	OUT OF PLANE
IP	IN PLANE
DIAG	DIAGONAL
DISP	DISPLACEMENT
ROT	ROTATION
PT	POINT
WP	WORK POINT
L	LOWER
U	UPPER

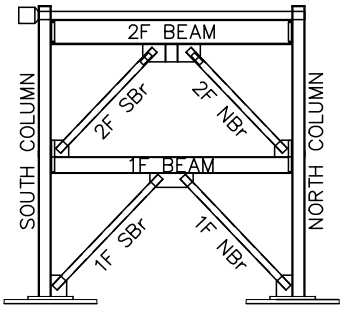

TNCBF1-N-HSS: NON-DUCTILE DETAILS/HSS BRACES

NEESR: SEISMIC REHAB. OF VULNERABLE BRACED FRAMES

DRAWN BY: ADS
DESIGNED BY: ADS
DATE: 6/27/2013
REVISED: 9/10/2014
CONTACT: ADSEN@UW.EDU

DWG: IN-3

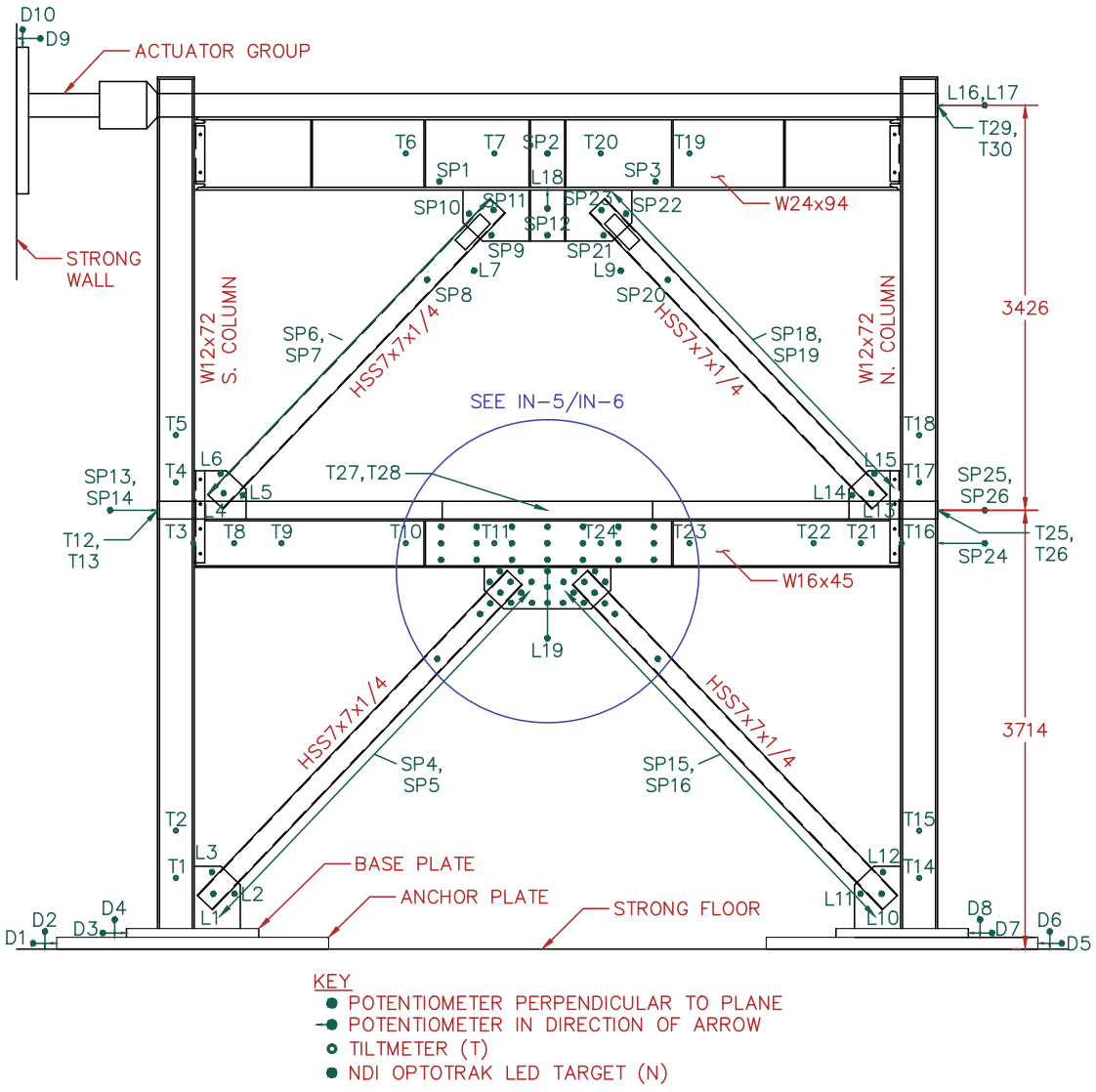

KEY

- POTENTIOMETER PERPENDICULAR TO PLANE
- POTENTIOMETER IN DIRECTION OF ARROW
- TILTMETER (T)
- NDI OPTOTRAK LED TARGET (N)

SCALE: 1mm = 50mm

TNCBF1-N-HSS: NON-DUCTILE DETAILS/HSS BRACES

NEESR: SEISMIC REHAB. OF VULNERABLE BRACED FRAMES

DWG: IN-4

DRAWN BY: ADS
DESIGNED BY: ADS
DATE: 6/27/2013
REVISED: 9/10/2014
CONTACT: ADSEN@UW.EDU

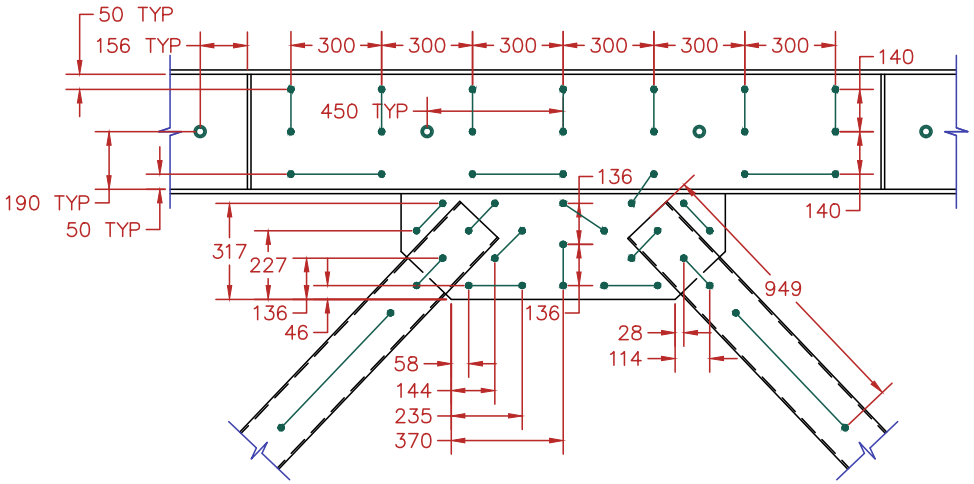

1F BEAM GUSSET PLATE LED LOCATION DETAIL

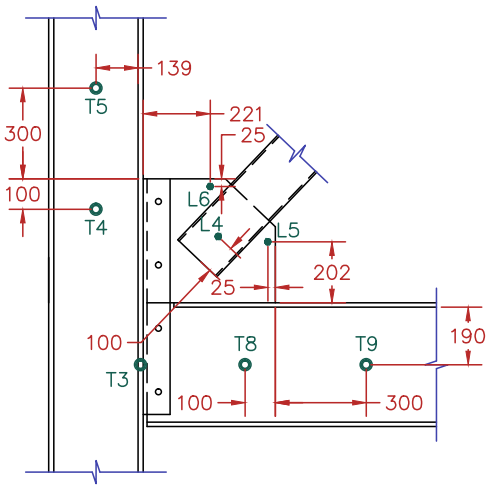

TYPICAL 1F BEAM AND 2F CORNER GUSSET PLATE INSTRUMENTATION DETAIL

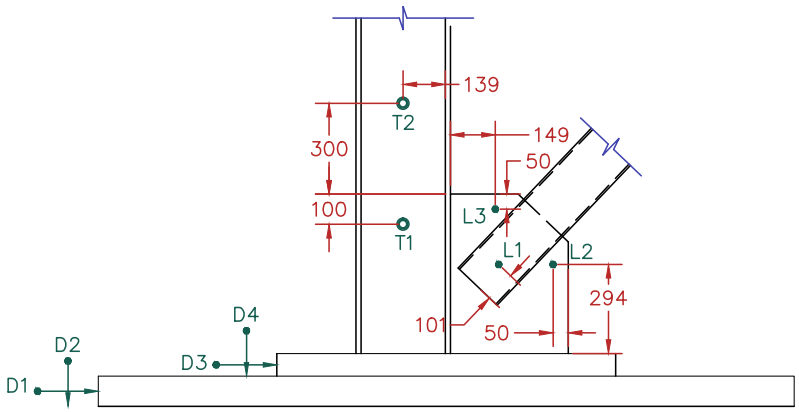

TYPICAL 1F CORNER GUSSET PLATE INSTRUMENTATION DETAIL

TNCBF1-N-HSS: NON-DUCTILE DETAILS/HSS BRACES

NEESR: SEISMIC REHAB. OF VULNERABLE BRACED FRAMES

DRAWN BY: ADS
DESIGNED BY: ADS
DATE: 6/27/2013
REVISED: 9/10/2014
CONTACT: ADSEN@UW.EDU

DWG: IN-5

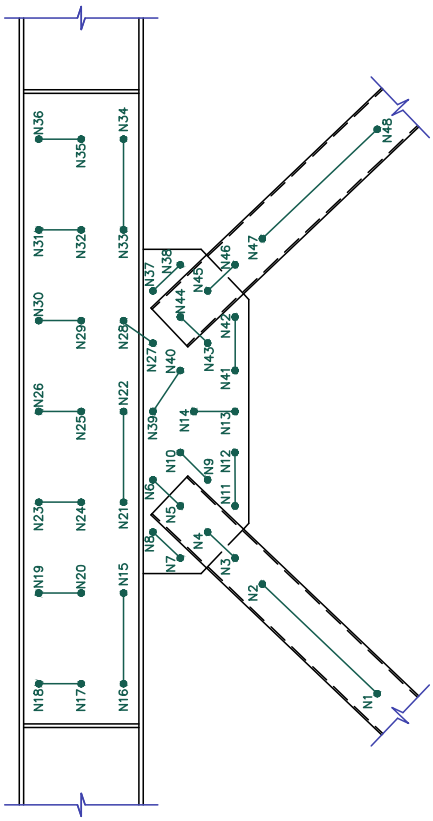

BOTTOM BEAM GUSSET PLATE LED NUMBERING

TNCBF1-N-HSS: NON-DUCTILE DETAILS/HSS BRACES

NEESR: SEISMIC REHAB. OF VULNERABLE BRACED FRAMES

DWG: IN-6

DRAWN BY: ADS
DESIGNED BY: ADS
DATE: 6/27/2013
REVISED: 9/10/2014
CONTACT: ADSEN@UW.EDU

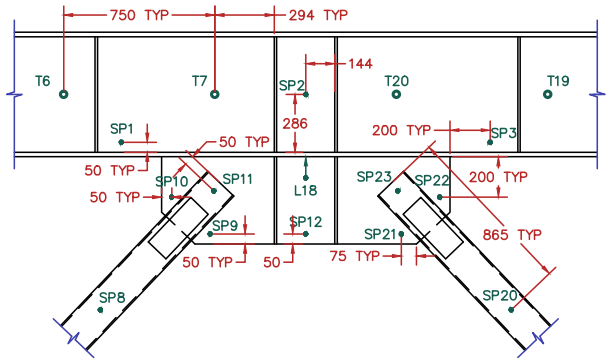

TOP BEAM GUSSET PLATE
INSTRUMENTATION DETAIL

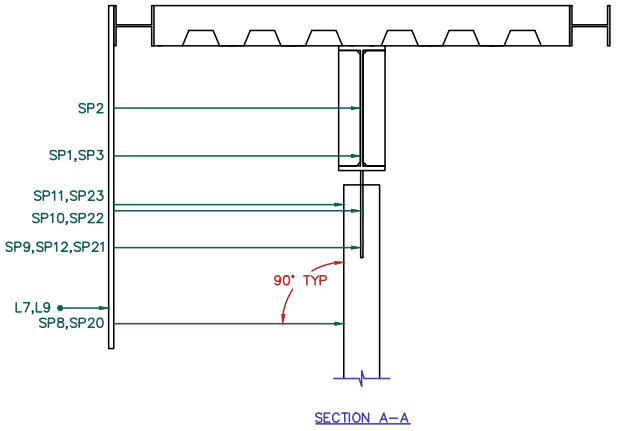

SECTION A–A

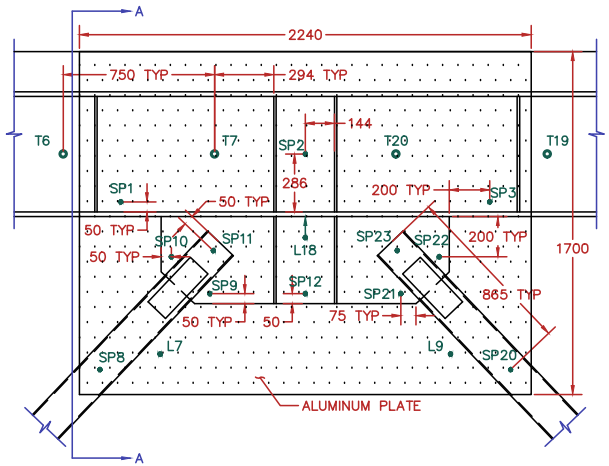

TNCBF1-N-HSS: NON-DUCTILE DETAILS/HSS BRACES	
NEESR: SEISMIC REHAB. OF VULNERABLE BRACED FRAMES	DWG: IN-7
DRAWN BY: ADS DESIGNED BY: ADS DATE: 6/27/2013 REVISED: 9/10/2014 CONTACT: ADSEN@UW.EDU	

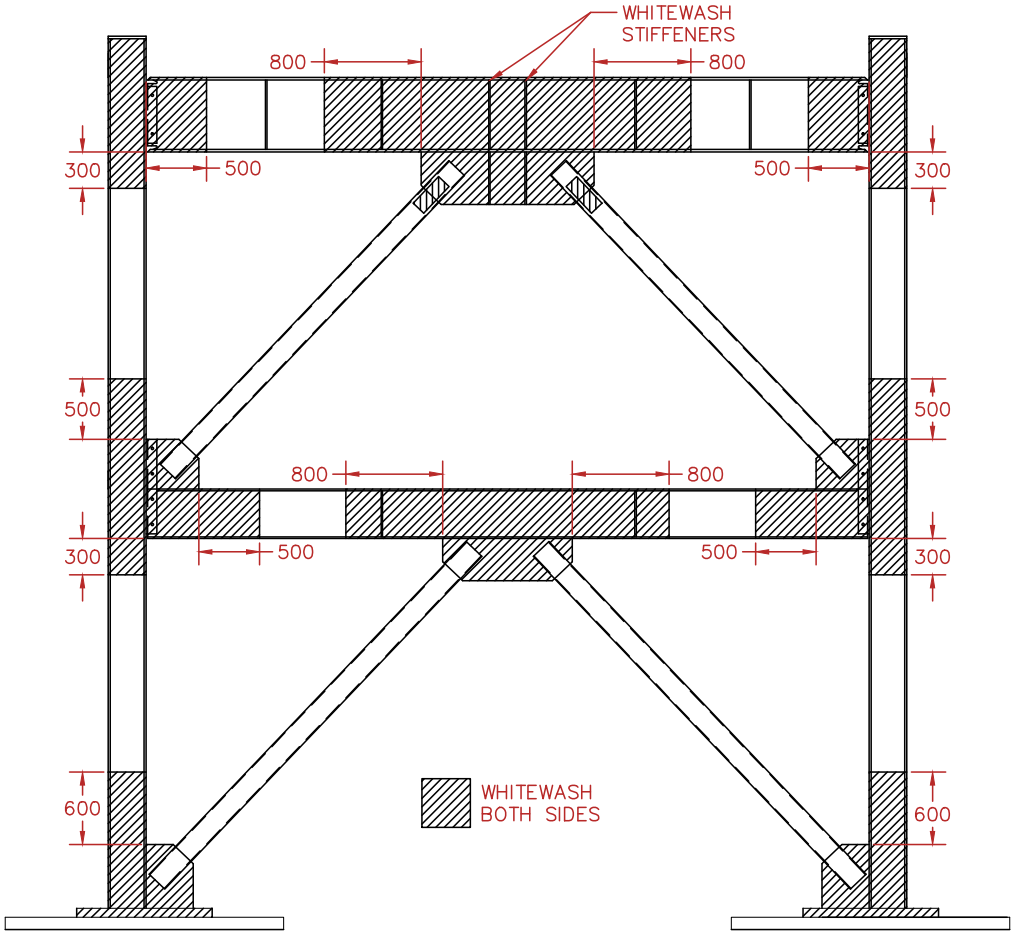

WHITEWASH PLAN
SCALE: 1mm = 50mm

TNCBF1-N-HSS: NON-DUCTILE DETAILS/HSS BRACES	
NEESR: SEISMIC REHAB. OF VULNERABLE BRACED FRAMES	DWG: IN-8
DRAWN BY: ADS DESIGNED BY: ADS DATE: 6/27/2013 REVISED: 9/10/2014 CONTACT: ADSEN@UW.EDU	

A.2 TNCBF1-R-HSS

The specimen drawings for TNCBF1-R-HSS are found below. This was the second specimen tested at NCREE in this test series and only the repair details are provided since no changes were made elsewhere.

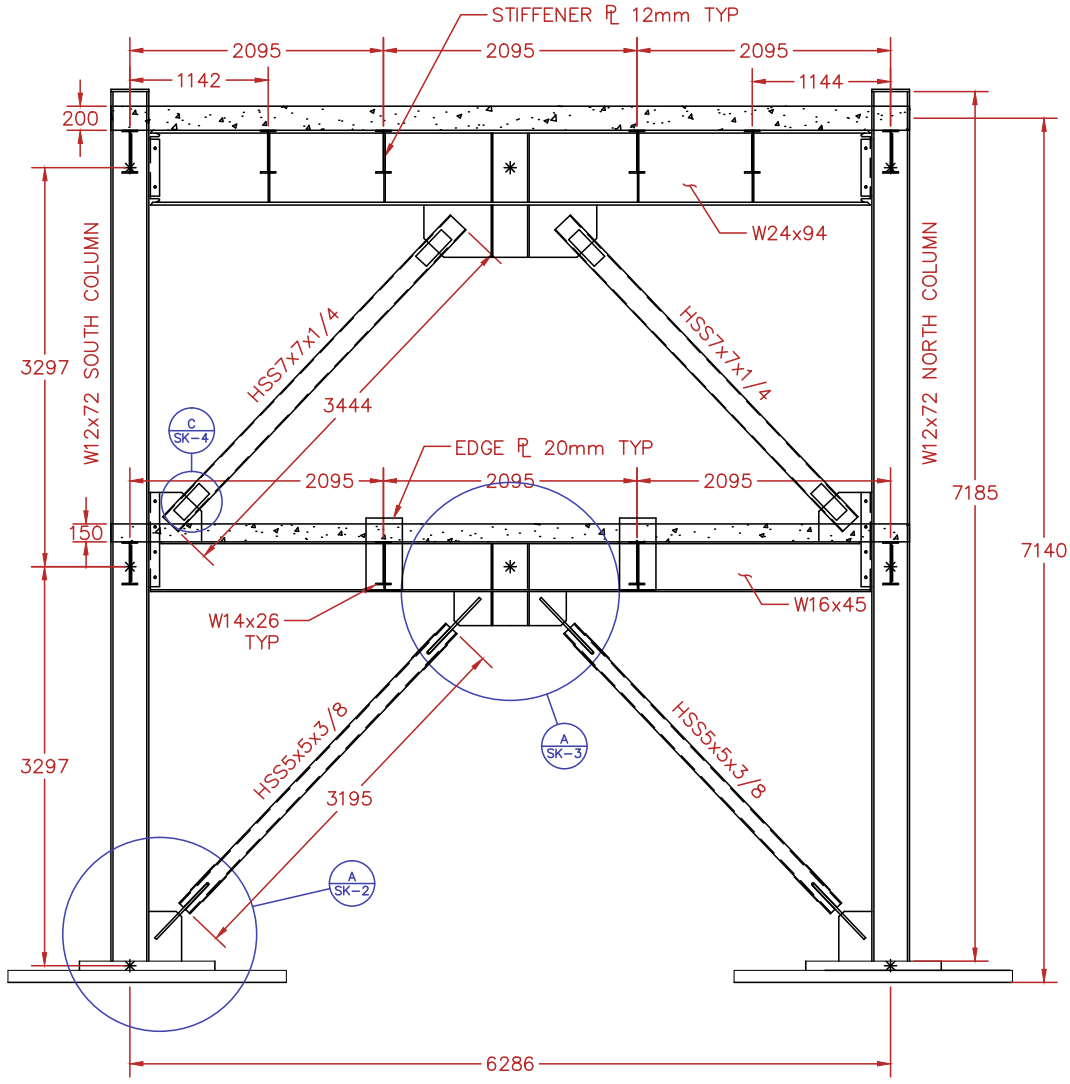

NOTES:
–EXISTING BOTTOM STORY BRACES AND GUSSET PLATES TO BE REMOVED
–BACK GOUGE SOUTH BOTTOM BEAM SHEAR TAB WELD DAMAGE AND REPAIR WITH 8mm FILLET WELD
–ALL WELDS TO SATISFY AISC DEMAND CRITICAL AWS E71T–1 OR EQUIVALENT

SCALE: 1mm = 50mm

TNCBF1-R-HSS: 1F IN-PLANE BUCKLING REPAIR/HSS BRACES

NEESR: SEISMIC REHAB. OF VULNERABLE BRACED FRAMES

DRAWN BY: ADS
DESIGNED BY: ADS
DATE: 7/26/2013
REVISED: 9/8/2014
CONTACT: ADSEN@UW.EDU

DWG: SK-1

A / SK–2

1F CORNER GUSSET PLATE REPAIR DETAIL

SCALE: 1mm = 20mm

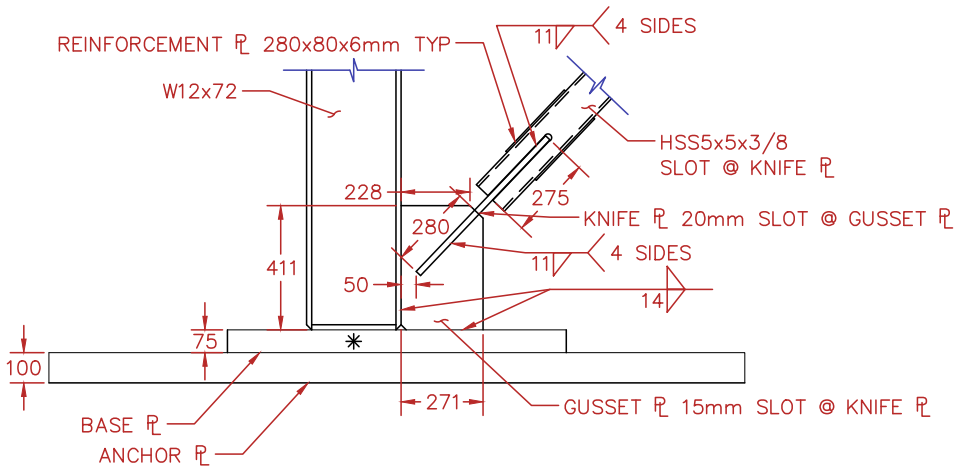

B / SK–2

1F CORNER GUSSET PLATE FABRICATION DETAIL

SCALE: 1mm = 20mm

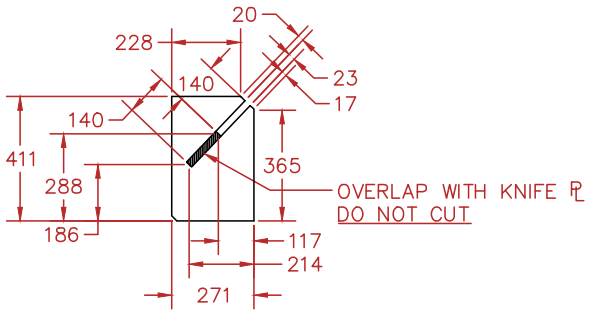

C / SK–2

1F BRACE SLOT DETAIL

SCALE: 1mm = 20mm

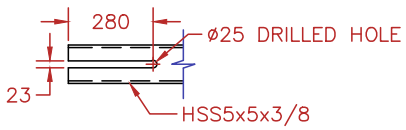

NOTES:
–ALL PLATE STEEL A572 GR 50 OR EQUIVALENT
–ALL BRACES TO BE A500 GR B/C OR EQUIVALENT
–ALL WELDS AS DESIGNATED IN SK–1

TNCBF1-R-HSS: 1F IN-PLANE BUCKLING REPAIR/HSS BRACES

NEESR: SEISMIC REHAB. OF VULNERABLE BRACED FRAMES

DWG: SK-2

DRAWN BY: ADS
DESIGNED BY: ADS
DATE: 7/26/2013
REVISED: 9/8/2014
CONTACT: ADSEN@UW.EDU

A
SK–3

1F MID–SPAN GUSSET PLATE REPAIR DETAIL
SCALE: 1mm = 20mm

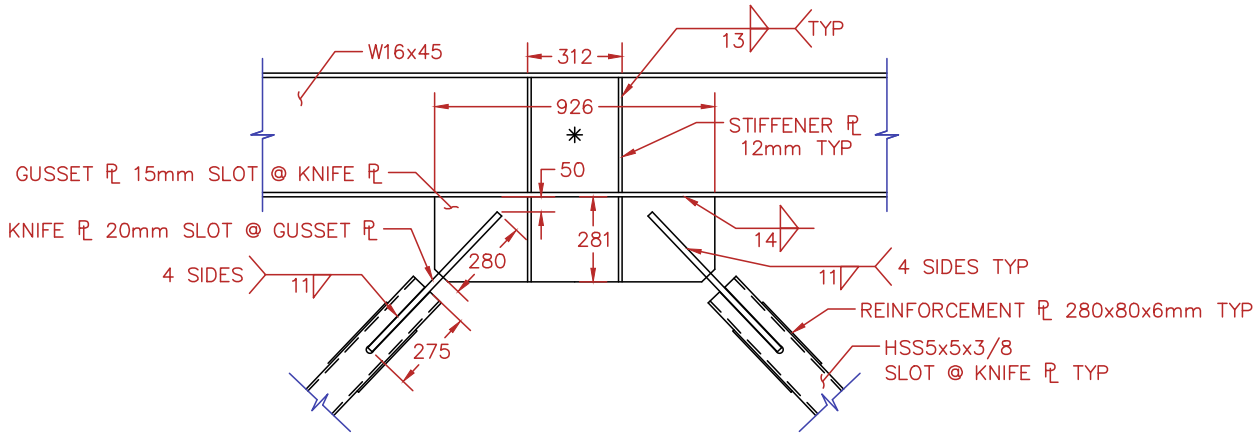

B
SK–3

1F MID–SPAN GUSSET PLATE FABRICATION DETAIL
SCALE: 1mm = 20mm

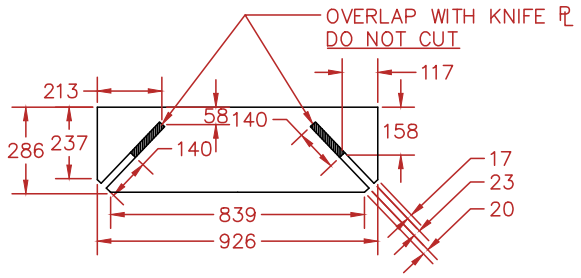

NOTES:
–ALL PLATE STEEL A572 GR 50 OR EQUIVALENT
–ALL BRACES TO BE A500 GR B/C OR EQUIVALENT
–ALL WELDS AS DESIGNATED IN SK–1

TNCBF1-R-HSS: 1F IN-PLANE BUCKLING REPAIR/HSS BRACES

NEESR: SEISMIC REHAB. OF VULNERABLE BRACED FRAMES

DRAWN BY: ADS
DESIGNED BY: ADS
DATE: 7/26/2013
REVISED: 9/8/2014
CONTACT: ADSEN@UW.EDU

DWG: SK-3

A
SK–4

KNIFE PLATE FABRICATION DETAIL
SCALE: 1mm = 20mm

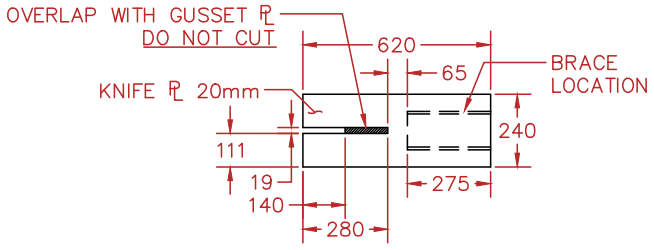

B
SK–4

KNIFE PLATE DETAIL
SCALE: 1mm = 20mm

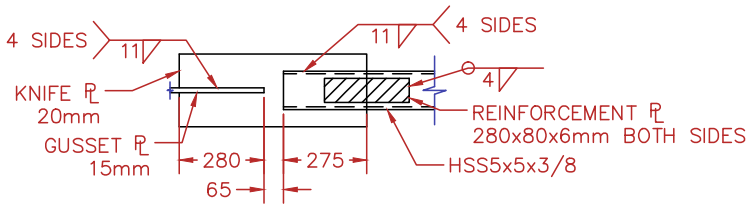

C
SK–4

2F NET SECTION REINFORCEMENT DETAIL
SCALE: 1mm = 20mm

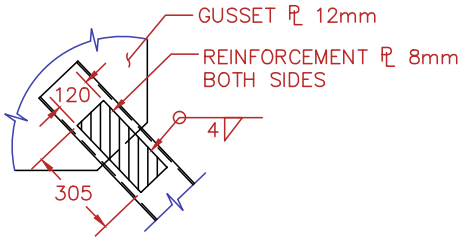

NOTES:
–ALL PLATE STEEL A572 GR 50 OR EQUIVALENT
–ALL BRACES TO BE A500 GR B/C OR EQUIVALENT
–ALL WELDS AS DESIGNATED IN SK–1

TNCBF1-R-HSS: 1F IN-PLANE BUCKLING REPAIR/HSS BRACES

NEESR: SEISMIC REHAB. OF VULNERABLE BRACED FRAMES

DWG: SK-4

DRAWN BY: ADS
DESIGNED BY: ADS
DATE: 7/26/2013
REVISED: 9/8/2014
CONTACT: ADSEN@UW.EDU

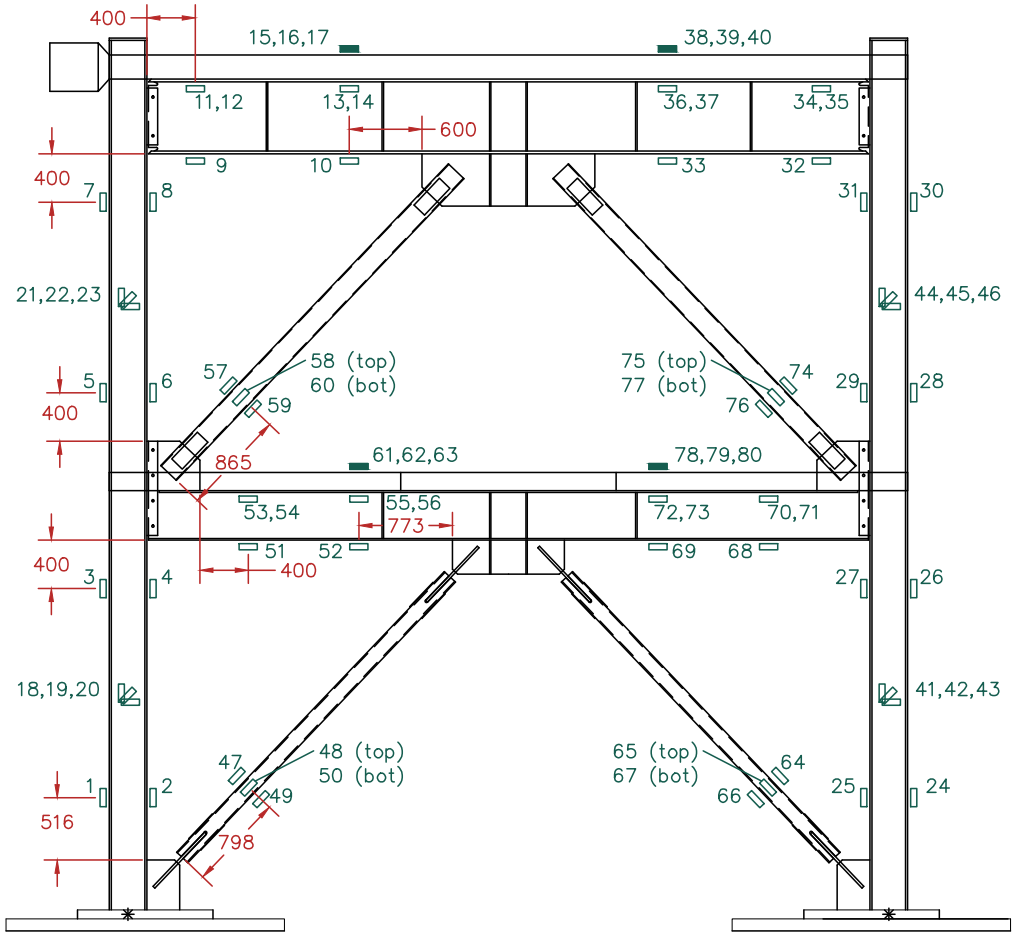

STRAIN GAUGE LAYOUT
SCALE: 1mm = 50mm

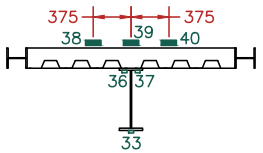

SECTION A–A

KEY
- STEEL UNIAXIAL STRAIN GAUGE
- CONCRETE UNIAXIAL STRAIN GAUGE
- TRIAXIAL STRAIN GAUGE

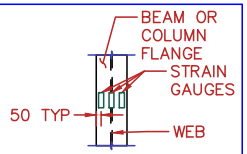

NOTE: LOCATE SG ON CENTER OF FLANGE OR UNDERSIDE OF FLANGE 50mm FROM EDGE AS NECESSARY.

	LABEL	LOCATION		LABEL	LOCATION
1	SG 1	S COLUMN	24	SG 24	N COLUMN
2	SG 2	S COLUMN	25	SG 25	N COLUMN
3	SG 3	S COLUMN	26	SG 26	N COLUMN
4	SG 4	S COLUMN	27	SG 27	N COLUMN
5	SG 5	S COLUMN	28	SG 28	N COLUMN
6	SG 6	S COLUMN	29	SG 29	N COLUMN
7	SG 7	S COLUMN	30	SG 30	N COLUMN
8	SG 8	S COLUMN	31	SG 31	N COLUMN
9	SG 9	S TOP BEAM	32	SG 32	N TOP BEAM
10	SG 10	S TOP BEAM	33	SG 33	N TOP BEAM
11	SG 11	S TOP BEAM*	34	SG 34	N TOP BEAM*
12	SG 12	S TOP BEAM*	35	SG 35	N TOP BEAM*
13	SG 13	S TOP BEAM*	36	SG 36	N TOP BEAM*
14	SG 14	S TOP BEAM*	37	SG 37	N TOP BEAM*
15	SG 15	S TOP SLAB	38	SG 38	N TOP SLAB
16	SG 16	S TOP SLAB	39	SG 39	N TOP SLAB
17	SG 17	S TOP SLAB	40	SG 40	N TOP SLAB
18	SG 18	S COL BOT 0°	41	SG 41	N COL BOT 0°
19	SG 19	S COL BOT 45°	42	SG 42	N COL BOT 45°
20	SG 20	S COL BOT 90°	43	SG 43	N COL BOT 90°
21	SG 21	S COL TOP 0°	44	SG 44	N COL TOP 0°
22	SG 22	S COL TOP 45°	45	SG 45	N COL TOP 45°
23	SG 23	S COL TOP 90°	46	SG 46	N COL TOP 90°

	LABEL	LOCATION		LABEL	LOCATION
47	SG 47	S BOT BRACE	64	SG 64	N BOT BRACE
48	SG 48	S BOT BRACE	65	SG 65	N BOT BRACE
49	SG 49	S BOT BRACE	66	SG 66	N BOT BRACE
50	SG 50	S BOT BRACE	67	SG 67	N BOT BRACE
51	SG 51	S BOT BEAM	68	SG 68	N BOT BEAM
52	SG 52	S BOT BEAM	69	SG 69	N BOT BEAM
53	SG 53	S BOT BEAM*	70	SG 70	N BOT BEAM*
54	SG 54	S BOT BEAM*	71	SG 71	N BOT BEAM*
55	SG 55	S BOT BEAM*	72	SG 72	N BOT BEAM*
56	SG 56	S BOT BEAM*	73	SG 73	N BOT BEAM*
57	SG 57	S TOP BRACE	74	SG 74	N TOP BRACE
58	SG 58	S TOP BRACE	75	SG 75	N TOP BRACE
59	SG 59	S TOP BRACE	76	SG 76	N TOP BRACE
60	SG 60	S TOP BRACE	77	SG 77	N TOP BRACE
61	SG 61	S BOT SLAB	78	SG 78	N BOT SLAB
62	SG 62	S BOT SLAB	79	SG 79	N BOT SLAB
63	SG 63	S BOT SLAB	80	SG 80	N BOT SLAB

* LOCATE STRAIN GAUGE AT UNDERSIDE OF BEAM FLANGE

TNCBF1-R-HSS: 1F IN-PLANE BUCKLING REPAIR/HSS BRACES

NEESR: SEISMIC REHAB. OF VULNERABLE BRACED FRAMES

DRAWN BY: ADS
DESIGNED BY: ADS
DATE: 7/26/2013
REVISED: 9/10/2014
CONTACT: ADSEN@UW.EDU

DWG: IN-1

KEY

- POTENTIOMETER PERPENDICULAR TO PLANE
- POTENTIOMETER IN DIRECTION OF ARROW
- TILTMETER (T)
- NDI OPTOTRAK LED TARGET (N)

ABBREVIATIONS

N	NORTH
S	SOUTH
E	EAST
W	WEST
BOT	BOTTOM
MID	MIDDLE
COL	COLUMN
BR	BRACE
PL	PLATE
OOP	OUT OF PLANE
IP	IN PLANE
DIAG	DIAGONAL
DISP	DISPLACEMENT
ROT	ROTATION
PT	POINT
WP	WORK POINT

TILTMETER DESIGNATIONS

○	DESCRIPTION	RANGE +/−
T1	1F S COL ROT L	5°
T2	1F S COL ROT L	10°
T3	1F S COL FLANGE AT BEAM	10°
T4	2F S COL ROT L	5°
T5	2F S COL ROT L	10°
T6	2F BEAM ROT MID S SIDE	10°
T7	2F BEAM ROT MID S SIDE	5°
T8	1F BEAM ROT S SIDE	5°
T9	1F BEAM ROT S SIDE	10°
T10	1F BEAM ROT MID S SIDE	5°
T11	1F BEAM ROT MID S SIDE	5°
T12	1F SLAB ROT S SIDE E	5°
T13	1F SLAB ROT S SIDE W	5°
T14	1F N COL ROT L	5°
T15	1F N COL ROT L	15°
T16	1F N COL FLANGE AT BEAM	10°
T17	2F N COL ROT L	10°
T18	2F N COL ROT L	10°
T19	2F BEAM ROT MID N SIDE	10°
T20	2F BEAM ROT MID N SIDE	5°
T21	1F BEAM ROT N SIDE	5°
T22	1F BEAM ROT N SIDE	10°
T23	1F BEAM ROT MID N SIDE	5°
T24	1F BEAM ROT MID N SIDE	5°
T25	1F SLAB ROT N SIDE E	5°
T26	1F SLAB ROT N SIDE W	5°
T27	1F SLAB ROT MID E	10°
T28	1F SLAB ROT MID W	10°
T29	2F SLAB ROT N SIDE E	5°
T30	2F SLAB ROT N SIDE W	5°
T31	S KP ROT AT GUSSET PL L	5°
T32	S KP ROT AT BRACE L	10°
T33	S KP ROT AT BRACE U	10°
T34	S KP ROT AT GUSSET PL U	5°
T35	N KP ROT AT GUSSET PL U	5°
T36	N KP ROT AT BRACE U	10°
T37	N KP ROT AT BRACE L	10°
T38	N KP ROT AT GUSSET PL L	5°

NDI OPTOTRAK LED DESIGNATIONS

●	DESCRIPTION	●	DESCRIPTION
N1	1F S BR IP QUARTER PT	N25	1F N BR IP QUARTER PT
N2	1F S BR IP	N26	1F N BR IP
N3	1F S BR IP	N27	1F N BR IP
N4	1F S BR IP	N28	1F N BR IP
N5	1F S BR IP	N29	1F N BR IP
N6	1F S BR IP	N30	1F N BR IP
N7	1F S BR IP	N31	1F N BR IP
N8	1F BEAM MID GP GRID	N32	1F BEAM MID GP GRID
N9	1F BEAM MID GP GRID	N33	1F BEAM MID GP GRID
N10	1F BEAM MID GP GRID	N34	1F BEAM MID WEB GRID
N11	1F BEAM MID GP GRID	N35	1F BEAM MID WEB GRID
N12	1F BEAM MID GP GRID	N36	1F BEAM MID WEB GRID
N13	1F BEAM MID WEB GRID	N37	1F BEAM MID WEB GRID
N14	1F BEAM MID WEB GRID	N38	1F BEAM MID WEB GRID
N15	1F BEAM MID WEB GRID	N39	1F BEAM MID WEB GRID
N16	1F BEAM MID WEB GRID	N40	1F BEAM MID WEB GRID
N17	1F BEAM MID WEB GRID	N41	1F BEAM MID WEB GRID
N18	1F BEAM MID WEB GRID	N42	1F BEAM MID WEB GRID
N19	1F BEAM MID WEB GRID	N43	1F BEAM MID WEB GRID
N20	1F BEAM MID WEB GRID	N44	1F BEAM MID WEB GRID
N21	1F BEAM MID WEB GRID	N45	1F BEAM MID WEB GRID
N22	1F BEAM MID WEB GRID	N46	1F BEAM MID WEB GRID
N23	1F BEAM MID WEB GRID	N47	1F BEAM MID WEB GRID
N24	1F BEAM MID WEB GRID	N48	1F BEAM MID WEB GRID

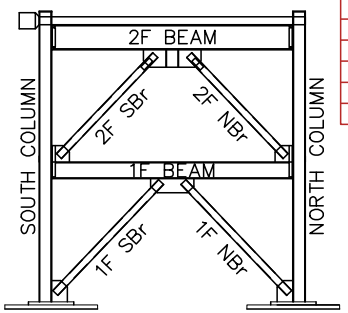

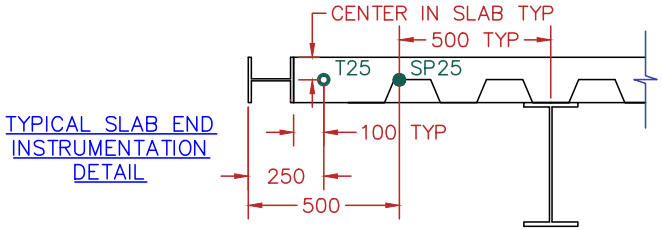

TYPICAL SLAB END INSTRUMENTATION DETAIL

NOTE: LOCATE INCLINOMETERS ON OUTSIDE EDGE OF EACH SLAB

TNCBF1-R-HSS: 1F IN-PLANE BUCKLING REPAIR/HSS BRACES

NEESR: SEISMIC REHAB. OF VULNERABLE BRACED FRAMES

DRAWN BY: ADS
DESIGNED BY: ADS
DATE: 7/26/2013
REVISED: 9/10/2014
CONTACT: ADSEN@UW.EDU

DWG: IN-2

POTENTIOMETER DESIGNATIONS

●	DESCRIPTION	TYPE	RANGE +/−	FREEDOM
L1	1F S COR GP OOP BOT	TML	100mm	
L2	1F S COR GP OOP TOP	TML	100mm	
L4	2F S COR GP OOP CENTER	TML	50mm	HORIZ
L5	2F S COR GP OOP EDGE	TML	100mm	HORIZ
L6	2F S COR GP OOP EDGE	TML	100mm	HORIZ
L7	ALUMINUM PL OOP S	TML	25mm	
L9	ALUMINUM PL OOP N	TML	25mm	
L10	1F N COR GP OOP BOT	TML	50mm	
L11	1F N COR GP OOP TOP	TML	100mm	
L13	2F N COR GP OOP CENTER	TML	50mm	HORIZ
L14	2F N COR GP OOP EDGE	TML	100mm	HORIZ
L15	2F N COR GP OOP EDGE	TML	100mm	HORIZ
L16	2F BEAM DRIFT E SIDE	TEMPO	250mm	
L17	2F BEAM DRIFT W SIDE	TEMPO	250mm	
L18	2F BEAM VERT DISP	TML	150mm	HORIZ
L19	1F BEAM VERT DISP	TML	150mm	HORIZ

●	DESCRIPTION	TYPE	RANGE +/−	FREEDOM
SP1	2F BEAM S OOP ROT	STRING	125mm	HORIZ
SP2	2F BEAM MID OOP	STRING	125mm	HORIZ
SP3	2F BEAM N OOP ROT	STRING	125mm	HORIZ
SP4	1F S BRACE DIAG/IP	STRING	250mm	HORIZ
SP5	1F S BRACE DIAG/IP	STRING	250mm	HORIZ
SP6	2F S BRACE DIAG/OOP	STRING	250mm	HORIZ
SP7	2F S BRACE DIAG/OOP	STRING	250mm	HORIZ
SP8	2F S BRACE QUARTER PT	STRING	250mm	HORIZ
SP9	2F S GP OOP BOT EDGE	STRING	125mm	HORIZ
SP10	2F S GP OOP S EDGE	STRING	125mm	HORIZ
SP11	2F S GP OOP CENTER	STRING	125mm	HORIZ
SP12	2F MID GP OOP	STRING	125mm	HORIZ
SP13	1F S BEAM DRIFT E SIDE	STRING	250mm	
SP14	1F S BEAM DRIFT W SIDE	STRING	250mm	
SP15	1F N BRACE DIAG/IP	STRING	250mm	HORIZ
SP16	1F N BOT BRACE DIAG/IP	STRING	250mm	HORIZ
SP18	2F N BRACE DIAG/OOP	STRING	250mm	HORIZ
SP19	2F N BRACE DIAG/OOP	STRING	250mm	HORIZ
SP20	2F N BRACE QUARTER PT	STRING	250mm	HORIZ
SP21	2F N GP OOP BOT EDGE	STRING	125mm	HORIZ
SP22	2F N GP OOP N EDGE	STRING	125mm	HORIZ
SP23	2F N GP OOP CENTER	STRING	125mm	HORIZ
SP24	1F N BOT BEAM DRIFT WP	STRING	250mm	
SP25	1F N BEAM DRIFT E SIDE	STRING	250mm	
SP26	1F N BEAM DRIFT W SIDE	STRING	250mm	
SP27	1F S BRACE OOP	STRING	125mm	
SP28	1F N BRACE OOP	STRING	250mm	

●	DESCRIPTION	TYPE	RANGE +/−	FREEDOM
D1	S ANCHOR PL SLIP	DIAL	25mm	
D2	S ANCHOR PL UPLIFT	DIAL	25mm	
D3	S BASE PL SLIP	DIAL	25mm	
D4	S BASE PL UPLIFT	DIAL	25mm	
D5	N ANCHOR PL SLIP	DIAL	25mm	
D6	N ANCHOR PL UPLIFT	DIAL	25mm	
D7	N BASE PL SLIP	DIAL	25mm	
D8	N BASE PL UPLIFT	DIAL	25mm	
D9	ACTUATOR BASE PL UPLIFT	DIAL	25mm	
D10	ACTUATOR BASE PL SLIP	DIAL	25mm	

ABBREVIATIONS

N	NORTH
S	SOUTH
E	EAST
W	WEST
BOT	BOTTOM
MID	MIDDLE
COL	COLUMN
BR	BRACE
PL	PLATE
OOP	OUT OF PLANE
IP	IN PLANE
DIAG	DIAGONAL
DISP	DISPLACEMENT
ROT	ROTATION
PT	POINT
WP	WORK POINT

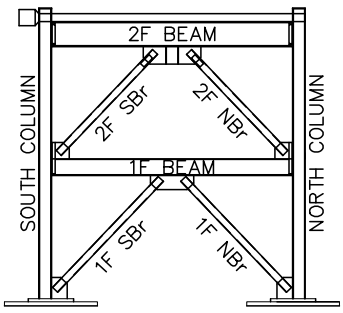

TNCBF1-R-HSS: 1F IN-PLANE BUCKLING REPAIR/HSS BRACES

NEESR: SEISMIC REHAB. OF VULNERABLE BRACED FRAMES

DRAWN BY: ADS
DESIGNED BY: ADS
DATE: 7/26/2013
REVISED: 9/10/2014
CONTACT: ADSEN@UW.EDU

DWG: IN-3

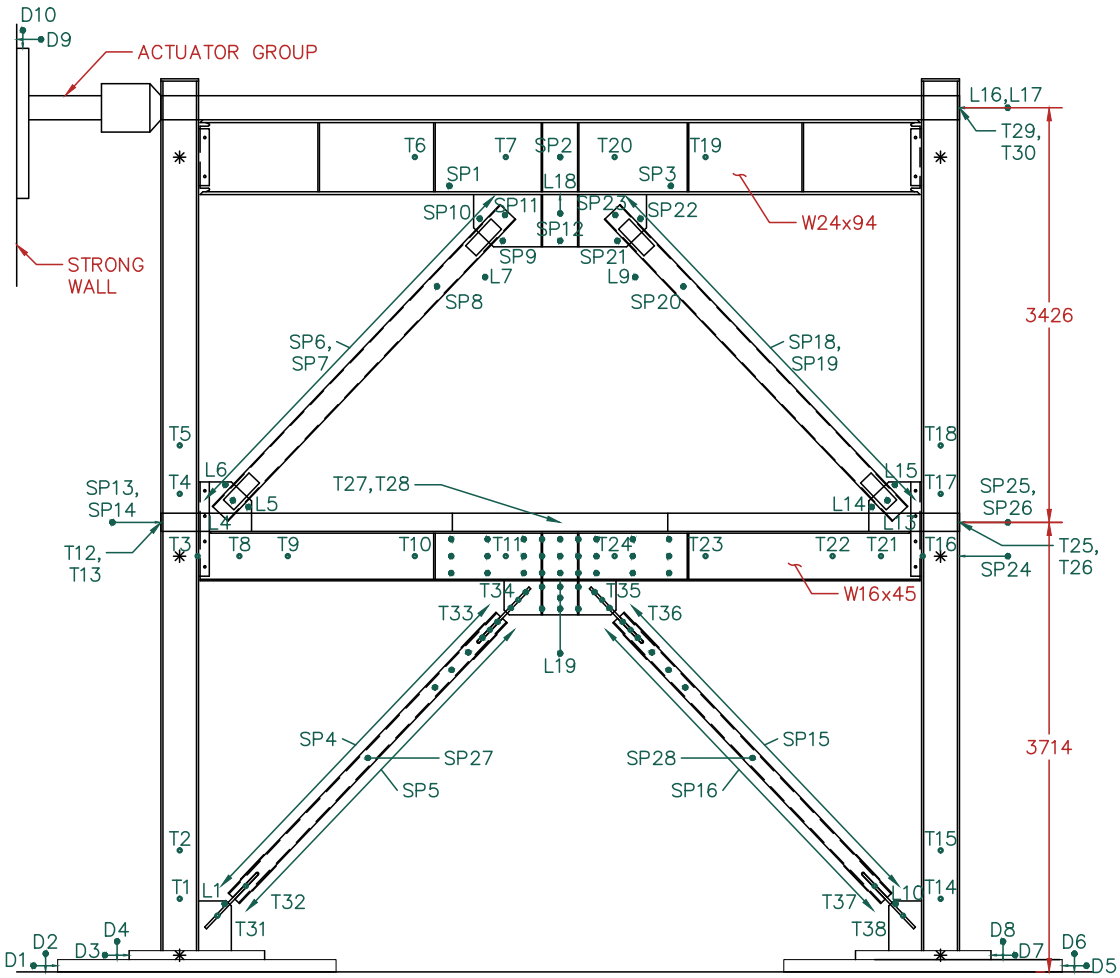

SCALE: 1mm = 50mm

TNCBF1-R-HSS: 1F IN-PLANE BUCKLING REPAIR/HSS BRACES

NEESR: SEISMIC REHAB. OF VULNERABLE BRACED FRAMES

DWG: IN-4

DRAWN BY: ADS
DESIGNED BY: ADS
DATE: 7/26/2013
REVISED: 9/10/2014
CONTACT: ADSEN@UW.EDU

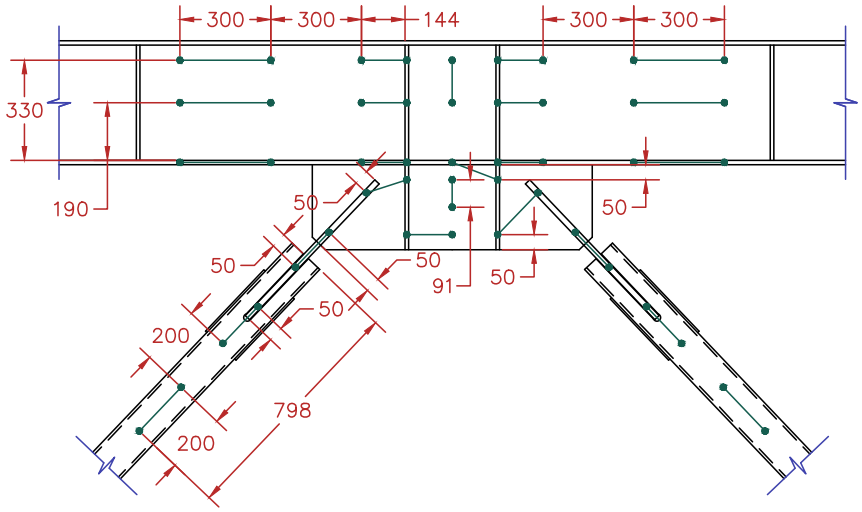

1F BEAM GUSSET PLATE LED LOCATION DETAIL

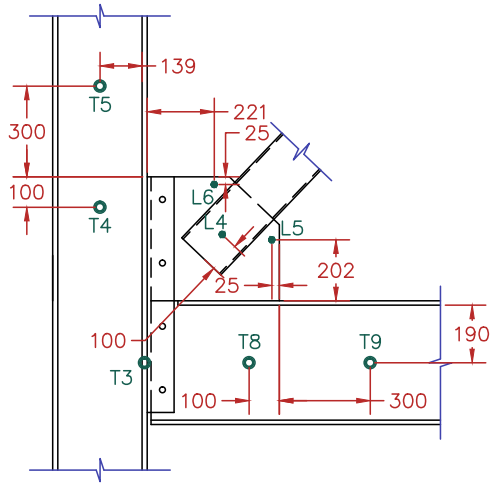

TYPICAL 1F BEAM AND 2F CORNER GUSSET PLATE INSTRUMENTATION DETAIL

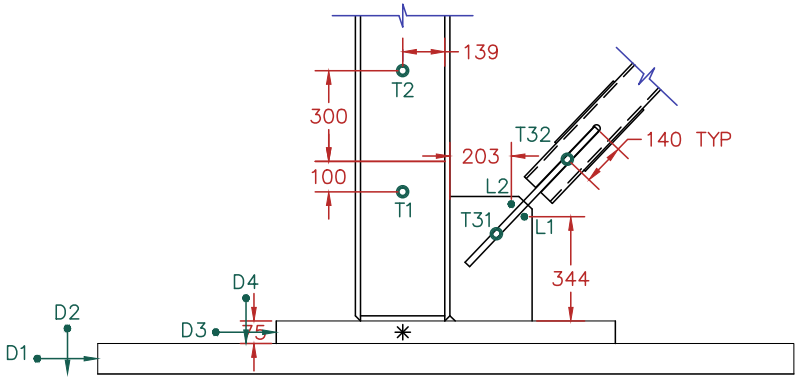

TYPICAL 1F CORNER GUSSET PLATE INSTRUMENTATION DETAIL

TNCBF1-R-HSS: 1F IN-PLANE BUCKLING REPAIR/HSS BRACES

NEESR: SEISMIC REHAB. OF VULNERABLE BRACED FRAMES

DWG: IN-5

DRAWN BY: ADS
DESIGNED BY: ADS
DATE: 7/26/2013
REVISED: 9/10/2014
CONTACT: ADSEN@UW.EDU

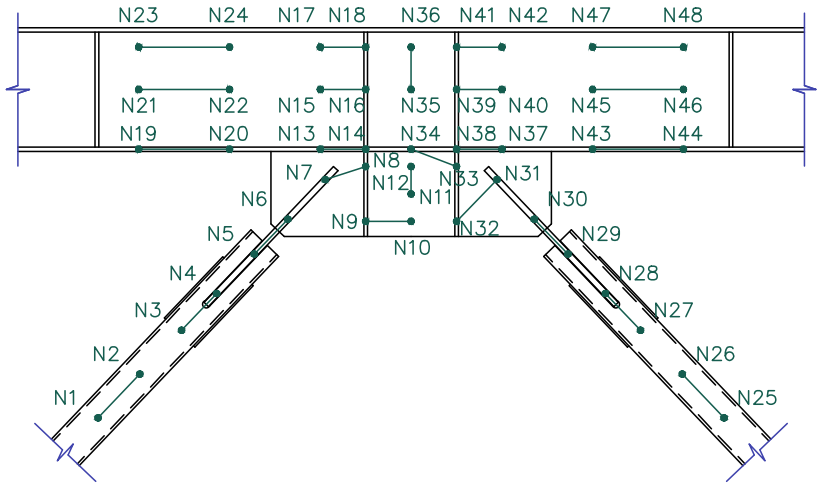

BOTTOM BEAM GUSSET PLATE LED NUMBERING

TNCBF1-R-HSS: 1F IN-PLANE BUCKLING REPAIR/HSS BRACES	
NEESR: SEISMIC REHAB. OF VULNERABLE BRACED FRAMES	DWG: IN-6
DRAWN BY: ADS DESIGNED BY: ADS DATE: 7/26/2013 REVISED: 9/10/2014 CONTACT: ADSEN@UW.EDU	

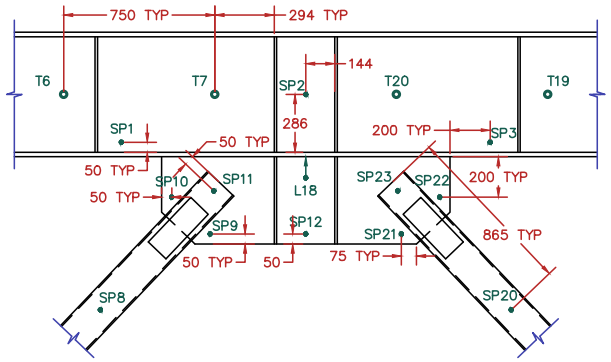

TOP BEAM GUSSET PLATE
INSTRUMENTATION DETAIL

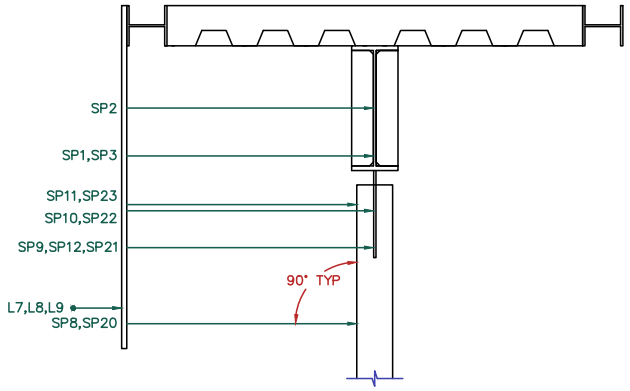

SECTION A–A

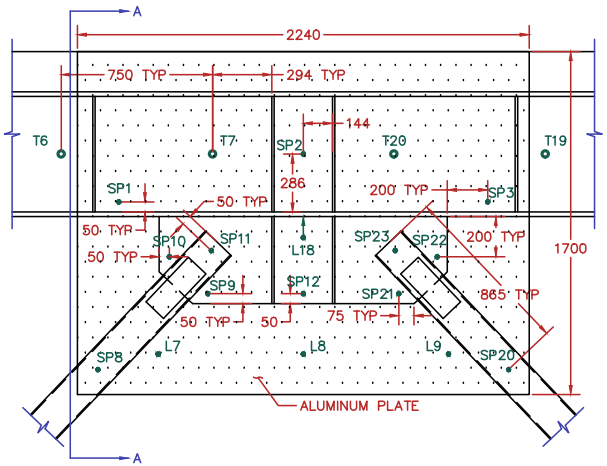

TNCBF1-R-HSS: 1F IN-PLANE BUCKLING REPAIR/HSS BRACES	
NEESR: SEISMIC REHAB. OF VULNERABLE BRACED FRAMES	DWG: IN-7
DRAWN BY: ADS DESIGNED BY: ADS DATE: 7/26/2013 REVISED: 9/10/2014 CONTACT: ADSEN@UW.EDU	

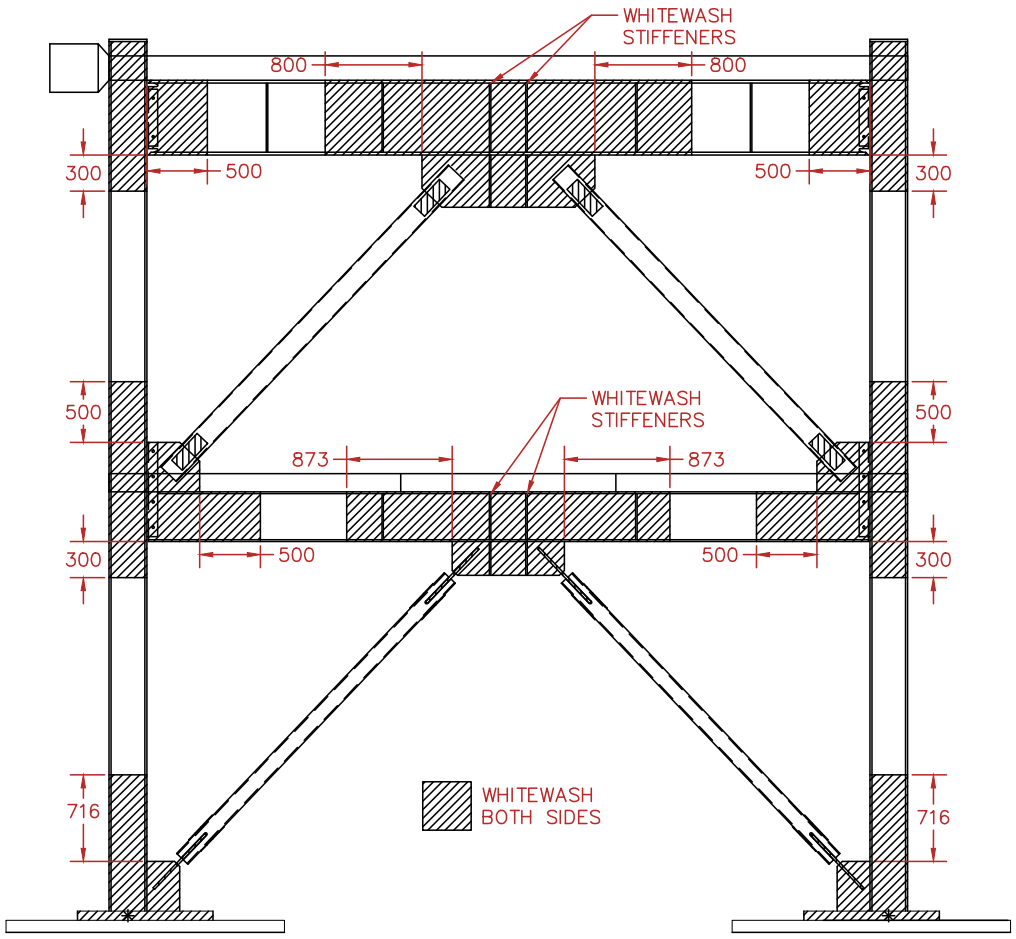

WHITEWASH PLAN
SCALE: 1mm = 50mm

TNCBF1-R-HSS: 1F IN-PLANE BUCKLING REPAIR/HSS BRACES	
NEESR: SEISMIC REHAB. OF VULNERABLE BRACED FRAMES	DWG: IN-8
DRAWN BY: ADS DESIGNED BY: ADS DATE: 7/26/2013 REVISED: 9/10/2014 CONTACT: ADSEN@UW.EDU	

A.3 TNCBF1-R-WF

The specimen drawings for TNCBF1-R-WF are found below. This was the third specimen tested at NCREE in this test series and only the repair details are provided since no changes were made elsewhere. The residual beam deflection from TNCBF1-R-HSS is drawn.

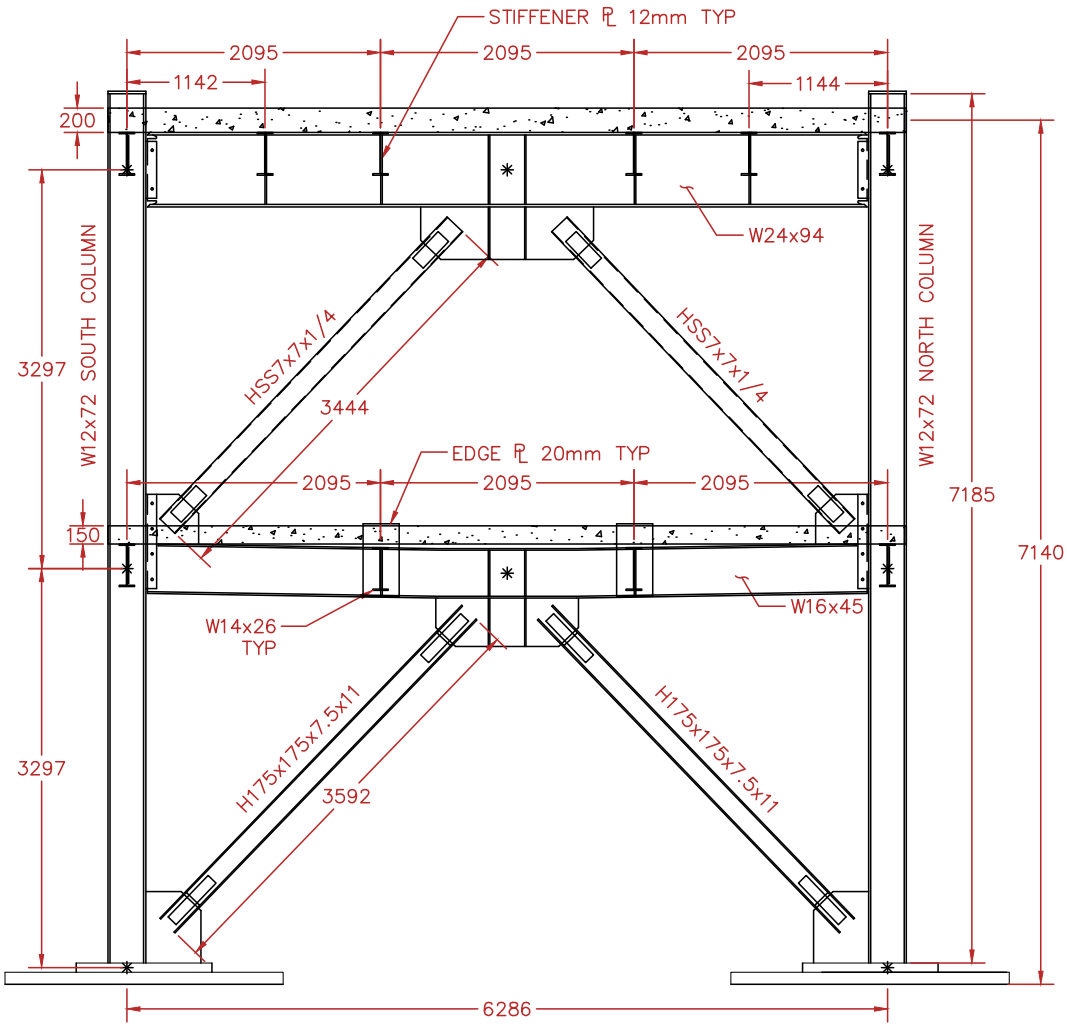

NOTES:
-EXISTING FIRST STORY BRACES, GUSSET PLATES, AND KNIFE PLATES TO BE REMOVED
-BACK GOUGE FIRST STORY BEAM-TO-SHEAR TAB WELD DAMAGE AND REPAIR WITH AT LEAST 8mm FILLET WELD
-ALL WELDS TO SATISFY AISC DEMAND CRITICAL AWS E71T-1 OR EQUIVALENT

SCALE: 1mm = 50mm

TNCBF1-R-WF: 1F REPAIR/WF BRACES

NEESR: SEISMIC REHAB. OF VULNERABLE BRACED FRAMES

DWG: SK-1

DRAWN BY: ADS
DESIGNED BY: ADS
DATE: 8/17/2013
REVISED: 9/8/2014
CONTACT: ADSEN@UW.EDU

A / SK–2

1F CORNER GUSSET PLATE REPAIR DETAIL

SCALE: 1mm = 20mm

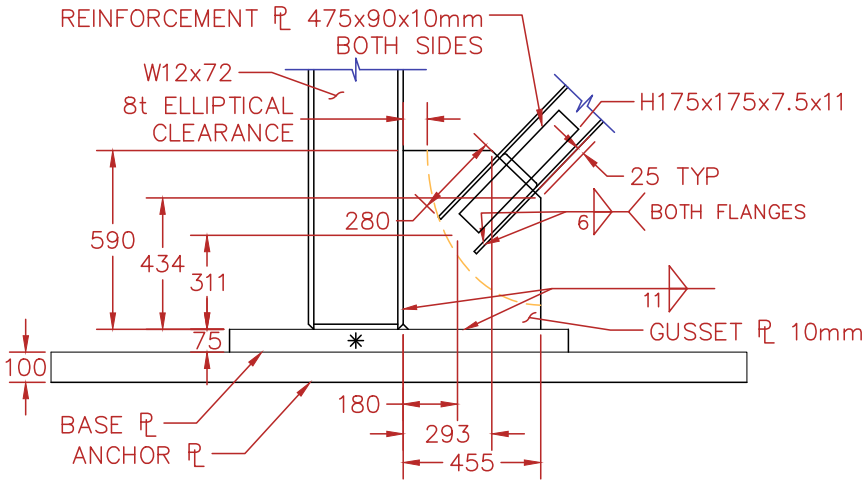

B / SK–2

1F BRACE NET SECTION REINFORCEMENT DETAIL

SCALE: 1mm = 20mm

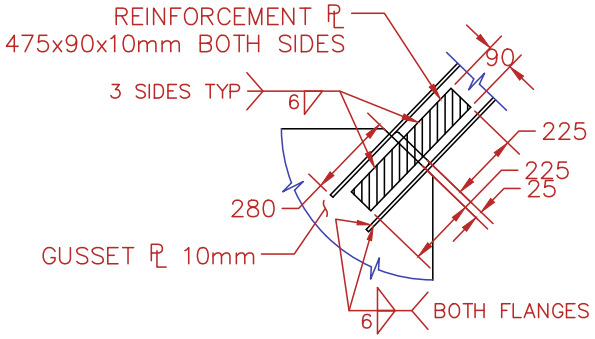

NOTES:
–ALL PLATE STEEL A572 GR 50 OR EQUIVALENT
–H175x175x7.5x11 BRACES TO BE SN400B
–ALL WELDS AS DESIGNATED IN SK–1

TNCBF1-R-WF: 1F REPAIR/WF BRACES

NEESR: SEISMIC REHAB. OF VULNERABLE BRACED FRAMES

DWG: SK-2

DRAWN BY: ADS
DESIGNED BY: ADS
DATE: 8/17/2013
REVISED: 9/8/2014
CONTACT: ADSEN@UW.EDU

A
SK–3

1F MID–SPAN GUSSET PLATE REPAIR DETAIL

SCALE: 1mm = 20mm

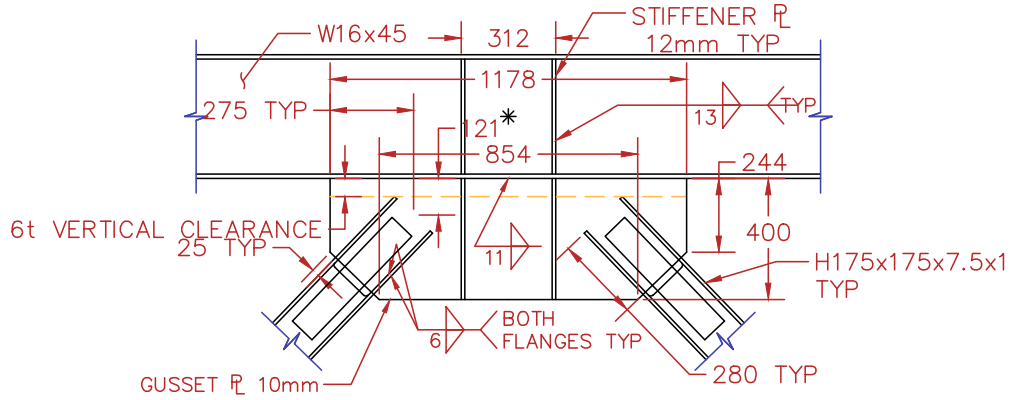

B
SK–3

1F BRACE WEB CUTOUT DETAIL

SCALE: 1mm = 15mm

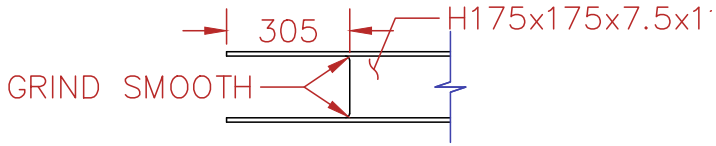

C
SK–3

1F BRACE SLOT DETAIL

SCALE: 1mm = 15mm

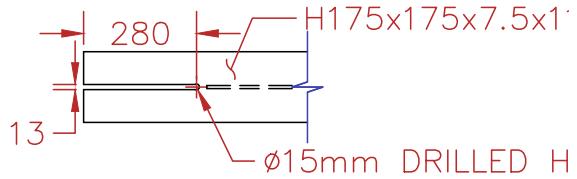

NOTES:
–ALL PLATE STEEL A572 GR 50 OR EQUIVALENT
–H175x175x7.5x11 BRACES TO BE SN400B
–ALL WELDS AS DESIGNATED IN SK–1

TNCBF1-R-WF: 1F REPAIR/WF BRACES

NEESR: SEISMIC REHAB. OF VULNERABLE BRACED FRAMES

DRAWN BY: ADS
DESIGNED BY: ADS
DATE: 8/17/2013
REVISED: 9/8/2014
CONTACT: ADSEN@UW.EDU

DWG: SK-3

A
SK–4

1F BEAM CUTOUT DETAIL
SCALE: 1mm = 20mm

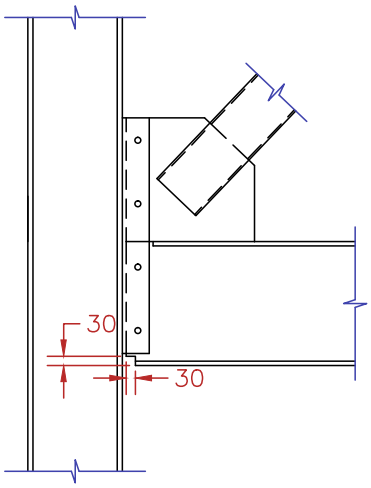

NOTES:
–ALL PLATE STEEL A572 GR 50 OR EQUIVALENT
–H175x175x7.5x11 BRACES TO BE SN400B
–ALL WELDS AS DESIGNATED IN SK–1

TNCBF1-R-WF: 1F REPAIR/WF BRACES

NEESR: SEISMIC REHAB. OF VULNERABLE BRACED FRAMES

DWG: SK-4

DRAWN BY: ADS
DESIGNED BY: ADS
DATE: 8/17/2013
REVISED: 9/8/2014
CONTACT: ADSEN@UW.EDU

A
SK–5

1F CORNER GUSSET PLATE
FABRICATION DETAIL
SCALE: 1mm = 15mm

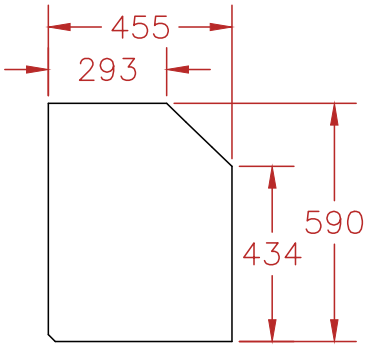

B
SK–5

1F MID–SPAN GUSSET PLATE
FABRICATION DETAIL
SCALE: 1mm = 15mm

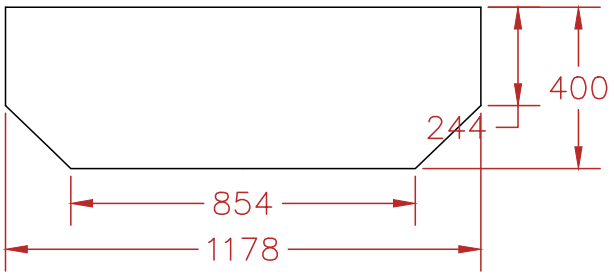

NOTES:
–ALL PLATE STEEL A572 GR 50 OR EQUIVALENT
–H175x175x7.5x11 BRACES TO BE SN400B
–ALL WELDS AS DESIGNATED IN SK–1

TNCBF1-R-WF: 1F REPAIR/WF BRACES

NEESR: SEISMIC REHAB. OF VULNERABLE BRACED FRAMES

DWG: SK-5

DRAWN BY: ADS
DESIGNED BY: ADS
DATE: 8/17/2013
REVISED: 9/8/2014
CONTACT: ADSEN@UW.EDU

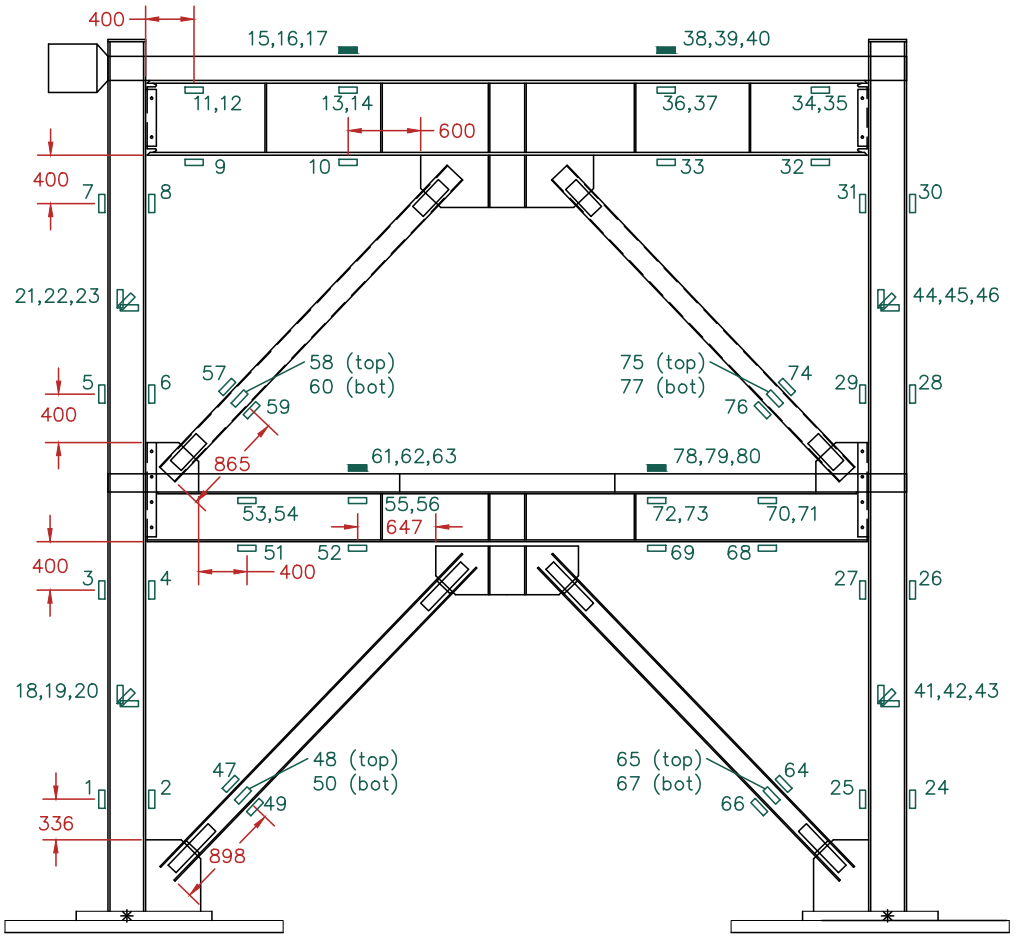

STRAIN GAUGE LAYOUT
SCALE: 1mm = 50mm

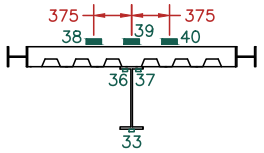

SECTION A–A

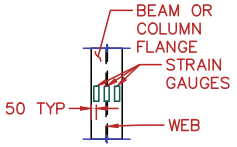

NOTE: LOCATE SG ON CENTER OF FLANGE OR UNDERSIDE OF FLANGE 50mm FROM EDGE AS NECESSARY.

KEY
- STEEL UNIAXIAL STRAIN GAUGE
- CONCRETE UNIAXIAL STRAIN GAUGE
- TRIAXIAL STRAIN GAUGE

	LABEL	LOCATION		LABEL	LOCATION
1	SG 1	S COLUMN	24	SG 24	N COLUMN
2	SG 2	S COLUMN	25	SG 25	N COLUMN
3	SG 3	S COLUMN	26	SG 26	N COLUMN
4	SG 4	S COLUMN	27	SG 27	N COLUMN
5	SG 5	S COLUMN	28	SG 28	N COLUMN
6	SG 6	S COLUMN	29	SG 29	N COLUMN
7	SG 7	S COLUMN	30	SG 30	N COLUMN
8	SG 8	S COLUMN	31	SG 31	N COLUMN
9	SG 9	S TOP BEAM	32	SG 32	N TOP BEAM
10	SG 10	S TOP BEAM	33	SG 33	N TOP BEAM
11	SG 11	S TOP BEAM*	34	SG 34	N TOP BEAM*
12	SG 12	S TOP BEAM*	35	SG 35	N TOP BEAM*
13	SG 13	S TOP BEAM*	36	SG 36	N TOP BEAM*
14	SG 14	S TOP BEAM*	37	SG 37	N TOP BEAM*
15	SG 15	S TOP SLAB	38	SG 38	N TOP SLAB
16	SG 16	S TOP SLAB	39	SG 39	N TOP SLAB
17	SG 17	S TOP SLAB	40	SG 40	N TOP SLAB
18	SG 18	S COL BOT 0°	41	SG 41	N COL BOT 0°
19	SG 19	S COL BOT 45°	42	SG 42	N COL BOT 45°
20	SG 20	S COL BOT 90°	43	SG 43	N COL BOT 90°
21	SG 21	S COL TOP 0°	44	SG 44	N COL TOP 0°
22	SG 22	S COL TOP 45°	45	SG 45	N COL TOP 45°
23	SG 23	S COL TOP 90°	46	SG 46	N COL TOP 90°
	LABEL	LOCATION		LABEL	LOCATION
47	SG 47	S BOT BRACE	64	SG 64	N BOT BRACE
48	SG 48	S BOT BRACE	65	SG 65	N BOT BRACE
49	SG 49	S BOT BRACE	66	SG 66	N BOT BRACE
50	SG 50	S BOT BRACE	67	SG 67	N BOT BRACE
51	SG 51	S BOT BEAM	68	SG 68	N BOT BEAM
52	SG 52	S BOT BEAM	69	SG 69	N BOT BEAM
53	SG 53	S BOT BEAM*	70	SG 70	N BOT BEAM*
54	SG 54	S BOT BEAM*	71	SG 71	N BOT BEAM*
55	SG 55	S BOT BEAM*	72	SG 72	N BOT BEAM*
56	SG 56	S BOT BEAM*	73	SG 73	N BOT BEAM*
57	SG 57	S TOP BRACE	74	SG 74	N TOP BRACE
58	SG 58	S TOP BRACE	75	SG 75	N TOP BRACE
59	SG 59	S TOP BRACE	76	SG 76	N TOP BRACE
60	SG 60	S TOP BRACE	77	SG 77	N TOP BRACE
61	SG 61	S BOT SLAB	78	SG 78	N BOT SLAB
62	SG 62	S BOT SLAB	79	SG 79	N BOT SLAB
63	SG 63	S BOT SLAB	80	SG 80	N BOT SLAB

* LOCATE STRAIN GAUGE AT UNDERSIDE OF BEAM FLANGE

TNCBF1-R-WF: 1F REPAIR/WF BRACES

NEESR: SEISMIC REHAB. OF VULNERABLE BRACED FRAMES

DWG: IN-1

DRAWN BY: ADS
DESIGNED BY: ADS
DATE: 8/23/2013
REVISED: 9/10/2014
CONTACT: ADSEN@UW.EDU

KEY

- POTENTIOMETER PERPENDICULAR TO PLANE
- POTENTIOMETER IN DIRECTION OF ARROW
- TILTMETER (T)
- NDI OPTOTRAK LED TARGET (N)

ABBREVIATIONS

N	NORTH
S	SOUTH
E	EAST
W	WEST
BOT	BOTTOM
MID	MIDDLE
COL	COLUMN
BR	BRACE
PL	PLATE
OOP	OUT OF PLANE
IP	IN PLANE
DIAG	DIAGONAL
DISP	DISPLACEMENT
ROT	ROTATION
PT	POINT
WP	WORK POINT

TILTMETER DESIGNATIONS

○	DESCRIPTION	RANGE +/−
T1	1F S COL ROT L	5°
T2	1F S COL ROT L	10°
T3	1F S COL FLANGE AT BEAM	10°
T4	2F S COL ROT L	5°
T5	2F S COL ROT L	10°
T6	2F BEAM ROT MID S SIDE	5°
T7	2F BEAM ROT MID S SIDE	5°
T8	1F BEAM ROT S SIDE	5°
T9	1F BEAM ROT S SIDE	10°
T10	1F BEAM ROT MID S SIDE	5°
T11	1F BEAM ROT MID S SIDE	5°
T12	1F SLAB ROT S SIDE E	5°
T13	1F SLAB ROT S SIDE W	5°
T14	1F N COL ROT L	5°
T15	1F N COL ROT L	15°
T16	1F N COL FLANGE AT BEAM	10°
T17	2F N COL ROT L	10°
T18	2F N COL ROT L	10°
T19	2F BEAM ROT MID N SIDE	10°
T20	2F BEAM ROT MID N SIDE	5°
T21	1F BEAM ROT N SIDE	5°
T22	1F BEAM ROT N SIDE	10°
T23	1F BEAM ROT MID N SIDE	5°
T24	1F BEAM ROT MID N SIDE	5°
T25	1F SLAB ROT N SIDE E	5°
T26	1F SLAB ROT N SIDE W	5°
T27	1F SLAB ROT MID E	10°
T28	1F SLAB ROT MID W	10°
T29	2F SLAB ROT N SIDE E	5°
T30	2F SLAB ROT N SIDE W	5°
T31	1F BEAM TORSIONAL ROT	10°

NDI OPTOTRAK LED DESIGNATIONS

●	DESCRIPTION	●	DESCRIPTION
N1	1F S BR OOP 1/4 PT	N25	1F N BR OOP 1/4 PT
N2	1F S BR OOP 1/4 PT	N26	1F N BR OOP 1/4 PT
N3	1F S BR OOP	N27	1F N BR OOP
N4	1F S BR OOP	N28	1F N BR OOP
N5	1F S BR OOP	N29	1F N BR OOP
N6	1F S BR OOP	N30	1F N BR OOP
N7	1F S BR OOP	N31	1F N BR OOP
N8	1F S BR OOP	N32	1F N BR OOP
N9	1F BEAM MID GP GRID	N33	1F BEAM MID GP GRID
N10	1F BEAM MID GP GRID	N34	1F BEAM MID GP GRID
N11	1F BEAM MID GP GRID	N35	1F BEAM MID GP GRID
N12	1F BEAM MID GP GRID	N36	1F BEAM MID WEB GRID
N13	1F BEAM MID GP GRID	N37	1F BEAM MID WEB GRID
N14	1F BEAM MID GP GRID	N38	1F BEAM MID WEB GRID
N15	1F BEAM MID WEB GRID	N39	1F BEAM MID WEB GRID
N16	1F BEAM MID WEB GRID	N40	1F BEAM MID WEB GRID
N17	1F BEAM MID WEB GRID	N41	1F BEAM MID WEB GRID
N18	1F BEAM MID WEB GRID	N42	1F BEAM MID WEB GRID
N19	1F BEAM MID WEB GRID	N43	1F BEAM MID WEB GRID
N20	1F BEAM MID WEB GRID	N44	1F BEAM MID WEB GRID
N21	1F BEAM MID WEB GRID	N45	1F BEAM MID WEB GRID
N22	1F BEAM MID WEB GRID	N46	1F BEAM MID WEB GRID
N23	1F BEAM MID WEB GRID	N47	1F BEAM MID WEB GRID
N24	1F BEAM MID WEB GRID	N48	1F BEAM MID WEB GRID

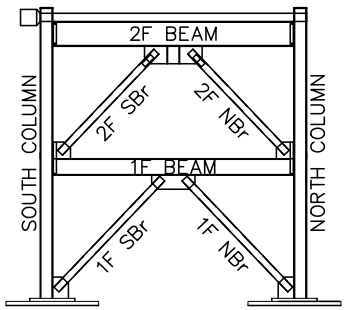

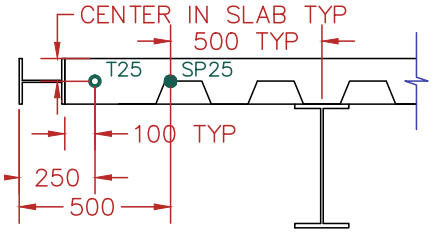

TYPICAL SLAB END INSTRUMENTATION DETAIL

NOTE: LOCATE INCLINOMETERS ON OUTSIDE EDGE OF EACH SLAB

TNCBF1-R-WF: 1F REPAIR/WF BRACES

NEESR: SEISMIC REHAB. OF VULNERABLE BRACED FRAMES

DRAWN BY: ADS
DESIGNED BY: ADS
DATE: 8/23/2013
REVISED: 9/10/2014
CONTACT: ADSEN@UW.EDU

DWG: IN-2

POTENTIOMETER DESIGNATIONS

●	DESCRIPTION	TYPE	RANGE +/−	FREEDOM
L1	1F S COR GP OOP BOT	TML	150mm	
L2	1F S COR GP OOP TOP	TML	150mm	
L4	2F S COR GP OOP CENTER	TML	50mm	HORIZ
L5	2F S COR GP OOP EDGE	TML	100mm	HORIZ
L6	2F S COR GP OOP EDGE	TML	100mm	HORIZ
L7	ALUMINUM PL OOP S	TML	25mm	
L9	ALUMINUM PL OOP N	TML	25mm	
L10	1F N COR GP OOP BOT	TML	150mm	
L11	1F N COR GP OOP TOP	TML	150mm	
L13	2F N COR GP OOP CENTER	TML	100mm	HORIZ
L14	2F N COR GP OOP EDGE	TML	100mm	HORIZ
L15	2F N COR GP OOP EDGE	TML	100mm	HORIZ
L16	2F BEAM DRIFT E SIDE	TEMPO	250mm	
L17	2F BEAM DRIFT W SIDE	TEMPO	250mm	
L18	2F BEAM VERT DISP	TML	150mm	HORIZ
L19	1F BEAM VERT DISP	TML	150mm	HORIZ

●	DESCRIPTION	TYPE	RANGE +/−	FREEDOM
SP1	2F BEAM S OOP ROT	STRING	125mm	HORIZ
SP2	2F BEAM MID OOP	STRING	125mm	HORIZ
SP3	2F BEAM N OOP ROT	STRING	125mm	HORIZ
SP4	1F S BRACE DIAG/OOP	STRING	250mm	HORIZ
SP5	1F S BRACE DIAG/OOP	STRING	250mm	HORIZ
SP6	2F S BRACE DIAG/OOP	STRING	250mm	HORIZ
SP7	2F S BRACE DIAG/OOP	STRING	250mm	HORIZ
SP8	2F S BRACE QUARTER PT	STRING	250mm	HORIZ
SP9	2F S GP OOP BOT EDGE	STRING	125mm	HORIZ
SP10	2F S GP OOP S EDGE	STRING	125mm	HORIZ
SP11	2F S GP OOP CENTER	STRING	125mm	HORIZ
SP12	2F MID GP OOP	STRING	125mm	HORIZ
SP13	1F S BEAM DRIFT E SIDE	STRING	250mm	
SP14	1F S BEAM DRIFT W SIDE	STRING	250mm	
SP15	1F N BRACE DIAG/IP	STRING	250mm	HORIZ
SP16	1F N BRACE DIAG/IP	STRING	250mm	HORIZ
SP18	2F N BRACE DIAG/OOP	STRING	250mm	HORIZ
SP19	2F N BRACE DIAG/OOP	STRING	250mm	HORIZ
SP20	2F N BRACE QUARTER PT	STRING	250mm	HORIZ
SP21	2F N GP OOP BOT EDGE	STRING	125mm	HORIZ
SP22	2F N GP OOP N EDGE	STRING	125mm	HORIZ
SP23	2F N GP OOP CENTER	STRING	125mm	HORIZ
SP24	1F N BEAM DRIFT WP	STRING	250mm	
SP25	1F N BEAM DRIFT E SIDE	STRING	250mm	
SP26	1F N BEAM DRIFT W SIDE	STRING	250mm	
SP27	1F S BRACE OOP	STRING	125mm	
SP28	1F N BRACE OOP	STRING	250mm	

●	DESCRIPTION	TYPE	RANGE +/−	FREEDOM
D1	S ANCHOR PL SLIP	DIAL	25mm	
D2	S ANCHOR PL UPLIFT	DIAL	25mm	
D3	S BASE PL SLIP	DIAL	25mm	
D4	S BASE PL UPLIFT	DIAL	25mm	
D5	N ANCHOR PL SLIP	DIAL	25mm	
D6	N ANCHOR PL UPLIFT	DIAL	25mm	
D7	N BASE PL SLIP	DIAL	25mm	
D8	N BASE PL UPLIFT	DIAL	25mm	
D9	ACTUATOR BASE PL UPLIFT	DIAL	25mm	
D10	ACTUATOR BASE PL SLIP	DIAL	25mm	

ABBREVIATIONS

N	NORTH
S	SOUTH
E	EAST
W	WEST
BOT	BOTTOM
MID	MIDDLE
COL	COLUMN
BR	BRACE
PL	PLATE
OOP	OUT OF PLANE
IP	IN PLANE
DIAG	DIAGONAL
DISP	DISPLACEMENT
ROT	ROTATION
PT	POINT
WP	WORK POINT

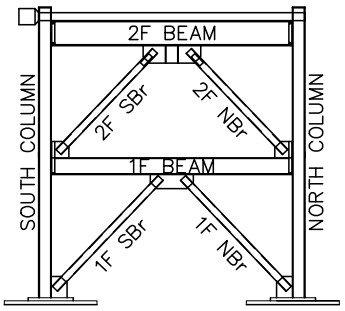

TNCBF1-R-WF: 1F REPAIR/WF BRACES

NEESR: SEISMIC REHAB. OF VULNERABLE BRACED FRAMES

DRAWN BY: ADS
DESIGNED BY: ADS
DATE: 8/23/2013
REVISED: 9/10/2014
CONTACT: ADSEN@UW.EDU

DWG: IN-3

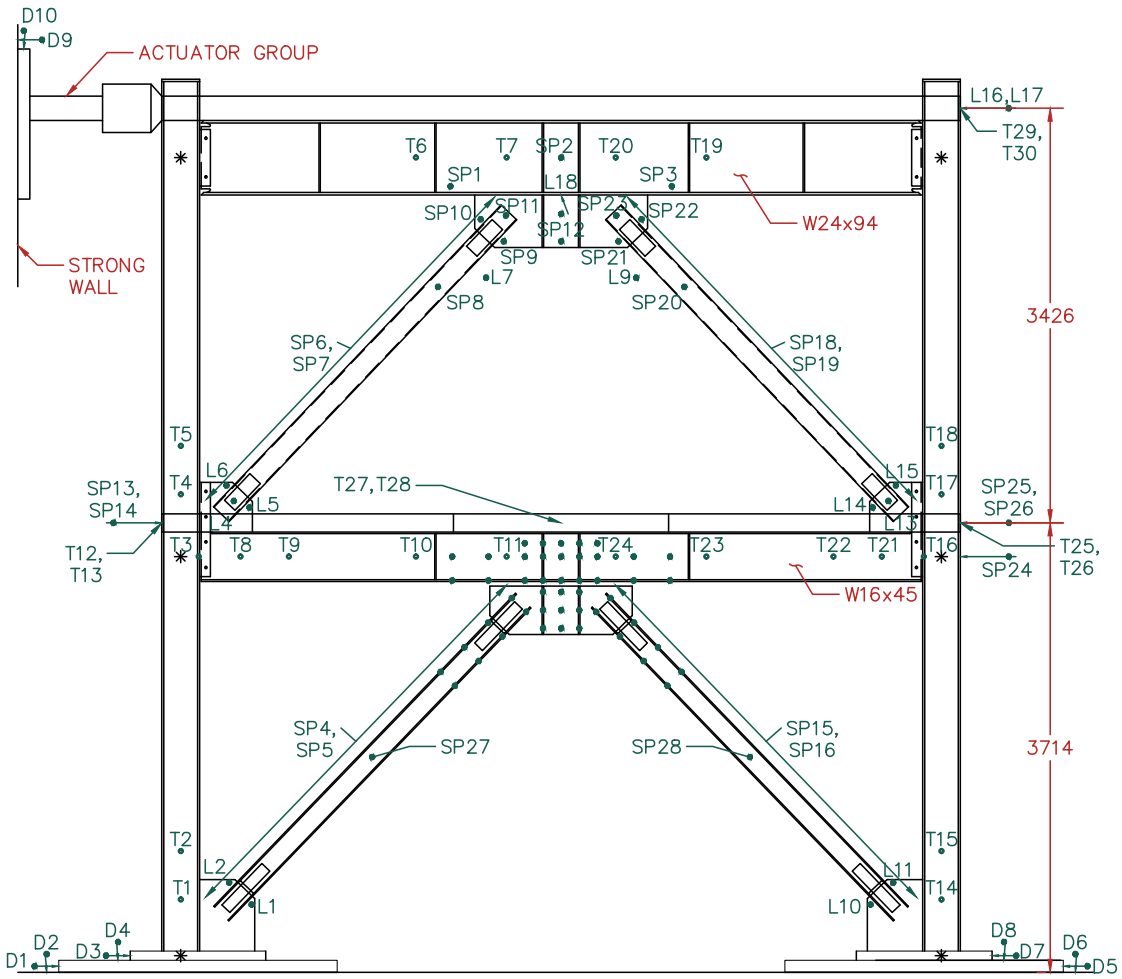

SCALE: 1mm = 50mm

TNCBF1-R-WF: 1F REPAIR/WF BRACES	
NEESR: SEISMIC REHAB. OF VULNERABLE BRACED FRAMES	DWG: IN-4
DRAWN BY: ADS DESIGNED BY: ADS DATE: 8/23/2013 REVISED: 9/10/2014 CONTACT: ADSEN@UW.EDU	

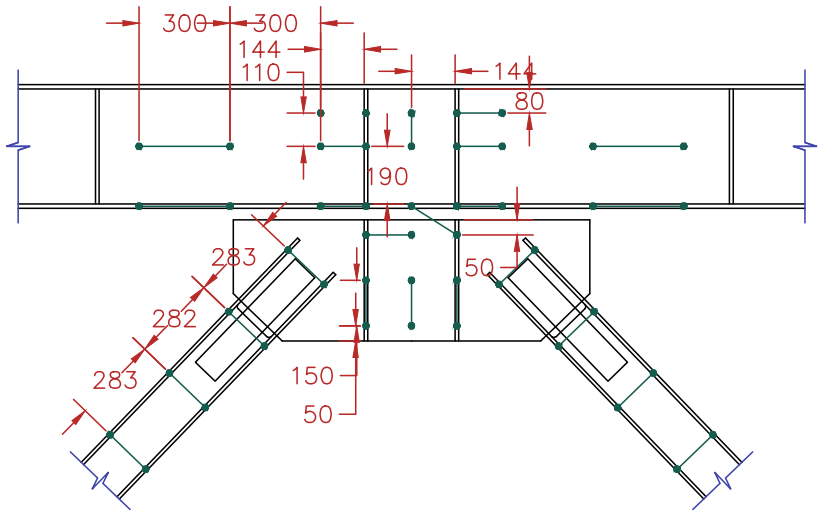

BOTTOM BEAM GUSSET PLATE LED LOCATION DETAIL

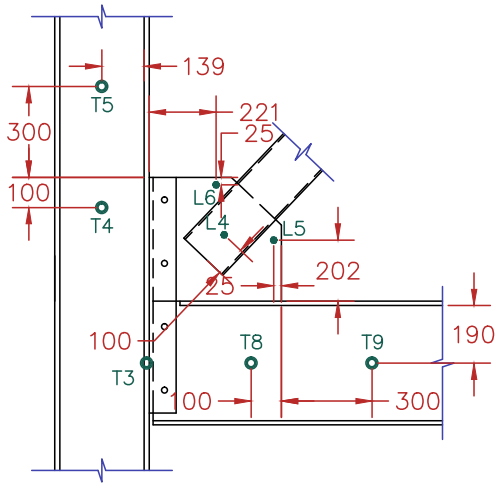

TYPICAL BEAM/COLUMN GUSSET PLATE INSTRUMENTATION DETAIL

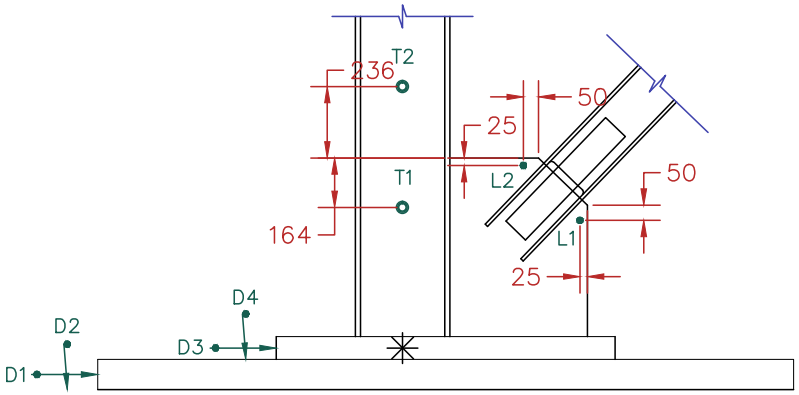

TYPICAL BASE GUSSET PLATE INSTRUMENTATION DETAIL

TNCBF1-R-WF: 1F REPAIR/WF BRACES

NEESR: SEISMIC REHAB. OF VULNERABLE BRACED FRAMES

DRAWN BY: ADS
DESIGNED BY: ADS
DATE: 8/23/2013
REVISED: 9/10/2014
CONTACT: ADSEN@UW.EDU

DWG: IN-5

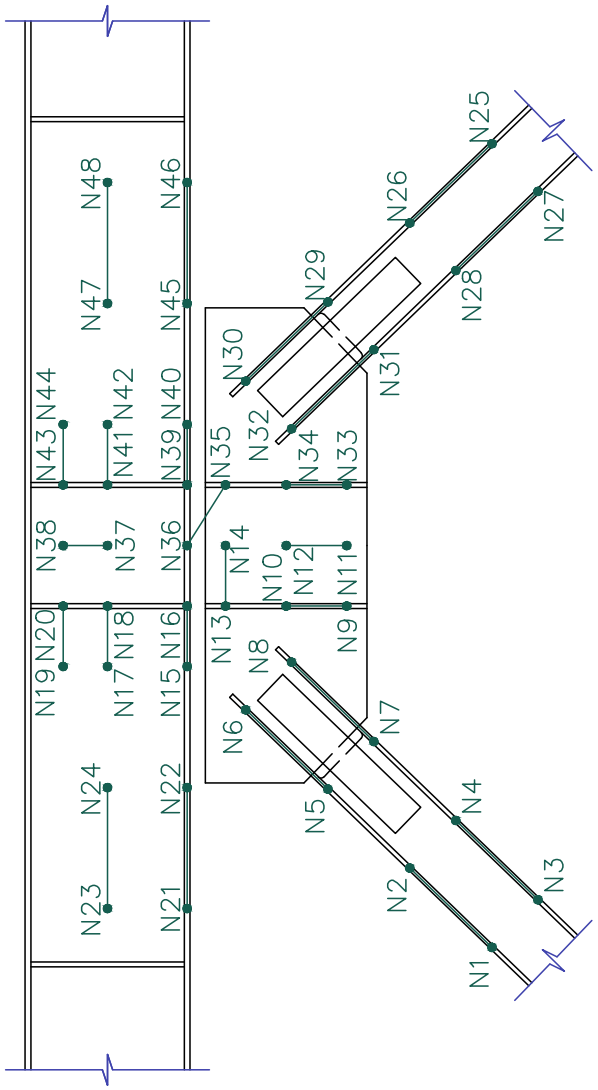

BOTTOM BEAM GUSSET PLATE LED NUMBERING

TNCBF1-R-WF: 1F REPAIR/WF BRACES

NEESR: SEISMIC REHAB. OF VULNERABLE BRACED FRAMES

DWG: IN-6

DRAWN BY: ADS
DESIGNED BY: ADS
DATE: 8/23/2013
REVISED: 9/10/2014
CONTACT: ADSEN@UW.EDU

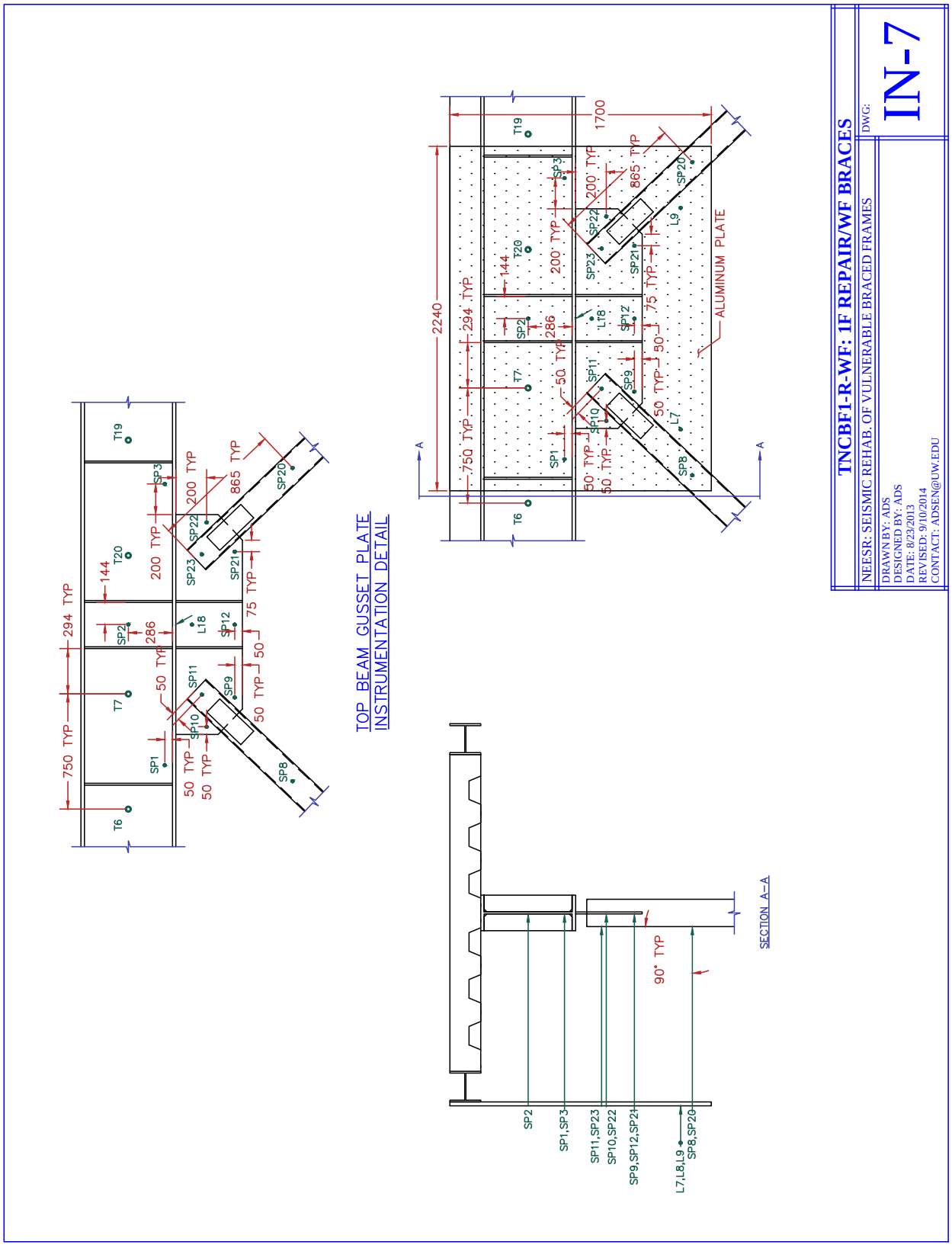
TNCBF1-R-WE: 1F REPAIR/WF BRACES
NEESR: SEISMIC REHAB. OF VULNERABLE BRACED FRAMES
DRAWN BY: ADS
DESIGNED BY: ADS
DATE: 8/23/2013
REVISED: 9/10/2014
CONTACT: ADSEN@UW.EDU
DWG:
IN-7
TOP BEAM GUSSET PLATE
INSTRUMENTATION DETAIL
ALUMINUM PLATE
SECTION A–A
90° TYP
SP2
SP1,SP3
SP11,SP23
SP10,SP22
SP9,SP12,SP21
L7,L8,L9
SP8,SP20
2240
1700
750 TYP
294 TYP
144
200 TYP
865 TYP
75 TYP
50 TYP
286

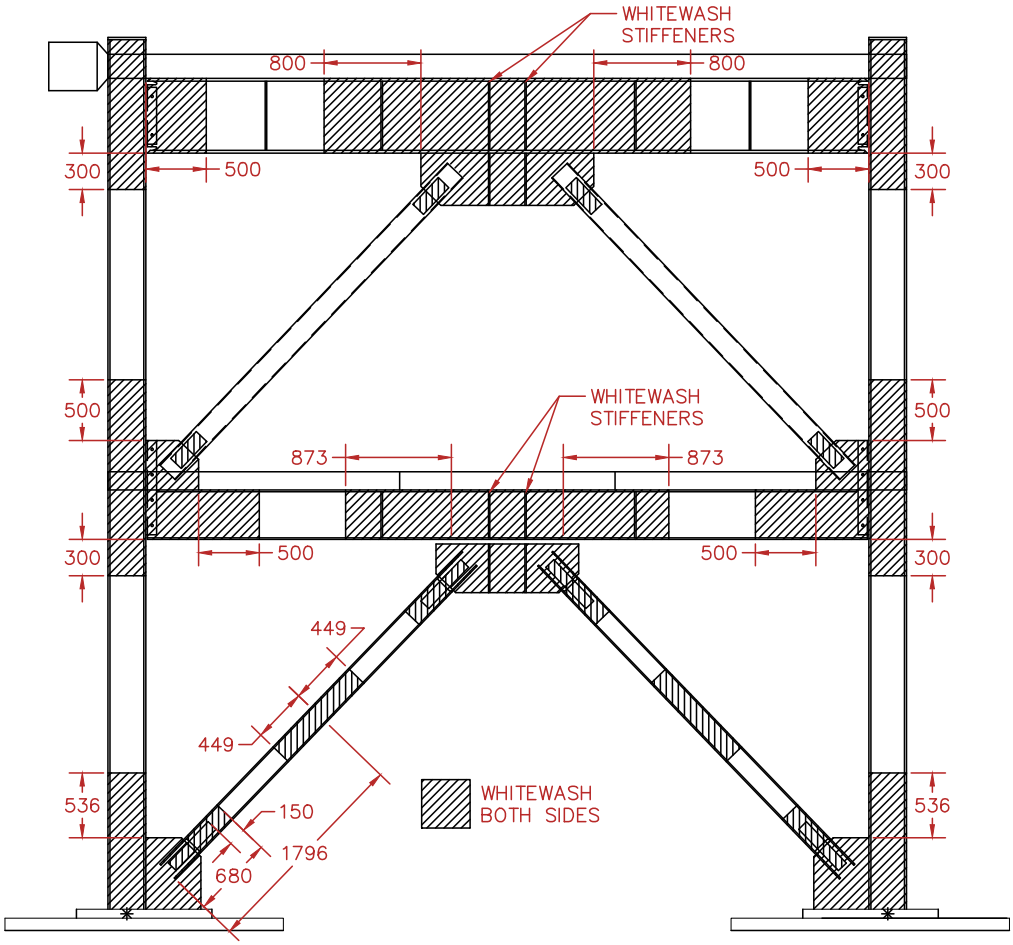

WHITEWASH PLAN
SCALE: 1mm = 50mm

TNCBF1-R-WF: 1F REPAIR/WF BRACES	
NEESR: SEISMIC REHAB. OF VULNERABLE BRACED FRAMES	DWG: IN-8
DRAWN BY: ADS DESIGNED BY: ADS DATE: 8/23/2013 REVISED: 9/10/2014 CONTACT: ADSEN@UW.EDU	

A.4 TNCBF2-D-HSS

The specimen drawings for TNCBF2-D-HSS are found below. This was the fourth specimen tested at NCREE in this test series and only the repair details are provided since no changes were made elsewhere.

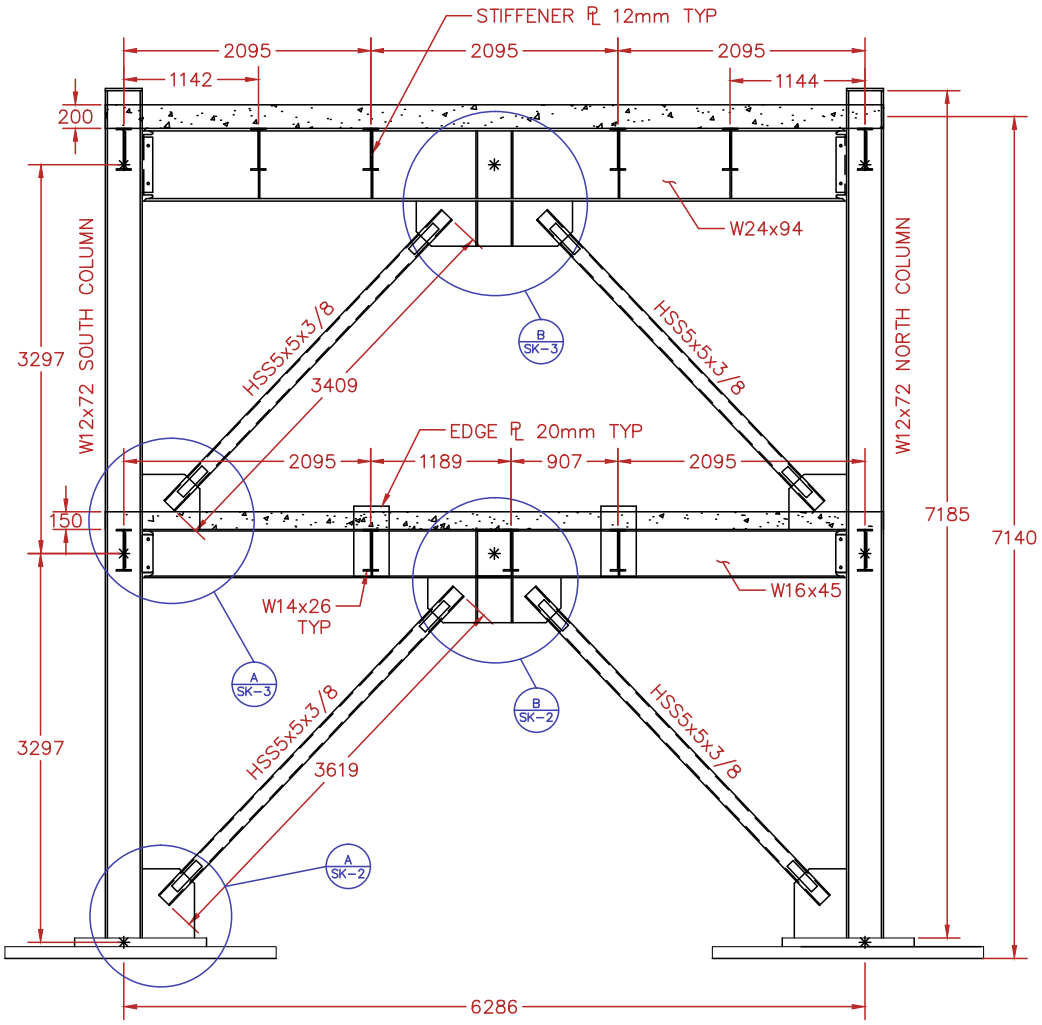

NOTES:
- EXISTING FIRST AND SECOND STORY BRACES AND GUSSET PLATES TO BE REMOVED
- EXISTING FIRST STORY BEAM AND SLAB TO BE REMOVED
- FIRST STORY SLAB TO HAVE SPECIFIED COMPRESSIVE STRENGTH OF 5.0 KSI
- ALL WELDS TO SATISFY AISC DEMAND CRITICAL AWS E71T-1 OR EQUIVALENT

TNCBF2-D-HSS: DUCTILE DETAILS/HSS BRACES

NEESR: SEISMIC REHAB. OF VULNERABLE BRACED FRAMES

DWG: SK-1

DRAWN BY: ADS, MAC
DESIGNED BY: ADS, MAC
DATE: 11/1/2013
REVISED: 9/8/2014
CONTACT: ADSEN@UW.EDU, MCLARKE3@UW.EDU

A
SK–2

1F CORNER GUSSET PLATE DETAIL
SCALE: 1mm = 20mm

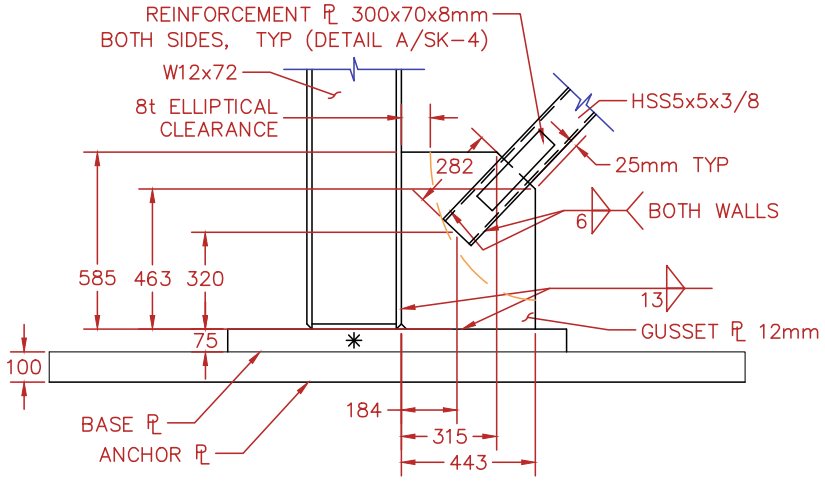

B
SK–2

1F MID–SPAN GUSSET PLATE DETAIL
SCALE: 1mm = 20mm

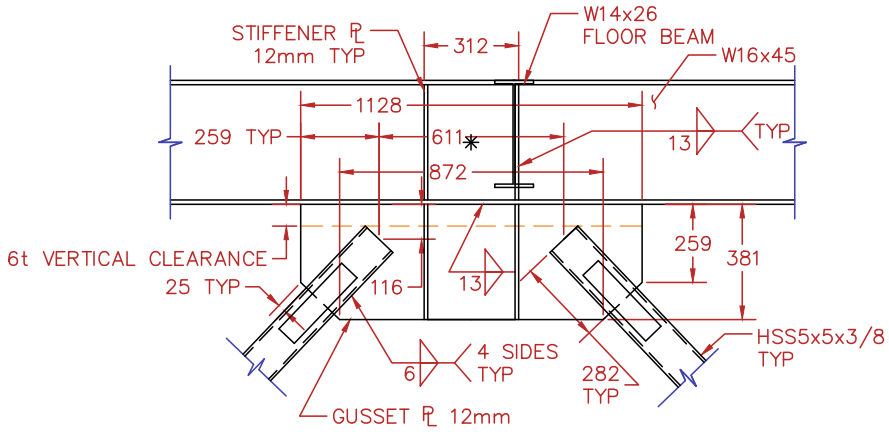

NOTES:
–ALL PLATE STEEL A572 GR 50 OR EQUIVALENT
–ALL BRACES TO BE A500 GR B/C
–ALL WELDS AS DESIGNATED IN SK–1

TNCBF2-D-HSS: DUCTILE DETAILS/HSS BRACES

NEESR: SEISMIC REHAB. OF VULNERABLE BRACED FRAMES

DWG: SK-2

DRAWN BY: ADS, MAC
DESIGNED BY: ADS, MAC
DATE: 11/1/2013
REVISED: 9/8/2014
CONTACT: ADSEN@UW.EDU, MCLARKE3@UW.EDU

A / SK–3

2F CORNER GUSSET PLATE DETAIL

SCALE: 1mm = 20mm

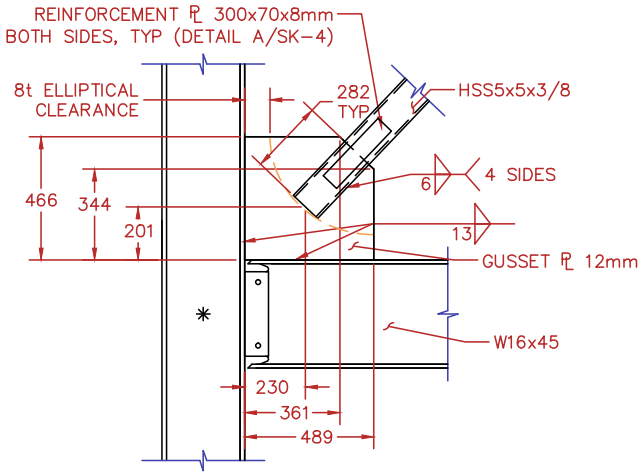

B / SK–3

2F MID–SPAN GUSSET PLATE DETAIL

SCALE: 1mm = 20mm

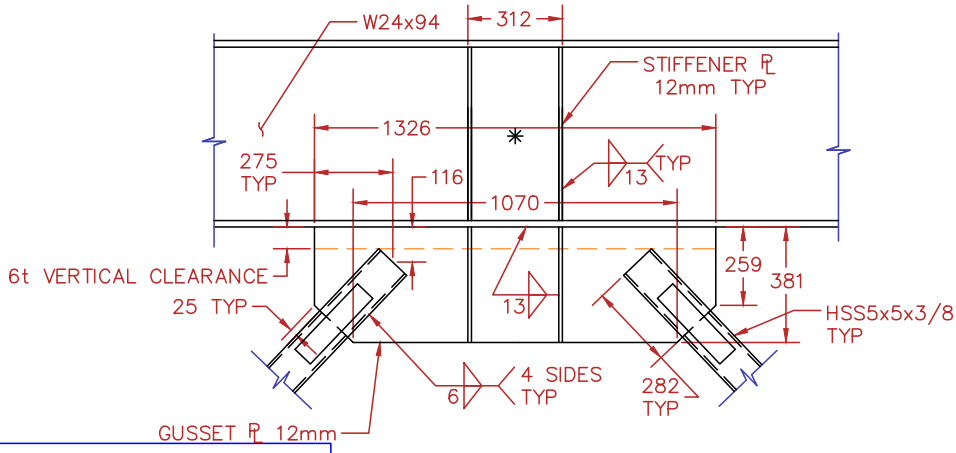

NOTES:
–ALL PLATE STEEL A572 GR 50 OR EQUIVALENT
–ALL BRACES TO BE A500 GR B/C
–ALL WELDS AS DESIGNATED IN SK–1

TNCBF2-D-HSS: DUCTILE DETAILS/HSS BRACES

NEESR: SEISMIC REHAB. OF VULNERABLE BRACED FRAMES

DWG: SK-3

DRAWN BY: ADS, MAC
DESIGNED BY: ADS, MAC
DATE: 11/1/2013
REVISED: 9/8/2014
CONTACT: ADSEN@UW.EDU, MCLARKE3@UW.EDU

A
SK–4

BRACE NET SECTION REINFORCEMENT DETAIL
SCALE: 1mm = 15mm

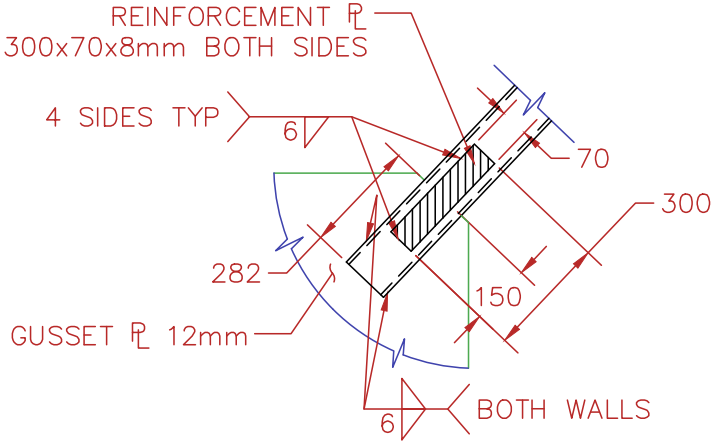

B
SK–4

BRACE SLOT DETAIL
SCALE: 1mm = 15mm

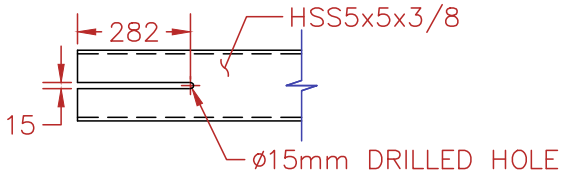

NOTES:
–ALL PLATE STEEL A572 GR 50 OR EQUIVALENT
–ALL BRACES TO BE A500 GR B/C
–ALL WELDS AS DESIGNATED IN SK–1

TNCBF2-D-HSS: DUCTILE DETAILS/HSS BRACES

NEESR: SEISMIC REHAB. OF VULNERABLE BRACED FRAMES

DWG: SK-4

DRAWN BY: ADS, MAC
DESIGNED BY: ADS, MAC
DATE: 11/1/2013
REVISED: 9/8/2014
CONTACT: ADSEN@UW.EDU, MCLARKE3@UW.EDU

A
SK–5

1F CORNER GUSSET PLATE
FABRICATION DETAIL

SCALE: 1mm = 15mm

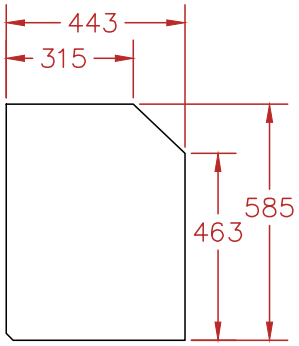

B
SK–5

1F MID–SPAN GUSSET PLATE
FABRICATION DETAIL

SCALE: 1mm = 15mm

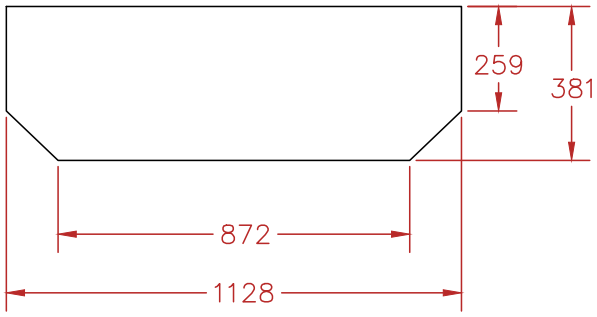

NOTES:
–ALL PLATE STEEL A572 GR 50 OR EQUIVALENT
–ALL BRACES TO BE A500 GR B/C
–ALL WELDS AS DESIGNATED IN SK–1

TNCBF2-D-HSS: DUCTILE DETAILS/HSS BRACES

NEESR: SEISMIC REHAB. OF VULNERABLE BRACED FRAMES

DWG: SK-5

DRAWN BY: ADS, MAC
DESIGNED BY: ADS, MAC
DATE: 11/1/2013
REVISED: 9/8/2014
CONTACT: ADSEN@UW.EDU, MCLARKE3@UW.EDU

A
SK–6

2F CORNER GUSSET PLATE
FABRICATION DETAIL
SCALE: 1mm = 15mm

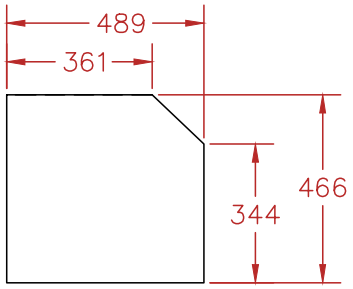

B
SK–6

2F MID–SPAN GUSSET PLATE
FABRICATION DETAIL
SCALE: 1mm = 15mm

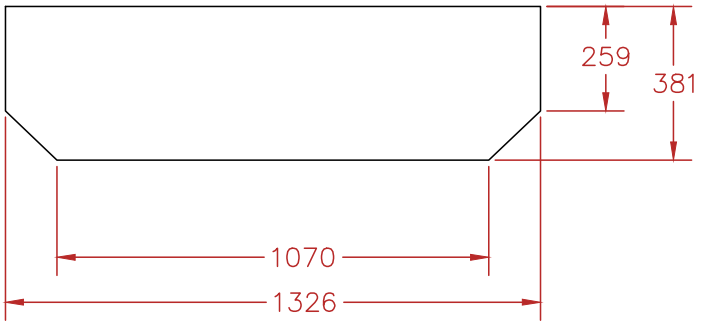

NOTES:
–ALL PLATE STEEL A572 GR 50 OR EQUIVALENT
–ALL BRACES TO BE A500 GR B/C
–ALL WELDS AS DESIGNATED IN SK–1

TNCBF2-D-HSS: DUCTILE DETAILS/HSS BRACES

NEESR: SEISMIC REHAB. OF VULNERABLE BRACED FRAMES

DWG: SK-6

DRAWN BY: ADS, MAC
DESIGNED BY: ADS, MAC
DATE: 11/1/2013
REVISED: 9/8/2014
CONTACT: ADSEN@UW.EDU, MCLARKE3@UW.EDU

A
SK–7

1F BEAM FABRICATION DETAIL
SCALE: 1mm = 50mm

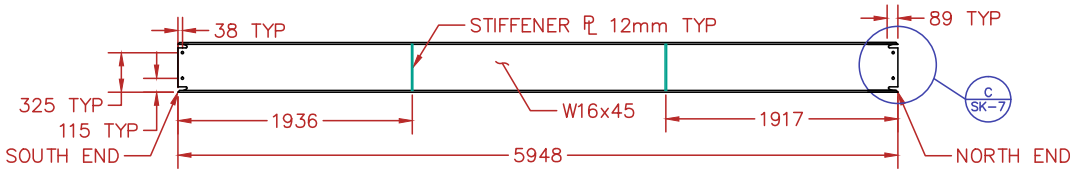

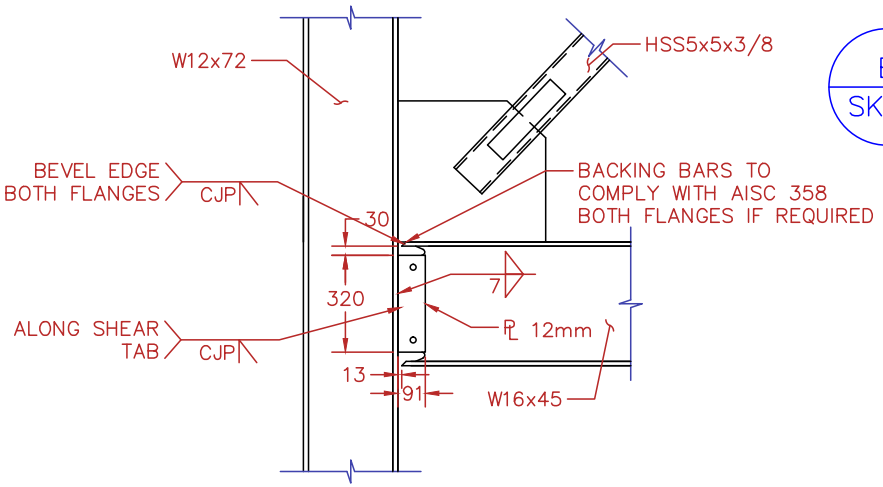

B
SK–7

1F BEAM–TO–COLUMN CONNECTION DETAIL
SCALE: 1mm = 20mm

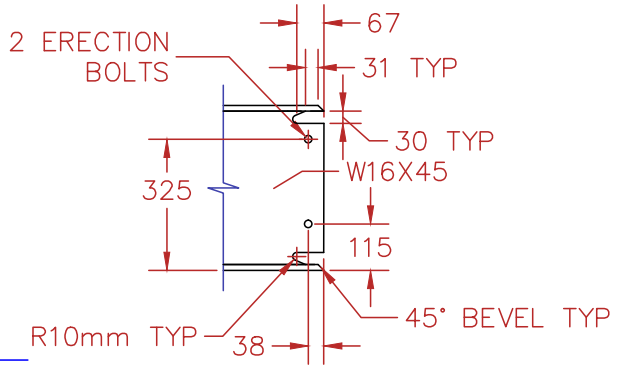

C
SK–7

1F BEAM END DETAIL
SCALE: 1mm = 15mm

NOTES:
–ALL PLATE STEEL A572 GR 50 OR EQUIVALENT
–ALL BRACES TO BE A500 GR B/C
–ALL WELDS AS DESIGNATED IN SK–1

TNCBF2-D-HSS: DUCTILE DETAILS/HSS BRACES

NEESR: SEISMIC REHAB. OF VULNERABLE BRACED FRAMES

DRAWN BY: ADS, MAC
DESIGNED BY: ADS, MAC
DATE: 11/1/2013
REVISED: 9/8/2014
CONTACT: ADSEN@UW.EDU, MCLARKE3@UW.EDU

DWG: SK-7

A
SK–2

1F BEAM/SLAB PLAN
SCALE: 1mm = 50mm

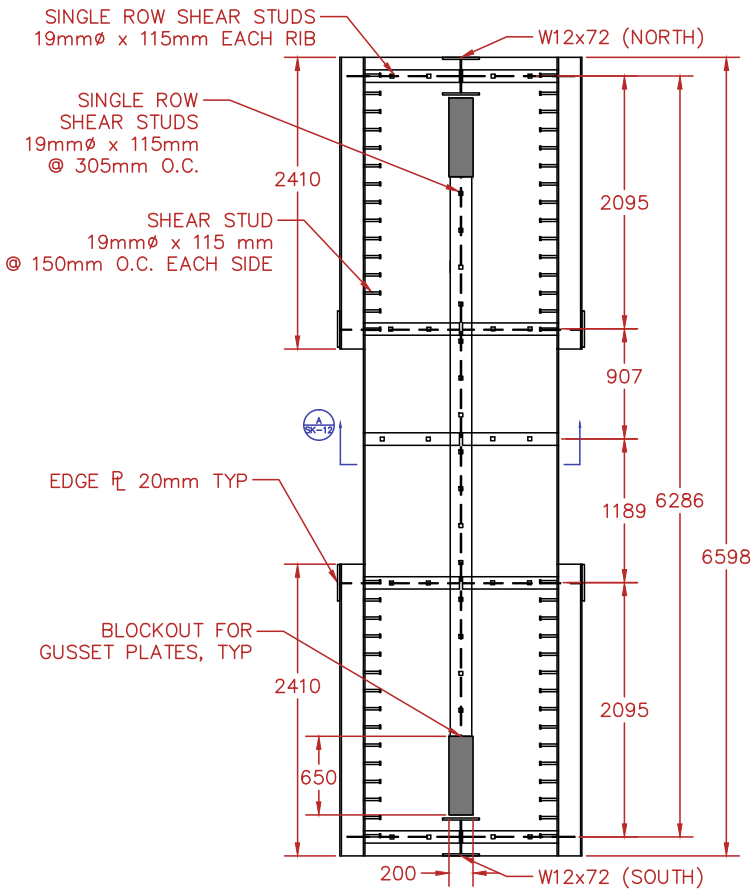

NOTES:
–ALL PLATE STEEL A572 GR 50 OR EQUIVALENT
–ALL BRACES TO BE A500 GR B/C
–ALL WELDS AS DESIGNATED IN SK–1

TNCBF2-D-HSS: DUCTILE DETAILS/HSS BRACES

NEESR: SEISMIC REHAB. OF VULNERABLE BRACED FRAMES

DWG: SK-8

DRAWN BY: ADS, MAC
DESIGNED BY: ADS, MAC
DATE: 11/1/2013
REVISED: 9/8/2014
CONTACT: ADSEN@UW.EDU, MCLARKE3@UW.EDU

A
SK–9

1F BEAM/SLAB SECTION
(INTERIOR FLOOR BEAMS)

SCALE: 1mm = 20mm

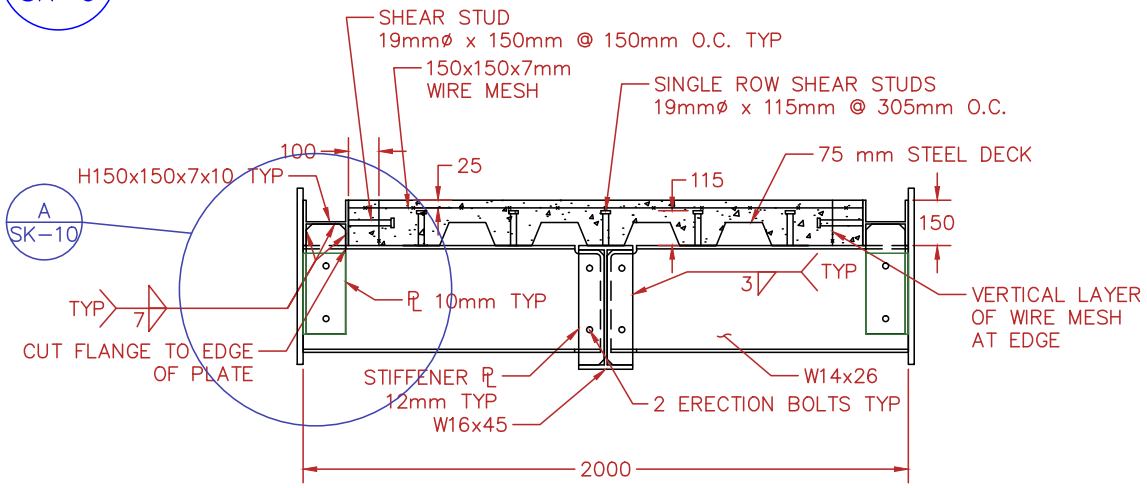

B
SK–9

1F SLAB DETAIL PLAN

SCALE: 1mm = 20mm

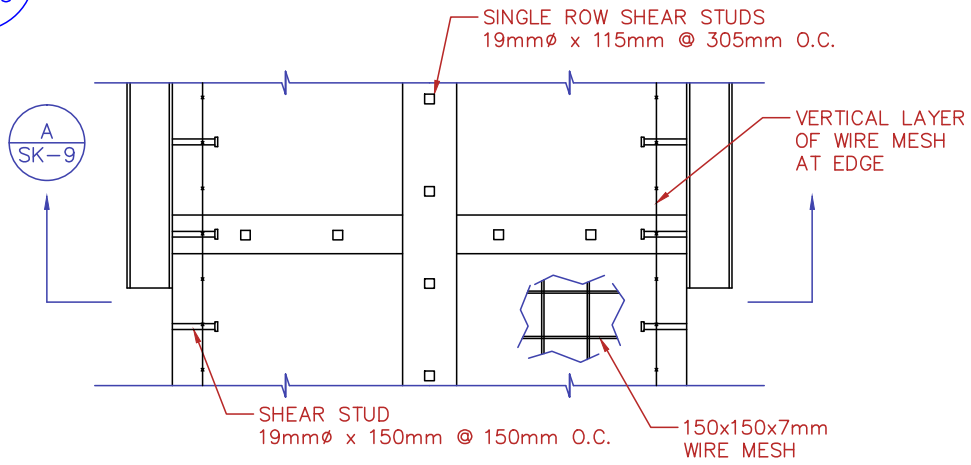

NOTES:
–ALL PLATE STEEL A572 GR 50 OR EQUIVALENT
–ALL BRACES TO BE A500 GR B/C
–ALL WELDS AS DESIGNATED IN SK–1

TNCBF2-D-HSS: DUCTILE DETAILS/HSS BRACES

NEESR: SEISMIC REHAB. OF VULNERABLE BRACED FRAMES

DWG: SK-9

DRAWN BY: ADS, MAC
DESIGNED BY: ADS, MAC
DATE: 11/1/2013
REVISED: 9/8/2014
CONTACT: ADSEN@UW.EDU, MCLARKE3@UW.EDU

A
SK–10

1F EDGE PLATE DETAIL
SCALE: 1mm = 20mm

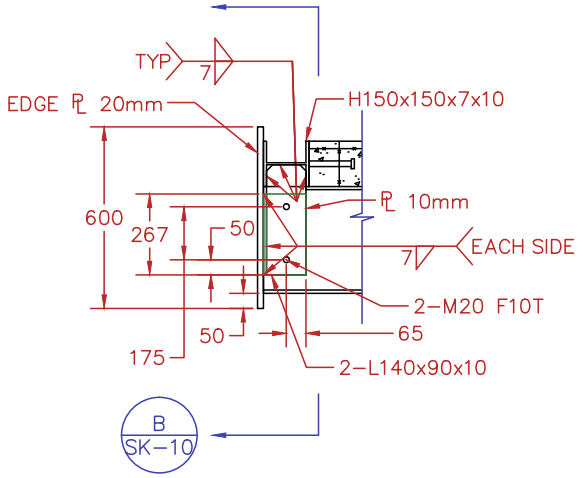

B
SK–10

1F INTERIOR FLOOR BEAM SECTION
SCALE: 1mm = 15mm

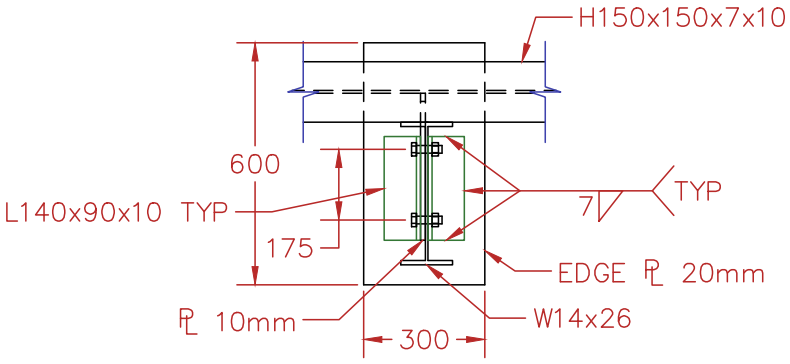

NOTES:
–ALL PLATE STEEL A572 GR 50 OR EQUIVALENT
–ALL BRACES TO BE A500 GR B/C
–ALL WELDS AS DESIGNATED IN SK–1

TNCBF2-D-HSS: DUCTILE DETAILS/HSS BRACES

NEESR: SEISMIC REHAB. OF VULNERABLE BRACED FRAMES

DWG: SK-10

DRAWN BY: ADS, MAC
DESIGNED BY: ADS, MAC
DATE: 11/1/2013
REVISED: 9/8/2014
CONTACT: ADSEN@UW.EDU, MCLARKE3@UW.EDU

A
SK–11

1F BEAM/SLAB SECTION
(EXTERIOR FLOOR BEAMS)

SCALE: 1mm = 20mm

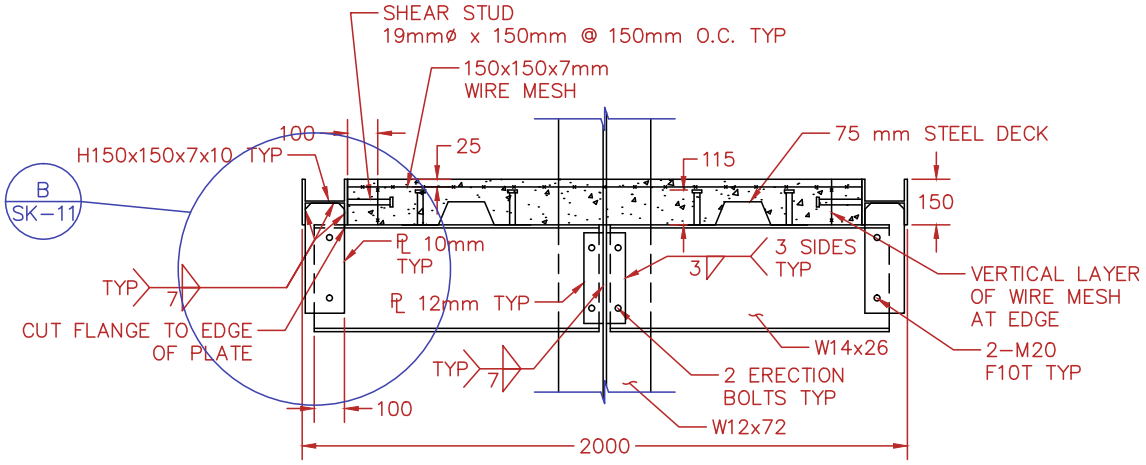

B
SK–11

1F FLOOR BEAM–TO–COLUMN CONNECTION

SCALE: 1mm = 20mm

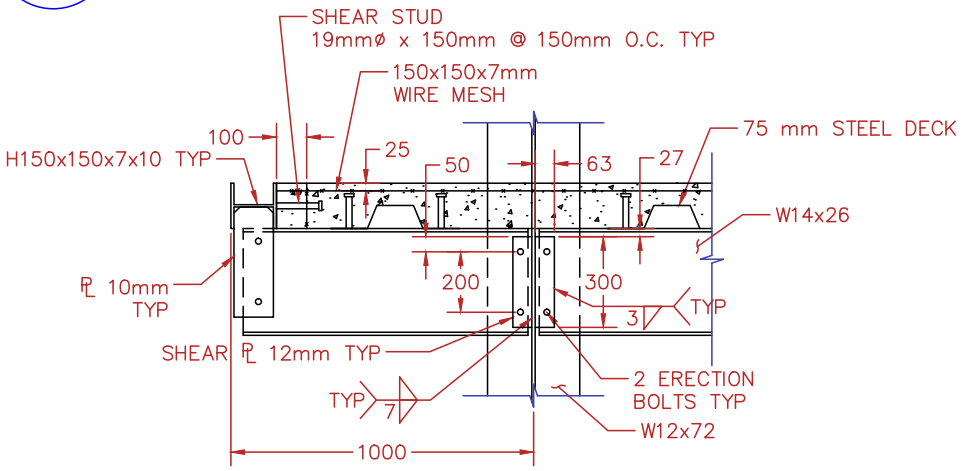

NOTES:
–ALL PLATE STEEL A572 GR 50 OR EQUIVALENT
–ALL BRACES TO BE A500 GR B/C
–ALL WELDS AS DESIGNATED IN SK–1

TNCBF2-D-HSS: DUCTILE DETAILS/HSS BRACES

NEESR: SEISMIC REHAB. OF VULNERABLE BRACED FRAMES

DWG: SK-11

DRAWN BY: ADS, MAC
DESIGNED BY: ADS, MAC
DATE: 11/1/2013
REVISED: 9/8/2014
CONTACT: ADSEN@UW.EDU, MCLARKE3@UW.EDU

A
SK–12

1F MID–SPAN FLOOR BEAM SECTION
SCALE: 1mm = 20mm

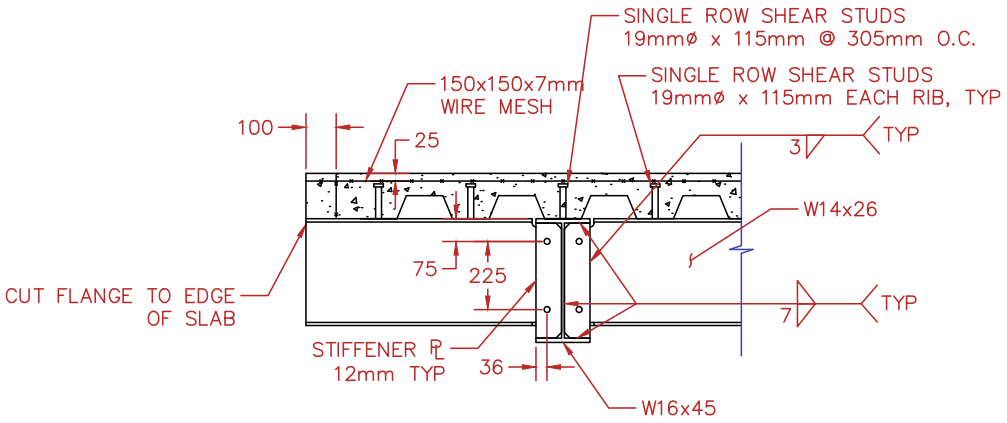

B
SK–12

1F MID–SPAN FLOOR BEAM
FABRICATION DETAIL
SCALE: 1mm = 15mm

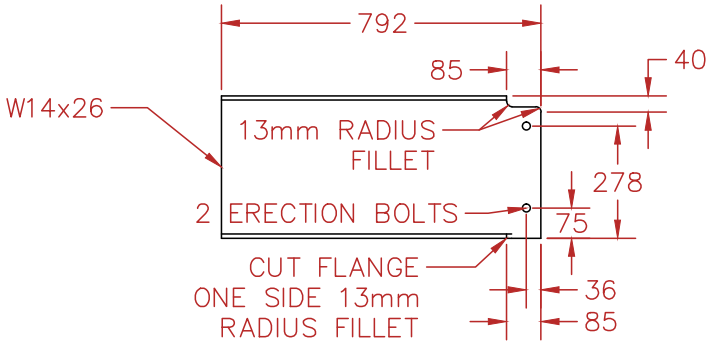

NOTES:
–ALL PLATE STEEL A572 GR 50 OR EQUIVALENT
–ALL BRACES TO BE A500 GR B/C
–ALL WELDS AS DESIGNATED IN SK–1

TNCBF2-D-HSS: DUCTILE DETAILS/HSS BRACES

NEESR: SEISMIC REHAB. OF VULNERABLE BRACED FRAMES

DWG: SK-12

DRAWN BY: ADS, MAC
DESIGNED BY: ADS, MAC
DATE: 11/1/2013
REVISED: 9/8/2014
CONTACT: ADSEN@UW.EDU, MCLARKE3@UW.EDU

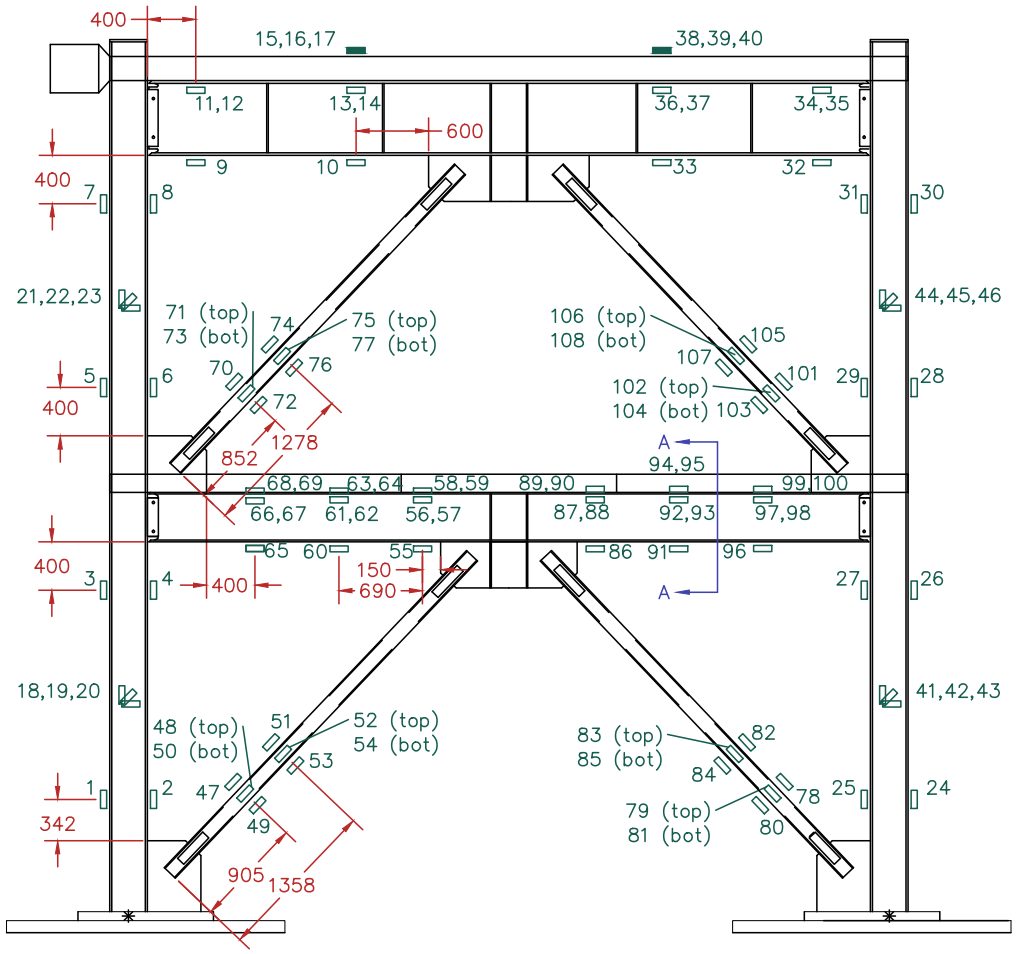

STRAIN GAUGE LAYOUT
SCALE: 1mm = 50mm

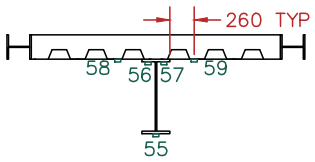

SECTION A–A

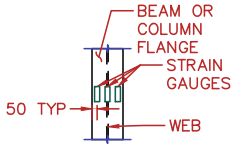

NOTE: LOCATE SG ON CENTER OF FLANGE OR UNDERSIDE OF FLANGE 50mm FROM EDGE AS NECESSARY.

TNCBF2-D-HSS: DUCTILE DETAILS/HSS BRACES

NEESR: SEISMIC REHAB. OF VULNERABLE BRACED FRAMES

DWG: IN-1

DRAWN BY: ADS, MAC
DESIGNED BY: ADS, MAC
DATE: 1/13/2013
REVISED: 9/10/2014
CONTACT: ADSEN@UW.EDU, MCLARKE3@UW.EDU

KEY
- STEEL UNIAXIAL STRAIN GAUGE
- CONCRETE UNIAXIAL STRAIN GAUGE
- TRIAXIAL STRAIN GAUGE

	LABEL	LOCATION		LABEL	LOCATION
1	SG 1	S COLUMN	24	SG 24	N COLUMN
2	SG 2	S COLUMN	25	SG 25	N COLUMN
3	SG 3	S COLUMN	26	SG 26	N COLUMN
4	SG 4	S COLUMN	27	SG 27	N COLUMN
5	SG 5	S COLUMN	28	SG 28	N COLUMN
6	SG 6	S COLUMN	29	SG 29	N COLUMN
7	SG 7	S COLUMN	30	SG 30	N COLUMN
8	SG 8	S COLUMN	31	SG 31	N COLUMN
9	SG 9	S TOP BEAM	32	SG 32	N TOP BEAM
10	SG 10	S TOP BEAM	33	SG 33	N TOP BEAM
11	SG 11	S TOP BEAM*	34	SG 34	N TOP BEAM*
12	SG 12	S TOP BEAM*	35	SG 35	N TOP BEAM*
13	SG 13	S TOP BEAM*	36	SG 36	N TOP BEAM*
14	SG 14	S TOP BEAM*	37	SG 37	N TOP BEAM*
15	SG 15	S TOP SLAB	38	SG 38	N TOP SLAB
16	SG 16	S TOP SLAB	39	SG 39	N TOP SLAB
17	SG 17	S TOP SLAB	40	SG 40	N TOP SLAB
18	SG 18	S COL BOT 0°	41	SG 41	N COL BOT 0°
19	SG 19	S COL BOT 45°	42	SG 42	N COL BOT 45°
20	SG 20	S COL BOT 90°	43	SG 43	N COL BOT 90°
21	SG 21	S COL TOP 0°	44	SG 44	N COL TOP 0°
22	SG 22	S COL TOP 45°	45	SG 45	N COL TOP 45°
23	SG 23	S COL TOP 90°	46	SG 46	N COL TOP 90°

	LABEL	LOCATION		LABEL	LOCATION
47	SG 47	S BOT BRACE L	78	SG 78	N BOT BRACE L
48	SG 48	S BOT BRACE L	79	SG 79	N BOT BRACE L
49	SG 49	S BOT BRACE L	80	SG 80	N BOT BRACE L
50	SG 50	S BOT BRACE L	81	SG 81	N BOT BRACE L
51	SG 51	S BOT BRACE U	82	SG 82	N BOT BRACE U
52	SG 52	S BOT BRACE U	83	SG 83	N BOT BRACE U
53	SG 53	S BOT BRACE U	84	SG 84	N BOT BRACE U
54	SG 54	S BOT BRACE U	85	SG 85	N BOT BRACE U
55	SG 55	S BOT BEAM	86	SG 86	N BOT BEAM
56	SG 56	S BOT BEAM*	87	SG 87	N BOT BEAM*
57	SG 57	S BOT BEAM*	88	SG 88	N BOT BEAM*
58	SG 58	S BOT BEAM**	89	SG 89	N BOT BEAM**
59	SG 59	S BOT BEAM**	90	SG 90	N BOT BEAM**
60	SG 60	S BOT BEAM	91	SG 91	N BOT BEAM
61	SG 61	S BOT BEAM*	92	SG 92	N BOT BEAM*
62	SG 62	S BOT BEAM*	93	SG 93	N BOT BEAM*
63	SG 63	S BOT BEAM**	94	SG 94	N BOT BEAM**
64	SG 64	S BOT BEAM**	95	SG 95	N BOT BEAM**
65	SG 65	S BOT BEAM	96	SG 96	N BOT BEAM
66	SG 66	S BOT BEAM*	97	SG 97	N BOT BEAM*
67	SG 67	S BOT BEAM*	98	SG 98	N BOT BEAM*
68	SG 68	S BOT BEAM**	99	SG 99	N BOT BEAM**
69	SG 69	S BOT BEAM**	100	SG 100	N BOT BEAM**
70	SG 70	S TOP BRACE L	101	SG 101	N TOP BRACE L
71	SG 71	S TOP BRACE L	102	SG 102	N TOP BRACE L
72	SG 72	S TOP BRACE L	103	SG 103	N TOP BRACE L
73	SG 73	S TOP BRACE L	104	SG 104	N TOP BRACE L
74	SG 74	S TOP BRACE U	105	SG 105	N TOP BRACE U
75	SG 75	S TOP BRACE U	106	SG 106	N TOP BRACE U
76	SG 76	S TOP BRACE U	107	SG 107	N TOP BRACE U
77	SG 77	S TOP BRACE U	108	SG 108	N TOP BRACE U

* LOCATE STRAIN GAUGE AT UNDERSIDE OF BEAM FLANGE
** LOCATE STRAIN GAUGE AT UNDERSIDE OF METAL DECK

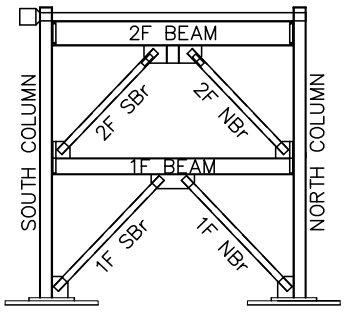

TNCBF2-D-HSS: DUCTILE DETAILS/HSS BRACES

NEESR: SEISMIC REHAB. OF VULNERABLE BRACED FRAMES

DWG: IN-2

DRAWN BY: ADS, MAC
DESIGNED BY: ADS, MAC
DATE: 1/13/2013
REVISED: 9/10/2014
CONTACT: ADSEN@UW.EDU, MCLARKE3@UW.EDU

KEY

- POTENTIOMETER PERPENDICULAR TO PLANE
- POTENTIOMETER IN DIRECTION OF ARROW
- TILTMETER (T)
- NDI OPTOTRAK LED TARGET (N)

ABBREVIATIONS

N	NORTH
S	SOUTH
E	EAST
W	WEST
BOT	BOTTOM
MID	MIDDLE
COL	COLUMN
BR	BRACE
PL	PLATE
OOP	OUT OF PLANE
IP	IN PLANE
DIAG	DIAGONAL
DISP	DISPLACEMENT
ROT	ROTATION
PT	POINT
WP	WORK POINT
L	LOWER
U	UPPER

TILTMETER DESIGNATIONS

○	DESCRIPTION	RANGE +/−
T1	1F S COL ROT L	5°
T2	1F S COL ROT L	10°
T3	1F S COL FLANGE AT BEAM	10°
T4	2F S COL ROT L	10°
T5	2F S COL ROT L	10°
T6	2F BEAM ROT MID S SIDE	3°
T7	2F BEAM ROT MID S SIDE	3°
T8	1F BEAM ROT S SIDE	5°
T9	1F BEAM ROT S SIDE	10°
T10	1F BEAM ROT MID S SIDE	15°
T11	1F BEAM ROT MID S SIDE	10°
T12	1F SLAB ROT S SIDE E	5°
T13	1F SLAB ROT S SIDE W	5°
T14	1F N COL ROT L	5°
T15	1F N COL ROT L	10°
T16	1F N COL FLANGE AT BEAM	10°
T17	2F N COL ROT L	15°
T18	2F N COL ROT L	15°
T19	2F BEAM ROT MID N SIDE	3°
T20	2F BEAM ROT MID N SIDE	3°
T21	1F BEAM ROT N SIDE	5°
T22	1F BEAM ROT N SIDE	15°
T23	1F BEAM ROT MID N SIDE	15°
T24	1F BEAM ROT MID N SIDE	15°
T25	1F SLAB ROT N SIDE E	5°
T26	1F SLAB ROT N SIDE W	5°
T27	1F SLAB ROT MID E	10°
T28	1F SLAB ROT MID W	10°
T29	2F SLAB ROT N SIDE E	10°
T30	2F SLAB ROT N SIDE W	5°
T31	1F BEAM TORSIONAL ROT	5°

NDI OPTOTRAK LED DESIGNATIONS

●	DESCRIPTION	●	DESCRIPTION
N1	1F S BR OOP 1/4 PT	N31	1F BEAM MID GRID
N2	1F S BR OOP	N32	1F FLOOR BEAM
N3	1F S BR OOP	N33	1F FLOOR BEAM
N4	1F S BR OOP	N34	1F FLOOR BEAM
N5	1F MID GP GIRD	N35	1F BEAM MID GRID
N6	1F MID GP GIRD	N36	1F BEAM MID GRID
N7	1F MID GP GIRD	N37	1F BEAM MID GRID
N8	1F S BR OOP	N38	1F BEAM MID GRID
N9	1F BEAM MID GRID	N39	1F BEAM MID GRID
N10	1F BEAM MID GRID	N40	1F METAL DECK
N11	1F BEAM MID GRID	N41	1F BEAM MID GRID
N12	1F BEAM MID GRID	N42	1F METAL DECK
N13	1F BEAM MID GRID	N43	1F MID GP GIRD
N14	1F METAL DECK	N44	1F MID GP GIRD
N15	1F BEAM MID GRID	N45	1F MID GP GIRD
N16	1F BEAM MID GRID	N46	1F MID GP GIRD
N17	1F BEAM MID GRID	N47	BOT BEAM MID WEB GRID
N18	1F METAL DECK	N48	BOT BEAM MID WEB GRID
N19	1F BEAM MID GRID	N49	1F N BR OOP 1/4 PT
N20	1F BEAM MID GRID	N50	1F N BR OOP
N21	1F BEAM MID GRID	N51	1F N BR OOP
N22	1F BEAM MID GRID	N52	1F N BR OOP
N23	1F BEAM MID GRID	N53	1F MID GP GIRD
N24	1F METAL DECK	N54	1F N BR OOP
N25	1F MID GP GIRD	N55	1F BEAM MID GRID
N26	1F MID GP GIRD	N56	1F BEAM MID GRID
N27	1F MID GP GIRD	N57	1F BEAM MID GRID
N28	1F MID GP GIRD	N58	1F BEAM MID GRID
N29	1F MID GP GIRD	N59	1F BEAM MID GRID
N30	1F BEAM MID GRID	N60	1F METAL DECK

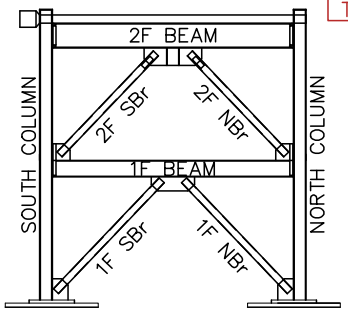

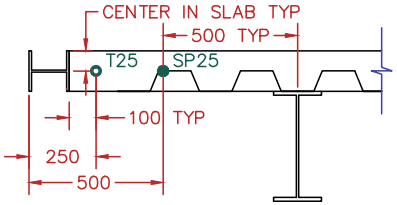

NOTE: LOCATE TILTMETERS ON OUTSIDE EDGE OF EACH SLAB

TYPICAL SLAB END INSTRUMENTATION DETAIL

TNCBF2-D-HSS: DUCTILE DETAILS/HSS BRACES

NEESR: SEISMIC REHAB. OF VULNERABLE BRACED FRAMES

DRAWN BY: ADS, MAC
DESIGNED BY: ADS, MAC
DATE: 1/13/2013
REVISED: 9/10/2014
CONTACT: ADSEN@UW.EDU, MCLARKE3@UW.EDU

DWG: IN-3

POTENTIOMETER DESIGNATIONS

●	DESCRIPTION	TYPE	RANGE +/−	FREEDOM
L1	1F S COR GP OOP BOT	TML	150mm	
L2	1F S COR GP OOP TOP	TML	150mm	
L3	1F S COR GP OOP CENTER	TML	100mm	
L4	2F S COR GP OOP CENTER	TML	50mm	HORIZ
L5	2F S COR GP OOP EDGE	TML	100mm	HORIZ
L6	2F S COR GP OOP EDGE	TML	100mm	HORIZ
L7	ALUMINUM PL OOP S	TML	25mm	
L9	ALUMINUM PL OOP N	TML	25mm	
L10	1F N COR GP OOP BOT	TML	150mm	
L11	1F N COR GP OOP TOP	TML	150mm	
L12	1F N COR GP OOP CENTER	TML	100mm	HORIZ
L13	2F N COR GP OOP CENTER	TML	50mm	HORIZ
L14	2F N COR GP OOP EDGE	TML	100mm	HORIZ
L15	2F N COR GP OOP EDGE	TML	100mm	HORIZ
L16	2F BEAM DRIFT E SIDE	TEMPO	250mm	
L17	2F BEAM DRIFT W SIDE	TEMPO	250mm	
L18	2F BEAM VERT DISP	TML	150mm	HORIZ
L19	1F BEAM VERT DISP	TML	150mm	HORIZ
●	DESCRIPTION	TYPE	RANGE +/−	FREEDOM
SP1	2F BEAM S OOP ROT	STRING	125mm	HORIZ
SP2	2F BEAM MID OOP	STRING	125mm	HORIZ
SP3	2F BEAM N OOP ROT	STRING	125mm	HORIZ
SP4	1F S BRACE DIAG/OOP	STRING	125mm	HORIZ
SP5	1F S BRACE DIAG/OOP	STRING	125mm	HORIZ
SP6	2F S BRACE DIAG/OOP	STRING	125mm	HORIZ
SP7	2F S BRACE DIAG/OOP	STRING	125mm	HORIZ
SP8	2F S BRACE MID PT	STRING	250mm	HORIZ
SP9	2F S GP OOP BOT EDGE	STRING	125mm	HORIZ
SP10	2F S GP OOP S EDGE	STRING	125mm	HORIZ
SP11	2F S GP OOP CENTER	STRING	125mm	HORIZ
SP12	2F MID GP OOP	STRING	125mm	HORIZ
SP13	1F S BEAM DRIFT E SIDE	STRING	250mm	
SP14	1F S BEAM DRIFT W SIDE	STRING	250mm	
SP15	1F N BRACE DIAG/IP	STRING	125mm	HORIZ
SP16	1F N BRACE DIAG/IP	STRING	125mm	HORIZ
SP18	2F N BRACE DIAG/OOP	STRING	125mm	HORIZ
SP19	2F N BRACE DIAG/OOP	STRING	125mm	HORIZ
SP20	2F N BRACE MID PT	STRING	250mm	HORIZ
SP21	2F N GP OOP BOT EDGE	STRING	125mm	HORIZ
SP22	2F N GP OOP N EDGE	STRING	125mm	HORIZ
SP23	2F N GP OOP CENTER	STRING	125mm	HORIZ
SP24	1F N BEAM DRIFT WP	STRING	250mm	
SP25	1F N BEAM DRIFT E SIDE	STRING	250mm	
SP26	1F N BEAM DRIFT W SIDE	STRING	250mm	
SP27	1F S BRACE MID PT	STRING	250mm	
SP28	1F N BRACE MID PT	STRING	250mm	
●	DESCRIPTION	TYPE	RANGE +/−	FREEDOM
D1	S ANCHOR PL SLIP	DIAL	25mm	
D2	S ANCHOR PL UPLIFT	DIAL	25mm	
D3	S BASE PL SLIP	DIAL	25mm	
D4	S BASE PL UPLIFT	DIAL	25mm	
D5	N ANCHOR PL SLIP	DIAL	25mm	
D6	N ANCHOR PL UPLIFT	DIAL	25mm	
D7	N BASE PL SLIP	DIAL	25mm	
D8	N BASE PL UPLIFT	DIAL	25mm	
D9	ACTUATOR BASE PL SLIP	DIAL	25mm	
D10	ACTUATOR BASE PL UPLIFT	DIAL	25mm	

ABBREVIATIONS

N	NORTH
S	SOUTH
E	EAST
W	WEST
BOT	BOTTOM
MID	MIDDLE
COL	COLUMN
BR	BRACE
PL	PLATE
OOP	OUT OF PLANE
IP	IN PLANE
DIAG	DIAGONAL
DISP	DISPLACEMENT
ROT	ROTATION
PT	POINT
WP	WORK POINT
L	LOWER
U	UPPER

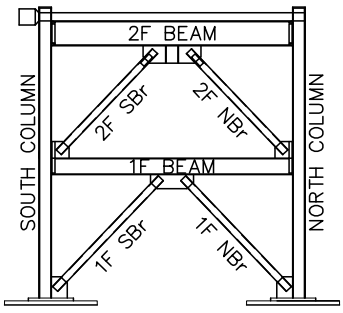

TNCBF2-D-HSS: DUCTILE DETAILS/HSS BRACES

NEESR: SEISMIC REHAB. OF VULNERABLE BRACED FRAMES

DWG: IN-4

DRAWN BY: ADS, MAC
DESIGNED BY: ADS, MAC
DATE: 1/13/2013
REVISED: 9/10/2014
CONTACT: ADSEN@UW.EDU, MCLARKE3@UW.EDU

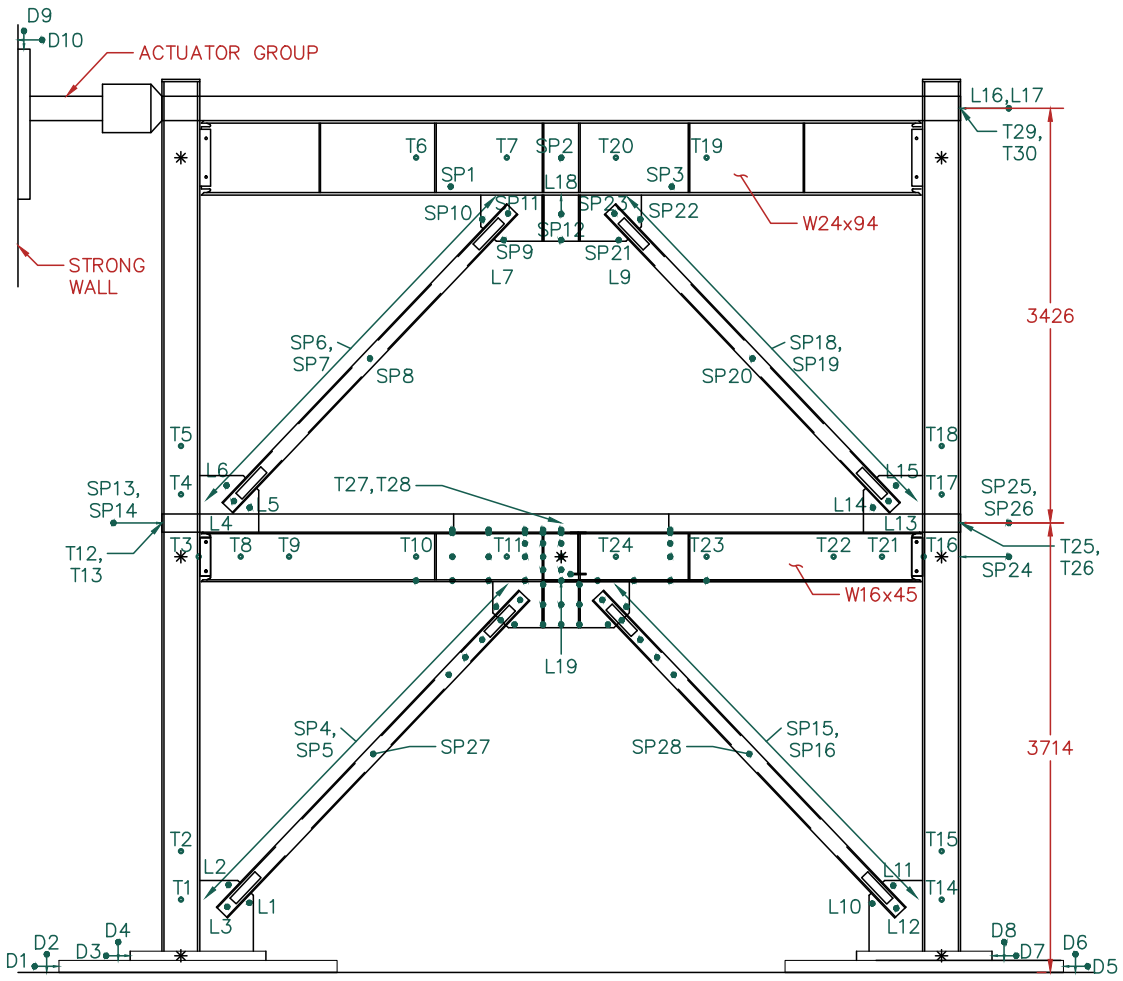

SCALE: 1mm = 50mm

TNCBF2-D-HSS: DUCTILE DETAILS/HSS BRACES

NEESR: SEISMIC REHAB. OF VULNERABLE BRACED FRAMES

DWG: IN-5

DRAWN BY: ADS, MAC
DESIGNED BY: ADS, MAC
DATE: 1/13/2013
REVISED: 9/10/2014
CONTACT: ADSEN@UW.EDU, MCLARKE3@UW.EDU

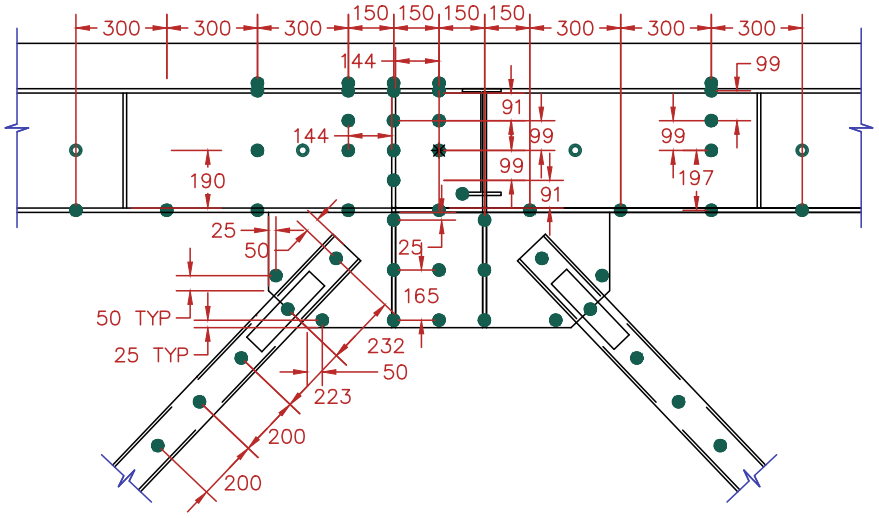

BOTTOM BEAM GUSSET PLATE LED LOCATION DETAIL

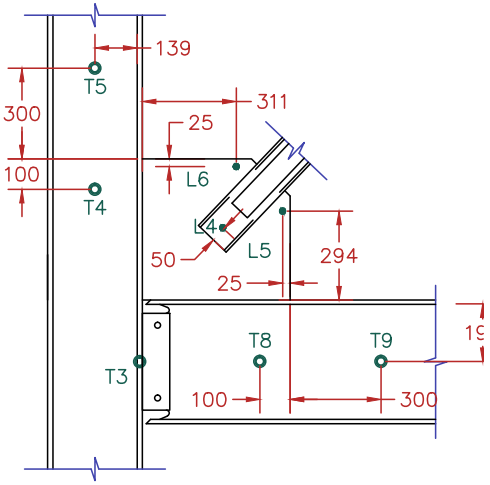

TYPICAL BEAM/COLUMN GUSSET PLATE INSTRUMENTATION DETAIL

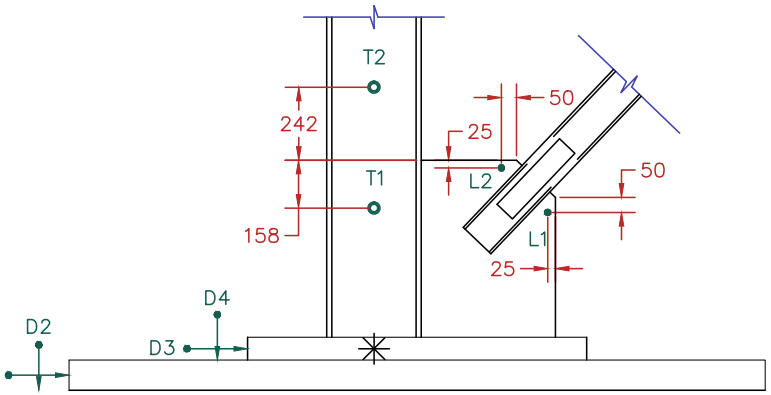

TYPICAL BASE GUSSET PLATE INSTRUMENTATION DETAIL

TNCBF2-D-HSS: DUCTILE DETAILS/HSS BRACES

NEESR: SEISMIC REHAB. OF VULNERABLE BRACED FRAMES

DRAWN BY: ADS, MAC
DESIGNED BY: ADS, MAC
DATE: 1/13/2013
REVISED: 9/10/2014
CONTACT: ADSEN@UW.EDU, MCLARKE3@UW.EDU

DWG: IN-6

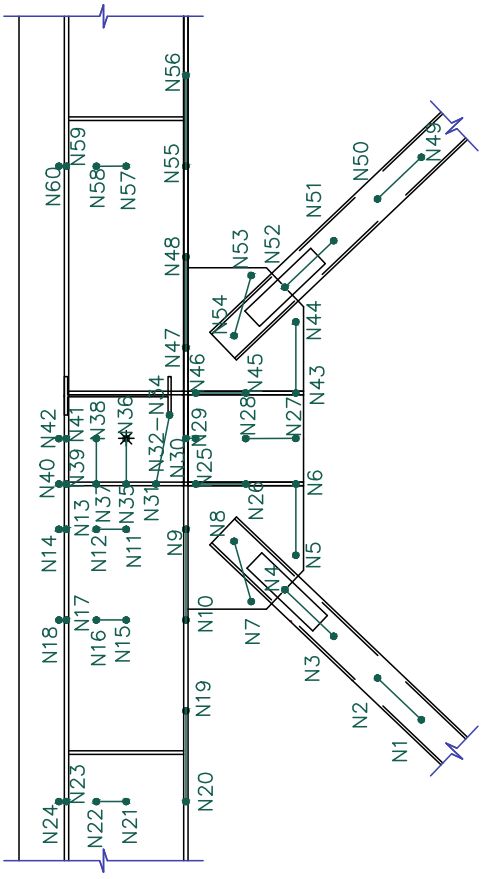

BOTTOM BEAM GUSSET PLATE LED NUMBERING

TNCBF2-D-HSS: DUCTILE DETAILS/HSS BRACES

NEESR: SEISMIC REHAB. OF VULNERABLE BRACED FRAMES

DRAWN BY: ADS, MAC
DESIGNED BY: ADS, MAC
DATE: 1/13/2013
REVISED: 9/10/2014
CONTACT: ADSEN@UW.EDU, MCLARKE3@UW.EDU

DWG: IN-7

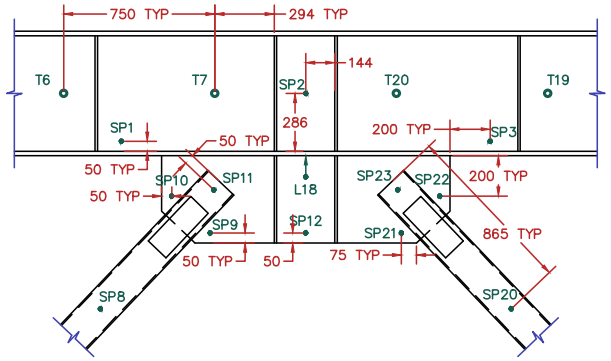

TOP BEAM GUSSET PLATE
INSTRUMENTATION DETAIL

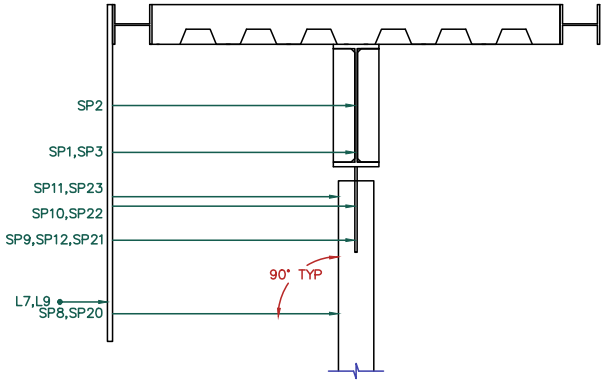

SECTION B–B

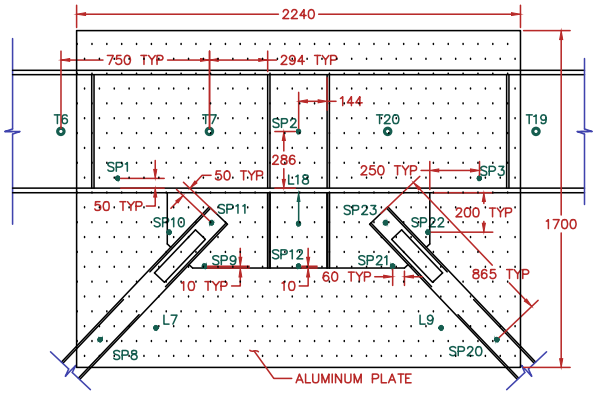

TNCBF2-D-HSS: DUCTILE DETAILS/HSS BRACES	
NEESR: SEISMIC REHAB. OF VULNERABLE BRACED FRAMES	DWG: IN-8
DRAWN BY: ADS, MAC DESIGNED BY: ADS, MAC DATE: 1/13/2013 REVISED: 9/10/2014 CONTACT: ADSEN@UW.EDU, MCLARKE3@UW.EDU	

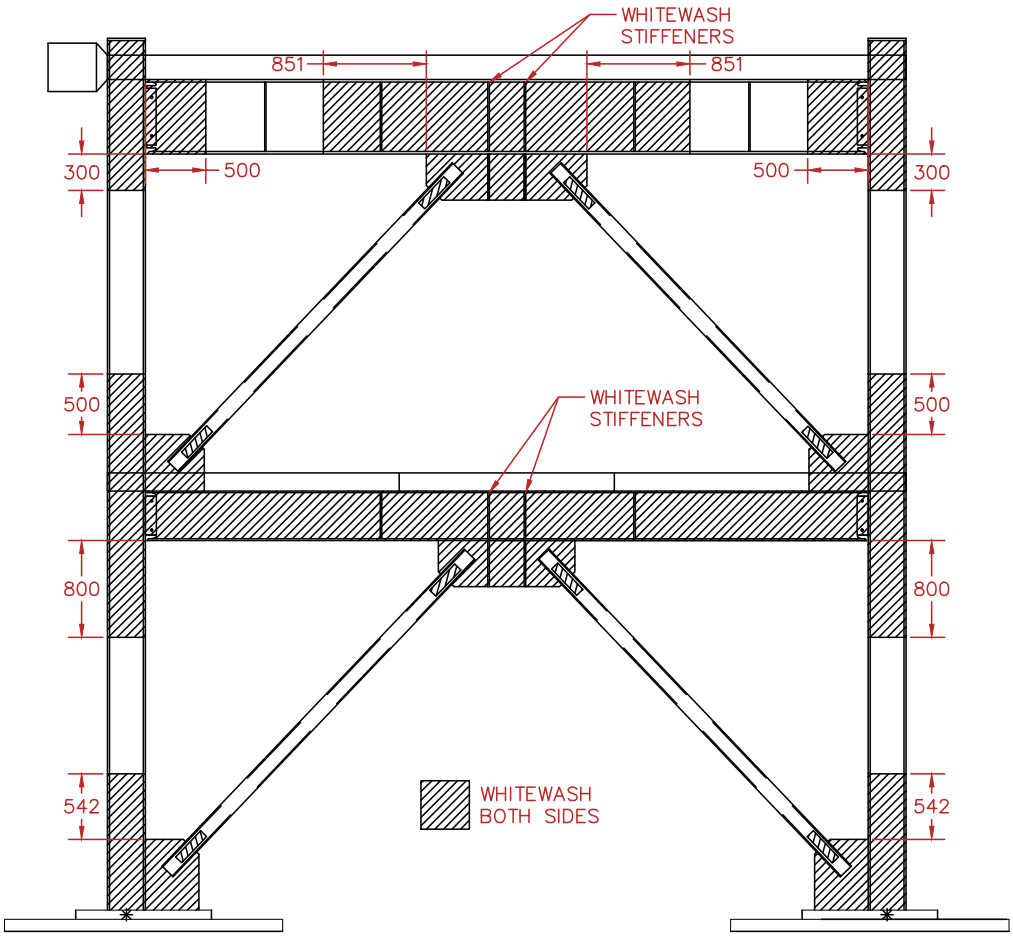

WHITEWASH PLAN
SCALE: 1mm = 50mm

TNCBF2-D-HSS: DUCTILE DETAILS/HSS BRACES	
NEESR: SEISMIC REHAB. OF VULNERABLE BRACED FRAMES	DWG: IN-9
DRAWN BY: ADS, MAC DESIGNED BY: ADS, MAC DATE: 1/13/2013 REVISED: 9/10/2014 CONTACT: ADSEN@UW.EDU, MCLARKE3@UW.EDU	

A.5 General Test Setup

The general test setup was designed by Chao-Hsien Li and An-Chien Wu, assistant research fellows at the National Center for Research on Earthquake Engineering (NCREE). These drawings include the design and setup of the out-of-plane reaction frame, actuator anchorage to the strong wall, and specimen anchorage to the strong floor.

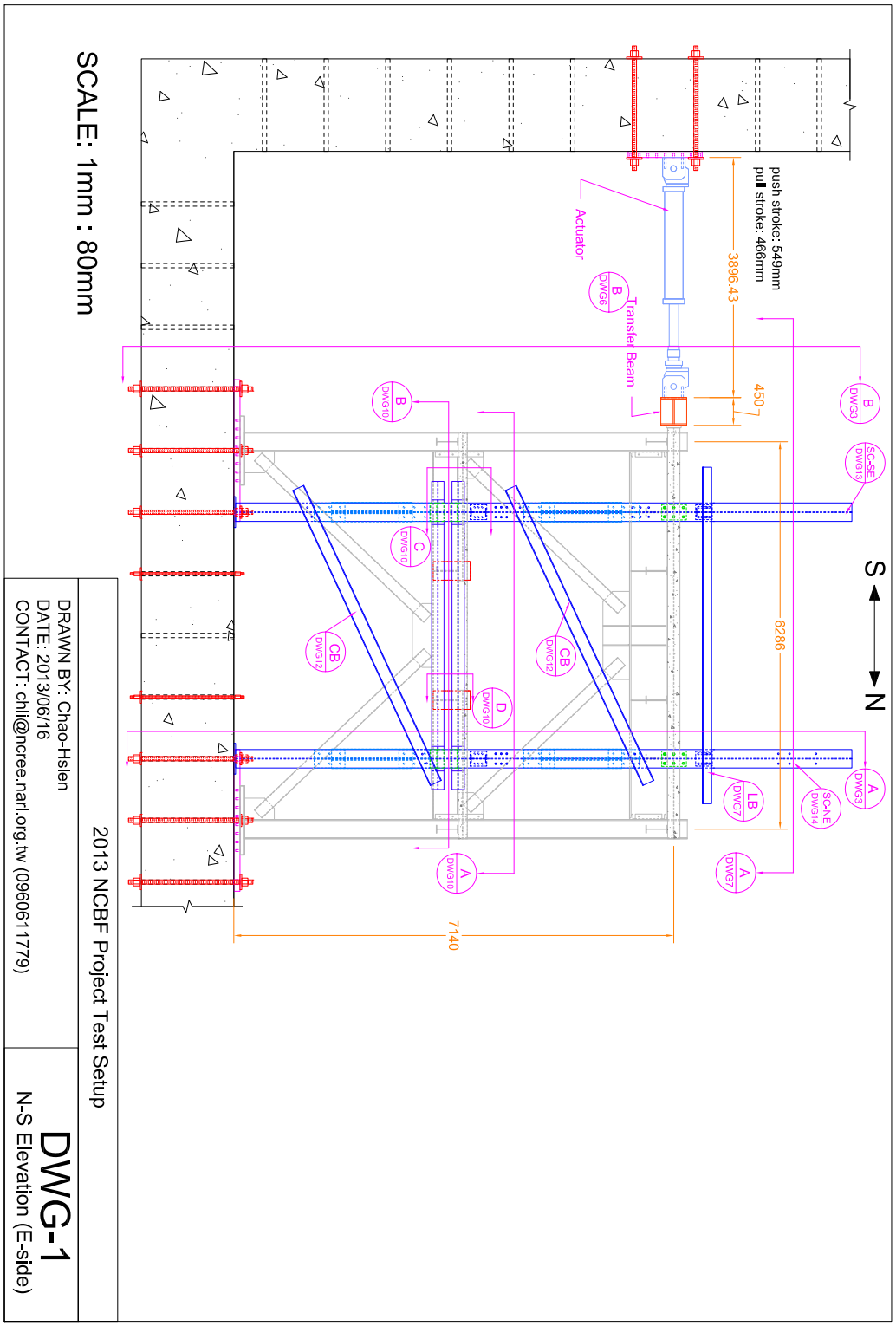

SCALE: 1mm : 80mm

2013 NCBF Project Test Setup

DRAWN BY: Chao-Hsien
DATE: 2013/06/16
CONTACT: chli@ncree.narl.org.tw (0960611779)

DWG-1

N-S Elevation (E-side)

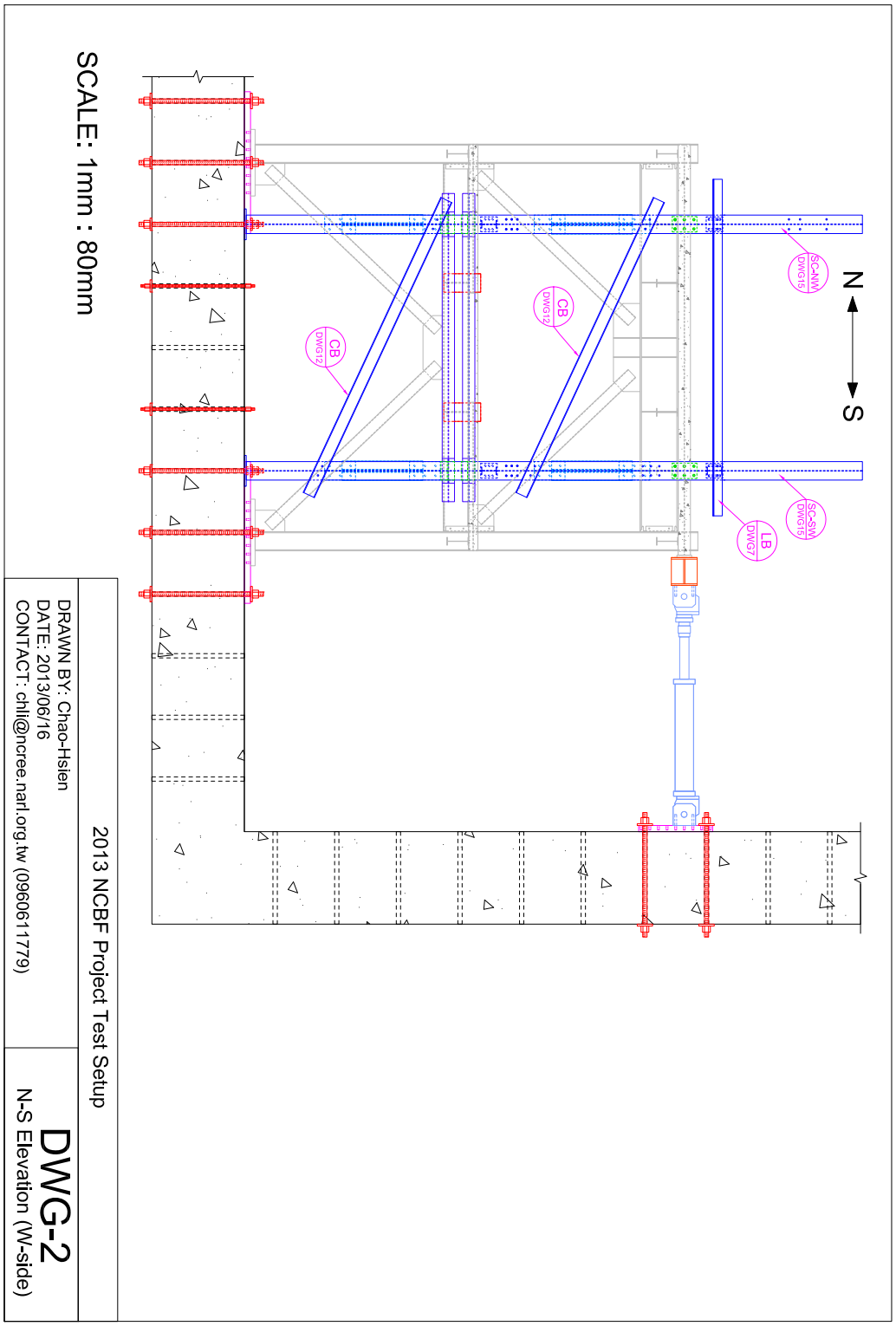

SCALE: 1mm : 80mm

2013 NCBF Project Test Setup

DRAWN BY: Chao-Hsien
DATE: 2013/06/16
CONTACT: chli@ncree.narl.org.tw (0960611779)

DWG-2

N-S Elevation (W-side)

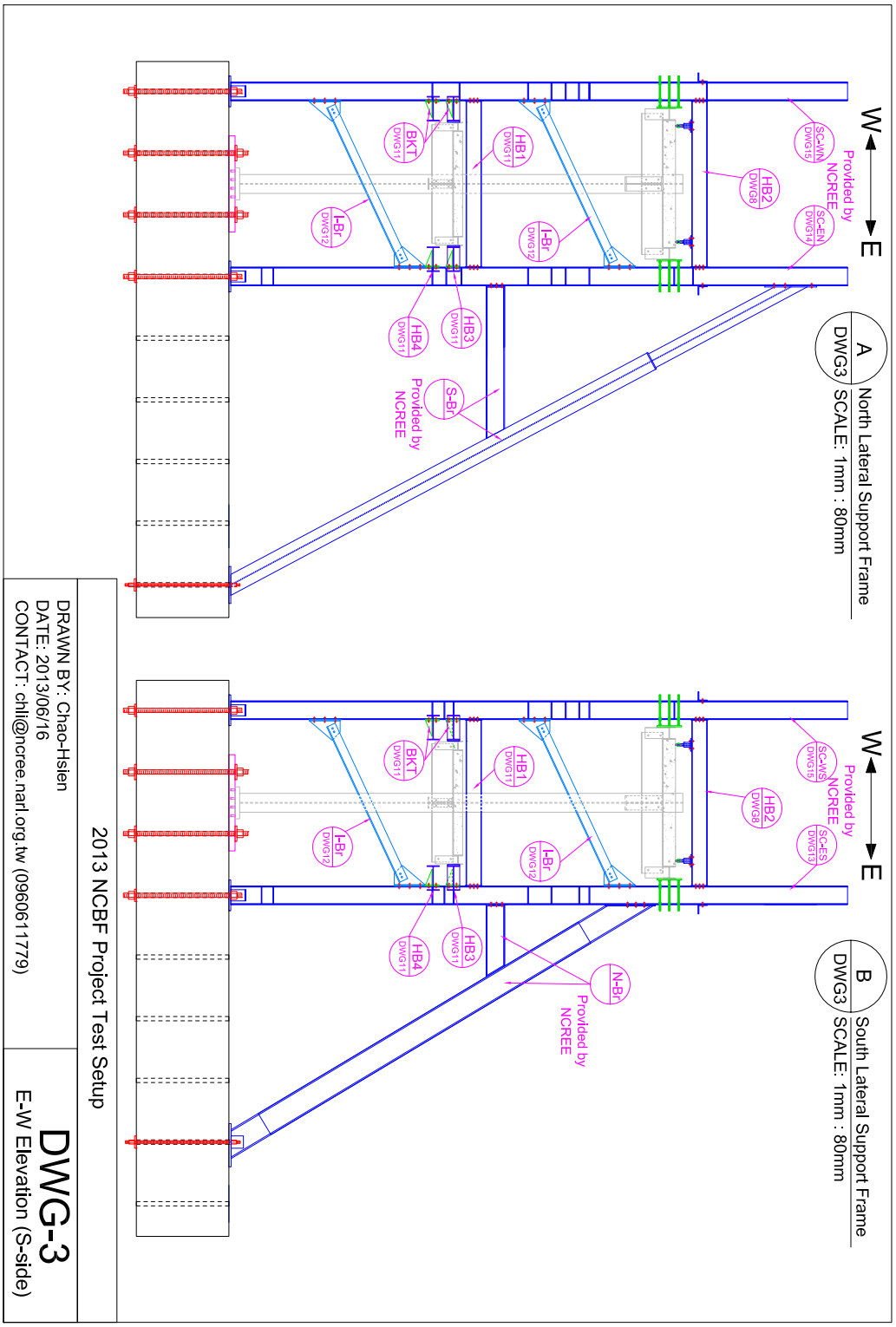
W
E
Provided by NCREE
SC-WN DWG15
SC-EN DWG14
HB2 DWG8
BKT DWG11
HB1 DWG11
I-Br DWG12
HB3 DWG11
HB4 DWG11
S-Br
A DWG3
North Lateral Support Frame
SCALE: 1mm : 80mm
SC-WS DWG15
SC-ES DWG13
N-Br
B DWG3
South Lateral Support Frame
SCALE: 1mm : 80mm
2013 NCBF Project Test Setup
DRAWN BY: Chao-Hsien
DATE: 2013/06/16
CONTACT: chli@ncree.narl.org.tw (0960611779)
DWG-3
E-W Elevation (S-side)

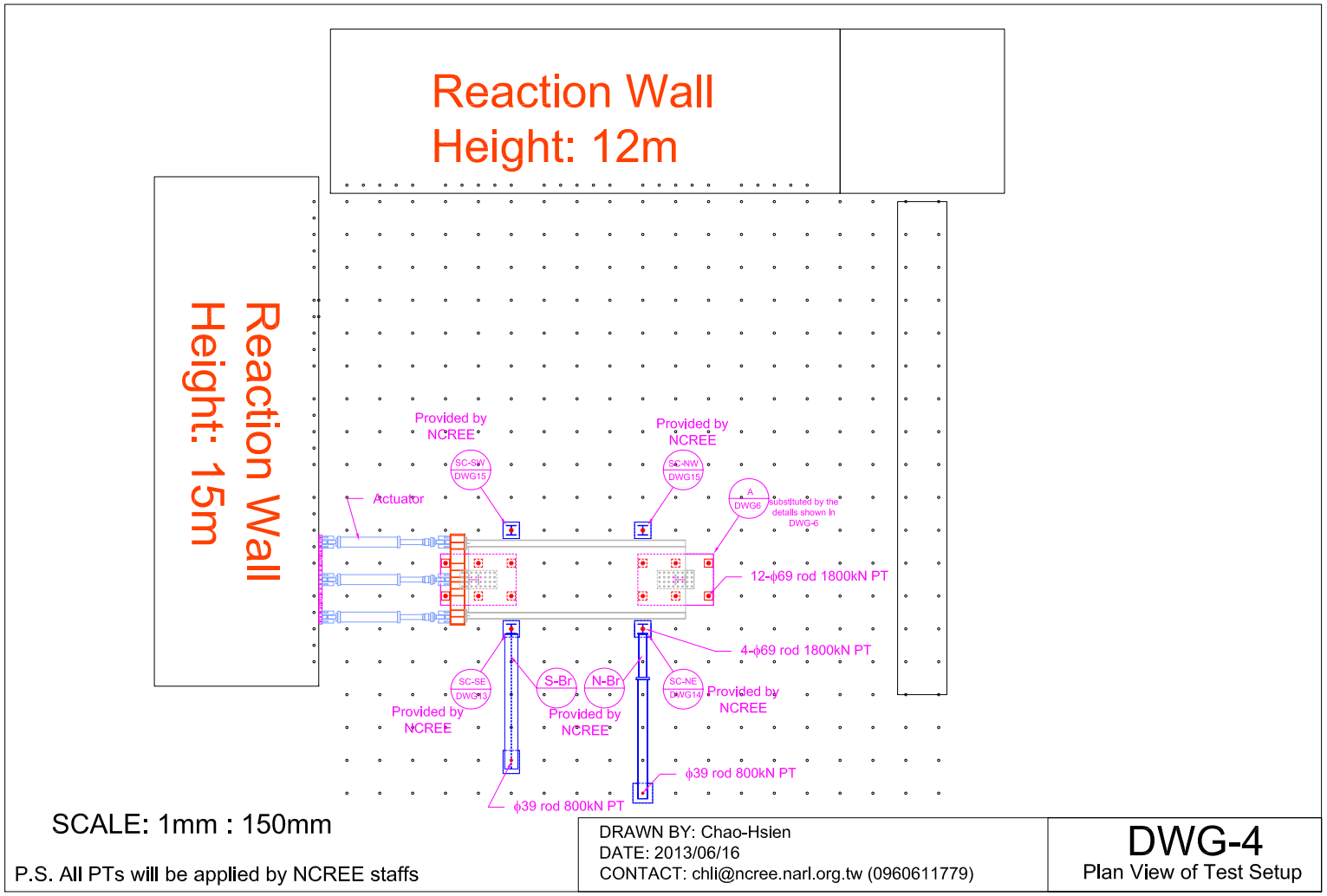

SCALE: 1mm : 150mm

P.S. All PTs will be applied by NCREE staffs

DRAWN BY: Chao-Hsien
DATE: 2013/06/16
CONTACT: chli@ncree.narl.org.tw (0960611779)

DWG-4
Plan View of Test Setup

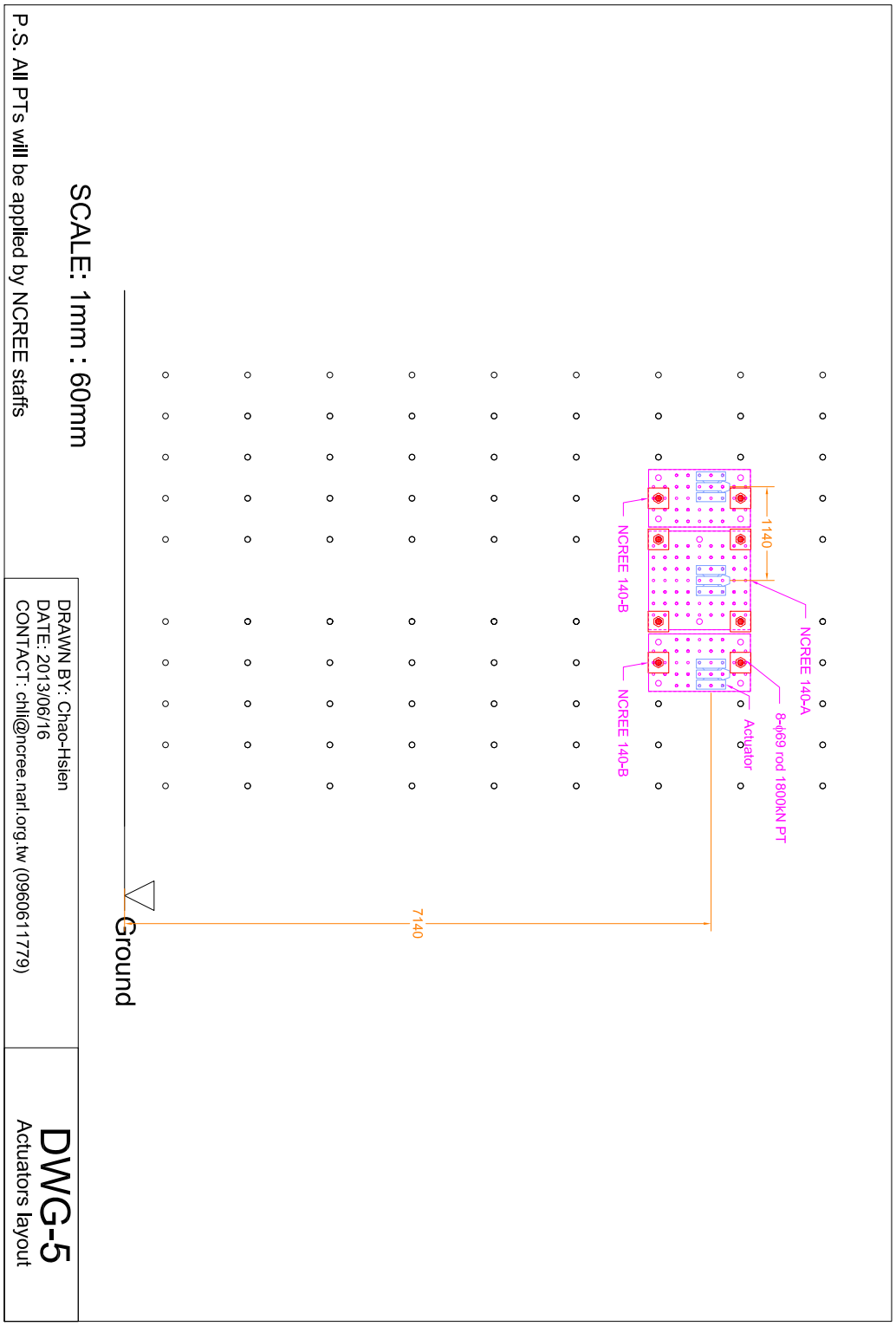

SCALE: 1mm : 60mm

P.S. All PTs will be applied by NCREE staffs

DRAWN BY: Chao-Hsien
DATE: 2013/06/16
CONTACT: chli@ncree.narl.org.tw (0960611779)

DWG-5

Actuators layout

A DWG6 Alternative base details
SCALE: 1mm : 40mm

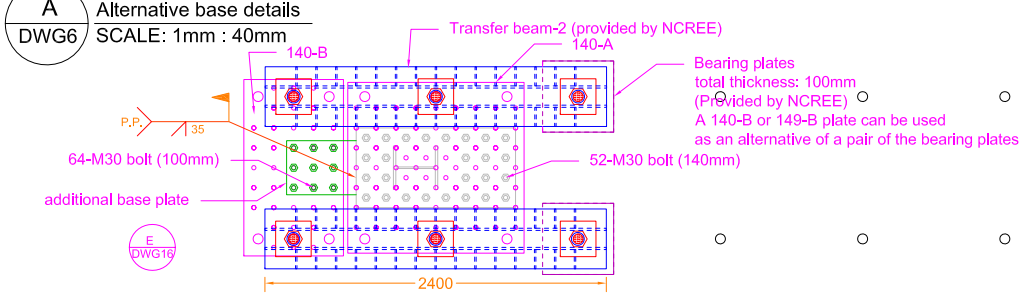

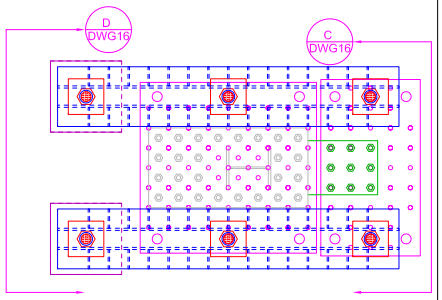

C DWG6 Column Base Details
SCALE: 1mm : 25mm

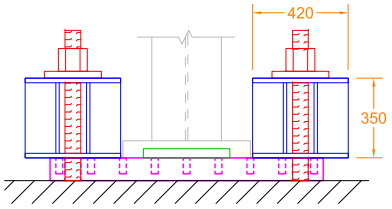

D DWG6 Column Base Details
SCALE: 1mm : 25mm

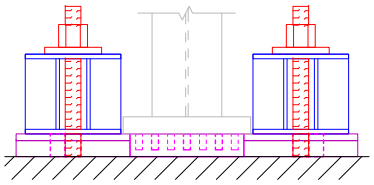

B DWG6 Holes on 140-A
SCALE: 1mm : 20mm

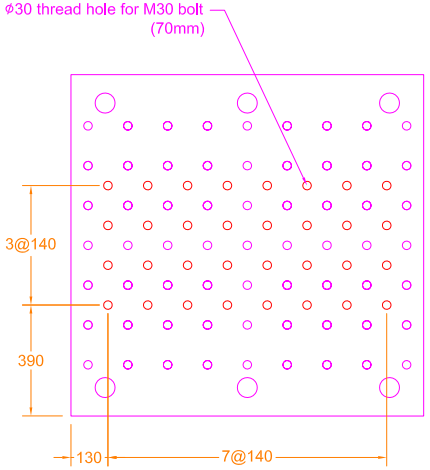

E DWG6 Additional base plate
SCALE: 1mm : 16mm

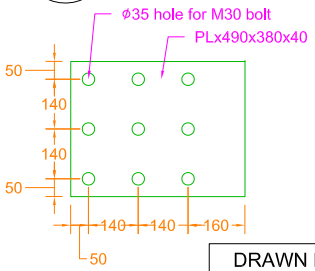

PLATES				
Name	Section	Material	Amount	
Additional Plate	PL490x380x40	A36	2	
BOLTS				
Dia./Class	Length (mm)	Cap Type	Nut/Washer	Amount
M30/F10T	140	Hex Head	1W	52
M30/F10T	100	Hex Head	1W	18
HOLE DRILLING				
64 holes on two 140-A plate. (32 on each)				

DRAWN BY: Chao-Hsien
DATE: 2013/06/16
CONTACT: chli@ncree.narl.org.tw (0960611779)

DWG-6
Column base details

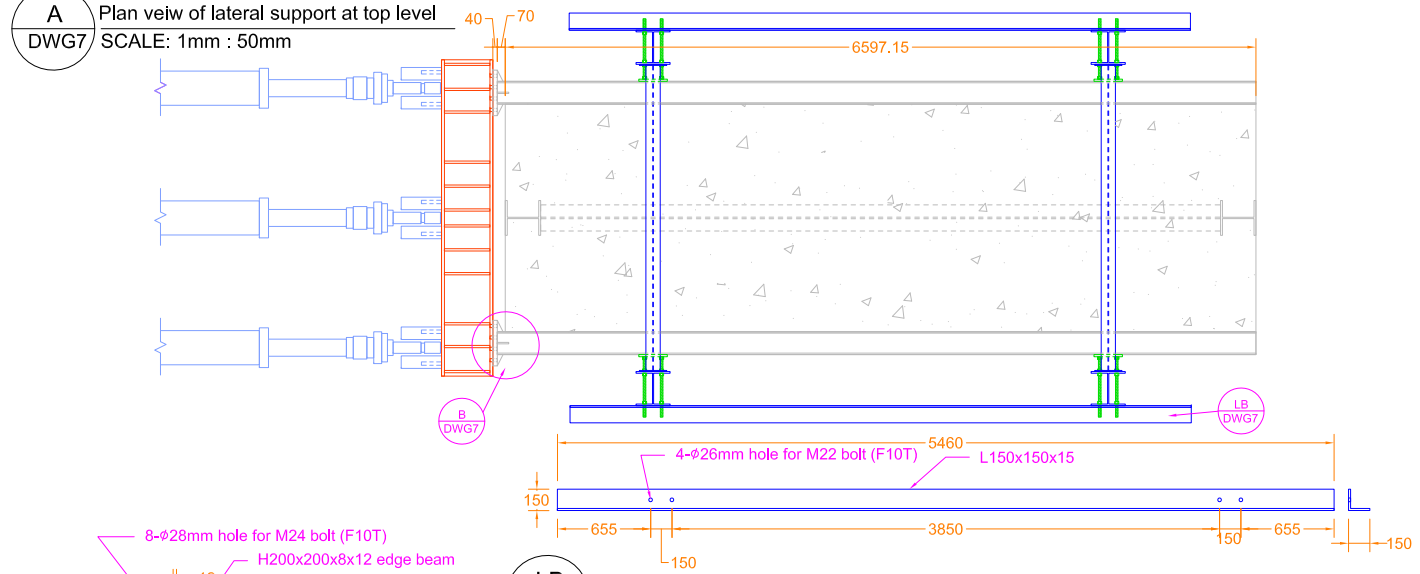

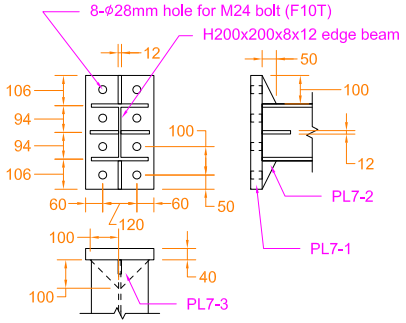

B
DWG7
Details at the edge beam's end
SCALE: 1mm : 20mm

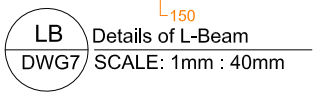

MEMBERS					
Name	Section	Material	Length (mm)	Amount	New/Exists
LB	L150x150x15	A36	5460	2	Exists
PLATES					
Name	Section	Material	Amount		
PL7-1	PL400x240x40	A36	2		
PL7-2	⊿100x50x12	A36	4		
PL7-3	⊿100x100x12	A36	4		
BOLTS					
Dia./Class	Length (mm)	Cap Type	Nut/Washer	Amount	
M24/F10T	110	Hex Head	1N2W	16	

DRAWN BY: Chao-Hsien
DATE: 2013/06/16
CONTACT: chli@ncree.narl.org.tw (0960611779)

DWG-7
Lateral Suppot at Top-1

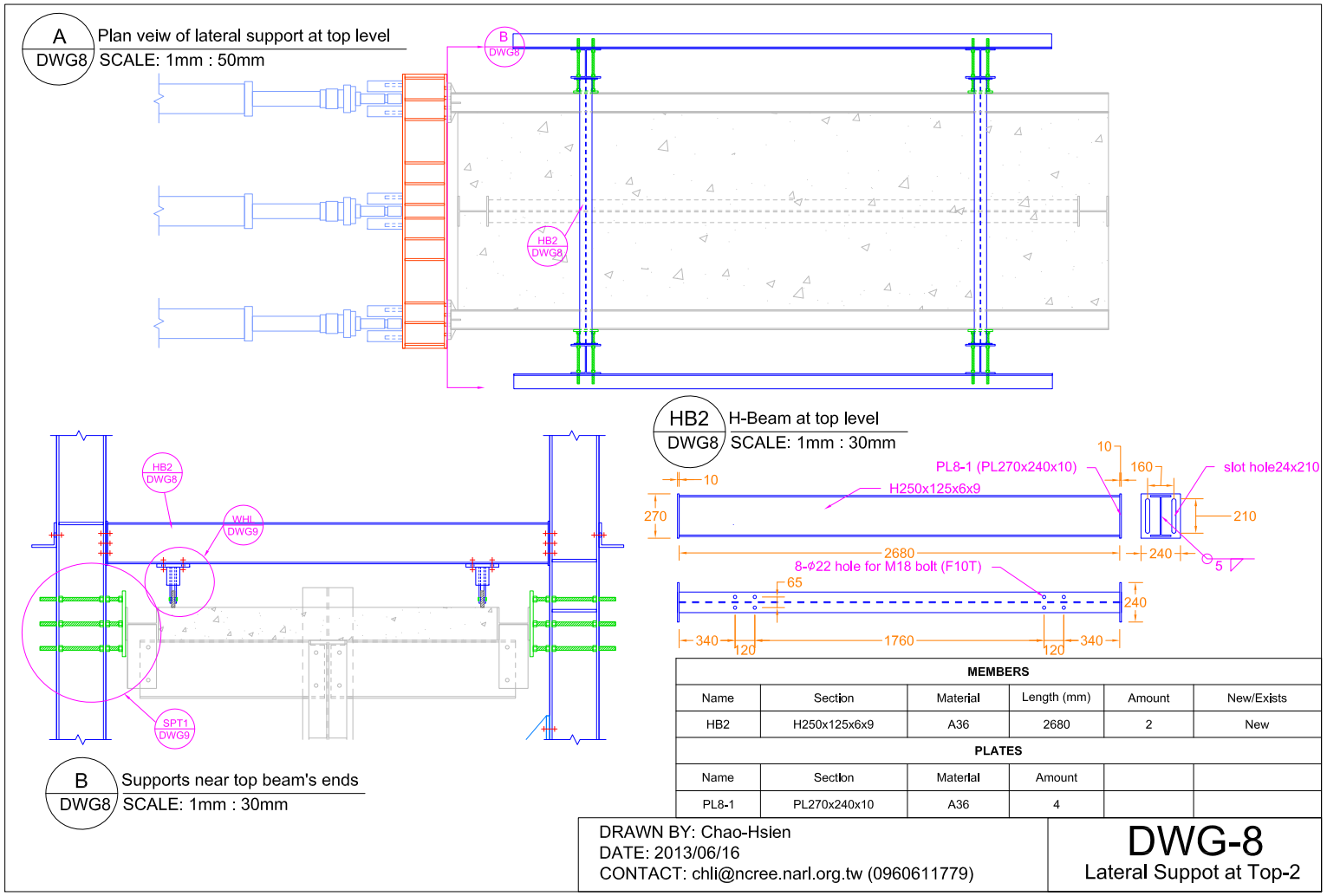

MEMBERS					
Name	Section	Material	Length (mm)	Amount	New/Exists
HB2	H250x125x6x9	A36	2680	2	New
PLATES					
Name	Section	Material	Amount		
PL8-1	PL270x240x10	A36	4		

DRAWN BY: Chao-Hsien
DATE: 2013/06/16
CONTACT: chli@ncree.narl.org.tw (0960611779)

DWG-8
Lateral Suppot at Top-2

A / DWG9 Combo of HB2 and wheels
SCALE: 1mm : 30mm

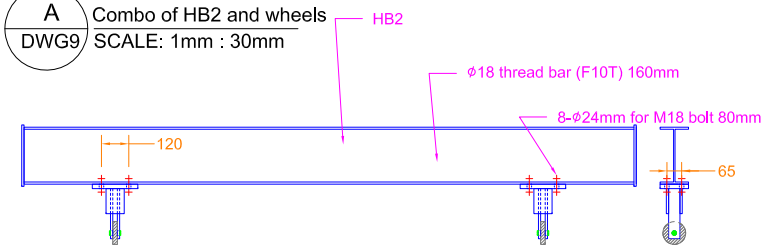

WHL / DWG9 Details for wheel
SCALE: 1mm : 10mm

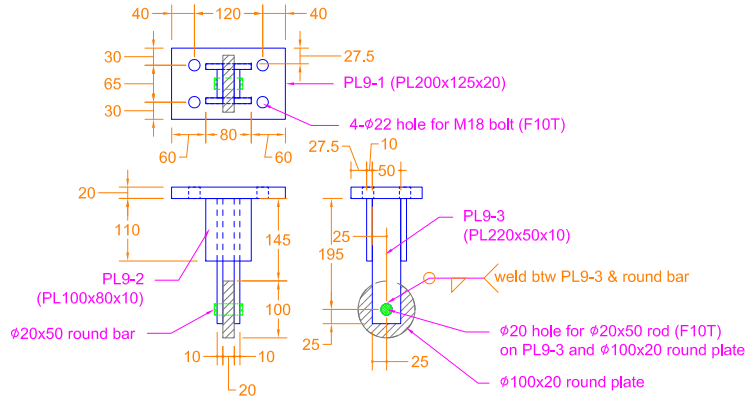

SPT1 / DWG9 Supporting plate at top level
SCALE: 1mm : 10mm

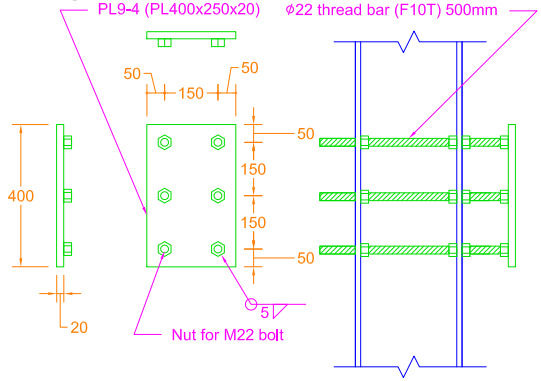

PLATES				
Name	Section	Material	Amount	
PL9-1	PL200x125x20	A36	4	
PL9-2	PL110x80x10	A36	8	
PL9-3	PL220x50x10	A36	8	
wheel	ϕ100x20 round plate	A36	4	
pin-rod	ϕ20x50 round bar	A36	4	
PL9-4	PL400x250x20	A36	4	
BOLTS				
Dia./Class	Length (mm)	Cap Type	Nut/Washer	Amount
ϕ22/F10T	500	thread bar	4N	24
M18/F10T	65	Hex Head	1N2W	16

DRAWN BY: Chao-Hsien
DATE: 2013/06/16
CONTACT: chli@ncree.narl.org.tw (0960611779)

DWG-9
Lateral Suppot at Top-4

A DWG10 Upper lateral support at middle level
SCALE: 1mm : 50mm

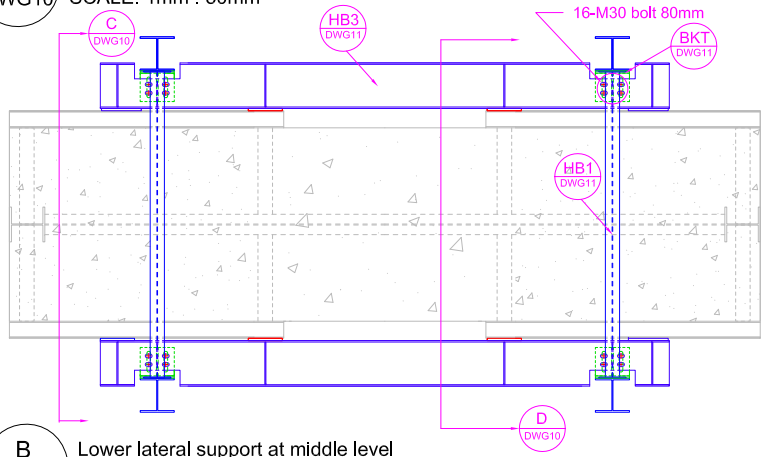

B DWG10 Lower lateral support at middle level
SCALE: 1mm : 50mm

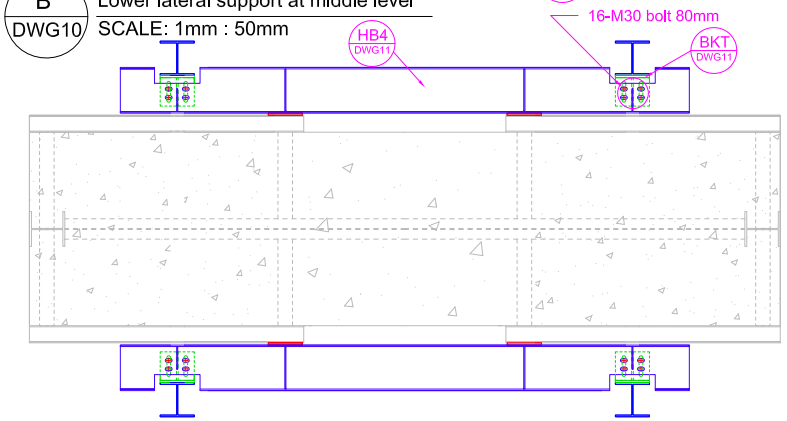

C DWG10 lateral support at middle level
near specimen's b-to-c connection
SCALE: 1mm : 30mm

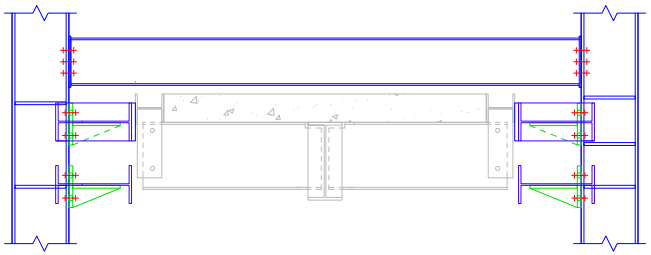

D DWG10 lateral support at middle level
near beam's ⅓ span
SCALE: 1mm : 30mm

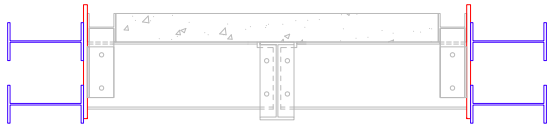

DRAWN BY: Chao-Hsien
DATE: 2013/06/16
CONTACT: chli@ncree.narl.org.tw (0960611779)

DWG-10
Lateral Suppot at Middle-1

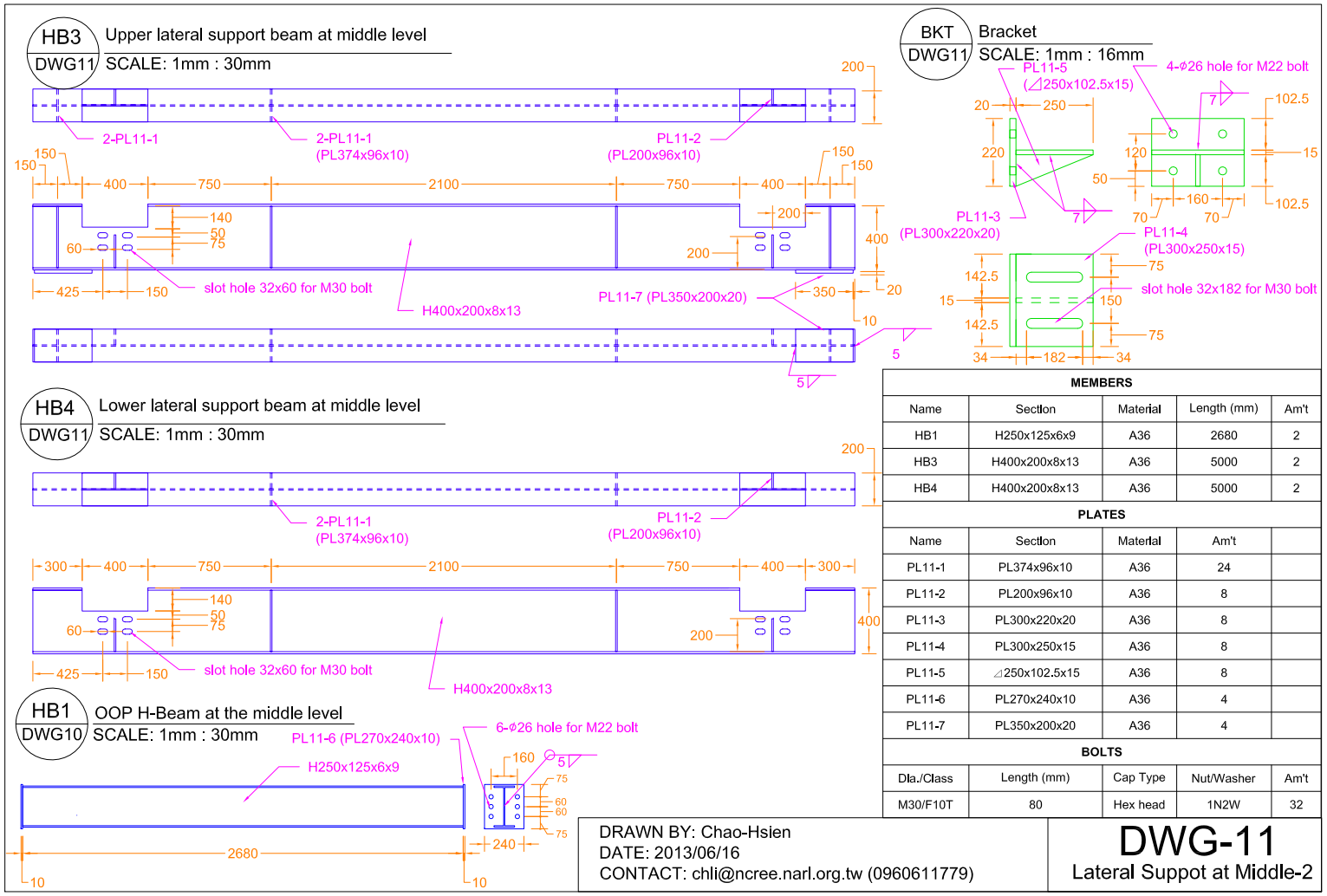

MEMBERS				
Name	Section	Material	Length (mm)	Am't
HB1	H250x125x6x9	A36	2680	2
HB3	H400x200x8x13	A36	5000	2
HB4	H400x200x8x13	A36	5000	2

PLATES			
Name	Section	Material	Am't
PL11-1	PL374x96x10	A36	24
PL11-2	PL200x96x10	A36	8
PL11-3	PL300x220x20	A36	8
PL11-4	PL300x250x15	A36	8
PL11-5	⊿250x102.5x15	A36	8
PL11-6	PL270x240x10	A36	4
PL11-7	PL350x200x20	A36	4

BOLTS				
Dia./Class	Length (mm)	Cap Type	Nut/Washer	Am't
M30/F10T	80	Hex head	1N2W	32

DRAWN BY: Chao-Hsien
DATE: 2013/06/16
CONTACT: chli@ncree.narl.org.tw (0960611779)

DWG-11
Lateral Suppot at Middle-2

CB
DWG12
Channel: in-plane brace
SCALE: 1mm : 25mm

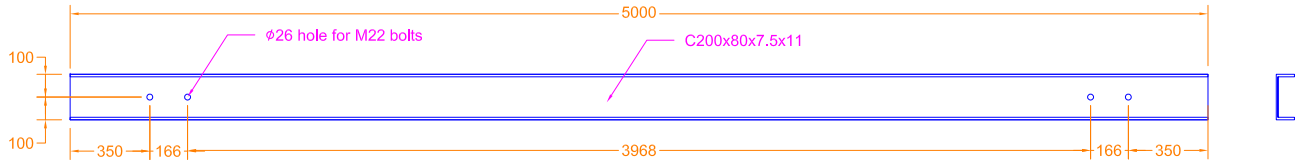

I-Br
DWG12
Combo of inner out-of-plane brace
SCALE: 1mm : 25mm

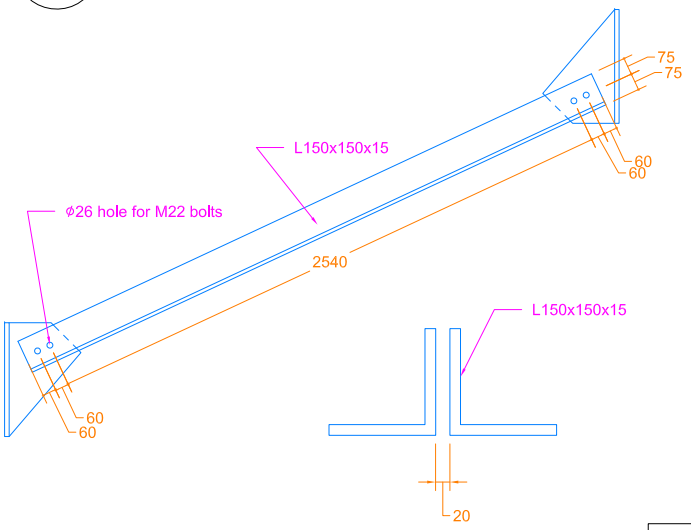

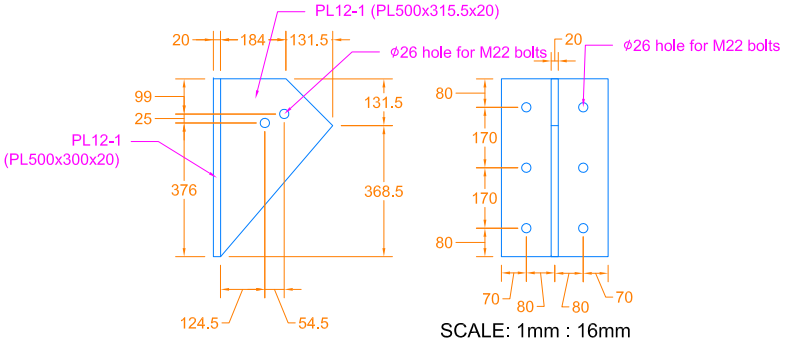

SCALE: 1mm : 16mm

MEMBERS					
Name	Section	Material	Length (mm)	Amount	New/Exists
CB	C200x80x7.5x11	A36	5000	4	Exists
I-Br	L150x150x15	A36	2780	8	3E/5N
PLATES					
Name	Section	Material	Amount		
PL12-1	PL500x300x20	A36	8		
PL12-2	PL500x315.5x20	A36	8		
BOLTS					
Dia./Class	Length (mm)	Cap Type	Nut/Washer	Amount	
M22/F10T	80	HEX HEAD	1N2W	16	

DRAWN BY: Chao-Hsien
DATE: 2013/06/16
CONTACT: chli@ncree.narl.org.tw (0960611779)

DWG-12
Brace Members in LS Frame

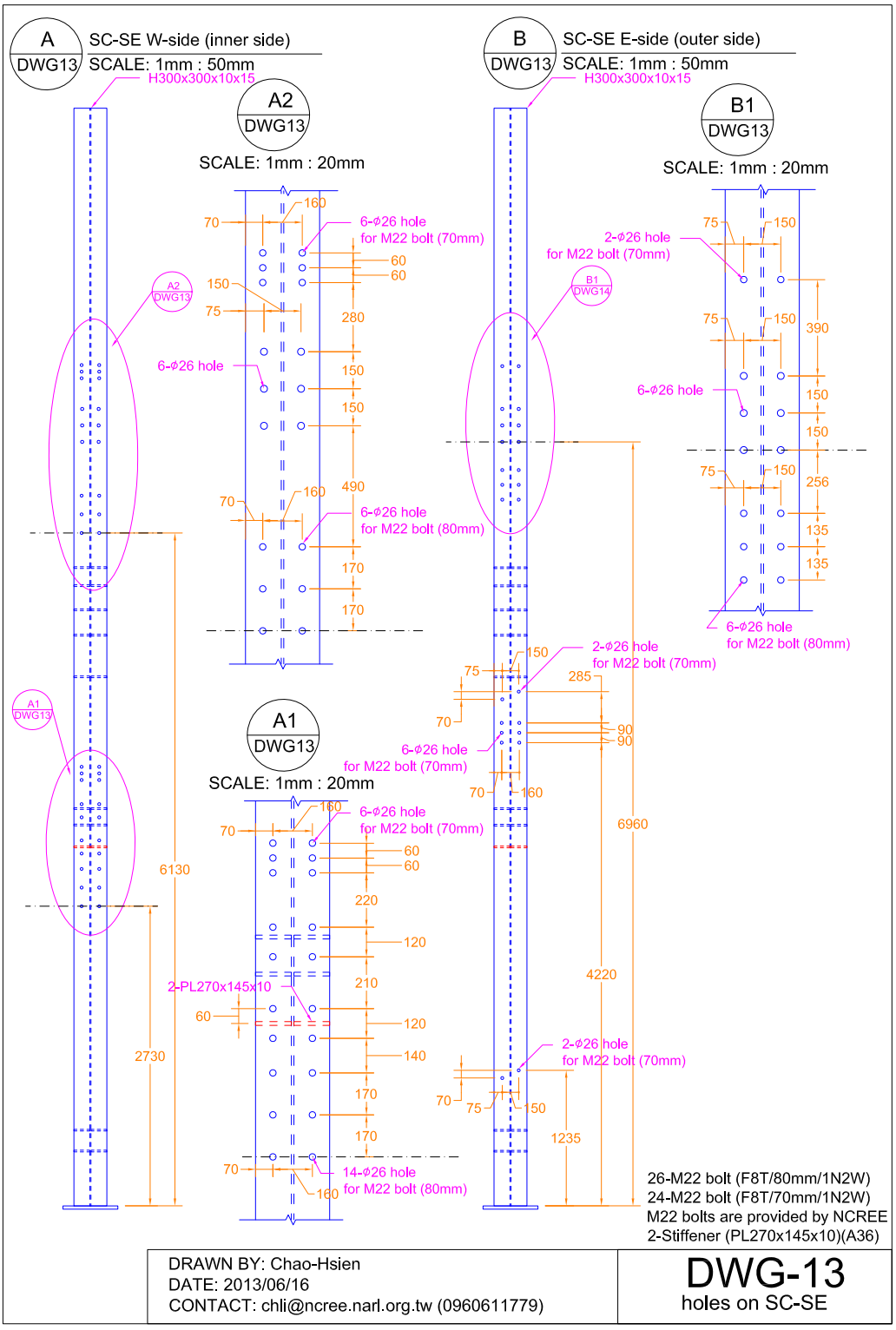
A
DWG13
SC-SE W-side (inner side)
SCALE: 1mm : 50mm
H300x300x10x15
A2
DWG13
SCALE: 1mm : 20mm
6-ϕ26 hole
for M22 bolt (70mm)
6-ϕ26 hole
6-ϕ26 hole
for M22 bolt (80mm)
A1
DWG13
SCALE: 1mm : 20mm
2-PL270x145x10
14-ϕ26 hole
for M22 bolt (80mm)
6130
2730
B
DWG13
SC-SE E-side (outer side)
SCALE: 1mm : 50mm
H300x300x10x15
B1
DWG13
SCALE: 1mm : 20mm
2-ϕ26 hole
for M22 bolt (70mm)
6-ϕ26 hole
6-ϕ26 hole
for M22 bolt (80mm)
2-ϕ26 hole
for M22 bolt (70mm)
6-ϕ26 hole
for M22 bolt (70mm)
2-ϕ26 hole
for M22 bolt (70mm)
6960
4220
1235
26-M22 bolt (F8T/80mm/1N2W)
24-M22 bolt (F8T/70mm/1N2W)
M22 bolts are provided by NCREE
2-Stiffener (PL270x145x10)(A36)
DRAWN BY: Chao-Hsien
DATE: 2013/06/16
CONTACT: chli@ncree.narl.org.tw (0960611779)
DWG-13
holes on SC-SE

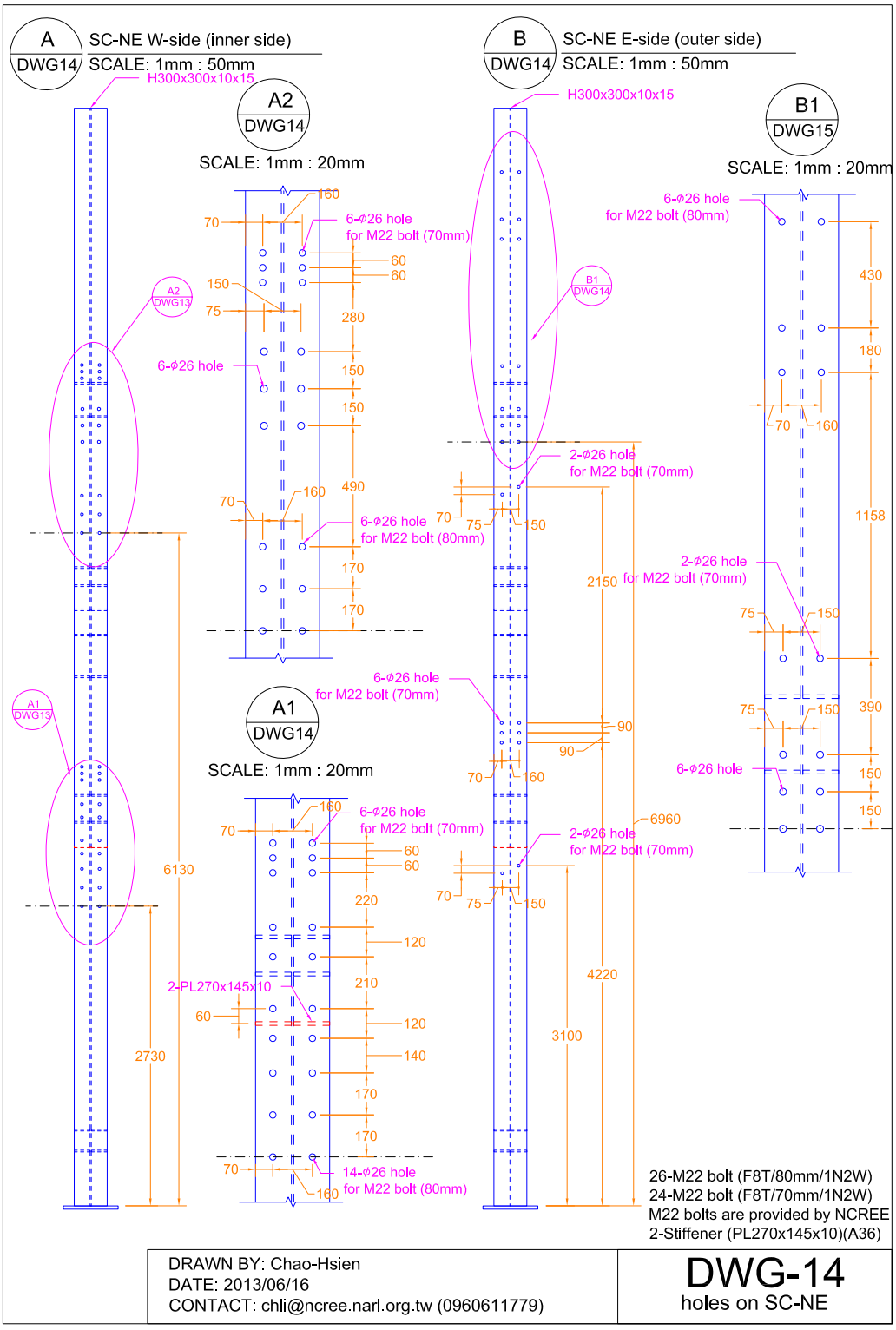
A
DWG14
SC-NE W-side (inner side)
SCALE: 1mm : 50mm
H300x300x10x15
A2
DWG14
SCALE: 1mm : 20mm
A1
DWG14
SCALE: 1mm : 20mm
B
DWG14
SC-NE E-side (outer side)
SCALE: 1mm : 50mm
H300x300x10x15
B1
DWG15
SCALE: 1mm : 20mm
A2 DWG13
A1 DWG13
B1 DWG14
6-ϕ26 hole
6-ϕ26 hole for M22 bolt (70mm)
6-ϕ26 hole for M22 bolt (80mm)
2-ϕ26 hole for M22 bolt (70mm)
14-ϕ26 hole for M22 bolt (80mm)
2-PL270x145x10
6130
2730
2150
6960
4220
3100
1158
26-M22 bolt (F8T/80mm/1N2W)
24-M22 bolt (F8T/70mm/1N2W)
M22 bolts are provided by NCREE
2-Stiffener (PL270x145x10)(A36)
DRAWN BY: Chao-Hsien
DATE: 2013/06/16
CONTACT: chli@ncree.narl.org.tw (0960611779)
DWG-14
holes on SC-NE

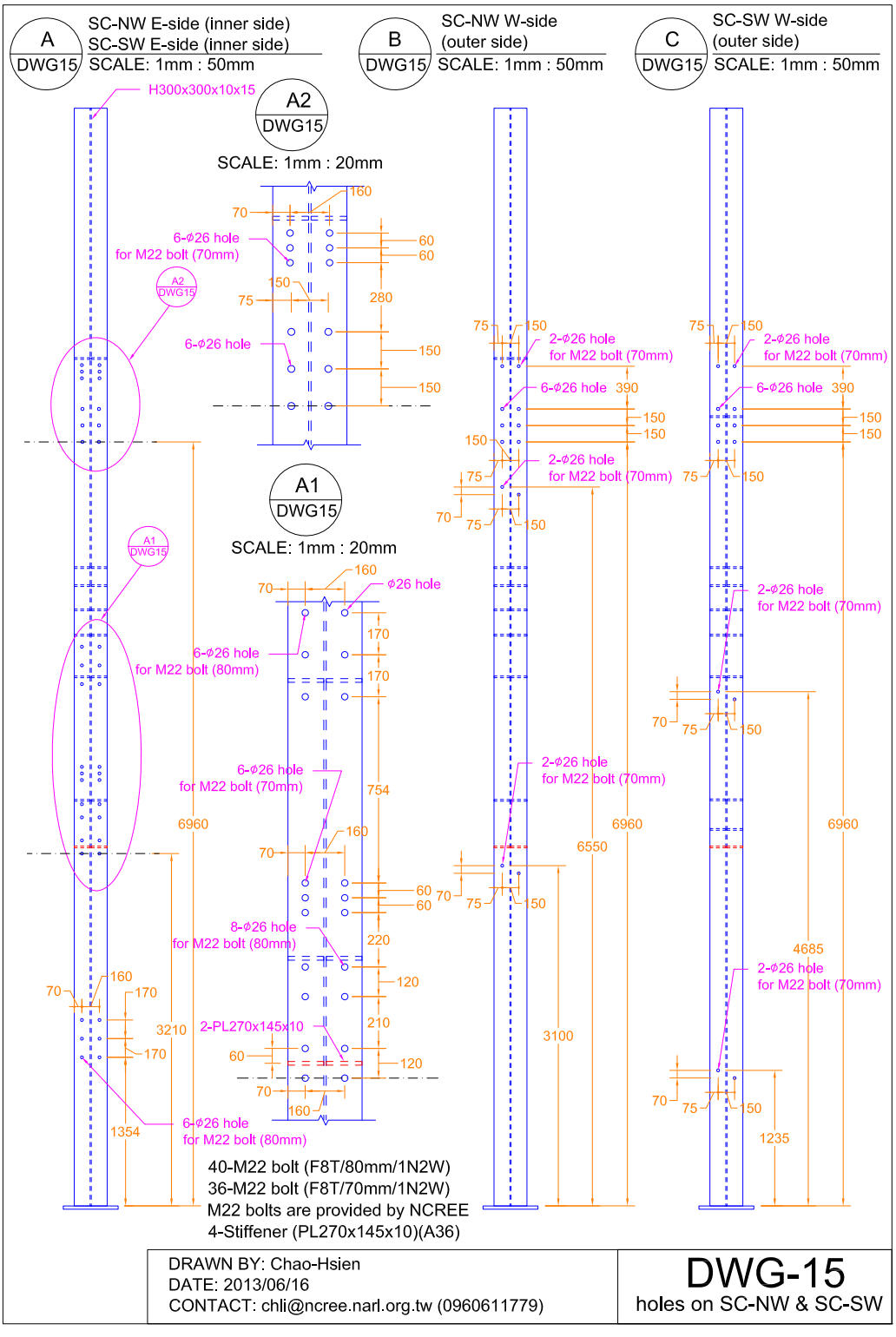
A
DWG15
SC-NW E-side (inner side)
SC-SW E-side (inner side)
SCALE: 1mm : 50mm
B
DWG15
SC-NW W-side
(outer side)
SCALE: 1mm : 50mm
C
DWG15
SC-SW W-side
(outer side)
SCALE: 1mm : 50mm
H300x300x10x15
A2
DWG15
SCALE: 1mm : 20mm
6-ϕ26 hole
for M22 bolt (70mm)
A1
DWG15
SCALE: 1mm : 20mm
ϕ26 hole
6-ϕ26 hole
for M22 bolt (80mm)
6-ϕ26 hole
for M22 bolt (70mm)
8-ϕ26 hole
for M22 bolt (80mm)
2-PL270x145x10
2-ϕ26 hole
for M22 bolt (70mm)
6-ϕ26 hole 390
6960
6550
3100
4685
3210
1354
1235
40-M22 bolt (F8T/80mm/1N2W)
36-M22 bolt (F8T/70mm/1N2W)
M22 bolts are provided by NCREE
4-Stiffener (PL270x145x10)(A36)
DRAWN BY: Chao-Hsien
DATE: 2013/06/16
CONTACT: chli@ncree.narl.org.tw (0960611779)
DWG-15
holes on SC-NW & SC-SW

Appendix B

SAMPLE CALCULATIONS

B.1 Sample Design Calculations

B.1.1 Brace Demands

Braces in CBFs are the main lateral force resisting elements in the system and are anticipated to undergo inelastic deformation to dissipate seismic energy. To ensure this behavior, the components comprising the rest of the system are designed to withstand the expected brace forces. The Seismic Provisions (AISC 2010a) outline two load cases: (i) a case in which the braces in tension reach their expected yield forces and the braces in compression reach their expected critical buckling loads and (ii) a post-buckled case the braces in tension reach their expected yield forces and the braces in compression have degraded to 30% of their expected critical buckling loads. The term "expected" indicates that material overstrength is considered. That is, in calculating brace demands, F_{y} is replaced with $R_{\mathrm{y}}F_{\mathrm{y}}$ and F_{u} is replaced with $R_{\mathrm{t}}F_{\mathrm{u}}$. Thus, the expected yield force of the brace in tension is given by Eq. B.1 and the expected critical buckling load is given by Eq. B.2. In the latter equation, F_{cre} is given by Eq. B.3 where F_{e} is defined in Eq. B.4.

$$P_{\mathrm{t}} = R_{\mathrm{y}}F_{\mathrm{y}}A_{\mathrm{g}} \tag{B.1}$$

$$P_{\mathrm{cr}} = F_{\mathrm{cre}}A_{\mathrm{g}} \tag{B.2}$$

$$F_{\mathrm{cre}} = \begin{cases} \left[0.658^{\frac{R_{\mathrm{y}}F_{\mathrm{y}}}{F_{\mathrm{e}}}}\right] R_{\mathrm{y}}F_{\mathrm{y}} & \text{if } \dfrac{KL}{r} \leq 4.71\sqrt{\dfrac{E}{R_{\mathrm{y}}F_{\mathrm{y}}}} \\ 0.877F_{\mathrm{e}} & \text{if } \dfrac{KL}{r} > 4.71\sqrt{\dfrac{E}{R_{\mathrm{y}}F_{\mathrm{y}}}} \end{cases} \tag{B.3}$$

$$F_{\mathrm{e}} = \frac{\pi^2 E}{\left(\frac{KL}{r}\right)^2} \tag{B.4}$$

For case (i) of loading described above, the horizontal and vertical loads at the brace intersection (beam mid-span) are described by Eqs. B.5 and B.6, where θ is the brace angle to the horizontal. The loading for case (ii) is defined by Eqs. B.7 and B.8. Note that V_{br} is directed positive downward.

$$H_{\mathrm{br}}^{(\mathrm{i})} = (P_{\mathrm{t}} + P_{\mathrm{cr}}) \cos\theta \tag{B.5}$$

$$V_{\mathrm{br}}^{(\mathrm{i})} = (P_{\mathrm{t}} - P_{\mathrm{cr}}) \sin\theta \tag{B.6}$$

$$H_{\mathrm{br}}^{(\mathrm{ii})} = (P_{\mathrm{t}} + 0.3P_{\mathrm{cr}}) \cos\theta \tag{B.7}$$

$$V_{\mathrm{br}}^{(\mathrm{ii})} = (P_{\mathrm{t}} - 0.3P_{\mathrm{cr}}) \sin\theta \tag{B.8}$$

In the remainder of this chapter, the measured brace yield and ultimate stresses will be used in the calculations directly (i.e., R_{y} and R_{t} are not necessary).

B.1.2 Connection Demand-to-Capacity Ratios

Brace Limit States

- **Block shear rupture**

$$DCR_{\mathrm{bs,br}} = \frac{P_{\mathrm{t}}}{\phi_{\mathrm{bs,br}} P_{\mathrm{bs,br}}} \tag{B.9}$$

$$P_{\mathrm{bs,br}} = 0.6 F_{\mathrm{u}} A_{\mathrm{nv}} \tag{B.10}$$

Example: TNCBF1-N-HSS (1F), AISC/BDP method

$$\begin{aligned} A_{\text{nv}} &= l_{\text{w}} t_{\text{br}} N_{\text{br}} \\ &= (254 \text{ mm})(5.92 \text{ mm})(4) \\ &= 6014.7 \text{ mm}^2 \end{aligned}$$

$$\begin{aligned} P_{\text{bs}} &= 0.6 F_{\text{u}} A_{\text{nv}} \\ &= 0.6(508 \text{ MPa})(6014.7 \text{ mm}^2) \\ &= 1833.3 \text{ kN} \end{aligned}$$

$$\begin{aligned} DCR_{\text{bs,br}} &= \frac{P_{\text{t}}}{\phi_{\text{bs,br}} P_{\text{bs,br}}} \\ &= \frac{1763 \text{ kN}}{(0.75)(1827.1 \text{ kN})} \\ &= \boxed{1.28} \end{aligned}$$

- **Net section rupture**

$$DCR_{\text{ns}} = \frac{P_{\text{t}}}{\phi_{\text{bs}} P_{\text{ns}}} \tag{B.11}$$

$$P_{\text{ns}} = U F_{\text{u}} A_{\text{n}} \tag{B.12}$$

Example: TNCBF1-N-HSS (1F), AISC method

$$\begin{aligned} A_{\mathrm{n}} &= A_{\mathrm{g}} - 2t_{\mathrm{slot}}t_{\mathrm{br}} \\ &= 3981\ \mathrm{mm}^2 - (2)(17\ \mathrm{mm})(5.92\ \mathrm{mm}) \\ &= 3779.7\ \mathrm{mm}^2 \end{aligned}$$

$$\begin{aligned} U &= 1 - \frac{\bar{x}}{l_{\mathrm{w}}} \\ &= 1 - \frac{66.7\ \mathrm{mm}}{254\ \mathrm{mm}} \\ &= 0.74 \end{aligned}$$

$$\begin{aligned} P_{\mathrm{ns}} &= UF_{\mathrm{u}}A_{\mathrm{n}} \\ &= (0.74)(508\ \mathrm{MPa})(3779.7\ \mathrm{mm}^2) \\ &= 1420.9\ \mathrm{kN} \end{aligned}$$

$$\begin{aligned} DCR_{\mathrm{ns}} &= \frac{P_{\mathrm{t}}}{\phi_{\mathrm{bs}}P_{\mathrm{ns}}} \\ &= \frac{1763\ \mathrm{kN}}{(0.75)(1420.9\ \mathrm{kN})} \\ &= \boxed{1.65} \end{aligned}$$

- **Splice weld rupture**

$$DCR_{\mathrm{sw}} = \frac{P_{\mathrm{t}}}{\phi_{\mathrm{sw}}P_{\mathrm{sw}}} \tag{B.13}$$

$$P_{\text{sw}} = 0.6F_{\text{EXX}}N_{\text{br}}0.707w_{\text{br}}l_{\text{w}} \tag{B.14}$$

Example: TNCBF1-N-HSS (1F), AISC method

$$\begin{aligned} P_{\text{sw}} &= (0.6)(482.6\text{ MPa})(4)(0.707)(11\text{ mm})(254\text{ mm}) \\ &= 2287.9\text{ kN} \end{aligned}$$

$$\begin{aligned} DCR_{\text{sw}} &= \frac{1763\text{ kN}}{(0.75)(2287.9\text{ kN})} \\ &= \boxed{1.03} \end{aligned}$$

Connection Limit States

- **Whitmore yielding**

$$DCR_{\text{wy}} = \frac{P_{\text{t}}}{\phi_{\text{wy}}P_{\text{wy}}} \tag{B.15}$$

$$P_{\text{wy}} = F_{\text{y}}B_{\text{w}}t_{\text{p}} \tag{B.16}$$

Example: TNCBF1-N-HSS (1F), AISC method

Note: The Whitmore length may extend into the beams and columns, as shown in Fig. B.1, so the beam and column web thicknesses and yield strengths may need to be considered in the calculation.

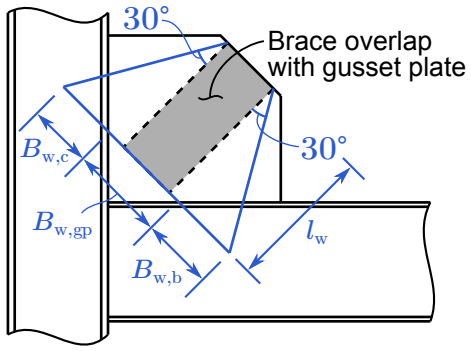

Figure B.1: Whitmore section diagram

$$A_{w,gp} = B_{w,gp}t_{gp} = (360\text{ mm})(12\text{ mm}) = 4320\text{ mm}^2$$
$$A_{w,c} = B_{w,c}t_c = (112\text{ mm})(10.9\text{ mm}) = 1221\text{ mm}^2$$
$$A_{w,b} = B_{w,b}t_b = (0\text{ mm})(8.8\text{ mm}) = 0\text{ mm}^2$$

$$\begin{aligned} P_{wy} &= F_{y,gp}A_{w,gp} + F_{y,c}A_{w,c} + F_{y,b}A_{w,b} \\ &= (337\text{ MPa})(4320\text{ mm}^2) + (395\text{ MPa})(1221\text{ mm}^2) + (414\text{ MPa})(0\text{ mm}^2) \\ &= 1938.1\text{ kN} \end{aligned}$$

$$\begin{aligned} DCR_{wy} &= \frac{P_t}{\phi_{wy}P_{wy}} \\ &= \frac{1763\text{ kN}}{(0.90)(1938.1\text{ kN})} \\ &= \boxed{1.01} \end{aligned}$$

- **Whitmore fracture**

$$DCR_{\text{wf}} = \frac{P_{\text{t}}}{\phi_{\text{wf}} P_{\text{wf}}} \tag{B.17}$$

$$P_{\text{wf}} = F_{\text{u}} B_{\text{w}} t_{\text{p}} \tag{B.18}$$

Example: TNCBF1-N-HSS (1F), AISC method

Note: The same Whitmore subareas (i.e., $A_{\text{w,gp}}$, $A_{\text{w,c}}$, and $A_{\text{w,b}}$) are used in the calculation for Whitmore fracture.

$$\begin{aligned} P_{\text{wy}} &= F_{\text{u,gp}} A_{\text{w,gp}} + F_{\text{u,c}} A_{\text{w,c}} + F_{\text{u,b}} A_{\text{w,b}} \\ &= (504 \text{ MPa})(4320 \text{ mm}^2) + (506 \text{ MPa})(1221 \text{ mm}^2) + (519 \text{ MPa})(0 \text{ mm}^2) \\ &= 2795.1 \text{ kN} \end{aligned}$$

$$\begin{aligned} DCR_{\text{wf}} &= \frac{P_{\text{t}}}{\phi_{\text{wf}} P_{\text{wf}}} \\ &= \frac{1763 \text{ kN}}{(0.75)(2795.1 \text{ kN})} \\ &= \boxed{0.84} \end{aligned}$$

- **Flexural buckling**

$$DCR_{\text{b}} = \frac{P_{\text{cr}}}{\phi_{\text{b}} P_{\text{b}}} \tag{B.19}$$

$$P_{\text{b}} = B_{\text{w}} t_{\text{p}} F_{\text{cr}} \tag{B.20}$$

Example: TNCBF1-N-HSS (1F), AISC method

Note: F_{cr} for the plate is calculated as in Eq. B.3. The buckling length can be taken as the average unbraced lengths of the gusset plate at the ends and middle of the Whitmore section. These dimensions are shown as l_1, l_2, and l_3 in Fig. B.2. When the Whitmore section falls outside the gusset plate, the lengths are can be taken as negative back from the Whitmore section to the gusset plate. For example, in Fig. B.2, l_1 and l_3 would have negative values.

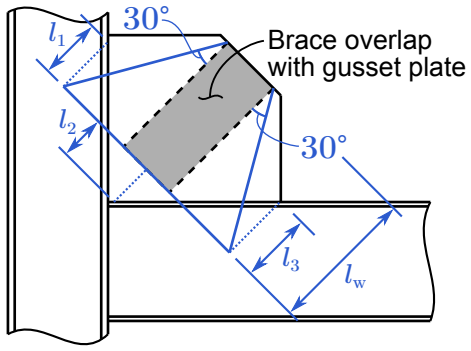

Figure B.2: Flexural buckling diagram based on Whitmore width

$$\begin{aligned} L_b &= \frac{l_1 + l_2 + l_3}{3} \\ &= \frac{-117 \text{ mm} + 127 \text{ mm} + 80 \text{ mm}}{3} \\ &= 30 \text{ mm} \end{aligned}$$

$$\begin{aligned} I_w &= I_{w,gp} + I_{w,c} + I_{w,b} \\ &= \frac{1}{12} B_{w,gp} t_{gp}^3 + \frac{1}{12} B_{w,c} t_c^3 + \frac{1}{12} B_{w,b} t_b^3 \\ &= \frac{1}{12}(360 \text{ mm})(12 \text{ mm})^3 + \frac{1}{12}(112 \text{ mm})(10.9 \text{ mm})^3 + \frac{1}{12}(0 \text{ mm})(8.8 \text{ mm}) \\ &= 63927 \text{ mm}^4 \end{aligned}$$

$$\begin{aligned} r_{\mathrm{w}} &= \sqrt{\frac{I_{\mathrm{w}}}{A_{\mathrm{w,gp}} + A_{\mathrm{w,c}} + A_{\mathrm{w,b}}}} \\ &= \sqrt{\frac{63927 \text{ mm}^4}{4320 \text{ mm}^2 + 1221 \text{ mm}^2 + 0 \text{ mm}^2}} \\ &= 3.40 \text{ mm} \end{aligned}$$

$$\begin{aligned} \frac{K_{\mathrm{w}} L_{\mathrm{b}}}{r_{\mathrm{w}}} &= \frac{(0.65)(30 \text{ mm})}{3.40 \text{ mm}} \\ &= 5.74 \end{aligned}$$

$$\begin{aligned} F_{\mathrm{y}} &= \frac{P_{\mathrm{wy}}}{A_{\mathrm{w,gp}} + A_{\mathrm{w,c}} + A_{\mathrm{w,b}}} \\ &= \frac{1938.1 \text{ kN}}{4320 \text{ mm}^2 + 1221 \text{ mm}^2 + 0 \text{ mm}^2} \\ &= 349.8 \text{ MPa} \end{aligned}$$

$$\begin{aligned} F_{\mathrm{e}} &= \frac{\pi^2 E}{\left(\frac{KL}{r}\right)^2} \\ &= \frac{\pi^2 (200 \times 10^3 \text{ MPa})}{5.74^2} \\ &= 59911 \text{ MPa} \end{aligned}$$

$$
\begin{aligned}
F_{\text{cr}} &= 0.658^{\frac{F_{\text{y}}}{F_{\text{e}}}} F_{\text{y}} \\
&= 0.658^{\frac{349.8\ \text{MPa}}{59911\ \text{MPa}}} (349.8\ \text{MPa}) \\
&= 348.9\ \text{MPa}
\end{aligned}
$$

- **Block shear rupture**

$$DCR_{\text{bs,gp}} = \frac{P_{\text{t}}}{\phi_{\text{bs,gp}} P_{\text{bs,gp}}} \tag{B.21}$$

$$P_{\text{bs,gp}} = \begin{cases} 0.6F_{\text{u}}A_{\text{nv}} + U_{\text{bs}}F_{\text{u}}A_{\text{nt}} \leq 0.6F_{\text{y}}A_{\text{gv}} + U_{\text{bs}}F_{\text{u}}A_{\text{nt}} & \text{(AISC)} \\ 0.6F_{\text{u}}A_{\text{nt}} + U_{\text{bs}}F_{\text{u}}A_{\text{nt}} & \text{(BDP)} \end{cases} \tag{B.22}$$

Example: TNCBF1-N-HSS (1F), AISC method

$$
\begin{aligned}
A_{\text{nv}} = A_{\text{gv}} &= 2l_w t_{\text{gp}} \\
&= (2)(254\ \text{mm})(12\ \text{mm}) \\
&= 6096\ \text{mm}^2
\end{aligned}
$$

$$
\begin{aligned}
A_{\text{nt}} &= b_{\text{br}} t_{\text{gp}} \\
&= (177.8\ \text{mm})(12\ \text{mm}) \\
&= 2134\ \text{mm}^2
\end{aligned}
$$

$$
\begin{aligned}
P_{\text{bs,gp}} &= 0.6F_{\text{u}}A_{\text{nv}} + U_{\text{bs}}F_{\text{u}}A_{\text{nt}} \leq 0.6F_{\text{y}}A_{\text{gv}} + U_{\text{bs}}F_{\text{u}}A_{\text{nt}} \\
&= (0.6)(504\text{ MPa})(6096\text{ mm}^2) + (1)(504\text{ MPa})(2134\text{ mm}^2) \leq \\
&\quad ...(0.6)(337\text{ MPa})(6096\text{ mm}^2) + (1)(504\text{ MPa})(2134\text{ mm}^2) \\
&= 2919 \leq 2308\text{ kN} \\
&= 2308\text{ kN}
\end{aligned}
$$

$$
\begin{aligned}
DCR_{\text{bs,gp}} &= \frac{P_{\text{t}}}{\phi_{\text{bs,gp}}P_{\text{bs,gp}}} \\
&= \frac{1763\text{ kN}}{(0.75)(2308\text{ kN})} \\
&= \boxed{1.02}
\end{aligned}
$$

- **Interface welds**

$$
DCR_{\text{wd,gp|b}} = \begin{cases} \dfrac{\sigma_{\text{eff}}}{\phi_{\text{w}}\sigma_{\text{w,gp|b}}} & \text{(AISC)} \\ \dfrac{F_{\text{y}}t_{\text{p}}}{\beta_{\text{w}}p_{\text{w,gp|b}}} & \text{(BDP)} \end{cases} \tag{B.23}
$$

$$
P_{\text{w,gp|b}} = 0.6F_{\text{EXX}}\left[1 + 0.5\sin^{1.5}\gamma\right]2L_{\text{w}}0.707w_1 \quad \text{(AISC)} \tag{B.24}
$$

$$
p_{\text{w,gp|b}} = 2(1.5)(0.6)F_{\text{EXX}}0.707w_1 \quad \text{(BDP)} \tag{B.25}
$$

Example: TNCBF1-N-HSS (1F corner), AISC method

Note: The Uniform Force Method (UFM) is used to calculate demand in the AISC method. Based on this, $H_{\text{b}} = 596.6$ kN, $V_{\text{b}} = 148.6$ kN, and $M_{\text{b}} = 3491$ kN-mm.

$$\begin{aligned} A_{\mathrm{w}} &= 2(0.707)w_1 L_{\mathrm{w}} \\ &= (2)(0.707)(8\text{ mm})(348\text{ mm}) \\ &= 3937\text{ mm}^2 \end{aligned}$$

$$\begin{aligned} S_{\mathrm{w}} &= \frac{2(0.707)w_1 L_{\mathrm{w}}^2}{6} \\ &= \frac{(2)(0.707)(8\text{ mm})(348\text{ mm})^2}{6} \\ &= 228321\text{ mm}^3 \end{aligned}$$

$$\begin{aligned} \sigma_{\mathrm{l}} &= \frac{H_{\mathrm{b}}}{A_{\mathrm{w}}} \\ &= \frac{596.6\text{ kN}}{3937\text{ mm}^2} \\ &= 151.5\text{ MPa} \end{aligned}$$

$$\begin{aligned} \sigma_{\mathrm{t}} &= \frac{V_{\mathrm{b}}}{A_{\mathrm{w}}} + \frac{M_{\mathrm{b}}}{S_{\mathrm{w}}} \\ &= \frac{148.6\text{ kN}}{3937\text{ mm}^2} + \frac{3491\text{ kN-mm}}{228321\text{ mm}^3} \\ &= 53.0\text{ MPa} \end{aligned}$$

$$\begin{aligned}\sigma_{\text{eff}} &= \sqrt{\sigma_{\text{l}}^2 + \sigma_{\text{t}}^2} \\ &= \sqrt{(151.5 \text{ MPa})^2 + (53.0 \text{ MPa})^2} \\ &= 160.5 \text{ MPa}\end{aligned}$$

$$\begin{aligned}\gamma &= \arctan\left(\frac{\sigma_{\text{t}}}{\sigma_{\text{l}}}\right) \\ &= \arctan\left(\frac{53.0 \text{ MPa}}{151.5 \text{ MPa}}\right) \\ &= 19.28^{\text{o}}\end{aligned}$$

$$\begin{aligned}\sigma_{\text{w,gp|b}} &= 0.6F_{\text{EXX}}\left[1 + 0.5\sin^{1.5}\gamma\right] \\ &= (0.6)(482.6 \text{ MPa})\left[1 + 0.5\sin^{1.5}(19.28^{\text{o}})\right] \\ &= 317.0 \text{ MPa}\end{aligned}$$

$$\begin{aligned}DCR_{\text{w,gp|b}} &= \frac{\sigma_{\text{eff}}}{\phi_{\text{w}}\sigma_{\text{w,gp|b}}} \\ &= \frac{160.5 \text{ MPa}}{(0.75)(317.0 \text{ MPa})} \\ &= \boxed{0.68}\end{aligned}$$

Example: TNCBF1-N-HSS, BDP method

$$
\begin{aligned}
p_{\mathrm{w,gp|b}} &= 2(1.5)(0.6)F_{\mathrm{EXX}}0.707w_1 \\
&= (2)(1.5)(0.6)(482.6\text{ MPa})(0.707)(8\text{ mm}) \\
&= 4.913\text{ kN/mm}
\end{aligned}
$$

$$
\begin{aligned}
DCR_{\mathrm{w,gp|b}} &= \frac{F_{\mathrm{y}}t_{\mathrm{p}}}{\beta_{\mathrm{w}}p_{\mathrm{w,gp|b}}} \\
&= \frac{(0.337\text{ GPa})(12\text{ mm})}{(0.75)(4.913\text{ kN/mm})} \\
&= \boxed{1.10}
\end{aligned}
$$

B.1.3 Beams

Axial-Flexural Interaction

$$
DCR_{\mathrm{b}} = \frac{H_{\mathrm{br}}}{\phi_{\mathrm{c}}P_{\mathrm{cr}}} + \frac{8}{9}\frac{M_{\mathrm{br}}}{\phi_{\mathrm{b}}M_{\mathrm{p}}} \tag{B.26}
$$

Example: TNCBF1-N-HSS (1F), load case (ii)

Note: The compressive and flexural capacities of the beam were calculated to be $P_{\mathrm{cr}} = 2788$ kN and $M_{\mathrm{p}} = 558343$ kN-mm, respectively.

$$
\begin{aligned}
M_{\mathrm{br}} &= \frac{V_{\mathrm{br}}L_{\mathrm{b}}}{4} \\
&= \frac{(949\text{ kN})(5948\text{ mm})}{4} \\
&= 1411163\text{ kN-mm}
\end{aligned}
$$

$$
\begin{aligned}
DCR_{\mathrm{b}} &= \frac{H_{\mathrm{br}}}{\phi_{\mathrm{c}} P_{\mathrm{cr}}} + \frac{M_{\mathrm{br}}}{\phi_{\mathrm{b}} M_{\mathrm{p}}} \\
&= \frac{764 \text{ kN}}{(0.9)(2788 \text{ kN})} + \frac{8}{9} \frac{1411163 \text{ kN-mm}}{(0.9)(558343 \text{ kN-mm})} \\
&= \boxed{2.80}
\end{aligned}
$$

BIBLIOGRAPHY

AISC (1997). "Seismic provisions for structural steel buildings." *AISC 341-97*, American Institute of Steel Construction, Chicago, IL.

AISC (2010a). "Seismic provisions for structural steel buildings." *AISC 341-10*, American Institute of Steel Construction, Chicago, IL.

AISC (2010b). "Specification for structural steel buildings." *AISC 360-10*, American Institute of Steel Construction, Chicago, IL.

AISC (2010c). "Steel construction manual." American Institute of Steel Construction, Chicago, IL.

CSA (1994). "Limit states design of steel structures." *CAN/CSA-S16.1-94*, Canadian Standards Association, Rexdale, Ontario.

Dassault Systèmes (2013). "Abaqus Unified FEA (Version 6.12-3).

Foutch, D. A., Goel, S. C., and Roeder, C. W. (1987). "Seismic testing of full-scale steel building–part i." *Journal of Structural Engineering*, 113(11), 2111–2129.

Fukuta, T., Nishiyama, I., Yamanouchi, H., and Kato, B. (1989). "Seismic performance of steel frames with inverted v braces." *Journal of Structural Engineering*, 115(8), 2016–2028.

Goel, S. C. (1992). "Cyclic post buckling behavior of steel bracing members." *Stability and Ductility of Steel Structures under Cyclic Loading*, CRC Press, Boca Raton, FL.

Hsiao, P. C. (2012). "Seismic performance evaluation of concentrically braced frames." Ph.D. thesis, University of Washington, Seattle.

ICBO (1988). "1988 Uniform Building Code." International Conference of Building Officials, Whittier, CA.

Johnson, M. M. (2014). "Seismic evaluation of bolted connections in non-seismic concentrically braced frames." M.S. thesis, Univeristy of Washington, Seattle.

Kelly, D. J., Bonneville, D. R., and Bartoletti, S. J. (2000). "1994 Northridge Earthquake: Damage to a four-story steel braced frame building and its subsequent upgrade." *Proceedings of the 12th World Conference on Earthquake Engineering*, Auckland, New Zealand.

Khatib, I. F., Mahin, S. A., and Pister, K. S. (1988). "Seismic behavior of concentrically braced steel frames." *PEER Report 1988/01*, Pacific Earthquake Engineeirng Research Center, Berkeley, CA.

Kotulka, B. A. (2007). "Analysis for a design guide on gusset plates used in special concentrically braced frames." M.S. thesis, University of Washington, Seattle.

Lehman, D. E., Roeder, C. W., Herman, D., Johnson, S., and Kotulka, B. (2008). "Improved seismic performance of gusset plate connections." *Journal of Structural Engineering*, 134(6), 890–901.

Liu, Z. and Goel, S. C. (1988). "Cyclic load behavior of concrete-filled tubular braces." *Journal of Structural Engineering*, 114(7), 1488–1506.

Lumpkin, E. J. (2009). "Enhanced seismic performance of multi-story special concentrically brace frames using a balanced design procedure." M.S. thesis, University of Washington, Seattle.

Lumpkin, E. J., Hsiao, P. C., Roeder, C. W., Lehman, D. E., Tsai, C. Y., Wu, A. C., Wei, C. Y., and Tsai, K. C. (2012). "Investigation of the seismic performance of three-story special concentrically braced frames." *Journal of Constructional Steel Research*, 77, 131–144.

NEES (2014). "NEEShub." *Project Warehouse*, <https://nees.org/> (Aug. 4, 2014).

Powell, J. A. (2010). "Evaluation of special concentrically braced frames for improved seismic performance and constructability." M.S. thesis, University of Washington, Seattle.

Rai, D. C. and Goel, S. C. (2003). "Seismic evaluation and upgrading of chevron braced frames." *Journal of Constructional Steel Research*, 59(8), 971–994.

Roeder, C. W. (1989). "Seismic behavior of concentrically braced frame." *Journal of Structural Engineering*, 115(8), 1837–1856.

Roeder, C. W., Lehman, D. E., Clark, K., Yoo, J. H., Tsai, K. C., Lin, C. H., and Wei, C. Y. (2011a). "Influence of gusset plate connections and braces on the seismic performance of x-braced frames." *Earthquake Engineering and Structural Dynamics*, 40(4), 355–374.

Roeder, C. W., Lumpkin, E. J., and Lehman, D. E. (2011b). "A balanced design procedure for special concentrically braced frame connections." *Journal of Constructional Steel Research*, 67(11), 1760–1772.

Roeder, C. W., Tsai, K. C., Lehman, D. E., Lien, Y. C., Lumpkin, E., Tsai, C. Y., Hsiao, P., and Ao, W. H. (2013). "In-plane buckling of special concentrically braced frames." *Engineering Journal* Submitted for publication.

Sloat, D. A. (2014). "Evaluation and retrofit of non-capacity designed braced frames." M.S. thesis, Univeristy of Washington, Seattle.

Tremblay, R., Haddad, M., Martinez, G., Richard, J., and Moffatt, K. (2008). "Inelastic cyclic testing of large size steel bracing members." *Proceedings of the 14th World Conference on Earthquake Engineering*, Beijing, China.

Tremblay, R. and Robert, N. (2000). "Seismic design of low- and medium-rise chevron braced steel frames." *Canadian Journal of Civil Engineering*, 27, 1192–1206.

Tremblay, R. and Robert, N. (2001). "Seismic performance of low- and medium-rise chevron braced steel frames." *Canadian Journal of Civil Engineering*, 28, 699–714.

Tsai, C. Y., Tsai, K. C., Lin, P. C., Ao, W. H., Roeder, C. W., Mahin, S. A., Lin, C. H., Yu, Y. J., Wang, K. J., Wu, A. C., Chen, J. C., and Lin, T. H. (2013). "Seismic design and hybrid tests of a full-scale 3-story concentrically braced frame using in-plane buckling braces." *Earthquake Spectra*, 29(3), 1043–1067.

Uriz, P. and Mahin, S. A. (2008). "Toward earthquake-resistance design of concentrically braced steel-frame structures." *PEER Report 2008/08*, Pacific Earthquake Engineeirng Research Center, Berkeley, CA.